2017

Testing the late-Holocene climate signal from ombrotrophic bogs in southernmost Chile and the Falkland Islands: a multi-proxy, multi-profile and multi-site approach

Rice, Emma May

Testing the late-Holocene climate signal from ombrotrophic bogs in southernmost Chile and the Falkland Islands: a multi-proxy, multi-profile and multi-site approach

by

EMMA MAY RICE

A thesis submitted to the University of Plymouth for the degree of

DOCTOR OF PHILOSOPHY

School of Geography, Earth and Environmental Sciences

September 2016

Testing the late-Holocene climate signal from ombrotrophic bogs in southernmost Chile and the Falkland Islands: a multi-proxy, multi-profile and multi-site approach

Emma May Rice

Peatlands in Southern South America (SSA), in the path of the Southern Westerly Wind belt (SWW), offer the potential of reliable palaeoclimate archives. This investigation aimed to test the late-Holocene climate signal related to variability of the SWW. Three sites were investigated: San Juan and Karukinka bog, southernmost Chile and San Carlos, a *Sphagnum* dominated bog, discovered in the Falkland Islands, to form a regional comparison. A multi-proxy approach was used, combining both palaeoecological and stable isotopic methods. At one site, Karukinka, intra-site replicability was tested across three profiles located along a microtopographical gradient. A low number of statistically significant correlations between proxies were evident. KAR-EM-1, the low-hummock profile, displayed the highest number of significant correlations, suggesting an optimal coring location. Chronological uncertainty in the high-hummock profile, KAR-EM-3, was the focus of discussion. Intra-site replicability between the palaeoecological records was improved by plotting the records against a 'master chronology', from the mid-hummock profile, KAR-EM-2, assuming a synchronous acrotelm-catotelm boundary across the profiles. The testate amoeba inferred depth to water table (WTD) reconstructions offered the highest intra-site coherence, while the stable isotope records suggested generally poor intra-site replicability. A semi-quantitative method of intra-site comparison was carried out which resulted in a number of climate scenarios. The inter-site comparison assessed correlations between the records from the three sites. A lack of significant correlations between the sites may have been due to regional climate variations and differences in the temporal resolution of the records. Robust climatic inferences were limited to the last 300 years. The WTD reconstructions displayed the highest inter-site coherence and suggested a drying trend after AD 1930 due to a southerly shift of the SWW. Late-Holocene climate variability was inferred from the palaeoecological records from Karukinka. Two periods were identified: a MCA period of generally wetter conditions (AD 750-1100) and a LIA period of overall drier conditions (~AD 1100-1900) during a southerly and northerly shifted SWW respectively, driven by solar variability and polar cell strengthening.

Acknowledgements

I would like to thank everybody who has made the completion of this thesis possible. Firstly, thank you to my supervisors, Prof. Neil Roberts and Dr Tim Daley, for their much needed advice and support throughout this PhD.

I would also like to thank NERC for providing funding for this project, without which fieldwork in Patagonia would not have been possible. I am very grateful to have had the opportunity to visit and undertake research in such a beautiful and interesting part of the world.

Thank you to members of the PATAGON and PARAD research groups, who I met on fieldwork and who provided an inspirational start to my PhD. In particular, Dr Tom Roland and Dr Simon van Bellen who introduced me to the wonderful world of peatlands! Thanks to Tim and Paola for their hard work in the field. Thank you to Dr Katie Head for technical support in the lab and thanks to various 8th floor lab buddies over the years.

Thank you to my family and friends, who provided strength and encouragement when I needed it the most. Thank you to Dr Kim Davies who turned up in the last year of my PhD - I'm not sure I would have seen it through without your support. Finally, thank you to my cat, Lola, for getting me out of bed every morning!

Author's declaration

At no time during the registration for the degree of Doctor of Philosophy has the author been registered for any other University award without prior agreement of the Graduate Sub-Committee.

Work submitted for this research degree at Plymouth University has not formed part of any other degree either at Plymouth University or at another establishment.

This study was financed by a NERC studentship.

Presentations and Conferences attended:

Rice, E. M., Daley, T. J. And Roberts, C. N., 2015 '*Testing the late-Holocene climatic signal from ombrotrophic bogs in southernmost Chile: an intra-site comparison of multi-proxy records*', 19th INQUA congress 'Quaternary Perspectives on Climate Change, Natural Hazards and Civilization', Nagoya, Japan. (Presentation)

Rice, E. M., 2013 '*Testing the late-Holocene climate signal from ombrotrophic bogs in southernmost Chile: a multi-proxy, multi-profile and multi-site approach'*, 18th QRA International Postgraduate Symposium, Southampton, UK. (Presentation)

Word count: 75,485

Signed ……

Date ……

List of contents

List of figures

List of tables

Chapter 1: Introduction

1.1 Project rationale

The strength and intensity of the circumglobal Southern Westerly Wind Belt (SWW) determines Southern Hemisphere (SH) mid-latitude weather systems, thus strongly influencing temperatures and precipitation in the mid-latitudes (Jones *et al*., 2009). A southerly shift of the mean annual latitude of this wind belt has been observed through the late 20th and early 21st centuries (Thompson and Solomon, 2002; Marshall, 2003) related to a positive index of the Southern Annular Mode (SAM) attributed to anthropogenic forcing (Section 2.1).

In comparison with the Northern Hemisphere (NH) relatively little is known about late-Holocene climate variability from the Southern Hemisphere (Wilmes *et al*., 2012) and is thus described as 'terra incognita' (Villalba *et al*., 2009) in terms of the relatively low density of proxy records available (Wilmes *et al*., 2012).

Southern South America (SSA) is the only continental landmass between 38°S and the Antarctic Circle which interrupts the SWW. Located in the present-day core of the SWW SSA is the ideal location for palaeoenvironmental reconstructions to track shifts in the strength and position of the SWW. To date, relatively few palaeoclimate records exist from this region especially of high enough resolution to establish natural variability in the absence of millennial scale orbital forcing (Section 2.2).

The use of peat as a palaeoclimate archive has long been established. Peatlands are now recognised as complex adaptive systems and the reinvigoration of early ideas of the dominance of autogenic, ecohydrological feedbacks, now questions the use of such palaeoclimate records. Despite this, many methods to reconstruct bog surface wetness (BSW) variability are now well established. The advantages of using a multi-proxy, multi-profile and multi-site approach may add to the debate around the dominance of autogenic and allogenic (climate) drivers of change in peatlands (Section 2.3).

1.2 Aim and research questions

In consideration of the research context, the aim of this investigation is *to* ***test the late-Holocene climate signal from ombrotrophic bogs in southernmost Chile and the Falkland Islands using a multi-proxy, multi-profile and multi-site approach.***

The following research questions will be considered:

1. **To what extent are there correlations between multiple proxies and multiple profiles from an ombrotrophic bog, Karukinka, in southernmost Chile?**
2. **To what extent are there correlations between multiple proxies from San Juan bog, Chile and from San Carlos bog, Falkland Islands?**
3. **Provided that these records have responded to recent (late 20th century) and late-Holocene (Medieval Climate Anomaly and Little Ice Age) climate variability related to shifts in the SWW, to what degree are there correlations between records from the multiple sites?**

Using a multi-proxy, multi-profile and multi-site approach it is hypothesised that correlations between these aspects will offer support for the use of ombrotrophic bogs from the region in inferring late-Holocene climate variability related to shifts in the SWW.

1.3 Thesis structure

Chapter 2 presents the research context of this thesis and involves three main themes:

1. Late-Holocene climate in southernmost Chile (and Falkland islands).
2. Climate signal from ombrotrophic bogs.
3. Multi-proxy, multi-profile and multi-site relating to the above

Chapter 3 presents the methodology of this thesis including the field methods, laboratory methods and statistical methods used to address the research questions. Chapter 4 presents the chronology of the profiles used in this thesis, the methods are reviewed and the chronological results are presented. Chapter 5 presents the

results of this thesis. The results from each profile are presented in this chapter plotted against depth to provide the context for subsequent chapters. Chapter 6 presents the first of two discussion chapters and presents the intra-site comparison of multi-proxy records from the KAR-EM profiles. Chapter 7 presents the second of two discussion chapters and presents the inter-site comparison of multi-proxy records from all profiles in the thesis to inform regional climate variability. Chapter 8 presents the conclusions of this thesis.

1.4 Frequently used acronyms

Terms that are frequently used throughout this thesis are given acronyms. On first use the full term is provided, followed by the acronym in brackets. The most frequently used are listed below.

BSW – Bog Surface Wetness
Cal BP – Calibrated years Before Present
DHI – Dupont Hydroclimatic Index
ENSO – El niño southern oscillation
KAR-EM-3 – High-hummock profile from Karukinka bog, Chile
KAR-EM-2 - Mid-hummock profile from Karukinka bog, Chile
KAR-EM-1 - Low-lawn profile from Karukinka bog, Chile
LIA – Little Ice Age
MCA – Medieval Climate Anomaly
SAN-EM-2 - Profile from San Juan bog, Chile
SCB-1 - Profile from San Carlos bog, Falkland Islands
SSA – Southern South America
SWW – Southern Westerly Wind belt
WTD – depth to the Water Table

Chapter 2: Research context

2.1 The Southern Westerly Wind Belt (SWW): Understanding modern variability

2.1.1 Modern climatology and intra-annual variability

An understanding of the modern climatology of South America is essential to the interpretation of palaeoclimate records from the continent (Garreaud, 2007; Garreaud and Aceituno, 2007; Garreaud *et al*., 2009; Garreaud *et al*., 2013). Southern Westerly Wind belt variability is extremely complex but is relatively well understood on the seasonal timescale (Garreaud, 2007; Garreaud *et al.*, 2013).

Meteorological stations are lacking and instrumental records are discontinuous and of poor quality in SSA making reconstructions of climate variability in the recent past difficult (Villalba *et al*., 2003; Moy *et al*., 2009). Instrumental records and reanalysis data have however, enabled an understanding of intra- and inter-annual climate variability in the region at least over the past ~50 years.

The SWW circulates globally around the southern mid-latitudes of the Earth's atmosphere between sub-tropical high pressure areas and Antarctic low pressure areas. These are a result of ocean-atmosphere interactions originating in the tropics (ITCZ (Intertropical Convergence Zone) and ENSO (El Niño Southern Oscillation)) and the high-latitudes (SAM (Southern Annular Mode) and AAO (Antarctic Oscillation)) respectively (Moy *et al*., 2009).

This dominant mode of variability in the Southern Hemisphere atmospheric circulation is known as the SAM or synonymously the Antarctic Oscillation (AAO) (Gong and Wang, 1999; Jones and Widmann, 2004; Sallée *et al*., 2010) and largely influences temperatures and precipitation in Antarctica and the Southern Hemisphere mid-latitudes (Jones *et al*., 2009).

On the seasonal timescale the principal driver of SWW variability originates in the tropics. The ITCZ, driven by solar radiation, transfers surplus heat energy from the tropics to the mid- and high- latitudes via atmospheric-ocean circulation systems. Via this mechanism the southeast Pacific subtropical anticyclone is shifted seasonally

causing differences in the pressure gradient with the circum-Antarctic low pressure belt. Thus, latitudinal Sea Surface Temperature (SST) gradients (see Figure 2.2A for latitudinal SST) in the Pacific and vertical atmospheric temperature gradients drive intra- and inter-annual scale variability of the position and intensity of the SWW (Kilian and Lamy, 2012). The mean annual core of the SWW currently lies between 50°–55°S (Lamy *et al*, 2010).

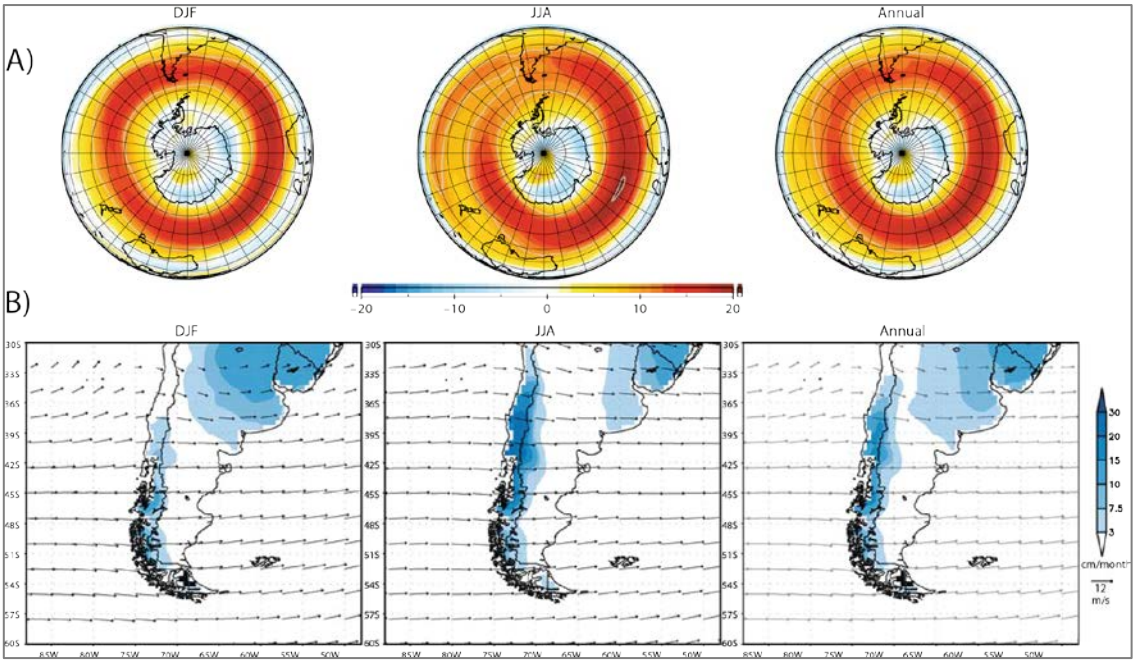

Figure 2.1. From **Moy *et al*. (2009)**. Annual and seasonal composite means of atmospheric circulation and precipitation 1980-2006 in Southern South America. **A)** DJF (Summer), JJA (Winter) and annual composite averages of 700 hPa zonal wind speed (m/s) using NCEP-NCAR reanalysis data. **B)** DJF, JJA and annual composite averages of U (700 hPa wind vectors) and precipitation (cm/month).

Figure 2.1 taken from Moy *et al*. (2009) uses NCEP-NCAR reanalysis data covering the period 1980-2006 to display annual and seasonal composite means of atmospheric circulation and precipitation over SSA (30-56ºS). Figure 2.1A shows how the ITCZ shifts the southeast Pacific subtropical anticyclone south in austral summer, strengthening the SWW as the pressure gradient is increased. The region of the steepest gradient determines the core of the SWW. The core of the SWW is thus between 49 and 53°S revealed by highest wind velocities in austral summer. It shifts north in austral winter decreasing the pressure gradient which weakens the SWW (Lamy *et al*., 2010) with a broader expansion and a northward displacement (Garreaud *et al*., 2009).

Figure 2.1B shows 700 hPa wind vectors and precipitation (cm/month) in the region. A correlation between the two is suggested by the synchrony between maximum precipitation and maximum SWW strength. This correlation between precipitation amount and 850 hPa (near –surface) zonal wind strength is further shown by Figure 2.2 (Garreaud, 2009; Garreaud *et al*., 2009; Garreaud *et al*., 2013). Garreaud *et al.* (2013) using interpolated weather station data find that there is a weaker correlation (r=0.2-0.4) between SWW strength and precipitation on the east side of the Andes compared to the hyperhumid west side. This correlation becomes more negative towards the Atlantic coast due to the provision of precipitation from Atlantic Ocean northerly air masses (Moy *et al*., 2009; Silvestri and Vera, 2009). In periods of weaker SWW there is an increase of precipitation in central and Eastern Patagonia.

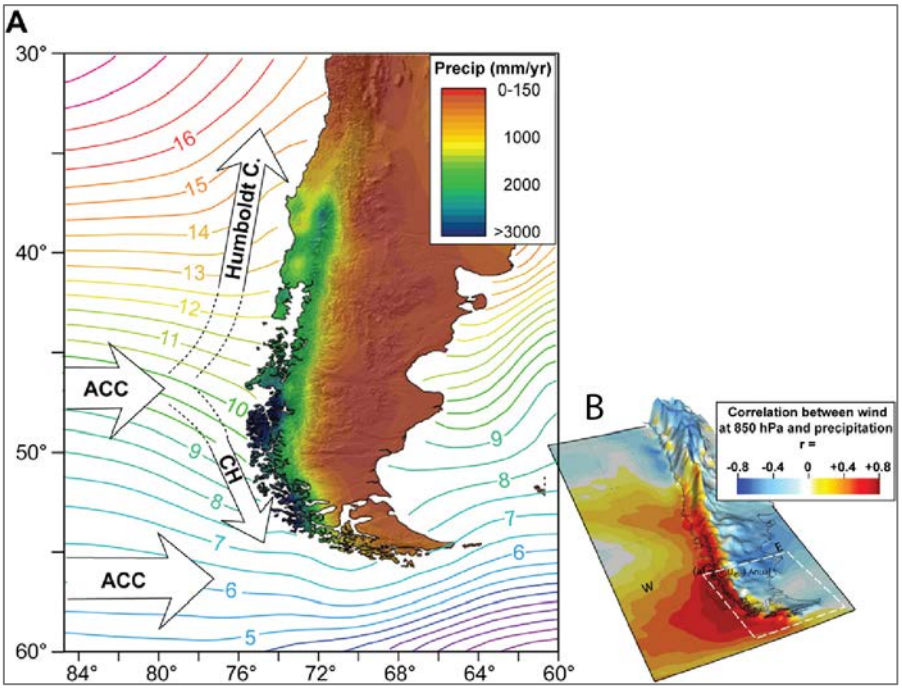

Figure 2.2. From **Kilian and Lamy (2012)**. **A)** Average annual precipitation in the region (data from New *et al*., 2002) with the modern annual mean SST of surrounding oceans (NOAA-CIRES Climate Diagnostics Centre http://www.cdc.noaa.gov/index.html). The ACC (Antarctic Circumpolar Current), Cape Horn and Humboldt currents are shown. **B)** Correlation between 850 hPa zonal wind and precipitation **(Garreaud *et al*., 2013).**

The influence of the Andes as a topographic barrier on precipitation in the region is demonstrated in Figure 2.2A. At ~53ºS a sharp precipitation gradient occurs from the superhumid Western Andes with annual precipitation amounts of 6000-10,000 mm with a subsequent rainshadow effect east of the Andes and precipitation amounts of

500 mm at Punta Arenas decreasing to amounts of 200mm towards the Atlantic coast (Garreaud *et al*., 2009). The precipitation gradient and resulting correlations between wind speed and precipitation are a fundamental consideration throughout this investigation.

Changes in Antarctic temperatures and the extent of Antarctic sea ice affects the pressure gradient therefore, the extent of sea ice influences the position of the SWW (Jones *et al*., 2009). Similarly, a southward shift of the SWW originating in the tropics shifts the ACC (Antarctic Circumpolar Current) southwards (Gille, 2014) causing sea ice expansion (Parkinson and Cavalieri, 2012). A positive feedback, this steepens the temperature gradient and leads to more intense SWW. Such feedbacks (both positive and negative) of the global ocean-atmosphere circulation are extremely important in understanding past, present and future climate variability.

The SWW is globally significant in that it affects global climate and oceanography (Kilian and Lamy, 2012). SWW changes affect the global thermohaline circulation (Marshall and Speer, 2012) and atmospheric CO_2 (Toggweiler *et al*., 2006). Wind-induced upwelling within the ACC forces deep water to the surface of the Southern Ocean reducing the Southern Ocean Carbon sink (Le Quéré *et al*., 2007; Moreno *et al*., 2010). However, Law *et al*. (2008) suggest that variations in SWW may actually result in increased Southern Ocean CO_2 sequestration efficiency. The shifting westerlies also have implications for global sea level rise predictions in that ocean water temperature changes can affect Antarctic ice sheet stability (Paruelo *et al*., 1998; Spence *et al*., 2014).

2.1.2 Inter-annual variability

Variability of the position and intensity of the SWW over inter-annual and inter-decadal timescales is less well understood. Inter-annual links between the El Niño – Southern Oscillation (ENSO) and SAM are evident (L'Heureux and Thompson, 2006; Sun *et al*., 2013). ENSO is the coupling of the oceanic and atmospheric systems primarily centred in the tropical-subtropical Pacific. Teleconnections throughout the global climate system make this phenomenon the most important ocean-atmosphere system, important in consideration of the strength and position of the SWW on decadal and sub-decadal time periods (Philander, 1990; Montecinos and Aceituno, 2003; Schneider and Gies, 2004; Turner, 2004). The ENSO phase cycle is

measured by means of the SOI (Southern Oscillation Index) which is the difference in air pressure between the West and East Pacific (Parker, 1983) and SSTs in the Niño 3.4 region (Trenberth, 1997). Figure 2.3 shows these phases of positive and negative SOI between AD 1970 to 2000 with negative SOI periods of el Niño and positive neutral and la Niña periods. It is thought that el Niño events have become more frequent over this time period with implications for its dominant areas of influence (Kwok and Comiso, 2002) and therefore must be taken into consideration when interpreting the forcing mechanisms of climate variability in SSA.

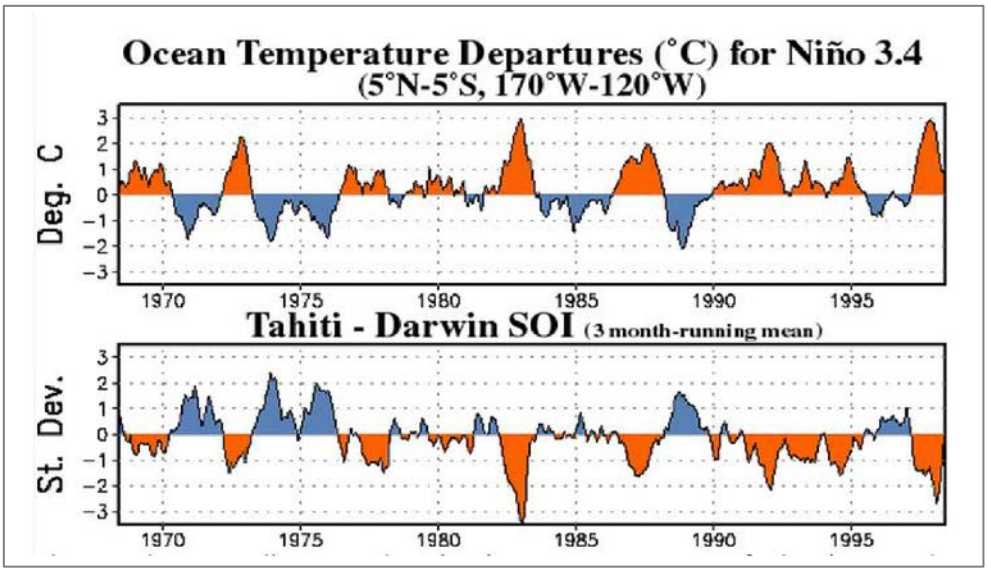

Figure 2.3. Ocean temperature departures in the Niño 3.4 region and the SOI (difference in air pressure between West and East Pacific) AD 1970-2000 (Climate Prediction Center, 2005).

Schneider and Gies (2004) find correlations between the SOI and SWW, suggesting that long-term ENSO variability may play a role in driving inter-annual SWW variability. The mean annual zonal wind speed is correlated with the mean annual SOI West of Chile between 50 and 55°S. Precipitation to the west of the Andes between latitudes 45 and 55°S is thus correlated with the SOI. During el Niño events a decrease in the mean zonal wind speed results in a ~15% reduction in precipitation in this region compared with normal and la Niña periods (Schneider and Gies, 2004). During el Niño years higher than average precipitation is recorded north of 38°S and lower than average between 38 and 41°S (Montecinos and Aceituno, 2003) and 45 and 55°S (Schneider and Gies, 2004). During la Niña years lower than average precipitation occurs north of 38°S and higher than average between 38 and 41°S (Montecinos and Aceituno, 2003) and 45 and 55°S (Schneider and Gies, 2004). On

the east side of the Andes however, the SOI and precipitation are insignificantly correlated, suggesting that ENSO has little effect on precipitation in this region (Schneider and Gies, 2004).

ENSO warm events are linked with negative trends in the SAM index and vice versa over the last 50 years (L'Heureux and Thompson, 2006; Wang and Cai, 2013). ENSO warm events result in the contraction of the Hadley cell due to an enhanced tropical temperature gradient, which then shifts the midlatitude jets equatorward (Sun *et al.*, 2013; Wang and Cai, 2013).

2.1.3 Recent observed SWW shifts

Through the late 20th and early 21st century, a shift in the mean annual latitude of the SWW core has been observed (Thompson and Solomon, 2002; Marshall, 2003) as a poleward shift of 300 hPa zonal wind between 1968 – 2001 (Garreaud, 2007; Garreaud *et al*., 2009). As such, between 55 and 70°S increased wind speeds have been observed and reduced wind speeds observed between 35 and 55°S (Garreaud *et al*., 2013). The observed shift is related to SAM indices which extend back to 1957. They reveal an increase in the positive phase of the SAM since this time (Gong and Wang, 1999; Limpasuvan and Hartmann, 1999; Marshall, 2003; Jones *et al*., 2009; Wilmes *et al*., 2012) related to a poleward shift and intensification of the SWW. Recent changes have been attributed to greenhouse gas accumulation (Hartmann *et al*., 2000; Marshall *et al*., 2004) and/or ozone depletion (Sexton, 2001; Thompson and Solomon, 2002; Gillett and Thompson, 2003; Kang *et al*., 2011; Polvani *et al*., 2011) (Section 2.1.4) the effects of which have been observed in natural ecosystems (Robinson and Erickson, 2015).

Instrumental precipitation data are available in the region covering the period AD 1950–2000. A spatial and temporal reconstruction of precipitation patterns of SSA (41-53°S) was carried out by Aravena and Luckman (2009). Figure 2.4 shows the annual rainfall averages since 1950. It appears that precipitation has decreased in Northwestern (41-44°S, both sides of Andes) and Central (45-47°S, West) Patagonia. A slight increase is evident in the Patagonian plains (43-50°S, East) over the period with no increase or decrease evident in the reconstruction from Southern Patagonia (51-53°S, East). Owing to the differences in correlation between zonal wind speed and precipitation this suggested intensification has resulted in regional spatial

heterogeneity of precipitation variability, highly dependent on location in terms of the sharp climate boundary formed by the Andes.

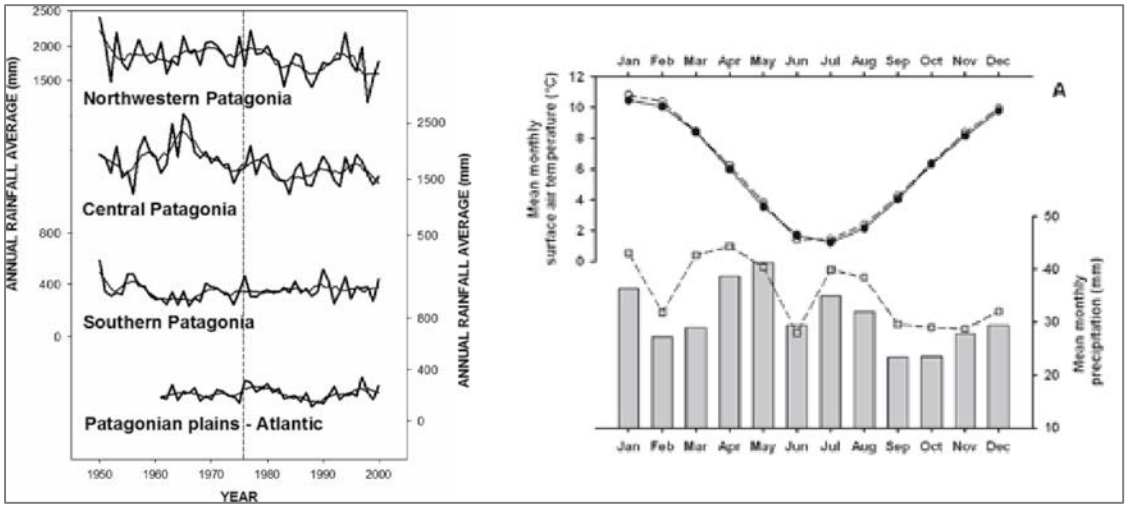

Figure 2.4. Left: From **Aravena and Luckman (2009)**. Annual rainfall averages of the regions mentioned in the text with a 10 year Gaussian filter. Right: From **Daley *et al*. (2012)** Punta Arenas instrumental data. Monthly mean precipitation amounts shown by grey bars (1961-1990) and grey squares (1981-2010). Monthly mean surface air temperatures shown by closed circles (1961-1990) and open circles (1981-2010).

The Punta Arenas instrumental data (mean monthly surface air temperatures and precipitation amounts) were analysed to compare two periods (1961-1990 and 1981-2010) (Figure 2.5). Comparison of the two time periods reveals that there have been no notable changes in the mean surface air temperature but increases in precipitation amount are evident (Daley *et al*., 2012). The positive correlation between zonal wind speed and precipitation at this meteorological station suggests that a southerly shift and intensification of the SWW has led to an increase in precipitation.

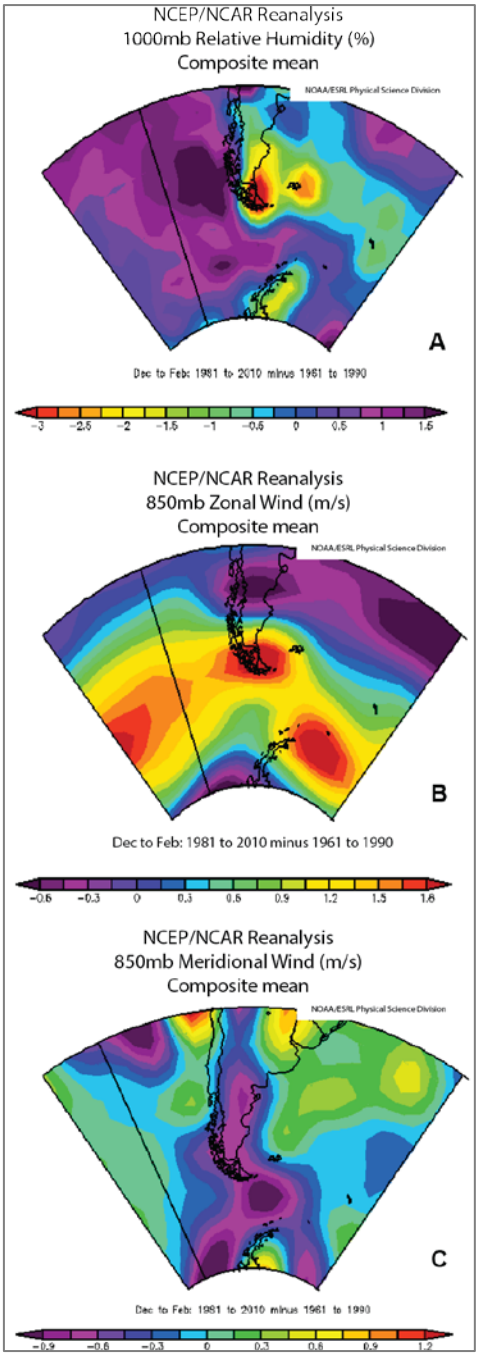

Figure 2.5. From **Daley *et al*. (2012)**. With reference to the 1961-1990 average showing the 1981-2010 anomaly for **A)** 1000 mb relative humidity (%) **B)** 850 mb zonal wind component (m/s) **C)** 850 mb meridional wind component (m/s). Note values with reference to key (A-positive, B and C-negative). Images from NOAA/ESRL Physical Sciences Division http://www.esrl.noaa.gov/psd/

Over the same two time periods a comparison was made using NCEP-NCAR reanalysis data of relative humidity, zonal and meridional wind. Figure 2.5 strongly supports a southward shifted and intensified SWW (shown by stronger (more positive values) zonal wind). This has led to increased relative humidity to the west

of the Andes between 40 and 55°S and due to a rainshadow effect a decrease to the east of the Andes between 50 and 55°S.

2.1.4 Anthropogenic drivers

Increasing greenhouse gas (GHG) concentrations due to human activity has influenced the climate system evidenced by an observed increase of global-mean surface temperature from 1951-2012 (Myrhe *et al.,* 2013). There has been a large focus on anthropogenically forced rapid increases in surface air temperature however, few studies have focused on the resulting precipitation variability on the global scale (Zhang *et al*., 2007; Min *et al*., 2011).

The shift to a positive SAM index (Thompson *et al*., 2000; Marshall, 2003; Fogt *et al*., 2009) (Section 2.1.3) is linked with cold polar temperatures, low geopotential height over Antarctica and strong zonal flow at 60°S (Thompson and Solomon, 2002).

Concurrent with the positive SAM is an associated poleward shift and intensification of the SWW (Polvani *et al*., 2011) evidenced by a decrease in precipitation at 45°S and an increase at 60°S in austral summer (Son *et al*., 2008; Sigmond *et al*., 2010). Also, an expansion of the Hadley cell and poleward extension of subtropical high pressure zones (Previdi and Liepert, 2007) resulted in an increase of subtropical precipitation (15-35°S) in austral summer between 1979 and 2000 (Kang *et al*., 2011).

Southward shifted and stronger westerlies have led to warming via warm advection from the Southern Ocean over Southern Patagonia and the Antarctic Peninsula, one of the fastest warming regions on earth (Kwok and Comiso, 2002; Pike *et al*., 2013) with implications for Antarctic sea ice extent (Section 2.2.6.1). The SAM trend can only account for ~50% of the warming occurring over the Peninsula suggesting that other climate mechanisms are also in place (Thompson and Solomon, 2002).

Models have attempted to assign the cause to stratospheric ozone depletion (Sexton, 2001; Polvani and Kushner, 2002; Gillett and Thompson, 2003; Shindell and Schmidt, 2004; Arblaster and Meehl, 2006). Owing to the increase of short-lived gases such as Sulphur dioxide, evidence for an Antarctic ozone hole is now well established (Trenberth *et al*., 1989; Jones and Shanklin, 1995; Forster and Shine, 1999; Zhou *et al*., 2000). Ozone depletion has resulted in photochemically induced stratospheric

cooling linked to recent tropospheric trends mentioned above (Thompson and Solomon, 2002).

In earlier models a poleward shift of the SWW is also evident in those studies including an anthropogenic increase of GHGs only (Shindell and Schmidt, 2004; Arblaster and Meehl, 2006) with resultant SST changes. The CAM3 model used by Polvani *et al*. (2011) compared with previous modelling studies uses actual observations of SSTs, sea ice extent, GHG concentrations and ozone fields. Comparison with other model simulations (Meehl *et al*., 2007; Son *et al*., 2008) suggests strongly robust results of the CAM3 model. Using this model they find that stratospheric ozone depletion is the dominant driver of SH atmospheric circulation changes between 1960 and 2000. This opposes atmosphere-ocean interactions and SSTs (Deser and Phillips, 2009) involving shifts of the ITCZ due to Arctic sea ice extent (Chiang and Bitz, 2005) and the Atlantic thermohaline circulation (Zhang and Delworth, 2005) dominant drivers in the Northern Hemisphere.

The cancelling out of the effects of increased GHG emissions by the recent recovery of stratospheric ozone has recently been suggested by model results (Son *et al*., 2010). Continual modelling of future climate scenarios based on an increased understanding of present observations may shed light on the matter (Polvani *et al*., 2011). A recent model suggests that the poleward shift of the SAM in response to recent and future global warming may not be evident owing to potential altitude changes of the Antarctic ice sheet and changes in sea ice extent (Chavaillaz *et al*., 2013).

A lack of knowledge of past variability of the SAM results in the need for high-resolution and precisely dated palaeoenvironmental records (Fletcher and Moreno, 2012). Southern South America is the only continental landmass between 38°S and the Antarctic Circle that interrupts the circum-global circulation of the SAM and resulting SWW. Sites in the core path of the SWW are preferable to obtain palaeoclimatic records as this area is subject to shifts in wind strength and precipitation regimes (Zolitschka *et al*., 2006) as a result of past variability in latitude and intensity of the SAM and SWW.

For this reason, SSA and Patagonia in particular have become increasingly important in palaeoclimatic research in the last 20 years. As it will be seen in the next

section, a major focus in this area has been on attempts to reconstruct changes in the behaviour of the SWW in the past including its latitudinal position and intensity (Kilian and Lamy, 2012). Reconstructing past variability provides a critical baseline against which future changes can be assessed (Moy *et al*., 2008). Equally, an understanding of the modern climatology and relatively shorter term changes of the SWW can help interpretation of longer term changes inferred from palaeoclimate records.

An observed poleward shift and intensification of the SWW is evident from instrumental data from SSA as increases to the West and decreases of precipitation to the east of the Andes. This result should be corroborated in high-resolution palaeoclimate records across the region depending on location within the precipitation gradient.

2.2 Late-Holocene palaeoclimate reconstructions

The following section will review key investigations that have been carried out in Patagonia, which is considered to be the region in southernmost South America extending between 40° and 55°S (Garreaud *et al*., 2013). Studies over these latitudes are most sensitive to SWW variability owing to their location in the zone of influence of the wind belt. These studies form the context of this investigation in enabling the assessment of the likely timing and direction of late-Holocene climate variability.

There is much potential for palaeoenvironmental reconstructions in Patagonia owing to the variety of palaeorecords available as will be made evident in this review. Compared with the Northern Hemisphere relatively few studies have been carried out in SSA but there has been an increase of palaeoclimate studies over the past 30 years in the region and records are now available across a range of spatial and temporal resolutions.

These most recent studies are concerned with using the modern correlation between zonal wind speed (925 hPa and 300 hPa) (SWW strength) and precipitation over SSA (e.g. Moy *et al*., 2009; Kilian and Lamy, 2012; Garreaud *et al*., 2013) to reconstruct past SWW variability, assuming that this relationship has held true over the reconstruction period. This correlation might suggest that the eastern side would

be less sensitive in recording SWW strength by reconstructing past precipitation. However, 85% of palaeoclimate-related studies have been carried out to the east of the Andes owing to the relative ease of accessibility and the abundance of naturally occurring sites from which palaeoclimate data can be obtained compared to the western side of the climate divide (Kilian and Lamy, 2012).

Since 2005 there has been a rapid increase in the number of publications containing palaeoclimate records (Kilian and Lamy, 2012). The most recent studies focus on SWW changes during the Last Glacial Maximum (Kohfeld *et al*., 2013; Sime *et al*., 2013). The majority of studies have focused on millennial- and centennial-scale Late Glacial and Holocene palaeoclimate reconstructions. One of the main criticisms of syntheses of these proxy reconstructions is the contrasting interpretations of the strength, extent and latitudinal position of the SWW throughout this time period (Kilian and Lamy, 2012). Controversy arises in the record of changes in SWW behaviour owing to opposing arguments based on records from both sides of the Andes and even intra-regional (W/E) differences. Evidence from the hyperhumid west side suggests either a southward shift and stronger core of the SWW (Lamy *et al*., 2010) or a weakening of the SWW (Moreno *et al*., 2010) in the early Holocene. Evidence from the east side suggests that there has been either no long-term trend or enhanced westerlies during the late-Holocene (Markgraf *et al*., 2003). These studies are important in modelling future climate scenarios however, variability over this time period is generally assumed to have been driven by seasonal insolation changes as a result of orbital variability (Milankovitch, 1941; Berger, 1988). Although the average annual insolation has decreased and summer insolation at 50°S has increased since 1000 cal BP (Berger and Loutre, 1991) the relationship between solar insolation and moisture balance has become weaker since 5000 cal BP thus suggesting the dominance of other drivers unrelated to longer term orbital forcing (McCarroll, 2010; Fletcher and Moreno, 2012) such as solar and volcanic drivers (Wilmes *et al*., 2012).

Two late-Holocene climate intervals largely found in Northern Hemisphere palaeoclimate records, now commonly known as the Medieval Climate Anomaly (MCA) and Little Ice Age (LIA), have also been found in Southern Hemisphere records (Stine, 1994). In Northern Hemisphere records these anomalies are usually present between ~AD 950 and 1250 (MCA) and ~AD 1400 and 1700 (LIA) (Mann *et*

al., 2009). However, there is still debate around the magnitude, timing and direction of these events in the Southern Hemisphere (Moy *et al*., 2008; Diaz *et al.*, 2011).

Despite the increase in palaeoclimate records from SSA, the majority of studies have focused on reconstructing centennial and millennial variability throughout the Holocene using a low sampling resolution. These records, therefore, may lack suitable chronologies when considering the late-Holocene. A shift to a focus of palaeoclimate reconstructions of the last 2000 years is now vital in order to isolate natural from anthropogenically forced climate change (Neukom and Gergis, 2012). It is for this reason that the IPCC focuses on the last 2000 years owing to the relative availability of data covering this time period (Masson-Delmotte *et al.*, 2013). Palaeoclimate records from the whole Southern Hemisphere covering the last 2000 years are severely lacking in comparison with Northern Hemisphere records (Stocker *et al*., 2013) and as a result existing Southern Hemisphere temperature reconstructions are based on comparatively few proxy records. These reconstructions use the hemispheric mean (Mann and Jones, 2003; Jones and Mann, 2004; Mann *et al*., 2008) potentially masking seasonal and regional scale changes leading to a need for records of high temporal and spatial resolution.

Numerous palaeoclimate archives are available in the region with most proxy records derived from glaciers, lake sediments, peatlands and tree rings. The following section aims to synthesise these existing records in order to provide an overview of climatic variability in the region in terms of SWW variability to provide a context for the recent shifts as reviewed in the previous section.

2.2.1 Glacial ice extent

The Northern and Southern Patagonian Ice Field and Cordillera Darwin Ice Field cover an extensive area, ~19,500 km^2, in SSA (Vimeux *et al*., 2009). The SWW supplies precipitation to these ice sheets and thus variability in the strength of the wind belt may be evident from reconstructions of glacial variability (Rignot *et al*., 2003). Glacial advances throughout the Holocene have been reconstructed from sites in the southernmost Andes. In consideration of late-Holocene climate variability most glacial studies focus on the timing of the deposition of moraines indicative of LIA glacier advances (Clapperton and Sugden, 1988; Villalba, 1994; Marden and Clapperton, 1995; Luckman and Villalba, 2001; Planas *et al*., 2002; Glasser *et al*.,

2004; Koch and Kilian, 2005; Strelin and Iturraspe, 2007; Strelin *et al*, 2011; Menounos *et al*., 2013). All offer support for a broad regional climate period during the 15th to late 19th centuries suggesting that the LIA glacial advances were due to precipitation and atmospheric temperature changes as a result of SWW variability.

2.2.2 Lake, marine and stalagmite records

Important sites discussed in the text are displayed in Figure 2.6 with a focus on the latitudinal extent 40-55°S.

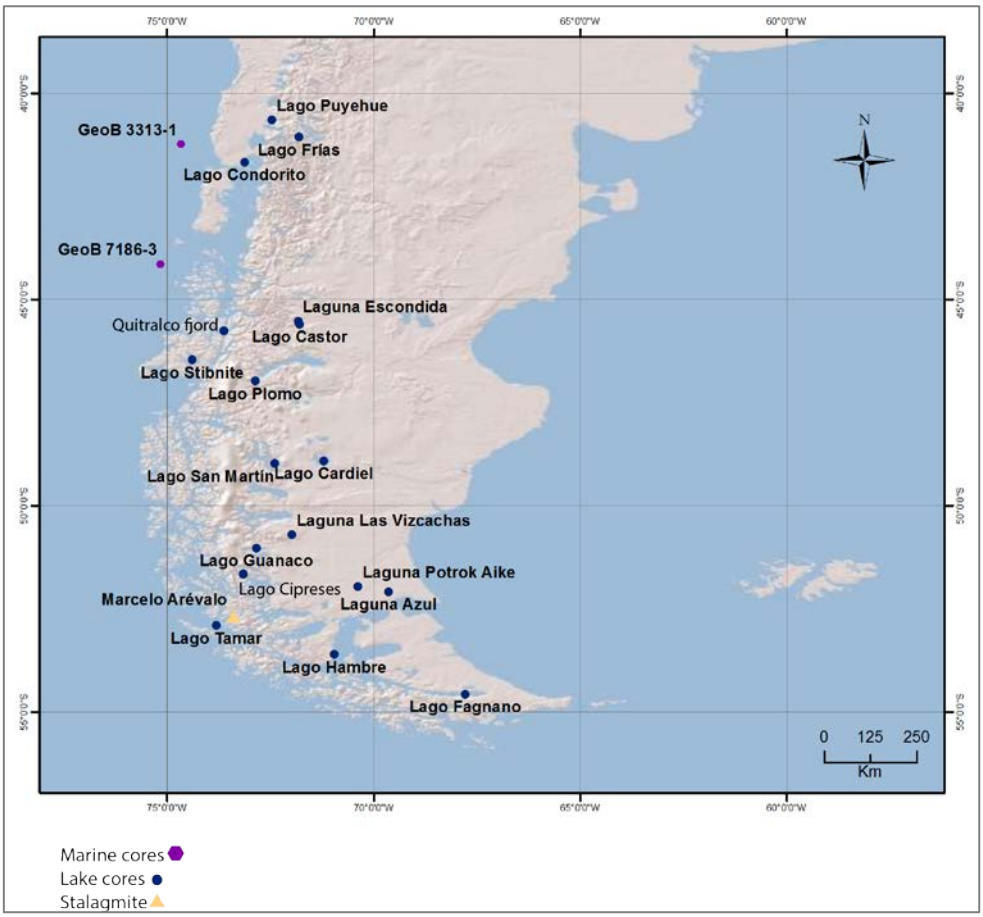

Figure 2.6. Location of study sites mentioned in section 2.2.2.

2.2.2.1 40-45°S

During the instrumental period, el Niño years are correlated with low precipitation (Boës and Fagel, 2008) suggesting that when considering palaeoclimate records from Northern Patagonia, ENSO is an important climate driver in the region. Ariztegui *et al*. (2007) investigated varve thickness in a sediment core from Lago Frías, finding a frequency of 2.5 to 3 years also suggesting a strong ENSO signal on

palaeoclimate records in the north of the region. Verification from the instrumental record supports a positive correlation between varve thickness and austral winter precipitation from Lago Puyehue.

A 600-year long varve thickness record highlighted a period of low winter precipitation via low varve thickness between AD 1400 and 1510 (Boës and Fagel, 2008), perhaps representing a late MCA period (Figure 2.7A). Thereafter, until ~AD 1630, varve thickness increases suggesting higher winter precipitation values during the LIA. Increased terrigenous supply to this lake between AD 1490 and 1700 is also indicative of a humid climate during this interval (Bertrand *et al*., 2005).

Marine records taken within this latitudinal band from the southeast Pacific at 41 ((GeoB 3313-1) Lamy *et al*., 2001; 2002) and 44°S ((GeoB 7186-3) Mohtadi *et al*., 2007) are displayed in Figure 2.7B. Variability in a record of iron content is interpreted to be a result of continental weathering as a result of the intensity of the SWW at this latitude. Periods of higher iron concentration indicate reduced precipitation and drier conditions with opposing conditions indicated by lower iron concentration. As shown in the record, periods at AD 1300 and AD 1700 indicate a southerly shift of the SWW during the MCA and a northward expansion of the SWW during the LIA respectively (Figure 2.7Bi). The alkenone-based Sea Surface Temperature (Figure 2.7Bii, iii) and Sea Surface Salinity records (Figure 2.7Biv) show a general decrease to present, interpreted as a northward expansion of the zonal systems (ACC and SWW) in recent decades. The authors suggest an ENSO signal is found in the record with strong ENSO events ~1300 cal BP followed by a northward (2° latitude) displacement of the SWW and ACC which resulted in strong la Niña conditions until ~800 cal BP at 44°S west of the Andes. Through a positive feedback the latitudinal thermal gradient steepened resulting in stronger zonal winds further steepening the E-W Pacific temperature gradient and the thermocline, reinforcing la Niña conditions (Mohtadi *et al*., 2007). The end of these conditions coincides with a minimum of solar activity associated with the LIA (Section 2.2.7.1).

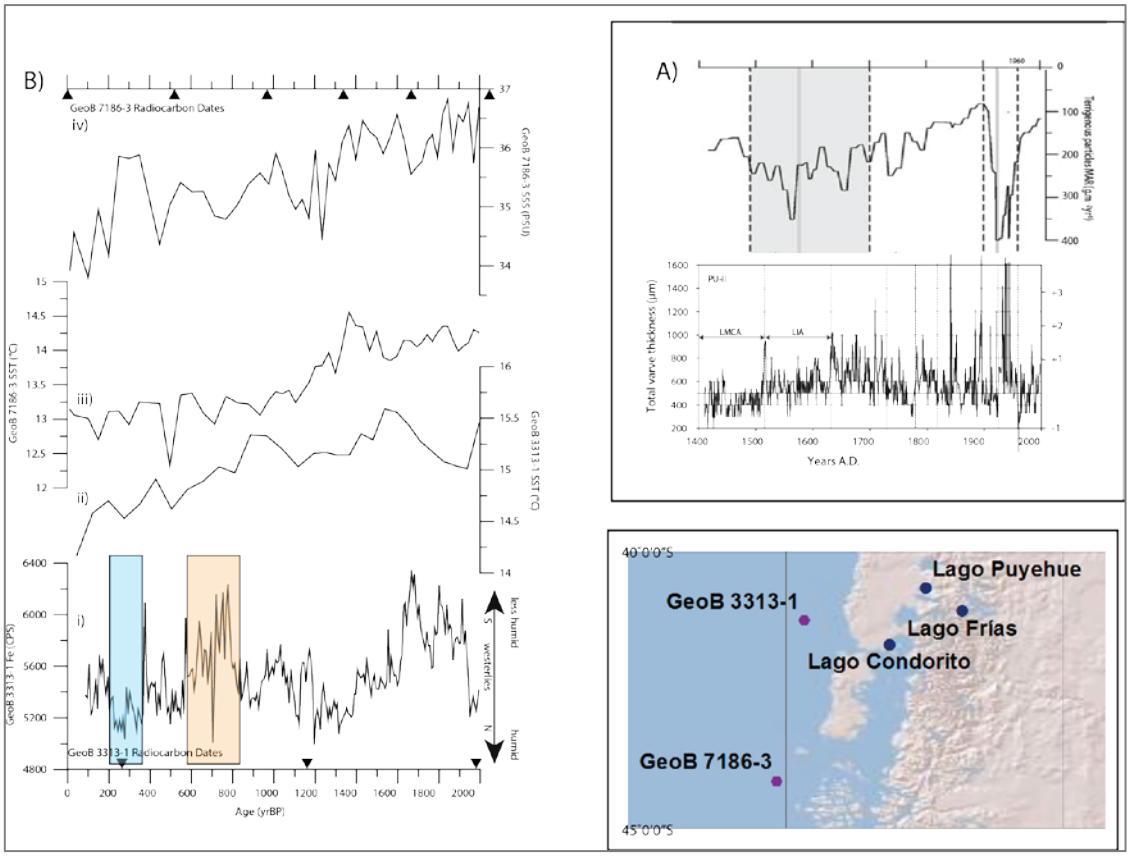

Figure 2.7. Location of palaeorecords mentioned in section 2.2.2.1 with a focus on 40-45˚S. **A)** Mass accumulation rates of sediment core PU-II-P5 **(Bertrand *et al*., 2005)** and total varve thickness of sediment core PU-II **(Boës and Fagel, 2008)** AD 1408-2000 both from Lago Puyehue. **B)** Edited from **Moy *et al*. (2009)** GeoB 3313-1 (41˚S): **i)** Iron content record; **ii)** Sea Surface Temperature reconstruction **(Lamy *et al*., 2001; 2002)**. GeoB 7186-3 (44˚S): **iii)** SST and **iv)** Sea Surface Salinity reconstruction **(Mohtadi *et al*., 2007)**. The orange box indicates higher Fe contents due to dry conditions of the MCA and the blue box indicates lower Fe contents due to wetter conditions of the LIA.

2.2.2.2 45-50°S

Work by Elbert *et al*. has increased the number of records from 40-50°S in recent years. The biogenic silica flux record of a sediment core from Laguna Escondida enabled an annual temperature anomaly reconstruction extending to AD 400 (Elbert *et al*., 2013a). Figure 2.8A displays the record from AD 1000 to present. Relative to the 20th century mean the record shows a warm period until ~AD 1150 and a subsequent colder period until ~AD 1500. Temperatures are more variable after this period and fluctuate above the mean until AD 1900 when there is a decrease, after this time, temperatures increase to current levels.

Bertrand *et al*. (2014) at Quitralco fjord (46°S) find evidence for a period of decreased precipitation seasonality (June July August : December January February precipitation) between AD 1200 and 1500 associated with a weakening of the SWW of the LIA (Figure 2.8B) at a time of lower sea surface temperatures in the southeast Pacific. Before this, precipitation seasonality was higher, implying a poleward SWW during the MCA.

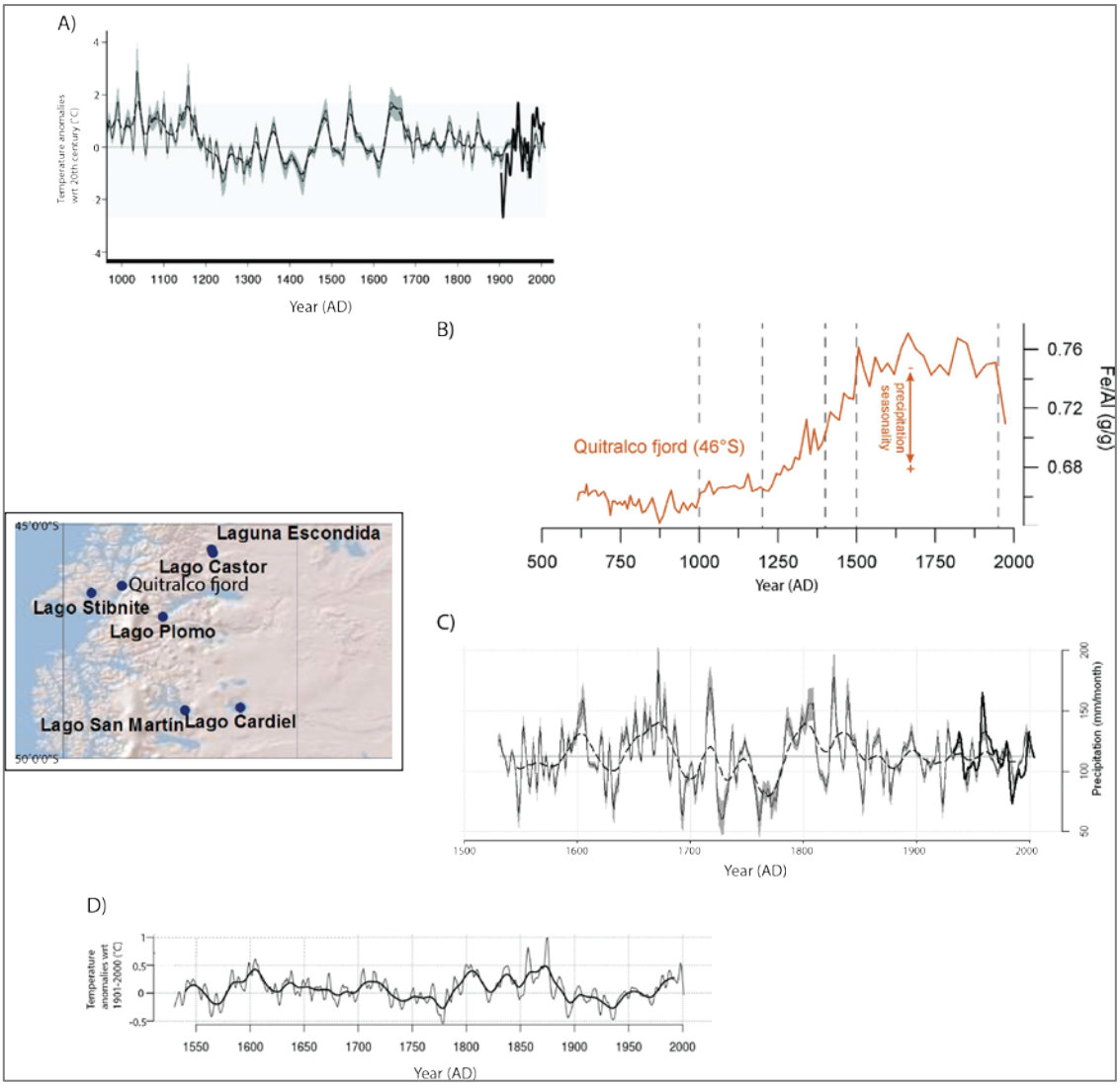

Figure 2.8. Location of palaeorecords mentioned in section 2.2.2.2 with a focus on 45-50˚S. **A)** Reconstruction of annual temperature anomalies from Laguna Escondida **(Elbert *et al*., 2013a)**. **B)** Fe/Al record from Quitralco Fjord as an indicator of precipitation seasonality driven by SWW shifts **(Bertrand *et al.*, 2014)**. **C)** Reconstruction of austral winter precipitation **(Elbert *et al*., 2012)** and **D)** austral warm season (SONDJF) temperature anomalies **(Elbert *et al*., 2013b)** both from Lago Plomo.

Two recent sediment records from Lago Plomo have provided a reconstruction of winter precipitation (Elbert *et al*., 2012) and warm season temperature anomalies (Elbert *et al*., 2013b) both extending to ~500 cal BP (Figure 2.8C and D). The high-resolution austral winter precipitation reconstruction based on the mass accumulation rate displays more humid conditions between AD 1600 and 1700 and a subsequent dry period until ~AD 1780. A similar pattern appears in the warm season temperature reconstruction in that a LIA period between AD 1700 and 1800 of lower temperatures (with reference to the 20th century mean) synchronous with lower winter precipitation occurs. Temperatures rise after AD 1960 to the end of the record.

A sedimentologic record from Lago Cardiel shows high late-Holocene variability in moisture although these records are difficult to compare with other records owing to poor chronological control (Markgraf *et al*., 2003). From the same lake a magnetic susceptibility record shows no evidence for contrasting conditions of the MCA and LIA in the last 1000 years (Gilli *et al*., 2005). However, a high-resolution isotope record from this lake (Gilli, 2003) finds hydrologic and solar variability to be correlated over the last 1870 years. From the same lake, Agosta *et al*. (2015) suggest that long-term precipitation is affected by Atlantic moisture transport, suggesting that records from this lake may not directly record SWW variability.

At a similar latitude to the West of the Andes, with a focus on the last 1000 years of the pollen record from Lago San Martín (Bamonte and Mancini, 2011), higher levels of herb taxa relative to shrubs indicate wetter conditions throughout until 100 cal BP, when a decrease in moisture availability is indicated by an assemblage dominated by grass steppe and higher levels of shrubs.

2.2.2.3 50-55°S

2.2.2.3.1 Westerly located records

A comparison of two proxy records from Lago Guanaco (Moy *et al*., 2008; Moreno *et al*., 2009) with a Western Antarctic ice core record (Kreutz *et al*., 1997) reveals synchronous SWW variability in the record thought to be indicative of the MCA and LIA in Patagonia (Figure 2.9).

A biogenic carbonate $\delta^{18}O$ reconstruction (Moy *et al*., 2008) is compared with a palaeovegetation index of *Nothofagus*:*Poaceae* ratios (Moreno *et al*., 2009).

Between ~900 and 700 cal BP higher than average $\delta^{18}O$ values indicate increased evaporation from the lake basin and a more negative palaeovegetation index, which indicates less precipitation, a period of weaker SWW and increased aridity characterises a period coincident with the MCA. The LIA is also characterised by higher than average $\delta^{18}O$ values and increased evaporation; however, the palaeovegetation index increases to a higher *Nothofagus*:*Poaceae* ratio indicative of an eastward expansion of *Nothofagus* dominated forests. This period is thus characterised by stronger westerlies resulting in higher evaporative losses but increased precipitation between 570-150 cal BP. This pattern is also displayed in the Na^+ ice core data from West Antarctica with higher levels indicative of stronger zonal flow.

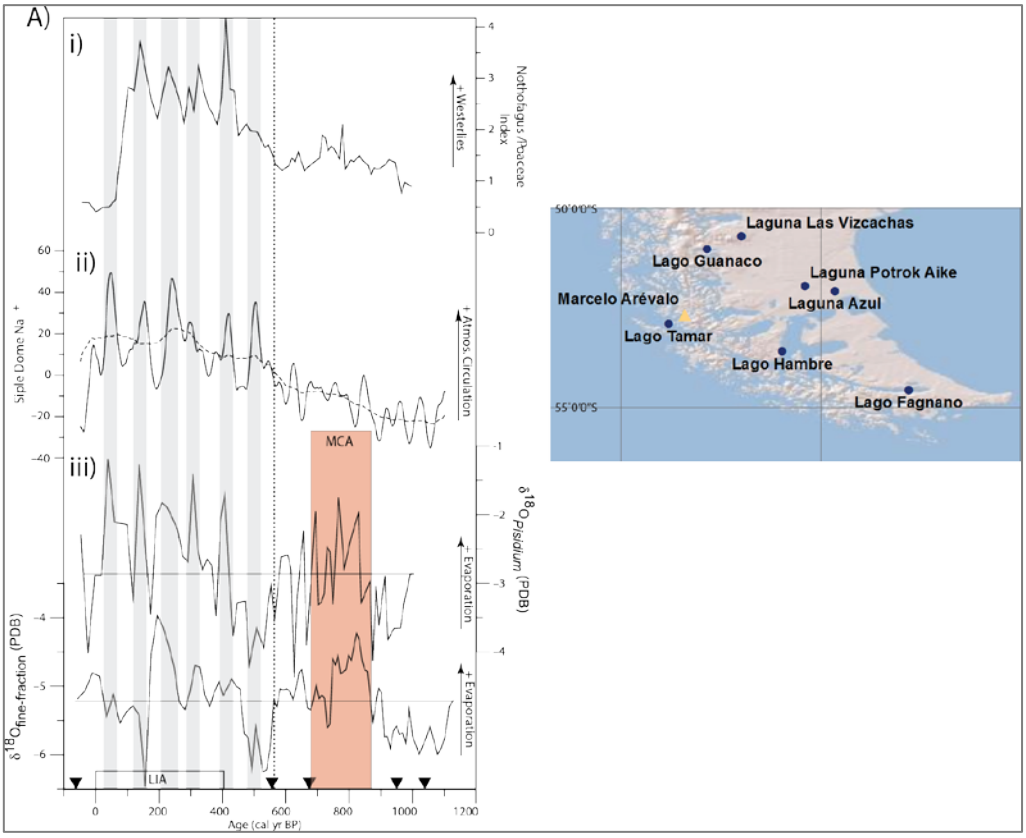

Figure 2.9. Comparison of records discussed in the section 2.2.2.3.1. **A)** Edited from **Moy *et al*. (2009) i)** *Nothofagus*:*Poaceae* ratio **(Moreno *et al*., 2009)** from Lago Guanaco. **ii)** Na+ concentration from Siple Dome **(Kreutz *et al*., 1997)**. **iii)** $\delta^{18}O$ Pisidium and $\delta^{18}O$ fine-fraction record from Lago Guanaco **(Moy *et al*., 2008)**.

A stratigraphic record from Lago Cipreses (51°S) covering the last 3000 years reveals dry/warm phases with 200-year durations, associated with positive phases of

the SAM, alternating with wet/cold phases (Moreno *et al*., 2014). A MCA dry/warm phase occurred between 1100 and 800 cal BP followed by a wet/cold LIA period from 800 and 60 cal BP. Since positive phases of the SAM are related to a southerly and intensified SWW, this record seems to contrast with the records from Lago Guanaco.

2.2.2.3.2 Easterly located records

Laguna las Vizcachas is the most northerly located lake within the classification of more easterly located records. A multi-proxy investigation of a sediment record covering the last 1600 years suggests variability in fluvial runoff over this period (Fey *et al*., 2009) (Figure 2.10A). A period of enhanced run off is indicative of stronger wind intensities and thus increased precipitation between ~AD 1100 and 1400, broadly synchronous with the MCA throughout the region. Furthermore, a LIA period is evident with cooler conditions between AD 1400-1650 in the diatom record and lower fluvial input. Fluvial input appears to have decreased to present in the Laguna las Vizcachas record owing to its relatively westerly position.

Many palaeoclimate records have been compiled from Laguna Potrok Aike (LPA) located in the Pali-Aike volcanic field. In line with the West-East Andean precipitation gradient the area receives 170 mm annual precipitation (Haberzettl *et al*., 2008). The modern negative correlation between zonal wind speed and precipitation (Figure 2.1 & 2.2) would suggest that the variability from these sites should be opposite in signal to variability further to the West where the correlation is more positive.

The las Vizcachas record (Fey *et al*., 2009) is compared with an early lake sediment record from LPA (Haberzettl *et al*., 2005). It is evident from the comparison that during the MCA conditions were opposite in direction between the two sites (Figure 2.10B). As evidenced in the Total Organic Carbon record at LPA there was an implied reduction in fluvial input and thus lake level between AD 1100 and 1400, with a subsequent increase during the LIA. The lake level dropped over the 20th century to present, which was also recorded in the las Vizcachas record. A MCA dry period is also evident in the fire record from LPA (Haberzettl *et al*., 2006); a natural fire event around AD 1400 occurred before the arrival of the Europeans during a period with favourable conditions for ignition in the area. In another LPA sediment record (Haberzettl *et al*., 2007), as indicated by the Total Inorganic Carbon, a moist period

occurs 950 and 750 cal BP, an intervening dry period until 530 cal BP with wetter conditions until 20 cal BP. This is also indicated by the Ti record, with higher values at times of increased minerogenic input and increased precipitation. This suggests that the LIA is evident in the record after 530 cal BP (Figure 2.10C). Another multi-proxy lake sediment record reveals centennial scale SWW strength variability and implications on precipitation (Mayr *et al*., 2007a). A decrease in AFT (Andean Forest Taxa) indicates that SWW strength was at a minimum at 800 cal BP, supported by a low C:N ratio indicative of a high lake level and higher Ti suggesting higher runoff. This all leads to the assumption of increased precipitation and lower evaporation at a time when weaker SWW allowed the penetration of northerly air masses (Figure 2.10D). A high lake level stand ~800 cal BP is supported by a decrease in the $\delta^{13}C_{org}$ values and an increase in $\delta^{15}N$ at this time (Figure 2.10E) (Mayr *et al*., 2009). Schabitz *et al*. (2013) found evidence of a MCA period of drier conditions between 1300 and 500 cal BP using a pollen-climate transfer function.

A lake sediment record from Laguna Azul located further south in the Pali-Aike volcanic field gives further evidence for a LIA period (Mayr *et al*., 2005) between AD 1400 and 1800 (Figure 2.10F). As well as changes in the vegetation index, $\delta^{13}C_{org}$ values rise during this time indicating a shift to cooler and wetter conditions with a resulting higher lake level. Thereafter, a shift in all records follows a fire event ~AD 1830, after which the record no longer reflects climatic conditions.

It is therefore assumed that in response to a southward shifted and intense SWW, drier conditions are evident at this location during the MCA as a result of foehn winds and increased evaporation from LPA (Schabitz *et al.*, 2013). As the SWW weakened, northerly and easterly air masses from the South West Atlantic were able to penetrate the area resulting in wetter conditions (Mendes *et al*., 2008) during the LIA. A recent synthesis of records from Patagonian sites located to the east of the Andes concluded that a MCA period was evident between 1600 and 750 cal BP during a poleward shift of the SWW followed by a northward shift of the SWW during a LIA period 750 and 200 cal BP (Sottile *et al.*, 2015). This is in agreement with SWW shifts during these periods from westerly located records (Moreno *et al*., 2014).

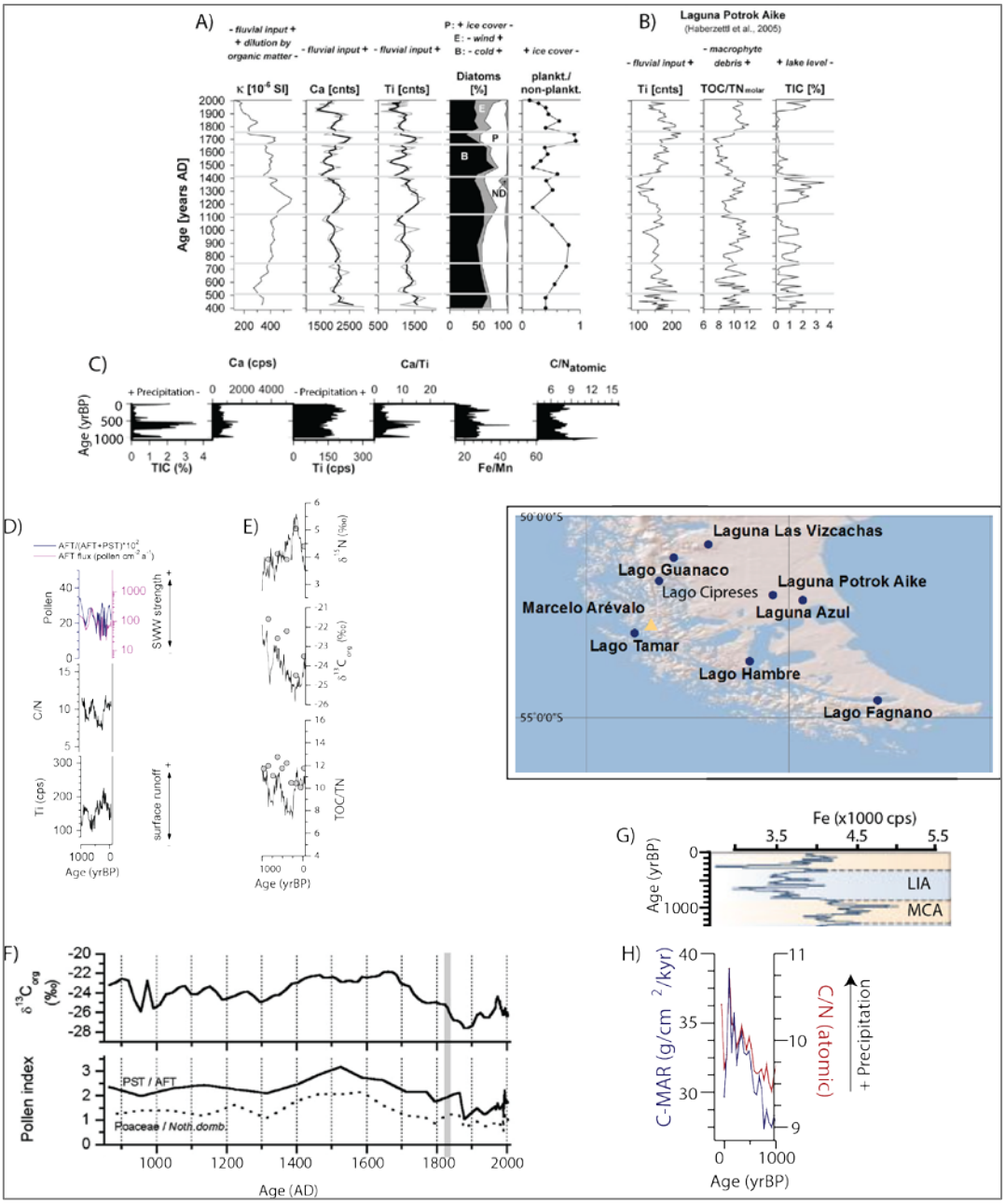

Figure 2.10. Location of palaeorecords mentioned in section 2.2.2.3.2 with a focus on 50-55˚S. **A)** Laguna las Vizcachas sediment record showing fluvial runoff and diatom record **(Fey *et al*., 2009)**. **B)** Laguna Potrok Aike sediment record **(Haberzettl *et al*., 2005)** (both edited from **Fey *et al*., 2009)**. LPA sediment records: **C) Haberzettl *et al*. (2007)**; **D) Mayr *et al*. (2007a)**. **E) Mayr *et al*. (2009)**. **F)** Laguna Azul δ^{13}org and pollen index **(Mayr *et al*., 2005)**. **G)** Lago Fagnano iron content record **(Waldmann *et al*., 2010)** and **H)** C:N and MAR record **(Moy *et al*., 2011)**.

From the same latitudinal band, precipitation (Schimpf *et al*., 2011) and temperature (Mühlinghaus *et al*., 2008) inferences have been gained from the investigation of stalagmites from Marcelo Arévalo located to the West of the Andes. Figure 2.11 taken from Schimpf *et al*. (2011) is a comparison of the stalagmite proxies with the Lago Guanaco $\delta^{18}O$ record (section 2.2.2.3.1) (Moy *et al*., 2008). All records indicate a humid MCA period 1200 to 700 cal BP which precedes an assumed LIA period from 700 to 100 cal BP of less humid conditions and temperatures 1.5 °C cooler than present. Three marine cores also located between 49 and 53ºS to the West of the Andes, find cooler alkenone-derived SSTs during the LIA at 600 to 250 cal BP (Caniupán *et al*., 2014).

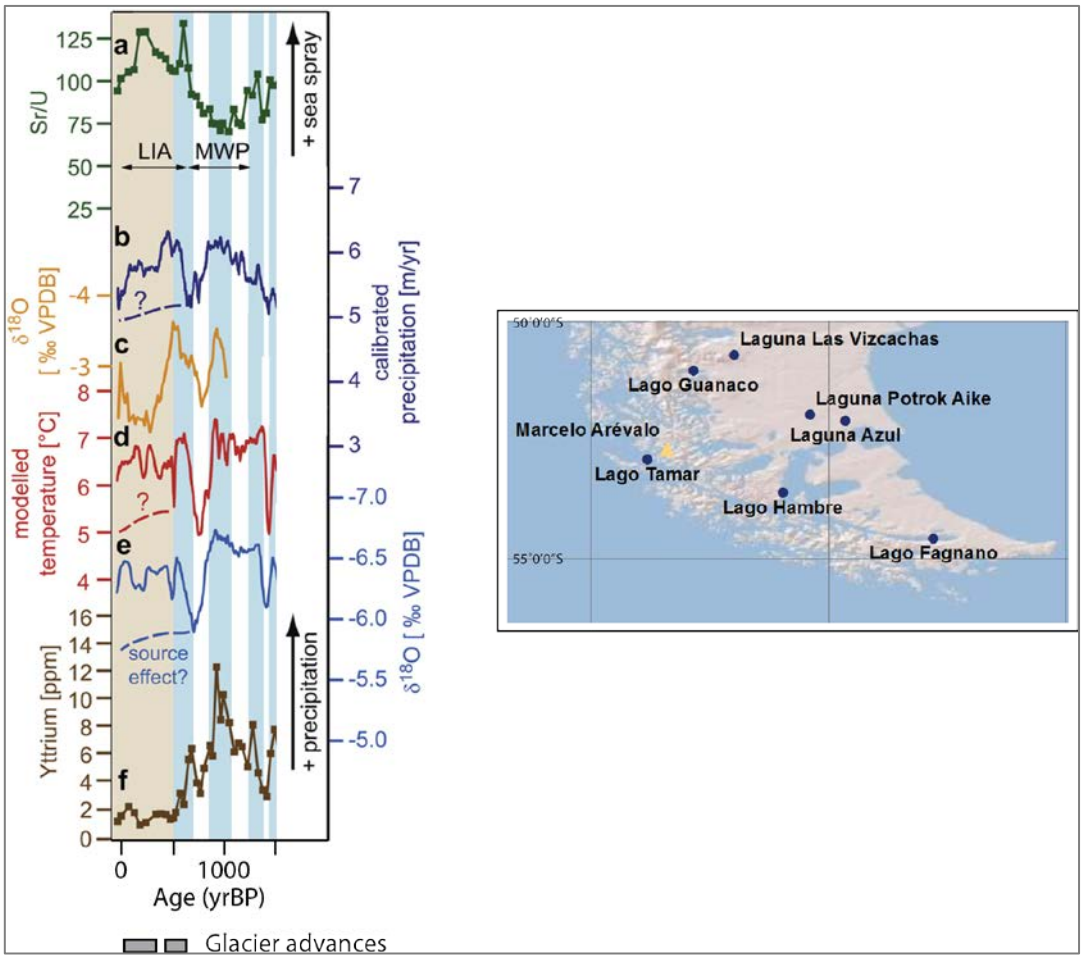

Figure 2.11. From **Schimpf *et al*. (2011)**. **A)** MA1 Sr/U ratios representing variability in sea spray deposition. **B)** MA1 Mg/Ca ratios **(Schimpf *et al*., 2011)**. **C)** Biogenic carbonate $\delta^{18}O$ indicating precipitation/ evaporation **(Moy *et al*.,2008)**. **D)** Temperature reconstruction using C and O isotopes from MA1. **E)** Smoothed mean $\delta^{18}O$ values and **F)** MA1 Yttrium content record all from **Schimpf *et al*. (2011)**.

2.2.2.3.3 Southerly located records

A mercury (Hg) record from a Lago Hambre sediment core (Hermanns and Biester, 2011) suggests that an increase in precipitation over the last 1000 years led to increased mercury accumulation throughout this period; a decrease in recent years would indicate a decrease in precipitation to present at this latitude.

A Lago Fagnano iron content record (Waldmann *et al*., 2010) indicates variability in the input of iron due to precipitation variability (Figure 2.10G). Higher iron content characterises the MCA with wetter conditions inferred until ~800 cal BP with a subsequent period of lower iron content until ~150 cal BP contemporaneous with the LIA and drier conditions. In contrast, from the same lake increased C:N ratios and MAR suggest wetter conditions during the LIA (Moy *et al*., 2011) (Figure 2.10H). A $\delta^{13}C$ record from the lake implies temperature variability, with lower temperatures during the MCA and higher temperatures during the LIA (Moy *et al*., 2011).

2.2.2.4 Synthesis of records

Figure 2.12 shows a synthesis of lake, marine and stalagmite records located between 40 and 55°S and the climate anomalies broadly contemporaneous with the Northern Hemisphere MCA and LIA. Although some of the lake records are of a low temporal resolution, inferences have been made of late-Holocene climate variability from all records. Figure 2.12 suggests that records discussed in this section display broadly regionally synchronous climate events with the majority of records implying a dry MCA and wetter LIA period. The more northerly records suggest that this pattern is a result of a more southerly and northerly shifted SWW respectively (Bertrand *et al*., 2005; Boës and Fagel, 2008). Records further to the south suggest similar directional shifts (Lago Cipreses., Lago Guanaco, LPA). The Laguna las Vizcachas and Lago Fagnano records show climate periods of opposite direction to the other records; it is most likely that this record is a local expression of the regional event. The stalagmite record also shows climate periods in the opposite direction with a wetter MCA and drier LIA period. It is, therefore, difficult to ascertain from the records already discussed whether regionally synchronous events did occur. The inclusion of other archives and proxies may be able to elucidate the timing and direction of these events.

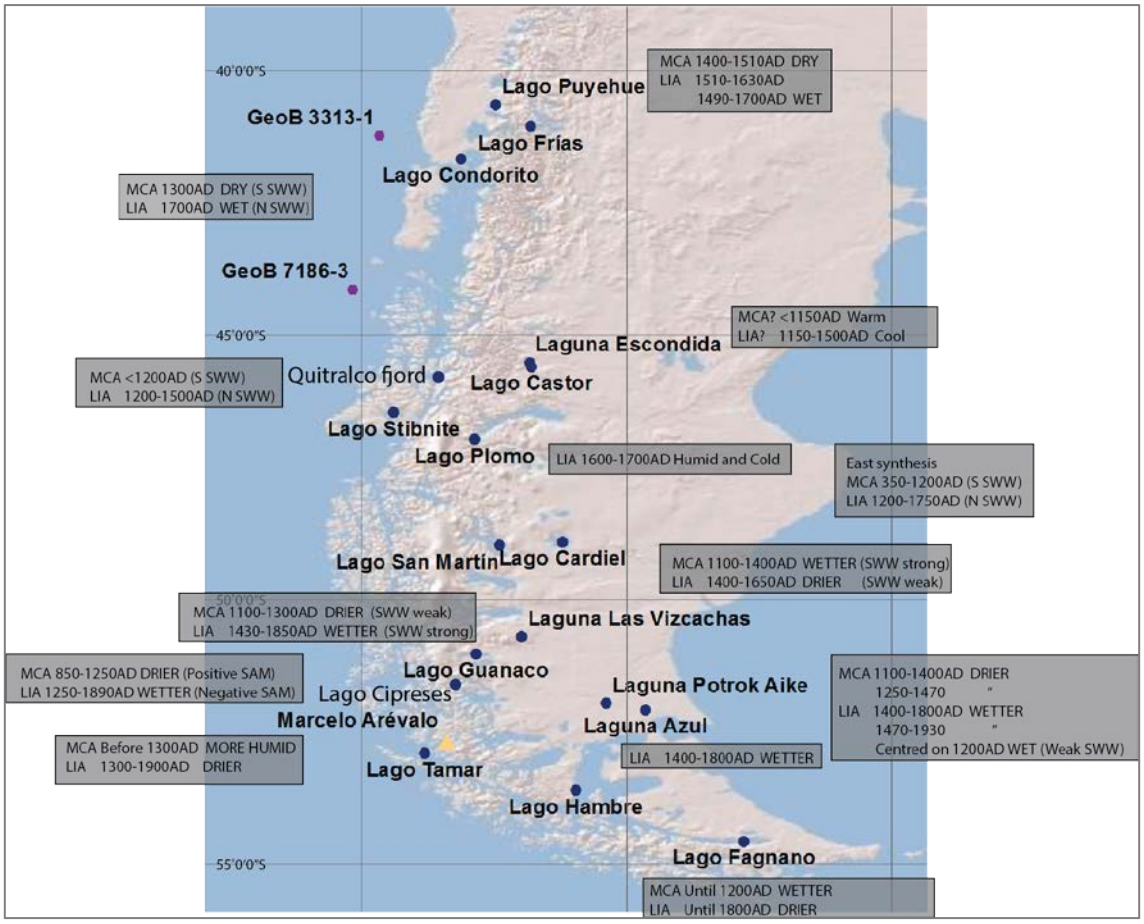

Figure 2.12. MCA and LIA events evident in lake, marine and stalagmite records.

2.2.3 Peat studies

The majority of peatland studies in Patagonia have focused on palaeoenvironmental reconstructions using pollen and charcoal to reconstruct major climatic events since the Last Glacial Maximum and subsequent Glacial-Interglacial transition (e.g. Heusser, 1989; 1995; 1998; Heusser *et al*., 2000; McCulloch and Davies, 2001; Villa-Martinez and Moreno, 2007; Musotto *et al*., 2016). The following section aims to review peat studies carried out in the region with a focus on 50-55°S. Peat studies are more common in this latitudinal band owing to the larger extent of peatlands (Section 2.3) (Yu *et al*., 2010). Records will be discussed, as with the lake studies, in a latitudinal order. The locations of study sites mentioned in this section are displayed in Figure 2.13.

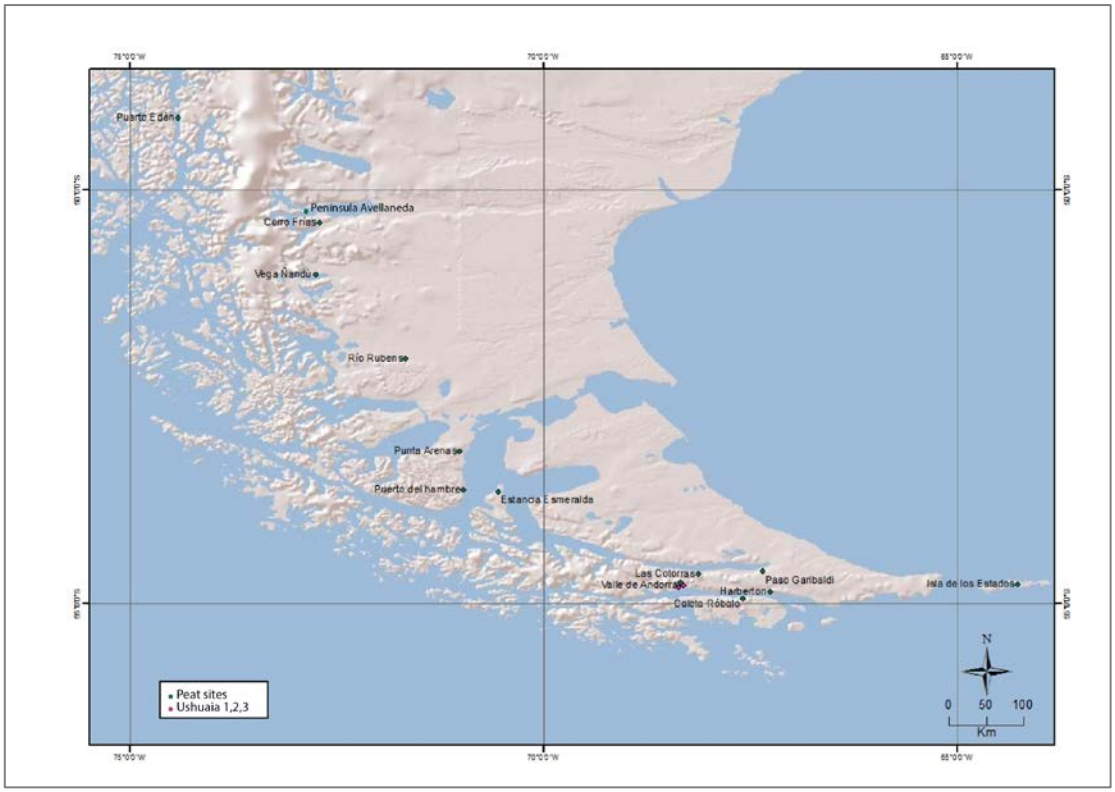

Figure 2.13. Location of peatland study sites mentioned in the text.

2.2.3.1 50-55°S

A peat record from Península Avellaneda using pollen, charcoal and sediment analyses from 50°S suggests decreased precipitation between ~550 cal BP and 50 cal BP due to a weakening of the SWW associated with the LIA with a preceding period associated with the MCA of wetter conditions due to a strengthening of the SWW (Echeverría *et al*., 2014).

At Cerro Frías, pollen records indicate a MCA period ~800 ^{14}C yr BP at which time a decrease in *Nothofagus* pollen and expansion of grass steppe occurred as a result of a decrease in annual precipitation (Figure 2.14A) (Mancini, 2009, Tonello *et al*., 2009). An increase in moisture and temperatures at ~250 ^{14}C yr BP (Mancini *et al*., 2002) is suggested by the recovery of *Nothofagus*, which subsequently declines after the arrival of Europeans (Mancini, 2009). This is also supported by a pollen record from Vega Ñandú bog (Figure 2.14B) (Villa-Martínez and Moreno, 2007) that showed fully developed *Nothofagus* forest until the last two centuries when it declines through deforestation and is followed by the introduction of *Rumex acetosella*.

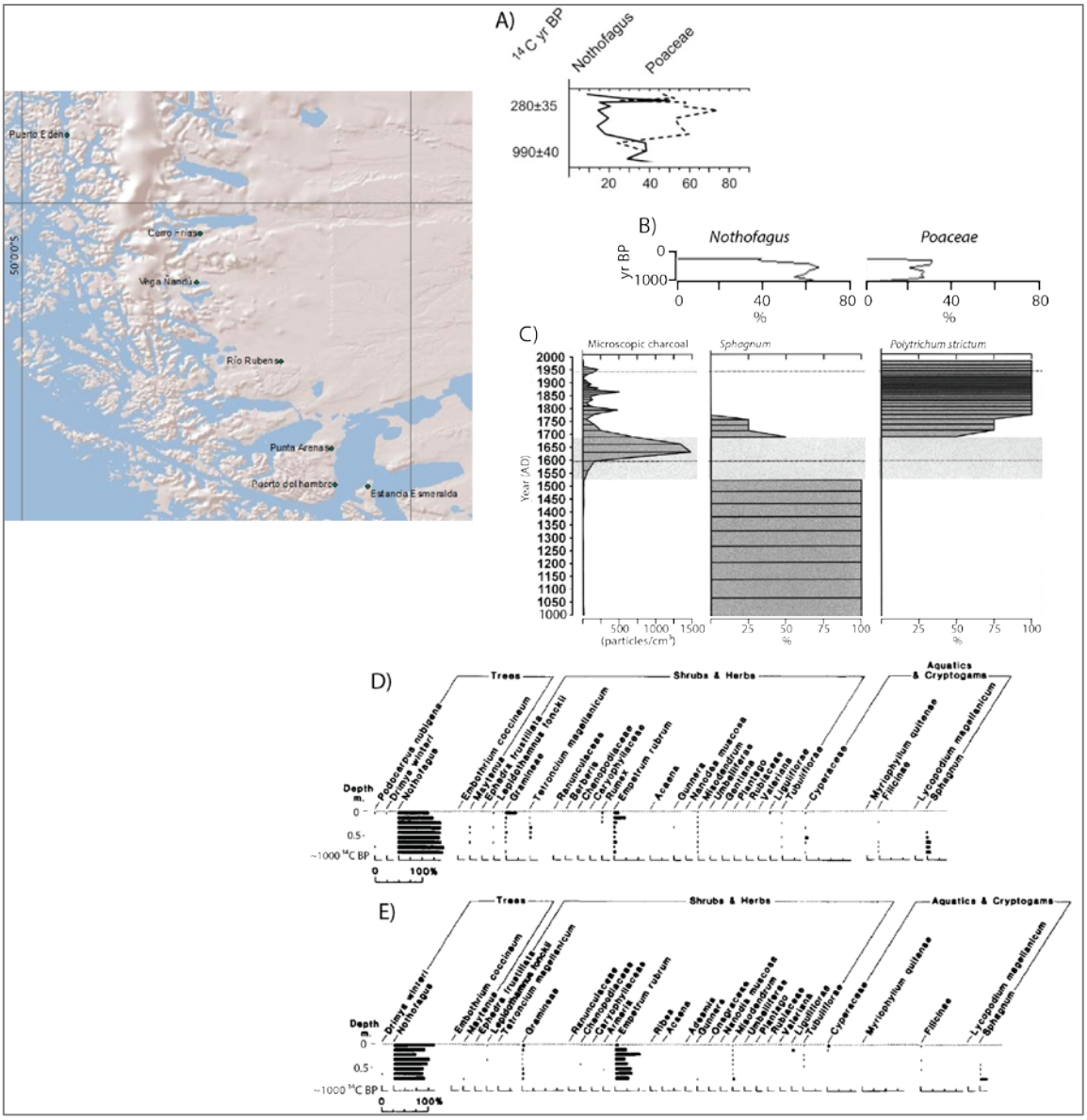

Figure 2.14. Location of peat study sites mentioned in section 2.2.3.1 with a focus on 50-54˚S. **A)** *Nothofagus* and *Poaceae* curves from Cerro Frías **(Mancini, 2009)**. **B)** *Nothofagus* and *Poaceae* curves from Vega Ñandú **(Villa-Martínez and Moreno, 2007)**. **C)** Microscopic charcoal and macrofossil record from Río Rubens **(Huber and Markgraf, 2003)**. **D)** Pollen record from Punta Arenas and **E)** Puerto del Hambre **(Heusser, 1995)**.

Human disturbance is also evident in the plant macrofossil and pollen records from Río Rubens (Figure 2.14C) (Huber and Markgraf, 2003; Huber *et al*., 2004; Markgraf and Huber, 2010). The plant macrofossil record shows a decrease of *Sphagnum* and subsequent increase of *Polytrichum strictum* (Huber and Markgraf, 2003) coincident with a peak in the charcoal record and a reduction of *Nothofagus* pollen after AD 1650. This was the only large variability since the beginning of the record (~5000 cal

BP), suggesting that climate conditions had been stable until European settlement and the resulting ecological disturbance. A pollen record from a site near Punta Arenas also finds a full expansion of *Nothofagus* until the arrival of Europeans (Figure 2.14D) (Heusser, 1995). A recent increase in the record of *Empetrum rubrum* may suggest surface drying of the bog. From the same study, the pollen record from Puerto del Hambre (Figure 2.14E) shows increasing *Nothofagus* suggesting that at this bog a local signal is evident with little deforestation of the surrounding area. A local signal of decreasing *E. rubrum* would suggest a shift in the opposite direction with wetter conditions at the surface. The two records were compared with a record from a mire located at 51°S 72°W where there had been drying over the last 1000 ^{14}C years. The signal here may be indicative of shifts in the SWW however, the records are of too low temporal resolution. A pollen record from the same bog finds decreasing *Nothofagus* and *E. rubrum* based on only two data points over the last 1000 ^{14}C years. From a site to the east, Estancia Esmeralda, the record shows a decrease from low to even lower *Nothofagus* values from three data points covering the same period. The comparatively lower values but similar patterns are a result of the precipitation gradient (McCulloch and Davies, 2001). These records may indicate decreasing precipitation over this gradient and time period.

The remaining peat study sites are at a similar latitude (54ºS) (Figure 2.15) and will be considered in longitudinal order from west to east to explore whether any correlation can be made between sites.

At this latitude the most westerly located sites are Ushuaia 1, 2 and 3 as investigated by Heusser (1998). Generally, the pollen records show an expansion of *Nothofagus* forest due to wetter and cooler conditions in the late-Holocene (Figure 2.15A). However, the records to present are variable between the three peatlands, with a general drying trend suggested by the increased presence of *Empetrum* at all sites. The chronology at each site varies making comparison difficult. Moreover, this comparison of pollen records from three closely located sites questions the validity of pollen to indicate climate variability owing to the differing results.

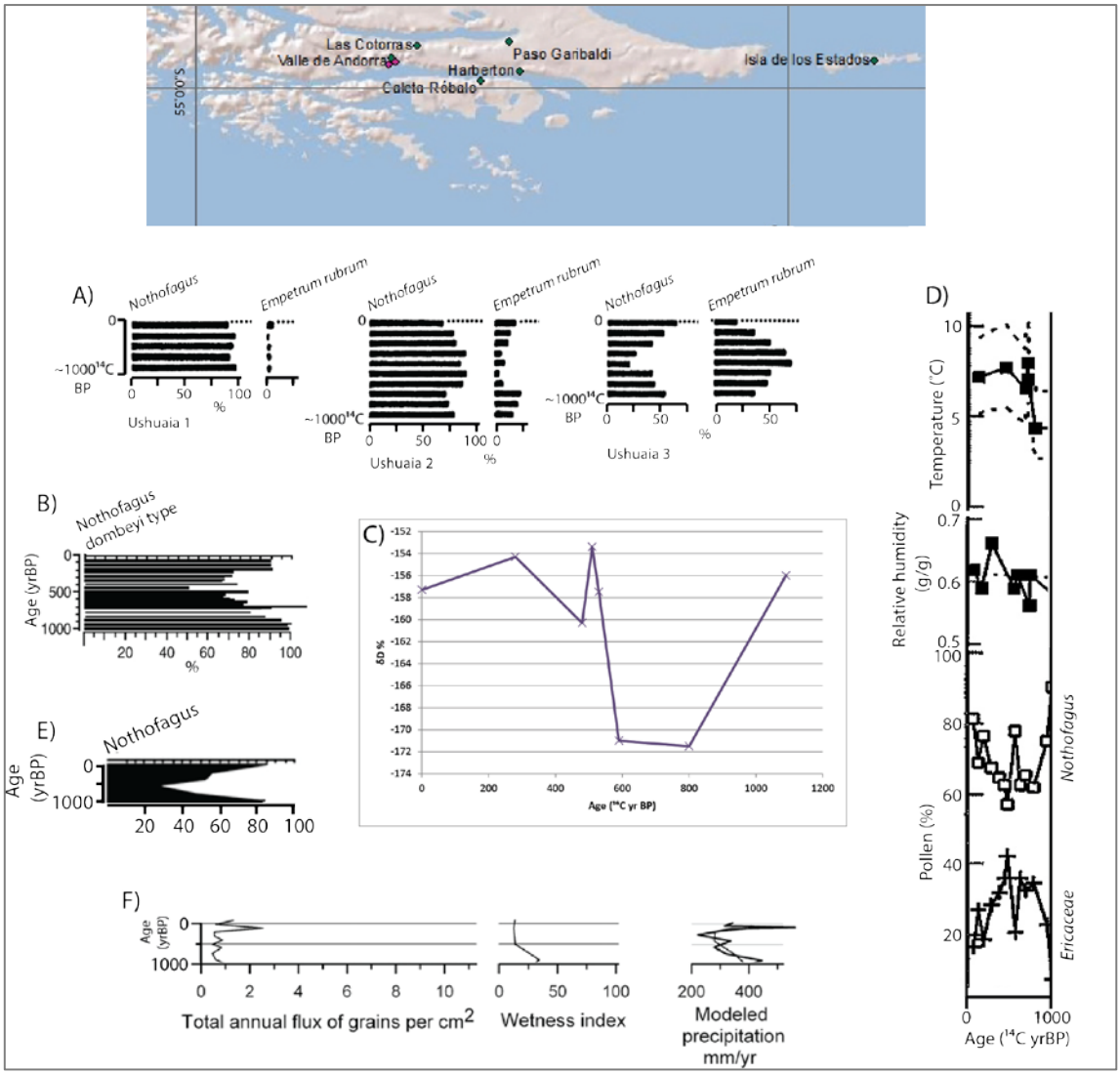

Figure 2.15. Peat records from ~54˚S. **A)** *Nothofagus* and *Empetrum rubrum* pollen records from Ushuaia 1, 2 and 3 **(Heusser, 1998)**. **B)** *Nothofagus dombeyi* pollen record from Las Cotorras **(Borromei *et al*., 2010)**. **C)** A stable hydrogen (D:H) isotope record from Harberton **(Kenny *et al*., 1999)**. **D)** Pollen data, inferred relative humidity and temperature from the stable hydrogen isotope record from Harberton **(Pendall *et al*., 2001)**. **E)** A *Nothofagus* pollen record from Isla de los estados **(Ponce *et al*., 2011)**. **F)** Also from Isla de los estados, a pollen inferred wind and wetness index and modelled precipitation **(Bjork *et al*., 2012)**.

A multi-proxy study was carried out at Valle de Andorra in which methods, until that time, usually applied to Northern Hemisphere bogs were used (Mauquoy *et al*., 2004). A record of plant macrofossils, pollen, fungal spores, testate amoebae and peat humification was compiled to provide a 1400-year record of inferred temperature and precipitation changes. The record revealed low local water tables between AD 960 and 1020, thought to be associated with the MCA with cooler and

wetter conditions apparent AD 1030-1100 and AD 1800-1930 perhaps a local signal of the Northern Hemisphere LIA and correlated with cooling at Law Dome, Antarctica. Another multi-proxy study from the same site investigated whether a climate anomaly centred at 2800 cal BP suggested by a shift to drier bog surface wetness was globally synchronous. They conclude that this cooling event caused by a solar down turn was globally synchronous suggesting global implications of a similar forcing event (Chambers *et al*., 2007). More recently, a peat record from the same site suggested a dry LIA period between AD 1675 and 1770 (Chambers *et al.*, 2014). The plant macrofossil data show an interruption in the *Sphagnum*-dominated record by increased Ericaceae remains alongside low light transmission values (high humification). The location of this site in terms of SWW influence is questioned based on whether the record demonstrates a western or eastern Andean response to variability.

Compared with other available records in the region a relatively higher resolution pollen record was constructed from Las Cotorras bog (Figure 2.15B) (Borromei *et al*., 2010). A decline of *Nothofagus* pollen at 1000 cal BP reaching a minimum between 680 and 300 cal BP is interpreted as a result of the cooler and wetter conditions of the LIA at this site.

Harberton bog is a key site in that multi-proxy records have to date been produced here using pollen and the stable isotopes of carbon and hydrogen (Markgraf, 1993; White *et al*., 1994; Markgraf *et al*., 1995; Kenny *et al*., 1999; Pendall *et al*., 2001). White *et al*. (1994) reconstruct atmospheric CO_2 content using the ratios of stable carbon isotopes (^{13}C:^{12}C) from mosses. This high-resolution study in terms of the last 14,000 ^{14}C years has only six data points covering the last 2000 ^{14}C years. Since this time a shift to less negative $\delta^{13}C$ values is evident and represents increasing relative humidity; a shift from the last data point to the surface to more negative $\delta^{13}C$ values is the result of decreasing humidity.

Using the same profile Kenny *et al*. (1999) reconstructed temperature variability over the last 14,000 ^{14}C years using stable hydrogen isotopes (D:H) of moss cellulose. Eight data points cover the last 1000 ^{14}C years (Figure 2.15C). More negative δD values are indicative of cooling while more positive values indicate warming. It appears that a cooling event ~800 ^{14}C yr BP may be synchronous with the LIA.

Pollen and stable hydrogen isotopes (D:H) from Harberton were used to reconstruct moisture and temperature variability over the last 16,000 years (Pendall *et al*., 2001). Figure 2.15D shows the *Nothofagus* and Ericaceae pollen results and the inferred relative humidity and temperature records. Cooler and less humid conditions are evident ~800 ^{14}C yr BP as suggested by the isotope and pollen data, after which conditions became progressively wetter and warmer towards present, suggested by the increase of *Nothofagus* and less negative δD values.

As shown in Figure 2.15E a decline of *Nothofagus* between 1000 and 700 cal BP in a record from the most easterly located site on Isla de los Estados is evident with an increase thereafter until present (Ponce *et al*., 2011). Similarly, Björck *et al*. (2012) used pollen data to create a wetness index and inferred wind strength from the annual pollen influx (Figure 2.15F). After 1000 cal BP the wetness index decreases along with the modelled precipitation during a time of inferred weaker SWW strength. A strengthening ~100 cal BP is suggested by a higher pollen influx and increase in modelled precipitation. It is difficult to ascertain from this record what has occurred recently, with the modelled precipitation apparently decreasing to present.

Despite the potential of peat as a palaeoclimate archive (Section 2.3) there have been relatively few studies in the region exploiting the range of proxies now available. In response to the lack of peatland palaeoclimate studies in SSA the PATAGOn research group (Palaeoclimate reconstructions from Tierra del Fuego to detect land-ocean-atmosphere interactions) aimed to develop a new regional network of palaeoclimate records over the past 2000 years using this archive. Records from five sites along the precipitation gradient are currently being investigated, with some sites further east in Argentina (Daley *et al*., 2012; van Bellen *et al*., 2014; 2016).

As well as the range of proxies available from Southern Patagonian peatlands already reviewed, anthropogenic Mercury and Lead accumulation and halogenide and heavy metal contents in the peat record have been investigated (Biester *et al*., 2002; 2003; 2006). Records of tephra layers from volcanic eruptions (Kilian *et al*., 2003) and atmospheric dust deposition (Sapkota *et al*., 2007; De Vleeschouwer *et al.*, 2014) have also been compiled from these peatlands.

2.2.3.2 Antarctic and Sub-Antarctic records

Pioneering work has recently been carried out on moss peat banks from the subantarctic islands (Van der Putten *et al*., 2009; 2012) and from the Antarctic Peninsula (Royles *et al*., 2012; 2013a; 2013b; 2016). These peat banks are semi-ombrotrophic thus relying primarily on precipitation but also to some extent on groundwater. They are dominated by *Polytrichum strictum* and *Chorisodontium aciphyllum*; Sphagna are rarely present owing to the high oceanicity of these study areas. These terrestrial archives provide important records of effective precipitation potentially resulting from the effect of SWW variability on the high latitudes.

Van der Putten *et al*. (2012) is a review of the plant macrofossil records from two subantarctic islands, South Georgia (54°S, 37°W) and Iles Crozet (46°25'S, 51°45'E). The records display millennial-scale Holocene changes with only four sampling points covering the last 1000 years, despite this; a shift in dominant vegetation 2000 years ago suggests cooler and wetter conditions since then. The authors suggest this may be a lagged response to the 2.8kyr BP cooling event, also found in the Chambers *et al*. (2007) record. Global in extent, this is thought to have been caused by a lowering of solar irradiation and resultant atmospheric (van Geel *et al*., 2000) or oceanic feedbacks (Renssen *et al*., 2006). The differing latitudinal locations of the islands in terms of the SWW explain the different signals evident in the records possibly resulting from regional manifestation of a global event.

2.2.2.3 Synthesis of records

There is now much potential for multi-proxy peatland palaeoclimate records in the region. The studies reviewed suggest that the majority of records are chronologically lacking and of low-resolution. The pollen records are useful for identifying ecological disturbance as a result of human settlement however, the majority are of too low a resolution to suggest late-Holocene natural climate variability.

Comparison between records is made difficult owing to the poor chronological control and differing interpretations between various peat proxies however, it can be seen that some correlated patterns may occur even between these low-resolution records. In terms of climate variability related to the MCA and LIA, more northerly records showed decreasing annual precipitation ~800 cal BP associated with the MCA and perhaps a later LIA period (~250 cal BP) of increasing precipitation

(Mancini, 2009). Further south, the records point to a LIA period of cooler and wetter conditions which vary in timing (1000 ^{14}C yr BP (White *et al*., 1994), 800 ^{14}C yr BP (Kenny *et al*., 1999; Pendall *et al*., 2001), 680-300 cal BP (Borromei *et al*., 2010)) whilst Chambers *et al.* (2014) find evidence of a drier LIA period ~230 cal BP. Records from Isla de los estados point to drier conditions from 1000 to 700 cal BP (Björck *et al*., 2012). Moreover, some show a drying trend until present (White *et al*. 1994; Heusser, 1998; McCulloch and Davies, 2001; Björck *et al*., 2012) whereas others show wetter conditions until present (Pendall *et al*., 2001; Markgraf and Huber, 2010). The differing results amongst these studies could be due to local responses to climate variability, questioning the reliability of using proxies from peat to reconstruct regional scale variability. The differences are more likely a result of incorrect interpretation of low-resolution studies that do not pick up late-Holocene low-frequency climate variability and also poor chronological control, which limits the comparison of records.

2.2.4 Tree-ring studies

Tree rings provide the majority of annually resolved climate reconstructions (Jones and Mann, 2004). Andean tree rings constitute the largest percentage of palaeoclimate data for SSA (Neukom *et al*., 2011) providing local- to regional-scale temperature reconstructions with annual resolution. The majority of records show periods contemporaneous with the Northern Hemisphere LIA suggesting climatic synchroneity between hemispheres however, the MCA is not always evident (Boninsegna *et al*., 2009). The significant and unprecedented increase in temperatures since AD 1850 is also evident in the majority of records (Boninsegna *et al*., 2009). Despite providing high-resolution palaeotemperature reconstructions, tree ring chronologies are limited in length with records only extending back to AD 1640 in Southern Patagonia. Also evident is the relatively low spatial resolution of records with the majority of reconstructions carried out using records from the West of the region. Reliability could be improved by increasing the records across a wider spatial gradient and more records are being produced further east in the region (Mundo *et al*., 2012) with a focus on the species *Araucaria araucana*. The dendrochronological records can be used in conjunction with other records from the region to aid interpretation of proxy response to late-Holocene climate variability. Climate model reconstructions may be able to assess the occurrence of synchronous climate

periods by combining a wide variety of temperature and precipitation proxies from the region.

2.2.5 Model reconstructions

Where previous sections aimed to review the results of various proxies from various archives, model reconstructions are now being used to perform regional reconstructions of temperature and precipitation using statistical methods on proxy and instrumental data.

2.2.5.1 Temperature

A statistical reconstruction of regional palaeotemperatures (between 20°S and 55°S) was carried out by Neukom *et al*. (2011). Using principal component regression of 22 (20) palaeotemperature proxies (tree ring, documentary and instrumental records) austral summer (winter) palaeotemperatures to AD 900 (AD 1706) were statistically reconstructed (Figure 2.16). These predictor sets were reduced from an evaluated set of 144 proxies. Climatic teleconnections between the reconstruction area and SAM and ENSO in the period AD 1950-2006, explain 38% of the mean annual temperature variability in the reconstruction area. This significant percentage explains the use of proxies from outside the reconstruction area (See Neukom *et al*., 2011 Table 1 and 2 for full list) in both predictor sets. To what extent the teleconnections account for temperature variability before the instrumental period must be considered and may in fact bias the reconstruction (Neukom *et al*., 2011).

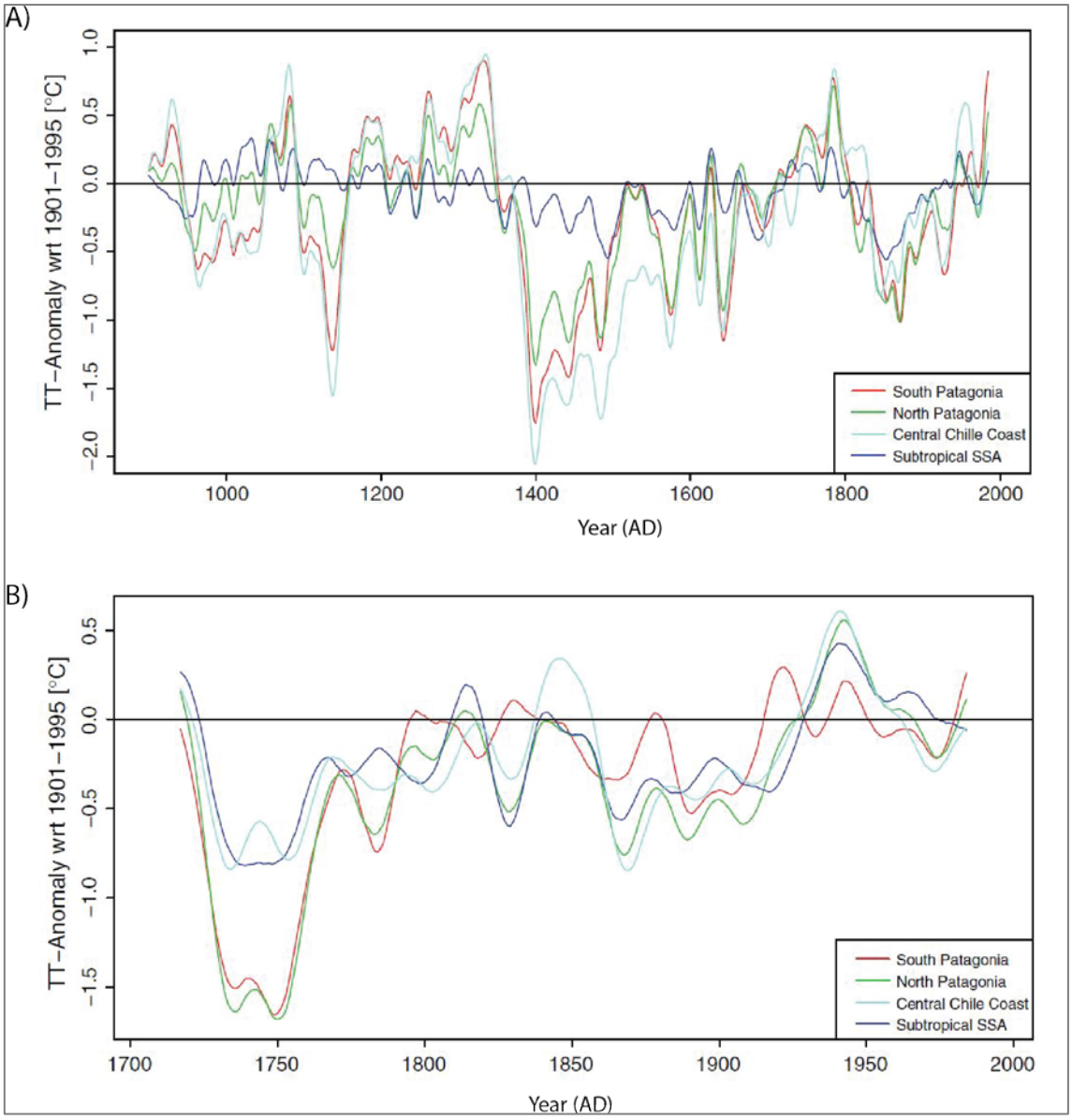

Figure 2.16. From **Neukom *et al*. (2011)**. **A)** 30-year Gaussian filtered summer temperature anomalies 900-1995 (with reference to 1901-1995) for the sub regions of SSA reconstructed by principal component regression. **B)** 30-year Gaussian filtered winter temperature anomalies 1706-1995 (with reference to 1901-1995) for the sub regions of SSA reconstructed using principal component regression.

The general trends in the summer temperature record (Figure 2.16A) suggest warm episodes until AD 1350, followed by a cold period between AD 1400 and 1650. Between AD 1710 and 1820 conditions were warmer with another subsequent cold period between AD 1820 and 1940. Since this time conditions have become warmer. The temperature anomaly of a 1.5 °C decrease around AD 1400 is significant in the summer temperature record and also that occurring after AD 1700 in the winter

record. These are associated with minima in sun activity (Figure 2.20). The records were verified using independent instrumental data of recent inter-annual and multi-decadal temperature variations and fit well with records of glacier fluctuations from SSA (Section 2.2.1), which are temperature sensitive. The difference in the amplitude of changes across the different sub-regions emphasises the caution that must be taken when comparing palaeorecords from these sub-regions with the results of this thesis. The reconstruction combined local and remote predictors to reconstruct regional climate variability. Southern Patagonian variability (red) must be viewed with caution as only a few proxies from SSA are used, missing variability on the smaller spatial scale. Using proxies from outside the region may impose unrealistic climate variability; however, regional reconstructions must be carried out in this way in the absence of more sufficient records.

Luterbacher *et al*. (2011) compared the austral summer temperature reconstruction of Neukom *et al*. (2011) with 3 AOGCM (Atmosphere-Ocean General Circulation Model) simulations for the last millennium (Figure 2.17) with a particular focus on the occurrence of the MCA and LIA in SSA (defined as 20-55°S).

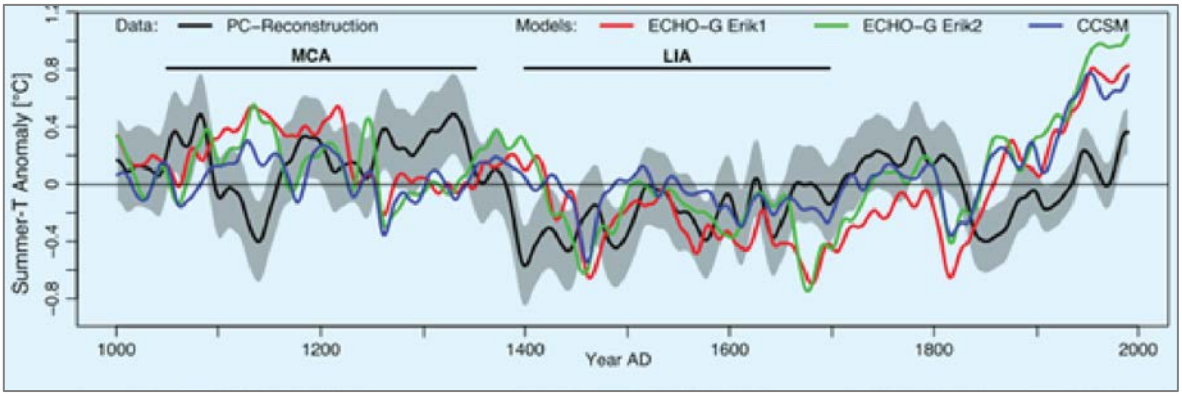

Figure 2.17. From **Luterbacher *et al*. (2011)**. Black line shows 30-year Gaussian filtered summer surface air temperature anomalies 1001-1990 (with reference to 1001-1700) with shaded area representing uncertainty (data from **Neukom *et al*., 2011)**. Coloured lines show the model simulations.

Warmer conditions of the MCA until ~AD 1350 and cooler conditions of the LIA until ~AD 1700 are evident in both the reconstruction and simulations, increasing the validity of such records. As proxy data are still lacking in the region, especially further south, the uncertainty of reconstructions is still high. As such, the most recent IPCC

report places medium confidence on warmer austral summer temperatures between AD 950 and 1350 than in the 20th century (Masson-Delmotte *et al.*, 2013). In order to reduce uncertainty more high-resolution records are needed.

A modification of the Neukom *et al*. (2011) proxy network in a continental temperature reconstruction (Pages 2k, 2013) removed the remote proxies used in the earlier reconstruction. New proxy records were included but each proxy record was from within South America; this should omit the bias produced in reconstructions due to remote proxies (Neukom *et al*., 2011). On the millennial-scale the South American reconstruction shows long-term cooling over the reconstruction period, with an intermittent warm period over the whole Southern Hemisphere between AD 1160 and 1370 and warming since the 20th century. Time series of volcanic and solar forcing were used in the reconstruction and suggest that in periods of strongest forcing, a resultant global cooling is evident. A warming period in the South American reconstruction during the most recent volcanic-solar downturn is opposite in direction to the other continental reconstructions. Globally synchronous MCA and LIA events are not revealed by the global continental reconstruction, which offers support for asynchroneity of climate events between the hemispheres. The reconstruction revealed warming in all regions since the 20th century apart from Antarctica where there has been cooling over this period, perhaps due to stratospheric ozone loss (Polvani *et al*., 2011) over Antarctica and associated global teleconnections of a resultant cooling.

2.2.5.2 Precipitation

Neukom *et al*. (2010) carried out the first gridded reconstruction of SSA precipitation variability on a multi-centennial scale. Independent predictors to Neukom *et al*. (2011) are used which consist of 33 (31) proxy records and 41 (42) instrumental data for summer (winter) reconstructions. The summer (winter) reconstruction extends back to AD 1498 (AD 1590) (Figure 2.18). Relative to the AD 1931-1995 mean climatology, between AD 1500 and 1600 summer precipitation reconstructions appear to be wetter (anomalies above the mean climatology) after which time until AD 1930 they are drier (anomalies below the mean climatology). Winter reconstructions are wetter from AD 1600 to 1900 (anomalies above the mean climatology). The record therefore suggests that between 20–55°S there has been an increase in summer

precipitation and a decrease in winter precipitation until the end of the record (20th century).

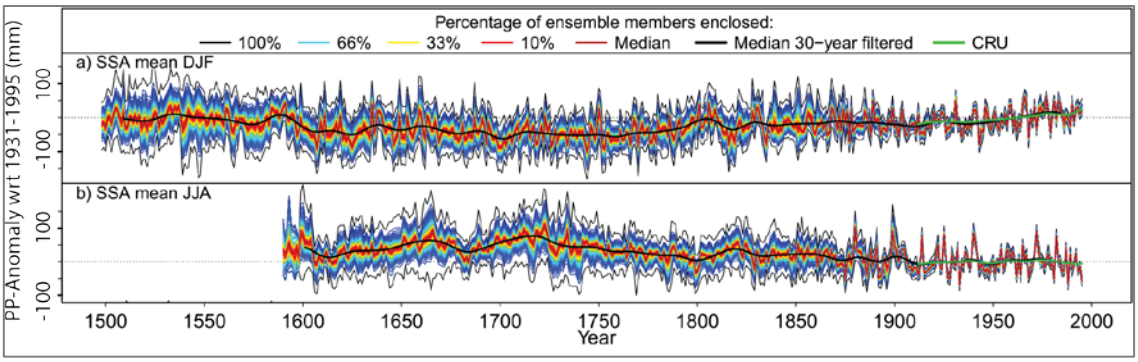

Figure 2.18. From **Neukom *et al*. (2010)**. In A and B; Percentage of ensemble members enclosed is represented by the different coloured areas according to the key. The 30-year Gaussian filtered ensemble mean is represented by the thick black line and the thick green line represents CRU gridded precipitation. **A)** Mean summer precipitation reconstruction 1498-1995. **B)** Mean winter precipitation reconstruction 1590-1995. Anomalies with reference to 1931-1995 average.

The decreasing uncertainty back in time is due to the decreasing number of predictors available; this would suggest that to decrease uncertainty more high-resolution records are needed. This study provides a good reconstruction of regional precipitation and general changes may aid interpretation of the results of this thesis. This regional reconstruction may miss smaller scale spatial variability, which is evident from reviewing records on an individual basis. The climate variability evident in such reconstructions could be used to infer SWW strength and intensity shifts on the basis of the correlation between wind strength and precipitation.

Figure 2.19 shows downscaled summer precipitation for the south-eastern region of Patagonia (Meyer and Wagner, 2008). A coarse general circulation model (GCM) was used with a further application of principal component regression to reconstruct precipitation variability. In very simple terms, and as has been attempted in previous sections, comparison with proxy data from the region suggests a drier and warmer MCA from AD 1150 to 1300 when the SWW shifted south (intensified). A wetter and cooler period characterised the LIA between AD 1550 and 1800 when the SWW is thought to have shifted north.

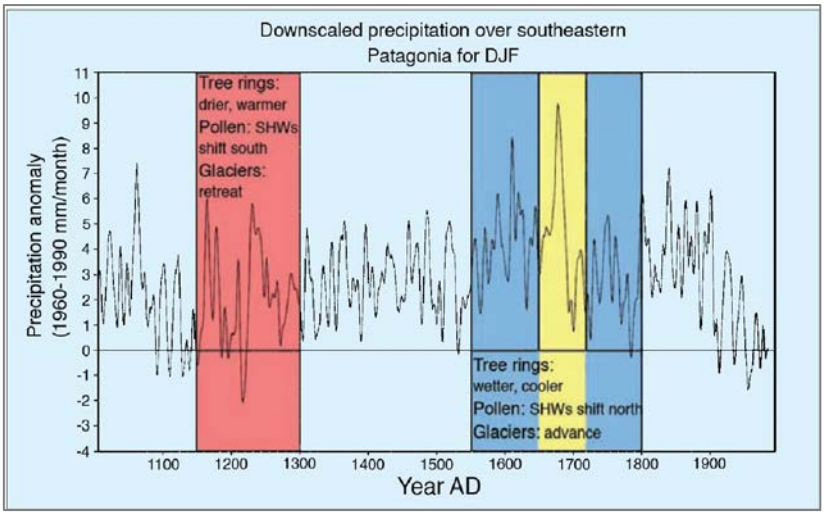

Figure 2.19. From **Meyer and Wagner (2008)**. Downscaled austral summer (DJF) precipitation, south-eastern Patagonia. Precipitation anomalies wrt 1960-1990 (zero line).

2.2.6 Antarctic climate variability

Finally, owing to its proximity to SSA and the influence of the SWW on Antarctic climate it is important to discuss briefly the role climate and palaeoclimate records from the continent may play in establishing SWW variability on the shorter and longer term.

2.2.6.1 Sea ice expansion

The atmosphere-ocean interactions mainly in the way of the SAM and ACC result in a circumpolar sea ice distribution around the Antarctic continent, the extent of which varies both intra- and inter-annually. Satellite observations over the last four decades record this variability (Parkinson and Cavalieri, 2012); however, more investigations into the natural variability of sea ice extent are important. Sea-ice proxies to understand the natural variability of sea ice cover over longer timescales would provide a baseline on which to assess direct observations of variability from anthropogenically forced climate change (de Vernal *et al*., 2013).

In contrast to rapid Arctic sea ice loss (Cavalieri and Parkinson, 2012) there has been an overall average increase in Antarctic sea ice extent since 1979 (Parkinson and Cavalieri, 2012). Model results (Turner *et al*., 2009) suggest that this recent increase may still be in the range of natural variability with implications for future climate predictions. Despite this overall positive trend there has been a sea ice loss

from the Bellingshausen and Amundsen seas (Parkinson and Cavalieri, 2012) coincident with warming over the Antarctic Peninsula.

Based on intra-annual observations during austral summer when the SWW is southward shifted there is a decrease of sea ice with an increase of sea ice in austral winter when the SWW is at its northerly extent. Sea-ice extent can, therefore, be linked to past indications of SWW strength.

2.2.6.2 ENSO and the southern high latitudes

Investigations into the linkage between ENSO and the southern high latitudes (Rind *et al*., 2001; Turner, 2004; Stammerjohn *et al*., 2008) suggest non-linear links via the atmosphere-ocean-sea ice system. In el Niño years there is an observed decrease in Pacific sea ice (West Antarctica) and an increase over the Weddel sea (East Antarctica) and the opposite trend in la Niña years (Rind *et al*., 2001). Stammerjohn *et al*. (2008) studied the ENSO-SAM-sea ice relationship over the period 1979 to 2004. In particular the Bellingshausen Sea ice response was particularly strong during el Niño years in a period of negative SAM index with later sea ice retreat and earlier sea ice advance and during la Niña years in a period of positive SAM index when the trend was reversed with earlier sea ice retreat and later sea ice advance. An anticorrelation between ENSO and SAM is suggested (Flantua *et al*., 2016) although the exact mechanism remains unclear. Recent studies have suggested longer term links between ENSO and SAM, with periods of negative (positive) SAM related to el Niño (la Niña) events and cooling (warming) on the Antarctic Peninsula (Fogt *et al*., 2011; Ding *et al*., 2012). It is suggested that these links are due to the effect of solar irradiance on tropical Pacific forcing (Yan *et al*., 2011; Ding and Steig, 2013; Emile-Geay *et al*., 2013; Sottile *et al*., 2015).

2.2.6.3 Longer term Antarctic perspective

A longer term perspective is provided by a review of Antarctic ice cores (Russell and McGregor, 2010). Records from the Western Antarctic peninsula can provide a longer term context for present warming (Aristarain *et al*, 2004; Steig *et al*., 2005; Thomas *et al*., 2008; Abram *et al*., 2013). An understanding of key climate processes of the late-Holocene may be provided by such investigations (Bentley *et al*., 2009; Mayewksi *et al*., 2009). Comparisons between palaeoclimate records from SSA and the Antarctic region also aid in interpretation of regional climate variability (e.g.

Björck *et al.,* 1996; Kreutz *et al*., 1997; Royles *et al*., 2012; Van der Putten *et al*., 2012; Strother *et al*., 2015) assumed to be driven by the same mechanisms (Section 2.2.7).

A West Antarctic ice core (79°S) records SWW variability using dust flux variability. A period of increased dust flux between AD 1050 and 1400 (synchronous with Northern Hemisphere MCA) suggests a southerly displaced and strengthened SWW. A decreased dust flux followed between ~AD 1430 until the late 20th century (Northern Hemisphere LIA), suggesting an equatorward shifted SWW (Koffman *et al*., 2014). As such, a longer term perspective inferred from high-resolution SSA palaeoclimate records will add to such reconstructions of regional climate variability.

The next section will focus on the potential climate forcings of SWW variability discussed in this section.

2.2.7 Late-Holocene climate forcing of SWW variability

As reviewed throughout this section, an increasing number of palaeoclimate records from SSA is beginning to establish a baseline of variability; however, owing to the relatively sparse network of palaeoclimate records from the Southern Hemisphere there remains a lot to be understood about the causes of late-Holocene climate variability in the region. Lower temporal resolution studies may not record relatively short but globally significant climate intervals (Moy *et al*., 2008) and regional complexities result in global inconsistencies (Jones and Mann, 2004) emphasising the need for high-resolution and regionally specific archives.

2.2.7.1 Natural climate variability

In the Northern Hemisphere it is suggested that higher solar output and fewer volcanic eruptions resulted in an apparent MCA and global warming in many records. Conversely the LIA is thought to have been caused by a reduction in solar output and an increase in volcanic eruptions leading to global cooling (Mann *et al*., 2009; Pages 2k, 2013).

The combined effects of external (solar and volcanic radiative) forcing as well as internal variability (ENSO) are considered in interpretation of late-Holocene palaeoclimate records from the Southern Hemisphere. Inter-hemispheric teleconnections can be assessed via comparison of Northern and Southern

Hemisphere palaeoclimate records and hypothesised forcing. In order to understand the reaction of the climate system to recent anthropogenic GHG forcing, establishing natural baseline variability and an understanding of the drivers of this variability is paramount.

It is hypothesised that if periods in the Southern Hemisphere correlate with the assumed MCA and LIA periods of the Northern Hemisphere then via inter-hemipsheric teleconnections solar variability may have caused assumed Southern Hemisphere natural climate variability. This may be tested by comparison of SSA palaeoclimate records with proxies of solar irradiance and volcanic eruptions (Wilmes *et al*., 2012).

Variability in total solar irradiance (TSI) (solar radiative energy hitting the upper atmosphere) is coincident with the Schwabe, Hale and Gleissberg sunspot cycles (~9-12, ~20-22, and ~72-90 years respectively) correlated with records of cosmogenic isotope production (^{14}C: Solanki *et al*., 2004 and ^{10}Be: Vonmoos *et al*., 2006; Steinhilber *et al*., 2009). These TSI changes are then amplified by ocean-atmosphere systems via global teleconnections. The mechanisms causing modern intra-annual variability (section 2.1.1) (ITCZ shifts) can be applied to past scenarios of solar variability that caused the mean annual position of the ITCZ to shift, with global impacts (Haug *et al*., 2001). The modern link between the ITCZ and ENSO is still not fully understood but reconstructions of late-Holocene ENSO variability (Moy *et al*., 2002; Cobb *et al*. 2003; Rein *et al*., 2004) allow the synchrony of global teleconnections to be assessed.

During the LIA, it is thought that a reduction in total solar irradiance caused a reduction in solar UV intensity, a decline of stratospheric ozone production and the absorption of less sunlight with a resultant cooling (van Geel *et al*., 2000). This affected the latitudinal extent of the Hadley cell, a reduction of which results in an equatorward shift of the SWW. The same reduction in total solar irradiance is thought to have caused cooling over the North Atlantic, sea- ice expanded and a positive oceanic feedback led to further cooling (Renssen *et al*., 2006).

Varma *et al*. (2010) correlated SWW variability (precipitation inferred SWW shifts (41ºS) (Lamy *et al*., 2001) with solar activity (^{10}Be and ^{14}C) on the centennial scale over the last 3000 years. Figure 2.20 shows coherent changes between the two. In

periods of lower solar activity equatorward shifts of SWW are suggested while during higher solar activity poleward shifts of SWW are inferred. Where correlations such as this occur it seems likely that variability in TSI has forced natural global climate variability. As reviewed in the previous section, records at different latitudes imply different SWW variability; for example, opposing Varma *et al*. (2010), Shulmeister *et al*. (2004) imply intensification of the SWW during the LIA.

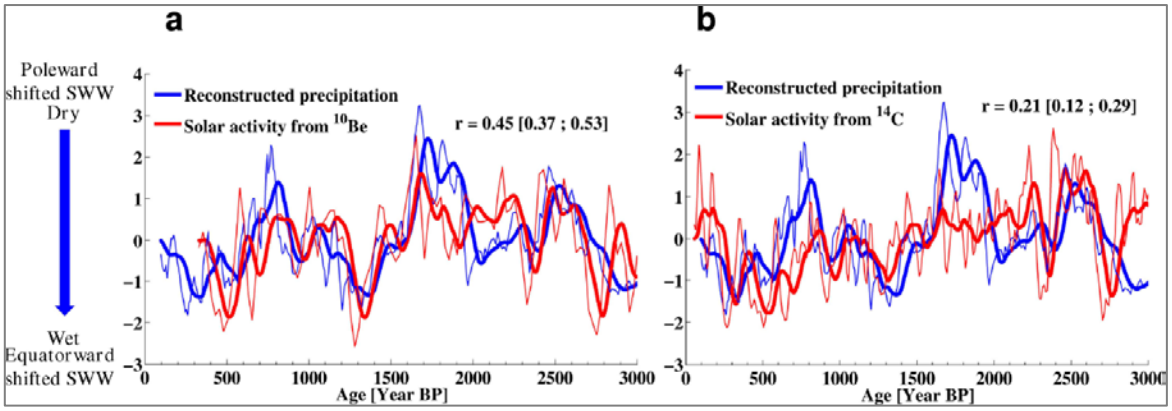

Figure 2.20. From **Varma *et al*. (2010)**. Precipitation inferred SWW variability from the marine iron content record **(Lamy *et al*., 2001)** see section 2.2.2.1. **A)** Solar activity based on ^{10}Be (Vonmoos *et al*., 2006) and **B)** ^{14}C **(Solanki *et al*., 2004)**. Thin lines show unsmoothed data and thick lines show 100-year running means.

Comparison of solar irradiance curves (Vieira *et al*., 2011; Steinhilber *et al*., 2009) with late-Holocene palaeoclimate proxy records can assess whether solar irradiance was a cause of SWW shifts. Wang *et al*. (2005) suggest that such relationships are complex and should be carefully considered. Non-linearity may arise because the cosmogenic isotopes taken to represent solar irradiance variability are not a direct measure of this (McCarroll, 2010).

An alternative hypothesis involves antiphase between Northern and Southern Hemisphere climate variability. A 20th century bipolar seesaw has been identified between Arctic and Antarctic temperatures (Chylek *et al*., 2010) linked by Atlantic Ocean circulation. Variability in the circulation is thought to have been responsible for a bipolar seesaw temperature pattern between the hemispheres during the last deglaciation (Lamy *et al*., 2007; Barker *et al*., 2009) and 8.2k yr event (Ljung *et al*., 2008).

Finally, Southern Hemisphere and Northern Hemisphere climate variability may not be correlated such that the aforementioned teleconnections with the NH could not explain the history of SH temperature changes.

2.2.7.2 Impact on atmospheric CO_2

In terms of natural variability, it is suggested that the SWW causes the upwelling of deep water in the Southern Ocean (Toggweiler *et al*., 2006; Anderson *et al.*, 2009; Toggweiler, 2009; Moreno *et al*., 2010; Mayr *et al*., 2013) with a resultant effect on atmospheric CO_2 concentrations. Whereas strengthening increases atmospheric CO_2 via increased upwelling, weakening slows upwelling and decreased ventilation of atmospheric CO_2. This feedback is important in light of the recent suggested strengthening of the SWW from increased CO_2 over the last 40 years (Arblaster and Meehl, 2006; Toggweiler and Russell, 2008) with addition of further atmospheric CO_2.

2.2.8 Summary of late-Holocene palaeoclimate studies

The current limitations of palaeoclimate reconstructions relate to the spatial limitation of records, inherent uncertainties of the records and problems of statistical comparisons between records as concluded in the latest IPCC report (Masson-Delmotte *et al.*, 2013).

From this review, it can generally be seen that broadly regionally synchronous MCA and LIA periods occurred in SSA. Despite spatial variability in the hydrological response, the lake, marine and stalagmite records suggested a southerly (northerly) shifted SWW during the MCA (LIA). Peat records point to cooler and wetter conditions at ~800 ^{14}C yr BP although these studies are limited by chronological uncertainty. Chambers *et al.* (2014) suggest a dry LIA period AD 1675-1770. Model reconstructions which include dendrochronological records suggest a warm and dry MCA period, perhaps due to a southward shifted SWW and a cool and wet LIA period (~AD 1350-1700) due to a northward shifted SWW.

Neukom and Gergis (2012) provide a review of Southern Hemisphere high-resolution palaeoclimate records, identifying 174 which can now provide improved hemisphere wide climate reconstructions. The majority of these records consist of tree ring chronologies and they emphasise the need for more high-resolution records from other archives. Similarly, from the previous section it is evident that existing

palaeoclimate records are of too low temporal resolution to establish recent natural climate variability.

Eastern South America is mentioned as an area in which many archives are available but have yet to be explored, emphasising the need for more records from this area in order to provide more detailed regional reconstructions (Neukom and Gergis, 2012). It seems that sites to the west and east of the Andes show generally consistent variability in terms of the precipitation gradient over time. However, where inconsistencies exist between archives this is most probably related to different depositional environments from contrasting environments and differing interpretations from a variety of proxies. Also, in consideration of latitudinal shifts of the SWW, this very complex system will have inevitably had an effect across the region. As such, whether records can predominantly reconstruct such shifts or whether they display local signals remains in question.

This section synthesised the existing palaeoclimate proxies and reconstructions from SSA. As well as providing a necessary comparison with the results of this investigation it has shown that gaps remain in terms of the spatial and temporal resolution of palaeoclimate records in the region. Despite the potential of peatland palaeoclimate records, which will be discussed in the following section, it has been seen that these archives remain little investigated in SSA.

2.3 Peatlands as palaeoclimate archives

Peatlands, also known as organic wetlands, are characterised by the accumulation of preserved organic matter (peat) underlying a living plant layer (Charman, 2002). Accumulation of peat occurs when net primary productivity (NPP) exceeds decomposition promoted by the favourable conditions that these landforms create. Wetness in the substratum creates anaerobic conditions and an inhibition of decay causing micro-organisms; the once living layer is then incorporated and vegetative remains are well preserved (Pennington, 1974). Analysis of this accumulated peat allows inferences to be made on past environmental changes (Barber, 1981). If these changes were driven by variations in climate conditions this assumes peatlands can provide an archive for past climate variability but as it will be seen in this section this is now debated. Peatlands cover 3% of the global land area (Yu *et*

al., 2010) thus providing a globally distributed terrestrial archive for potential records of climate variability.

As Figure 2.21 shows, the majority of peatlands are located in the Northern Hemisphere owing to the more extensive land cover. Extensive peatlands in SSA offer the potential of such records to be exploited in the Southern Hemisphere. It is clear from this figure that climate is a key factor in the modern global distribution of peatlands. The conditions necessary for peat accumulation include sufficient precipitation and adequate temperatures to enable plant growth alongside waterlogged conditions to inhibit decomposition in the catotelm zone (Charman, 2002). Their global distribution is clearly related to these conditions, such as rain days per annum (Lindsay *et al*., 1988). This distribution would suggest that climate plays a key role in the ecology and function of peatlands, even over time; it is for this reason that palaeoclimate proxies from peat have been extensively used in recent decades (Chambers *et al*., 2012).

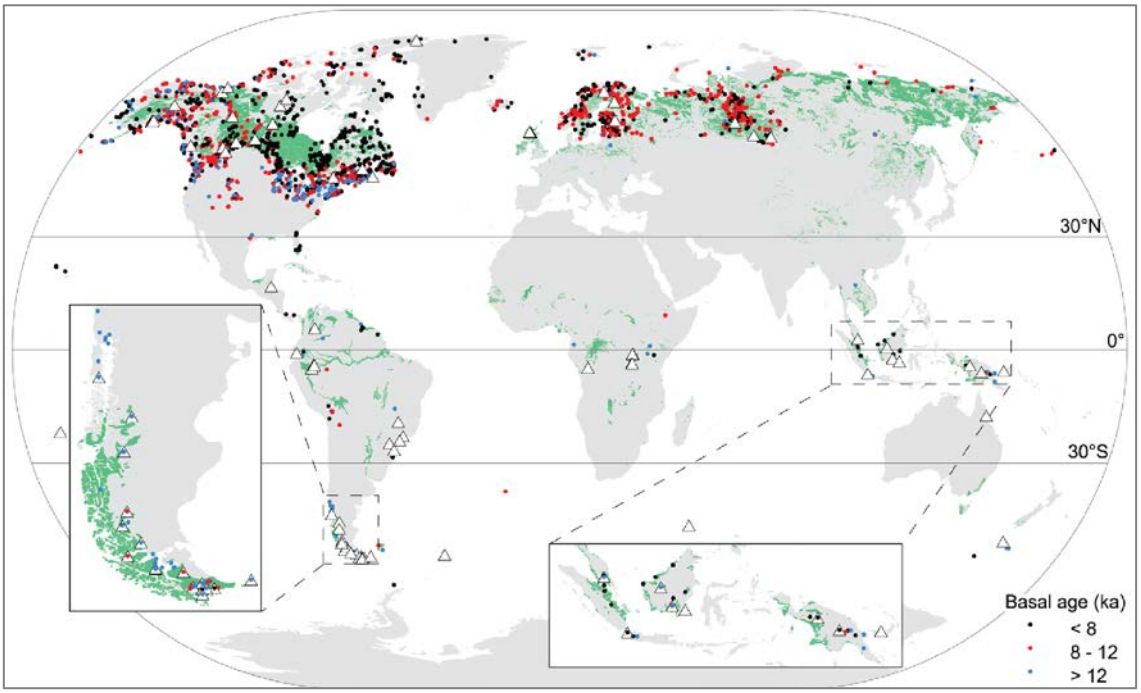

Figure 2.21. From **Yu *et al*. (2010)**. Map of global peatland distribution and peatland study sites. Small dots show basal ages and the large triangles are sites at which detailed carbon accumulation rates are available.

2.3.1 Historical development of peat as a palaeoclimate archive

Changes in the stratigraphy of peat profiles from ombrotrophic peatlands have now been used as a palaeoclimate proxy for over 30 years. Raised bogs, one type of ombrotrophic peatland, have a convex profile and receive water and nutrients solely from atmospheric inputs and it is for this reason that the majority of studies to reconstruct hydroclimatic variability use profiles obtained from raised bogs. The basic water balance of an ombrotrophic peatland depends on the influx (precipitation), efflux (evapotranspiration) and changes in storage being balanced (Eggelsman *et al*., 1993), directly linking climate with bog hydrology. Peatland surfaces are usually characterised by microtopographic differences. These microforms, differentiated by the terms hummock and hollow, are functionally different (Malmer and Wallén, 1999; Kettridge and Baird, 2010). Characteristically lying above the mean peatland surface level, hummocks are composed of dry-adapted plant species isolated from the mean water table level. Hollows lie below the mean surface level as depressions and also usually lie below the mean water table level and thus are characterised by wet-adapted plant species (Loisel and Yu, 2013). These microforms are often termed microtopographic gradients owing to the more often than not smooth transitional gradient from hummock to hollow, separated by a lawn area. The development and function of these microforms is still not fully understood.

Owing to observations of this microtopographic variability and darker and lighter bands in exposed peat profiles, Von Post and Sernander in 1910 proposed the cyclic regeneration theory (also Osvald, 1923). It was thought that autogenic (internal) processes were responsible for this cyclic pattern between hummock and hollow microforms evident throughout the stratigraphy and that the pattern was related to ontological development, with little consideration of allogenic (external) forcing. This theory was empirically tested by Barber (1981) in comparison of macrofossil analyses of multiple peat profiles from Bolton Fell Moss, Cumbria with an independent climate record (Lamb, 1977). Clear links between summer wetness and winter severity in Lamb's record and stratigraphic changes in the plant macrofossil record suggested an allogenic cause of change. This stratigraphic change was preferably described as the phasic theory of peat growth (Barber, 1981) in which hollows expand in wet periods and hummocks expand in dry periods. This early work

formed the basis for the development of palaeoclimate records from peatlands. The implication of Barber's phasic theory is that hummocks and hollows remain in the same position over time and hummocks, therefore, may provide a 'complacent' climate signal (Barber *et al*., 1998). The interface between a hummock and hollow would be the most climatically sensitive location from which to discover stratigraphic changes. Pool layers are more likely to be found in these locations (green/yellow muds with *Sphagnum cuspidatum*) (Aaby, 1976) (See Figure 3.2).

2.3.2 Ombrotrophic raised bogs: complex adaptive systems

It has until recently been generally accepted in the literature (Morris *et al*., 2011a) that ombrotrophic bogs are diplotelmic, with two layers, first hypothesised by Ivanov (1953) and Ingram (1978). This was followed by the conceptual models of Ingram (1982) (Groundwater Mound Hypothesis (GMH)) and Clymo (1984) (model of limits to peat bog growth (BGM)). The acrotelm, an active and permeable near surface layer, is above the lowest water table level. This layer is aerated with rapid rates of litter decay. The thickness of this layer depends on the seasonally fluctuating depth to water table differences of microforms (Belyea, 1999). The lower inactive layer, the catotelm, is saturated and anoxic with very slow rates of peat decay. It is assumed by the GMH and BGM that the catotelm controls the peat system dynamics. Central to palaeoclimate investigations of ombrotrophic peatlands is the assumption of this diplotelmic layering.

The basic assumption of the BGM is that decayed litter is transferred from the acrotelm to the catotelm at a constant rate. Once the litter is in the catotelm layer the rate of decay is slower and as a result the peat accumulation rate slows as the bog develops towards a limit to growth. This addition of litter to the catotelm was assumed to be constant across the microtopographic gradient (Belyea and Clymo, 1999). Large differences between the surface and the water table across the bog would be evident if this were not the case (Belyea and Clymo, 1999). NPP and the cumulative rate of loss by acrotelm decay (CRD_A) vary across microforms (Wallén *et al*., 1988; Clymo, 1965; Belyea, 1996). This control on peat accumulation is thought to be due to species differences between hummocks and hollows, with higher NPP on hummocks and lower NPP in hollows (Johnson and Damman, 1991).

The resulting deeper and shallower acrotelm of hummocks and hollows respectively result in differing CRD_A across microtopographic gradients (higher and lower decomposition in hollows and hummocks respectively). Belyea and Clymo (1999) suggest that the RSC (rate of submergence by the catotelm) is the same across microforms. This suggests that horizontal heterogeneity is not represented by this model but supports the notion that hummocks and hollows have been persistent throughout the peat stratigraphy, remaining in the same place over time but expanding and contracting (Aaby, 1976; Barber, 1981).

The GMH (Ingram, 1982) assumes that the low hydraulic conductivity of the catotelm underneath the acrotelm is the cause of the dome shape of raised bogs. Clymo and Bryant (2008) suggested a polytelmic model with four structural layers, with the addition of the mesotelm (layer between the acrotelm and catotelm influenced by water table fluctuations) and the pectotelm (surface plant layer) to expand the original diplotelmic model.

These models are based on rigid vertical boundaries defined by the lowest drought water table. Morris *et al*. (2011a) question the validity of these highly simplified one-dimensional models arguing that their simplicity cannot explain these peatland complex adaptive systems (Belyea and Baird, 2006). Peatlands are now understood to be ecohydrological systems with the interaction of feedbacks between ecology, biogeochemistry and hydrology (Belyea, 2009; Eppinga *et al*., 2009a; b) varying on spatial and temporal scales (Belyea and Baird, 2006; Ise *et al*., 2008; Belyea; 2009).

Morris *et al*. (2011a) suggest the use of the terms hot spot, a three-dimensional zone where ecohydrological feedback rates are elevated, and cold spot, where these feedbacks are inhibited. *Sphagnum* hummocks, for example, have been described as cold spots (Benscoter *et al*., 2011). The interactive feedbacks inherent to these hot and cold spots are explained in detail in Morris *et al*. (2011b) and provide a more flexible and complex framework to enable understanding of these dynamic systems. Despite the potential redundancy of the traditional diplotelmic model and the terms acrotelm and catotelm, this terminology will continue to be used throughout this thesis in order to maintain consistency and ease of understanding.

Ecohydrological feedbacks result in microtopographical differences on peatlands (Baird *et al.*, 2008) and the importance of peatland microtopography on overall

peatland functioning is recognised; however, investigation into the processes across microtopographical gradients is lacking (Branham and Strack, 2014).

2.3.3 Autogenic and allogenic drivers of change

It is suggested that early in succession allogenic factors are dominant until a bog reaches ombrotrophic status after which time long-term autogenic development (Charman *et al*., 2006) predominates and the bog is thought to self-regulate (Dise, 2009). Allogenic factors will still remain important especially in forcing the system (Rydin and Jeglum, 2006).

Changes in peat properties are generally accepted to be indicative of allogenic influences (e.g climate); it is now argued that these changes may be caused by autogenic influences resulting from ecohydrological feedbacks occurring throughout an entire period of climatic stability. Negative ecohydrological feedbacks enable peatlands to resist external forcing (self-dampening and stabilizing) (Belyea and Baird, 2006; Belyea, 2009) whereas positive ecohydrological feedbacks (self-reinforcing and destabilizing) respond disproportionately to external forcing (Belyea and Clymo, 2001). Results of a theoretical model (Morris *et al*., 2011b) displayed a negative feedback to changes in temperature and rainfall regimes (allogenic drivers) suggesting resistance of peatlands to external change. This finding, therefore, has implications for the use of peat as a palaeoclimate proxy (Morris *et al*., 2011b, Swindles *et al*., 2012a). It is important to note that the time frame of such changes applies to millennial-scale development of peatlands and to what extent this can be applied to the centennial and decadal timescales is questionable.

Ground penetrating radar (GPR) reflects the boundaries between stratigraphical layers (Worsfold *et al*., 1986; Warner *et al*., 1990; Comas and Slater, 2009) and has enabled the development of a conceptual model of peatland development at Cors Fochno raised bog, Wales (Kettridge *et al*.,2012). The model suggests that horizontal bands of differential peat composition (hummock and hollow) built up diagonally over time at this site owing to internal feedbacks and self-organisation. This appears to support the cyclic regeneration theory reinvigorating early autogenic ideas. In order to carry out a detailed description of the stratigraphy of an entire peatland, multiple cores would be necessary, which is time-consuming and invasive. Exposed peat faces, as were used in early investigations, are rarely available

nowadays. GPR is a suitable alternative and such investigations across a wide range of peatlands could reveal more about peatland development.

Mathematical models of peatland development have now been developed and take into consideration the complex adaptive nature of peatlands (Baird *et al*., 2012; Morris *et al*., 2013). As these continue to develop with the inclusion of three dimensional processes, an increased understanding of peatland development could either inhibit or promote the use of peatlands as palaeoclimate archives.

The inherent uncertainties of models in explaining such complex systems including inability to explain all internal feedbacks offers support to the continuing use of peatlands as palaeoclimate archives. It is however, important to consider the effect of ecohydrological feedbacks when interpreting palaeoclimate results. It is also important to note that the vast majority of these peat accumulation studies have been carried out on Northern Hemisphere peatlands; whether the same feedbacks are applicable to Southern Hemisphere peatlands remains under investigation. Despite the recent debate about allogenic and autogenic causes of change, high-resolution and well dated profiles from peatlands will continue to add to the debate.

2.3.4 Palaeohydrological methods to reconstruct Bog Surface Wetness from ombrotrophic bogs

Owing to the close link between climate and ombrotrophic bog hydrology it is possible to record effective precipitation changes indirectly by inferring bog surface wetness (BSW) and bog water table depth changes from biological and chemical proxies (Barber and Langdon, 2007; Charman, 2007; Charman *et al*., 2009). Until recently the control of BSW remained a contentious issue in the literature. The relative dominance of temperature (Schoning *et al*., 2005; Barber and Langdon, 2007) and precipitation (Hendon & Charman, 2004; Charman, 2007) has been considered. The growing season (summer) moisture deficit, in terms of both length and severity, is now suggested as the primary control of BSW change in ombrotrophic bogs (Charman, 2007; Charman *et al*., 2009; Booth *et al*., 2010). Changes resulting from evapotranspiration - a function of temperature, relative humidity and wind speed (Charman, 2002) - are suggested to be secondary (Charman, 2007; Charman *et al*., 2009). The use of proxy-climate data from

ombrotrophic bogs is now well established (Chambers *et al*., 2012). The majority of work has to date been carried out in North America and Europe but these methods are increasingly being applied to tropical and southern peatlands (e.g. Mauquoy *et al*., 2004).

2.3.4.1 Plant macrofossil analysis

Following the work of Barber (1981) a large literature now exists surrounding the use of plant macrofossil analysis in peatland palaeoclimate records underpinning the majority of such studies. Waterlogged conditions prevent the decay of mosses and other plant macrofossils and these well preserved remains are usually identifiable to species level. Autogenic deposition and incorporation into the catotelm means that the plant macrofossils identified will represent the vegetation community growing throughout time at that position within the bog.

Plant macrofossils can elucidate peatland successional development (Hughes *et al*., 2000; Hughes and Barber, 2004) and mire surface wetness (Swindles *et al*., 2007; Mauquoy *et al*., 2008) through the uniformitarian assumption that the ecological niches of species found down core remain the same until the modern day (Väliranta *et al.*, 2007). Inferences can then be made about past moisture availability controlling the vegetation composition through time. As an example, if hummock species of *Sphagnum, Calluna vulgaris* and *Empetrum nigrum* are found in the stratigraphy this would be indicative of a dry phase with a low water table, whereas hollow wet-adapted species of *Sphagnum* and *Eriophorum angustifolium* would be indicative of a wet phase with a higher water table (Chambers *et al*., 2012). The method now used (section 3.4.2.1) is more objective than earlier work and development of statistical analysis techniques allows a quantitative approach. Plant macrofossil data are usually converted to a single index of BSW to aid interpretation (Daley and Barber, 2012).

Limitations of the method are evident in the application to peat records on sites where a single *Sphagnum* species dominates throughout the record (Mauquoy *et al*., 2004; Chambers *et al.*, 2007). The dominance of species that are wet and dry adapted such as *Sphagnum magellanicum* may lead to a complacent signal despite climatic variability. Plant macrofossil analysis should, therefore, always be used alongside other proxies to form multi-proxy analyses owing to the recent debate

about ecohydrological feedbacks. Other proxies unaffected by these feedbacks may be able to establish a climate signal even if vegetation does not respond to hydrological variability.

2.3.4.2 Humification analysis

Peat humification analysis aims to assess the degree of decomposition of peatland vegetation. This method has been used as a palaeoclimate proxy on the premise that the degree of peat humification is directly related to BSW variability. Assuming that water table variability controls acrotelm thickness and CRD_A (Section 2.3.3), aerobic conditions promoting decomposition in this zone will vary. Wet periods with a higher water table will decrease the thickness of the acrotelm with plant matter in this zone exposed to less aerobic decay before it is incorporated into the catotelm. In dry periods the opposite is assumed.

A variety of methods now exists for quantifying decomposition (Chambers *et al.*, 2011; Hansson *et al*., 2013) following early work by Blackford and Chambers (1993). A higher degree of peat decomposition results in darker humic acids; the extraction of these acids using sodium hydroxide (NaOH) and subsequent measurement by colorimetric methods can provide a record of wetness. The results of colorimetric analysis are presented as a percentage of light transmission through the extracted acids. Darker humic acids are produced in drier periods and result in lower values owing to lower light transmission, where the opposite is true for wetter periods and higher values (Chambers *et al.,* 2014).

The slow decay of material in the catotelm may result in a long-term decay signal through a peat profile; where such a long-term trend is evident the % light transmission values can be detrended (Borgmark and Wastegard, 2008). Non-climatic variability may be introduced when a climate shift causes the vegetation composition to change (as is assumed by plant macrofossil analysis) and the differing decay rates of taxa within the composition introduces bias. This method should only be used where vegetation composition is relatively uniform throughout the peat stratigraphy (Yeloff and Mauquoy, 2008; Hughes *et al*., 2012) and as part of multi-proxy analyses (Chambers *et al*., 2012).

2.3.4.3 Testate amoeba analysis

Testate amoebae (Protozoa: Rhizopoda) are 'shellforming non-marine taxa of single celled protists' (Charman, 2001) and produce decay-resistant and morphologically distinct shells (Booth *et al*., 2010). These organisms live on the surface and in the sub-surface of peatlands with their tests becoming incorporated in the stratigraphy according to peat accumulation. High reproduction rates make them very responsive to environmental variability (Charman, 2007; Charman *et al*., 2009; Chambers *et al*., 2012).

Testate amoeba assemblages were first related to peat soil moisture in the 80s with work in the 90s including other environmental variables such as WTD and pH of soil water (Tolonen *et al*., 1992; 1994; Warner and Charman, 1994; Charman, 1997; Charman and Warner, 1997; Woodland *et al*., 1998; Bobrov *et al*., 1999; Charman *et al*., 1999). An uniformitarian assumption is also applied to this method in that modern testate amoeba distributions and their response to soil moisture and water table variability are applied to fossil communities.

Hydroclimatic variability is now quantified through the use of transfer functions and the well-established link between modern WTD (depth to the water table from the surface) and testate amoeba assemblages (Swindles *et al*., 2010) following the uniformitarian assumption. Modern training data sets relate present-day testate amoeba communities to a range of environmental variables including depth to water table, pH and conductivity using ordination methods. Regression models are applied and methods of cross validation test the prediction ability of the modern training data set. Where water table is demonstrated to be the dominant control on testate amoeba assemblages, past water table variability can then be quantitatively inferred. Transfer functions from many Northern Hemisphere locations now exist (Woodland *et al*., 1998; Charman *et al*., 2007; Payne and Mitchell, 2007; Booth, 2008; Lamentowicz *et al*., 2008; Payne *et al*., 2008; Swindles *et al*., 2009; Markel *et al*., 2010; Amesbury *et al*., 2013; Lamarre *et al*., 2013).

Testate amoeba taxonomy remains unclear leading to discrepancies in the interpretation of sub-fossil testate amoebae (Charman *et al*., 2000). The identification guide by Charman *et al*. (2000) aimed to establish a standard taxonomy for the identification of sub-fossil peatland testate amoebae in order to ensure repeatability

between observers. All common taxa of European and North American peat are included in the guide however, there is still no globally applicable identification guide owing to the lack of inclusion of Southern Hemisphere taxa for example where both cosmopolitan and regionally specific taxa are found (Mauquoy *et al*., 2004). The application of transfer functions is for this reason regionally specific (Turner *et al*., 2013). van Bellen *et al*. (2014) developed the first regional transfer function for SSA.

Owing to the uniformitarian nature of the method, morphological variability through time may make the application of modern taxa to fossil communities difficult although many fossil peat taxa are thought to be morphologically stable (Charman *et al.*, 2000). The differential decomposition of tests has also recently been questioned with perhaps better preserved taxa more represented and thus biasing palaeohydrological records although Mitchell *et al*. (2008) suggest that this has minimal effects. An issue still unresolved is the lack of modern analogue for the fossil species *Difflugia pulex*, the optima and range of which are still debated (Charman *et al*., 2007; Sullivan and Booth, 2011).

Transfer functions have been criticised in light of recent ecological theory and emphasis is now placed on an understanding of spatial autocorrelation, neutral effects and complex dynamics in the application of transfer functions to palaeoenvironmental reconstructions (Belyea, 2007; Amesbury *et al*., 2013).

Verification through the comparison of water table inferences with instrumental data (Charman *et al*., 2004; Booth, 2010; Lamentowicz *et al*., 2010; Amesbury *et al*., 2012; Charman *et al*., 2012) offers support for the accuracy and reliability of testate amoebae to reconstruct palaeohydrological variability. This is demonstrated by Figure 2.22 where near synchrony is evident between the testate amoeba inferred water table variability and the Palmer Drought Severity Index (Chambers *et al*., 2012).

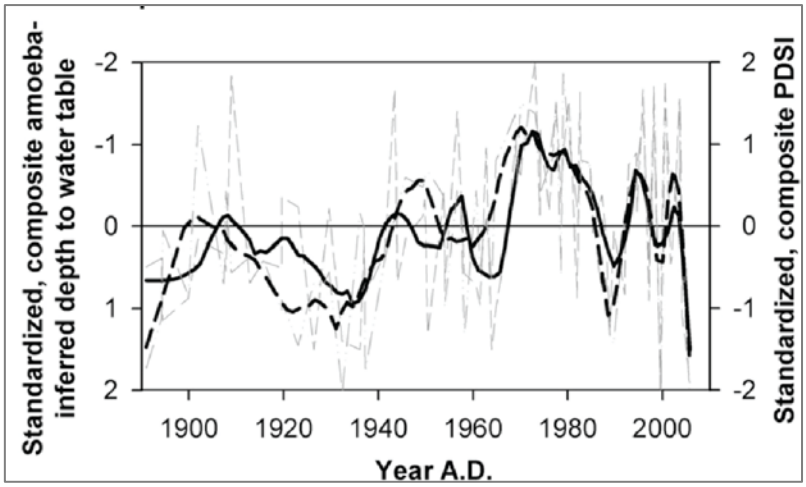

Figure 2.22. From **Chambers *et al*. (2012)**. A palaeohydrological reconstruction (testate amoebae inferred depth to water table) (faint continuous line) and instrumental data (Palmer Drought Severity Index) (faint dashed line). Decadal scale smoothing is shown by the thick lines (Continuous and dashed respectively). Data from Booth (2010).

2.3.4.4 Stable Oxygen isotope analysis

The stable oxygen isotope composition of *Sphagnum* cellulose has also been successfully used as a proxy of BSW (Daley, 2007; Daley *et al.*, 2010; Daley *et al.*, 2016).

Measurements of the isotopic composition of natural waters are expressed relative to a standard (VSMOW – Vienna Standard Mean Ocean Water) (Coplen *et al*., 2002) which is the mean isotopic composition of ocean water (Craig, 1961a) and values are expressed in delta notation (δ per mil deviation). The isotopic composition of Oxygen is expressed as enrichment or depletion of the heavy isotope (^{18}O) relative to the standard. If the sample were enriched in ^{18}O a higher $^{18}O/^{16}O$ ratio would be expressed as a higher $\delta^{18}O$ value and vice versa (Faure and Mensing, 2005).

Oxygen isotope ratios are tracers of water through the hydrologic cycle from its origin and through the phase transitions and transport it undertakes (Criss, 1999) this results in precipitation at any given location having its own ‘signature’ or ‘fingerprint’ (IAEA, 2013). Worldwide spatial and temporal variability of the isotopic composition of precipitation is a result of fractionation effects related to latitude, altitude, distance from the coast, amount of precipitation and surface air temperature (Dansgaard, 1964; Rozanski *et al*., 1997).

In line with uniformitarianism, understanding the modern-day relationship between isotope and meteorological data is paramount for interpretation of past relationships (Dansgaard, 1964; Rozanski *et al*, 1992; Daley *et al*., 2012), which is then important for predicting future changes. The Global Network for Isotopes in Precipitation (GNIP) database has included monthly measurements of the 18-oxygen isotopic composition of precipitation since 1961 and is available at www.iaea.org/water.

Establishing this modern-day relationship in the area of interest of this thesis is paramount in interpretation of palaeoisotopic data. This relationship was assessed by Daley *et al*. (2012) through analysis of the stable isotope values in precipitation ($\delta^{18}O$ and δD) recorded as part of the Global Network for Isotopes in Precipitation (GNIP) from Punta Arenas, Chile (AD 1990-2008) and Ushuaia, Argentina (AD 1982-2002). These data were compared with mean monthly surface air temperature and precipitation data from the same sites on a longer time scale AD 1890-present (Punta Arenas) and AD 1931-present (Ushuaia). Owing to the complex nature of the isotopic composition of precipitation, in comparing mean monthly precipitation and temperature with $\delta^{18}O$ of precipitation a statistically significant relationship is not found.

Despite this, the results support existing evidence of a southward retraction and increase in the zonal wind speed of the SWW over the last 30 years (Garreaud 2007; 2009). This zonal wind speed increase should have caused an isotopic rain shadow effect on the leeward side of the Andes with lower $\delta^{18}O$ values but this has not been observed. The explanation for this may be related to evaporation of raindrops as they fall through drier air (Dansgaard, 1964) or to increased influence of northerly air masses (Stern and Blisniuk, 2002) and additional evaporation over Seno Otway a ~50 km expanse of open sea leading to higher than expected $\delta^{18}O$ and δD values.

At Punta Arenas there has been an increase in the seasonal difference between summer and winter $\delta^{18}O$ values. An increase in relative humidity over the southeast Pacific Ocean is evident in the decline in *d* of summer precipitation. At Ushuaia an increase in the mean annual amount of precipitation has resulted in a fall in $\delta^{18}O$ values. Owing to the paucity of both meteorological and GNIP data most relationships in the study were not statistically significant.

The relationship between water isotopes and climate suggests that archives from which palaeoisotope records can be derived will enable extension of the GNIP records. $\delta^{18}O$, δD and $\delta^{13}C$ records from tree rings have been compiled to indicate palaeoclimate conditions (Roden *et al*., 2000; Waterhouse *et al*., 2002; Anderson *et al*., 2002; McCarroll and Loader, 2004; Loader *et al*., 2013) offering support for the link between temperature and/or humidity and plant cellulose (El Bilali and Patterson, 2012). The organic compound cellulose ($C_6H_{10}O_5$) is the most abundant biopolymer in nature (Loader *et al*., 2014) and is isotopically stable (El Bilali and Pattareson, 2012) and is thus ideal for use in isotopic investigation.

The advantage of *Sphagnum* over vascular plants in isotopic studies is their lack of roots and functioning guard cells which prevents control of water loss and gas exchange (Loader *et al*., 2007). Via photosynthesis, meteoric water is simply incorporated to cellulose; growth is linked to growing season precipitation, owing to the suspension of photosynthesis when water availability is low. It is thought that the isotopic signature of the source water does not undergo any significant change before assimilation and cellulose synthesis plant water fractionation is environmentally controlled (Ménot-Combes *et al*., 2002). Also, habitat preferences usually of 100% relative humidity (Clymo and Hayward, 1982) led Zanazzi and Mora (2005) to assume a simple calculation of the isotopic composition of *Sphagnum* cellulose.

Equation 2.1. Calculation of the isotopic composition of *Sphagnum* cellulose.

$$\delta cell = \delta sw + \varepsilon b$$

ε_b ,the biochemical enrichment factor, related to the hydration of carbonyl groups during photosynthesis, is now well established as 27±3‰ for oxygen isotopes (Brenninkmeijer *et al*., 1982; Aravena and Warner, 1992; Zanazzi and Mora, 2005; Tillman *et al*., 2010; Skrzypek *et al*., 2011). This enrichment is independent of temperature (DeNiro and Epstein, 1979; 1981; Sternberg *et al*., 1986).

Sphagnum leaf water derived directly from precipitation is assumed to be the source water used for cellulose synthesis. It is, therefore, considered that *Sphagnum* mosses can record the isotopic composition of their source water, which provides a record of climate variability and changes in bog hydrology (Moschen *et al*., 2009).

From recent work in the Northern Hemisphere a common forcing is suggested by largely correlated $\delta^{18}O$ values in *Sphagnum* cellulose with BSW changes derived from palaeoecological proxies (Daley, 2007; Daley *et al*., 2009; 2010) (see Figure 2.23).

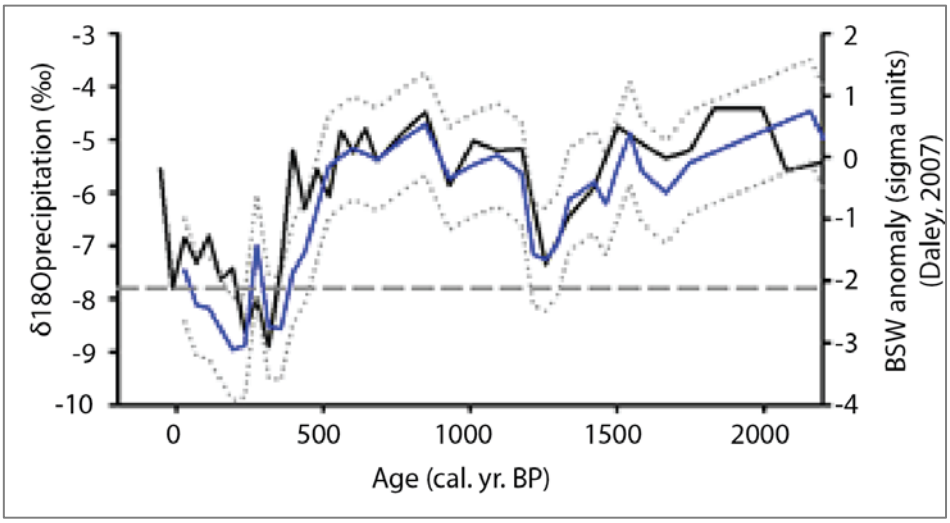

Figure 2.23. From **Daley *et al*. (2010)**. Data from Walton Moss, Northern England. The black line shows ecologically inferred BSW **(Daley, 2007)** and the blue line shows $\delta^{18}O$ composition of precipitation (from *Sphagnum* cellulose) **(Daley *et al*., 2010)** for the last 2000 years. The grey dotted lines show ±1‰ $\delta^{18}O$. The grey dashed line shows the modern mean annual $\delta^{18}O$.

$\delta^{13}C$ and $\delta^{18}O$ values from a single or mixture of different *Sphagnum* species provide more accurate reconstructions compared with bulk peat cellulose (Ménot and Burns, 2001; El Bilali and Patterson, 2012). There is also evidence of intra-genus stable isotopic differences which must be considered. Various *Sphagnum* species with differing physiologies (evapotranspiration) are characteristic of the differing microenvironments of peatlands (Ingram, 1982). The amplitude of the isotopic response of *Sphagnum* cellulose to climatic conditions is, thus, species dependent (Ménot and Burns, 2001; Ménot-Combes *et al*., 2002) based on their microtopographic position (Price *et al*., 1997). Modern *Sphagnum* samples taken along these microtopographic gradients reveal additional biochemical evaporative effects resulting in higher $\delta^{18}O$ values (^{18}O enriched) in species from hummock tops (Ménot- Combes *et al*., 2002; Zanazzi and Mora, 2005). Values vary between 27±3‰ on hummock tops and 27±1‰ in hollows (Zanazzi and Mora, 2005) emphasising the need for species-specific analyses. A more recent investigation found a statistically insignificant offset of 0.1‰ between *Sphagnum* species at the same levels. This

would oppose suggestions of the segregation of different *Sphagnum* species before isotopic analysis (El Bilali and Patterson, 2012). In light of earlier studies, it is still preferable to isolate a single *Sphagnum* species for isotopic analysis.

Following the advice of earlier studies of the need for species-specific analyses, Royles *et al*. (2013b) from moss peat banks in Antarctica found that from surface samples of *Chorisodontium aciphyllum* there was evidence of a 5‰ $\delta^{18}O$ enrichment of leaf water before cellulose synthesis in comparison with modern precipitation. It should be noted that this moss is physiologically different from *Sphagnum* but it may question the use of moss to reconstruct the isotopic composition of precipitation.

A 'space-for-time' calibration was undertaken along a 10 m NNW oriented hummock-hollow transect at Parrillar bog, Southern Patagonia (Loader *et al*., 2016). Based on different WTD from the surface, temperature and humidity were measured over 5 days. *Sphagnum magellanicum* capitula were taken from the same points along the transect and the leaf water was sampled in order to compare the stable (oxygen and hydrogen) isotopic composition with the stable (carbon, oxygen and hydrogen) isotopic composition of cellulose from the same plants. A wider amplitude of temperature and relative humidity was evident from hummocks than from hollows owing to generally higher exposure of hummock microforms; such variability across the microtopography if present throughout the duration of the record may have influenced longer term stable isotopic records resulting in amplitude differences across the microtopography. Despite correlation between leaf water and cellulose stable oxygen isotope composition they find evidence for evaporative enrichment of the leaf water used for cellulose formation, which does not support the 27‰ enrichment suggested by DeNiro and Epstein (1981). Both atmospheric and local scale drivers influence the $\delta^{18}O$ of cellulose. Further investigation is needed before assuming that growing season precipitation is directly represented by the $\delta^{18}O$ of cellulose.

To date, few studies exist that have tested the effect of the modern microtopographic gradient on the isotopic composition of moss. It is also unknown whether variability associated with the microtopographic gradient is maintained over time especially considering the recent debate about autogenic and allogenic drivers of ecological change. This led to **Research Question 1** in which it is aimed to test amplitude

differences with regards to these differing evaporative effects. It is hypothesised that a core from a hummock, lawn and near-hollow location should show similar allogenic driven ecological changes, which if synchronous with isotopic changes should occur similarly across the microtopography but in light of differing evaporative effects the hummock profile would show changes of a higher amplitude with changes of a lower amplitude further down the microtopographic gradient.

With consideration of the previous sections, the isotopic composition of precipitation is an indicator of the rain-out history of an air mass (Cole *et al*., 1999) and the fractionation processes from the moisture source to final site of measurement in the hydrological cycle. Although complex and indirect inferences can be made from past changes in the isotopic composition of precipitation they are not directly palaeothermometers or palaeo-rain gauges (Araguás-Araguás *et al*., 2000; Daley *et al*., 2012).

2.3.4.5 Stable Carbon isotope records

The stable carbon isotope composition of *Sphagnum* cellulose has also been successfully used as a proxy of BSW (Price *et al*., 1997; Loader *et al*., 2007; De Vleeschouwer *et al*., 2012). Stable carbon isotope measurements are expressed as per mil (‰) deviations from a standard (VPDB - Vienna PeeDee Belemnite) (Coplen, 1995). Values are expressed as enrichment or depletion of the heavy isotope (^{13}C) relative to the standard. A sample enriched in ^{13}C, with a higher $^{13}C/^{12}C$ ratio is expressed as a higher (less negative) $\delta^{13}C$ value.

Carbon is incorporated into the *Sphagnum* cellulose through the diffusion of CO_2 into hyaline cells that surround the photosynthetic cells (Ménot and Burns, 2001). In wetter/drier conditions the presence/absence of a water film on *Sphagnum* leaves results in the differential diffusion of CO_2 and fractionation (Farquhar *et al*., 1982; Ménot and Burns, 2001). This process model is based on the work by Rice (2000) and Loisel *et al*. (2009). Loisel *et al*. (2009) find that lower (more negative) $\delta^{13}C$ values of modern *Sphagnum* are found in locations with high WTD (depth to water table) and higher (less negative) $\delta^{13}C$ values are found in locations with low WTD (depth to water table).

Supporting this interpretation, a clear relationship is found between the stable carbon isotope composition of *S.magellanicum* cellulose with WTD, relative humidity and temperature from the Southern Patagonian 'space-for-time' calibration (Loader *et al*., 2016). The stable carbon isotope values of cellulose across the transect ranged from -24.6‰ to -27.5‰ with lower WTD related to less negative $\delta^{13}C$ values and vice versa. Based on this interpretation, variability between more and less negative values over time could be used to infer relatively drier and wetter conditions respectively.

With a move towards species-specific isotopic analyses it is also suggested that certain components of *Sphagnum* should be used for isotopic analysis (McClymont *et al*., 2010). Significant offsets between the stable carbon and oxygen isotope values of *Sphagnum* branch and stem components from down core peat records have been found (Moschen *et al.*, 2009; Tillman *et al.*, 2010). Separation and analysis of specific components reduces the error associated with the analysis of multiple components or whole plant material. Owing to the excellent preservation of stems down core, these are now preferable in longer term isotopic reconstructions (McClymont *et al*., 2010). The use of stable isotopes from *Sphagnum* cellulose in peat records is now well established. A species-specific isotopic analysis of *Sphagnum* stems from a peatland with suitable microtopographic gradients will be able to test intra-site variability between late-Holocene records.

2.3.5 Multi-proxy; Multi-profile; Multi-site approach

2.3.5.1 Multi-site

Many studies now forming a network of a combination of multi-proxy, multi-profile and multi-site records have enabled major regional climate shifts to be inferred across Northwestern Europe and North America (Aaby, 1976; Chambers *et al*., 1997; Charman *et al*., 1999; Mauquoy and Barber, 1999a; Mauquoy and Barber, 1999b; Barber *et al*., 2000; Ellis and Tallis, 2000; Hughes *et al*., 2000; Chiverrell, 2001; Hendon *et al*., 2001; Mauquoy and Barber, 2002; Mauquoy *et al*., 2002; Barber *et al*., 2003; Langdon *et al*., 2003; Barber *et al*., 2004; Langdon *et al*., 2004; Langdon and Barber, 2005; Charman *et al*., 2006; Hughes *et al*., 2006; Swindles *et al*., 2007; Mauquoy *et al*., 2008; Daley and Barber, 2012; Hughes *et al*., 2012; Roland *et al*.,

2013). Using conventional AMS ^{14}C and ^{210}Pb dating with the addition of AMS wiggle match dating (van Geel and Mook, 1989) and the use of tephrochronology, robust chronologies have been created enabling such regional comparisons to be made. Where regional correspondence and even synchroneity across each aspect of this network is evident, this offers strong support for an allogenic driver. Further support is offered when records are linked to solar variability (e.g. Mauquoy and Yeloff, 2008) and resulting impacts on ocean-atmosphere systems (van Geel *et al*., 1996; van Geel and Renssen, 1998). However, these studies are all undertaken at different classifications of ombrotrophic bogs (raised and blanket bogs); the differential sensitivity of ombrotrophic bogs has been suggested as a cause of the discrepancies between records from a number of sites (Mauquoy and Barber, 2002).The majority of these studies reveal a LIA period (Daley and Barber, 2012) that may have been globally synchronous.

A variety of proxies displaying synchronous changes in the peat record is encouraging and it is now suggested that all peat studies should use a multi-proxy approach in order to validate results from one proxy using independent palaeoclimate evidence such as stable isotopes or other biological proxies (Birks *et al*., 2010) decreasing uncertainty associated with single-proxy records (Väliranta *et al*., 2012). Published studies using multiple proxies are increasingly being used (Blundell and Barber, 2005; Loisel and Garneau, 2010). Normalisation of data to one scale aids interpretation and comparison between proxies (Charman *et al*., 2006; Hughes *et al*., 2006). Similar temporal resolution of records ensures that any climate signal that is captured can be compared.

Assessment of periodicities in peat records offers support for an allogenic climate driver (Swindles *et al*., 2012b). Testate amoeba and humification records from two sites in Northern Ireland were statistically tested with periodicities evident in at least one proxy from each site. Coherence is evident between the records and where discrepancies exist they are the suggested result of ecohydrological feedbacks, proxies responding to allogenic forcing in a non-linear manner and chronological errors (Swindles *et al*., 2012b). Comparison of such multi-proxy records between sites is a robust test of the dominance of allogenic and autogenic control on peat records.

As such, oscillations at different periodicities between inferred wet and dry BSW across a number of sites would suggest that internal processes at the intra-site scale may be the dominant influence (Loisel and Yu, 2013). Furthermore, where correlations are not found between such peat records and other palaeoclimate records autogenic controls are dominant. This does not make peatlands as archives of palaeoclimate variability redundant, only that interpretation of such records must always take such allogenic and autogenic processes into consideration.

However, limitations still remain in the use of multi-proxy analyses of peat. For example, different proxies respond differently to environmental changes resulting in contrasting results and asynchronous trends in the record, making interpretation of the record difficult (Chambers *et al*., 2012). Hughes *et al*. (2006) chose the majority indication of changes but this should be avoided. It is also important to choose the proxy that will produce the most reliable palaeoclimate record when making this decision the appropriate strengths and limitations of each proxy must be considered.

2.3.5.2 Spatially specific records

In terms of the microtopographic gradients discussed (Section 2.3.4) and associated debate about allogenic and autogenic drivers of change, few studies exist which specifically test this on the spatial scale.

2.3.5.2.1 Multi-profile

As Charman *et al*. (2006) note, it is now pertinent, instead of replicating records from within and across sites, to collect records in regions from which relatively few exist. However, owing to the uncertainties surrounding proxy records and questions around autogenic controls on peatland processes, multiple profiles within the same peatland are useful to identify surface wetness variability most likely linked to climate. With coherent changes across multiple cores offering support for a common influence (Belyea, 2009; Belyea and Malmer, 2004) intra- site replicate cores are now desired (Amesbury *et al*., 2012). The potential of multiple cores was recognised in early studies (Moore, 1977; Barber, 1981; Smart, 1982; Svensson, 1988a; b) using plant macrofossil analysis. The replicability of records on the intra-site scale (Barber *et al*., 1998) was later tested to discover whether, for example when taking a core of 5-10 cm diameter, this is representative of stratigraphic changes across the

bog as a whole. Ten short core profiles were taken from two adjacent bogs in Cumbria, England (Bolton Fell Moss and Walton Moss) and subjected to plant macrofossil analysis. Inferred hydrological changes were found to occur coherently across the profiles and also across other records from the same sites (Barber *et al*., 1998). Such replication at the intra-site scale offers support for an allogenic driver of large-scale BSW variability.

2.3.5.2.2 Multi-proxy, multi-profile

Hansson *et al*. (2013) investigated intra-site variability across three short cores (~70 cm) taken from hummock locations at Store Moss bog in south-central Sweden using bulk density, light transmission and the C:N ratio across the three cores as proxies of decomposition. Statistical analyses found general similarities within each proxy across the three cores. The exact location of the three cores used in this study is not documented; only stated as three hummock cores, this could give rise to the minor differences within each proxy. Different aspects of the decomposition process are displayed by each proxy across the three cores; this has implications as to which proxy of decomposition is best placed in studies of climate reconstruction.

2.3.6 Summary

This section introduced the use of peatlands as palaeoclimate archives. Peatlands are globally distributed and compared with other archives are relatively easy logistically from which to obtain core profiles. The reinvigoration of early ideas and the potentially shifting paradigm of autogenic processes as the dominant driver of change may now question the use of palaeoclimate proxies from peat. Many peat records have successfully reconstructed regional climate change in Northwest Europe and North America using a combination of multi-proxy, multi-profile and multi-site records. More detailed, high-resolution multi-proxy records from multiple profiles from multiple sites will surely give further evidence for a common allogenic control, an example now to be followed in other regions of the world.

2.3.7 Patagonian Peatlands

The majority of peatland studies in the region have thus far been focused on peatlands on the island of Tierra del Fuego. Darwin (1839) made the first

observations of the presence and distribution of bogs in Tierra del Fuego along the coastal areas of the Beagle Channel and also on the Falkland Islands (Roig, 2004). Bonarelli (1917) and Guiñazú (1934) carried out the first peatland surveys in order to exploit them for alternative energy. The next major study of regional distribution was carried out by Auer (1965). There is now a move towards application of techniques, commonly applied from Northern Hemisphere peatlands, to the peatlands in SSA (Mauquoy *et al*., 2004; Chambers *et al*., 2007; Chambers *et al.*, 2014; van Bellen *et al.*, 2016).

There are currently 45,000 km^2 of peatlands in Patagonia accounting for ~25% of the land area (Figure 2.21) (Loisel, 2012; Yu *et al*., 2010). Loisel (2012) in an investigation of carbon sequestration in Patagonian peatlands found that these peatlands are a carbon sink for 7.6 GtC. The bogs in the region all developed from lakes or fens (Grootjans *et al*., 2010). These bogs formed where mean annual precipitation is between 800 and 6000 mm falling evenly throughout the year and where temperatures fluctuate around an annual mean of less than 8ºC (Charman, 2002), ideal conditions for peat formation. It is for this reason that *Sphagnum* bogs occur in areas of deciduous forests (Grootjans *et al*., 2010).

Sphagnum magellanicum dominates the surface vegetation of Patagonian peatlands, forming large hummocks some as high as 90 cm above the water table in the majority of these peatlands (Grootjans *et al.*, 2010). This species is able to hold water through capillary action and can thus grow to substantial heights above the water table (Grootjans *et al.*, 2010). The surface vegetation is dominated by *Empetrum rubrum*, *Nothofagus antarctica* and *Marsippospermum grandiflorum* on hummock tops. *Sphagnum falcatulum* and *Sphagnum fimbriatum* fringe pools and both *S.magellanicum* and *Sphagnum acutifolium* inhabit drier lawn and hummock positions (Villagrán and Barrera, 2002).

The potential of these peatlands as palaeoclimate archives is evident (Pendall *et al*., 2001; Mauquoy *et al*., 2004; Chambers *et al*., 2007; 2014). These pioneering studies revealed excellent preservation of plant macrofossils in records where peat accumulation rates were high (0.5-1 cm per year). This, together with the extent of Patagonian peatlands, demonstrates the potential for the development of high temporal resolution proxy records using peat. Loisel (2012) however, found a lack of

correlation between climate (temperature and precipitation) and peat accumulation in these peatlands suggesting the dominance of autogenic processes (Belyea and Baird, 2006; Swindles *et al*, 2012a).

These peatlands have developed under different conditions to Northern Hemisphere peatlands (Loisel and Yu, 2013) which questions the assumed relationship between climate and bog hydrology and the summer water deficit as a control of BSW/water table depth variability in Northern Hemisphere peatlands. Loisel and Yu (2013) investigated the climate controls on Patagonian peatlands through analysis of the modern climate space of these peatlands using gridded climate data. The following general conditions were found:

-Relatively higher mean annual temperatures (3-9 °C)

-Wider range of mean annual precipitation (owing to the precipitation gradient)

-Wide range of mean annual relative humidity

-Lower temperature seasonality (~12 °C)

-Mean monthly temperatures above 0 °C throughout the year

-Cooler conditions in warmest month of the year

-Even distribution of precipitation throughout the year

-Evapotranspiration is limited in these conditions and the growing seasons are longer.

These conditions are thought to create the extreme microtopographical gradients present on the modern surfaces of these peatlands through higher productivity and limited decomposition in the acrotelm (Baumann, 2006). The summer moisture deficit as a control on BSW variability in the region is questioned by the year round supply of precipitation and because of low species diversity the system may have been able to self-regulate via ecohydrological feedbacks (Section 2.3.3).

This suggests that variability in proxy records may have been caused by autogenic rather than allogenic drivers; thus, the drivers of hydrological change from Patagonian peatlands need to be further investigated.

2.3.7.1 Southern South America: Peat isotope studies

The spatial distribution of the isotopic composition of precipitation over SSA is primarily affected by orography with the Andes cordillera acting as a barrier to the SWW (Stern and Blisniuk, 2002). As an air mass reaches mountainous regions, adiabatic cooling related to increasing altitude results in increasing rainout and depletion of the heavier isotopes from the air mass. The altitude effect is very influential on the isotopic composition of precipitation in the Andean region of South America with the range stretching from 10°N to 50°S (Rozanski and Araguás-Araguás, 1995). Orographic precipitation on the windward side of the Andes results in an orographic rain shadow on the leeward side. This produces an isotopic rain shadow effect with depleted $\delta^{18}O$ and δD values to the east of the Andes (Siegenthaler and Oeschger, 1980; Stern and Blisniuk, 2002). It is estimated that there may be as much as a 4‰ rain shadow effect (Stern and Blisniuk, 2002).

Pioneering studies using isotopes in peat archives from SSA were carried out by White *et al*. (1994), Kenny *et al*. (1999) and Pendall *et al*. (2001) as reviewed in section 2.2.3.1. All of these studies are located near Ushuaia with no relevant studies further west to date. Palaeoisotopic data from *Sphagnum* cellulose to investigate changes over the last 3000 years is being obtained as part of the PATAGOn project in order to extend current GNIP data which have been compared with instrumental data in Daley *et al*. (2012).

Owing to the dominance of *S.magellanicum* throughout the stratigraphy, Patagonian peatlands are ideal for the species-specific isotopic analyses and are also characterised by substantial microtopographic gradients.

2.4 Summary

In summary, **Section 2.1 and 2.2** assessed the likely timing and direction of recent and late-Holocene climate variability, which may also be evident in the records in this investigation (**Research Questions 1-3**).

Section 2.3 explored the potential of peatlands as palaeoclimate archives and reviewed the methods most commonly used to reconstruct BSW. This formed the

basis for **Research Questions 1 and 2** in which correlations between multiple proxies in individual profiles are hypothesised.

This chapter has, therefore, formed the basis for the overall research question: can ombrotrophic bogs from the region provide reliable reconstructions of climate related SWW shifts? Correlations between proxies (palaeoecological and species-specific stable isotope records), between profiles (in consideration of microtopographical differences) and between sites would offer support for the use of peatlands as palaeoclimate archives. The methodological basis of the investigation will be considered in the following chapter.

Chapter 3: Methodology

3.1 Introduction

In order to achieve the aim of this investigation, to *test the late-Holocene climate signal from ombrotrophic bogs in southernmost Chile and the Falkland Islands*, the following research questions will be addressed:

1. To what extent are there correlations between multiple proxies and multiple profiles from an ombrotrophic bog, Karukinka, in southernmost Chile?
2. To what extent are there correlations between multiple proxies from San Juan bog, Chile and from San Carlos bog, Falkland Islands?
3. Provided that these records have responded to recent (late 20th century) and late-Holocene (Medieval Climate Anomaly and Little Ice Age) climate variability related to shifts in the SWW, to what degree are there correlations between records from the multiple sites?

These research questions will be addressed through the following objectives:

1. To carry out palaeoecological and stable isotope analysis from profiles from three sites, Karukinka and San Juan bog, Chile and San Carlos bog, Falkland Islands and assess the correlation between the multiple proxies within each profile.
2. To assess the correlation between multi-proxy records from three profiles taken across a microtopographic gradient at Karukinka bog, Chile and test intra-site replicability based on age.
3. To assess the correlation between multi-proxy records across the three sites, Karukinka and San Juan bog, Chile and San Carlos bog, Falkland Islands, based on age.

This chapter will discuss the methodology of this investigation including field methods, laboratory methods and statistical methods necessary for achievement of the objectives.

3.2 Site Selection

Fieldwork was carried out in the austral summer of 2013. Three sites were chosen in consideration of their location within the precipitation gradient, correlation between zonal wind speed and precipitation (figure 2.1b & 2.2a), relative humidity anomaly (figure 2.5) and the hypothesised gradient in isotopic values (section 2.3.7.1). The site locations are displayed in figure 3.1 and table 3.1 summarises site details.

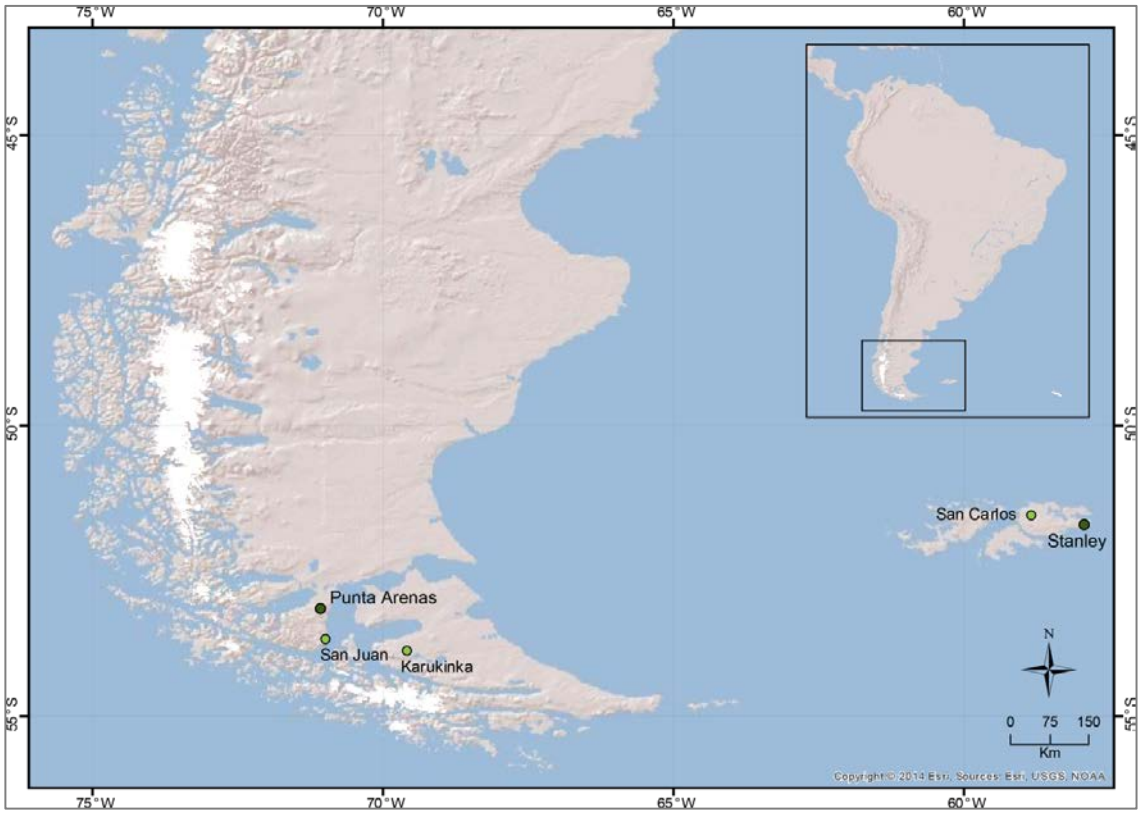

Figure 3.1. Location of study sites.

Table 3.1. Details of the sites in this investigation.

Site name	Location	Elevation	Average annual precipitation
San Juan bog	53°39'4.82°S, 70°57'57.38°W	8 m.a.s.l	~500 mm
Karukinka bog	53°51'36.14°S, 69°34'39.11°W	228 m.a.s.l	~500 mm
San Carlos bog	51°30'28.24°S, 58°49'16.45°W	8 m.a.s.l	~200 mm

The first site, San Juan bog, is located on the Brunswick peninsula on mainland Chile. Alongside a larger peatland, which is being exploited for peat resources, San Juan is a smaller peatland in pristine condition. The second site, ~150 km east, Karukinka bog is located further east within Karukinka Natural Park on Chilean Tierra

del Fuego. The ~290 square miles of peatlands within the park are in pristine condition owing to its relative inaccessibility and status as a natural park since 2004. These sites are both located east of the Andean divide. The final site, ~1200 km to the east, San Carlos bog, is located on East Falkland Island. Although historically peatlands on the island were exploited, with peat forming the majority of the island's energy resource, *Sphagnum* bogs had not previously been recorded in the Falkland Islands. San Carlos bog was in pristine condition when discovered in February 2013. The sites are all ombrotrophic and *S.magellanicum* dominates the surface vegetation along extreme microtopographic gradients from lawns to high hummocks (some 90 cm+ above the water table).

3.3 Field methods: Core location, extraction and storage

3.3.1 Core location: Surface microtopography

The core location forms a crucial part of the methodology. At each site an appropriate sampling microform (hummock) was chosen based on a number of criteria. They include prevailing wind direction, steepness of the gradient between hummock and pool, absence of shrubby vegetation and central location within the bog to ensure ombrotrophy and maximum peat depth.

At Karukinka the general surface patterning seems to be a result of the southern westerly winds with the longest length of pools (generally located behind hummocks) orientated in the direction of the prevailing winds (South West to North East). Interestingly, the same length of each pool appears to be perpendicular to the direction of the overall slope of the bog with the highest part of the bog in the northwest and the lowest part in the southeast. However, as mentioned, the hummock was at a mid-location within the bog and should not be affected by surface flow. Similar surface patterning has been investigated by Couwenberg and Jousten (2005). A levelling survey of the bog surface in the immediate vicinity of the chosen sampling microform was undertaken in order to reproduce the surface microtopography digitally. Around a radius from the centre of the chosen hummock, elevation measurements were taken relative to a single datum line at 10 cm intervals to 270 cm and subsequently every 20 cm. The digging of various wells in the context of the hummock also enabled the water table depth at these points to be measured.

Using these data Rockworks (v. 15) allowed the generation of a surface microtopography model from Karukinka (see figure 3.3).

With regard to the phasic theory, the best location from which to extract a core for palaeohydrological reconstruction was suggested to be from the most climatically sensitive area between a hummock and hollow microform (Barber *et al.*, 1998). This assumes that hummocks and hollows have remained in the same place throughout time (Barber, 1981; Van der Molen and Hoekstra, 1988) with expansion and contraction of hummocks in dry and wet periods respectively and vice versa in hollows.

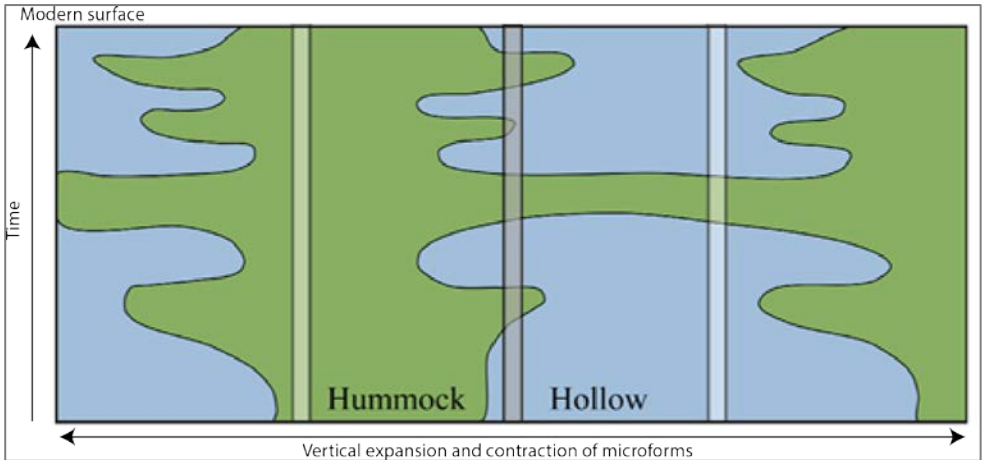

Figure 3.2. Hummock and hollow microforms through time (bottom – top) with the expansion of hummock areas (green areas) in dry periods and the expansion of hollow areas (blue areas) in wet periods. The grey rectangle shows the location of assumed highest sensitivity. Edited from **De Vleeschouwer *et al.* (2010a).**

Figure 3.2 from De Vleeschouwer *et al.* (2010a) demonstrates the sensitivity of the suggested core location. Evidence of this was found at Parrillar bog, Chile, where vegetation on the surface hollow was seen to be expanding over a dried-out pool (plate 3.1). Recent renewed interest in the cyclic regeneration theory and the migration of microforms over time (Kettridge *et al.*, 2012) has obvious implications for selection of a core location. As demonstrated by figure 3.2 hummocks are suggested to be insensitive to climate variability in terms of vegetation response. Core locations were chosen in response to the hypotheses to be tested relating to the hydroclimatic and stable isotopic signal along a hummock-hollow microtopographic gradient.

Plate 3.1. Demonstration of the phasic theory on the modern surface at Parrillar bog, Chile where hummock vegetation has expanded over a now dry hollow.

3.3.2 Core extraction

3.3.2.1 Karukinka

Peat cores were collected in February 2013 using monolith tins (10 cm x 10 cm x 50 cm) and a Russian corer (50 cm length, 11 cm diameter). As shown by figures 3.3 and 3.4, three profiles were obtained in terms of the microtopographic gradient, with high hummock (KAR-EM-3), mid-hummock (KAR-EM-2) and low-lawn (KAR-EM-1) locations represented. The surface vegetation along the gradient is shown in figure 3.4. The low-lawn location is dominated by *S.magellanicum* with *Tetroncium magellanicum*, *Marsippospermum grandiflorum* and *Empetrum rubrum.* The mid-hummock/lawn location is also dominated by *S.magellanicum* with *E.rubrum*. The high hummock is dominated by *S.magellanicum* with *E.rubrum* and *N.antarctica*. Each profile consisted of a top monolith section (surface to 50 cm depth) these were extracted by inserting the monolith tins through the surface and then the lids were inserted to contain each peat monolith fully. Whilst the monoliths remained in situ the peat faces were exposed by digging a trench in turn in front of each profile location and then each lower overlapping section (KAR-EM-1B, 45-85 cm; KAR-EM-2B, 45-95 cm; KAR-EM-3B, no overlap, 50-100 cm) was extracted by inserting each monolith tin into the exposed face. Peat depth probing was carried out at this site

and at ~5 m below the surface contact with a layer of clay was made, suggesting the potential of this site for longer peat records. For the purpose of this investigation, 150 cm depth was deemed appropriate to encompass the late-Holocene.

Each upper monolith tin was carefully sawed around and removed, the peat above each lower section was removed and the tin lids placed to enclose fully the lower sections, then removed in the same way as the upper sections. The conventional method of core extraction involves taking Russian core sections from two adjacent coring locations (usually within 20 cm of each other) to avoid coring through disturbed peat. Through the use of monolith tins extracted from peat faces there is improved down-core stratigraphic consistency in this study. A lower Russian core section was taken for each profile to the left of the trenches before disturbance had occurred (KAR-EM-1C, 80-130 cm; KAR-EM-2C, 80-130 cm; KAR-EM-3C, no overlap, 100-150 cm). The peat monolith section faces were exposed and photographed and the lids replaced. Each section was then labelled, wrapped in cling film and plastic sheeting. The Russian core sections were photographed while still on the Russian core blade and then transferred to split PVC pipes (also lined with cellophane) and wrapped in plastic sheeting. To avoid disturbance to the stratigraphy all cores were kept in a horizontal position in solid wooden boxes during transport and shipment back to the UK where they have since been stored in the Plymouth University cold stores. The monolith tins used for the upper sections were made of steel and galvanised with zinc, the low pH of peat led to the rapid corrosion of the zinc coating during transportation of the cores to the UK. Small areas of oxidised material were present on these sections; as such they were immediately transferred intact to plastic containers to prevent further corrosion.

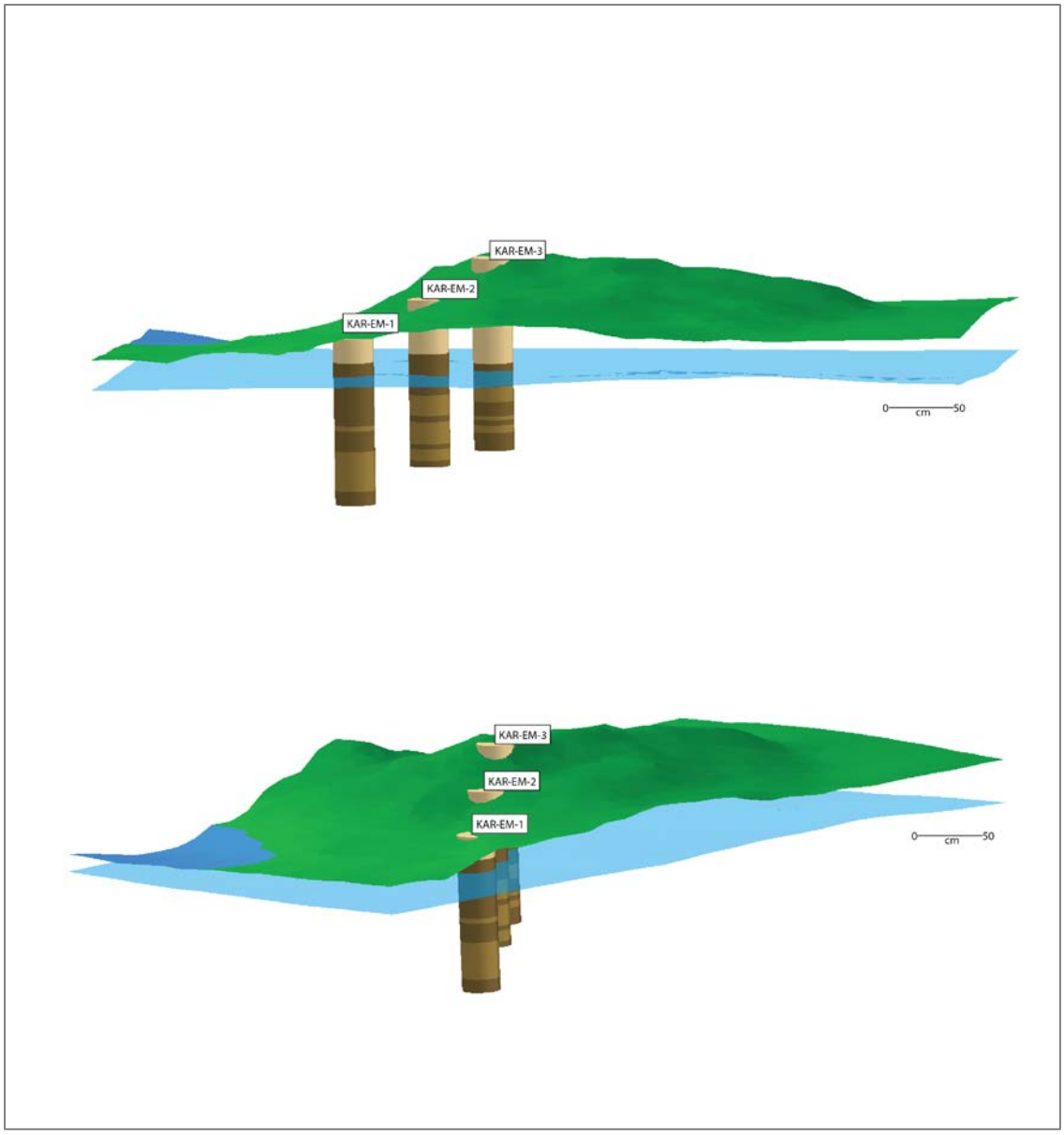

Figure 3.3. Surface microtopography model of the Karukinka core location using survey data. The core transect is shown in the context of the hummock. The approximate boundary of the nearby pool is shown as well as the approximate water table depth interpolated from well locations.

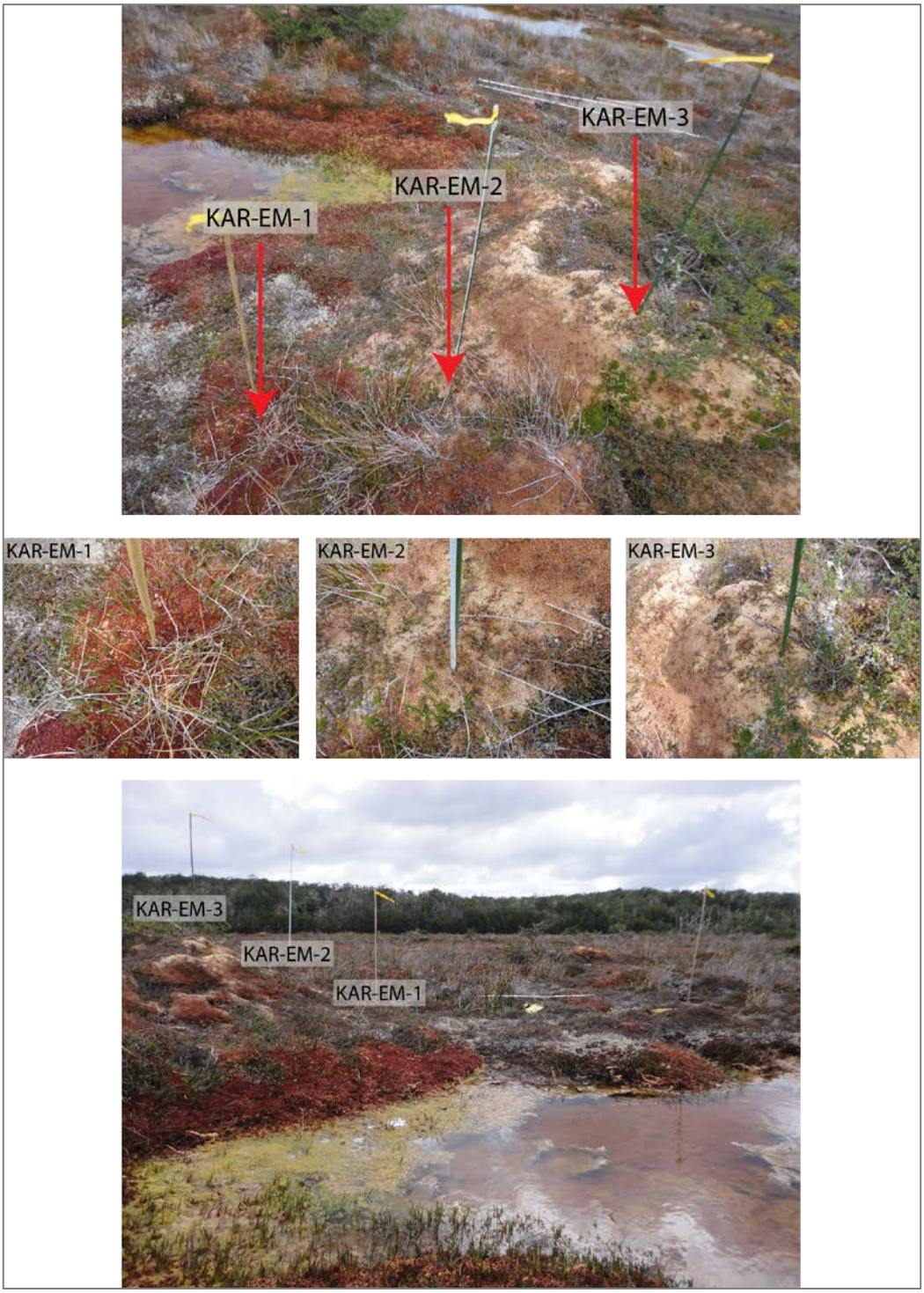

Figure 3.4. Karukinka bog. Location of KAR-EM-3, KAR-EM-2 and KAR-EM-1 along the microtopographic gradient and respective surface vegetation.

3.3.2.2 San Juan

The same procedure was followed in extraction of cores from San Juan. The preliminary plant macrofossil analysis carried out on the cores from Karukinka was used to ascertain which core location seemed to be the most sensitive to potential climate variability. As the results suggested that the core at a mid-hummock location was the most sensitive this was also chosen for analysis at San Juan. This core, SAN-EM-2, consists of an upper monolith section (SAN-EM-2A, 0-50 cm) and two lower Russian core sections (SAN-EM-2B, 45-95 cm AND 2C, 85-135 cm). Peat depth was greater than 135cm however, this was thought to be sufficient for the purposes of the investigation. Figure 3.5 shows the location of SAN-EM-2 in terms of the microtopographic gradient, taken from the northern transect of the hummock close to a pool. The surface vegetation at the core location (figure 3.5) is dominated by *Sphagnum magellanicum* with *Tetroncium magellanicum* and *Empetrum rubrum*.

3.3.2.3 San Carlos

Owing to time constraints a survey of the site was not possible. Core SCB-1 was taken at a mid-hummock location from San Carlos bog (Figure 3.6). The surface vegetation of the bog is dominated by *S.magellanicum* and a dense covering of *E.rubrum* shrubs; a *Sphagnum*-dominated hummock was chosen for core extraction. Other vegetation present on the hummock includes *Hymenophyllum caespitosum, Gaultheria pumila, Oreobulis obtusangulus, Gunnera magellanica and Myrteola nummularia*. This core consists of an upper monolith section (0-50 cm) and lower Russian core sections (40-90 cm, 80-130 cm, 120-170 cm). The core is *Sphagnum* dominated to a depth of 80 cm followed by herbaceous compacted peat to the base.

Figure 3.5. San Juan bog. Location of SAN-EM-2 along the microtopographic gradient and surface vegetation.

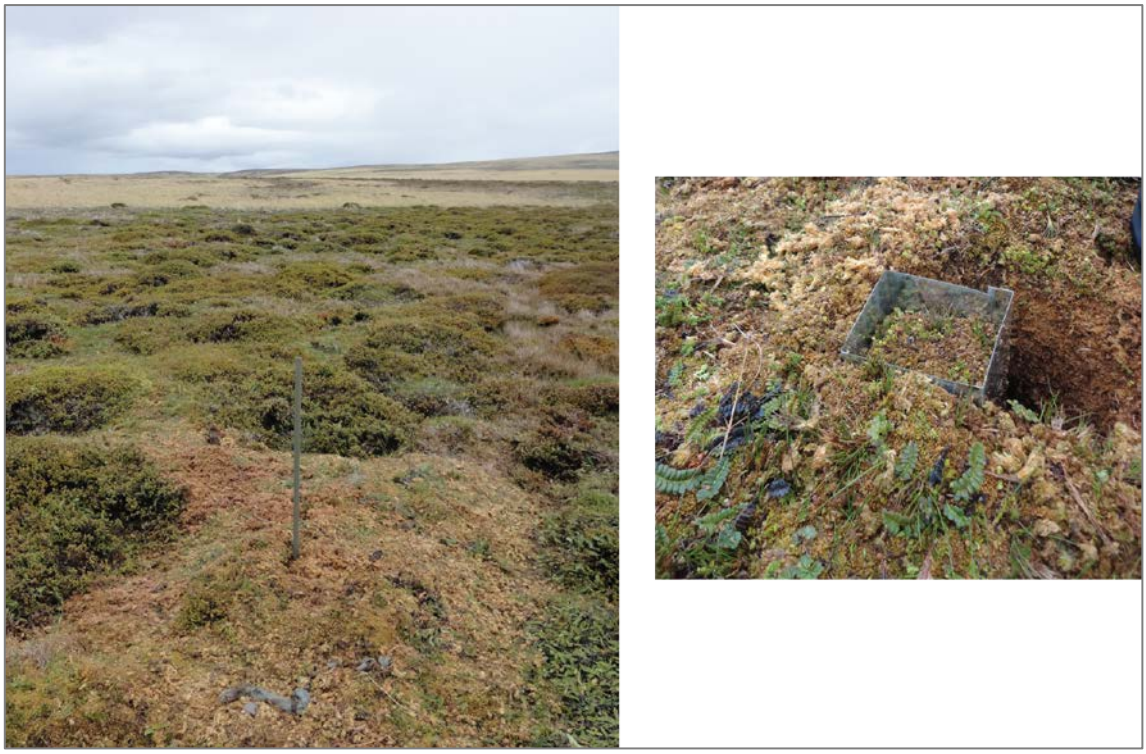

Figure 3.6. San Carlos bog. Location from which SCB-1 was taken and surface vegetation.

3.4 Laboratory methods

3.4.1 Sampling procedure

As reviewed, differential peat accumulation rates exist across the microtopographic gradient (Belyea and Clymo, 2001), so an appropriate sub-sampling procedure was considered. Patagonian peatlands generally accumulate rapidly (1 cm = ~10years) (Pendall *et al.*, 2001) and in the absence of dates to determine peat accumulation rates in this study an initial sampling resolution of 4 cm was carried out with levels of finer resolution sampling where necessary. The differential accumulation rates across the microtopographic gradient were kept in mind and a 4 cm resolution was carried out for consistency until the ages of the base of the profiles were established.

There is not yet consensus on the most efficient and precise method of sub-sampling peat cores. The conventional method following early work by Barber uses fine dissecting equipment, such as a scalpel for more humified layers and scissors for the looser *Sphagnum* of the acrotelm to minimise loss. This method was used in this study to sub-sample the Chilean cores from Karukinka bog and San Juan bog. The core from San Carlos bog was sub-sampled at the ECOLAB (University of Toulouse)

by freezing the core and cutting it with a band-saw at 1 cm resolution. This is potentially a more precise and efficient sub-sampling method (Givelet *et al.*, 2004; De Vleeschouwer *et al.*, 2010a; Hansson *et al.*, 2013)

3.4.2 Palaeohydrological methods

This section reviews the methods used to reconstruct palaeohydrological variability from the peat cores in this investigation. Plant macrofossil analysis was chosen to establish vegetation change over the period of interest and indicate BSW variability using statistical methods. Humification analysis was chosen to assess the degree of decomposition of peat throughout the records. Testate amoeba analysis was further chosen to quantify BSW variability via the use of a recently developed transfer function of water table depth. These palaeoecological proxies provide a context in which to interpret the stable isotope analysis, which was chosen in response to questions regarding evaporative effects over microtopographic gradients (Section 2.3.4.4).

3.4.2.1 Plant macrofossil analysis

Preparation of samples for plant macrofossil analysis followed the Mauquoy *et al.* (2010) protocol. Each core was initially subsampled contiguously every 1 cm; using a dissecting kit, scissors were used to sub sample the fresh *Sphagnum* in the acrotelm layer whilst a scalpel was used in the more humified layers of the catotelm. 4 cm^3 of material per sample was measured accurately using a graduated cylinder and water displacement. Samples were then sieved using a 125 µm sieve and deionised water. Mauquoy *et al.* (2010) emphasise the need to keep the plant material just below the water level in order to prevent any damage that could inhibit correct identification. In order to maintain consistency between samples the same amount of water was used to sieve each sample. After sieving, the samples were carefully placed into Sterilin tubes, labelled accordingly and filled with deionised water; they were then kept in the refrigerator until they were needed for analysis.

In order to determine the abundance of plant macrofossils within a sample, traditionally ordinal values have been applied with values ranging from 1 (rare) to 5 (abundant) (Barber, 1981) as well as detailed and total counts of plant macrofossils present in a sample (Janssens, 1983). Large variation in plant macrofossils between sequences may demand a total count as was done by Van der Putten *et al.* (2012)

although this is very labour intensive. The Quadrat and Leaf Count (QLC) technique, developed and applied by Barber *et al.* (1994), is a combination of the traditional techniques. A percentage estimate is used of the presence of different plant macrofossils and then numbers of any seeds, fruits or charcoal present are tallied. In this investigation the QLC was used as opposed to either traditional technique as QLC is also now the most commonly used technique in palaeoclimate investigations involving plant macrofossil analysis. Bias may be a result of the subjectivity of this procedure (Barber *et al.*, 2000); however, the technique has been successfully used. Further, Mauquoy *et al.* (2004) and Chambers *et al.* (2007) used the same techniques as are applied to similar studies of northwest European peat in investigations at Valle de Andorra bog.

Each sample was analysed using an Olympus SZ stereo microscope. As explained in Mauquoy *et al.* (2010) each sample was placed in a petri dish with sufficient water to float the sample. For each sample 15 views were counted in a systematic way starting from the top left. In each view, the volume percentage of the main peat components is estimated, forming the 'Quadrat' component of the technique. The main peat components identified are displayed in the results section but include *Sphagnum*, Ericaceae and monocot remains. As well as volume percentage, a brief description of each sample was noted to aid with interpretation. Detailed identification can be carried out by mounting monocot leaves on microscope slides and analysing under X100-X400 magnification, forming the 'Leaf Count' component of the technique. Similarly, where possible, 100 *Sphagnum* leaves should be identified and expressed as the percentage of identified *Sphagnum* alongside the percentage *Sphagnum* abundance. In the case of Patagonian peatlands however, *Sphagnum magellanicum* is dominant throughout the record so the individual expressions may not be necessary. Additionally, *Sphagnum* remains are well preserved in these samples with leaves attached to the stems, so identification to section or species level can simply be made by eye. A 100 leaf count may result in bias through the selective nature of pulling leaves from intact *Sphagnum* remains for identification as opposed to less well preserved remains from which 100 leaves would be selected at random for identification. As mentioned, fruits, seeds, charcoal and individual leaves should be tallied (n) for each sample. In this study, in some samples, there were a high number of e.g. *Empetrum rubrum* leaves so it was

thought necessary to include these in the percentage abundance of the whole sample.

The Mire and Peat Macros guide (Mauquoy and Van Geel, 2007) was followed for the identification of the main peat components. Preservation in the upper section of each profile allowed identification to species level of the main components. Daniels and Eddy (1990) and Atherton *et al.* (2010) were used to identify *Sphagnum magellanicum* identifiable by the morphological characteristics of the hyaline cells. Robertson (2000) was used for non-*Sphagnum* bryophytes along with the Grosse-Brauckmann (1972; 1974) guides for vascular species. The presence of well-preserved species at the surface enabled identification of more degraded plant macrofossils deeper in the profiles.

Following analysis, the samples were returned to Sterilin tubes, refilled with deionised water and returned to the refrigerator where they were stored for subsequent stable isotope analysis.

3.4.2.2 Humification analysis

Peat samples of ~2 cm^3 were processed following the standard method by Chambers *et al.* (2011). To ensure operator-independence the samples were all analysed within a uniform time window (Caseldine *et al.*, 2000; Chambers *et al.,* 2012). A Cecil 1011 spectrophotometer, set to 540 nm, was used to analyse three cuvettes of pipetted solution. The percentage light transmission was averaged across the three readings to give a final value for each sample. This method was applied to the three profiles from Karukinka and the San Juan profile to agree with the sampling resolution of the other proxies. Humification analysis was not carried out for San Carlos owing to time constraints. Long-term trends in humification data were removed by detrending the record (Borgmark and Wastegard, 2008).

3.4.2.3 Testate amoeba analysis

Testate amoeba samples were prepared following Booth *et al.* (2010). Initially a low-resolution sub-sampling was carried out, every 4 cm. The samples were extracted from the exposed right-hand edge left from the plant macrofossil sub-sampling. Again, the top layer was removed and the section accurately measured to ensure the

samples were taken at the respective depths compared with the plant macrofossil samples. Samples 2 cm^3 in volume were extracted and placed in beakers, the beakers were filled with deionised water to 100 ml. One tablet of *Lycopodium clavatum* spores per cm^3 was added to each sample (Stockmarr, 1971) to calculate test concentration and the beaker placed on a hot plate and contents stirred. Samples were boiled for 10 minutes to disaggregate the material and left over night. Each sample was then washed through a 300 µm and 15 µm sieve. A consistent amount of water was used to wash each sample. A small amount of vibration (tapping the hand on the edge of the sieve) encouraged the passage of water through the 15 µm sieve speeding up the sieving process. The material remaining on the 15 µm sieve was placed carefully in Sterilin tubes; with the addition of deionised water the samples were stored at this point. When the samples were needed they were centrifuged at 3000 rpm for 5 minutes to concentrate the sample in the bottom of the tube. After this, excess water was removed using a scientific pipette until a layer of water remained on the sample. The samples were then stirred gently to ensure non-bias of sample picked up in the next step. Using a pipette, a couple of drops of sample were placed onto microscope slides. Non-permanent slides were made for each sample using glycerol; these slides were disposed of after counts had been made.

The slides were analysed using an Olympus CX41 microscope. An initial scan of the slide was carried out at X200 and then systematically analysed at 400X starting at the top left of the slide. It was traditionally recommended to count 150 tests per sample for statistical validity (Warner, 1990; Woodland, 1996) however, owing to time constraints 100 tests were identified per sample which is thought to be sufficient for application of transfer functions to palaeorecords (Payne and Mitchell, 2009). In some cases counts of 100 were not possible owing to extremely low test concentrations; these samples are coloured grey in the stratigraphic diagrams. Samples with counts as low as 50 can still be used for statistical analysis (Charman *et al.*, 1999; Payne and Mitchell, 2009).

The identification key of North American peat testate amoebae was used (Booth, 2008); which is a modification of Charman *et al.* (2000). An unpublished key (Mitchell, 2003) was used for the identification of *Nebela* taxa originally described by Deflandre

(1936). The Southern Hemisphere restricted taxa were identified following van Bellen *et al.* (2014) who used Vucetich (1978), Smith *et al.* (2008) and Jung (1942). To calculate the test concentration per sample the following equation adapted from Mertens *et al.* (2009) was used:

Equation 3.1. Calculation of test concentration.

$$C = \frac{\left(\frac{L_a}{L_t}\right)}{v \times T_a}$$

,where C is the concentration of tests per cm^3, L_a the total *Lycopodium* spores added, L_t the total *Lycopodium* spores counted, v the volume of the sample and T_a the total number of tests counted.

3.4.2.4 Stable isotope analysis

Where possible the sub-sampling resolution of samples for stable isotope analysis generally followed that of plant macrofossil, humification and testate amoeba analysis to allow direct comparison between the proxies. Extensive experimentation of *Sphagnum* stable isotopic methods was carried out by Daley (2007). The methodological findings included the importance of the isolation of *Sphagnum* from the peat matrix as reviewed in section (2.3.4.4).

For each sample plant macrofossil analysis was first carried out and the same sample was subjected to micromanipulation (picking) of *Sphagnum* remains. Leaves were detached and the pure *Sphagnum* stems retained to form each sample for isotopic analysis of the *Sphagnum* stem cellulose (as in Markel *et al.*, 2010). The necessity of using *Sphagnum* stems for isotopic analysis is demonstrated by statistically significant differences between the $\delta^{13}C$ values of *Sphagnum* stems and branches (Loader *et al.*, 2007). Stems were picked until an adequate number had been collected to form the necessary weight for isotopic analysis. Loader *et al.* (2013; 2016) find evidence of inter-plant isotopic variability, which suggests that more stems

in a sample will result in better precision. The number of stems was not counted in this investigation and so an estimation of plant-associated uncertainty is not possible.

The preliminary plant macrofossil analysis demonstrated that the Patagonian cores were ideal for the cellulose stable isotope analysis in that a single species, *Sphagnum magellanicum*, is almost consistently present throughout the stratigraphy of all profiles.

3.4.2.4.1 α-cellulose extraction

After the stems had been picked, alpha-cellulose was extracted using the following method by Rinne *et al.* (2005), modified by Daley (2007). Each sub-sample of stems was placed in glass Soxlet vessels (extraction tubes). These vessels have a material chamber ~2 cm^3 and of equal diameter a coarse (p1) glass sinter filter. The vessels were suspended in a water bath heated to 80 °C. Acidified $NaClO_2$ (aq) was made using 600 ml of double distilled water mixed with 8.55 g of sodium Chlorite. 6 ml of acetic acid was mixed in just before the whole solution was added to each vessel (ensuring saturation of whole sample) and left to react for 50 minutes. The samples were then filtered *in vacuo* (by creating a vacuum) to remove the solution. This bleaching process was repeated to a total of five times resulting in delignification of the samples. After this the samples were washed once with boiling double distilled water and filtered *in vacuo*. Samples were washed in this way a further four times with room temperature double distilled water to ensure the removal of any remaining bleaching solution. 2 ml of 10% sodium hydroxide (NaOH) (made by mixing NaOH and 600 ml of double distilled water) was added to each sample and suspended in the water bath at 70 °C for 45 minutes and again, filtered *in vacuo* to remove short chain celluloses (hemicellulose). The samples were washed through three times with double distilled water and filtered *in vacuo.* The water bath was then heated to 80 °C and a final two sodium chlorite bleaching processes were carried out after which the samples were subjected to a further five double distilled water washes.

After the bleaching process, samples were transferred to 2 ml plastic Eppendorf tubes and filled with double distilled water using a scientific pipette. An ultrasonic probe (2 mm) was used to homogenise the alpha-cellulose. This was repeated until the liquid was of a homogenous translucent appearance. The samples were left in

the freezer overnight with aluminium foil placed over the tubes pierced to allow moisture to escape. Samples were then freeze dried over for ~48 hours. Samples were then weighed in silver capsules (1±0.1 mg) for pyrolysis ($\delta^{18}O$) and tin capsules (0.10±0.02 mg) for combustion ($\delta^{13}C$). Following this, samples were ready for mass spectrometric analysis.

3.4.2.4.2 Stable isotope accelerator mass spectrometry

Methods of continuous flow isotope ratio mass spectrometry (CF-IRMS) are continually being developed. Using this online measurement of stable isotope ratios, the cellulose is transformed to carbon dioxide by combustion and carbon monoxide by high-temperature pyrolysis for the analysis of $\delta^{13}C$ and $\delta^{18}O$ respectively. This is followed immediately by mass spectrometry by transportation of the gas along a helium gas stream. The gas is then ionised in the mass spectrometer and accelerated through a magnetic field. Isotopes of different masses are deflected differently off the magnetic field and collected in Faraday cups.

In an attempt to reduce the amount of material and time needed for the analysis of oxygen and carbon stable isotopes, investigation into the simultaneous measurement of these isotopes has been carried out in recent years (McCarroll and Loader, 2004; Woodley *et al.*, 2012; Loader *et al.* 2014). Woodley *et al.* (2012) investigated the potential use of high temperature pyrolysis of cellulose to allow for the simultaneous measurement of oxygen and carbon stable isotope ratios as opposed to individual measurements using pyrolysis and combustion respectively. Discrepancies were found between the $\delta^{13}C$ results using pyrolysis and combustion especially after anthropogenic CO_2 increases ~AD 1900. After this time the values derived using combustion became increasingly negative, diverging from the values using pyrolysis. In the case of divergence a pyrolysis adjustment can be applied to ensure a robust $\delta^{13}C$ record (Young *et al.*, 2011) supporting the efficiency of such simultaneous measurements. Loader *et al.* (2014) have further developed the means to measure oxygen, carbon and hydrogen stable isotopes simultaneously using an automated equilibration unit interfaced with an elemental analyser and IRMS. The initial aim of this investigation was to use this method of simultaneous measurement but time constraints restricted its use.

Stable carbon isotope analysis was carried out at Plymouth University using an Isoprime isotope ratio mass spectrometer. Certified standards were analysed alongside samples for the correction of measured values to an international scale. The final $\delta^{13}C$ values are expressed as per mille (‰) deviations from the VPDB (Vienna PeeDee Belemnite) standard (Coplen, 1995). Alongside the $\delta^{13}C$ analysis the USGS40 standard was analysed as well as the IAEA-CH-3 (cellulose, $\delta^{13}C_{VPDB}$= -24.724‰) standard. A two-point calibration equation (y=0.912x-13.128) was used to calibrate the measured values (Ke *et al.*, 2014). The two points were the known values of both USGS24 (graphite, $\delta^{13}C_{VPDB}$= -16.049‰) and USGS40 (graphite, $\delta^{13}C_{VPDB}$= -26.389‰) and measured values of these standards. This equation was used to calibrate all measured $\delta^{13}C$ values.

Four runs were carried out, the accuracy of which is assessed by the comparison of the mean ±1σ of all measured and known values of standards across runs (Jardine and Cunjack, 2005). This comparison of the IAEA-CH-3 was assessed and owing to similarity in values between runs an offset correction between runs was not necessary to allow comparison of the resulting $\delta^{13}C$ values used in this investigation.

The analytical error was calculated by taking the mean and standard deviation of all calibrated $\delta^{13}C$ values from each of the standards used in the respective runs (IAEA-CH-3 N=18 in runs one-three, N=4 in run four, USGS40 N=22 in runs one-three, N=3 in run four). The average of the standard deviation of the calibrated $\delta^{13}C$ values was found to be ±0.32‰ for the Karukinka and San Juan $\delta^{13}C$ values and is higher than the ±0.19‰ calculated for the San Carlos $\delta^{13}C$ values owing to an outlier in the USGS40 calibrated values in run one.

Stable oxygen isotope analysis was conducted by Iso-analytical Ltd. using pyrolysis and a Europa Scientific 20-20 IRMS. Final $\delta^{18}O$ values are expressed as deviations from the VSMOW (Vienna Standard Mean Ocean Water) standard (Coplen, 1995). The certified standards used were IA-R006 (cane sugar, $\delta^{18}O_{VSMOW}$ 35.23‰) and IAEA-CH-3 (cellulose, $\delta^{18}O_{VSMOW}$ 32.20‰). IA-R006, IAEA-CH-3, IAEA-CH-6 and IAEA-601 test samples were also measured for quality control and the means and 1σ were all within the accepted values of each standard. The analytical error was

calculated by taking the standard deviation of the measured IAEA-CH-3 $\delta^{18}O$ values (N=41), which was ±0.19‰ for all $\delta^{18}O$ results in this investigation.

3.4.2.4.3 Correction of $\delta^{13}C$ results

Industrialisation (~AD 1760) has resulted in a decrease of the $\delta^{13}C$ values of atmospheric CO_2 (McCarroll and Loader, 2004) to the present day by ~2‰ due to the burning of coal and oil which are ^{13}C depleted (Keeling, 1979; Tans *et al.*, 1979). This has resulted in a similar decrease in values in terrestrial $\delta^{13}C$ records. To account for this the Suess correction has been used to de-trend records which exhibit this trend from industrialisation to the present day (Francey *et al,* 1999). Following McCarroll and Loader (2004) values from terrestrial $\delta^{13}C$ records are corrected against a pre-industrial (AD 1850) standard of -6.4‰ using a high-resolution record of $\delta^{13}C$ values of atmospheric CO_2 derived from Antarctic ice cores (Francey *et al.*, 1999). This record extends from AD 1980 to 1997 and values after AD 1997 are extrapolated to give annual correction values (Appendix I). Correction of the record relies on an accurate chronology to ensure that the correct value is assigned to the correct year. Chronological uncertainty makes this difficult due to the range of ages per sampling point. A comparison was made between corrected values based on the weighted mean age of each sampling point and an average of the correction values for the range of ages per sampling point. Differences between the two were within the measurement error of the original values owing to the relatively low correction values before AD 1900; therefore, the former record was chosen for final comparison with the raw values presented in Chapter 5.

3.5 Statistical analysis of the multivariate proxy data

Stratigraphic diagrams of the palaeoecological data were produced using the rioja package in R (Juggins, 2015). The same package was used for zonation of the stratigraphic diagrams via the method of Constrained Incremental Sum of Squares (CONISS; Grimm, 1987). The broken stick model (Bennett, 1996) was used to determine the number of zones of each diagram. For ease of interpretation of the multivariate data and for comparison between the multi-proxy, multi-profile and multi-site records, various statistical techniques were used and are reviewed in this section.

Ordination in palaeoecology aims to order multivariate data consisting of multiple species and samples to assess ecological distance within the data. Indirect gradient analysis assesses the similarities within the data to aid interpretation, whereas direct gradient analysis orders the data in relation to a measured environmental variable. Methods of indirect gradient analysis include Principal Components Analysis (PCA), Detrended Correspondence Analysis (DCA) (Hill and Gauch, 1980) and Non-metric multidimensional scaling (Nmds) (Minchin, 1987). These methods reduce the multi-dimensionality of data and, using a linear or unimodal species response model, explore an underlying structure in the data, which may be determined by latent environmental variables (Legendre and Gallagher, 2001; Legendre and Legendre, 2012).

When selecting an ordination method an appropriate ecological distance measure must be chosen. Some methods represent the percentage variance of axes (PCA, DCA), whereas other methods compare the various ecological distances between the original data and the ordination data (Nmds) (Kindt and Coe, 2005). These methods were investigated in order to relate species composition in the plant macrofossil and testate amoeba data with environmental gradients. These techniques can be used to transform the multivariate data to a more easily interpretable single index of BSW, assuming that the axis accounting for most variability in the data is related to bog hydrology (Barber *et al.*, 1994; Sillasoo *et al.*, 2007).

Studies aiming to do this via the use of plant macrofossil and testate amoeba records have mainly used DCA and DHI (Dupont Hydroclimatic Index; Dupont and Brenninkmeijer, 1984, Dupont, 1986) (e.g. Blundell *et al.*, 2008; Turner *et al.*, 2013) and DCA and transfer functions (Charman *et al.*, 2009; Amesbury *et al.*, 2012) respectively, to transform the data to an index of hydrological variability.

3.5.1 Plant macrofossil analysis

The majority of peatland palaeoecological studies using plant macrofossil analysis have been carried out in northwest Europe and North America. DCA and DHI have often been used in these studies to condense the multivariate plant macrofossil data to a more easily interpretable index of BSW. The potential of plant macrofossil

transfer functions to reconstruct BSW/WTD variability quantitatively has also recently been investigated (Väliranta *et al.*, 2007; Mitchell *et al.*, 2013).

A range of techniques was tested in this investigation to explore which method was the most appropriate for conversion to a BSW index. The most appropriate method and any necessary transformations were dependent on the individual datasets. Each dataset is discussed in Chapter 5. The same criteria were followed in the application of techniques to each dataset.

First a DCA was carried out to test the underlying gradient length. The influence of both the removal of rare species (<5% abundance) and downweighting of rare species were assessed and in most cases were found to alter the gradient lengths only slightly so were deemed unnecessary in this case. In the absence of environmental variables the homogeneity of data can be assessed using DCA. The beta diversity (species turnover) is measured by the length of the gradients (individual ordination axes) and standard deviation around the mean. Lepš & Šmilauer (2003) state that if the value of the longest gradient is more than 4σ a unimodal method should be used since a large value indicates heterogeneous data and high beta diversity. On the contrary if the value of the longest gradient is less than 3σ this suggests homogenous data and low beta diversity; in this case a linear response model is appropriate. If using a linear response model certain transformations of the data matrix may be necessary (Legendre and Gallagher, 2001). Both the Hellinger distance and chord distance methods of data transformation were tested with the plant macrofossil datasets. As the respective PCA axis-one scores were found to be similar the Hellinger transformation was used as this is the most commonly used square root method to transform percentage data (Ramette, 2007). The influence of the removal of rare species was assessed in each case using a transformation-based PCA. The option with the highest axis-one eigenvalue was ultimately chosen. All options resulted in very similar axis-one scores and the direction of change was uniform in all cases. The vegan package in R was used to carry out both DCA (decorana function) and PCA (rda function). The decostand function was used for data transformation with method="Hellinger".

In cases where an environmental gradient is difficult to infer using DCA and PCA DHI, a method based on weighted averaging by assigning values to different components based on ecological knowledge, can be used alongside ordinations. Conversion of the plant macrofossil data to a single line of BSW using this method was found to agree better with other proxy records from NW European bogs than DCA and Nmds (Daley and Barber, 2012).

Using the values assigned to similar species by Daley and Barber (2012) the values for weighted averaging are displayed in table 3.2. *Eriophorum* species are not present in Patagonian peatlands (Mauquoy and Bennet, 2006). Values assigned to these species in northern European reconstructions were assigned to species found in the Patagonian records of similar modern-day habitat preference.

Table 3.2. Dupont Hydroclimatic Index values for application to Patagonian sites.

Sphagnum magellanicum	3
Liverwort sp.	3
Brown moss undif.	6
Ericaceae roots undif.	8
Ericaceae wood undif.	8
Empetrum rubrum stems/leaves	8
Nothofagus antarctica leaves	8
Monocot leaves undif.	7
Monocot roots undif.	7
Monocot node undif.	7
Unidentified Organic Matter	8
Tetroncium magellanicum	3

Table 3.3. Dupont Hydroclimatic Index values for application to San Carlos bog.

Sphagnum magellanicum	3
Monocot leaves undif.	7
Monocot roots undif.	7
Monocot node undif.	7
Wood undif.	8
UOM	8
Dicot roots	8
Dicot leaves undif.	8
Myrteola nummularia	8
Empetrum rubrum	8
Gaultheria pumila	8

For each sample a DHI value is derived using the following equation:

Equation 3.2. Calculation of the DHI value of each sample.

$$(x_1 + w_1 + x_2 + w_2 \ldots x_n + w_n)/(w_1 + w_2 \ldots w_n) = \sum(\boldsymbol{x_i} + \boldsymbol{w_i})/\sum \boldsymbol{x_i}$$

,where x_i is the species percentage abundance of each sample $(i = 1 \ldots n)$, w_i is each species' weighting (displayed in table 3.2). Each species percentage abundance is multiplied by its weighting; the sum of this for each sampling level is then divided by the sum of the total species percentage abundance for each sampling level.

Care must be taken in assigning values based on habitat preferences from studies in the Northern Hemisphere owing to potential differences with similar species in the Southern Hemisphere. DHI may not be useful where *Sphagnum* is only identified to section or where only one species is present throughout the record as various species are assigned different values. These values range from 1 for *Sphagnum* sect. *Cuspidata* (a wet adapted species), 3 for *S.magellanicum* (an apparently wet adapted species) to 6 for *Sphagnum* sect. *Acutifolia* (relatively dry adapted) (Daley and Barber, 2012). The dominance of *S.magellanicum* throughout the record may suggest that this is an intermediate species and the influence of a different weighting was assessed. Changing the weight does not influence either the direction of change or, ultimately, the z scores; therefore a value of 3 was appropriate.

The validity of each record as an index of BSW was tested by comparing the PCA axis-one values with the DHI records plotted against depth from each profile.

3.5.2 Testate amoeba analysis

The most common methods of transformation of testate amoeba records from peatlands to an index of hydrological variability are DCA and transfer functions. Using the same criteria as discussed in section 3.5.1, first a DCA of the data was applied to test the gradient length with the appropriate model (unimodal/linear response) applied based on this value (>4σ/<3σ respectively). DCA (decorana

function) and PCA (rda function) were carried out using the vegan package in R. Transformation of the data for use with a linear response model (PCA) was carried out where necessary. The decostand function was used for data transformation with method="Hellinger".

As well as the above ordination methods the data have been transformed using a transfer function. The training data set from southern South America (van Bellen *et al.*, 2014) was applied to the testate amoeba percentage abundance data (also see section 2.4.5.3). The training data set consists of 154 modern samples taken from five southern South American bogs, two of which, Karukinka bog and San Juan bog are sites in this study. These samples were taken over two field seasons with 99 taken in 2012 and 55 taken in 2013. Surface samples were taken along the microtopographical gradient, with five transects from hummock to pool to establish uncertainty. Corresponding measurements of pH, electrical conductivity and depth to water table were carried out from each sampling point. Each sample was processed and 150 tests were counted. Rare taxa (found in less than five samples) were not included in the training data set to improve model performance. DCA assessed relationships amongst the taxa and Canonical Correspondence Analysis (CCA) assessed the relationship with the measured environmental variables. A variety of regression models was tested with the Weighted Averaging Partial Least Squares (WA-PLS) model performing best. The RMSEP values from Leave-One-Out and bootstrap cross validation of this model were high (13.51 and 14.01 cm respectively) compared with other transfer functions of this type owing to the wide range of water table depths (~16 cm). Of the variability in the testate amoeba assemblages 16.6% in the 2012 and 15% in the 2012 and 2013 datasets was explained by measured water table depth. These values are the norm in peatland testate amoeba transfer function development (van Bellen *et al.*, 2016).

Caution must be taken when applying the transfer function to fossil data sets from sites not included in the modern training data set owing to the potential inconsistencies between taxa in each. This is similar to the application of a supra-regional transfer function where a regional transfer function would be more appropriate (Turner *et al.*, 2013). The application of this regional transfer function is appropriate at Karukinka bog and San Juan bog owing to the inclusion of transects

from these sites in the modern training data set. It was applied with caution to the San Carlos bog fossil data set but despite the absence of this site in the modern training data set, there were consistencies in the taxa present with the southern South American sites. Some taxa were excluded before application of the transfer function to the records as they were not present in the training data set.

The WTD reconstructions resulting from application of the transfer function were compared with the axis-one scores of the ordinations from each profile to assess similarities between these measures of hydrological variability.

3.6 Multi-proxy comparison

Following assessment of the most appropriate representation of hydrological variability from the plant macrofossil and testate amoeba data, a multi-proxy comparison of the palaeoecological records could be carried out. These records along with the humification records (humification not available for San Carlos) were standardised using the following equation removing magnitude differences between records by using the z-score calculation (Ramette, 2007).

Equation 3.3. Calculation of sample z-scores.

$$z = \frac{X - \mu}{\sigma}$$

where z = standardised value, X= original value, μ= mean of all X and σ= standard deviation of X.

These records were then compared based on depth for visual similarities. Normally distributed data are necessary for parametric statistical tests however, none of the palaeoecological records evidenced normal distributions. Spearman's rank correlation coefficient was used to explore correlations between the palaeoecological records in the individual profiles. Correlations are based on the depths at which there were observations in both of the proxies being compared to ensure this the pairwise.complete.obs command was used in R when carrying out statistical analysis.

A perfect association between the ranked data from each record would give an r_s value of +1 with the palaeoecological records demonstrating similar variability through time with a common forcing.

Standardisation of the stable carbon and oxygen isotope records was not carried out and these were instead compared with each other. Pearson product-moment correlation coefficient was carried out between these records as the data displayed a normal distribution.

3.7 Multi- profile and multi-site comparison

Each proxy record from each of the KAR-EM profiles was compared to form the intra-site aspect of the investigation. The raw plant macrofossil data from each profile were used in a PCA ordination to assess similarities between the profiles based on their corresponding plant macrofossil zones. The DHI values from the three profiles were compared based on actual depth and depth relative to the surface of KAR-EM-3 to assess which of the two methods of displaying the records drew the most similarities. The humification records are compared both based on actual depth and relative depth. DCA was applied to the raw testate amoeba data from each profile and similarities between samples across the profiles according to testate amoeba zone were assessed. The WTD reconstruction records from the three profiles were compared based on actual and relative depth. Similarly, the stable carbon and stable oxygen isotope records were compared plotted against actual and relative depth.

A comparison of the proxy records plotted against depth was carried out to assess visual similarities between the records which could be used as tie points in an attempt to tune the chronology of each record based on apparently synchronous events. Spearman's rank correlation coefficient explored intra-site correlations between the palaeoecological data from each profile (DHI values, humification and WTD reconstruction). Pearson's correlation coefficient explored intra-site correlations between the raw stable isotope records from each profile. Correlations were carried out in R using the pairwise.complete.obs command to ensure correlation of observed values across the actual depths of the profiles (Appendix II).

The proxy records from each profile were compared and plotted relative to the surveyed datum height (top of hummock) and therefore the surface of KAR-EM-3 is 0 cm, the surface of KAR-EM-2 is 34 cm below this and the surface of KAR-EM-1 is 60 cm below the surface of KAR-EM-3. Visual similarities between the records were assessed plotted in this way. Correlations across the three profiles were made difficult by the absence of observations at synchronous depths across the three profiles. The sampling depths of KAR-EM-2 were used as the standard against which observations from intervening sampling depths in KAR-EM-3 and KAR-EM-1 could be compared. (See Appendix II for the number of observations from each profile that could be used for correlation and the number of those observations that are original values, the rest being two-point averages of intervening depths). As above, Spearman's rank and Pearson's correlation coefficient were used in R with the pairwise.complete.obs command.

Accumulation differences across the profiles question the comparison of the three based on both actual and relative depth; however, this enables comparison based on both depth and chronology in subsequent chapters to assess the accuracy of the developed chronology and the timing of variability.

Owing to differences in the ages of each profile, correlation across records was difficult through the lack of chronologically synchronous sampling points. 50- and 20-year bins were used to enable intra-site correlation between proxy records. This was carried out by taking the mid-point age of each sampling point and manually binning the data into 50- and 20-year periods (… 1963-2013; …1993-2013). In instances where more than one sampling point occurred these values would be averaged across the time period. Depending on the distribution of the data sets, Spearman's rank and Pearson's correlation coefficient were used in R with the pairwise.complete.obs command. (See Appendix II for the number of original observations (the non-averaged results) and number of pairwise observations).

The SAN-EM-2 and SCB-1 data were binned into the same 50- and 20-year periods as was carried out for the intra-site comparison to allow comparison of data across sites. The final inter-site comparison compares the data based on 20-year periods. This is because the number of original observations from SAN-EM-2 and SCB-1 was

too low owing to the averaging of original observations within 50-year time periods. Significant correlations (at the 0.05 significance level) are shown by an asterisk and highlighted (see Chapters 5 and 6 for full results).

Robust chronologies were a pre-requisite for both multi-profile and multi-site comparisons. The development of chronological records for each of the profiles in this investigation is discussed in the following chapter.

Chapter 4: Chronology

4.1 Introduction

This chapter aims to review the techniques underlying the construction of peat chronologies in this investigation; the results using these techniques are then presented, followed by the final age-depth models developed for each profile. Understanding the timing of variability throughout a peat record is critical and is dependent on accurate chronological control. Chronological errors limit the comparison and correlation of peat records both within peatlands and across multiple sites. Such comparisons are facilitated by the use of multiple chronological techniques.

4.2 Radiometric dating

Radiometric dating allows the production of an absolute time scale and the potential for comparison of variability between different records (Smart and Frances, 1991). The principles and methodologies of radiocarbon (^{14}C) and lead 210 (^{210}Pb) dating are reviewed in the following sections. These techniques were applied to all profiles in this investigation and the chronological results are presented in sections 4.2.1.3 and 4.2.2.3. The statistical development of age-depth models is discussed in section 4.3 to establish a chronology for each profile.

4.2.1 Radiocarbon (^{14}C) dating

4.2.1.1 Principles

Radiocarbon dating was used as the main chronological technique in this investigation. It is the most commonly used dating technique in peatland studies owing to 50% of peat being composed of carbon (Charman, 2002). It is a well-established technique relying on a few assumptions. Cosmic rays strike nitrogen atoms in the atmosphere forming the unstable radioisotope ^{14}C (carbon-14); this radioisotope is incorporated into plants via photosynthesis at which point the ratio of ^{14}C to the stable isotopes of carbon is the same as the atmosphere. This fixation ceases when the plant dies and ^{14}C begins to decay back to nitrogen-14, with half of its atoms decayed (half-life) after 5730±40 (Godwin, 1962) years relative to the stable isotopes of carbon (^{12}C, ^{13}C). This measurable ratio is indicative of when a

plant died; therefore, measurement of samples taken from a stratigraphic sequence can be used to establish an absolute time scale. A full review of the technique can be found in Olsson (1986) and Turetsky *et al*. (2004).

Conventional ^{14}C dating techniques involved the analysis of large bulk peat samples using gas proportional counting or liquid scintillation spectrometry to measure ^{14}C activity. Accelerator mass spectrometry is now commonly used on much reduced samples (1 g) to measure ^{14}C concentration by atomic mass separation (Piotrowska *et al.*, 2011). The reduction in sample size necessary for this technique allows for the isolation and dating of above-ground components in peat, which provide a more accurate age estimation of the sample depth. The reservoir effect, in which plant remains for dating have fixed old carbon dioxide, is a common problem when using bulk peat samples (Kilian *et al*., 1995; 2000). Isolation of the above ground components of individual species for dating reduces potential differences in the ^{14}C concentration of different species (through different fractionation processes), although Nilsson *et al.* (2001) found no differences in the ^{14}C content of *Sphagnum* species. More accurate age estimations can thus be established through the appropriate selection of material for dating.

Appropriate calibration is necessary to avoid the introduction of inaccuracy to the method. Comparison of the ^{14}C content of tree rings with cave deposits of known calendar age suggests that there have been fluctuations in the ratio of ^{14}C to the stable isotopes of carbon in the atmosphere over time (Stuiver *et al*., 1998). Calibration curves reflecting these fluctuations have been produced to allow conversion of uncalibrated radiocarbon dates to calendar years before present (cal BP) however, plateaus and steep sections of the curves limit the accurate calibration of radiocarbon dates (Blackwell and Buck, 2008). Atmospheric ^{14}C varies globally with Northern and Southern Hemisphere calibration curves now extending to 50,000 cal BP (IntCal13 Reimer *et al.*, 2013; SHCal13 Hogg *et al.*, 2013).

A plateau on the calibration curves over the last ~300 years has been the result of industrialisation and the burning of coal and oil in which all ^{14}C has decayed and ^{13}C is depleted relative to atmospheric concentration (Keeling, 1979; Tans *et al*., 1979).

The use of ^{14}C dating is, therefore, less appropriate for dating recent peat deposits (Le Roux and Marshall, 2011).

Radiocarbon dates are expressed as cal BP with present placed at 1950 owing to the natural level of ^{14}C in the atmosphere (~100%) being increased to 200% in the Northern Hemisphere and 170% in the Southern Hemisphere resulting from nuclear weapons testing in 1955 (Hua and Barbetti, 2004). Where ^{14}C enrichment is >100% modern (100% is 1950) one of various post-bomb calibration curves can be used (Reimer and Reimer, 2004; Hua *et al*., 2013) as well as wiggle matching to the higher ^{14}C enrichment in recent peat deposited over the last 50 years (Clymo *et al*., 1990). Wiggle matching uses the wiggles of the calibration curve to match closely spaced radiocarbon dates of peat (van Geel and Mook, 1989) but relies on acquiring sufficient radiocarbon dates at a high cost (Blaauw *et al*., 2003).

Radiocarbon dates are statistically calibrated based on the probability density distribution, at 95.4% probability, on the calibration curve. Fluctuations in the calibration curve result in a (non-Gaussian) range of calendar ages for each sampling depth. Plateaus result in large probability distributions in calibrated ages and steep sections lead to overly precise ages. Statistical programs can be used to calibrate single dates to produce such probability-based age ranges (e.g. OxCal: Bronk Ramsey, 1995; CALIB: Stuiver and Reimer, 2006).

A sequence of radiocarbon dates can be used to develop an age-depth model in which the dates are calibrated and the age of intervening depths are statistically estimated using classical age modelling (Blaauw, 2010) or Bayesian methods (Blaauw and Christen, 2005; Bronk Ramsey, 2008).

Clam (Classical Age Modelling) is a non-Bayesian method of age-depth modelling (Blaauw, 2010) in R. This method can be used to explore a variety of models including linear interpolation, linear or polynomial regression and cubic or smoothed splines. Blaauw and Christen (2005) note the disadvantages of classical age-depth modelling. Using these methods, the presence of outliers result in unrealistically abrupt changes in sedimentation; the midpoints of each calibrated age are used in model development despite it not necessarily being the most likely age. Classical

age-depth modelling does not consider potential memory between the ages of depths, and normal uncertainty distributions are assumed (despite non-Gaussian age ranges); hence, uncertainty between depths is poorly determined.

The use of Bayesian statistics requires a high sampling resolution and multiple ^{14}C dates. However, the same is true for classical age-depth models where none of the available methods is inherently efficient in creating age-depth models with low uncertainty (Telford *et al*., 2004a). Reliable age-depth models are increasingly being produced using Bayesian methods (e.g. Charman *et al.*, 2013; 2015; Crann *et al.*, 2015).

One such approach, Bacon in R (Bayesian accumulation histories for deposits) (Blaauw and Christen, 2011) uses a Markov Chain Monte Carlo self-adjusting sampling algorithm (Christen and Fox, 2011) that runs through thousands of iterations of the full calibrated probability distribution and uses prior information about accumulation rates to develop robust age-depth models. The weighted average of all iterations at each depth provides the ultimate age-depth line throughout the profile. The weighted mean ages and 2σ errors are produced as an output - an improvement of the intercept method of generating mid-points of radiocarbon dates (Telford *et al.*, 2004b).

In this investigation age-depth models were initially developed in Clam but owing to the low ^{14}C sampling resolution unrealistic abrupt changes were evident at dated levels and uncertainty between these levels was unrealistically low. The ability to provide prior information about accumulation rates and memory between calibrated radiocarbon dates in Bacon warrants its use in this investigation. Despite relatively higher age uncertainties the resulting models were more realistic in their age estimation.

4.2.1.2 Methods

A reasonable number of radiocarbon dates is necessary to control a peat record chronologically. Before proxy analysis, rangefinder AMS radiocarbon dates were obtained in order to establish the ages of the base of the KAR-EM, SAN-EM-2 and SCB-1 profiles. Subsequent to proxy analysis, 11 AMS radiocarbon dates were

applied to the three profiles from Karukinka. These dates were not evenly spaced throughout the profiles but were chosen based on attempting to establish the timing of significant changes in the proxy records (Telford *et al.,* 2004a).

All dated material consisted of *Sphagnum* stems that grew *in situ* and should therefore be representative and robust. Care was taken to remove any contaminants from the stems under magnification. The samples were then stored in Sterilin tubes in deionised water prior to analysis. These samples were processed by the NERC Radiocarbon Facility, East Kilbride under the allocation numbers; 1740.1013 and 1903.0415. Pre-treatment of all samples involved digestion in 2M HCl (80 °C, 8 hours) before being washed with deioinised water, dried and homogenised. A known weight of the pre-treated sample was heated with CuO in a sealed quartz tube with total carbon being recovered as CO_2 and converted to graphite by Fe/Zn reduction. The results were returned as conventional radiocarbon years BP (AD 1950=present) and % modern ^{14}C with ±1σ analytical error (Displayed in section 4.2.1.3). The returned dates were calibrated online using OxCalv4.2.4 (Bronk Ramsey, 2013) using the SHCal13 calibration curve (Hogg *et al.*, 2013) to establish the presence of outliers in consideration of the final chronology of each profile. The calibrated ages can also be assessed alongside alternative techniques aiming to resolve surface layers of peat profiles chronologically, as reviewed in section 4.2.2.

4.2.1.3 Radiocarbon results

This section presents the results from radiocarbon dating of samples from all profiles in this investigation. These dates are incorporated in the age-depth models presented at the end of this chapter. The results from the KAR-EM profiles are first presented followed by the results from SAN-EM-2 and SCB-1.

4.2.1.3.1 KAR-EM-3

Table 4.1 presents the radiocarbon results from KAR-EM-3. The conventional ^{14}C ages were calibrated online using OxCal and the resulting probability-based age ranges are presented. An initial age of the base of this profile (129.5 cm) was obtained before the record was extended for proxy analysis which returned a ^{14}C age

of 114 ^{14}C BP. This age was relatively young compared with the age obtained at 82.5 cm which attempted to resolve the acrotelm-catotelm boundary in the profile estimated to be 971±37 ^{14}C BP. When calibrated it is clear that these ages are problematic with the presence of older material at 82.5 cm or the presence of younger material at 129.5 cm. After extension of the proxy record, a further application returned an age of 1637±37^{14}C BP of the base of the profile which was more realistic in comparison with the other records; however, ages above and below the acrotelm-catotelm boundary at 66.5 and 101.5 cm were relatively young, 122±37 and 161±35 ^{14}C BP respectively. These two ages as well as the age from 129.5 cm are calibrated on the same section, a plateau, on the calibration curve. Inconsistencies exist between the returned ages of this profile; however, both comparison with the other profiles from the site and also the incorporation of the ^{210}Pb ages can aid development of the KAR-EM-3 age-depth model.

Table 4.1. Radiocarbon dating results from KAR-EM-3 samples.

Publication code	**Depth**	**^{14}C Enrichment (% Modern ±1σ)**	**Conventional ^{14}C Age (years BP ±1σ)**	**δ^{13}C VPDB‰ ± 0.1**	**Calibrated age (AD) (Probability distribution)**
SUERC-62500	66.5 cm	98.49 ± 0.45	122 ± 37	-29.1 ‰	1803-1950 (77.3%) 1685-1730 (18.1%)
SUERC-51683	82.5 cm	88.62 ± 0.40	971 ± 37	-27.9 ‰	1026-1190 (95.4%)
SUERC-62499	101.5 cm	98.01 ± 0.43	161 ± 35	-29.0 ‰	1796-1950 (64.1%) 1672-1744 (27.9%) 1759-1780 (3.4%)
SUERC-51684	129.5 cm	98.59 ± 0.43	114 ± 35	-27.8 ‰	1805-1950 (79.8%) 1691-1728 (15.6%)
SUERC-62498	149.5 cm	81.57 ± 0.37	1637 ± 37	-29.2 ‰	382-548 (93.9%) 560-570 (1.5%)

4.2.1.3.2 KAR-EM-2

Table 4.2 displays the radiocarbon results from KAR-EM-2. The probability-based age ranges resulted from online calibration of the conventional ^{14}C ages using OxCal. The age of the profile at 129.5 cm (1603±37 ^{14}C BP) is similar to the age of the base

of KAR-EM-3 with no age reversals apparent in this profile suggesting continuous accumulation throughout. The age at 38.5 cm was calibrated on the same calibration curve plateau as the ages in KAR-EM-3, as discussed above, which results in a wider probability-based age range at this depth. However, the ^{210}Pb ages may be used to constrain this depth in the development of the final KAR-EM-2 age-depth model.

Table 4.2. Radiocarbon dating results from KAR-EM-2 samples.

Publication code	**Depth**	**^{14}C Enrichment (% Modern ±1σ)**	**Conventional ^{14}C Age (years BP ±1σ)**	**δ^{13}C VPDB‰ ± 0.1**	**Calibrated age (AD) (Probability distribution)**
SUERC-51681	38.5 cm	98.54 ± 0.45	118 ± 37	-29.2 ‰	1804-1950 (78.1%) 1687-1729 (17.3%)
SUERC-62502	65.5 cm	89.60 ± 0.41	882 ± 37	-28.3 ‰	1148-1274 (94.5%) 1070-1077 (0.9%)
SUERC-62501	85.5 cm	87.48 ± 0.40	1075 ± 37	-28.2 ‰	962-1050 (76.3%)
SUERC-51682	129.5 cm	81.91 ± 0.38	1603 ± 37	-28.6 ‰	415-584 (95.4%)

4.2.1.3.3 KAR-EM-1

Table 4.3 presents the radiocarbon results from KAR-EM-1. The conventional ^{14}C ages were calibrated online using OxCal and the resulting probability-based age ranges are presented. The age at 129.5 cm (1719±37 ^{14}C BP) is similar to that of the base of KAR-EM-3 and KAR-EM-2 and there are no apparent age reversals in the profile. None of the ages was calibrated on a plateau on the calibration curve. The sample from 14.5 cm has a Post-1950 age suggested by the 111% ^{14}C enrichment and this level returned no probability-based age ranges, despite this it was possible to incorporate it into the final KAR-EM-1 age-depth model. Comparison with the other profiles and incorporation of the ^{210}Pb ages will help to constrain this profile chronologically.

Table 4.3. Radiocarbon dating results from KAR-EM-1 samples.

Publication code	Depth	^{14}C Enrichment (% Modern ±1σ)	Conventional ^{14}C Age (years BP ±1σ)	δ^{13}C VPDB‰ ± 0.1	Calibrated age (AD) (Probability distribution)
SUERC-51677	14.5 cm	111.37 ± 0.51	Post-1950	-29.4 ‰	n/a
SUERC-62508	42.5 cm	91.10 ± 0.40	749 ± 35	-28.5 ‰	1261-1321 (64.1%) 1350-1387 (26.4%)
SUERC-62504	69.5 cm	88.24 ± 0.38	1005 ± 35	-28.3 ‰	1017-1160 (95.4%)
SUERC-62503	101.5 cm	81.61 ± 0.37	1632 ± 37	-30.1 ‰	387-549 (93.2%)
SUERC-51680	129.5 cm	80.74 ± 0.37	1719 ± 37	-27.8 ‰	246-437 (95.4%)

4.2.1.3.4 SAN-EM-2

Table 4.4 displays the result of the radiocarbon date taken from the base of SAN-EM-2. The probability-based age ranges were calculated using the conventional ^{14}C ages using the online calibration tool, OxCal. Owing to the recent nature of this profile the probability-based ages show a bimodal distribution. It was only possible to obtain the age of the base of this profile, placing importance on the ^{210}Pb profile from SAN-EM-2 for the development of the final age-depth model.

Table 4.4. Radiocarbon dating results from SAN-EM-2.

Publication code	Depth	^{14}C Enrichment (% Modern ±1σ)	Conventional ^{14}C Age (years BP ±1σ)	δ^{13}C VPDB‰ ± 0.1	Calibrated age (AD) (Probability distribution)
SUERC-51675	129.5 cm	94.99 ± 0.43	413 ± 37	-28.1 ‰	1448-1525 (51.6%) 1535-1627 (43.8%)

4.2.1.3.5 SCB-1

Only one radiocarbon date was obtained for SCB-1 and the result is presented in table 4.5. OxCal was used to calibrate the conventional ^{14}C age and to provide the probability-based age distributions. As with some of the other radiocarbon ages with almost 100% modern ^{14}C enrichment, problems concerning the recent plateau in the calibration curve occur. This calibration results in very high age uncertainty at this

depth. As in SAN-EM-2 the ^{210}Pb age profile is particularly important from SCB-1 owing to problems arising from the dating of recent peat layers.

Table 4.5. Radiocarbon dating results from SCB-1.

Publication code	Depth	^{14}C Enrichment (% Modern ±1σ)	Conventional ^{14}C Age (years BP ±1σ)	δ^{13}C VPDB‰ ± 0.1	Calibrated age (AD) (Probability distribution)
SUERC-51676	76.5 cm	98.11 ± 0.45	153 ± 37	-27.6 ‰	1796-1950 (68%) 1672-1743 (26.3%) 1771-1779 (1.1%)

4.2.2 Lead (^{210}Pb) dating

4.2.2.1 Principles

Owing to the limitations of the method of radiocarbon dating particularly associated with the last 200 years, alternative methods must be used to date the surface layers of peat profiles.

The radioisotope ^{210}Pb (lead-210), a natural radionuclide within the ^{238}U decay series (table 4.6) and with a half-life of 22.26 years has the potential to date recent peat deposits. Lead 210 is usually undetectable after 7 half-lives (156.1 years) offering a potential tool for dating sediments that have accumulated during this time period. This method is reviewed by Le Roux and Marshall (2011). ^{238}U, present in land masses, decays to ^{222}Rn which diffuses into the atmosphere continuing the decay series to ^{210}Pb which is then removed from the atmosphere by precipitation (Appleby, 2001).

Table 4.6. The ^{238}U decay series.

	4.51x10^{9}years	1602 years	3.82 days	22.26 years	138.4 days	
^{238}U	>	^{226}Ra >	^{222}Rn >	^{210}Pb >	^{210}Po >	^{206}Pb

Radiogenic Pb fallout may be insufficient to conduct ^{210}Pb analysis in southern South America (Preiss *et al*., 1996). Areas where ^{222}Rn emissions and annual rainfall are high have the highest ^{210}Pb activity (Le Roux and Marshall, 2011).

The SWW and its control on precipitation poses a challenge for the use of this technique in its zone of influence. ^{210}Pb is depleted from air masses owing to higher deposition on the windward side of the Andes resulting in low ^{210}Pb activity on the leeward side (Le Roux and Marshall, 2011). Mean annual rainfall is also assumed to be constant in the supply of ^{210}Pb, so variability in mean annual rainfall potentially caused by migration and/or intensification of the SWW may limit the use of this method (Appleby, 2008).

Furthermore, the lack of continental landmass to the west of southern South America results in low concentration of ^{210}Pb in precipitation owing to the lack of diffusion of ^{222}Rn into the atmosphere (Appleby, 2008). Despite the low atmospheric fluxes particularly in Polar Regions there is evidence for success of this method (Appleby *et al*., 1995).

The mechanism by which ^{210}Pb can be used for dating sediments from terrestrial archives depends on the supply of the radioisotope either by supported ^{210}Pb (in-situ decay of ^{226}Ra) or unsupported ^{210}Pb (as above, from the atmospheric flux) (Appleby, 2001; Le Roux and Marshall, 2011).

^{210}Pb in peat is the unsupported fraction that binds to atmospheric particles, and falls onto land either as dry or wet deposition (precipitation). It is distributed on the peat surface and binds to organic matter by physical entrapment (Schnitzer, 1982); it is then buried with exponential radioactive decay over time enabling its use as a chronological tool (Appleby, 2001).

Water table fluctuation may affect the redox potential in peat and thus the post-depositional mobility of Pb (Oldfield *et al*., 1995; Clymo and Hayward, 1982) leading to potentially high ^{210}Pb activity around the zone of water table fluctuation (MacKenzie *et al.*, 1998). This is important to consider if the period spanning the last ~200 years is predicted to pass through the acrotelm-catotelm boundary/ zone of water table fluctuation. Despite this, Vile *et al.* (1999) find an absence of Pb mobility

in *Sphagnum* peat offering support for the immobilisation of ^{210}Pb once bound to *Sphagnum* capitula at the peat surface and this technique has been used successfully to resolve the age of recent peat deposits (De Vleeschouwer *et al.*, 2010b; Parry *et al.*, 2013).

4.2.2.2 Methods

^{210}Pb dating should always be used alongside other dating techniques (Oldfield *et al*., 1995) and is used in this investigation alongside radiocarbon dating and ^{137}Cs. ^{210}Pb activity can be measured by alpha, beta or gamma spectrometry (Turetsky *et al.*, 2004) and may form complementary analyses. Alpha spectrometry was able to provide surface chronologies of each core in this investigation although gamma spectrometry was initially used to enable simultaneous measurement of ^{210}Pb and ^{137}Cs.

Radioisotope analysis of the upper sections of the KAR-EM profiles was carried out using gamma spectrometry at the ISO9001: 2008 certified Plymouth University Consolidated Radioisotope Facility (CoRiF). The approximate depth necessary to encompass the potential range covered by ^{210}Pb dating was estimated using the initial age-depth models based on the rangefinder radiocarbon dates.

The sections were frozen and 10 cm sub-sections were extracted from the intact core and sub-sampled at 1 cm resolution using a bread knife whilst the sections were still frozen. The sample volumes were then measured using a Vernier caliper (De Vleeschouwer *et al.*, 2010a) for bulk density calculations (for use of the model for age calculation). Samples were placed in bags and their wet weight was recorded. They were frozen for 48 hours and freeze dried for ~72 hours and their dry weights recorded. The dried samples were then transferred to pre-weighed 50 ml petri dishes, which were packed full where possible, weighed to calculate final sample weight and sealed with insulating tape.

The samples were then left for 28 days to allow equilibration between ^{214}Pb and ^{226}Ra, necessary to calculate the fraction of supported ^{210}Pb potentially contained in atmospheric dust wind-transported to the peat surface (Appleby, 2001).

Total ^{210}Pb activity concentration was then determined through measurement of gamma ray emissions alongside ^{137}Cs, ^{214}Pb and ^{241}Am using a low-background EG&G ORTEC planar (GEM-FX8530-S N-type) Hyper Pure Germanium Gamma spectrometer. Calibration was carried out using a peat sample provided by Eckert and Ziegler Analytics and quality control was carried out using IAEA international standards. The samples were generally run for around 2 days (~160,000 seconds). The simultaneous measurement of other radionuclides alongside ^{210}Pb is an advantage of gamma analysis as well as its relatively short sample preparation time and the non-destructive nature of the technique (Ebaid and Khater, 2006). Activity needs to be sufficiently high at the surface to allow for analytical uncertainty (Le Roux and Marshall, 2011). If activity at the surface was 100 Bq kg^{-1} this would be reduced to 12.5 Bq kg^{-1} after 3 half-lives, which is lower than the typical analytical uncertainty.

The results are presented on a spectrum showing the number of photons emitted at a particular energy (^{210}Pb: 46.5keV, ^{241}Am: 59.5, ^{214}Pb: 352 keV, ^{137}Cs: 662 keV) given in the number of counts per channel in Bq kg^{-1} (Becquerel) (Appleby, 2001). The results of gamma analysis of the KAR-EM profiles are discussed in section 4.2.3.3.1. The results were omitted from the final age-depth models owing to activity concentrations being below the detection limit and high analytical uncertainty (>100% throughout the profiles).

Alpha spectrometry offers an alternative measurement for the application of ^{210}Pb dating of sediments in which ^{210}Pb concentrations are below the detection limit of gamma analysis. As shown in table 4.6, ^{210}Pb decays to ^{210}Po which decays to a stable state as ^{206}Pb by emission of an alpha particle (half-life of 138 days). Alpha spectrometry is sensitive to the alpha emissions from the decay of ^{210}Po which is measured as a proxy of ^{210}Pb (Le Roux and Marshall, 2011).

This technique requires laborious acid digestion resulting in the destruction of samples and although the simultaneous measurement of alternative radionuclides is not offered by the technique, the potential for calculation of ^{210}Pb activity for use with dating models warrants its use (Holynska *et al*., 1998; Fiałkiewicz-Kozieł *et al.*, 2014).

Preparation and analysis using alpha spectrometry was carried out at Exeter University. The same samples prepared for and analysed using gamma spectrometry were used for alpha analysis. For each sample ~0.5 g of the peat powder was weighed into pre-labelled glass beakers and 1 ml of ^{209}Po spike was added (to ensure no loss of ^{210}Po during sample preparation). To break down organic matter 10 ml of concentrated nitric acid (HNO3) was added and the samples were brought to dryness on a hotplate. 10 ml of 30% Hydrogen peroxide (H_2O_2) was added and left on a low heat for an hour, the heat was then increased and the samples were brought to dryness. 5 ml of 6M hydrochloric acid (HCL) was added and brought to dryness, this step was repeated once. 5 ml of 6M HCL was added to each sample before each sample was washed into centrifuge tubes using 0.5M HCL. The samples were centrifuged and the supernatant was poured into plating jars containing pre-prepared suspended silver planchets. The jars were filled with 0.5M HCL and 0.2 g of ascorbic acid was added (Method modified by N. Sanderson (University of Exeter)). The jars were left on a magnetic stirring table for 24 hours to ensure deposition of ^{210}Po on the planchets. Planchets were measured in an alpha counter for a minimum of 24 hours and until a minimum of 400 counts had been reached.

4.2.2.3 Lead 210 results

This section presents the results from both gamma and alpha analysis using Lead210 and the process to age calculation for use in the ultimate age-depth models presented at the end of this chapter.

4.2.3.3.1 Gamma results

Gamma analysis offered the potential of synchronous ^{210}Pb, ^{214}Pb, ^{137}Cs and ^{241}Am measurement. The ^{210}Pb excess records from the KAR-EM profiles are presented in figure 4.1. The ^{210}Pb excess was calculated by subtracting the supported ^{210}Pb (via measurement of ^{214}Pb) from the total ^{210}Pb activity concentration to give the unsupported ^{210}Pb fraction.

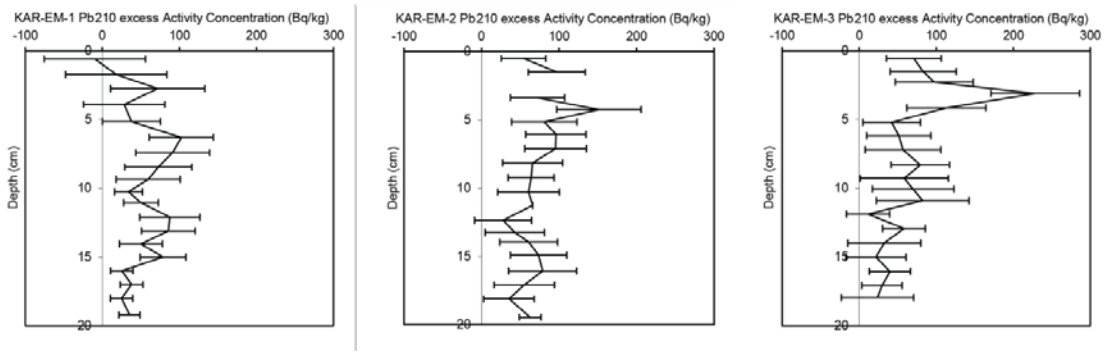

Figure 4.1. The ^{210}Pb excess records from the KAR-EM profiles using gamma analysis.

For use with age calculation ^{210}Pb activity must be sufficient at the surface (Le Roux and Marshall, 2011). In previous studies, using this technique on ombrotrophic peatlands located in granitic landscapes, values of 1000±100 Bq kg^{-1} are evident (Parry *et al*., 2013). Below the surface, an exponential curve is required, at the end of which total ^{210}Pb excess reaches 0 where there is equilibrium between ^{226}Ra (^{214}Pb) and ^{210}Pb (Noller, 2000). Uncertainties associated with gamma counting are usually around ±15-25 Bq kg^{-1} and where activity concentrations are low the uncertainty is too high for use with age calculation models. As displayed in figure 4.1 none of the profiles has high activity concentrations at the surface and rather increases are evident just below the surface. Moreover, the associated uncertainties are regularly ~60 Bq kg^{-1} much higher than the generally accepted analytical error. ^{210}Pb analysis was reported to be unsuccessful at a nearby site, Andorra bog owing to low radon source in the region (Chambers *et al.*, 2014). Low overall concentrations and high uncertainties resulted in the refutation of the KAR-EM ^{210}Pb records using gamma analysis.

^{210}Pb dates may be validated by pinpointing the ^{137}Cs peak (AD 1964 (Olsson, 1986)) and accompanying increases of ^{241}Am. Nuclear weapons testing resulted in deposition of these fallout radionuclides which may have been incorporated into terrestrial records (Appleby, 2001). Despite the refutation of the ^{210}Pb records, simultaneous measurement of ^{137}Cs was possible and the ^{137}Cs records from the KAR-EM and SAN-EM profiles are presented in figure 4.2.

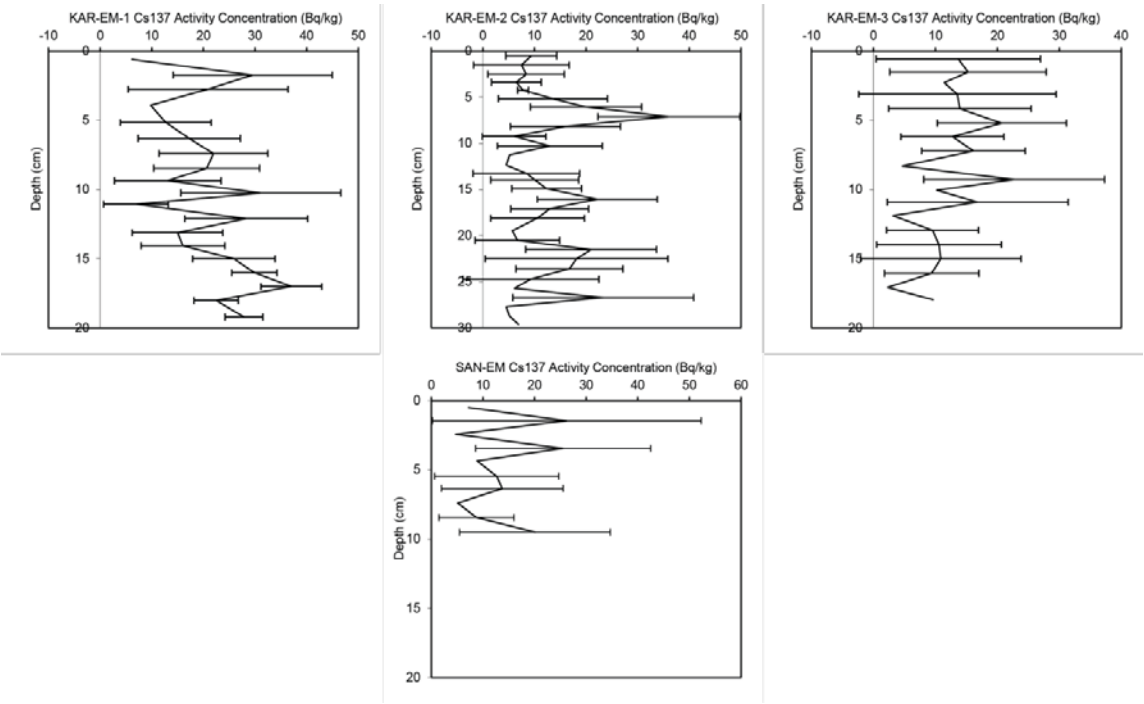

Figure 4.2. ^{137}Cs records from KAR-EM profiles and SAN-EM-2 using gamma analysis.

In Northern Hemisphere peatlands high ^{137}Cs activity concentrations around the caesium peak are expected (Cambray *et al*., 1980) in order to be used as a calibration point, often reaching levels around 120±20 Bq kg^{-1} (Parry *et al*., 2013). Relatively low ^{137}Cs activity concentrations are found across the three KAR-EM profiles and SAN-EM profile. This may be due to the less prominent ^{137}Cs spike in the Southern Hemisphere, although it is has been used successfully in the Southern Hemisphere (Walling and Quine, 1992; Hancock *et al.*, 2011). A potential caesium peak is evident in KAR-EM-2 around 7 cm depth although this is not present in the other two profiles. The maximum peak of ^{137}Cs activity has been assigned to AD 1965 (Walling and Quine, 1995) suggesting that this peak could date to AD 1965. Whether it is plausible for 7 cm growth in 50 years must be assessed (section 6.3). The activity concentrations of ^{241}Am were below the detection limit throughout the profiles and cannot be used for validation of the caesium peak. For correct calibration, uncertainties of 50% or less are expected; however, uncertainties higher than 100% are clear throughout the three records. Moreover, there is high variability in activity concentrations. Although caesium particulate matter can be bound to

Sphagnum tissue by cation exchange (Dragovic *et al.*, 2004; Vinichuk *et al.,* 2011) it is soluble and thus mobile in peat (MacKenzie *et al.,* 1998).

It was intended to carry out a multi-profile analysis of the KAR-EM ^{210}Pb and ^{137}Cs records as has been done at Northern Hemisphere sites (Rosén *et al*., 2009; Parry *et al*., 2013; Van der Plicht *et al*., 2013) but due to low concentrations and high uncertainties this has not been possible using gamma analysis.

4.2.3.3.2 Alpha results

Alpha spectrometry measures the ^{209}Po and ^{210}Pb counts. The corrected ^{210}Pb is then divided by the corrected ^{209}Po. This value is multiplied by the result of the division of the ^{209}Po spike specific activity (91.77 mBq) by the dry weight of each sample to give the ^{210}Pb activity (Bq kg^{-1}) of each sample. The ^{210}Pb activity records from each profile are presented in figure 4.3.

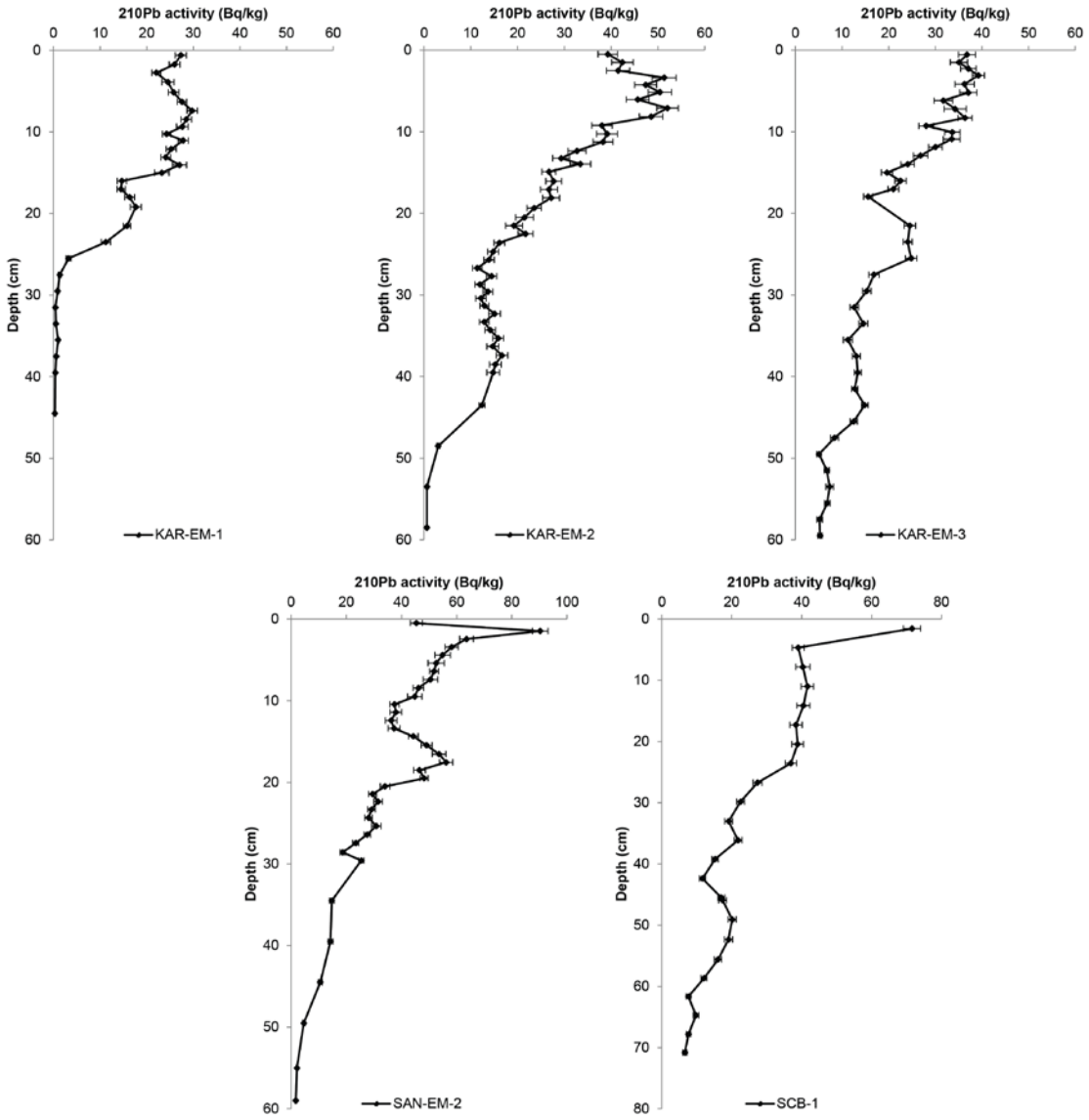

Figure 4.3. The ^{210}Pb activity records from KAR-EM-1, KAR-EM-2, KAR-EM-3, SAN-EM-2 and SCB-1 using alpha analysis.

^{210}Pb concentrations are low at the surface of all profiles as is expected for low radon source areas (Appleby, 2008) but a clear exponential curve is displayed in each profile with low uncertainties. In KAR-EM-3 ^{210}Pb activity is ~37 Bq kg^{-1} at the surface, decreasing to ~30 Bq kg^{-1} at 12 cm, further decreasing to 15 Bq kg^{-1} to 28 cm and decreases to ~10 Bq kg^{-1} at 45 cm. Below 50 cm ^{210}Pb activity drops to ~5 Bq kg^{-1} and remains at this level until the base of sampling depth; as such this level is chosen as the equilibrium depth (A(0)). In KAR-EM-2 ^{210}Pb activity is ~40 Bq kg^{-1} at the surface, there is a slight increase to ~52 Bq kg^{-1} at 7 cm but below this values decrease steadily from 40 to 20 Bq kg^{-1} between 10 and 20 cm. Below 20 cm activity

is around 10 Bq kg^{-1}, decreasing to below 10 Bq kg^{-1} after 40 cm. Activity is close to 0 below 54 cm and this is set as the equilibrium depth. In KAR-EM-1 activity is ~27 Bq kg^{-1} at the surface increasing slightly to 30 Bq kg^{-1} at 7 cm. There is a slight decrease until 15 cm, a more rapid decrease to ~15 Bq kg^{-1}, followed by a further decrease to values close to 0 after 30 cm. The equilibrium depth in this profile is taken as the average of ^{210}Pb activity from samples below this depth until the base. Activity at the surface of KAR-EM-3 and KAR-EM-2 are similar (37 and 40 Bq kg^{-1} respectively) and the two profiles have similar equilibrium depths (50 and 54 cm respectively). Activity at the surface of KAR-EM-1 is lower (27 Bq kg^{-1}) and the equilibrium depth is also lower (average below 60 cm) than the other profiles. This suggests differential accumulation rates across the microtopography.

In SAN-EM-2 ^{210}Pb activity is ~45 Bq kg^{-1} at the surface increasing to 90 Bq kg^{-1} just below the surface. After this there is a decrease in activity to 37 Bq kg^{-1} at 10 cm, an increase to ~56 Bq kg^{-1} with activity decreasing below this to 25 Bq kg^{-1} at 30 cm. Activity decreases gradually until reaching a value close to 0 at 60 cm, set as the equilibrium depth. In SCB-1 activity is ~72 Bq kg^{-1} decreasing to ~40 Bq kg^{-1} immediately below this. Activity remains at this level until 22 cm, below this, activity decreases to ~15 Bq kg^{-1} at 40 cm reaching a fairly uniform level below 63 cm. 72 cm has been set as the equilibrium depth despite the activity at this level being ~6 Bq kg^{-1}. Reaching values closer to 0 is preferable (see section 4.2.3.3.3) but was not possible here. Regional differences in ^{210}Pb activity are evident between the different sites with slightly higher activity in the surface of SAN-EM-2 compared with the KAR-EM profiles and a significantly higher activity at the surface of SCB-1.

4.2.3.3.3 Age calculation

The most common model for age calculation using ^{210}Pb activity is the Constant Rate of Supply (CRS) model (Appleby and Oldfield, 1978; Appleby *et al.*, 1979), which assumes that the ^{210}Pb flux has remained the same through time whilst sediment accumulation may have varied.

For a full explanation of the equations used in the CRS model the reader is referred to Appleby (2001). Firstly, **m (x)** the cumulative dry mass (g cm^{-2}) is calculated for

the section of the core below the level to be dated using the bulk density measurements. **C(x)** the cumulative unsupported ^{210}Pb (Bq kg^{-1}) is calculated by subtracting **A(0)** (the ^{210}Pb activity at **x(eq)** the depth of equilibrium) from the ^{210}Pb activity of contiguous samples above this depth. **x(eq)** is the depth at which there is secular equilibrium between the unsupported (^{210}Pb) and supported (^{209}Po) fractions at a constant level and must be carefully selected. **Â(x)**, the total unsupported ^{210}Pb inventory, is then calculated using **m(x)** (Bq kg^{-1}) and **C(x)** (g cm^{-2}) with the results multiplied by 10 to give units in Bq m^{-2}. **A(x)**, the residual unsupported ^{210}Pb, is calculated by subtracting **Â(x)** from **A(0)**. Age is calculated using the following formula: 1/**^{210}Pb decay constant***natural logarithm (**A(0)**/**A(x)**). Age is then subtracted from the year of coring to give the year of each sample.

Age calculations of the ^{210}Pb activity profiles were carried out using the CRS model. The resulting ^{210}Pb age-depth profiles from each core are presented in figure 4.4 and figure 4.6. The KAR-EM-3 profile extends 151 years to AD 1862 and the KAR-EM-1 profile extends 146 years to AD 1867. The KAR-EM-2 profile extends comparably less than the other profiles to AD 1909. The potential ^{137}Cs peak at 7 cm can be disregarded as the age calculated for this depth is AD 2003 with AD 1965 located ~30 cm.

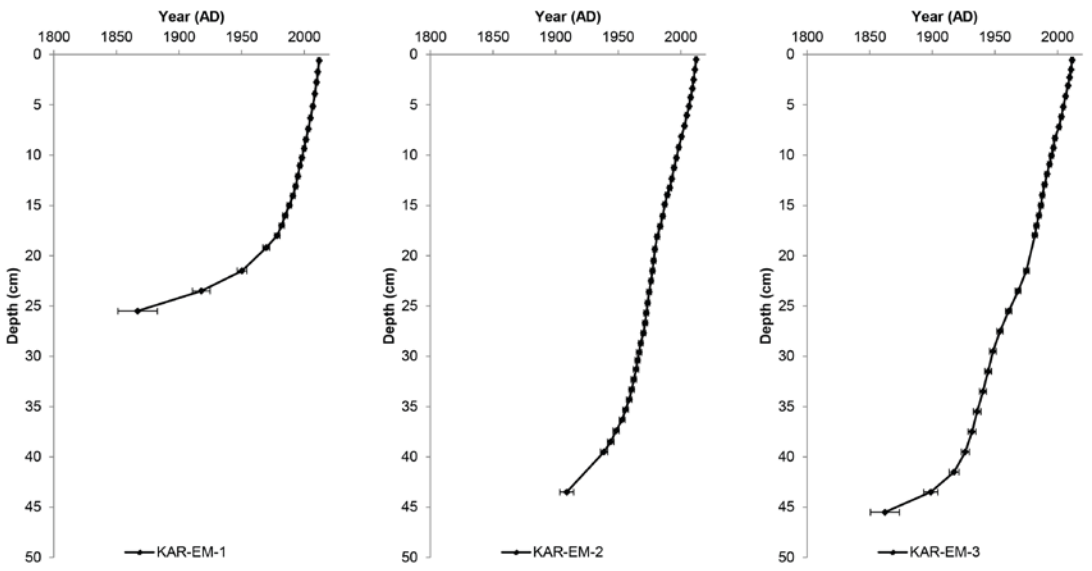

Figure 4.4. The ^{210}Pb age-depth profiles from KAR-EM-1, KAR-EM-2 and KAR-EM-3.

The comparison of the three profiles in figure 4.5 reveals a similar accumulation rate of ~1.76 yr/cm from the surface until 17 cm (~AD 1983) in all three profiles. Below this depth the accumulation differs between the profiles. In KAR-EM-3 between 17 and 41 cm accumulation is ~2.67 yr/cm, slowing to 13.75 yr/cm between 41 and 45 cm. In KAR-EM-2 between 17-34 cm is ~1.47 yr/cm slowing to 5.56 yr/cm between 34 and 43 cm. In KAR-EM-1 between 17 and 25 cm the accumulation rate is much slower than the other two profiles at 15.86 yr/cm.

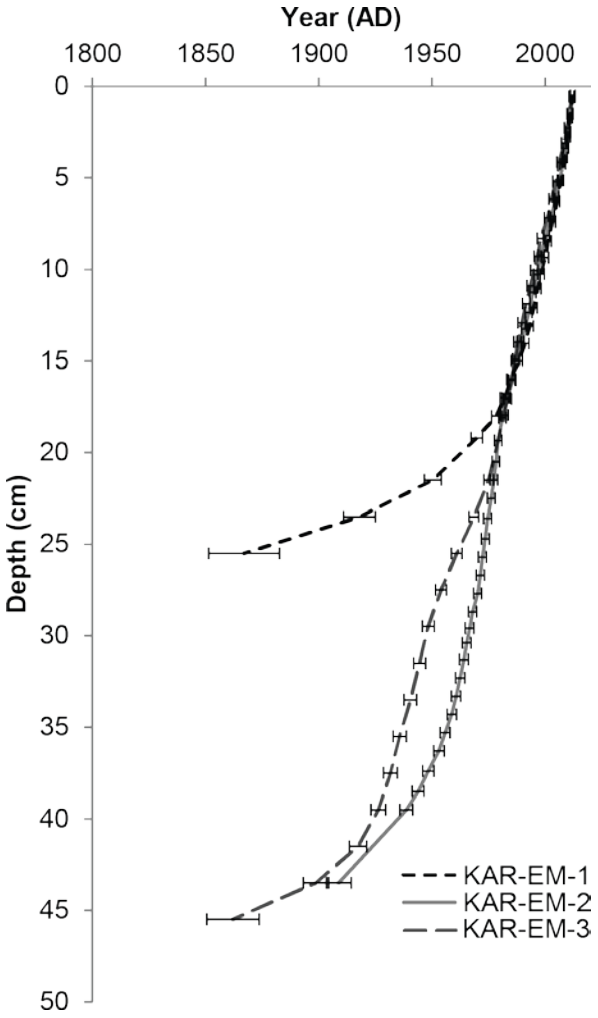

Figure 4.5. Comparison of the KAR-EM ^{210}Pb age-depth profiles.

The SAN-EM-2 profile extends 150 years to AD 1863 and accumulates steadily to this point. The SCB-1 profile is the longest record extending 197 years to AD 1817.

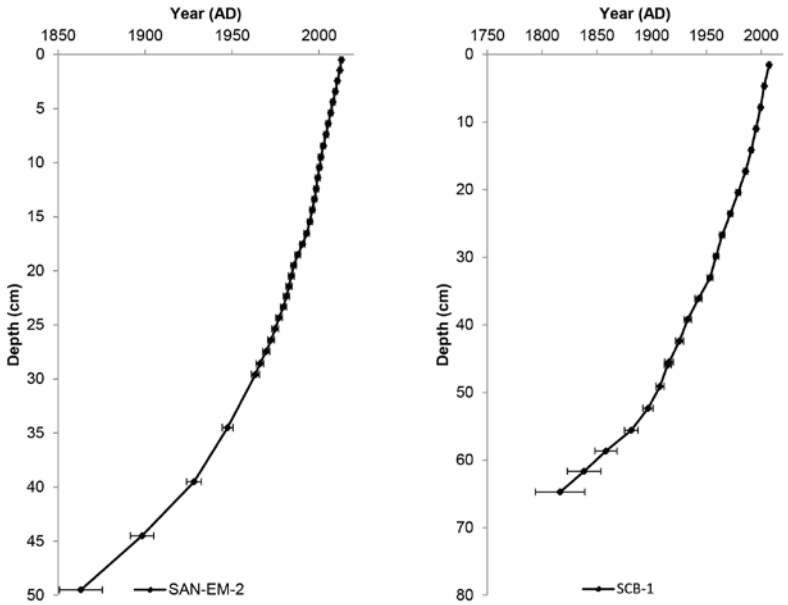

Figure 4.6. The ^{210}Pb age-depth profiles from SAN-EM-2 and SCB-1.

The calculated ages can be incorporated into the final age-depth models using the calibrated radiocarbon ages. Development of these models for each profile will be discussed in the next section.

4.3 Age-depth modelling

The development of age-depth models of the profiles in this investigation relied on the ^{14}C and ^{210}Pb results as presented in the previous sections. This section presents the process carried out to reach the final age-depth models for each profile to provide a chronology against which the proxy records can be assessed. Bacon in R (Blaauw and Christen, 2011) has been used to develop the final age-depth models for each profile. The KAR-EM age-depth models are first presented followed by the age-depth models from SAN-EM-2 and SCB-1. Finally, the KAR-EM age-depth models are compared to provide the context for the multi-profile comparison of proxy records and the age-depth models from all profiles are compared to provide the context for the multi-site aspect of the investigation. Appendix III displays alternative age-depth models for the Karukinka profiles which exclude the ^{210}Pb ages and one 14C date from KAR-EM-3 and the implications on the final interpretation are discussed.

4.3.1 KAR-EM-3

As discussed in section 4.2.1.3.1 inconsistencies are evident between the radiocarbon ages from KAR-EM-3. Three age-depth models were subsequently produced using the different combinations of ^{14}C ages alongside the ^{210}Pb ages presented in section 4.2.3.3.2.

All received ^{14}C ages were included in the first model, presented in figure 4.7. Development of age-depth models in Bacon relies on prior information about peat accumulation rate and memory between calibrated radiocarbon ages. The green curves are the priors for accumulation rate (years per cm) and memory, Blaauw and Mauquoy (2012) was followed as an example of these priors. Shown in red text, mean accumulation was set to 10 years per cm with a shape of 1.5; this is a relatively strong constraint on this accumulation rate (constraint can be up to 2) as peat accumulation rates of around 10 years per cm are common in the region (Pendall *et al.*, 2001; Mauquoy *et al.*, 2004). Mean memory of accumulation rate can be set between 0 (0% memory) to 1 (100% memory) between levels. Prior information about memory between levels is difficult to ascertain so this was set to a

midpoint of 0.5 (50%) memory and memory strength was set to 4 (strong constraint on mean memory). The respective grey histograms show the posterior distributions for accumulation rate and memory. Various combinations of accumulation rate and memory were tested, the best model resulting in the best agreement between the prior and posterior distributions.

The dark blue distributions show the 5 calibrated ^{14}C dates with the turquoise distributions showing the modelled ^{210}Pb ages. The red line connecting the calibrated ages is the weighted mean age of ~6000 iterations (top left graph of MCMC iterations) with the outer dashed lines showing the 95% confidence intervals (2σ).

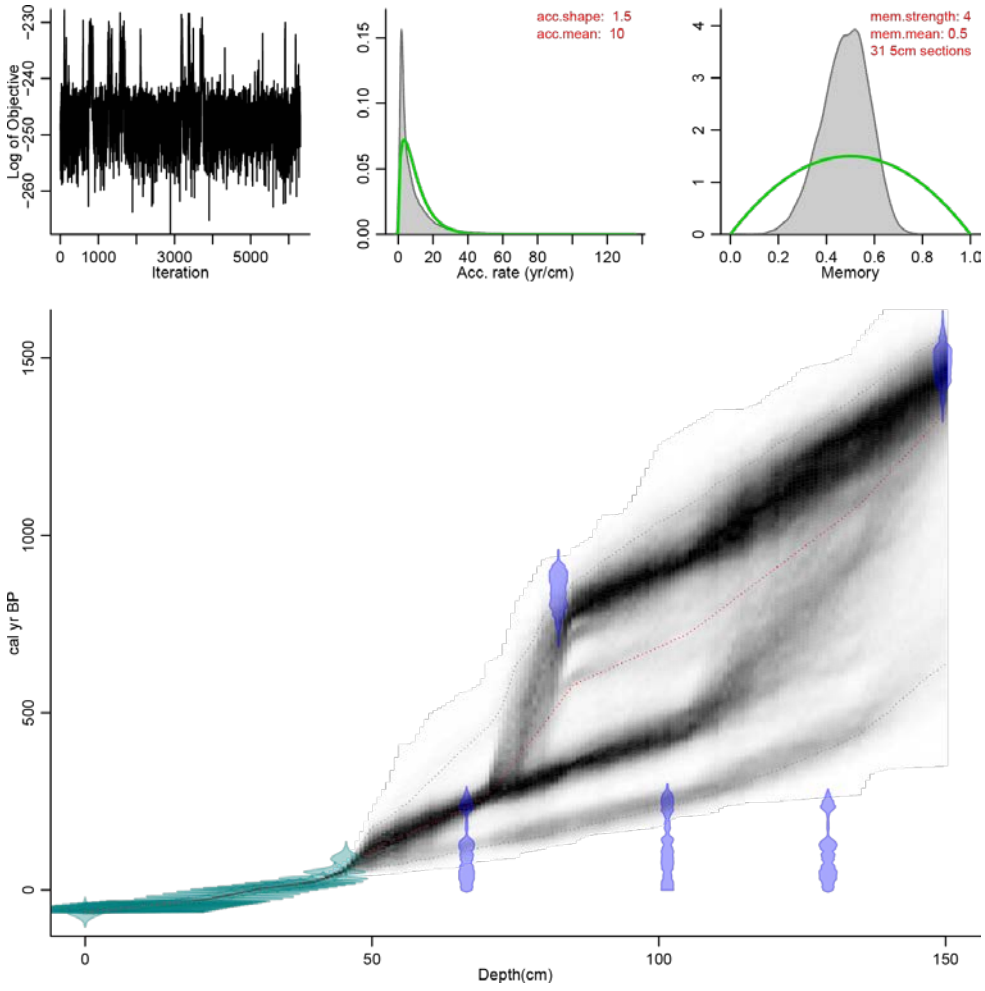

Figure 4.7. The initial age-depth model including all ^{210}Pb ages and all ^{14}C ages from KAR-EM-3 (KAREM3ALL).

The dates from 101.5 cm and 129.5 cm appear to be outliers with the calibrated ages at these levels similar to the date at 66.5 cm owing to the plateau on the calibration curve. The ^{210}Pb ages suggest that the model follows an increasing trajectory just before 50 cm forcing the weighted mean through the less probable section of the probability distribution of the calibrated age at 66.5 cm. After this the model chooses the date at 82.5 cm as the most probable based on the prior information and the age at the base (149.5 cm). The model attempts to include the younger ages resulting in high uncertainty (grey shading) around the weighted mean particularly towards the younger section of the uncertainty. Exclusion of the dates at 101.5 cm and 129.5 cm seems the most likely scenario as these dates would suggest unrealistically fast accumulation rates however, it may be that the relatively older date at 82.5 cm is an outlier. This potential outlier has been removed from the model in figure 4.8.

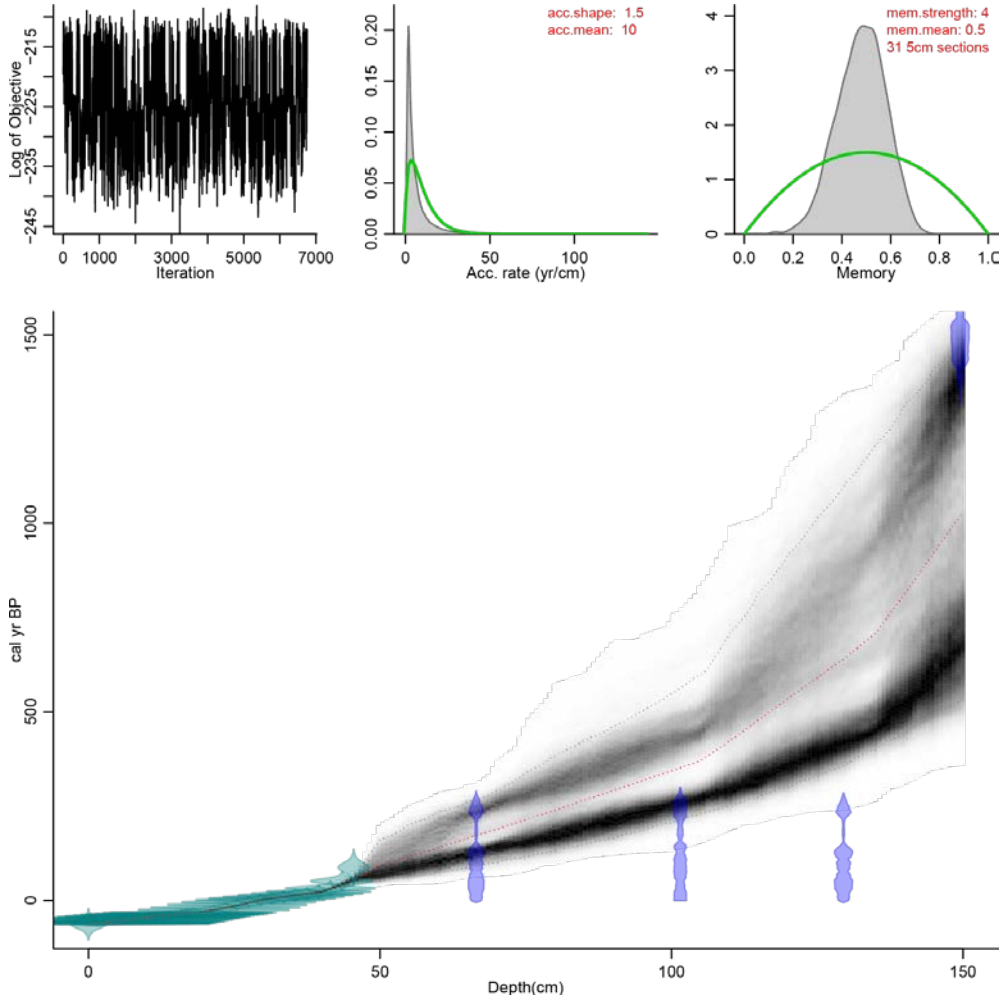

Figure 4.8. The second age-depth model including all ^{210}Pb ages and ^{14}C ages, excluding the potential outlier, 971±37 ^{14}C BP. (KAREM3 outlier removed).

Removing the older date from the model results in relatively lower uncertainty around the weighted mean between 50 and 110 cm; however, the basal age does not allow the weighted mean to pass through the date at 129.5 cm and results in higher uncertainty between 110 and 150 cm than the rest of the model. The trajectory of the ^{210}Pb age profile would suggest that a uniform accumulation towards the base of the profile is more likely rather than rapid accumulation until 129.5 cm followed by a sharp 'elbow' and extremely slow accumulation over the remaining 20 cm. The final age-depth model, therefore, excluded the dates at 101.5 cm and 129.5 cm and included the date from 82.5 cm (figure 4.9).

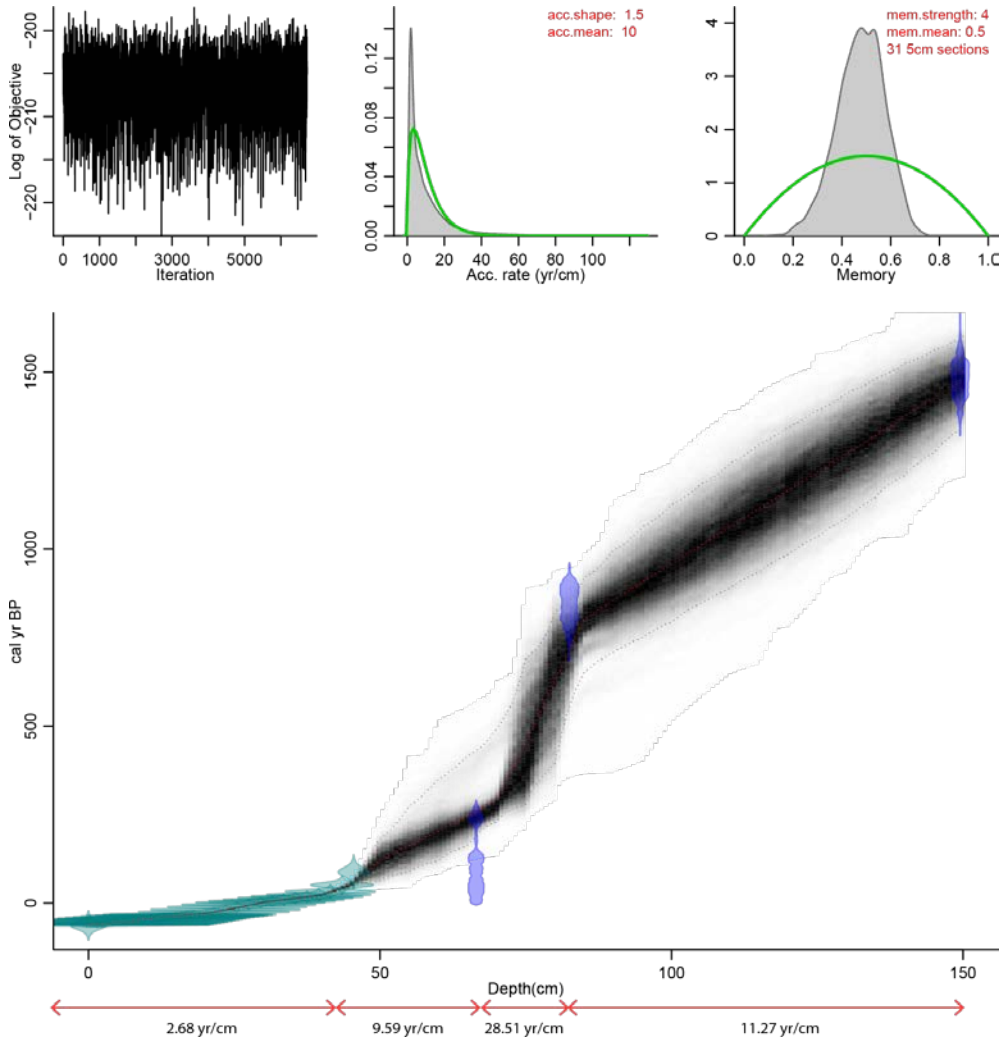

Figure 4.9. The final age-depth model including all ^{210}Pb ages and ^{14}C ages from KAR-EM-3, excluding the outliers 161±35 and 114±35 ^{14}C BP. Red arrows beneath the model show calculated accumulation rates throughout the profile. (KAREM3FINAL).

Table 4.7. Radiocarbon dates and OxCal calibrated ages from KAR-EM-3. The weighted mean and range of ages based on the final Bacon age-depth model (figure 4.9) are presented.

Depth	**Conventional ^{14}C Age (years BP ±1σ)**	**Calibrated age (AD) (Probability distribution)**	**Bacon age estimates**	
			Weighted mean (AD)	Range (AD) (95% error)
66.5 cm	122 ± 37	1803-1950 (77.3%) 1685-1730 (18.1%)	1690	1619-1860
82.5 cm	971 ± 37	1026-1190 (95.4%)	1234	1082-1369
101.5 cm	161 ± 35	1796-1950 (64.1%) 1672-1744 (27.9%) 1759-1780 (3.4%)	974	819-1133
129.5 cm	114 ± 35	1805-1950 (79.8%) 1691-1728 (15.6%)	683	510-843
149.5 cm	1637 ± 37	382-548 (93.9%) 560-570 (1.5%)	478	341-601

Exclusion of the two outliers results in a more realistic age-depth model with relatively more uniform accumulation and much lower age uncertainties than the previous models. The calculated mean accumulation rates are shown in figure 4.9. From the base until 82 cm the accumulation rate is ~11 years per cm; the weighted mean line traverses the younger section of the calibrated age range after which accumulation slows to ~29 years per cm until 66 cm, when the weighted mean traverses the older section of the calibrated age range. The accumulation rate is ~10 years per cm until the beginning of the ^{210}Pb age profile, after which accumulation until the surface is faster at ~2 years per cm.

Table 4.7 compares the conventional ^{14}C ages, the original probability-based age ranges calibrated using OxCal and the age estimates for all depths from which ^{14}C ages were obtained. The exclusion of the outliers resulted in older age ranges at 101.5 cm and 129.5 cm compared with the original calibrated ages. This material consisting of *Sphagnum* remains has most likely been dragged down from the surface especially as both samples were taken from the lower Russian core section (KAR-EM-3C). The Bacon age estimates differ from the original calibrated ages from the remaining samples owing to the influence of the ^{210}Pb age profile and the accumulation rate prior information on the final age-depth model. The weighted mean traverses the calibrated ages based on this information, which appears to be a realistic representation of accumulation in this profile.

After selection of the final age-depth model the model output can be used to infer the ages at which proxy observations are available. The default age output in Bacon is in cal BP (as shown by the age-depth model figure); these ages are converted to years AD/BC with reference to AD 1950 with associated errors in figure 4.10 at 0.5 cm resolution.

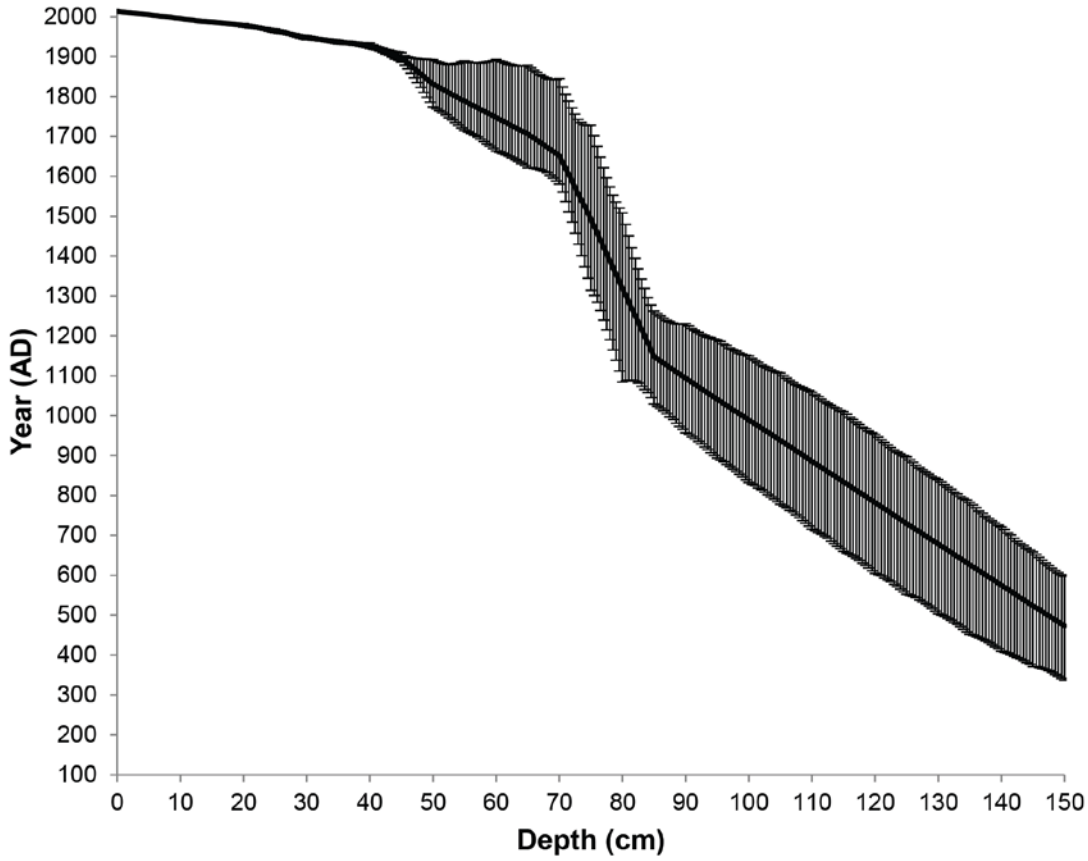

Figure 4.10. The KAR-EM-3 age-depth profile converted to years AD at 0.5 cm resolution with 95% confidence intervals displayed.

Further to figure 4.9, figure 4.10 displays the variable accumulation rates throughout the profile with the slowdown in accumulation between 82 and 66 cm. Uncertainties are high around the weighted mean age line with an average uncertainty of ±140 years throughout the profile until the beginning of the ^{210}Pb ages where uncertainty averages ±3 years. Further to this the ages from depths at which proxy observations are available can be inferred to inform on the timing of variability throughout the record. The proxy data are plotted against the inferred ages from the chronologies presented in this chapter throughout chapters 6 and 7.

4.3.2 KAR-EM-2

The absence of age reversals and outliers in the ^{14}C ages from KAR-EM-2 resulted in direct incorporation of all ages in the final age-depth model (figure 4.11).

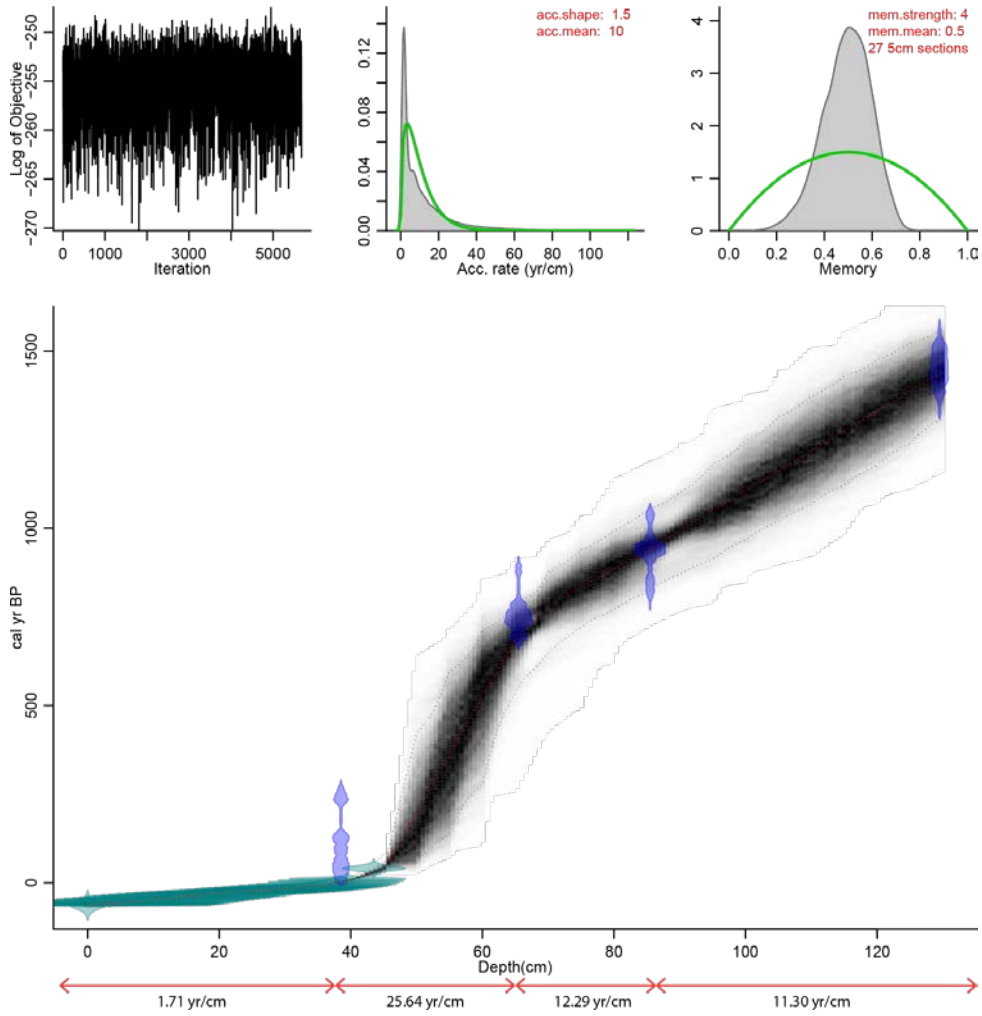

Figure 4.11. The final age-depth model including all ^{210}Pb ages and ^{14}C ages from KAR-EM-2. Red arrows beneath the model show calculated accumulation rates throughout the profile.

Table 4.8. Radiocarbon dates and OxCal calibrated ages from KAR-EM-2. The weighted mean and range of ages based on the final Bacon age-depth model (figure 4.11) are presented.

Depth	**Conventional ^{14}C Age (years BP ±1σ)**	**Calibrated age (AD) (Probability distribution)**	**Bacon age estimates**	
			Weighted mean (AD)	Range (AD) (95% error)
38.5 cm	118 ± 37	1804-1950 (78.1%) 1687-1729 (17.3%)	1947	1944-1950
65.5 cm	882 ± 37	1148-1274 (94.5%) 1070-1077 (0.9%)	1255	1109-1353
85.5 cm	1075 ± 37	962-1050 (76.3%)	1009	896-1121
129.5 cm	1603 ± 37	415-584 (95.4%)	512	378-632

As discussed in section 4.3.1 each model was run using various combinations of prior information and the prior information was kept uniform across the KAR-EM profiles for consistency, despite differential accumulation rates expected across the microtopography. This combination of prior information resulted in the best agreement between the prior and posterior distributions and a reasonable age-depth model with realistic accumulation rates resulted (figure 4.11). The four calibrated ^{14}C dates are shown by the dark blue distributions and the ^{210}Pb ages are shown by the turquoise distributions. The weighted mean age (red dashed line) resulting from >5000 iterations runs through the shaded grey area with the dashed lines delimiting 95% confidence intervals (2σ).

The mean accumulation rates, shown below the age-depth model, demonstrate a steady accumulation of around 12 years per cm from the base to 66 cm with the weighted mean line passing through the highest probability distribution at 85 cm and the younger section of the calibrated age distribution at 66 cm. After this the accumulation rate slows to 26 years per cm until 39 cm. The weighted mean line is forced through the youngest section of the calibrated age at 39 cm owing to the influence of the ^{210}Pb age profile but is still within the probability based age range of this depth. Between 39 cm and the surface more rapid accumulation of 2 years per cm is evident.

The conventional ^{14}C ages, the original probability-based age ranges calibrated using OxCal and the age estimates for all depths from which ^{14}C ages were obtained are compared in table 4.8. All of the weighted mean ages calculated in Bacon are

within the original calibrated ages and the final age-depth model provides a likely representation of peat accumulation in this profile.

The model output from the final age-depth model in Bacon has been converted from cal. BP to years AD/BC with reference to AD 1950 in figure 4.12. Ages have been inferred at 0.5 cm resolution and the 95% confidence intervals are displayed.

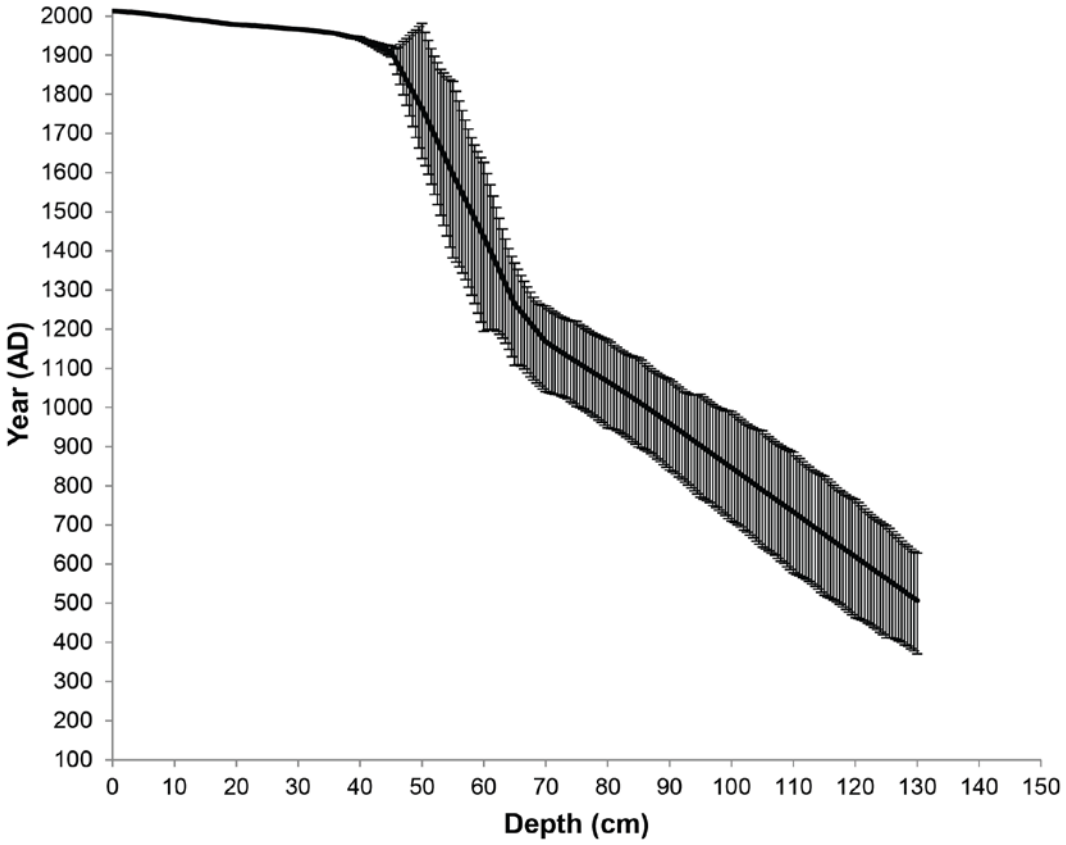

Figure 4.12. The KAR-EM-2 age-depth profile converted to years AD at 0.5 cm resolution with 95% confidence intervals displayed.

Figure 4.12 further displays the slowdown in accumulation rate between 66-39 cm with the average age uncertainty around the weighted mean age line decreasing from ±130 years throughout the majority of the profile to ±2 years from ~50 cm to the surface. Ages can be inferred using the model output to estimate the timing of variability in proxy records. The proxy records are, thus, plotted against age in chapters 6 and 7.

4.3.3 KAR-EM-1

All ^{14}C and ^{210}Pb ages were incorporated in the final age-depth model (figure 4.13) including the sample (14.5 cm) that returned a >100% modern ^{14}C enrichment result. The p.MC.age function produced a conventional ^{14}C age for this depth of -865±37 and using the Southern Hemisphere post-bomb calibration curve (SHZ1_2; Hua *et al.*, 2013) this age was incorporated into the final age-depth model.

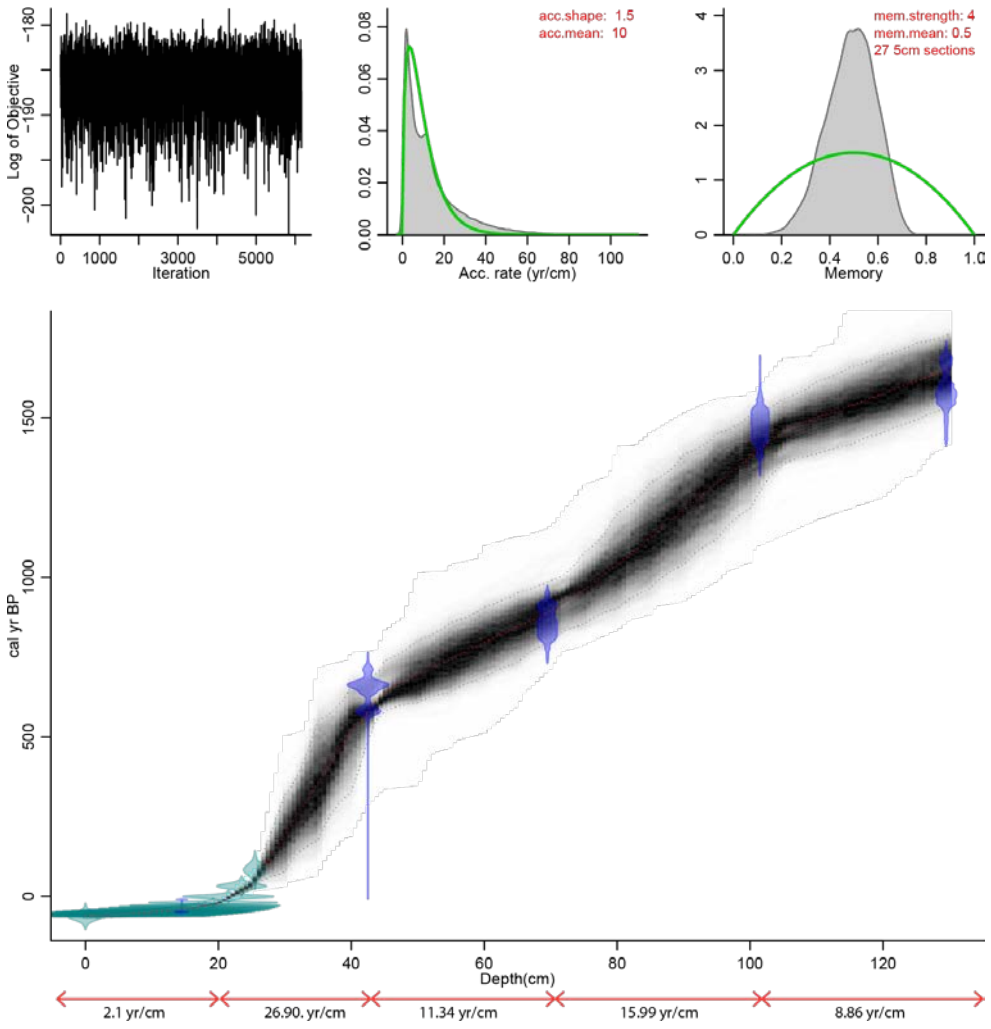

Figure 4.13. The final age-depth model including all ^{210}Pb ages and ^{14}C ages from KAR-EM-1. Red arrows beneath the model show calculated accumulation rates throughout the profile.

Table 4.9. Radiocarbon dates and OxCal calibrated ages from KAR-EM-1. The weighted mean and range of ages based on the final Bacon age-depth model (figure 4.13) are presented. The age estimate from 14.5 cm is displayed in red, derived using the p.MC.age function in Bacon.

Depth	**Conventional ^{14}C Age (years BP ±1σ)**	**Calibrated age (AD) (Probability distribution)**	**Bacon age estimates**	
			Weighted mean (AD)	Range (AD) (95% error)
14.5 cm	-865 ± 37	n/a	1991	1989-1993
42.5 cm	749 ± 35	1261-1321 (64.1%) 1350-1387 (26.4%)	1366	1323-1421
69.5 cm	1005 ± 35	1017-1160 (95.4%)	1060	961-1156
101.5 cm	1632 ± 37	387-549 (93.2%)	548	413-667
129.5 cm	1719 ± 37	246-437 (95.4%)	300	184-410

The same prior information was applied to this profile as in the other KAR-EM profiles resulting in the best agreement between the prior and posterior distributions. The resulting age-depth model suggests that the prior information was appropriate with realistic and smooth accumulation rates evident. The dark blue distributions are the 5 calibrated ^{14}C dates and the ^{210}Pb ages are displayed by the turquoise distributions. >6000 iterations resulted in the weighted mean age (red dashed line) traversing the calibrated ^{14}C ages with the grey shaded area delimited by the 95% confidence intervals (2σ).

The accumulation rates shown below the age-depth model are fairly uniform between the base of the core until around 43 cm depth at an average rate of 12 years per cm. The weighted mean age line is forced through a relatively young section of the calibrated age at 42.5 cm despite lower probability in response to the prior information. The probability distribution of this date extends to 0 (1950); as shown in table 4.9 the total probability distribution of this age is equal to 90.5%, whereas the remaining distribution although of a low probability may be an age extending to 1950. The accumulation rate slows to an average of 27 years per cm until 20 cm after which accumulation is rapid to the surface at an average rate of 2 years per cm.

Table 4.9 displays the conventional ^{14}C ages, the original probability based age ranges calibrated using OxCal and the age estimates for all depths from which ^{14}C ages were obtained. The weighted mean ages from Bacon are all within the range of

the original calibrated ages and the ultimate age from 14.5 cm fits well with the ^{210}Pb age profile with the weighted mean age line passing through this date. The final-age-depth model represents a realistic and steadily accumulating peat profile.

The cal. BP model output has been converted to years AD/BC in figure 4.14. Ages are inferred at a resolution of 0.5 cm and the 95% confidence intervals are displayed.

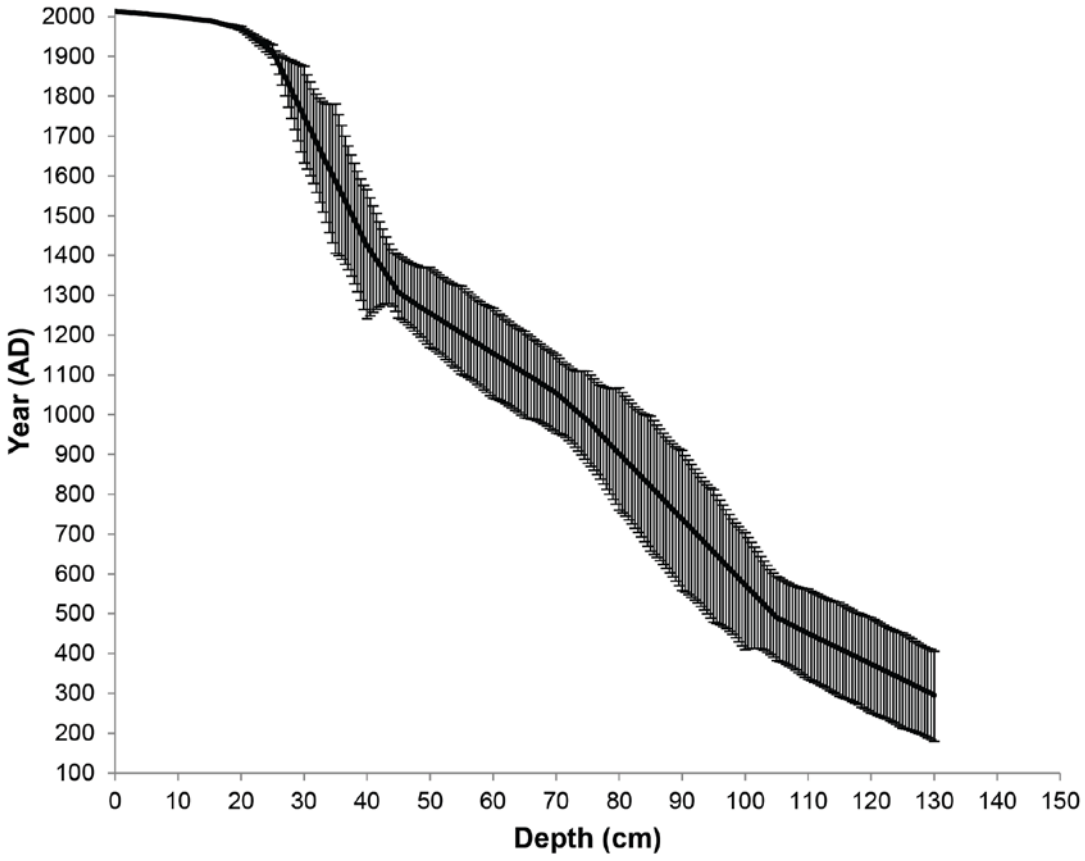

Figure 4.14. The KAR-EM-1 age-depth profile converted to years AD at 0.5 cm resolution with 95% confidence intervals displayed.

Figure 4.14 further displays the slowdown in accumulation between 44-20 cm in this profile. Uncertainty around the weighted mean age line is high throughout the majority of the profile at ±120 years until ~20 cm when it decreases to ±2 years

through the ^{210}Pb age profile. The model output is then used in chapters 6 and 7 throughout which the proxy records are plotted against age.

4.3.4 SAN-EM-2

The ^{14}C age at the base and all ^{210}Pb ages were incorporated in the final age-depth model from SAN-EM-2 (figure 4.15).

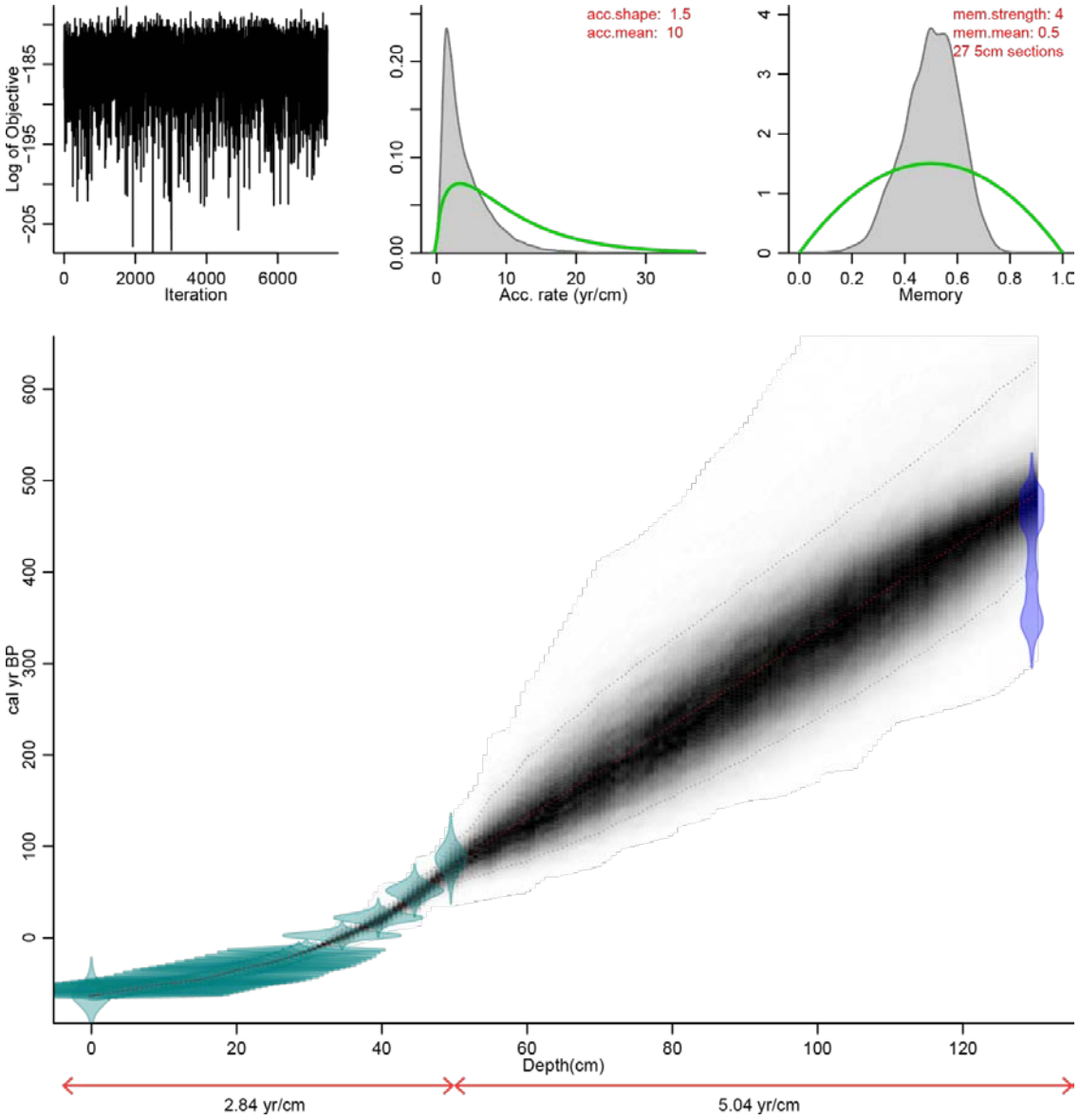

Figure 4.15. The final age-depth model including all ^{210}Pb ages and the ^{14}C age from SAN-EM-2. Red arrows beneath the model show calculated accumulation rates throughout the profile.

Table 4.10. Radiocarbon date and OxCal calibrated ranges from SAN-EM-2. The weighted mean and range of ages based on the final Bacon age-depth model (figure 4.15) are presented.

Depth	**Conventional ^{14}C Age (years BP ±1σ)**	**Calibrated age (AD) (Probability distribution)**	**Bacon age estimates**	
			Weighted mean (AD)	Range (AD) (95% error)
129.5 cm	413 ± 37	1448-1525 (51.6%) 1535-1627 (43.8%)	1470	1391-1610

The prior information from the KAR-EM age-depth profiles was also appropriate for this profile owing to the location of San Juan Bog in the same region and is therefore assumed to have similar accumulation rates. The dark blue distribution shows the only calibrated ^{14}C date from the base of the profile and the turquoise distributions show the ^{210}Pb ages. The weighted mean age line (red dashed line) resulted from >6000 model iterations and the 95% confidence intervals (2σ) are shown.

Compared with the KAR-EM profiles this profile is relatively young with a weighted mean age at the base of AD 1470. Owing to the lack of ^{14}C dates between the base of the profile and the ^{210}Pb dates the weighted mean age line connects the section of highest probability from 129.5 cm to the lowest ^{210}Pb date (~50 cm) with high uncertainties around the weighted mean. The red arrows below the age-depth model show the mean accumulation rates for the profile and display faster accumulation rates than the KAR-EM profiles. From the base until 50 cm the mean accumulation rate is ~5 years per cm. Through the ^{210}Pb age profile the accumulation rate is ~3 years per cm to the surface.

Table 4.10 displays the conventional ^{14}C age, the original probability based age ranges calibrated using OxCal and the Bacon age estimate from the sample at 129.5 cm. The Bacon age estimate falls within the range of the original highest probability age estimates. The final age-depth model, despite the high uncertainties between 50 and 130 cm, represents a steadily accumulating peat profile and the final chronology can be applied to the proxy records.

Figure 4.16 presents the model output from the final SAN-EM-2 Bacon age-depth model presented as years AD/BC at 0.5 cm resolution. The 95% confidence intervals around the weighted mean age line are displayed.

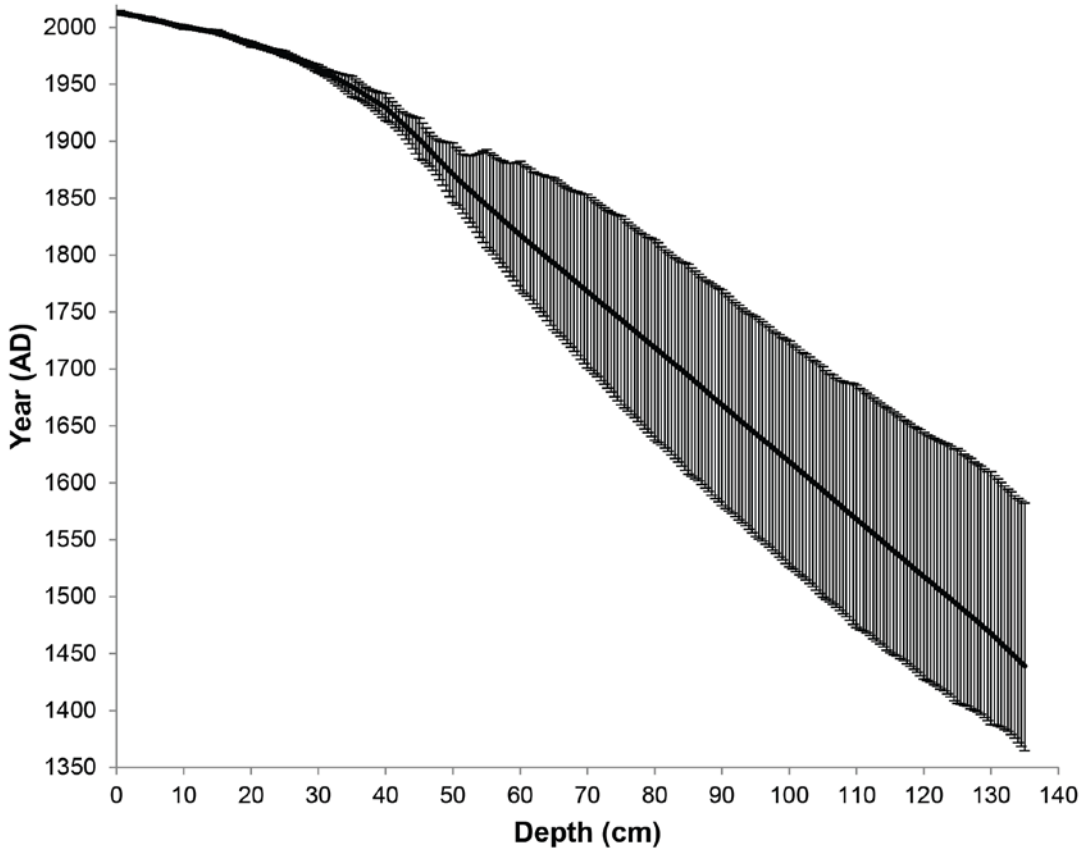

Figure 4.16. The SAN-EM-2 age-depth profile converted to years AD at 0.5 cm resolution with 95% confidence intervals displayed.

Figure 4.16 further displays steady accumulation throughout the profile. The uncertainty around the weighted mean age line decreases from the base throughout the profile from an average of ±80 years until ~50 cm after which the average uncertainty decreases to ±3 years to the surface. The model output is used in chapter 7 in which the SAN-EM-2 proxy records are plotted against age.

4.3.5 SCB-1

As discussed in section 4.2.1.3.5, only one ^{14}C date was obtained for SCB-1 and this date has been used to constrain the base of the section of interest in this profile alongside the ^{210}Pb ages. The final-age-depth model is presented in figure 4.17.

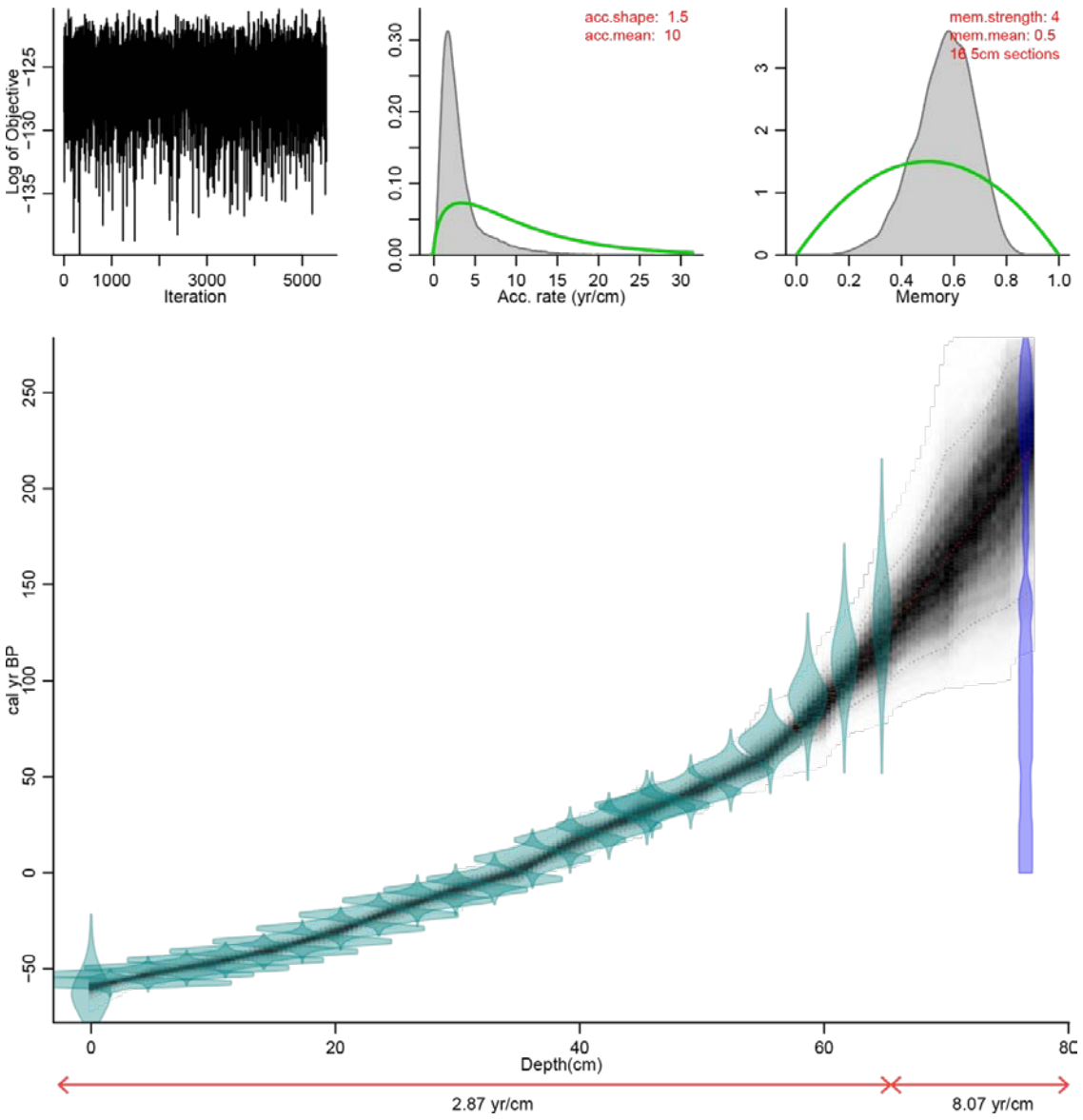

Figure 4.17. The final age-depth model including all ^{210}Pb ages and the ^{14}C ages from SCB-1. Red arrows beneath the model show calculated accumulation rates throughout the profile.

Table 4.11. Radiocarbon date and OxCal calibrated ranges from SCB-1. The weighted mean and range of ages based on the final Bacon age-depth model (figure 4.17) are presented.

Depth	**Conventional ^{14}C Age (years BP ±1σ)**	**Calibrated age (AD) (Probability distribution)**	**Bacon age estimates**	
			Weighted mean (AD)	Range (AD) (95% error)
76.5 cm	153 ± 37	1796-1950 (68%) 1672-1743 (26.3%) 1771-1779 (1.1%)	1734	1660-1790

San Carlos bog, despite its location further east from the other sites, is assumed to have a similar accumulation history as the other sites and the same prior information was thought to be appropriate. The only ^{14}C date from the profile is shown by the dark blue distribution and the turquoise distributions show the ^{210}Pb ages. >5000 model iterations resulted in the weighted mean age line (red dashed line) with the 95% confidence intervals (2σ) displayed.

The calibrated age at 76.5 cm has a high probability distribution owing to the recent plateau in the calibration curve resulting in high uncertainty between this depth and the depth of the lowest ^{210}Pb age. The weighted mean average line goes through the older section of the probability distribution following the trajectory of the ^{210}Pb age profile. The mean accumulation rate is ~8 years per cm until ~65 cm after which it is faster at ~3 years per cm. The ^{210}Pb age profile is vital from this profile and has resulted in a final age-depth model which suggests a steadily accumulating peat profile despite its shorter extent compared with the other profiles in the investigation.

The cal. BP ages have been converted to AD/BC in figure 4.18 and ages have been inferred at 0.5 cm resolution. The 95% confidence intervals around the weighted mean age line are presented. Plant macrofossil and testate amoeba samples were analysed from depths below the extent of the age-depth model. Ages have been extrapolated using polynomial regression and the extension of the age-depth profile is shown in red.

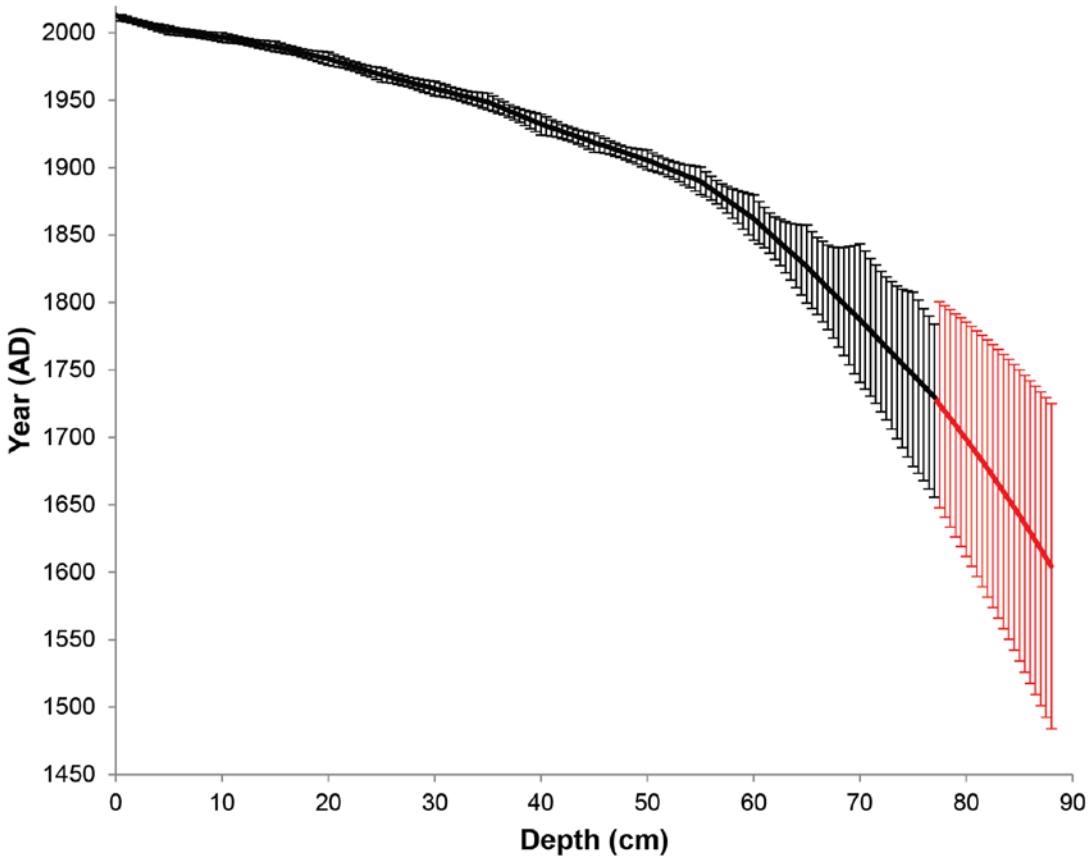

Figure 4.18. The SCB-1 age-depth profile converted to years AD at 0.5 cm resolution with 95% confidence intervals displayed.

The uncertainty around the weighted mean age line decreases from an average of ±40 years between the base and ~58 cm to ±5 years until the surface. The final chronology is used in chapter 7 against which the SCB-1 proxy records are plotted.

4.3.6 Intra-site comparison

The resulting age-depth lines from the individual KAR-EM profiles as presented in sections 4.3.1-4.3.3 are compared in figure 4.19. This allows comparison of the accumulation rates and associated age uncertainties from each profile.

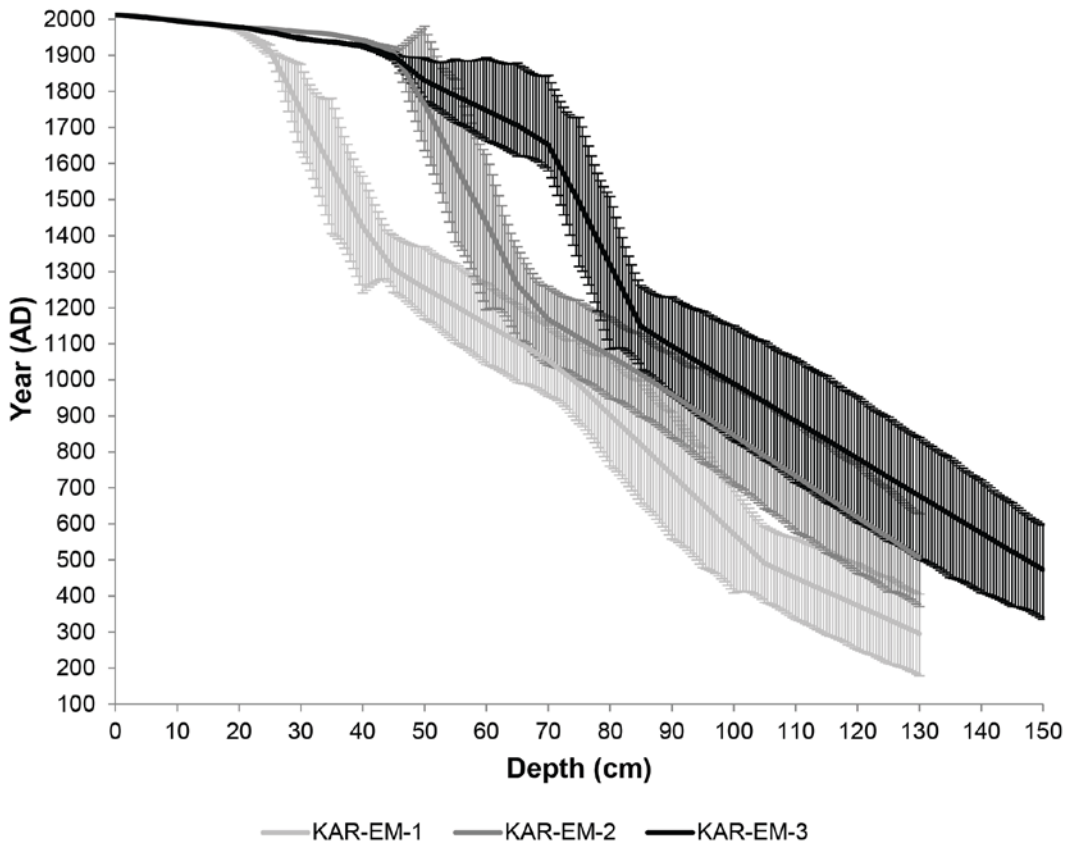

Figure 4.19. Comparison of the KAR-EM age-depth profiles presented in years AD. 95% confidence intervals displayed.

Owing to continual processes of accumulation, decomposition and compaction within peatlands, depth is not linearly related to age. These processes are variable across the microtopography resulting in differing age-depth relationships and this will be discussed further in section 6.3. The three profiles display similar accumulation rates of ~12 years per cm from the base of each profile until 82 cm (AD 1251) in KAR-EM-3, 66 cm (AD 1245) in KAR-EM-2 and 43 cm (AD 1354) in KAR-EM-1. Above this the slowdown in accumulation is evident across all profiles to a rate of ~28 years per cm from 82-66 cm (AD 1251-1695) in KAR-EM-3, 66-39 cm (AD 1245-1946) in KAR-EM-2 and 43-20 cm (AD 1354-1971) in KAR-EM-1. There is a higher average uncertainty in KAR-EM-3 (±140 years) than KAR-EM-2 (±130 years) and relatively lower average uncertainty in KAR-EM-1 (±120 years) owing to the higher constraint of more evenly spaced radiocarbon dates in this profile.

There is an overlap of uncertainty between KAR-EM-3 and KAR-EM-2 profiles between 130-80 cm. Above this there is a switch with the uncertainty of KAR-EM-2 and KAR-EM-1 overlapping between 80 and 60 cm. The uncertainties of KAR-EM-3 and KAR-EM-2 overlap between 60 and 50 cm with these two records remaining of similar age and accumulation rate from 50 cm to the surface (AD 1942 and AD 1927 to present respectively). The profiles are only similar after 20 cm (KAR-EM-1: AD 1971, KAR-EM-2: AD 1978, KAR-EM-3: AD 1979) and display similar uncertainties through ^{210}Pb age sections ~ ±2 years to the surface.

The weighted mean ages (mean lines of each profile) are overall younger in KAR-EM-3, overall relatively older in KAR-EM-2 and older still in KAR-EM-1. This holds true from the base of the profiles until 50 cm when the KAR-EM-3 and KAR-EM-2 profiles become of a similar age with KAR-EM-1 significantly older at this depth (AD 1250) with the three profiles of a similar age above 20 cm.

The comparison of the age-depth models from the KAR-EM profiles forms the basis for comparison of the proxy records from each of the profiles plotted against the individual age profiles. With the similarities between the profiles considered, tuning of the records within the age uncertainties may be possible in order to verify the chronology and this will be considered in the discussion (Chapter 6) subsequent to the presentation of the raw proxy data from each profile (Chapter 5). More specifically throughout Chapter 5 the KAR-EM proxy records are plotted against depth to explore intra-site similarities between the records forming the basis of potential intra-site tuning between records. Circular reasoning is introduced with the determination of a chronology against which proxy records can be plotted (Blaauw *et al.*, 2003) related to climate-related accumulation differences between profiles that are themselves being assessed for climate variability (Clarke *et al.*, 2012). This has been assessed through the comparison of the final chronology from each profile and will be further assessed throughout the remaining chapters.

4.3.7 Inter-site comparison

After consideration of the intra-site comparison of the KAR-EM profiles in figure 4.19, figure 4.20 compares the KAR-EM, SAN-EM-2 and SCB-1 age-depth models.

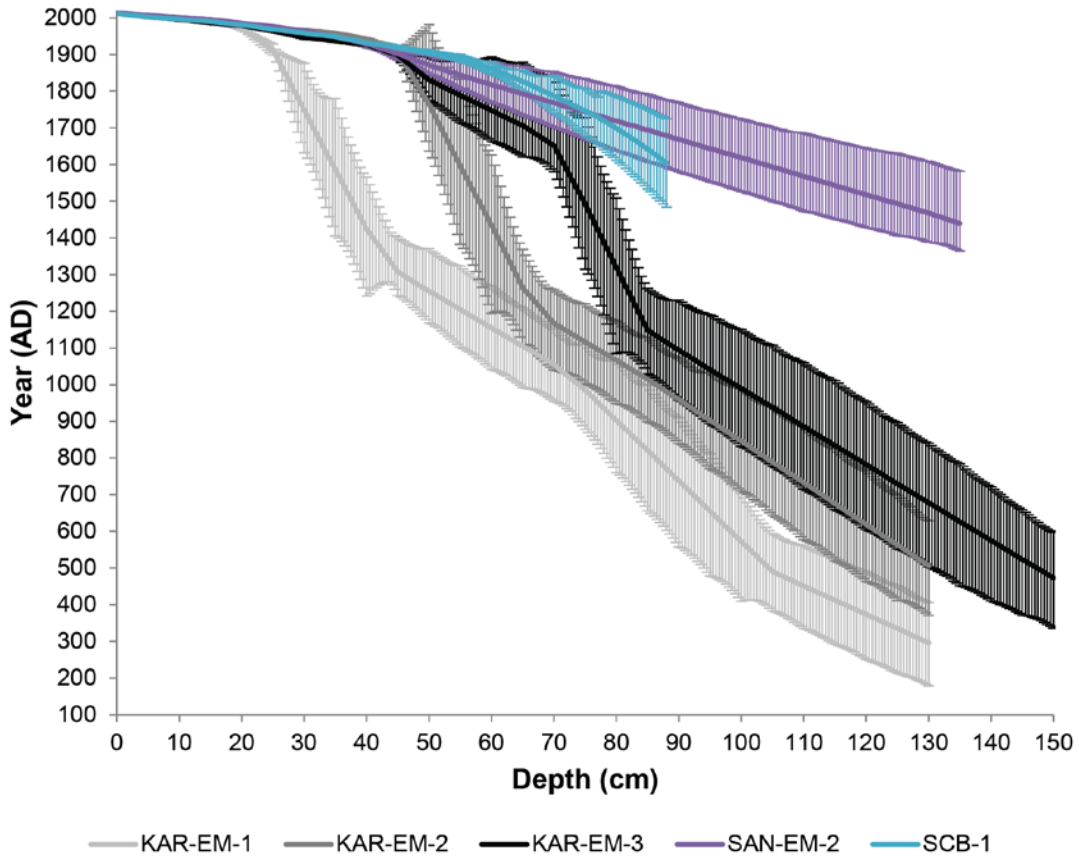

Figure 4.20. Comparison of the KAR-EM, SAN-EM-2 and SCB-1 age-depth profiles presented in years AD from AD 100 to present. 95% confidence intervals displayed.

As it can be seen these two profiles forming the inter-site aspect of the investigation have accumulated relatively quickly compared with the KAR-EM profiles. SAN-EM-2, despite the similar length of this profile with the KAR-EM profiles is estimated to have a basal age ~AD 1500 - much younger than the basal ages of the KAR-EM profiles. The average uncertainty around the weighted mean is ±80 years from the base to 50 cm, much lower than that of the KAR-EM profiles with a more rapid accumulation of 5 years per cm between these depths. Above 50 cm uncertainty decreases to ±3 years to the surface and the accumulation rate is similar to that of the KAR-EM profiles. The SCB-1 record is only 80 cm long and has accumulated much more rapidly than the other profiles in the investigation. Figure 4.21 presents the age-depth models covering the period from AD 1350 to present.

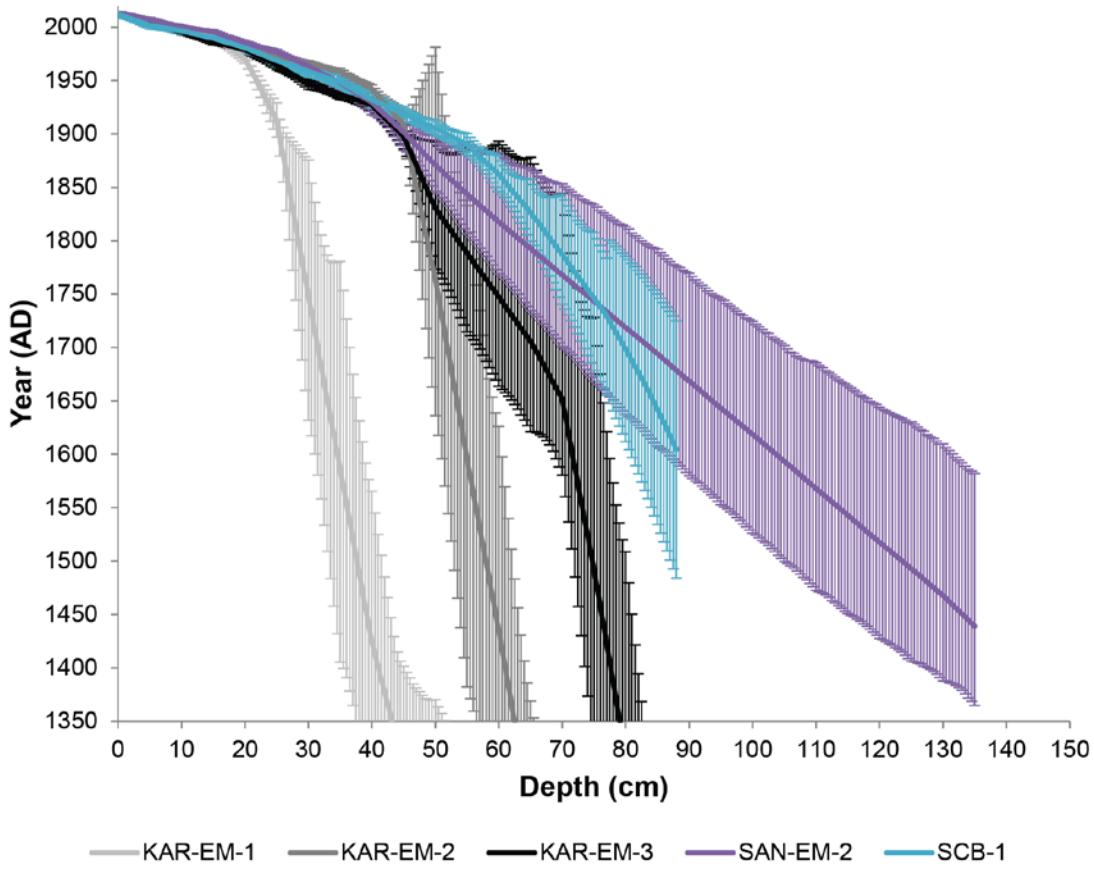

Figure 4.21. Comparison of the KAR-EM, SAN-EM-2 and SCB-1 age-depth profiles presented in years AD from AD 1350 to present. 95% confidence intervals displayed.

Much faster accumulation rates are evident in SCB-1 of 8 years per cm from the base until 58 cm and of 3 years per cm to the surface. Uncertainties are lower than in the other profiles, ±40 years until 58 cm and ±5 years to the surface, relatively higher than in the KAR-EM and SAN-EM-2 profiles. An inter-site comparison of the proxy records plotted against age is carried out in chapter 7.

Chapter 5: Results

The results will first be presented from the three profiles from Karukinka, KAR-EM-3, KAR-EM-2 and KAR-EM-1, in section 5.1. The results are then presented from the second Chilean site, San Juan (SAN-EM-2) in section 5.2 followed by the results from the final site in the Falkland Islands (SCB-1) in section 5.3.

5.1 Karukinka

The results from the three profiles from Karukinka are presented in this section. An overview of the profiles with a stratigraphic description is presented, followed by the palaeoecological results with a final multi-proxy comparison of the plant macrofossil, testate amoeba and humification results from each profile. Finally, the stable isotope results are presented. All results are plotted against depth with the approximate ages of zone boundaries displayed on the plant macrofossil and testate amoeba diagrams. At the end of each section, as discussed in section 3.7, similarities between the KAR-EM profiles have been assessed by aligning the proxy records based on actual depth and relative depth to the surface of KAR-EM-3, irrespective of age. This is before consideration of the timing of variability in the profiles which will be considered in Chapters 6 and 7.

5.1.2 Profile stratigraphies

5.1.2.1 Stratigraphic description

The profiles from Karukinka are presented in figure 5.1. The photographed profiles are presented alongside a simplified description, which follows the Von Post scale of peat decomposition (von Post and Granlund, 1926; in Kettridge *et al.*, 2012); the profiles are dominated by variability between *Sphagnum* peat (H1: undecomposed and unaltered plant structure) and humified *Sphagnum* peat (H4: weakly decomposed and remains identifiable).

In KAR-EM-3 there appear to be oscillations between more and less humified peat in the lower section until 100 cm, after which there is a prolonged period of more humified peat until ~82 cm. Similarly in KAR-EM-2 there are layers of more and less humified peat until 74 cm, followed by a larger section of humified peat until 42 cm.

In KAR-EM-1 there is a section of humified peat until 119 cm followed by a prolonged period of less humified peat until 88 cm. There is a subsequent period of humified peat for ~70 cm punctuated by a section of less humified peat between 72 and 68 cm. This period of humified peat persists until 19 cm. There is a clear boundary in each profile (demarcated by the red box) which is characteristic of the acrotelm-catotelm boundary (Belyea and Clymo, 1999; Morris *et al.*, 2011a). Above this, undecomposed *Sphagnum* remains persist until the surface. This basic overview of the profile stratigraphies provides the context for both the palaeoecological and stable isotope analysis.

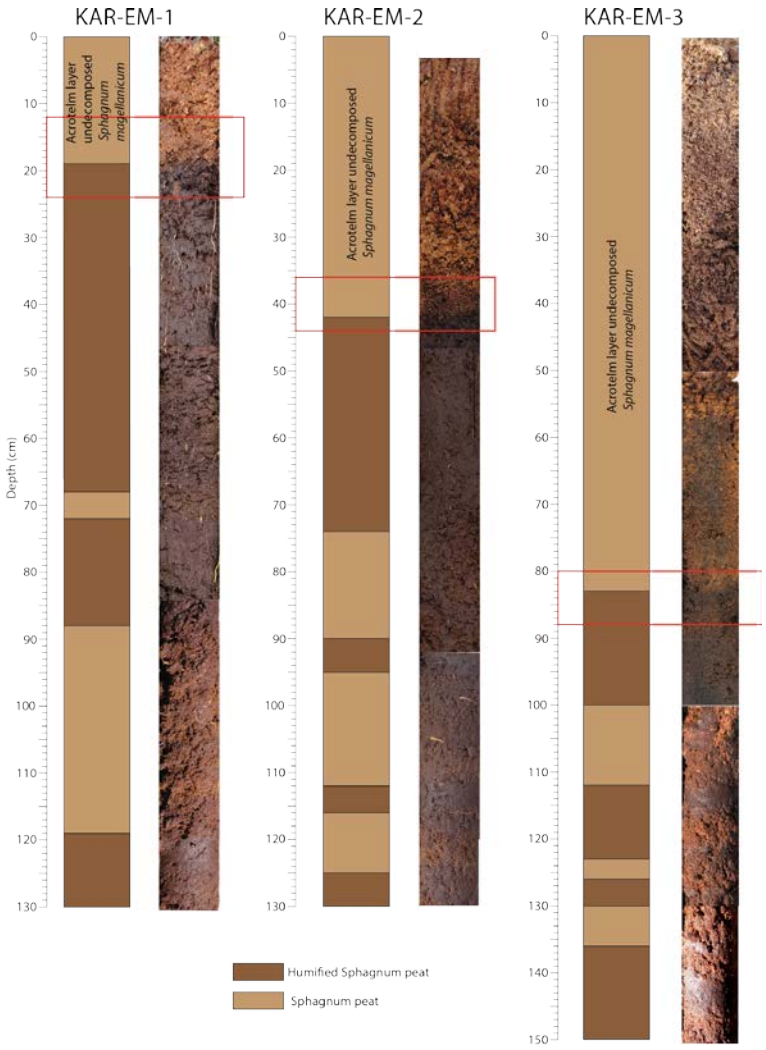

Figure 5.1. Depth based stratigraphic variability of KAR-EM-1, KAR-EM-2 and KAR-EM-3. The red boxes mark the proposed acrotelm-catotelm boundary in each profile.

5.1.2.2 Intra-site comparison of profile stratigraphies

Figure 5.2 presents the stratigraphies of the three profiles compared based on the actual depths of each profile (figure 5.2a) and plotted relative to the surface of KAR-EM-3 (figure 5.2b) prior to chronological development. Assuming that the upper sections, located above the potentially synchronous acrotelm-catotelm boundary, of undecomposed *Sphagnum* are tied, figure 5.2b displays the stratigraphic units tied below this boundary (A-H) (also see Table 5.1 for depths of units). Stratigraphic changes in each profile seem better related when displayed in this way. There is an extended period of humification in each profile below the acrotelm-catotelm boundary (~80 cm) with decreasing extent from KAR-EM-1 to KAR-EM-3. Below this there is higher variability between *Sphagnum* peat and humified *Sphagnum* peat in KAR-EM-2 and KAR-EM-3 than in KAR-EM-1. Comparing against actual depth disregards the role of the acrotelm-catotelm boundary and associated processes of accumulation and decomposition which differ across the microtopography. Tying these stratigraphic units forms the basis for tying the profiles in Chapter 6. Comparison of the humification profiles would provide a more detailed overview of intra-site variability for comparison with the other proxies which will be considered in the following sections.

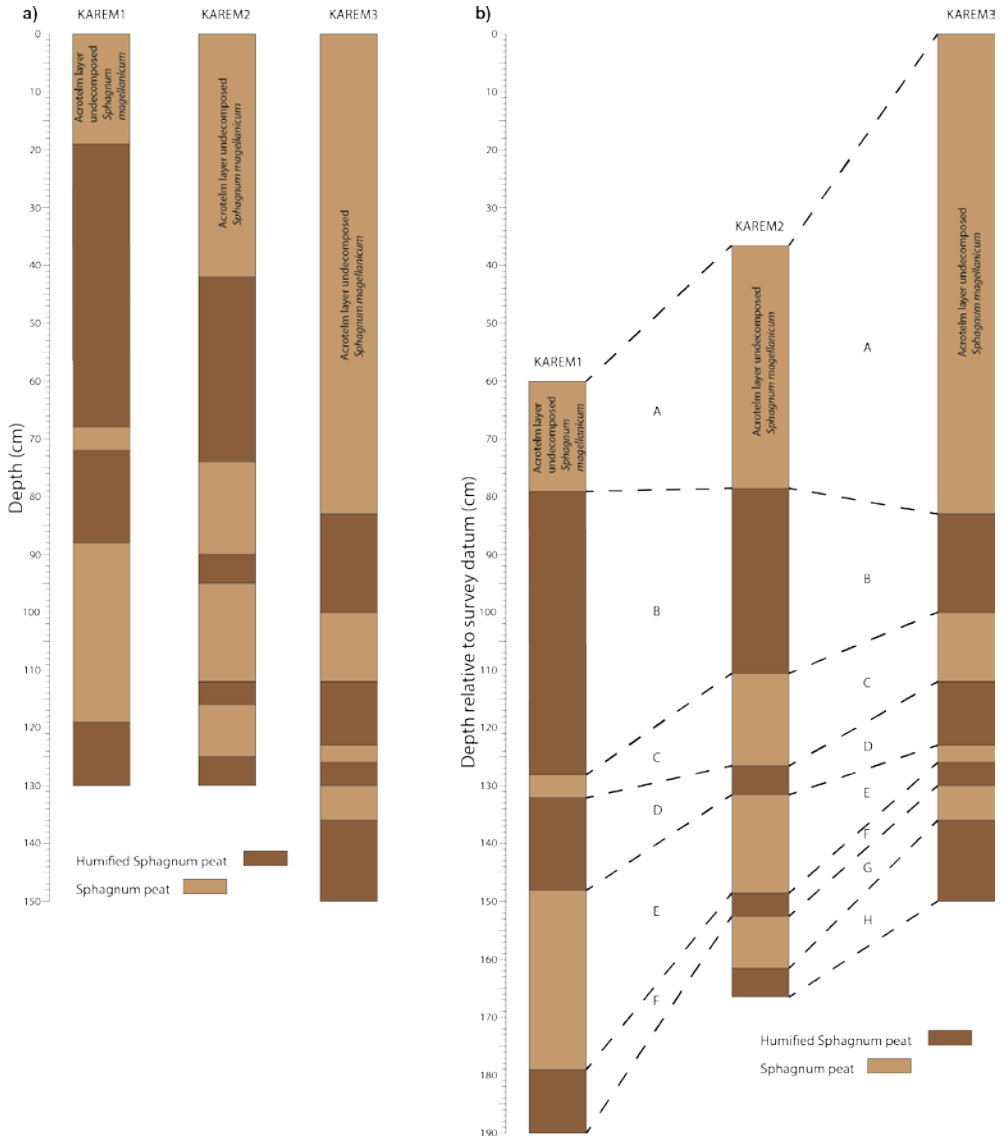

Figure 5.2. Comparison of the KAR-EM profile stratigraphies plotted against the actual depths of each profile (a) and plotted relative to the surface of KAR-EM-3 (b). Stratigraphic units are tied in 5.2b.

Table 5.1. Depths of the stratigraphic units tied in Figure 5.2b.

	KAR-EM-1		KAR-EM-2		KAR-EM-3
Unit	Actual depth	Relative (+60cm)	Actual depth	Relative (+34cm)	Actual depth
A	0-19	60-79	0-42	34-76	0-82
B	19-68	79-128	42-74	76-108	82-100
C	68-72	128-132	74-90	108-124	100-112
D	72-88	132-148	90-95	124-129	112-123
E	88-119	148-179	95-112	129-146	123-126
F	119-130	179-190	112-116	146-150	126-130
G			116-125	150-159	130-136
H			125-130	159-164	136-150

5.1.3 Palaeoecological results

5.1.3.1 Plant macrofossil results

The plant macrofossil diagrams from KAR-EM-3, KAR-EM-2 and KAR-EM-1 are presented in figure 5.3, 5.4 and 5.5 respectively. Table 5.2 presents a summary description of the plant macrofossil zones identified and the depths and approximate ages of the zone boundaries.

Sphagnum forms the main component throughout all of the peat records presented and a single species, *Sphagnum magellanicum* dominates. This could suggest insensitivity of the records to climate variability as major climatic events are assumed to cause shifts between *Sphagnum* species evident in plant macrofossil records (Barber *et al.*, 1994). Despite this dominance there is evidence of variability in each profile.

In the basal zone of KAR-EM-3, 3-Ma, there is an oscillation between *Sphagnum* dominance and the dominance of UOM. UOM dominates at the beginning of the zone alongside monocot roots and towards the end of the zone above 100 cm there are three peaks in both UOM and Ericaceae roots where *Sphagnum* becomes less abundant. Similarly in KAR-EM-2 the highest variability in the record is found in zones 2-Ma and 2-Mb. In zone 2-Ma there are two depths (112 cm and 92 cm) at which *Sphagnum* does not dominate and is replaced by Ericaceae and monocot roots and UOM. At the beginning of zone 2-Mb (AD 1116) Ericaceae roots first dominate, followed by *S.magellanicum*, then in the middle of the zone monocot roots increase at the same time as a peak in UOM. *S.magellanicum* dominates again before a peak of Ericaceae roots at the end of the zone. In KAR-EM-1 *S.magellanicum* dominates in the basal zone, 1-Ma, decreasing towards the end of the zone (AD 999). In zone 1-Mb *S.magellanicum* is absent at 72 cm and is at lower abundances throughout the zone alongside monocot roots and UOM.

The acrotelm-catotelm boundary is evident in each profile and a higher sampling resolution (every 1 cm) captured variability in this part of each profile. In KAR-EM-3 this is at ~83 cm at the zone boundary to 3-Mb (AD 1216) and is characterised by a low percentage of *Sphagnum* and dominance of Ericaceae roots. In KAR-EM-2 the

zone boundary between 2-Mb and 2-Mc (AD 1942) intersects the higher resolution analysis around the acrotelm-catotelm boundary throughout which *S.magellanicum* is dominant alongside Ericaceae roots and UOM. The boundary in KAR-EM-1 is characterised by the absence of *S.magellanicum* in zone 1-Mc (AD 1880-1986) where Ericaceae and monocot roots and UOM dominate.

After the acrotelm-catotelm boundary *Sphagnum* returns to dominance in the surface zones 3-Mc, 2-Mc and 1-Md. In KAR-EM-3 and KAR-EM-2 there is a slight decrease of *S.magellanicum* towards the surface owing to the increasing presence of identifiable surface vegetation in these profiles

.

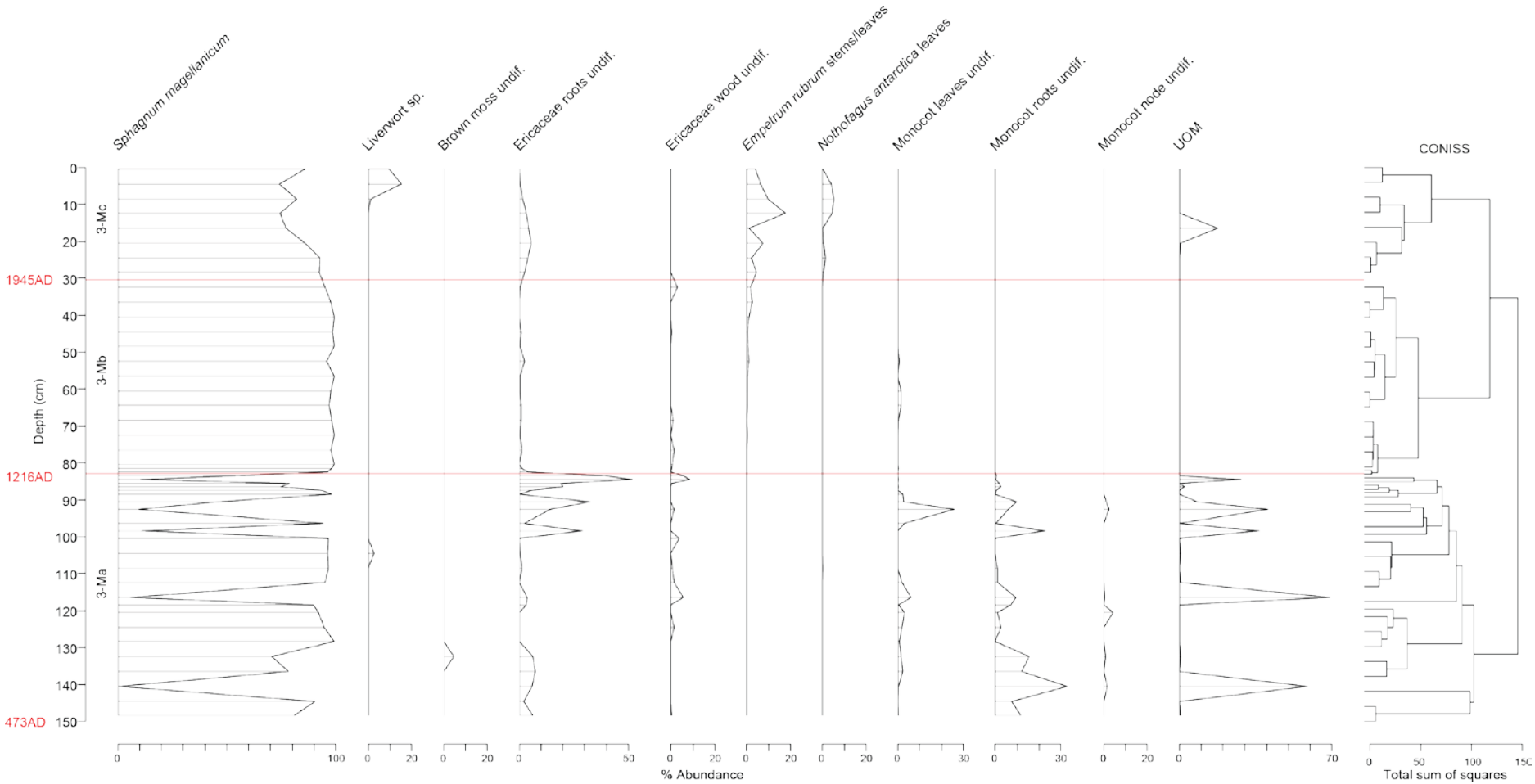

Figure 5.3. KAR-EM-3 plant macrofossil diagram plotted against depth, displaying plant macrofossil zones based on CONISS (red lines) with approximate ages of zone boundaries presented.

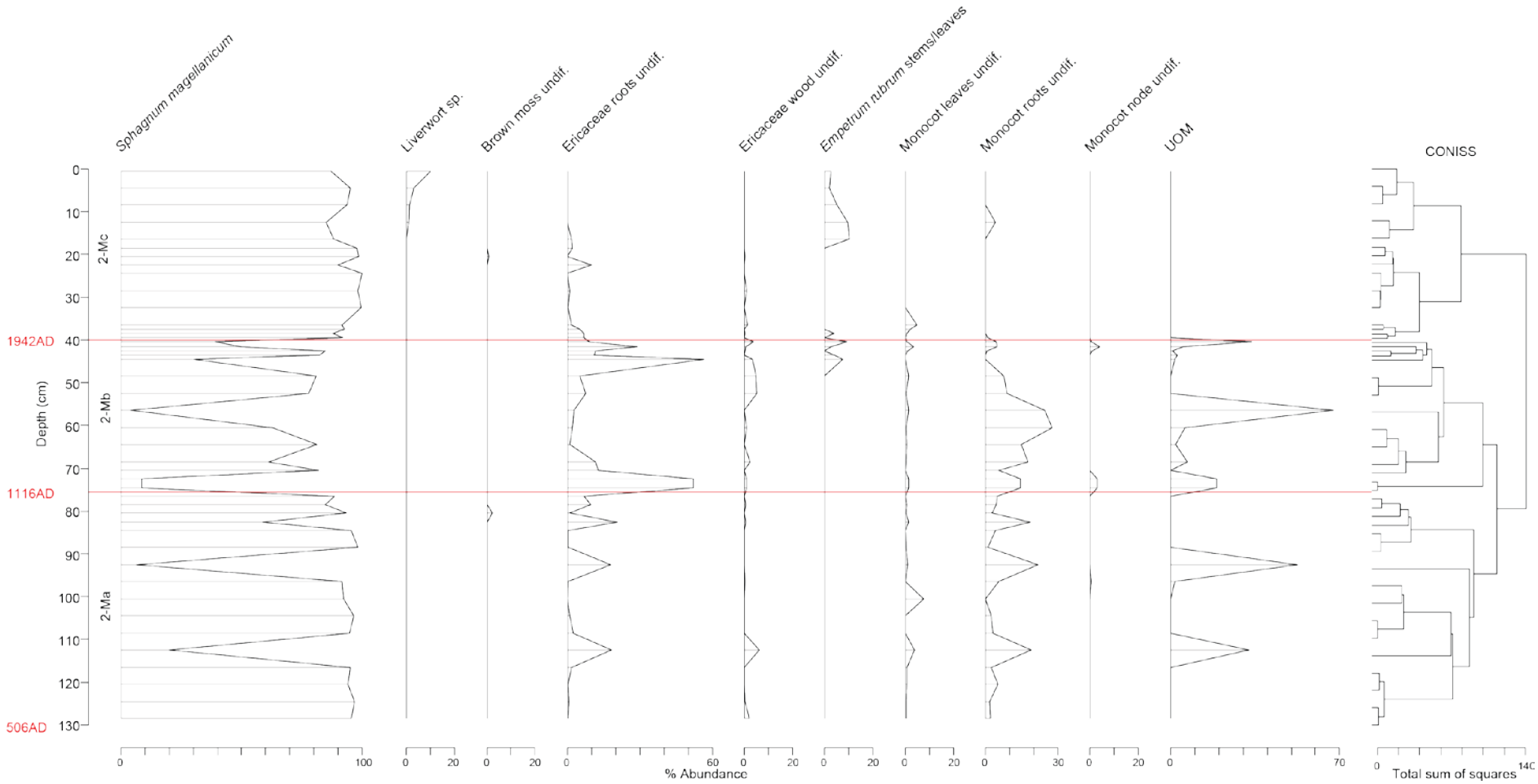

Figure 5.4. KAR-EM-2 plant macrofossil diagram plotted against depth, displaying plant macrofossil zones based on CONISS with approximate ages of zone boundaries presented.

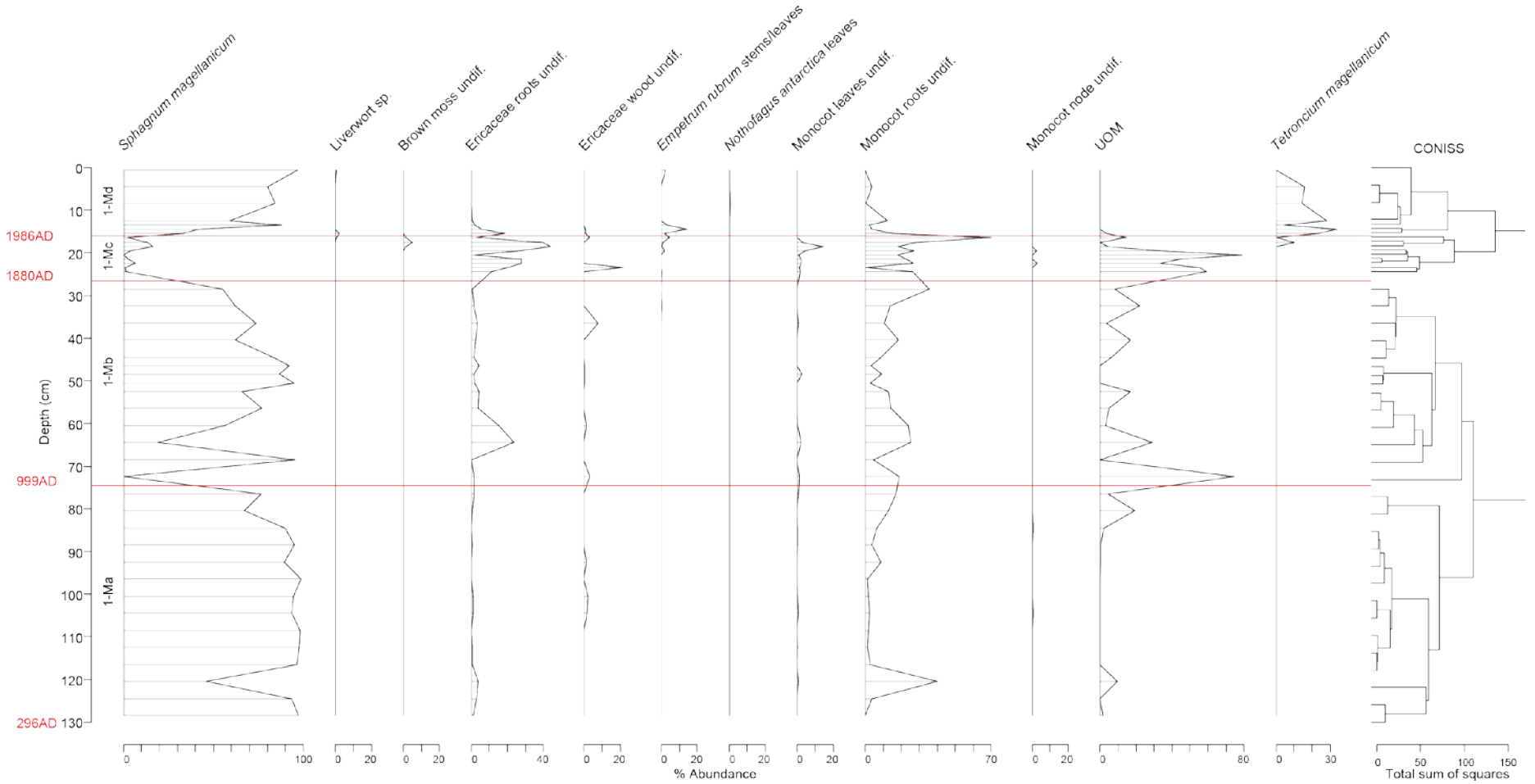

Figure 5.5. KAR-EM-1 plant macrofossil diagram plotted against depth, displaying plant macrofossil zones based on CONISS with approximate ages of zone boundaries presented.

Table 5.2. Summary description of the plant macrofossil zones from the Karukinka profiles; KAR-EM-3, KAR-EM-2 and KAR-EM-1.

Zone	Depth (cm)	Plant macrofossil zone description	Age cal BP (AD)
KAR-EM-3			
3-Ma	150-83	Throughout this zone *Sphagnum magellanicum* is largely dominant. At the beginning of the zone, where there is a decrease of *S.magellanicum* there are peaks of Unidentified Organic Matter (UOM). Towards the end of the zone, the decrease of *S.magellanicum* corresponds to an increase of ericaceous roots as well as UOM. There is a peak of monocot leaves undifferentiated towards the end of the zone and monocot roots are present throughout the zone. This is the zone of most variability in the record with repeated oscillations between the dominance of *S.magellanicum*, ericaceous roots and UOM. The end of this zone coincides with the well-defined boundary between the acrotelm and catotelm layers at ~83 cm in which *S.magellanicum* decreases and ericaceous roots and UOM dominate.	1476-734 cal BP (AD 473-1216)
3-Mb	83-31	This zone is dominated by *S.magellanicum* with high percentages persisting throughout resulting in the absence of other plant macrofossil components throughout this zone. *Empetrum rubrum* remains begin to increase towards the end of the zone.	734-49 cal BP (AD 1216-1945)
3-Mc	31-0	*S.magellanicum* is dominant at the beginning of this zone with the increasing presence of *E.rubrum* and *N.antarctica* towards the end of the zone. *S.magellanicum* dominates at the surface.	4.9 - -63 cal BP (AD 1945-2013)
KAR-EM-2			
2-Ma	130-75	Zone of high variability with the oscillation between the dominance of *S.magellanicum* and UOM. Ericaceous and monocot roots also contribute to the macrofossil count at the levels where *S.magellanicum* decreases.	1444-834 cal BP (AD 506-1116)
2-Mb	75-40	Lower levels of *S.magellanicum* are found in this zone. Ericaceous roots peak at the beginning and end of the zone. There is a mid-zone peak of monocot roots and UOM. Low abundance of Ericaceae wood	834-8 cal BP (AD 1116-1942)

		throughout the zone. The end of this zone corresponds to the boundary between the acrotelm and catotelm layers ~40 cm where *S.magellanicum* decreases and ericaceous roots and UOM dominate.	
2-Mc	40-0	Dominance of *S. magellanicum* throughout the zone. *E.rubrum* increases in the middle of the zone and decreases towards the surface. *S. magellanicum* dominates at the surface with low abundance of *Liverwort sp*.	8 - -63 cal BP (AD 1942-2013)
KAR-EM-1			
1-Ma	130-74	*S.magellanicum* dominates throughout this zone. There is a peak of monocot roots at the beginning of the zone and there is an increase of both monocot roots and UOM towards the end of the zone.	1654-951 cal BP (AD 296-999)
1-Mb	74-26	*S.magellanicum* levels are lower but dominant throughout this zone. *S.magellanicum* is lower due higher levels of monocot roots and UOM throughout the zone.	951-70 cal BP (AD 999-1880)
1-Mc	26-16	*S.magellanicum* levels are low in this zone alongside the highest levels of ericaceous and monocot roots and UOM. The boundary between the acrotelm and catotelm falls in this zone.	70- -36 cal BP (AD 1880-1986)
1-Md	16-0	*S.magellanicum* rises to dominance from the previous zone towards the surface. *Tetroncium magellanicum* also increases in this zone but declines towards the surface.	-36 - -63 cal BP (AD 1986-2013)

As discussed in section 3.5.1, statistical methods were assessed with the ultimate aim of reducing the dimensionality of the multivariate plant macrofossil data for conversion to a line of BSW variability. The results of DCA are shown in table 5.3. The DCA axis-one gradient length of each dataset was less than 3σ and a linear response model could, therefore, be used on each dataset (Ter Braak and Prentice, 1988; Lepš & Šmilauer, 2003). The results of the PCA of the KAR-EM-3, KAR-EM-2 and KAR-EM-1 datasets are presented in table 5.4 with the proportion of the total variance of axis-one relatively high at 38.80%, 37.95% and 36.49% respectively. Using a screeplot axis-one was the only significant axis in each dataset. Bi-plots of axis-one and -two sample and species scores of each dataset are presented in figure 5.6. Each point is a sample based on depth and points are coloured according to the plant macrofossil zones as indicated.

Table 5.3. Results of DCA of KAR-EM-3, KAR-EM-2 and KAR-EM-1 plant macrofossil data.

KAR-EM-3 (No down-weighting or removal of rare species)			
	Axis 1	Axis 2	Axis 3
Eigenvalues	0.6366	0.1486	0.09893
% accounted for by axis	51.44%	12.01%	7.99%
Gradient lengths	2.3318	0.8022	0.73809
KAR-EM-2 (Down-weighting and removal of rare species)			
	Axis 1	Axis 2	Axis 3
Eigenvalues	0.5138	0.1847	0.07625
% accounted for by axis	57.64%	20.72%	8.55%
Gradient lengths	2.1137	1.66732	0.66181
KAR-EM-1 (Down-weighting and removal of rare species)			
	Axis 1	Axis 2	Axis 3
Eigenvalues	0.5838	0.2944	0.16392
% accounted for by axis	46.70%	23.55%	13.11%
Gradient lengths	2.3319	1.3234	1.21791

Table 5.4. Results of PCA of KAR-EM-3, KAR-EM-2 and KAR-EM-1 plant macrofossil data.

KAR-EM-3 (No removal of rare species, Hellinger transformed)			
	Axis 1	Axis 2	Axis 3
Eigenvalues	4.0134	1.9408	1.3964
% accounted for by axis	36.49%	17.64%	12.69%
Scree plot (Broken stick)	Significant	-	-
KAR-EM-2 (No removal of rare species, Hellinger transformed)			
	Axis 1	Axis 2	Axis 3
Eigenvalues	3.795	1.521	1.021
% accounted for by axis	37.95%	15.27%	10.21%
Screeplot (Broken stick)	Significant	-	-
KAR-EM-1 (Removal of rare species, Hellinger transformed)			
	Axis 1	Axis 2	Axis 3
Eigenvalues	3.492	1.761	1.16
% accounted for by axis	38.80%	19.57%	12.89%
Screeplot (Broken stick)	Significant	-	-

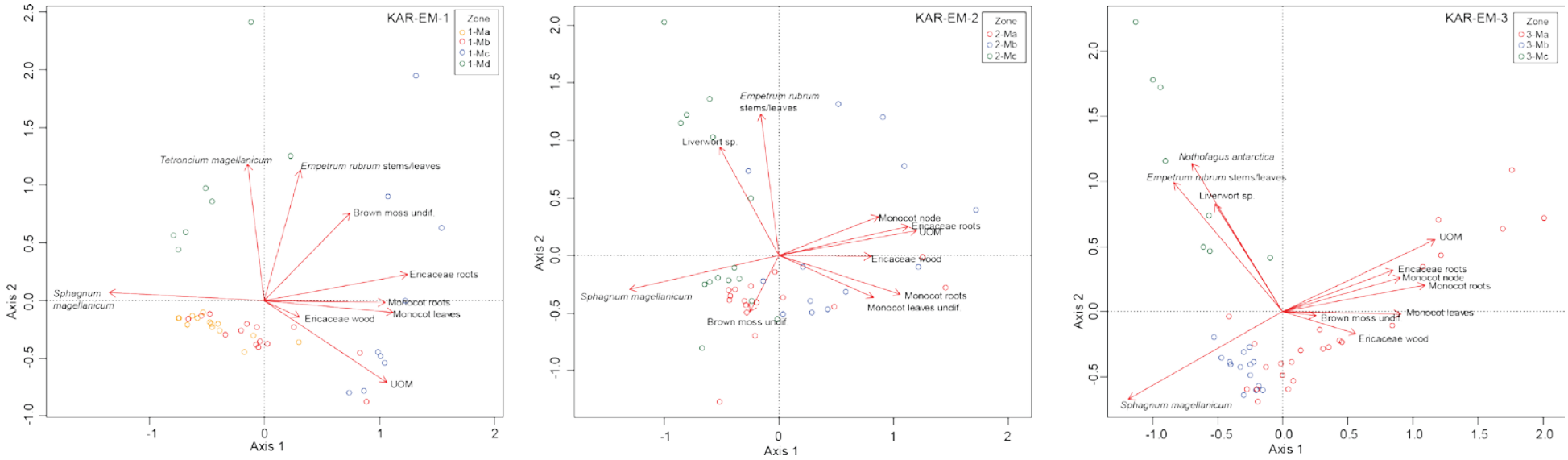

Figure 5.6. Bi-plot of PCA axis-one and -two species (Red arrows) and sample scores (points coloured according to CONISS plant macrofossil zone) of KAR-EM-1, KAR-EM-2 and KAR-EM-3 plant macrofossil data.

In the KAR-EM-3 plant macrofossil data *S.magellanicum*, monocot roots and UOM are most strongly correlated with the first principal component. These variables, located at opposite ends of the axis respond in the opposite direction to each other. Points located at the lower end of axis-one have a high abundance of *S.magellanicum* and points located at the higher end of axis-one have a high abundance of monocot roots and UOM. Samples located in zone 3-Ma (red points) are composed mainly of these three variables and are scattered between the two ends of axis-one. Samples located in 3-Mb (blue points) are mostly dominated by *S.magellanicum* and are located at the lower end of axis-one. Samples in the surface zone, 3-Mc (green points) are dominated by *S.magellanicum* alongside *E.rubrum* and *N.antarctica*, with these two variables most strongly correlated with axis-two. Most of these samples are located at the high end of this axis as these variables increase towards the surface.

S.magellanicum, Ericaceae roots, monocot roots and UOM are most correlated with the first principal component of the KAR-EM-2 plant macrofossil data. *S.magellanicum* is located at the lower end of axis-one with the other dominant variables at the opposite end. Samples in 2-Ma (red points) are mostly dominated by *S.magellanicum* and are located at the lower end of axis-one. Samples in 2-Mb (blue points) are scattered between the middle and higher end of axis-one owing to the shifts between the four dominant variables in this zone. Samples in 2-Mc (green points) are dominated by *S.magellanicum* and located at the lower end of axis-one. *E.rubrum* is most strongly correlated with axis-two, thus, some samples in 2-Mb and 2-Mc are located at the higher end of this axis.

In the KAR-EM-1 plant macrofossil data *S.magellanicum*, Ericaceae roots and monocot leaves are most correlated with the first principal component. *S.magellanicum* is located at the lower end of axis-one with the remaining dominant variables at the opposite end. Samples in 1-Ma (orange points) and 1-Mb (red points) are grouped at the lower end of axis-one owing to the dominance of *S.magellanicum* in these samples. Samples in 1-Mc (blue points) are located at the other end of the axis reflecting the low abundance of *S.magellanicum* in these samples and increase of the other dominant variables. Samples in 1-Mc (green points) are grouped at the

lower end of axis-one and are also located at the higher end of axis-two owing to the correlation of *E.rubrum* and *T.magellanicum* with this axis.

Separation along axis-one in the PCA of *S.magellanicum* and other components seems to represent a wetness gradient in each profile, with *S.magellanicum* a wetter indicator located at the negative end of axis-one and the other components drier indicators located at the positive end of the axis. In figure 5.7, as an indication of wetness variability throughout the record the PCA axis-one scores (a diagrams) are displayed alongside bog surface wetness lines (b diagrams), derived by conversion of the raw plant macrofossil data using the Dupont Hydroclimatic Index. Both records are normalised for comparison to represent wetness variability (c diagrams).

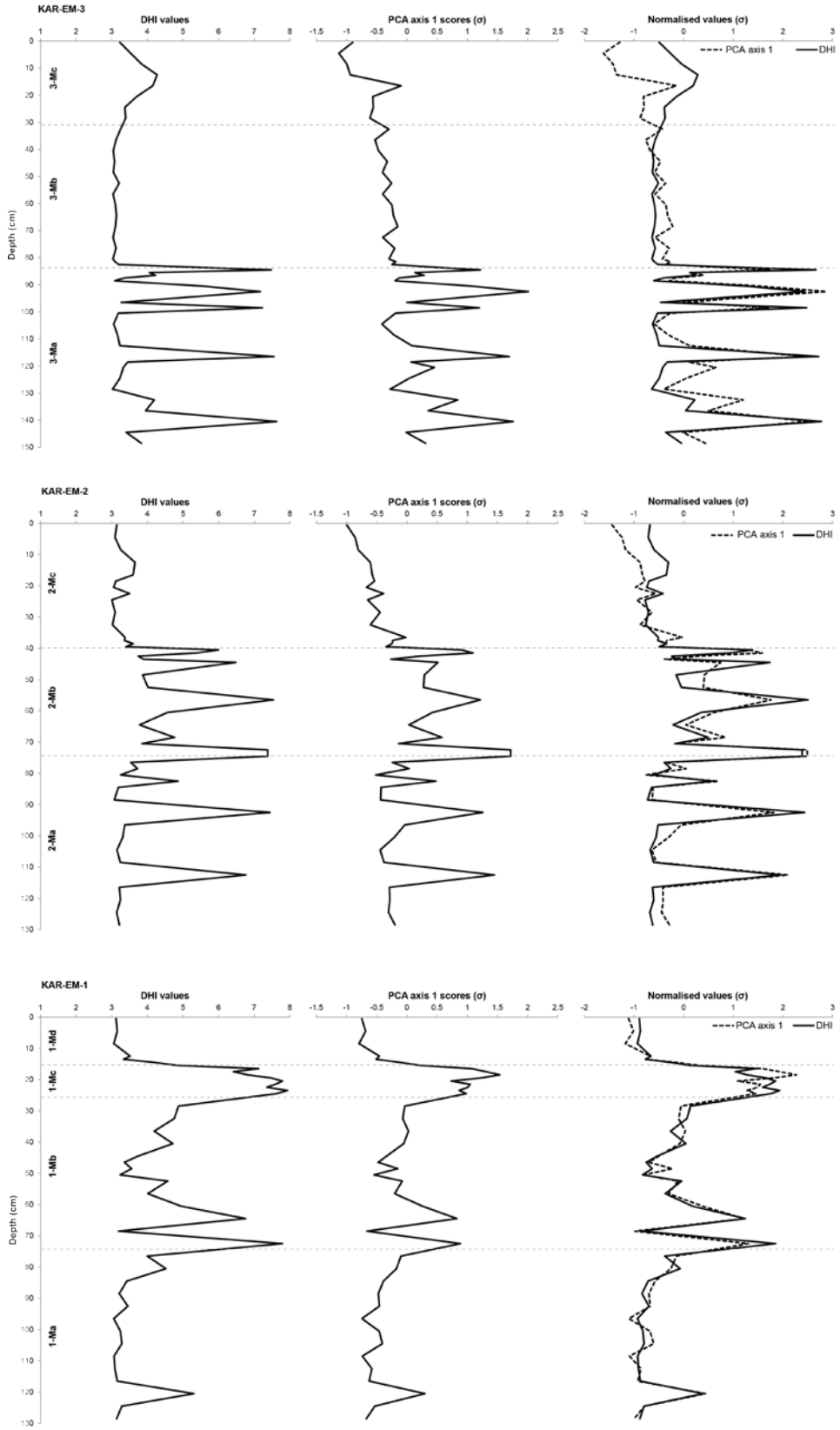

Figure 5.7. Bog surface wetness anomaly curves from the KAR-EM-3, KAR-EM-2 and KAR-EM-1 plant macrofossil data transformed using the Dupont Hydroclimatic Index (a) and the axis-one scores of Principal Components Analysis (b). These two records are then normalised and compared (c). The plant macrofossil zones are displayed.

In KAR-EM-3, oscillations between low and high DHI values represent the zone of highest variability in 3-Ma. The peaks to higher values are representations of the dominance of UOM, ericaceous and monocot roots, which have high DHI weightings (8) at depths where *S.magellanicum* decreases. The persistent low values above the acrotelm-catotelm boundary throughout zones 3-Mb and 3-Mc reflect the dominance of *S.magellanicum,* which has a low DHI weighting (3). The PCA axis-one scores display much the same results with peaks in scores reflecting the presence of components located at the higher end of axis-one with a similar persistence in lower values after the acrotelm-catotelm boundary reflecting the dominance of *S.magellanicum* located at the lower end of axis-one.

The variability in plant macrofossil composition in 2-Ma and 2-Mb is demonstrated well by the switch between low and high DHI values in these zones. The high values are depths at which Ericaceae/monocot roots and UOM dominate, whereas low values represent periods of dominance of *S.magellanicum* which has a low weighting particularly after the acrotelm-catotelm boundary and through zone 2-Mc. Similar variability is demonstrated by the PCA axis-one scores as a result of the location of *S.magellanicum* at the lower end of axis-one and the other components at the higher end of axis-one.

The DHI values are low throughout zone 1-Ma, reflecting the dominance of *S.magellanicum* apart from a peak to higher values at 120 cm representing an increase of monocot roots at this depth. There is a peak to the highest DHI value (7.8) in zone 1-Mb at 72 cm where *S.magellanicum* is absent and UOM dominates and again at 64 cm where Ericaceae roots, monocot roots and UOM dominate. Values remain low throughout the zone until a rise to higher values in zone 1-Mc, reflecting the low abundance of *S.magellanicum* in the acrotelm-catotelm boundary. Values are low again in zone 1-Md to the surface. The PCA axis-one scores are very similar to the DHI record apart from at 18 cm when there is a peak to the highest scores in the record. This difference is driven by the dominance of Ericaceae roots at this depth and the higher correlation of this variable with axis-one than the other variables and thus having a higher influence on this record.

The normalised records (c diagrams) are very similar with slight differences in the magnitude of change related to a difference in the separation of the components along the respective wetness gradients but the direction of change is generally uniform.

In Zone 3-Mc and 2-Mc, the 2 normalised records separate as the PCA axis-one scores become more negative, this may be due to the correlation of surface vegetation with axis-two and a lack of contribution of these samples to axis-one scores, whereas they are included in the DHI record.

Inconsistencies between the two records result from the unknown underlying latent environmental variable, which could be hydrological, of the PCA. The DHI records are chosen for comparison with the other proxies owing to a representation of the data based on ecological knowledge and not an underlying latent environmental variable. All components are included at each depth whereas all components are not represented by the PCA axis-one scores.

5.1.3.2 Intra-site comparison of plant macrofossil records

5.1.3.2.1 Multivariate statistical analysis of plant macrofossil records

Figure 5.8 presents a biplot of the axis-one and -two scores resulting from a PCA of the raw plant macrofossil KAR-EM records (Figures 5.3-5.5). The symbols for each profile are coloured according to the corresponding plant macrofossil zone.

Table 5.5. Results of PCA of plant macrofossil data from all KAR-EM profiles.

	Axis 1	Axis 2	Axis 3
Eigenvalues	2.9854	1.7967	1.2493
% accounted for by axis	27.14%	16.33%	11.36%

The majority of samples across the three profiles are correlated with axis-one and are spread along this axis, which accounts for 27.14% of the total variance (table 5.5). Of these samples the majority are located at the lower end of the axis in the direction of *S.magellanicum* owing to the dominance of this species in the KAR-EM profiles; samples from zone 3-Mb are particularly clustered for this reason. Samples

located at the higher end of the axis are dominated by Ericaceae and monocot roots and UOM and are from zones 1-Mc, 1-Mb, 2-Ma and 3-Ma, which have similar species composition. The green samples are correlated with axis-two in which surface vegetation is important in the surface zones of all three profiles.

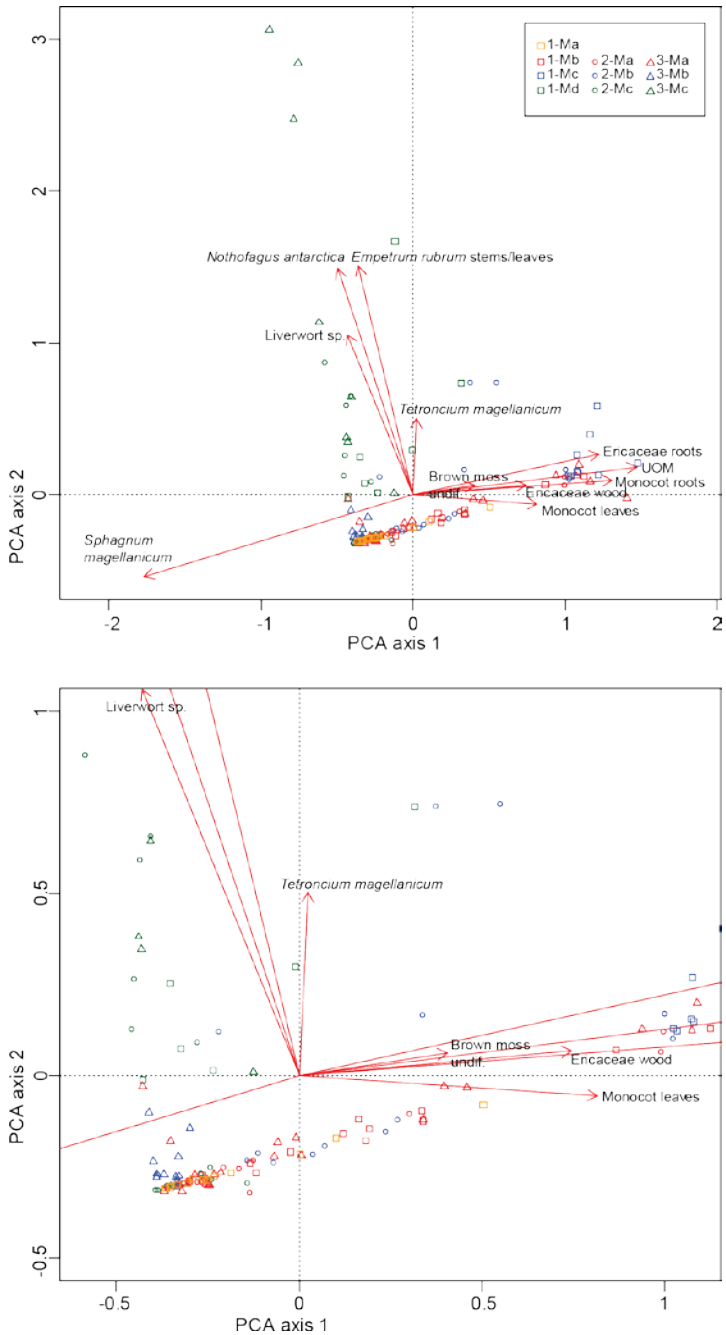

Figure 5.8. Biplot of the PCA axis-one and -two scores based on the raw plant macrofossil data from the KAR-EM profiles.

5.1.3.2.2 Intra-site comparison of DHI values

A comparison of the DHI values from each profile is displayed in figure 5.9. Figure 5.9a plots the DHI values against the actual depths of each profile. The lowest zones in KAR-EM-3 (3-Ma) and KAR-EM-2 (2Ma and 2Mb) are highly variable with little variability in the lowest zone of KAR-EM-1 (1-Ma). Above this, in this profile, there is higher variability through zones 1-Mb and 1-Mc. In zones 3-Mb and c, 2-Mc and 1-Md *Sphagnum* dominates, resulting in low variability across these zones. Between 110 and 100 cm all three records are in agreement and there is agreement between KAR-EM-3 and KAR-EM-2 at 92 cm and between KAR-EM-2 and KAR-EM-1 between 80 and 70 cm; however, plotted in this way there is little synchroneity between all records. This is further demonstrated by the correlations between the profiles based on DHI values displayed in table 5.6. Although a higher negative correlation is found between KAR-EM-3 and KAR-EM-2, the profiles are generally weakly correlated based on actual depth.

Table 5.6. Spearman's rank correlation coefficient between DHI values of profiles plotted against actual depth and plotted relative to the surface of KAR-EM-3 (α=0.05).

	KAR-EM-3 vs. KAR-EM-2	KAR-EM-3 vs. KAR-EM-1	KAR-EM-2 vs. KAR-EM-1
Actual depth			
r_s	-0.337	-0.083	0.035
Relative depth			
r_s	0.093	0.279	*0.348

Figure 5.9b plots the DHI values relative to the surface of KAR-EM-3. The three records are highly variable below 80 cm; above this values remain low to the surface in KAR-EM-3. There is a synchronous shift to lower values at ~74 cm in KAR-EM-2 and KAR-EM-1 with the three records synchronous above this towards the surface. Although plotting the profiles relative to the surface of KAR-EM-3 does not result in more general similarity between the records, the acrotelm-catotelm boundary in each profile is synchronous across the three. Positive correlations result from comparison of the profiles plotted relative to the surface of KAR-EM-3 (table 5.6); however, correlation in this way relies on interpolating between sampling depths in KAR-EM-3 and KAR-EM-1 (See section 3.7).

The mean DHI value decreases from KAR-EM-3 to KAR-EM-1 (KAR-EM-3:3.90, KAR-EM-2:4.08, KAR-EM-1:4.64) and all have a similar range of variability (4.5-5). Differential accumulation rates across the three profiles suggest that chronologically constrained records must be compared.

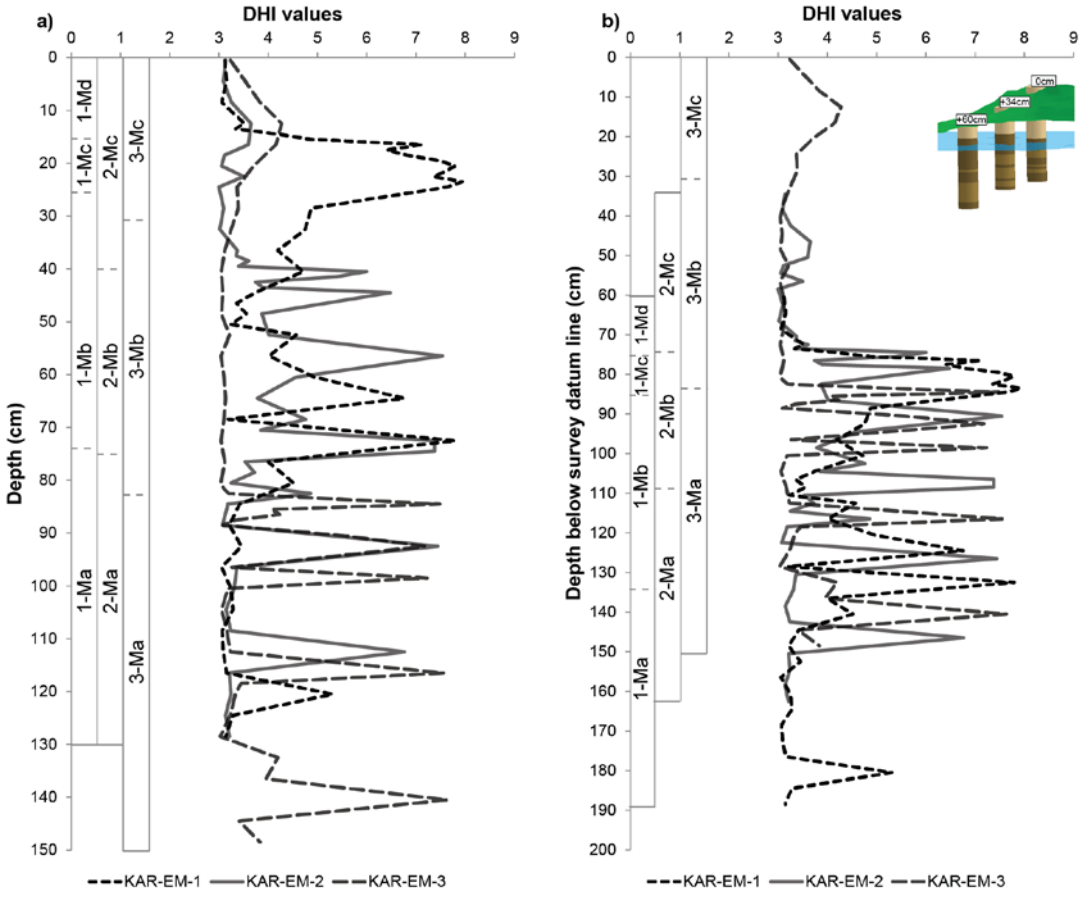

Figure 5.9. Comparison of the DHI values from each KAR-EM profile. DHI values are plotted against the actual depths of each profile (a) and relative to the surface of KAR-EM-3 (b).

5.1.3.3 Humification results

The raw humification data from KAR-EM-3, KAR-EM-2 and KAR-EM-1 are presented in figure 5.10 and show variability of % light transmission. The mean values of the records are 49.76%, 38.39% and 42.38% respectively.

In KAR-EM-3 most variability in the record is present in the basal zone 3-Ma in which there is a peak to higher % light transmission at 104 cm. At the zone boundary to 3-Mb, % light transmission decreases; this coincides with the acrotelm-catotelm

boundary. Above this boundary, values increase and remain at ~60% throughout zone 3-Mb reflecting the presence of undecomposed remains in the acrotelm. There is a drop in values in zone 3-Mc with a peak to low values at 18 cm; after this there is an increase in values towards the surface.

In KAR-EM-2 there is higher variability in zone 2-Ma, with two peaks to lower % light transmission at 112 cm (16%) and 92 cm (22%). Zone 2-Mb shows less variability with values below the mean ~30% throughout the zone. At the acrotelm-catotelm boundary there is a shift to lower % light transmission to 22% after which values become higher towards the surface through zone 2-Mc.

In KAR-EM-1 values are uniform around the mean (42.38%) throughout zones 1-Ma and 1-Mb, apart from a peak at 68 cm to ~50%. There is a switch from values around the mean to higher values in zone 1-Mc to 56.6% at the end of the zone. Values increase through zone 1-Md to 86.5% at the surface.

The slight trend from the base to the surface resulting from the long-term decay of peat in the saturated catotelm zone resulted in the need to detrend the records. The detrended and normalised records are presented alongside the raw data and will be compared with other proxies in section 5.4.1.

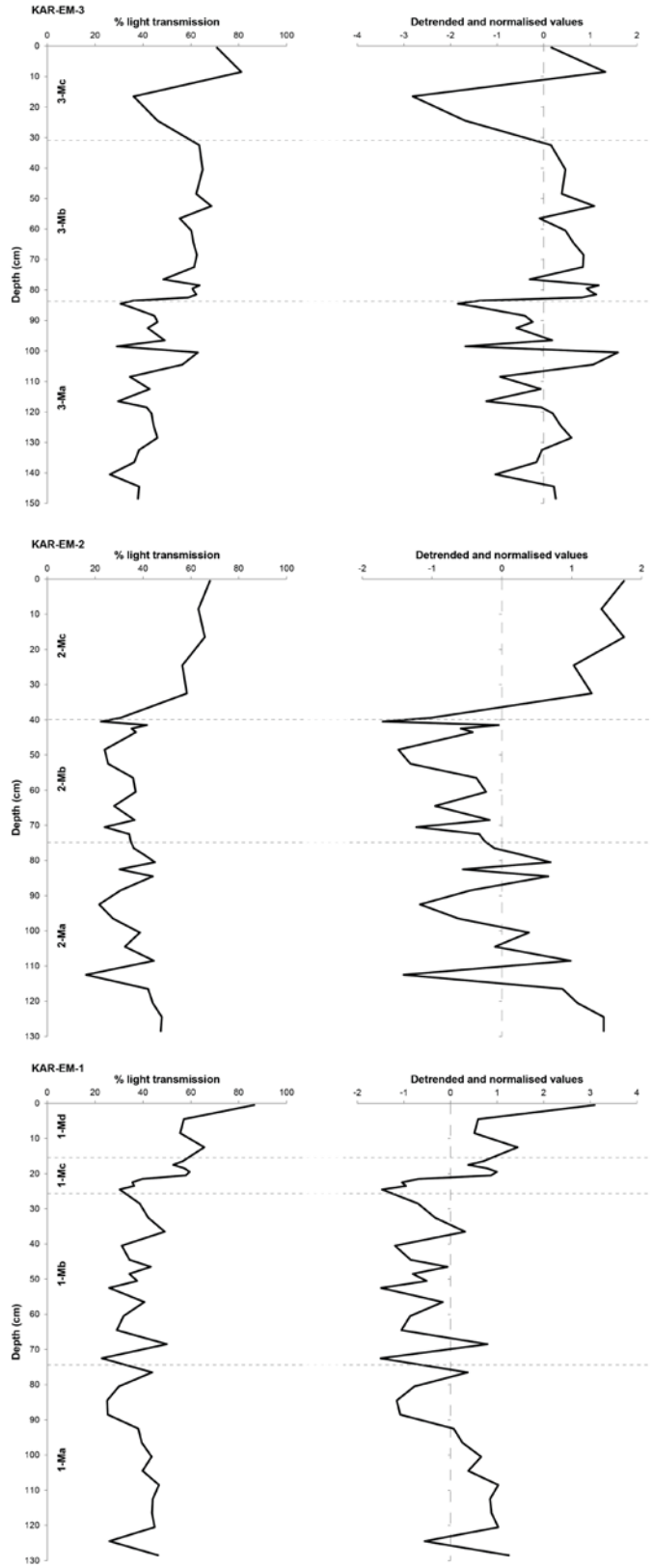

Figure 5.10. The raw humification data (graphs on left) and the detrended and normalised humification records (graphs on right) from KAR-EM-3, KAR-EM-2 ns KAR-EM-1. Plant macrofossil zones are displayed.

5.1.3.4 Intra-site comparison of humification records

Figure 5.11 presents an intra-site comparison of humification values. The stratigraphic descriptions as presented in figure 5.2 are displayed alongside the diagrams. The humification results are a quantitative measure to complement the qualitative approach to stratigraphic description.

Figure 5.11a plots the values from each profile based on the actual sample depths. KAR-EM-3 has a higher mean value (49.76%) than KAR-EM-2 (38.39%) and KAR-EM-1 (42.38%), explained by the higher presence of undecomposed matter in KAR-EM-3, the comparably lower presence of undecomposed matter in KAR-EM-1 and the higher variability between the two in KAR-EM-2. This is also indicated by the lower range of variability (between maximum and minimum value) in KAR-EM-3 (54.97%) than in KAR-EM-1 (63.67%). The highest % light transmission value in each profile is at the surface with the lowest values at very different depths (KAR-EM-3: 140 cm, KAR-EM-2: 112 cm and KAR-EM-1: 72 cm). The three records are dissimilar below 80 cm; above this there is better similarity between KAR-EM-2 and KAR-EM-1 alongside higher values in KAR-EM-3. Above ~35 cm all records shift to higher % light transmission values towards the surface. Plotted in this way the changes across the three records are not generally synchronous. The agreement between KAR-EM-2 and KAR-EM-1 is demonstrated by the positive correlation between the two shown in table 5.7 alongside disagreement between the other profiles.

Table 5.7. Spearman's rank correlation coefficient between the humification records from profiles plotted against actual depth and plotted relative to the surface of KAR-EM-3 (α=0.05).

	KAR-EM-3 vs. KAR-EM-2	KAR-EM-3 vs. KAR-EM-1	KAR-EM-2 vs. KAR-EM-1
Actual depth			
r_s	-0.156	-0.091	*0.495
Relative depth			
r_s	-0.196	-0.039	0.141

When plotted relative to the surface of KAR-EM-3 (figure 5.11b) there is better visual agreement between the records but this does not result in stronger correlations between the profiles (table 5.7). In fact, the correlation between KAR-EM-2 and KAR-EM-1 is weaker.

The lowest values in each record are more closely spaced (between 150-130 cm). The shift to lower % light transmission values is synchronous across the three profiles just below 80 cm with a shift to higher values in all records above this boundary. Above 100 cm the KAR-EM-3 and KAR-EM-1 records are synchronous until 70 cm with KAR-EM-2 displaying a similar trend but at lower values. The records, plotted against the chronology to assess the synchroneity between the stratigraphic shifts, are displayed in Figure ***.

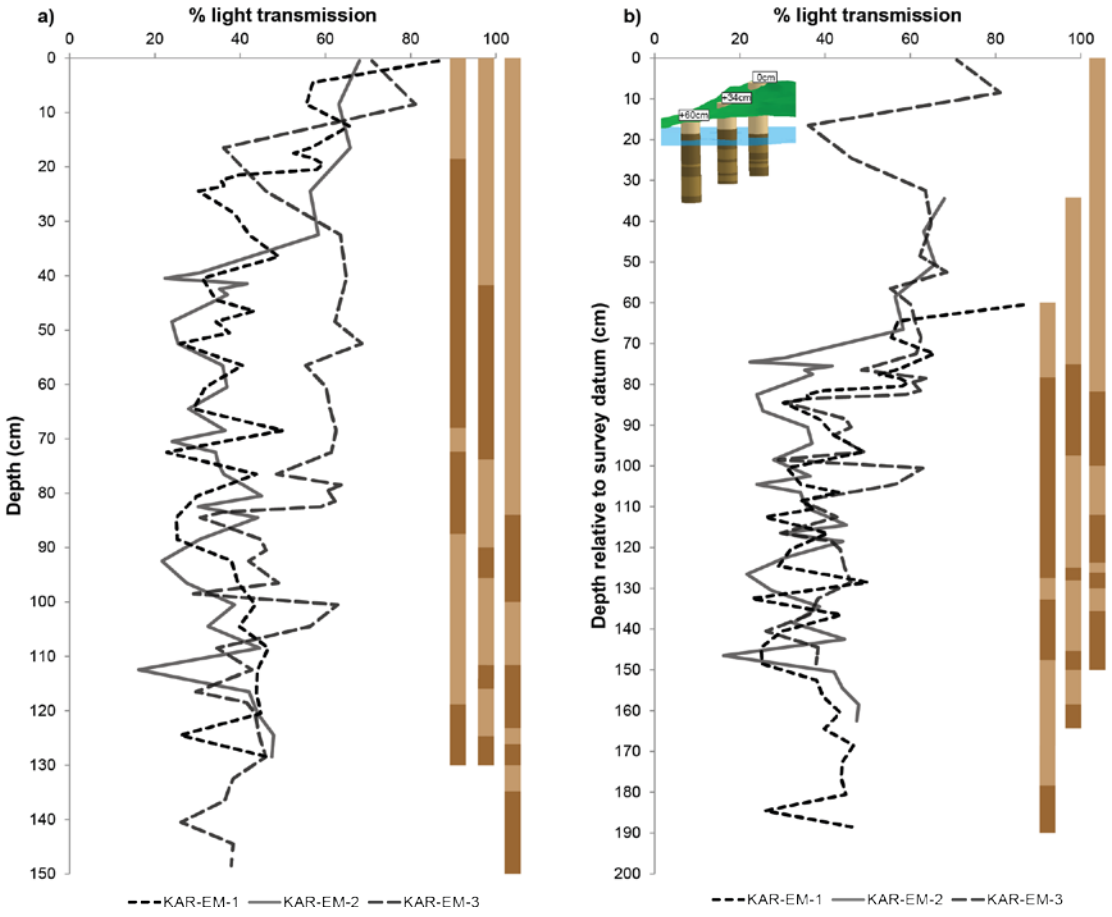

Figure 5.11. Comparison of the humification values from each KAR-EM profile. Humification values are plotted against the actual depths of each profile (a) and relative to the surface of KAR-EM-3 (b).

5.1.3.5 Testate amoeba results

The testate amoeba diagrams from KAR-EM-3, KAR-EM-2 and KAR-EM-1 are presented in figure 5.12, 5.13 and 5.14 respectively. A summary description of the testate amoeba zones as well as the depths and approximate ages of the zone boundaries is presented in table 5.8.

Of the taxa included in the transfer function and subsequent water table depth reconstruction, xerophilous to hygrophilous taxa are displayed from left to right on the stratigraphic diagrams. On the far right of each diagram are the taxa that are not included in the transfer function and subsequent water table depth reconstruction. Test concentration per cm^3 and taxonomic diversity are displayed next to the stratigraphic diagrams for reference. In some cases a count of 100 tests was not achieved (displayed by dashed lines); however, a sufficient number of taxa were identified within the lower counts

With reference to figure 5.12, zone 3-Ta (AD 473-1652) has the most variability in the record in which *D.pulex* is the dominant taxon. Taxonomic diversity is higher in this zone than upper zones, with the presence of many taxa in relatively low abundances. Test concentration is also highest in this zone. *D.pristis* type dominates in Zone 3-Tb (AD 1652-1858) where taxonomic diversity and test concentration is lower than the previous zone. Between the depths 50 to 12 cm (AD 1858-1990) testate amoebae are absent. In the surface zone, 3-Tc (AD 1990-2013), test concentration remains low and taxonomic diversity is lowest with the dominance of *A.muscorum* throughout this zone. In KAR-EM-2 (figure 5.13) zone 2-Ta is dominated by *D.pulex*, test concentration is uniform throughout the zone apart from a peak at 112 cm. Taxonomic diversity increases towards the end of the zone (73 cm, AD 1137). There is a large peak in test concentration at 72 cm to ~19,000 tests per cm^3 but test concentration remains uniform after this. *D.pulex* is, again, dominant throughout zone 2-Tb with taxonomic diversity increasing towards the end of the zone (38 cm, AD 1949). *D.pulex* decreases at the beginning of zone 2-Tc and *D.pristis* type increases. Taxonomic diversity decreases throughout the zone and test concentration is lowest in this zone. *A.muscorum* increases to dominance after 12 cm (AD 1992). With reference to figure 5.14, test concentration and taxonomic diversity is highly variable throughout this record, with 2 peaks to high concentrations at 16 cm and 88 cm. *D.pulex* dominates through zones 1-Ta, 1-Tb and 1-Tc until AD 1880 when this species decreases and *A.muscorum* becomes dominant to the surface.

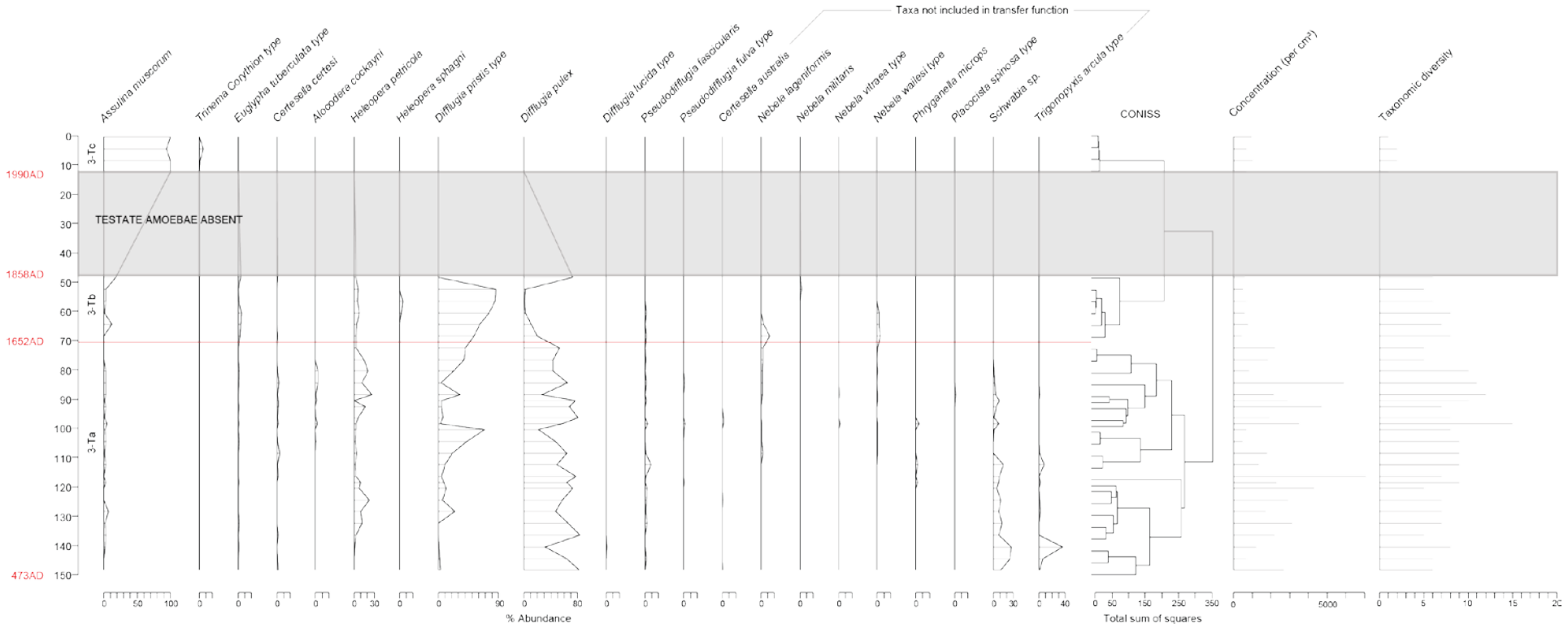

Figure 5.12. KAR-EM-3 testate amoeba diagram plotted against depth, displaying testate amoeba zones based on CONISS with approximate ages of zone boundaries presented. Concentration and taxonomic diversity presented. Note zone in which no testate amoebae were present.

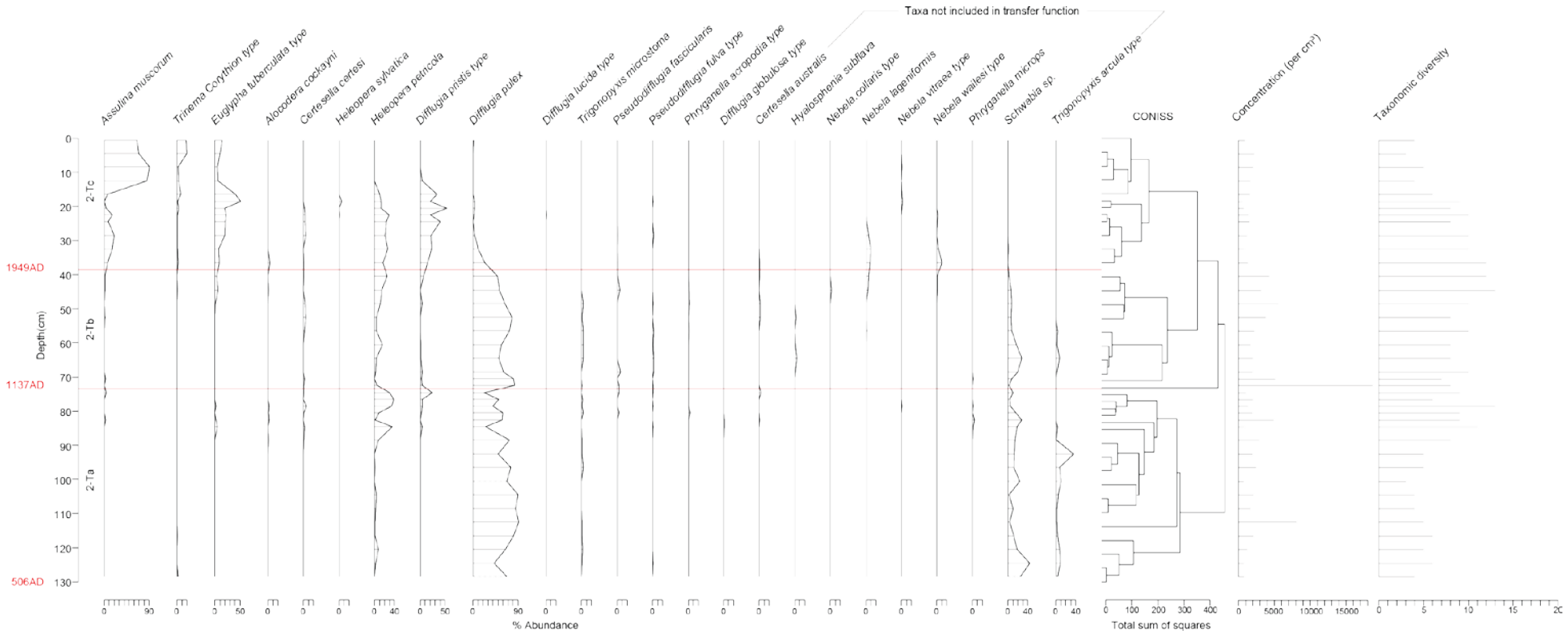

Figure 5.13. KAR-EM-2 testate amoeba diagram plotted against depth, displaying testate amoeba zones based on CONISS with approximate ages of zone boundaries presented. Concentration and taxonomic diversity presented.

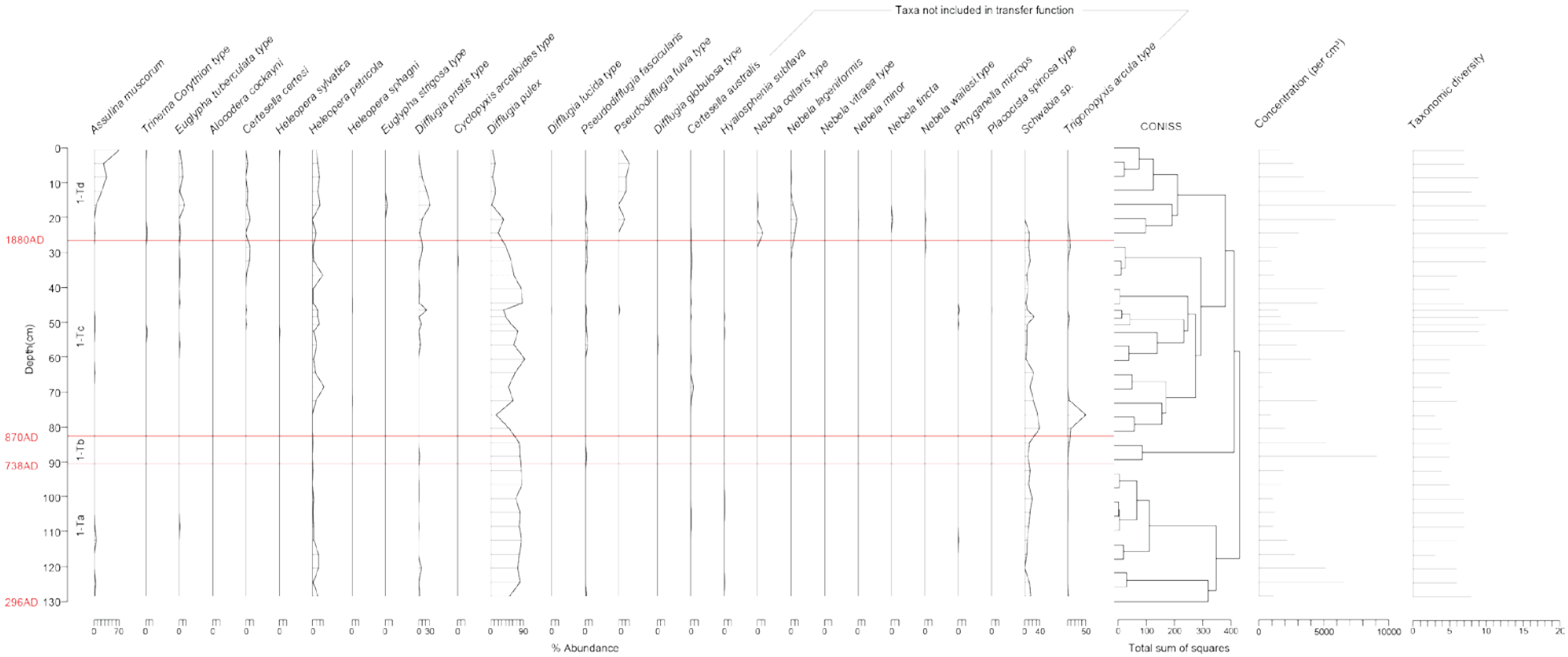

Figure 5.14. KAR-EM-1 testate amoeba diagram plotted against depth, displaying testate amoeba zones based on CONISS with approximate ages of zone boundaries presented. Concentration and taxonomic diversity presented.

Table 5.8. Summary description of the testate amoeba zones from the Karukinka profiles; KAR-EM-3, KAR-EM-2 and KAR-EM-1.

Zone	Depth (cm)	Testate amoeba zone description	Age cal BP (AD)
KAR-EM-3			
3-Ta	150-70	Zone of high variability in which *Difflugia pulex* dominates throughout. There is a peak of *Trigonopyxis arcula* at the beginning of the zone. *Schwabia* sp. is present throughout the zone but decreases and becomes absent towards the end of the zone. There is a mid-zone peak of *Difflugia pristis* type with an increase towards the end of the zone. *Heleopera petricola* also contributes to the assemblage throughout this zone. *Assulina muscorum* is present in low numbers throughout the zone. Taxonomic diversity is highest throughout this zone, especially towards the end. Test concentration peaks at 120 cm and 84 cm and is higher than in other zones.	1476-298 cal BP (AD 473-1652)
3-Tb	70-48	*D.pulex* decreases at the beginning of the zone and *D.pristis* type increases to dominance. *D.pulex* and *A.muscorum* increase at the end of the zone before the next zone where testate amoebae are absent. Taxonomic diversity is lower than in the previous zone. Test concentration is low in this zone.	298-93 cal BP (AD 1652-1858)
Absence of testate amoebae	48-13	At 4 cm resolution no testate amoebae were found between these depths.	93- -40BP (AD 1858-1990)
3-Tc	13-0	Dominance of *A.muscorum* in this zone with almost 100% abundance throughout the zone. *Trinema/Corythion* type is present towards the end of the zone. Taxonomic diversity is lowest in this zone. Test concentration remains as low as in 3-Tb.	-40- -63 cal BP (AD 1990-2013)
KAR-EM-2			
2-Ta	130-73	*D.pulex* dominates throughout. The highest percentage of *Schwabia* sp. is found at the beginning of the zone and remains present throughout. *H.petricola* is present throughout and rises towards the	1444-813 cal BP (AD 506-

		end of the zone. *T. arcula* is present throughout the zone with a peak ~92 cm. Test concentration is fairly uniform throughout the zone with a peak at 112 cm. Taxonomic diversity increases towards the end of the zone.	1137)
2-Tb	73-38	*D.pulex* dominates throughout the zone and decreases towards the end. *Schwabia* sp. decreases throughout the zone. *D.pristis* type and *H.petricola* increase towards the end of the zone. There is a peak of test concentration at the beginning of the zone with ~19000 tests per cm^3 concentration is otherwise uniform throughout the zone. Taxonomic diversity increases towards the end of the zone.	813-1 cal BP (AD 1137-1949)
2-Tc	38-0	*D.pulex* decreases to absence at the beginning of the zone. *Euglypha tuberculata* type and *D.pristis* type increase from the beginning of the zone until there is a rise to dominance of *A.muscorum*. Test concentration is lower than previous zones. Taxonomic diversity decreases throughout the zone.	1- -63 cal BP (AD 1949-2013)
KAR-EM-1			
1-Ta	130-90	*D.pulex* dominates throughout the zone. *H.petricola* and *Schwabia* sp. contribute to the assemblage. Taxonomic diversity is uniform throughout the zone. Test concentration decreases throughout this zone.	1654-1213 cal BP (AD 296-738)
1-Tb	90-82	This short zone is dominated by *D.pristis*. Taxonomic diversity is similar to the previous zone. There is a peak of test concentration with numbers reaching ~10,000 tests per cm^3 at 88 cm.	1213-1080 cal BP (AD 738-870)
1-Tc	82-26	The abundance of *D.pulex* is lower than previous zones, *H.petricola* contribute to the assemblage and *Schwabia* sp. Taxonomic diversity and test concentration increase around the middle of the zone.	1080-70 cal BP (AD 870-1880)
1-Td	26-0	*D.pulex* decreases from previous levels. E. tuberculata type, *H.petricola*, *D.pristis* type and *Pseudodifflugia fulva* type contribute to the assemblage of this zone. There is a marked increase of *A.muscorum* towards the surface. Taxonomic diversity is uniform	70- -63 cal BP (AD 1880-2013)

		throughout this zone. Test concentration peaks at the beginning of the zone with ~10,000 tests per cm^3 at 16 cm.	

The results of the DCA of the KAR-EM-3, KAR-EM-2 and KAR-EM-1 are displayed in table 5.9. The axis-one gradient length of less than 3σ from the KAR-EM-3 dataset resulted in the use of a linear response model. The axis-one gradient length between 3-4σ in the KAR-EM-1 dataset suggests that a unimodal or linear response model can be used, for consistency with the other records a linear response model was used. The results of the PCA of these two datasets are presented in table 5.10; high taxonomic diversity and a high influence of rare species on PCA axis-one scores resulted in removal of rare species. The DCA of the KAR-EM-2 dataset resulted in an axis-one gradient length of more than 4σ which warrants the use of a unimodal response model (Ter Braak and Prentice, 1988; Lepš & Šmilauer, 2003).

Bi-plots of the PCA axis-one and -two sample and species scores from KAR-EM-1 and KAR-EM-3 and a bi-plot of DCA axis-one and -two sample and species scores from KAR-EM-2 are presented in figure 5.15. Points are coloured according to their corresponding testate amoeba zone. The PCA of the KAR-EM-3 dataset resulted in two significant axes: axis-one (34.44%) and -two (26.11%). Axis-one of the KAR-EM-2 dataset has a sufficiently high eigenvalue of 0.7699 (Ter Braak, 1995) and accounts for 42.05% of variability in the data. The PCA of the KAR-EM-1 dataset resulted in only one significant axis, axis-one, accounting for 32.65% of the variance in the data.

Table 5.9. Results of DCA of KAR-EM-3, KAR-EM-2 and KAR-EM-1 testate amoeba data.

KAR-EM-3 (Down-weighting and removal of rare species)			
	Axis 1	Axis 2	Axis 3
Eigenvalues	0.8114	0.4720	0.11226
% accounted for by axis	48.74%	28.35%	6.74%
Gradient lengths	2.7430	2.5048	0.78601
KAR-EM-2 (Down-weighting and removal of rare species)			
	Axis 1	Axis 2	Axis 3
Eigenvalues	0.7699	0.14289	0.1372
% accounted for by axis	42.05%	7.81%	7.50%
Gradient lengths	4.2192	1.12691	1.3179
KAR-EM-1 (Down-weighting and removal of rare species)			
	Axis 1	Axis 2	Axis 3
Eigenvalues	0.5333	0.1645	0.10490
% accounted for by axis	35.83%	11.06%	7.05%
Gradient lengths	3.5150	1.2989	1.25791

Table 5.10. Results of PCA of KAR-EM-3 KAR-EM-2 and KAR-EM-1 testate amoeba data.

KAR-EM-3 (Removal of rare species, Hellinger transformed)			
	Axis 1	Axis 2	Axis 3
Eigenvalues	3.0092	2.3498	0.9301
% accounted for by axis	34.44%	26.11%	10.33%
Screeplot (Broken stick)	Significant	Significant	-
KAR-EM-1 (Removal of rare species, Hellinger transformed)			
	Axis 1	Axis 2	Axis 3
Eigenvalues	4.571	2.394	1.445
% accounted for by axis	32.65%	17.10%	10.32%
Screeplot (Broken stick)	Significant	-	-

With reference to the KAR-EM-3 PCA bi-plot, *A.muscorum* and *D.pulex* are most correlated with axis-one and are located at opposite ends of the axis. Samples in 3-Ta are located at the higher end of axis-one as the species composition is dominated by *D.pulex* and samples in 3-Tc are located at the opposite end with the dominance

of *A.muscorum* in this zone. *D.pristis* type is most correlated with axis-two and samples in 3-Tb are located at the higher end of this axis and are dominated by *D.pristis* type. Samples in 3-Ta are spread along this axis. Inferring a hydrological gradient from either axis is difficult owing to the significance of both axis-one and -two and the lack of separation of taxa along either of the axes.

Similarly, *D.pulex* and *A.muscorum* are located at opposite ends of axis-one of the bi-plot of the DCA of KAR-EM-2 dataset. Samples in 2-Ta and 2-Tb are located at the lower end of axis-one with samples in 2-Tc located towards the higher end of the axis. This separation could suggest that axis-one represents a wetness gradient; however, *H.petricola* and *D.pristis* type should be in opposite positions according to their currently known ecological preferences.

D.pulex and *E.tuberculata* type are most strongly correlated with axis-one of the PCA of the KAR-EM-1 dataset, located at opposite ends of the axis. Samples are highly spread in the multidimensional space with groupings by zone not clearly apparent. The majority of samples are located at the higher end of axis-one, owing to the dominance of *D.pulex* throughout the record and may display uniform conditions. Samples in zone 1-Td are located at the opposite end of the axis due to the shift from dominance of *D.pulex* to dominance of *A.muscorum* towards the surface, potentially indicating a shift to drier conditions if this axis represents a wetness gradient. A wetness gradient may be represented by the shift in species composition from the lower zones to the surface zone.

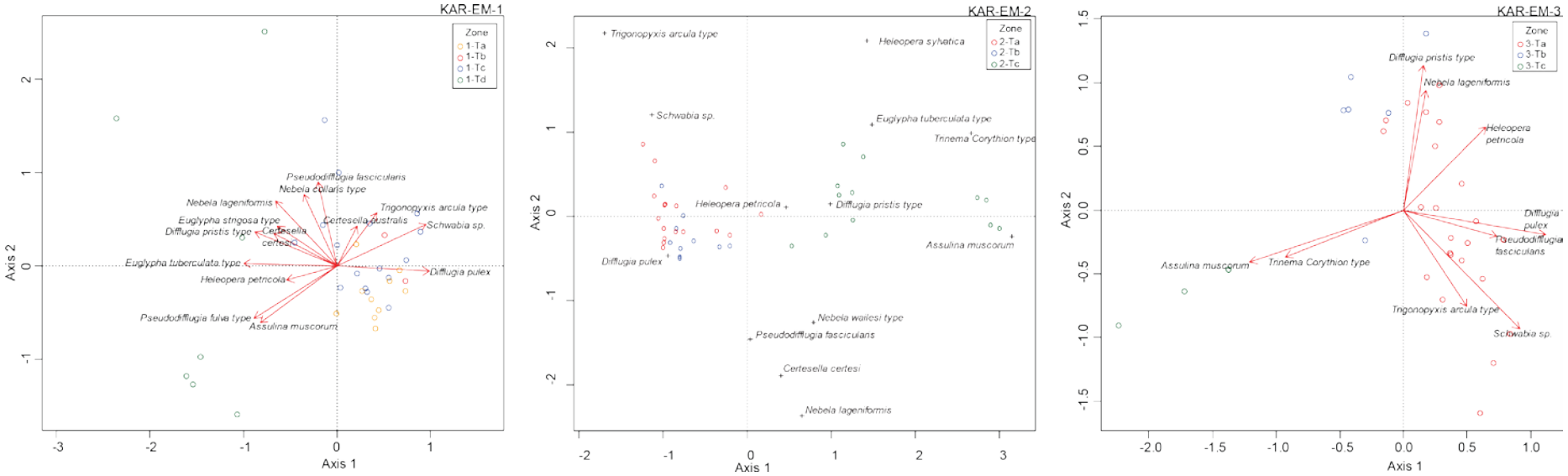

Figure 5.15. Bi-plot of PCA axis-one and -two species (Red arrows) and sample scores (points coloured according to CONISS testate amoeba zone) of KAR-EM-1 and KAR-EM-3 testate amoeba data. Bi-plot of DCA axis-one and -two species and sample scores (points coloured according to CONISS testate amoeba zone) of KAR-EM-2 testate amoeba data.

Separation of taxa along axis-one may suggest that this axis represents a hydrological gradient; the KAR-EM-3 and KAR-EM-1 PCA axis-one scores and KAR-EM-2 DCA axis-one scores are compared with the WTD reconstruction in figure 5.16.

The water table depth (WTD) reconstruction from each profile was derived by application of the Patagonian WA-PLS transfer function to the raw testate amoeba data (Section 3.5.2) and these records are shown to the left of the figure. These records are presented as WTD in cm units with each sample point representing the reconstructed depth to the water table from the surface. The dashed lines are the associated WTD errors (~16 cm). The testate amoeba zones are displayed on the diagrams for reference. The mean reconstructed WTD for KAR-EM-3, KAR-EM-2 and KAR-EM-1 is 24.02 cm, 23.96 cm and 16.65 cm respectively.

In zone 3-Ta, the WTD persists at a level around 15 cm until 90 cm after which the depth increases to a level around 20 cm to the end of the zone. In zone 3-Tb, the WTD is at a higher level around 30 cm dropping slightly before the zone in which testate amoebae are absent. After this zone at 12 cm, the WTD is increased to the highest level in the record in zone 3-Tc towards the surface at a level around 66 cm. The shifts between the zones are, again, a reflection of the shift in species composition from *D.pulex* – *D.pristis* type – *A.muscorum* from the base to the surface with their respective environmental preferences influencing the WTD reconstruction. The PCA axis-one scores are displayed. In zone 3-Ta there is little variability just above the mean, reflecting the dominance of *D.pulex* located at the higher end of axis-one. There is a peak to lower scores at 106 cm which is driven by a peak of *D.pristis* type, correlated with axis-two, within this zone. There is a slight trend to decreased scores through this zone. In zone 3-Tb there is a decreasing trend reflecting the dominance of *D.pristis* type with values below the mean. In the surface zone, values are well below the mean and reflect the switch to dominance of *A.muscorum*, located at the lower end of axis-one. The peak reflects the small increase of *Trinema/Corythion* type which is correlated with and located at the lower end of axis-one. The two normalised records are compared and are shown to the right of the figure. The record of PCA axis-one scores diverges at 106 cm and also at the end of zone 3-Tb with the shifts in the same direction but of higher magnitude.

The two records diverge in zone 3-Tc as *Trinema/Corythion* type drives the peak in PCA axis-one scores in this zone and have less influence on the WTD reconstruction.

Throughout zone 2-Ta the WTD remains ~10 cm until the end of the zone where there are 2 shifts to higher WTD (~26 cm) at 84 cm and 76 cm. WTD decreases to ~10 cm in zone 2-Tb increasing towards the end of the zone to ~21 cm at the boundary to zone 2-Tc. WTD continues to increase throughout this zone to ~64 cm at the surface. These WTD shifts reflect the shift in dominant species from *D.pulex* in zone 2-Ta to the end of 2-Tb, to the dominance of *D.pristis* type in zone 2-Tc and *A.muscorum* towards the surface. The peaks in zone 2-Ta reflect a rise in *H. petricola*. An almost identical record is shown by DCA axis-one scores which suggests that this may be a record of wetness variability, representing shifts in dominant species. The correspondence between the two records is displayed by comparison of the normalised records. The two records are both good representations of the raw testate amoeba data.

Through zones 1-Ta and 1-Tb WTD is uniform at ~9 cm reflecting the dominance of *D.pulex*, apart from a shift to higher WTD at 68 cm (~20 cm) where there is a higher abundance of *H.petricola*. WTD rises to ~26 cm towards the end of zone 1-Tc (26 cm). WTD increases throughout zone 1-Td to 54 cm at the surface reflecting the shift to *A.muscorum* in this zone. The PCA axis-one scores are presented and both the normalised records are compared. The two records correspond well owing to the dominant variables driving the PCA axis-one scores. However, there is a divergence between the two records in the surface zone, particularly where there is no apparent shift to higher PCA scores at 20 cm (note the reversal of the PCA axis-one scores axis) and a shift to lower PCA scores of higher magnitude than the shift in WTD at 16 cm. There is also a divergence between the two records to the surface where the WTD reconstruction displays a shift to higher values whereas the PCA scores shift to higher values relative to the mean of the record. These differences are due to the differences in the importance of the taxa in the two analyses.

Despite similarities between the normalised records the WTD reconstructions are constrained by modern data and therefore provide a more reliable quantification of wetness variability and will be compared with the other proxy records.

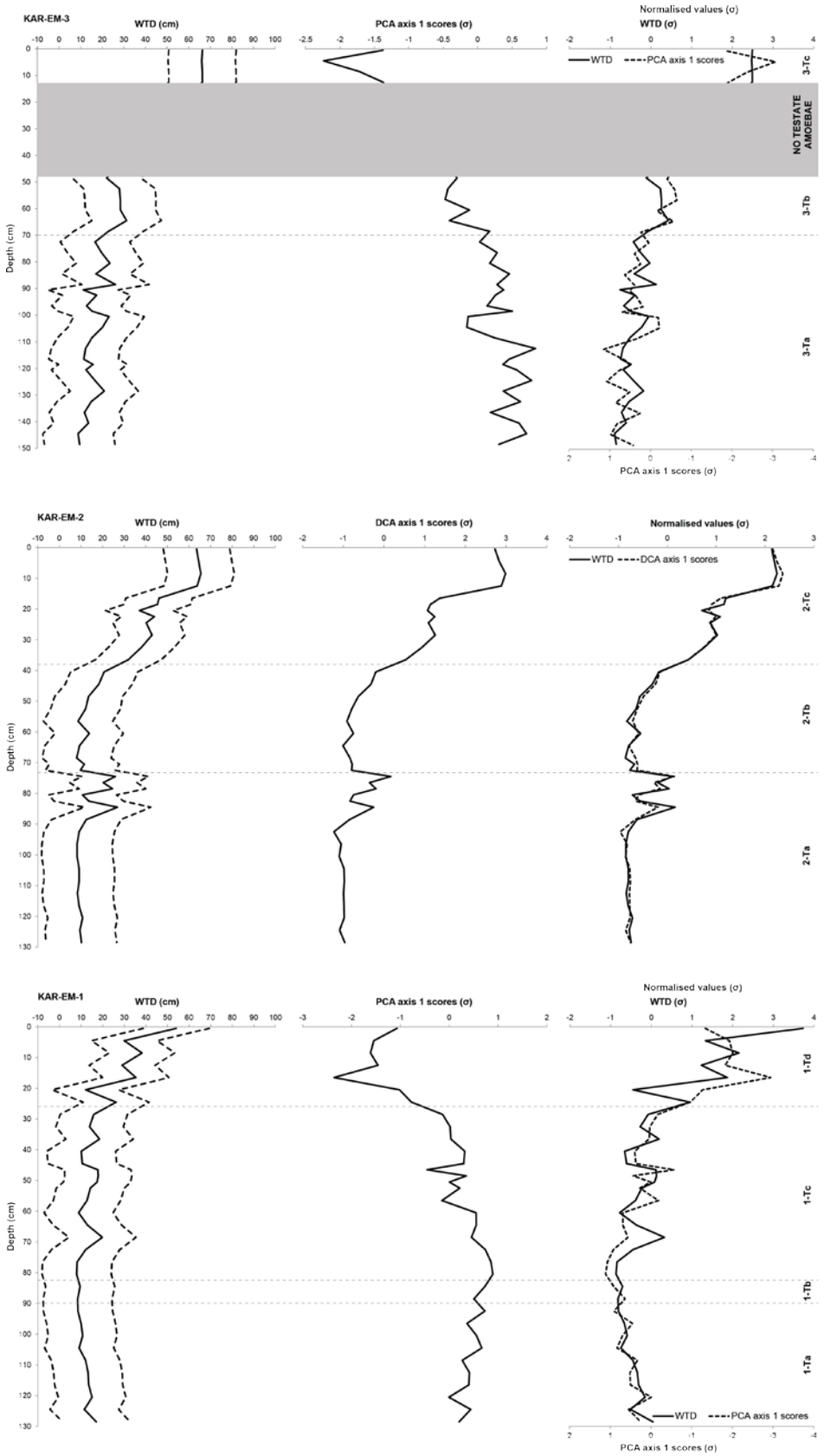

Figure 5.16. Bog surface wetness anomaly curves from the KAR-EM-3, KAR-EM-2 and KAR-EM-1 testate amoeba data transformed to water table depth reconstruction (a) and respective axis-one scores (b). The two normalised records are compared (c). Testate amoeba zones are displayed. Note zone in which no testate amoebae were present.

5.1.3.6 Intra-site comparison of testate amoeba records

5.1.3.6.1 Multivariate statistical analysis of testate amoeba records

A bi-plot of the DCA axis-one and -two scores of the testate amoeba data from all three KAR-EM profiles is displayed in figure 5.17. A DCA was carried out because the sufficient gradient length of the first axis (4.0920) enabled the use of a unimodal response model. 14 ‘rare species’ were removed because of low abundances. Each sample’s symbol and colour relates to the corresponding profile and testate amoeba zone. Axis-one accounts for 33.48% of the total variance in the data (table 5.11) and samples are spread along this principal axis. There is separation along this axis of surface samples dominated by *A.muscorum* etc. at the higher end of the axis with the majority of samples located at the lower end of the axis and dominated by *D.pulex*. A cluster of samples from 3-Ta is located between *D.pulex* and *D.pristis* type and a cluster from 3-Tb is located close to *D.pristis* type suggesting the difference in species composition of these two zones compared with the other profiles.

Table 5.11. Results of DCA of testate amoeba data from all three KAR-EM profiles.

	Axis 1	Axis 2	Axis 3
Eigenvalues	0.6899	0.2122	0.28949
% accounted for by axis	33.48%	10.30%	14.05%
Gradient lengths	4.0920	1.8304	2.1490

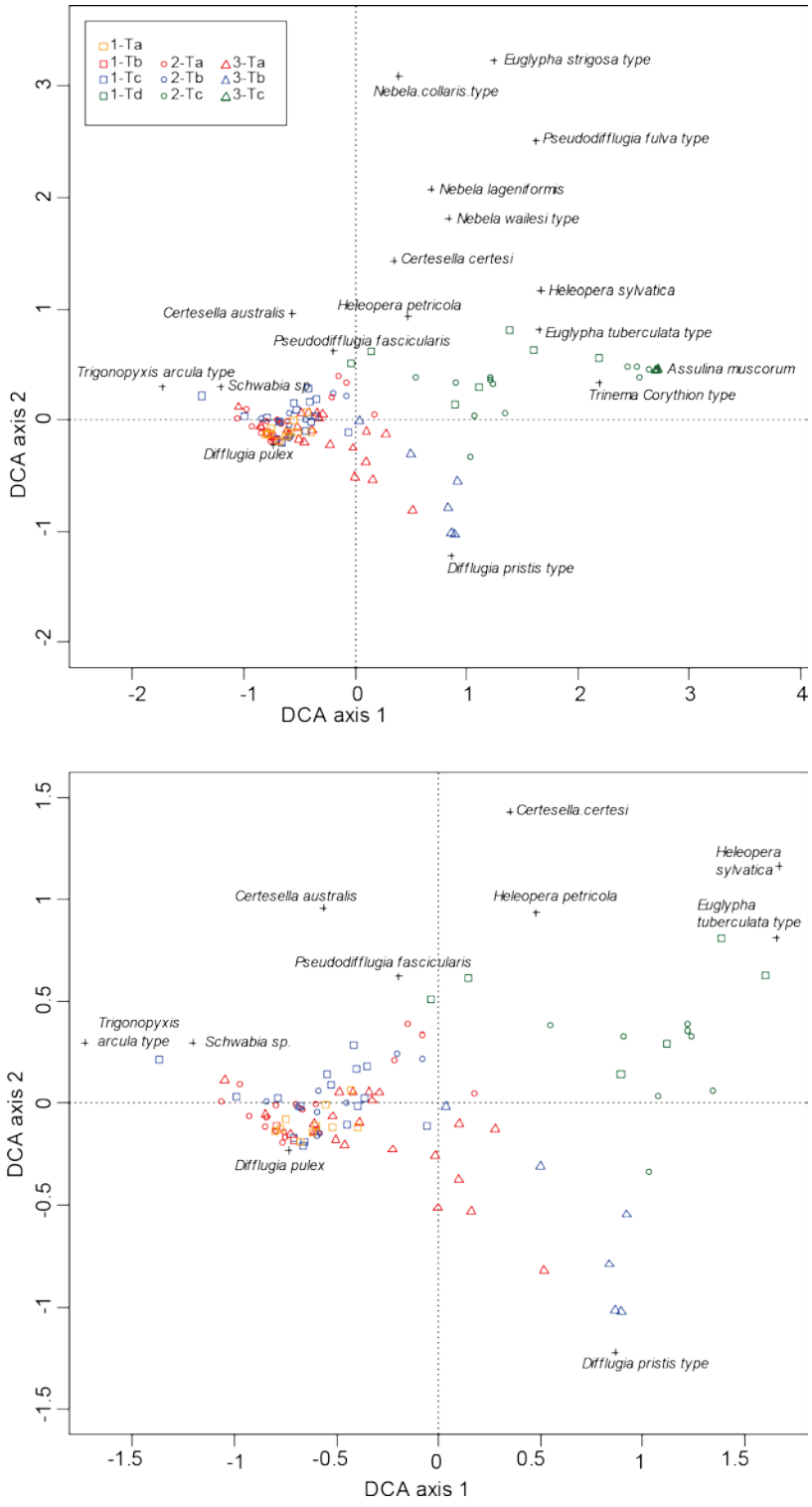

Figure 5.17. Bi-plot of the DCA axis-one and -two scores of the testate amoeba data from the KAR-EM profiles.

5.1.3.6.2 Intra-site comparison of WTD reconstructions

Figure 5.18 presents the WTD reconstruction from each profile. The WTD reconstruction plotted against the actual depth of each profile is displayed in figure 5.18a. The WTD error of each record is similar ~16 cm and little variability in the records leads to overlap of the error ranges of the records apart from separation of the records towards the surface. KAR-EM-3 and KAR-EM-2 have similar mean values (24.02 cm and 23.96 cm) with a lower mean value from the KAR-EM-1 reconstruction (16.65 cm). Below 90 cm all 3 records are at a similar level (10-20 cm). Between 90 and 70 cm KAR-EM-1 remains at the same level and KAR-EM-2 and KAR-EM-3 are similar in their shifts to higher values. Between 70-50 cm KAR-EM-1 and KAR-EM-2 are at a similar level with KAR-EM-3 at a higher level than the other two records. Above 50 cm there is a trend to higher WTD in all three records; the shift in KAR-EM-1 is lower compared with the other two records rising to ~54 cm WTD at the surface. The increase in KAR-EM-2 and KAR-EM-3 is similar with both records rising to ~65 cm WTD at the surface. A shift to lower WTD at 20 cm is registered in the record from both KAR-EM-1 and KAR-EM-2. A positive correlation is evident between all profiles (table 5.12) with the highest correlation between KAR-EM-3 vs. KAR-EM-2 and KAR-EM-2 vs. KAR-EM-1. A slightly lower correlation is found between KAR-EM-3 vs. KAR-EM-1 and evidences spatial dissimilarity of the records.

Table 5.12. Spearman's rank correlation coefficient between WTD reconstructions of profiles plotted against actual depth and plotted relative to the surface of KAR-EM-3 (α=0.05).

	KAR-EM-3 vs. KAR-EM-2	KAR-EM-3 vs. KAR-EM-1	KAR-EM-2 vs. KAR-EM-1
Actual depth			
r_s	*0.527	0.327	*0.451
Relative depth			
r_s	*0.592	*0.632	*0.642

The WTD reconstruction is plotted relative to the surface of KAR-EM-3 in figure 5.18b. This results in better similarity between the records with better overlap between the error ranges. Plotted in this way a higher positive correlation between records is also demonstrated in table 5.12 (also see section 3.7).

KAR-EM-1 and KAR-EM-3 show a shift to higher WTD at 130 cm. Between 120 and 105 cm KAR-EM-1 and KAR-EM-3 are similar whereas there are shifts to higher WTD values in KAR-EM-2. Above this all three records are variable but all increase to higher WTD values to their respective surfaces. There is better agreement between the records in figure 5.18a above 70 cm and better agreement between the records in figure 5.18b below 70 cm. This suggests that the three records must be compared based on their chronology.

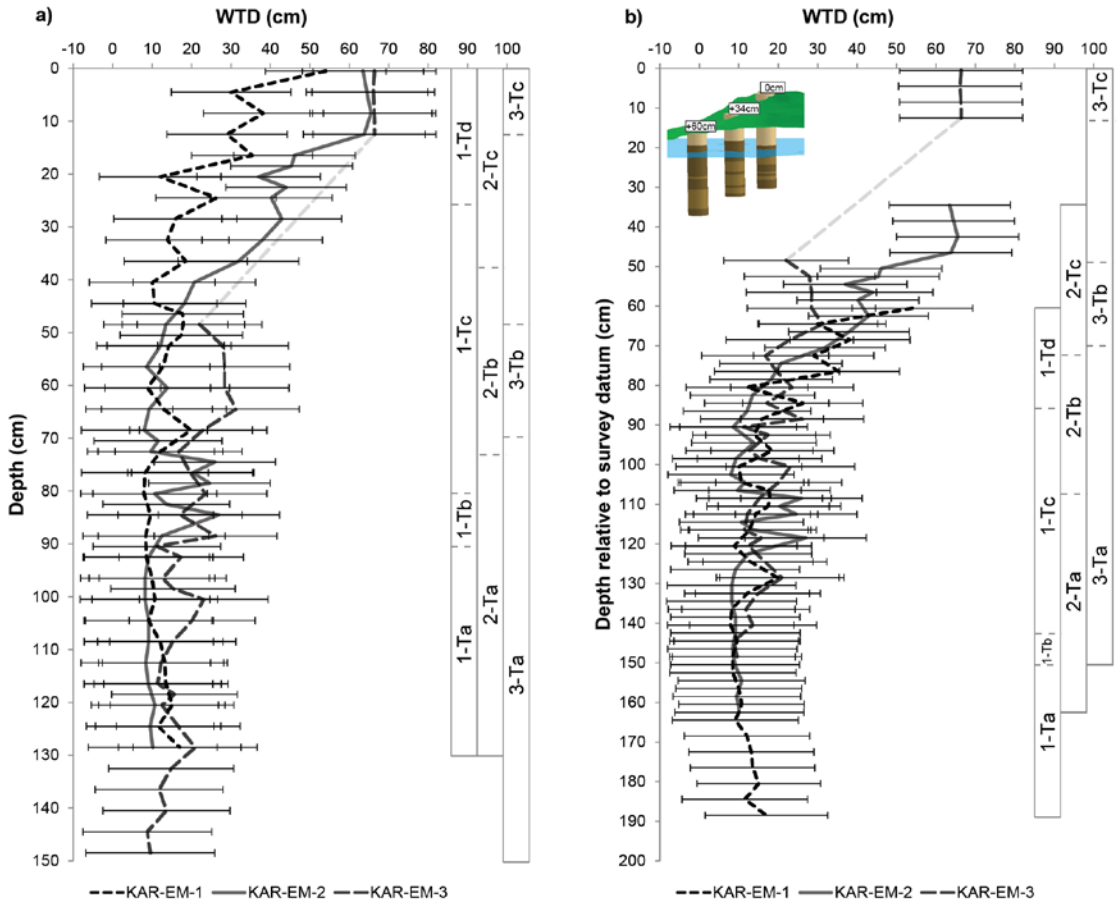

Figure 5.18. Comparison of the WTD reconstructions from each KAR-EM profile. WTD values are plotted against the actual depths of each profile (a) and relative to the surface of KAR-EM-3 (b).

5.1.3.7 Multi-proxy comparison of palaeoecological records

Figure 5.19 displays the normalised palaeoecological records plotted against depth from KAR-EM-1, KAR-EM-2 and KAR-EM-3, providing a multi-proxy comparison of

the records from each profile. The smaller graphs displayed below provide a pairwise comparison between two of the three proxies for ease of interpretation with the correlations below corresponding to those proxies. The normalised testate amoeba and plant macrofossil records are plotted on the primary axis while the normalised humification record is plotted on the secondary axis, which has been reversed for consistency with the direction of hydrological variability. The profile stratigraphies are presented alongside the main diagram and variability is discussed with reference to the plant macrofossil zones.

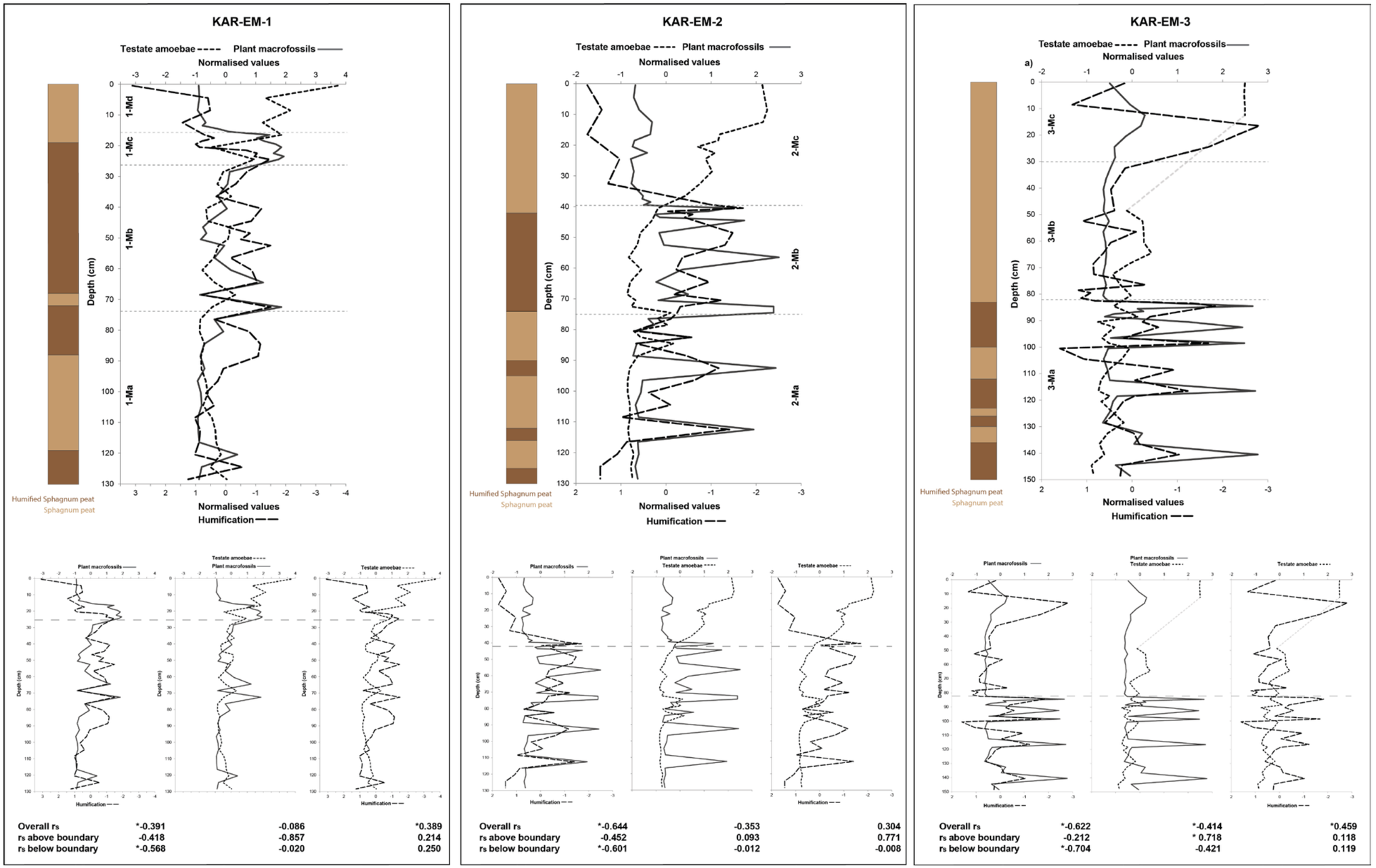

Figure 5.19. Multiproxy comparison of the KAR-EM-1, KAR-EM-2 and KAR-EM-3 palaeoecological records. The normalised testate amoeba and plant macrofossil records are on the primary axis. The normalised humification record is presented on the secondary axis which has been reversed.

5.1.3.7.1 KAR-EM-3 multi-proxy comparison

Zone 3-Ma displays the most variability especially in the plant macrofossil and humification records reflecting the shifts in the stratigraphy. The testate amoeba record is relatively less sensitive to the shifts in the stratigraphy with little variability in this record in zone 3-Ma. Above the acrotelm-catotelm boundary at 83 cm in zone 3-Mb the records are less variable than zone 3-Ma, reflecting the uniform stratigraphy and insensitivity of the proxies in this zone. In zone 3-Mc, there is a shift in the humification record at 18 cm that is not registered in the plant macrofossil record. After a zone with the absence of tests above 12 cm there is a positive excursion of the WTD record that is not registered by the other proxies.

The best correlation is found between the plant macrofossil and humification records (r_s= *-0.62) with good agreement evident between these records. Higher DHI values generally occur alongside lower % transmission values (more humified) which are both indicative of drier conditions. A negative correlation (r_s= *-0.41) is found between the plant macrofossil and testate amoeba records. This is due to the sensitivity of the plant macrofossil record and relative insensitivity of the testate amoeba record in the lower zone and the subsequent insensitivity of the plant macrofossil record and the corresponding excursion of the WTD reconstruction in the upper zones. Higher DHI values generally occur alongside low WTD values and vice versa. A positive correlation (r_s= *0.46) is found between the testate amoeba and humification records. Higher WTD values generally occur alongside higher % transmission values (less humified). A negative correlation would be expected between the two records with higher WTD values occurring alongside lower % transmission values (more humified) in drier conditions. There is a lack of agreement between the three records except where all three are insensitive in zone 3-Mb, which is uninformative in terms of indicating climatic variability.

A comparison of the correlation below and above the acrotelm-catotelm boundary (grey dashed line) at 83 cm demonstrates the difference in variability in the proxy records above and below this boundary. Below this boundary there is a stronger negative correlation (r_s= *-0.70) than above the boundary (r_s= -0.21) between the plant macrofossil and humification records. There is a negative correlation below the

boundary (r_s= -0.42) and positive correlation above the boundary (r_s= *0.72) between the plant macrofossil and testate amoeba records. This difference may be due to the lack of data points in the WTD reconstruction above the boundary. There is a weak positive correlation (r_s= 0.12) above and below the boundary between the testate amoeba and humification records.

5.1.3.7.2 KAR-EM-2 multi-proxy comparison

There is high variability in zones 2-Ma and 2-Mb, which reflects variability in the stratigraphic description. In these lower zones the plant macrofossil and humification records are more sensitive than the testate amoeba record which shows little variability. In zone 2-Mc above the acrotelm-catotelm boundary at 42 cm the plant macrofossil and humification records are less variable than the lower zones while the testate amoeba record shifts in the opposite direction to the other proxies.

The plant macrofossil and humification records show the best correlation between proxies (r_s= *-0.64) with higher DHI values generally occurring alongside lower % transmission values as expected in drier conditions. There is better agreement between the two records in zone 2-Ma and 2-Mc than in zone 2-Mb, with the two records responding in opposite directions in this zone. A weak negative correlation (r_s= -0.35) is found between the plant macrofossil and testate amoeba record with lower WTD values occurring alongside higher DHI values. A positive correlation between the two would be expected but the negative correlation may be explained by the relative lack of sensitivity of the testate amoeba record in the lower zones and the positive excursion of this record in zone 2-Mc. A weak positive correlation (r_s= 0.30) is found between the humification and testate amoeba records. Unexpectedly, lower WTD values occur alongside lower % transmission values (more humified). If relatively wet conditions were to be inferred from lower WTD values, higher % transmission values (less humified) and a negative correlation would be expected. Despite general agreement between the plant macrofossil and humification records, the testate amoeba record does not agree with the other records either in magnitude or direction of variability. There is perhaps agreement between the three towards the end of zone 2-Ma where all three records show low magnitude variability between 80 and 70 cm.

The correlation below and above the acrotelm-catotelm boundary (grey dashed line) at 42 cm is compared to demonstrate how variability differs above and below this boundary. There is a stronger negative correlation below the boundary (r_s= *-0.60) than above (r_s= -0.45) between the plant macrofossil and humification records. Separation by the boundary results in little correlation between the plant macrofossil and testate amoeba records both below (r_s= -0.01) and above (r_s= 0.09) the boundary. Below the boundary there is almost no correlation (r_s= -0.01) between the testate amoeba and humification records but a strong positive correlation above the boundary (r_s= 0.77).

5.1.3.7.3 KAR-EM-1 multi-proxy comparison

There is generally little variability around the mean of all records in zones 1-Ma and 1-Mb. This may reflect the lack of variability in the stratigraphy. At the acrotelm-catotelm boundary in zone 1-Mc there is a shift in all records. DHI values increase in this zone and decrease in zone 1-Md to the surface. Both the humification and testate amoeba records display shifts to lower values in zone 1-Mc with a subsequent increase in values in both records through zone 1-Md to the surface but with opposing directional shifts according to hydrological interpretation.

A negative correlation (r_s= *-0.39) is found between the plant macrofossil and humification records. The two records show synchronous variability between 76-64 cm with higher DHI values occurring alongside lower % transmission values throughout the record. There is almost no correlation (r_s= -0.09) between the testate amoeba and plant macrofossil records. Both records are insensitive and show little variability around the mean value. A positive correlation (r_s=*0.39) is found between the testate amoeba and humification records. Unexpectedly, higher WTD values occur alongside higher % transmission values.

A comparison of the correlation below and above the acrotelm-catotelm boundary at ~26 cm in this profile demonstrates how variability in the proxy records differs above and below this boundary. The negative correlation above the boundary is slightly reduced (r_s= -0.42) compared with below the boundary (r_s= *-0.57) between the plant macrofossil and testate amoeba records. There is no correlation below this boundary (r_s= -0.02) but a strong negative correlation above the boundary (r_s= -0.86) between

the testate amoeba and plant macrofossil records. There is a similar correlation between the testate amoeba and humification records both above (r_s= 0.21) and below (r_s= 0.25) the boundary.

5.1.4 Stable isotope results

5.1.4.1 Stable carbon isotope results

Figure 5.20 presents the stable carbon isotope results from KAR-EM-1, KAR-EM-2 and KAR-EM-3. A surface trend is evident in all profiles to more negative $\delta^{13}C$ values related to industrialisation and a decrease in $\delta^{13}C$ values of atmospheric CO_2. To account for this the records have been corrected with the original values displayed by the dashed lines. The appropriate annual correction was applied to each point using the respective profile chronologies. The error bars (±0.32‰) are based on standards run alongside the samples (Section 3.4.2.4). The mean values of the corrected KAR-EM-3, KAR-EM-2 and KAR-EM-1 stable carbon isotope records are -27.36‰, -27.69‰ and -27.81‰ respectively. Correction resulted in slightly less negative means across all records.

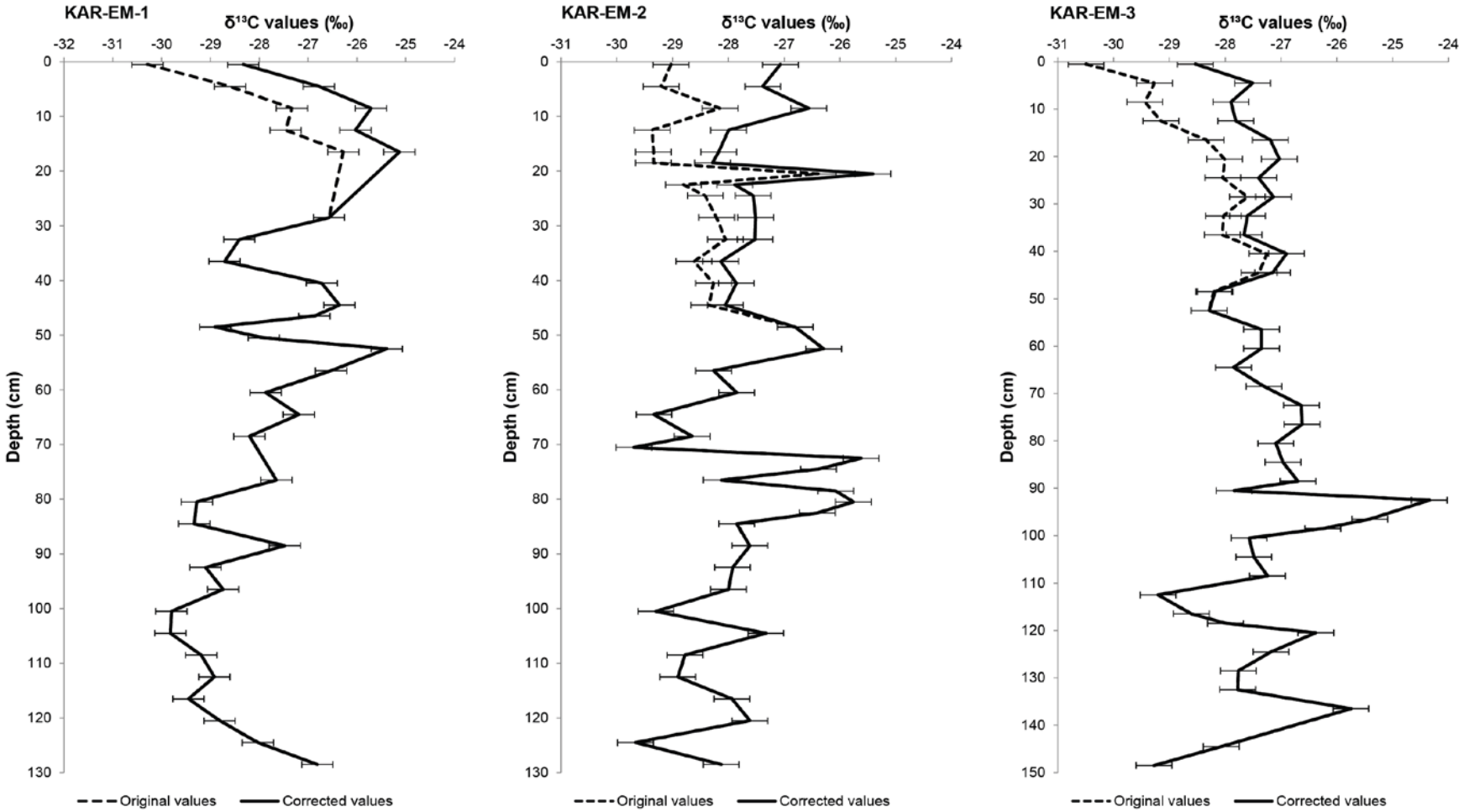

Figure 5.20. The KAR-EM-1, KAR-EM-2 and KAR-EM-3 corrected stable carbon isotope records. Original surface values before correction are displayed by the dashed lines.

With reference to the KAR-EM-3 stable carbon isotope record, from the base there is a general trend to less negative values until 92 cm (-24.34‰) apart from an excursion to more negative values (-29.20‰) at 112 cm. Before correction, after the least negative value at 92 cm there was a persistent negative trend of 6.16‰ to -30.50‰ at the surface. The sampling point closest to the 1850 pre-industrial standard is AD 1851 at 48 cm and the record has been corrected above this depth. After correction the largest shift (4.94‰) is found between the base of the record (148 cm: -29.28‰) and 92 cm (-24.34‰). After removal of the surface trend, the record fluctuates slightly around the mean between 92 cm and the surface, with a slight shift to more negative values at the surface.

With reference to the KAR-EM-2 stable carbon isotope record, values become less negative from the base of the record until 72 cm (-25.62‰). This is followed by a sharp decrease to the most negative value (-29.70‰) at 70 cm. There is an increase to less negative values until 52 cm. Before correction above this there was a shift to ~-29‰ at the surface. The stable carbon isotope record has been corrected above 44 cm as this was the sampling point closest to the 1850 pre-industrial standard (AD 1913). The sampling point below this, 48 cm, has a pre-industrial age of AD 1808. The trend to more negative values above 52 cm towards the surface has been removed as a result of correction. The record is generally around the mean until the single point shift at 20 cm where the least negative value (-25.41‰) is found. The largest range of variability in the record is between 72-20 cm (4.29‰). (This is a single point shift and may be an anomalous result, if this were the case the largest range (4.08‰) would be between 72-70 cm). Above this there is a shift to slightly less negative values towards the surface.

With reference to the KAR-EM-1 stable carbon isotope record, there is a decrease in values from the base until the most negative value at 104 cm (-29.82‰), after which there is a general shift to less negative values until 52 cm (-25.39‰). Above this there is a gradual shift to more negative values until 36 cm punctuated by a sharp shift to more negative values at 48 cm (-28.90‰). Between 36 and 16 cm there is a shift to less negative values. Above this, before correction, there was a shift to more negative values to -30.29‰ at the surface. The record has been corrected above 16 cm as this was the sampling point closest to the 1850 pre-industrial standard (AD

1984). Owing to a lack of *Sphagnum* stems at the sampling resolution through the acrotelm-catotelm boundary the next sampling point (28 cm) is of pre-industrial age (1798). The least negative value in the record is at 16 cm (-25.13‰) resulting in the largest range of variability between 104 and 16 cm of 4.69‰. Above 16 cm there is a shift to more negative values to -28.33‰ at the surface.

5.1.4.2 Intra-site comparison of stable carbon isotope records

Figure 5.21 displays the intra-site comparison of the stable carbon isotope records. Figure 5.21a displays the records plotted against the actual depth of each profile. Both the raw data and the corrected records are presented. Correction was applied to KAR-EM-3 and KAR-EM-2 at a similar depth (48 cm and 44 cm respectively) with KAR-EM-1 corrected above 16 cm. The mean values of the uncorrected records are slightly higher (KAR-EM-3: -27.64‰, KAR-EM-2: -28.05‰, KAR-EM-1: -28.06‰) with higher ranges between the minimum and maximum values (KAR-EM-3: 6.16‰, KAR-EM-2: 4.08‰, KAR-EM-1: 4.90‰) compared with the corresponding mean values and ranges of the corrected records (KAR-EM-3: -27.36‰, KAR-EM-2: -27.69‰, KAR-EM-1: -27.81‰), (KAR-EM-3: 4.94‰, KAR-EM-2: 4.29‰, KAR-EM-1: 4.69‰). From the base of the records KAR-EM-3 and KAR-EM-2 show a general shift to less negative values until 92 cm and 72 cm respectively whereas KAR-EM-1 shifts to more negative values until 100 cm before shifting to less negative values until 52 cm. Above these respective depths before correction there was a shift to more negative values to the surface that, after correction, results in a fluctuation of the stable carbon isotope values around the mean to the surface. In KAR-EM-2 above 72 cm, after the shift to more negative values at 70 cm there is a shift to less negative values until 52 cm, above this before correction there was a shift to more negative values to the surface but this trend was removed by correction and values generally fluctuate around the mean until the surface. In KAR-EM-1 above 52 cm after a shift to more negative values there is a shift to less negative values until 16 cm which has been made larger as a result of correction with the shift to more negative values to the surface still evident. The records seem to be showing similar general trends; however, when plotted as in figure 5.21a there are no clear synchronous shifts across all three records with the maximum and minimum values

of each record not in proximity. Additionally, there is generally little correlation between the profiles (table 5.13).

Table 5.13. Pearson's correlation coefficient between the stable carbon isotope records of profiles plotted against actual depth and plotted relative to the surface of KAR-EM-3 (α=0.05).

	KAR-EM-3 vs. KAR-EM-2	KAR-EM-3 vs. KAR-EM-1	KAR-EM-2 vs. KAR-EM-1
Actual depth			
r^2	0.040	-0.120	0.142
Relative depth			
r^2	-0.227	-0.333	0.329

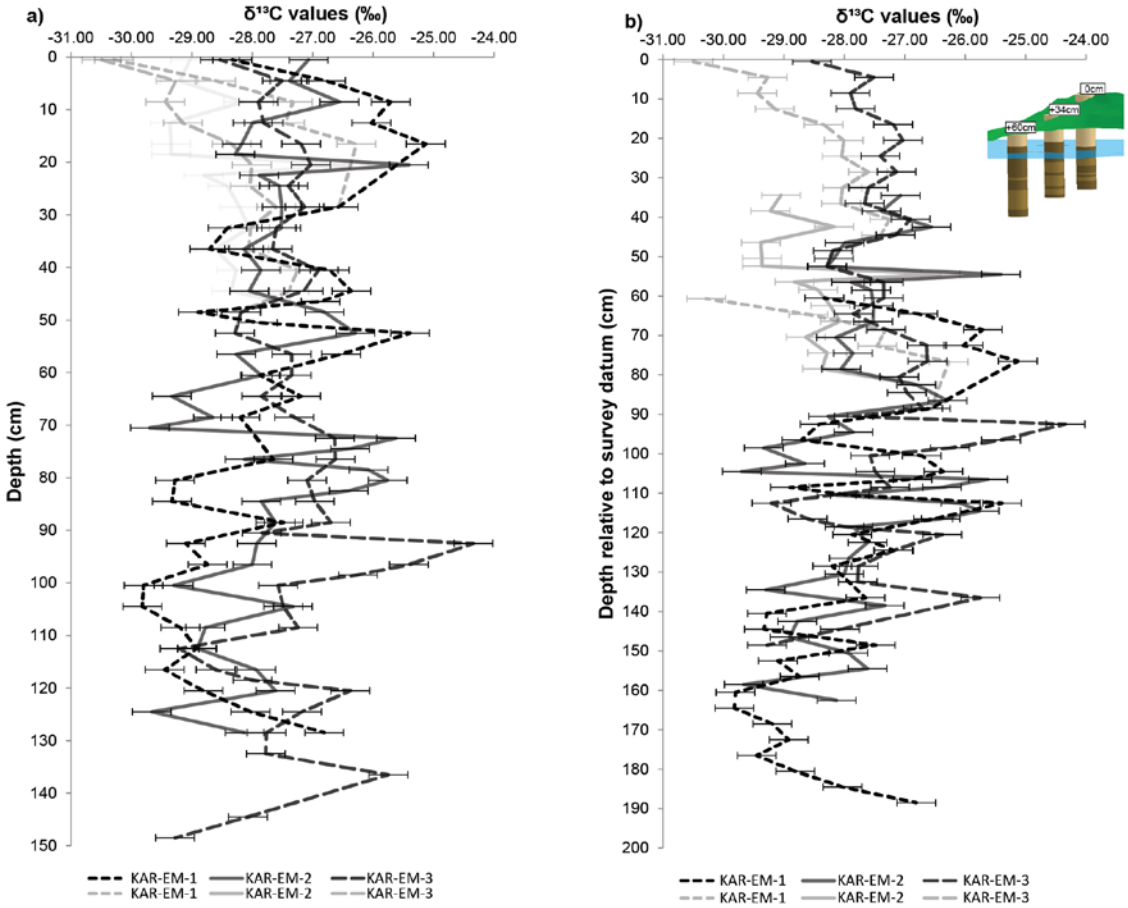

Figure 5.21. Comparison of the stable carbon isotope records from each KAR-EM profile. Stable carbon isotope values are plotted against the actual depths of each profile (a) and relative to the surface of KAR-EM-3 (b).

There is better agreement between the records when they are plotted relative to the surface of KAR-EM-3 (figure 5.21b). The correction is applied at a more similar depth

in KAR-EM-1 and KAR-EM-2 plotted in this way (76 cm and 78 cm respectively) with KAR-EM-3 corrected above 48 cm. The general trend to less negative values is evident between 165 and 110 cm. Despite this, between 120 and 110 cm KAR-EM-1 and KAR-EM-2 shift to less negative values while KAR-EM-3 shifts to more negative values. Between 100 and 90 cm there is a shift to the least negative value in KAR-EM-3 at a similar level to a shift to more negative values in KAR-EM-1 and just below this between 110 and 100 cm is the shift to the most negative value (after correction) in KAR-EM-2. Between 90 and 60 cm KAR-EM-1 and KAR-EM-2 show opposite shifts where KAR-EM-3 is in between the two. Above 55 cm the records from KAR-EM-3 and KAR-EM-2 are synchronous after correction. The maximum and minimum values in each profile are more closely related than in figure 5.21a. Correlations between the records plotted relative to the surface of KAR-EM-3 are also significantly improved (table 5.13). Despite synchronous variability as discussed above it is important to consider these records based on their respective chronologies.

5.1.4.3 Stable oxygen isotope results

Figure 5.22 presents the KAR-EM-1, KAR-EM2 and KAR-EM-3 stable oxygen isotope records. The error bars (±0.19‰) were calculated from the related standards (Section 3.4.2.4). The mean values of the KAR-EM-3, KAR-EM-2 and KAR-EM-1 are similar at 21.11‰, 21.11‰ and 20.92% respectively.

With reference to the KAR-EM-3 stable oxygen isotope record, there is a peak to higher $\delta^{18}O$ values (22.17‰) at 136 cm after which the values remain just below the mean until 104 cm. After this there is a gradual decrease in values to 19.67‰ at 64 cm, the lowest value in the record. Values gradually increase to 22.74‰ at 16 cm, the highest in the record. The trend between 64 cm and 16 cm is the largest in the record with a 3.07‰ shift and these are the largest excursions from the mean in the record (-1.44‰ and +1.63‰ respectively). Values decrease and remain around the mean towards the surface.

There is higher variability around the mean in the KAR-EM-2 stable oxygen isotope record. From the base there is a general decrease of values to 84 cm. There is a peak to the highest value in the record (22.78‰) at 78 cm and a peak to the lowest

value in the record (19.73‰) at 76 cm. This represents the largest shift in the record of 3.05‰. Above this there is a general trend to higher values until 48 cm (22.30‰), a trend to lower values to 20 cm (19.66‰) apart from a single peak at 24 cm to 21.91‰. Above 20 cm there is a shift to higher values towards the surface (21.67‰) apart from a single peak to lower values at 4 cm to 19.67‰.

With reference to the KAR-EM-1 stable oxygen isotope record, values begin around the mean decreasing until 104 cm (19.56‰) and then increasing to 92 cm (22.44‰). Above this there is a shift to lower values until 64 cm (20.38‰) followed by an increase until 52 cm to the highest value in the record (22.46‰). After this there is a general trend to lower values at the surface (19.46‰). Within this decrease there are three sharp shifts to lower values at 48 cm (20.71‰), 36 cm (19.98‰) and 4 cm (18.56‰). The shift of 3.9‰ between 52 cm and 4 cm to the lowest value in the record is the largest shift in the record.

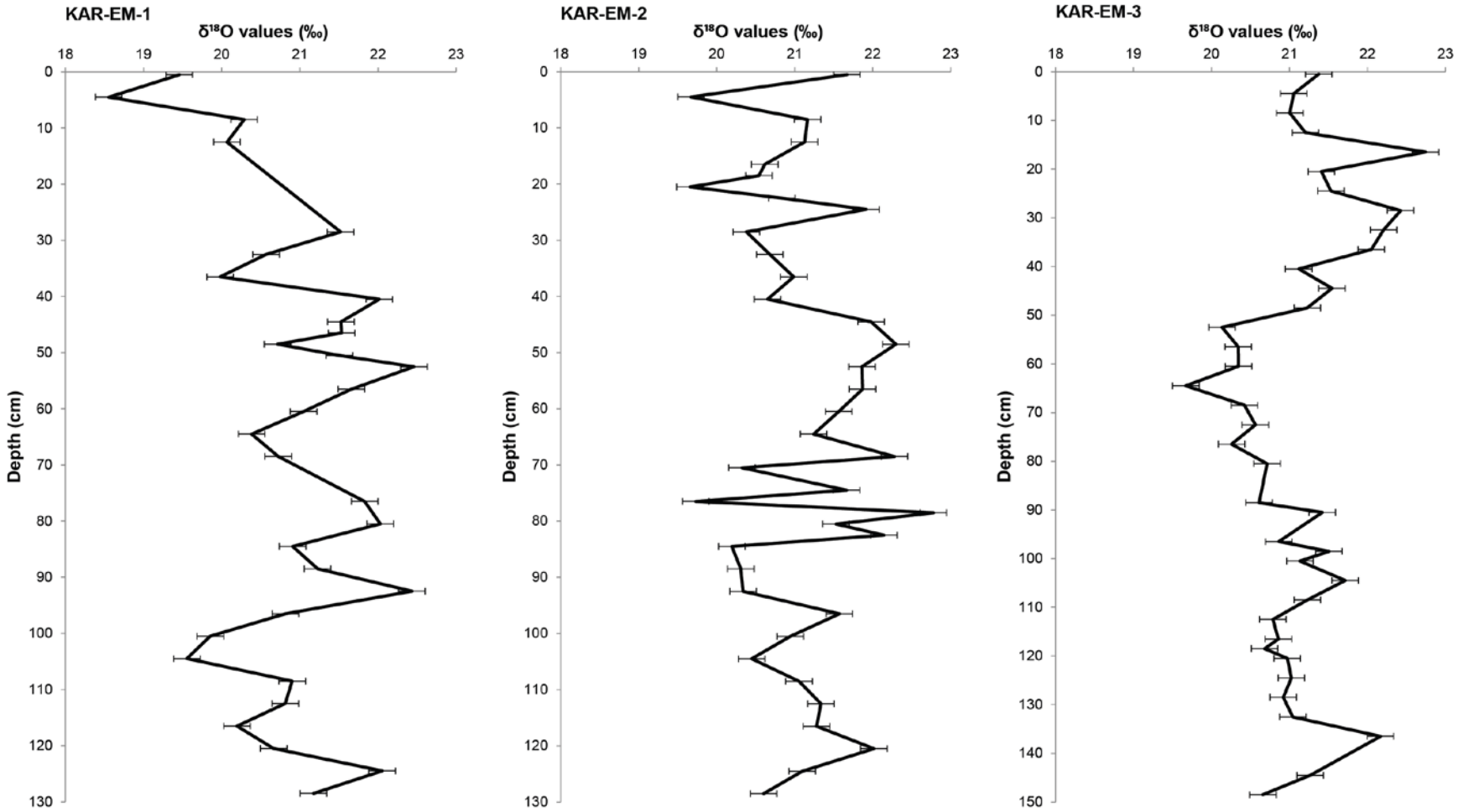

Figure 5.22. The KAR-EM-1, KAR-EM-2 and KAR-EM-3 stable oxygen isotope records.

5.1.4.4 Intra-site comparison of stable oxygen isotope records

Figure 5.23 presents the intra-site comparison of the stable oxygen isotope records. The records from each profile are plotted against actual depth in figure 5.23a. KAR-EM-3 and KAR-EM-2 both have mean values of 21.11‰ with a slightly lower mean value from KAR-EM-1 of 20.92‰. Plotted in this way there is no clear synchronous variability between the records. At 104 cm values in KAR-EM-1 and KAR-EM-2 decrease at the same time as an increase in KAR-EM-3. Between ~84 cm and 70 cm there is an increase to higher values in KAR-EM-1 and KAR-EM-2 which is not present in KAR-EM-3. At 64 cm there is a decrease in values in all three records before a general increase in all three to ~42 cm. Above this, there is a marked decrease in values in KAR-EM-1, a slight decrease in values in KAR-EM-2 and a less clear shift in KAR-EM-3 to the surface. The largest shifts in each record are not closely related based on actual depth (KAR-EM-3: 64-16 cm 3.07‰, KAR-EM-2: 76-78 cm 3.05‰, KAR-EM-1: 4-52 cm 3.9‰). Negative correlations are found between KAR-EM-3 and the other profiles suggesting dissimilarity of this profile (table 5.14). KAR-EM-2 and KAR-EM-1 may be more similar in directional change, displaying a weak positive correlation.

Table 5.14. Pearson's correlation coefficient between stable oxygen isotope records of profiles plotted against actual depth and plotted relative to the surface of KAR-EM-3 (α=0.05).

	KAR-EM-3 vs. KAR-EM-2	KAR-EM-3 vs. KAR-EM-1	KAR-EM-2 vs. KAR-EM-1
Actual depth			
r^2	-0.247	-0.274	0.102
Relative depth			
r^2	0.170	*0.591	0.402

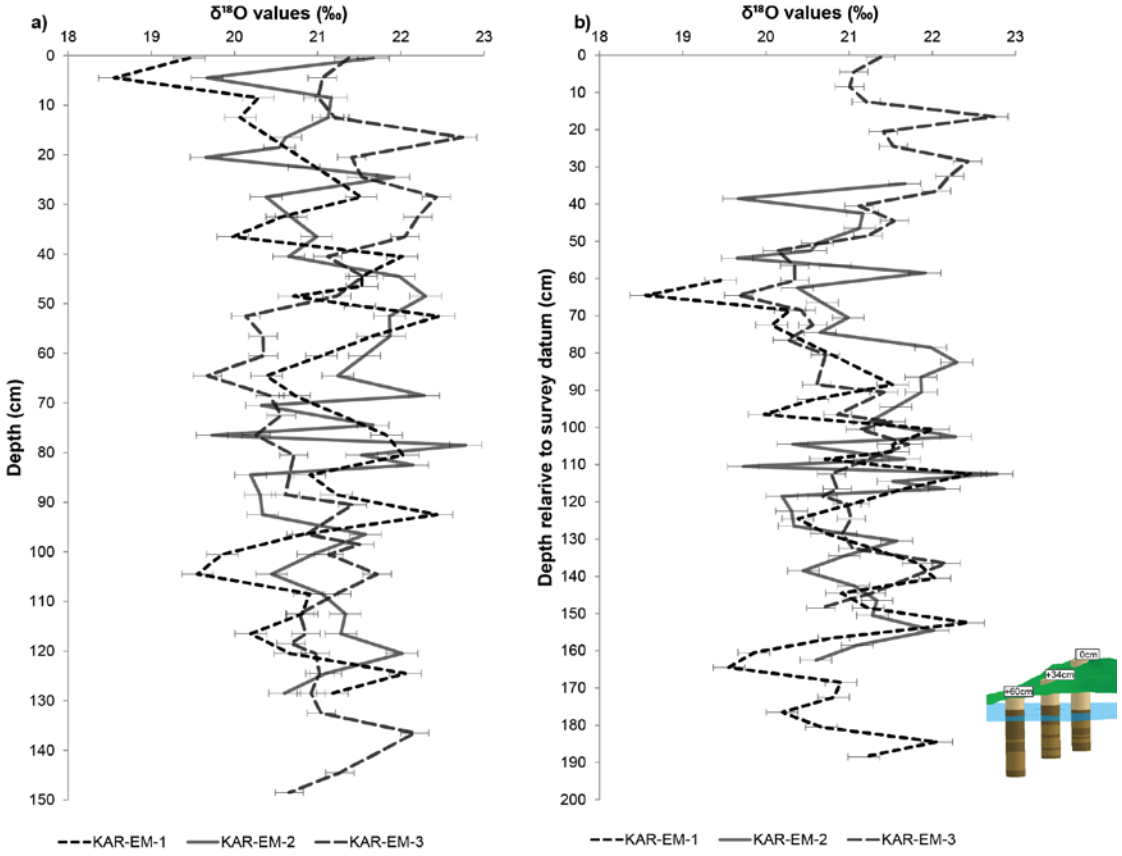

Figure 5.23. Comparison of the stable oxygen isotope records from each KAR-EM profile. Stable oxygen isotope values are plotted against the actual depths of each profile (a) and relative to the surface of KAR-EM-3 (b).

Plotted relative to the surface of KAR-EM-3 (figure 5.23b), there is better agreement between the three records. Between 160-145 cm there is good agreement between KAR-EM-1 and KAR-EM-2; however, above this between 145-130 cm KAR-EM-3 and KAR-EM-1 are synchronous with an opposite shift in KAR-EM-2. Between 130-100 cm variability in KAR-EM-1 and KAR-EM-2 is similar where values in KAR-EM-three remain around the mean. After an increase, between 90-65 cm there is a synchronous decrease in values in all three records. Above this there is an increase in all records to the surface. Compared relative to the surface of KAR-EM-3 correlations between the records are altered (table 5.14) with the highest positive correlation between KAR-EM-3 and KAR-EM-1. Comparison of these records based on their individual time-scales may further improve agreement between the records in a more accurate manner in consideration of differential accumulation rates.

5.1.4.5 Comparison of stable carbon and stable oxygen isotope records

Figure 5.24 compares the corrected stable carbon and stable oxygen isotope records from KAR-EM-1, KAR-EM-2 and KAR-EM-3. The records are plotted against depth and where necessary are discussed with reference to the plant macrofossil zones. The b graphs compare the two records with the axis of the stable carbon isotope record reversed in order to compare the two records based on a hydrological interpretation.

With reference to the comparison of records from KAR-EM-3, the stable carbon isotope record has a larger range of variability (148-92 cm: 4.94‰) compared with the stable oxygen isotope record (64-16 cm: 3.07‰). There is almost no correlation between the two records (r^2=0.002). The peak at 136 cm is evident in both records and there are an additional three peaks in the $\delta^{13}C$ record below 92 cm which are not evident in the $\delta^{18}O$ record. The stable carbon isotope record fluctuates around the mean between 92 cm and the surface whereas there is a decrease in values in the stable oxygen isotope record until 64 cm and a subsequent increase in values until 16 cm. Both records move to relatively lower values above 16 cm to the surface. Similarity in the direction of variability between the records is not improved when the stable carbon isotope axis is reversed owing to the relative insensitivity of the stable carbon isotope record compared with the stable oxygen isotope record. Reversal of this axis results in disagreement between the records at 136 cm.

With reference to the comparison of records from KAR-EM-2, the stable carbon isotope record has a larger range of maximum variability (72-20 cm: 4.29‰) compared with the stable oxygen isotope record (78-76 cm: 3.05‰). The two records are very weakly positively correlated (r^2=0.032) and based on depth, general agreement between the records is not evident. There is a period where variability in the two records is similar between 84 and 64 cm (intersected by 2-Ma and 2-Mb zone boundary) with a fluctuation between less negative $\delta^{13}C$ values (higher $\delta^{18}O$ values) and more negative $\delta^{13}C$ values (lower $\delta^{18}O$ values). This is also the zone in which the highest and lowest values are found in both records. Above 64 cm the two records generally agree with disagreement at some depths particularly at 20 cm when the two records are opposite (higher $\delta^{18}O$ values and less negative $\delta^{13}C$

values). Reversal of the stable carbon isotope axis results in disagreement between the two records, especially between 84 and 64 cm; however, at 20 cm the two records are in agreement.

With reference to the comparison of records from KAR-EM-1, the stable carbon isotope record has a larger range of maximum variability (104-16 cm: 4.69‰) compared with the stable oxygen isotope record (52-4 cm: 3.9‰). There is a very weak positive correlation between the two records (r^2=0.050); despite this there is general agreement of variability where higher $\delta^{18}O$ values occur alongside higher (less negative) $\delta^{13}C$ values and lower $\delta^{18}O$ values occur alongside lower (more negative) $\delta^{13}C$ values throughout the record. There is particular agreement between 60 and 28 cm (Zone 1-Mb). Above this the stable oxygen isotope record shifts to lower values to the surface whereas the stable carbon isotope record moves to less negative values until 16 cm after which values are more negative to the surface. Reversal of the stable carbon isotope axis results in disagreement between the two records with higher $\delta^{18}O$ values occurring alongside lower (more negative) $\delta^{13}C$ and lower $\delta^{18}O$ values occurring alongside higher (less negative) $\delta^{13}C$ values.

In each case reversal of the stable carbon isotope axis does not improve similarity in the direction of variability between the records. Comparison with the other proxies may aid interpretation of the stable isotope records.

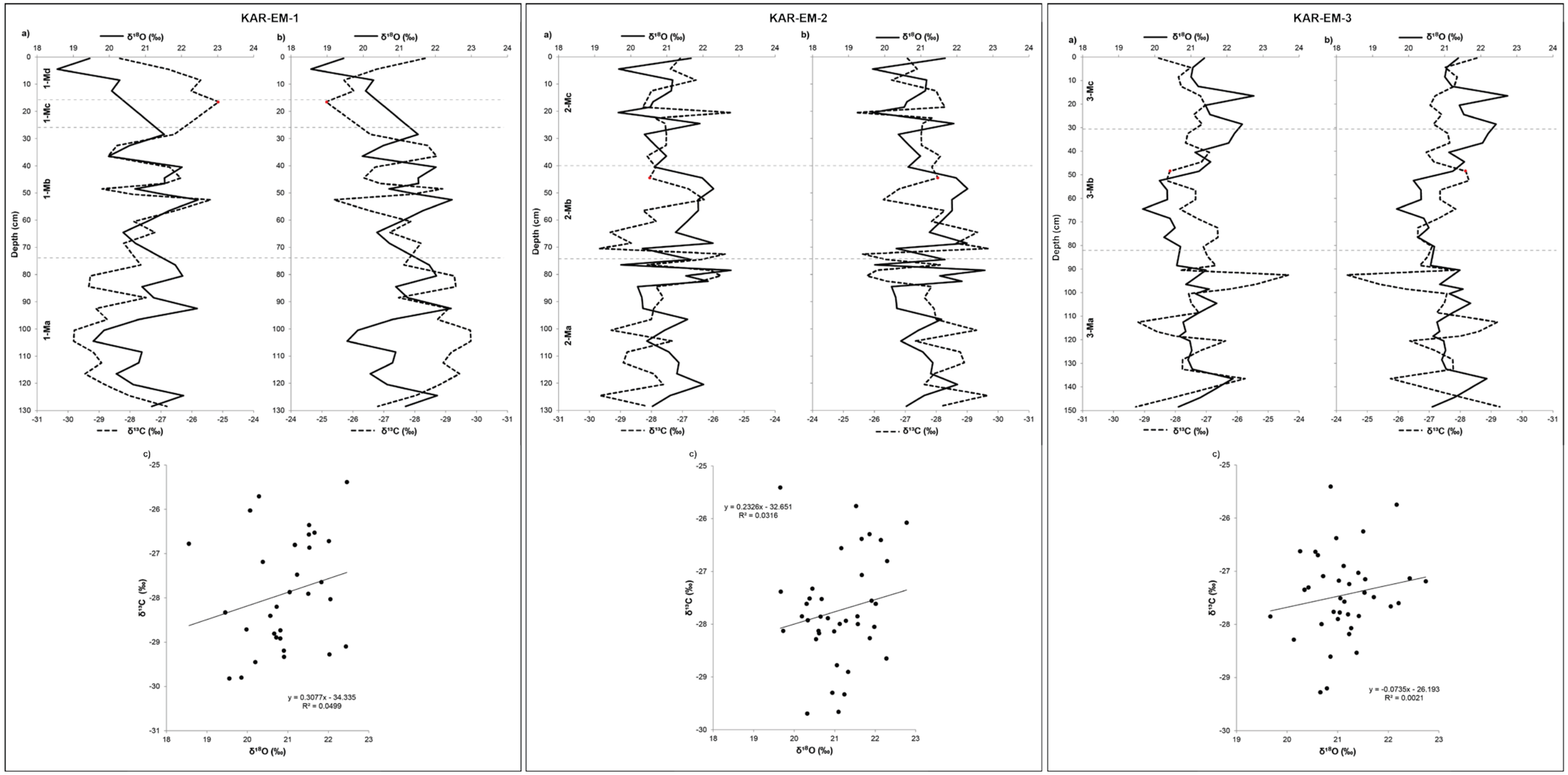

Figure 5.24. Comparison of the KAR-EM-1, KAR-EM-2 and KAR-EM-3 corrected stable carbon and stable oxygen isotope records (a graphs). Comparison of the two with the stable carbon isotope axis reversed (b graphs). A scatterplot of the two records from each profile (c graphs).

5.2 San Juan

5.2.1 SAN-EM-2

The results from SAN-EM-2 are presented in the following section. Firstly, the profile and stratigraphic description are displayed, followed by presentation of the palaeoecological results: plant macrofossil, humification and testate amoeba records and a multi-proxy comparison of these records. Following this the stable isotope results are presented. All records are plotted against depth. The approximate ages of zone boundaries are displayed on the plant macrofossil and testate amoeba diagrams.

The photographed SAN-EM-2 profile is presented alongside the diagram of stratigraphic description in figure 5.25. The majority of the profile is dominated by *Sphagnum* peat with periods of humified peat occurring from the base until ~115 cm and between 48 and ~26 cm. Demarcated by the red box the gradual shift from humified to undecomposed *Sphagnum* peat at ~26 cm is the acrotelm- catotelm boundary (Belyea and Clymo, 1999; Morris *et al.*, 2011a).

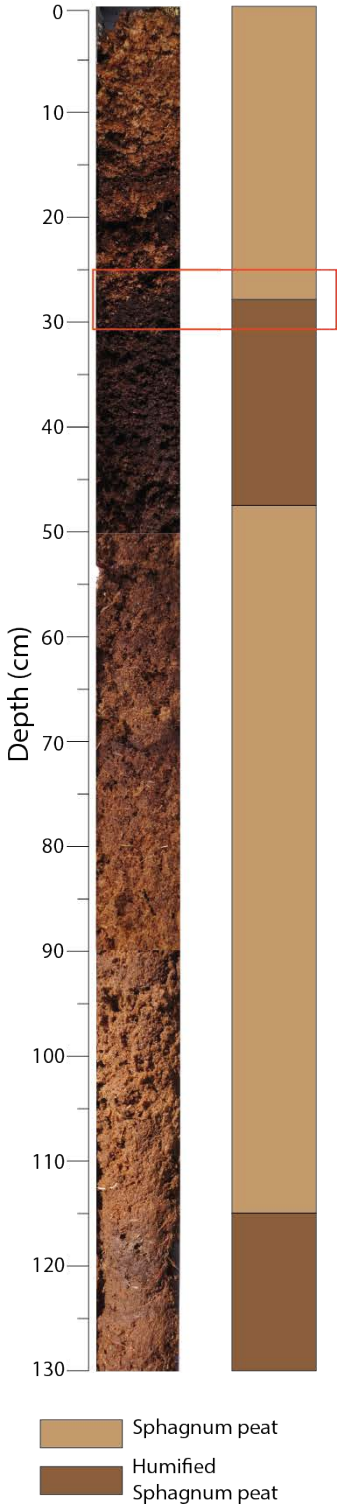

Figure 5.25. Depth based stratigraphic variability of SAN-EM-2. The red box marks the proposed acrotelm-catotelm boundary.

5.2.1.1 Palaeoecological results

5.2.1.1.1 Plant macrofossil results

The plant macrofossil results from SAN-EM-2 are presented in figure 5.26. Table 5.15 presents a summary description of the plant macrofossil zones and the depths and approximate ages of the zone boundaries.

One species of *Sphagnum* dominates throughout, *S.magellanicum.* The most significant variability in this profile is found in zones SJMc and SJMd where *S.magellanicum* decreases to below 10% in zone SJMd. This is characteristic of the acrotelm-catotelm boundary where Ericaceae roots and UOM dominate particularly before the zone boundary to SJMe (AD 1974). *S.magellanicum* dominates throughout zone SJMe to the surface.

The data were subject to multivariate statistical analysis to provide a BSW index. The DCA results, with removal and down-weighting of rare species, are displayed in table 5.16. A linear response model can be used owing to the axis-one gradient length being less than 3σ and the results of a PCA of the dataset are presented in table 5.17. Rare species were removed and the data were Hellinger-transformed before the PCA. Figure 5.27 presents a bi-plot of the axis-one and -two sample and species scores.

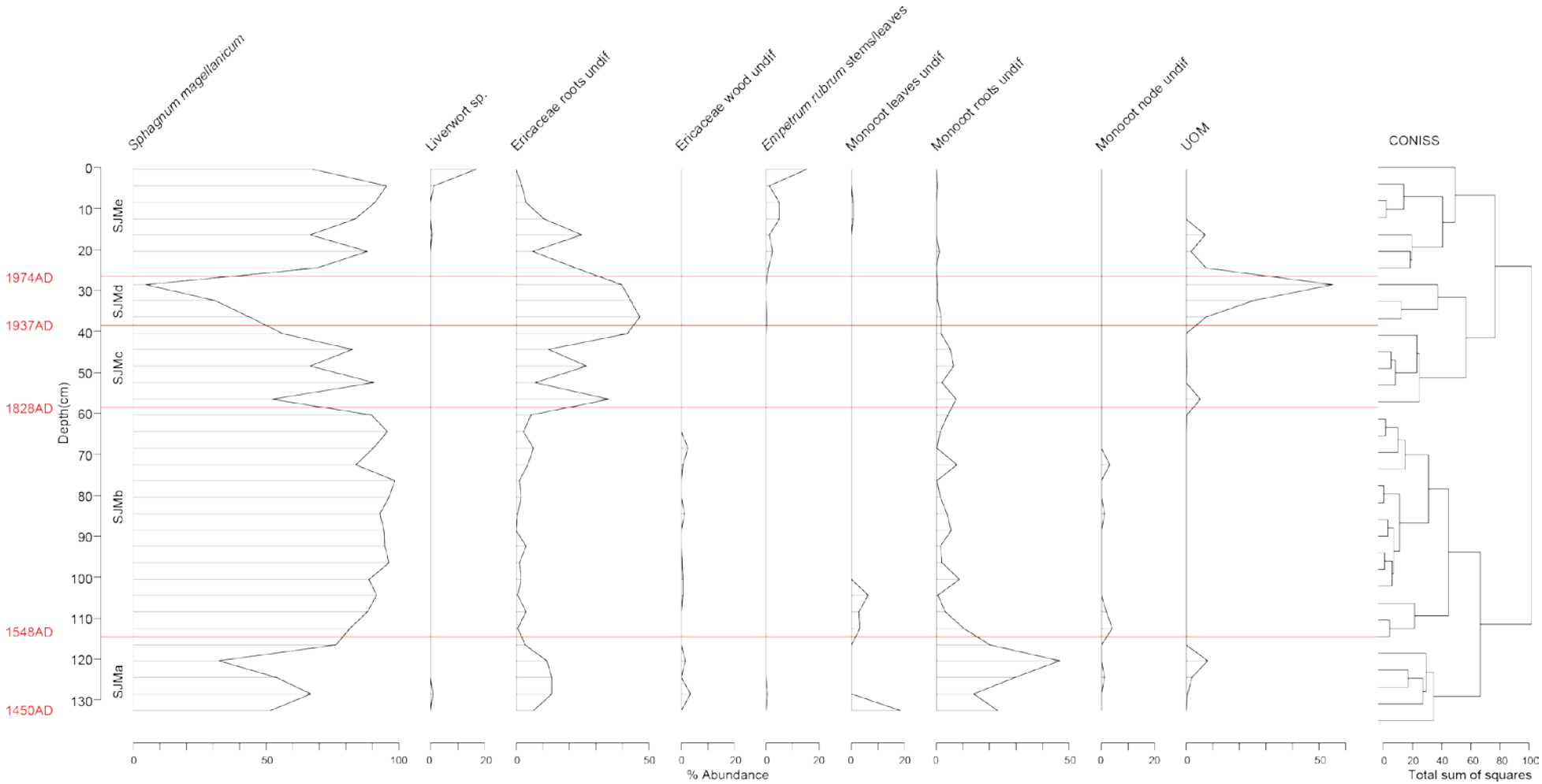

Figure 5.26. SAN-EM-2 plant macrofossil diagram plotted against depth, displaying plant macrofossil zones based on CONISS with approximate ages of zone boundaries presented.

Table 5.15. Summary description of SAN-EM-2 plant macrofossil zones.

Zone	Depth (cm)	Plant macrofossil zone description	Age cal BP (AD)
SJMa	133-114	*S.magellanicum* dominates throughout this zone alongside monocot roots undif. and Ericaceae roots. *S.magellanicum* decreases and monocot roots undif. dominate at 120 cm.	500-402 cal BP (AD 1450-1548)
SJMb	114-58	*Sphagnum* dominates and is at high abundance throughout the zone. Ericaceae and monocot roots undif. are present but low in abundance.	402-122 cal BP (AD 1548-1828)
SJMc	58-38	*S.magellanicum* decreases in this zone as Ericaceae roots undif. increases.	122-13 cal BP (AD 1828-1937)
SJMd	38-26	*S.magellanicum* continues to decrease in this zone to below 10% abundance. Ericaceae roots undif. dominates throughout the zone. UOM increases throughout the zone to dominance towards the end of the zone.	13- -24 cal BP (AD 1937-1974)
SJMe	26-0	*S.magellanicum* returns to high abundance in this zone and dominates throughout as Ericaceae roots undif. decreases. *Liverwort* sp. and *E.rubrum* increase towards the surface.	-24 - -63 cal BP (AD 1974-2013)

Table 5.16. Results of DCA of SAN-EM-2 plant macrofossil data.

	Axis 1	Axis 2	Axis 3
Eigenvalues	0.3624	0.1600	0.07456
% accounted for by axis	47.14%	20.81%	9.70%
Gradient lengths	2.0054	1.0550	0.71683

Table 5.17. Results of PCA of SAN-EM-2 plant macrofossil data.

	Axis 1	Axis 2	Axis 3
Eigenvalues	2.6425	1.9535	1.0494
% accounted for by axis	37.75%	27.91%	14.99%
Screeplot (Broken stick)	Significant	Significant	-

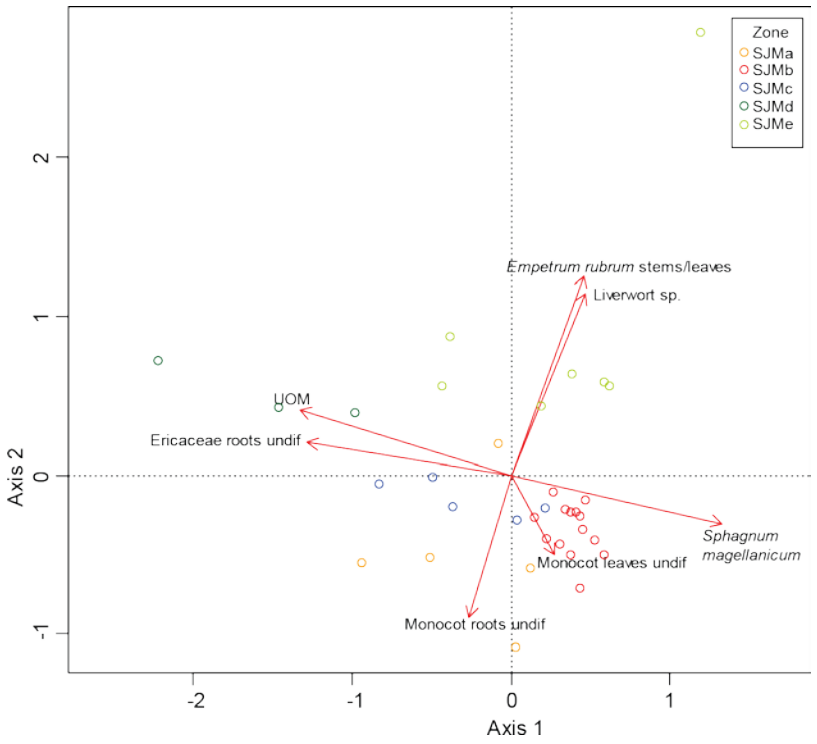

Figure 5.27. Bi-plot of PCA axis-one and -two species (Red arrows) and sample scores (points coloured according to CONISS plant macrofossil zone) of SAN-EM-2 plant macrofossil data.

Two significant axes result from the PCA of the plant macrofossil data with axis-one accounting for 36.49% of the total variance in the plant macrofossil data and axis-two accounting for 27.91%. *S.magellanicum*, Ericaceae roots and UOM are most strongly correlated with the first principal component with *Liverwort* sp. and *E.rubrum* most strongly correlated with axis-two. *S.magellanicum* is located at the higher end of axis-one with the other dominant variables located at the lower end of this axis. Grouping of samples according to zone is evident in the data. The difference in species composition between zone SJMb, with the dominance of *S.magellanicum*, and zones SJMa and SJMc in which *S.magellanicum* is less abundant is clear. Samples in SJMd are dominated by UOM and Ericaceae roots, supporting figure 5.26. Samples in zone SJMe move towards the higher end of axis-two owing to the dominance of *Liverwort* sp. and *E.rubrum* in these samples. This grouping of samples based on zone and the separation of *S.magellanicum* and Ericaceae roots and UOM along axis-one supports the representation of a wetness gradient along this axis.

The PCA axis-one scores (figure 5.28b) may be used to represent wetness variability and are displayed alongside the Dupont Hydroclimatic Index (figure 5.28a) of the SAN-EM-2 plant macrofossil data and the two are normalised for comparison (figure 5.28c).

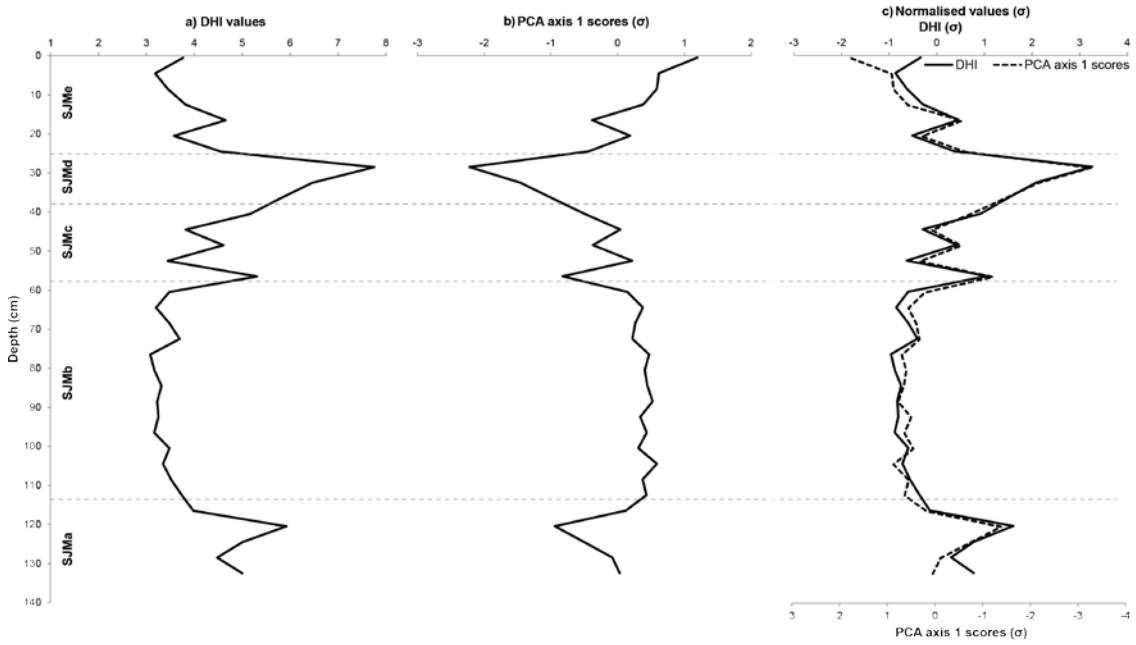

Figure 5.28. Bog surface wetness anomaly curves from the SAN-EM-2 plant macrofossil data transformed using the Dupont Hydroclimatic Index (a) and the axis-one scores of Principal Components Analysis (b). The two records are normalised and compared (c).

The dominance of *S.magellanicum* throughout zones SJMa and SJMb result in low DHI values in these zones apart from a peak to higher values in zone SJMa at 120 cm. This reflects the rise in monocot roots and a decrease of *S.magellanicum*. There is a peak to the highest DHI value in the record in SJMd at 28 cm, where *S.magellanicum* is low in abundance. After this peak there are uniform values towards the surface. The PCA axis-one scores are almost identical and only differ in zone SJMe towards the surface in which PCA axis-one scores reflect the presence of surface vegetation. The surface components are not correlated with axis-one but are accounted for in the DHI record and this record is a better representation of wetness variability.

5.2.1.1.2 Humification results

Figure 5.29 displays the raw humification data as (% light transmission) and the detrended and normalised record with the raw data and the plant macrofossil zone boundaries displayed. The mean value of this record is 53.33% with only small variability around the mean throughout the record. From the base there is a general increase to higher values until 84 cm after which there is a decrease until just before the zone boundary to SJMc to the lowest value of 33.73%. Above this there is an increase until the surface to 75.23% apart from a peak to lower values at the zone boundary between zones SJMd and SJMe (26 cm). The detrended and normalised record is compared with other proxy records in section 5.3.1.2.

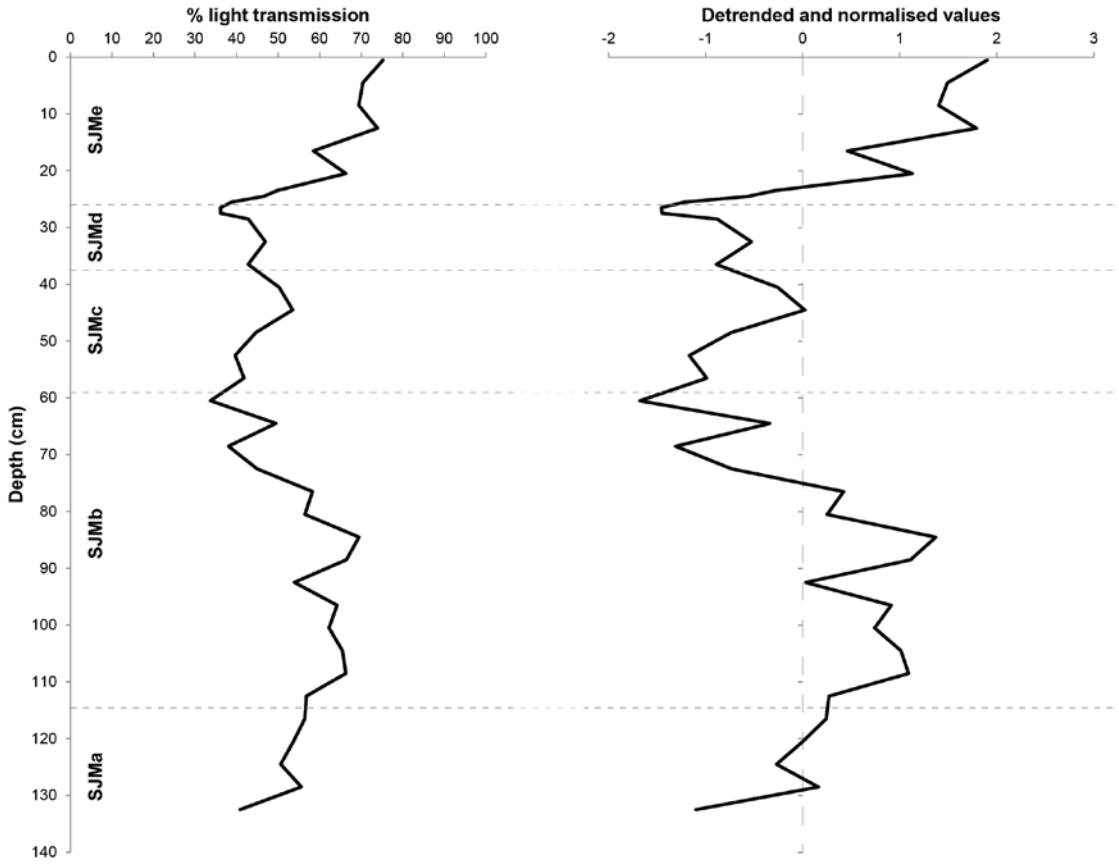

Figure 5.29. The raw humification data and the detrended and normalised humification record from SAN-EM-2. Plant macrofossil zones are displayed.

5.2.1.1.3 Testate amoeba results

Figure 5.30 presents the testate amoeba results from SAN-EM-2 and a summary description of the zones and depths and approximate ages of zone boundaries are displayed in table 5.18. Xerophilous to hygrophilous taxa included in the transfer function and water table reconstruction are displayed from left to right on the diagram (taxa that are not included are grouped on the right hand side of the diagram). Test concentration per cm^3 and taxonomic diversity are displayed on the far right of the diagram.

The most significant shifts in this record occur in zone SJTa at 96 cm with the shift from dominance of *H.petricola*, to *D.pulex* after which this taxon dominates through zone SJTa, SJTb, SJTc into SJTd until 24 cm and after this *A.muscorum* dominates to the surface. The zones reflect the variability in test concentration, with low concentration in zone SJTa until AD 1748. Test concentration is high throughout zone SJTb. There is a peak in test concentration in zone SJTc (AD 1919-1951) to ~12,000 tests per cm^3 and is lower in the surface zone.

Owing to the dominance of *D.pulex* in the San Juan samples between 88-25 cm, and the uncertainty associated with this taxon in terms of WTD reconstruction, a few samples were re-counted (32-33 cm, 40-41 cm, 48-49 cm). It was aimed to reduce the relative abundances of *D. pulex* in order to characterise the assemblage by allowing for rare taxa. Even after doubling the count total the relative abundance of *D.pulex* still remained dominant (88-82%, 91-93%, 95-91% respectively). These small changes in relative abundance greatly increased counting time. Payne and Mitchell (2009) conclude that counting more samples (higher resolution) is more time efficient than increasing count totals.

A DCA of the data (with removal of rare species and down-weighting) was carried out and the results are displayed in table 5.19. At a value only slightly above 3σ, the axis-one gradient length warrants the use of a linear response model. The results of the PCA are presented in table 5.20. Rare species were removed and the data were Hellinger-transformed before analysis. A bi-plot of the axis-one and -two sample and species scores is presented (figure 5.31).

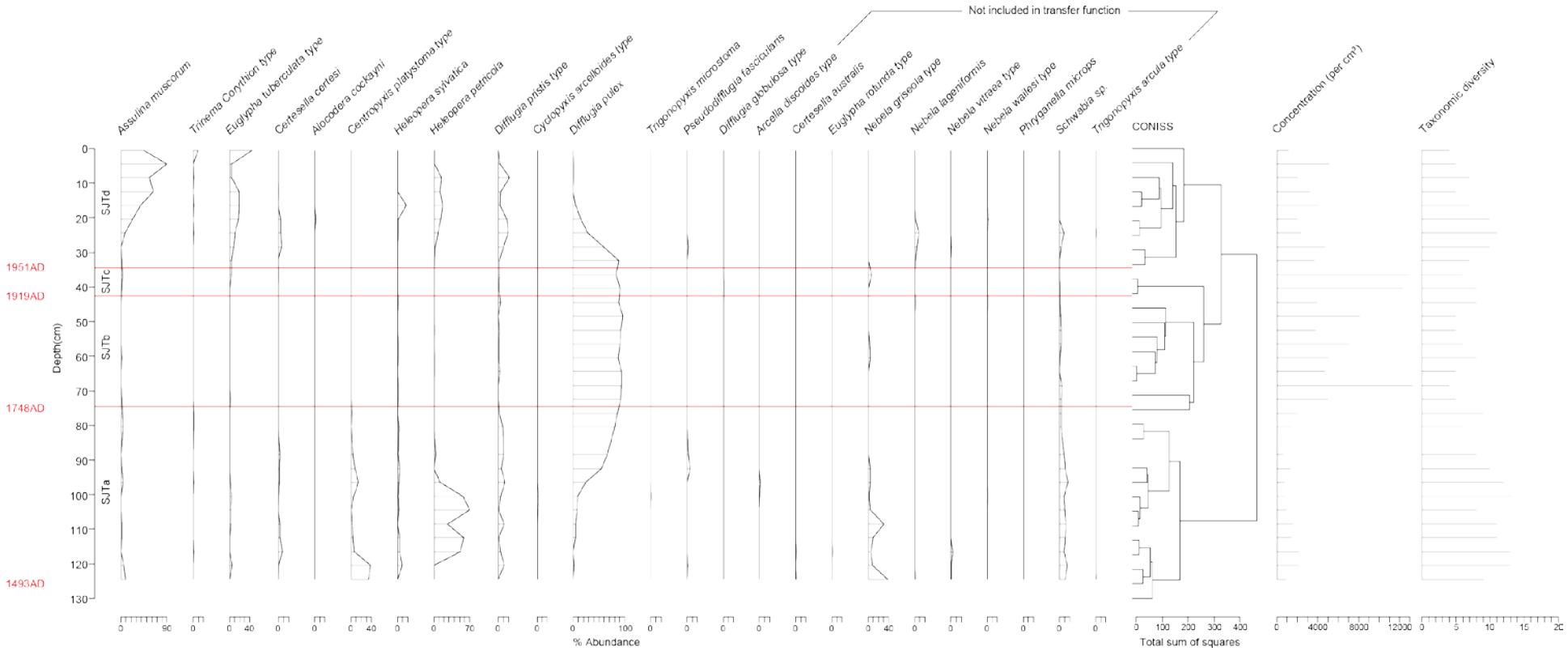

Figure 5.30. SAN-EM-2 testate amoeba diagram plotted against depth, displaying testate amoeba zones based on CONISS with approximate ages of zone boundaries presented. Concentration and taxonomic diversity presented.

Table 5.18. Summary description of SAN-EM-2 testate amoeba zones.

Zone	Depth (cm)	Testate amoeba zone description	Age cal BP (AD)
SJTa	125-74	*H.petricola* dominates at the beginning of the zone with high taxonomic diversity but other taxa are in low abundance. *D.pulex* increases at 96 cm and dominates throughout the zone. Test concentration is lowest in this zone.	457-202 cal BP (AD 1493-1748)
SJTb	74-42	*D.pulex* dominates in this zone which has the lowest taxonomic diversity. There is a peak in test concentration at the beginning of the zone and it is generally high throughout.	202-31 cal BP (AD 1748-1919)
SJTc	42-34	There are only 2 samples in this short zone which is dominated by *D.pulex* with low taxonomic diversity. Both samples have high test concentrations.	31 - -1 cal BP (AD 1919-1951)
SJTd	34-0	*D.pulex* decreases gradually until 24 cm when *A.muscorum* increases to dominance until the surface.	-1 - -63 cal BP (AD 1951-2013)

Table 5.19. Results of DCA of SAN-EM-2 testate amoeba data.

	Axis 1	Axis 2	Axis 3
Eigenvalues	0.6688	0.3156	0.36418
% accounted for by axis	34.17%	16.13%	18.60%
Gradient lengths	3.0309	2.2743	2.15924

Table 5.20. Results of PCA of SAN-EM-2 testate amoeba data.

	Axis 1	Axis 2	Axis 3
Eigenvalues	3.455	2.919	1.699
% accounted for by axis	26.58%	22.46%	13.07%
Screeplot (Broken stick)	Significant	Significant	Significant

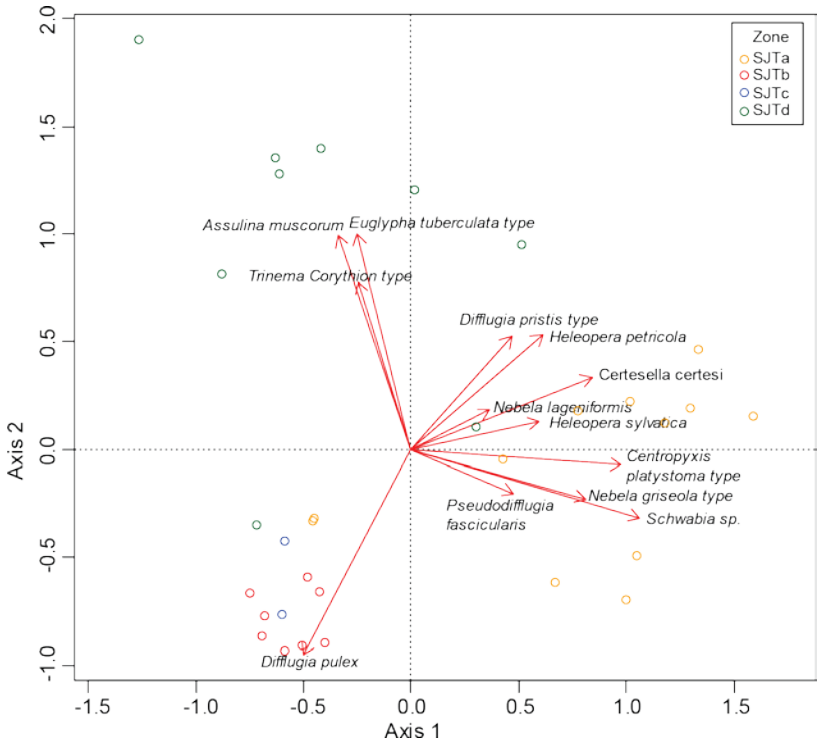

Figure 5.31. Bi-plot of PCA axis-one and -two species (Red arrows) and sample scores (points coloured according to CONISS testate amoeba zone) of SAN-EM-2 testate amoeba data.

The screeplot shows that there are three significant axes resulting from the PCA. The first and second axes account for a total of 49.04% of total variance in the data. *Schwabia sp.* and *Centropyxis platystoma* type are most strongly correlated with axis-one despite their low abundances in the profile. Despite accounting for less of the total variance than axis-one, axis-two seems to be the dominant axis with *D.pulex*, *E.tuberculata* and *A.muscorum* most strongly correlated with this axis. *D.pulex* is located at the lower end of this axis and samples are grouped around this taxon; however, a clear grouping based on zone is not evident. Samples in SJTa are spread along the higher end of axis-one owing to high taxonomic diversity. Samples in SJTd are grouped at the higher end of axis-two owing to the dominance of *E.tuberculata* and *A.muscorum* in these surface samples. Axis-one poorly represents the data but axis-two may represent a wetness gradient owing to separation of the dominant taxa along this axis.

The PCA axis-one and -two scores are presented alongside the WTD reconstruction in figure 5.32 for comparison. The Patagonian WA-PLS transfer function was applied to the SAN-EM-2 testate amoeba data and the resulting WTD reconstruction is presented in figure 5.32a with each sample representing reconstructed depth to the water table from the surface in cm units. The reconstruction error is shown by the dashed lines. The zones on the diagram correspond to the testate amoeba zones (figure 5.30).

The mean WTD is 27.66 cm; values are above the mean at the base of the record in zone SJTa at around 38 cm depth until 92 cm when there is a shift to lower values. These values persist at ~10 cm between 92 and 32 cm into zone SJTc and reflect the dominance of *D.pulex*. Above 32 cm there is a shift to higher values from low values ~10 cm at the beginning of SJTd to 61.05 cm at the surface reflecting the shift in species composition from the dominance of *D.pulex* to the dominance of *A.muscorum*. PCA axis-one and -two scores are displayed alongside the WTD reconstruction (figure 5.32b). The general trend in the three records is the same with higher values in the basal zone with a shift to lower values. The PCA axis-one scores show lower values in the surface zone, this is because of the lack of correlation of the taxa in zone SJTd with this axis. The axis-one scores, therefore, do not seem to be representing wetness variability. The axis-two scores are similar to the WTD reconstruction, owing to the correlation of *D.pulex*, at one end of the axis, and *E.tuberculata* and *A.muscorum*, at the other end, with axis-two representing a wetness gradient. The WTD reconstruction better represents a wetness gradient as it is constrained by modern hydrological data. As such, the normalised WTD record will be compared with other proxies (figure 5.33).

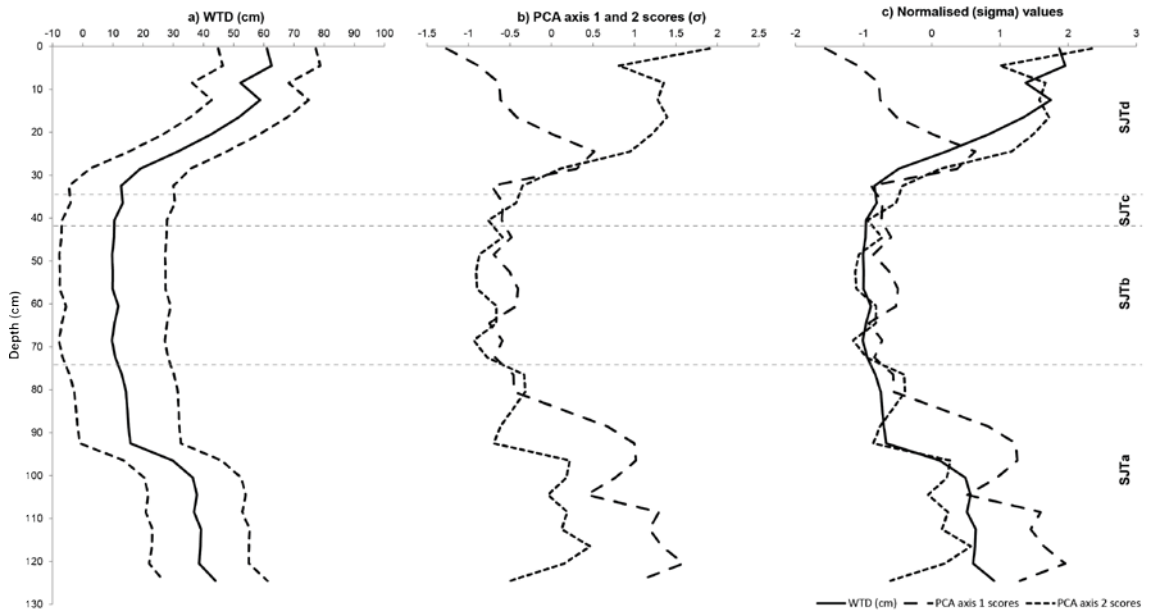

Figure 5.32. Bog surface wetness anomaly curves from the SAN-EM-2 testate amoeba data transformed to water table depth reconstruction (a) and PCA axis-one scores (b) and the two normalised records are compared (c). Testate amoeba zones are displayed.

5.2.1.2 Multi-proxy comparison of palaeoecological records

Figure 5.33 displays the multi-proxy comparison of the SAN-EM-2 normalised palaeoecological records plotted against depth. The primary axis displays the normalised testate amoeba and plant macrofossil records and the secondary axis displays the (reversed) normalised humification record. The plant macrofossil zones and stratigraphic description are displayed for reference. From the base of the records until 84 cm the three display a similar direction of change. Above this until the end of zone SJMb the testate amoeba record remains at a similar level whereas the humification and plant macrofossil records move in the opposite direction. Above this these two records show a similar directional shift to the surface whereas the testate amoeba record remains at the same level as before, shifting to increased values in zone SJMe, an opposite shift to the other records. Both the humification and plant macrofossil records reflect the shifts in the stratigraphy between more and less humified peat.

Comparisons between the different combinations of proxies are displayed in figures 5.33ai – 5.33aiii. The plant macrofossil and humification records are negatively

correlated (r_s= *-0.43) and are in good agreement visually, with higher DHI values generally occurring alongside lower % transmission values. The testate amoeba and plant macrofossil records show almost no correlation (r_s= -0.03) and this may be a result of relative insensitivity of the testate amoeba record. The testate amoeba and humification records are positively correlated (r_s= *0.76) with higher WTD values occurring alongside higher % transmission values.

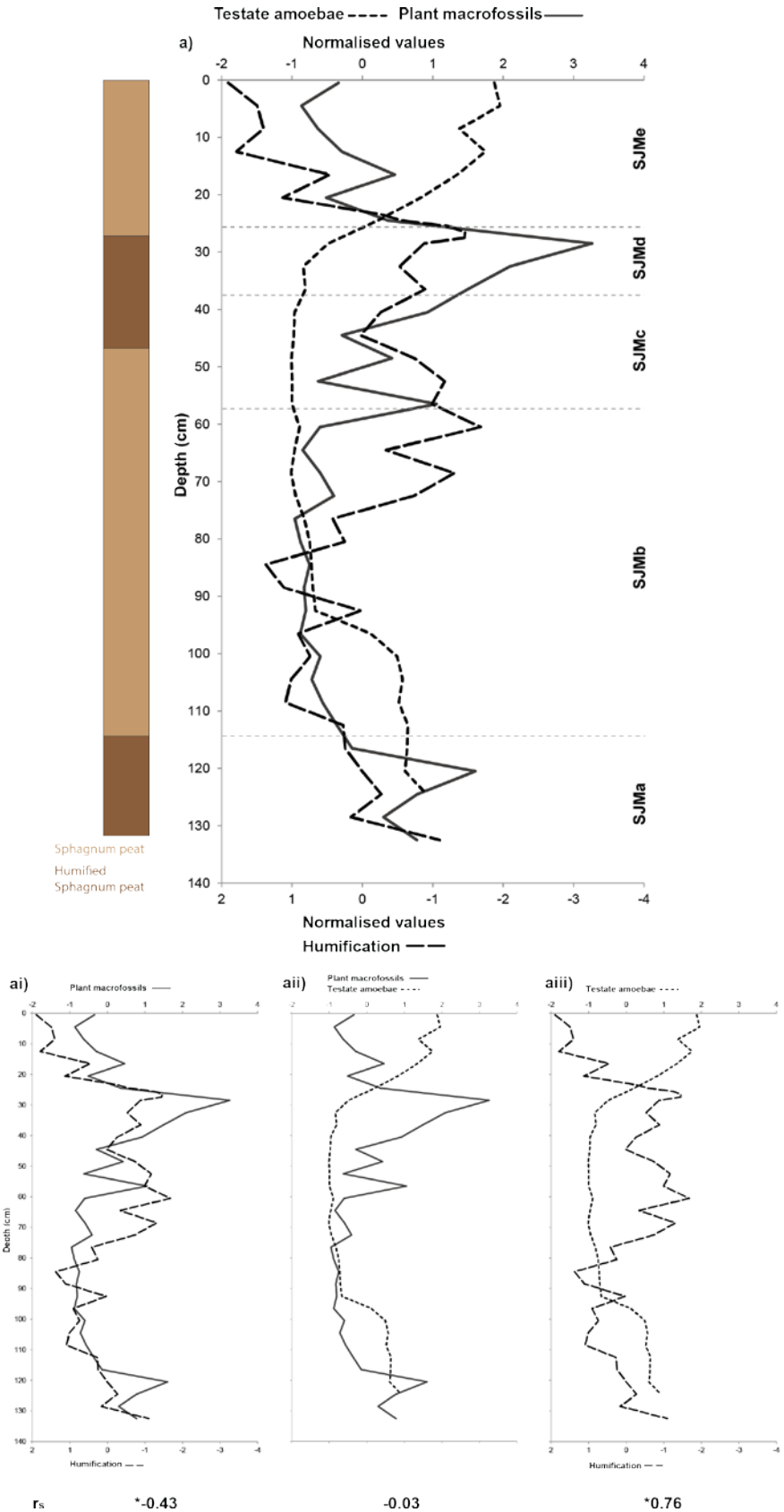

Figure 5.33. Multiproxy comparison of the SAN-EM-2 palaeoecological records. The normalised testate amoeba and plant macrofossil records are on the primary axis. The normalised humification record is presented on the secondary axis which has been reversed.

5.2.1.3 Stable isotope results

5.2.1.3.1 Stable carbon isotope results

Figure 5.34 presents the stable carbon isotope results from SAN-EM-2 with 1σ error bars shown (0.32‰). Values peak above and below the mean value (-27.56‰) throughout the record. The shift to the least negative value at 112 cm (-25.55 ‰) is one example with the largest range of variability (3.97‰) in the record between this depth and a general shift to more negative values until the most negative value at 52 cm (-29.52‰). The SAN-EM-2 chronology allowed identification of the closest sampling point to the 1850 pre-industrial standard, AD 1857 at 52 cm. Despite only showing a slight shift to more negative values towards the surface, a pre-requisite for correction, the record has been corrected above 52 cm. Above this there is a shift to less negative values, except an excursion to a more negative value at 28 cm, until 20 cm. Above 20 cm there is a shift to more negative values before a shift to less negative values towards the surface.

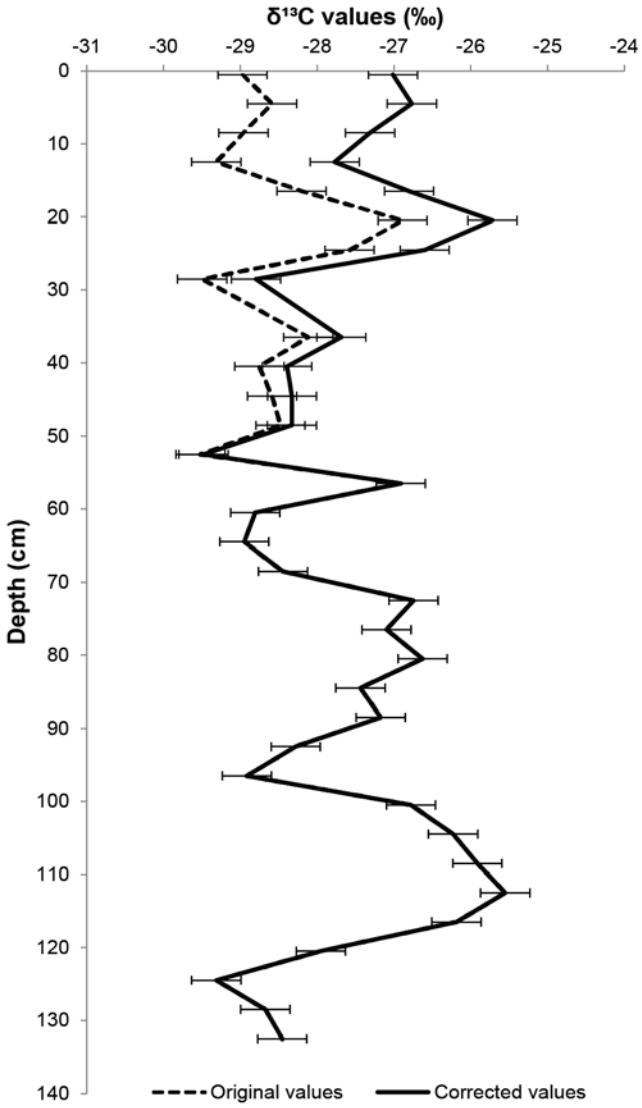

Figure 5.34. The SAN-EM-2 corrected stable carbon isotope records. Original surface values before correction are displayed by the dashed lines.

5.2.1.3.2 Stable oxygen isotope results

The stable oxygen isotope record from SAN-EM-2 is presented in figure 5.35. 1σ error bars are displayed (±0.17‰). The mean value of this record is 22.68‰. From the base of the record there is a general shift to higher values, to the highest value in the record at 56 cm (24‰). During this shift there are two peaks to lower values at 96 cm (21.74‰) and 68 cm (21.73‰). Above 56 cm there is a general shift to lower values to the surface apart from a shift of 2.61‰ to the lowest value in the record at 44 cm (21.39‰) before returning to a higher value at 36 cm and a continued general trend to lower values to the surface.

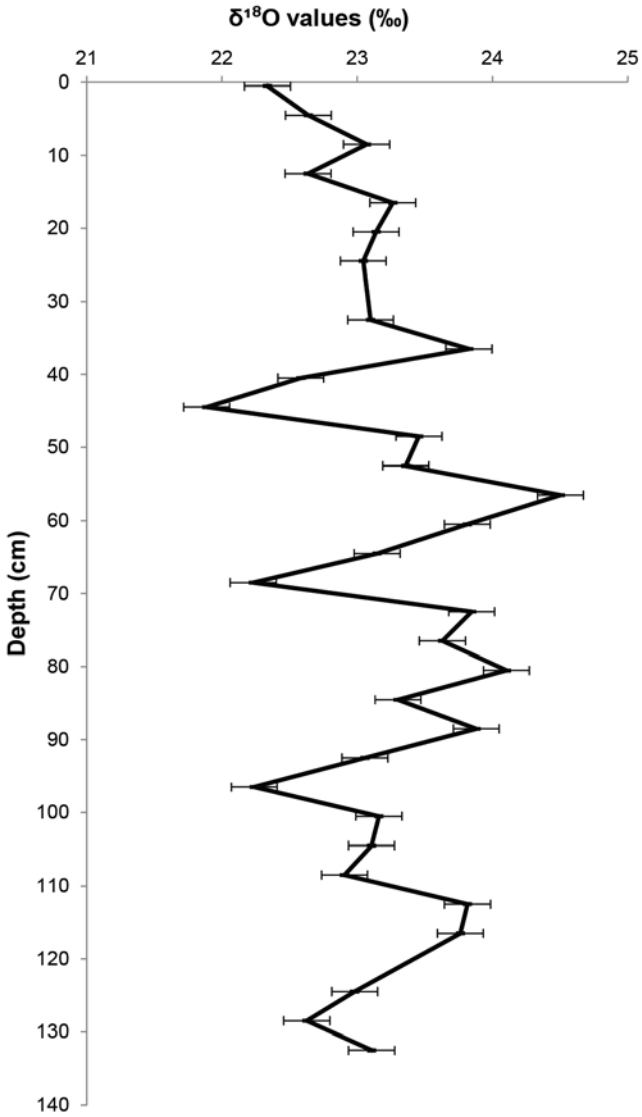

Figure 5.35. The SAN-EM-2 stable oxygen isotope results.

5.2.1.3.3 Comparison of stable carbon and stable oxygen isotope records

Figure 5.36 compares the corrected stable carbon isotope record with the stable oxygen isotope records from SAN-EM-2. The stable carbon isotope record has a higher range of maximum variability (3.97‰) compared with the stable oxygen isotope record (2.61‰). There is a weak positive correlation between the two records (r^2=0.11). Despite good agreement between the records between 100-50 cm in zone SJMb the records generally disagree above 50 cm to the surface. Reversal of the stable carbon isotope axis results in greater disagreement in the direction of variability throughout the records.

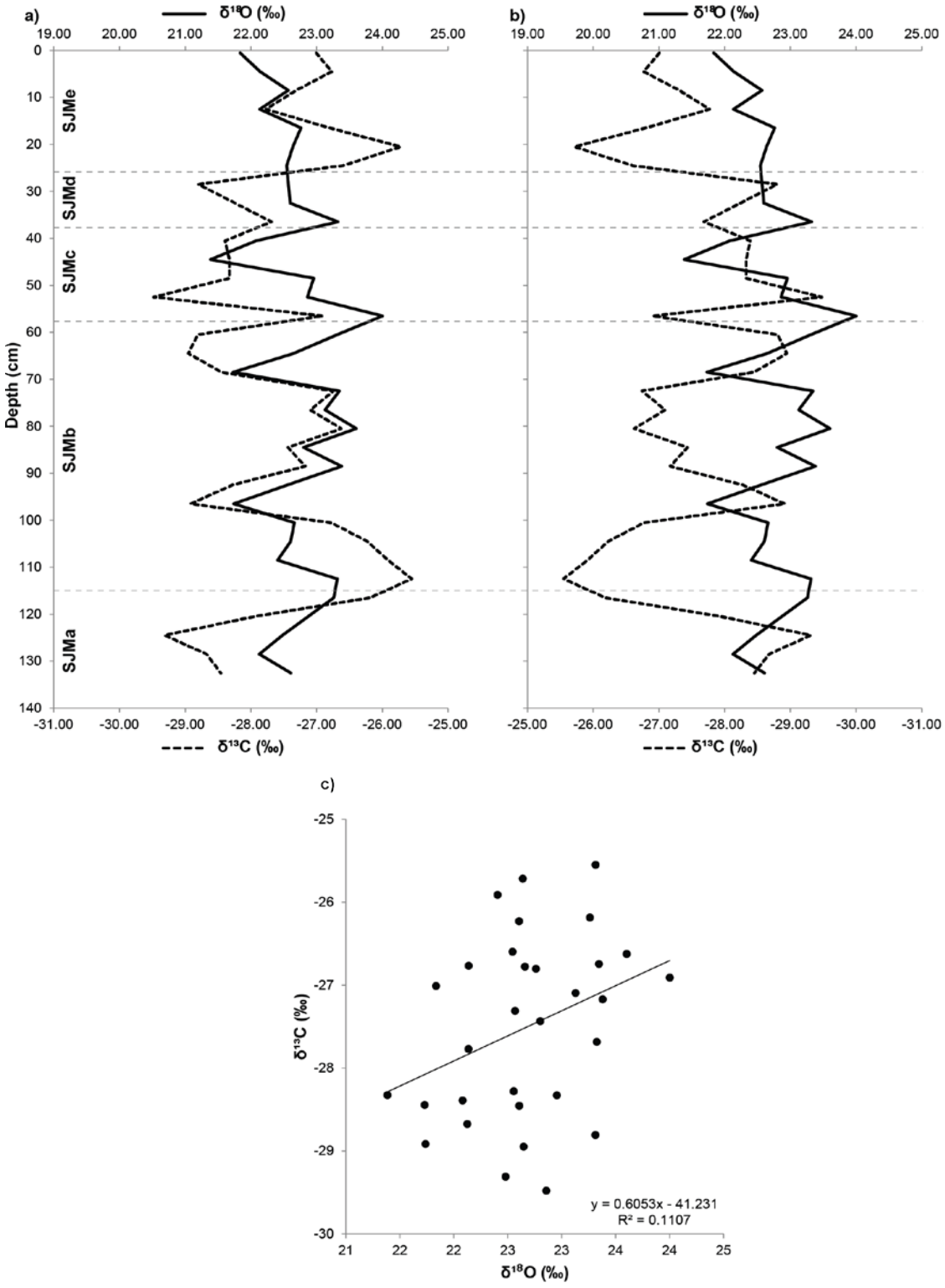

Figure 5.36. Comparison of the SAN-EM-2 corrected stable carbon and stable oxygen isotope records (a). The stable carbon isotope axis is reversed in (b). The scatterplot compares the two records (c).

5.3 San Carlos

This final section presents the results from SCB-1. The profile and stratigraphic description are presented, followed by the palaeoecological results and a multi-proxy comparison of the plant macrofossil and testate amoeba results. The stable isotope results are then presented. All records are plotted against depth. The approximate ages of zone boundaries are displayed on the plant macrofossil and testate amoeba diagrams.

The SCB-1 profile is presented in figure 5.37. The photographed sections and stratigraphic description are displayed. The profile consists of two sections, a lower section of herbaceous compacted peat from the base to 80 cm and an upper section above this throughout which *Sphagnum* peat dominates with a section of more humified peat between 80 and 60 cm. The upper section has been the focus in this investigation owing to the dominance of *Sphagnum* and the importance of this genus in terms of the stable isotopic aspect of the investigation.

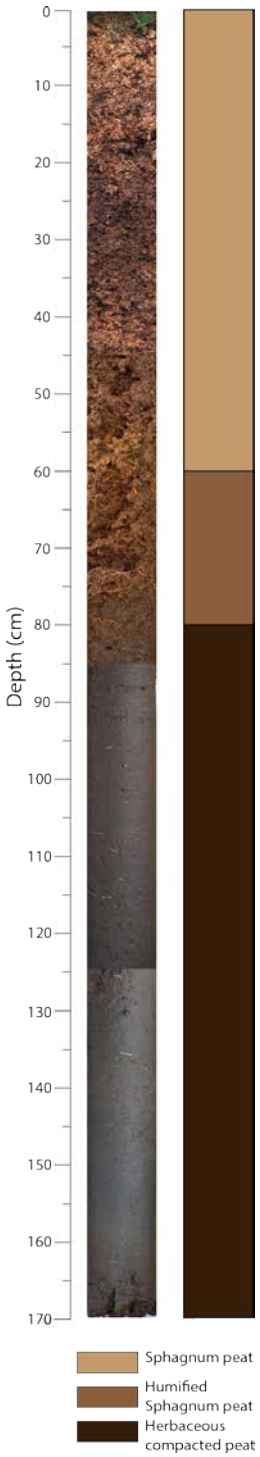

Figure 5.37. Depth based stratigraphic variability of SCB-1.

5.3.1 SCB-1

5.3.1.1 Palaeoecological results

5.3.1.1.1 Plant macrofossil results

The SCB-1 plant macrofossil results are presented in figure 5.38. Table 5.21 provides a summary description of the plant macrofossil zones, the depths and approximate ages of zone boundaries.

Note that the approximate ages of the zone boundaries of SCMa and the lower zone boundary of SCMb are not available due to these depths being outside of the age-depth model with ages only available above 77 cm (see section 4.3.5). *Sphagnum* dominates throughout all zones apart from the basal zone and only one species of *Sphagnum* is present, *S.magellanicum*. The only major shift in the profile is between the basal zone SCMa and SCMb, ~81 cm, where *S.magellanicum* rises from absence to dominance. The age of this boundary is not dated but is suggested to be before AD 1730 (age at 77 cm). There is a decrease of *S.magellanicum* after the zone boundary between SCMb and SCMc (AD 1771), dominating the zone at ~90% throughout SCMc. *S.magellanicum* is slightly lower after the zone boundary to SCMd (AD 1978) owing to the presence of surface vegetation (monocot and Ericaceae components).

Statistical methods are used to transform the raw multivariate plant macrofossil data to a univariate line of BSW variability. Table 5.22 presents the results of the DCA after the removal from and down-weighting of rare species in the dataset. The axis-one gradient length of much lower than 3σ necessitated the use of a linear response model (Ter Braak and Prentice, 1988; Lepš & Šmilauer, 2003).

The PCA results are displayed in table 5.23, rare species were removed and a Hellinger transformation was carried out on the data set resulting in the bi-plot of axis-one and -two sample and species scores as presented in figure 5.39.

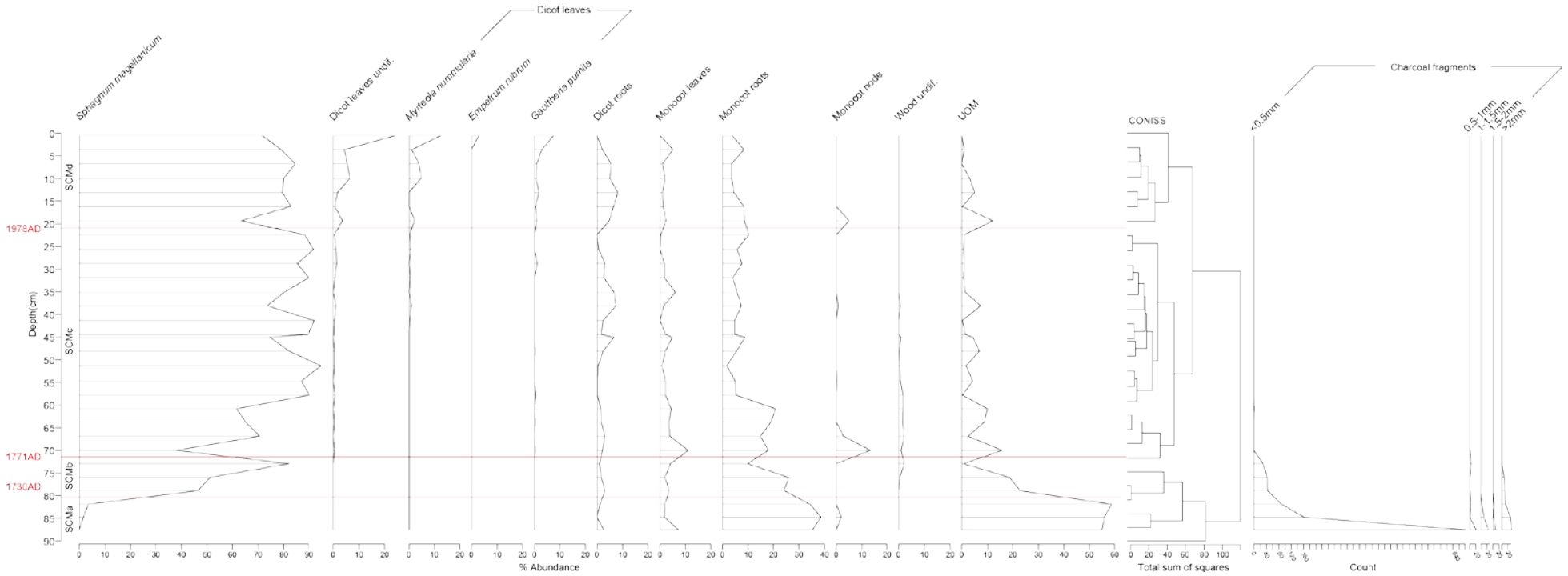

Figure 5.38. SCB-1 plant macrofossil diagram plotted against depth, displaying plant macrofossil zones based on CONISS with approximate ages of zone boundaries presented.

Table 5.21. Summary description of SCB-1 plant macrofossil zones.

Zone	Depth (cm)	Plant macrofossil zone description	Age cal BP (AD)
SCMa	88-81	In this zone *S.magellanicum* is very low alongside high levels of monocot roots and UOM. Charcoal fragments <0.5mm are high throughout the zone alongside lower counts of larger fragments.	N/A
SCMb	81-72	*S.magellanicum* increases throughout the zone to 80% at the end of the zone. Monocot roots and UOM decrease throughout the zone. Charcoal fragments <0.5mm are lower in this zone alongside even lower counts of larger fragments than the previous zone.	>220 – 179 cal BP (<AD 1730 – 1771)
SCMc	72-21	*S.magellanicum* is at ~40% abundance at the beginning of the zone and increases to 90% thereafter remaining at this level throughout the zone. The abundance of monocot roots decrease from ~20% at the beginning of the zone to <10% throughout the rest of the zone alongside low levels of UOM.	179- -28 cal BP (AD 1771-1978)
SCMd	21-0	There are slightly lower levels of *S.magellanicum* in this zone ~80% throughout alongside low % of monocot and dicot roots. Dicot leaves increase towards the surface due to the presence of identifiable surface vegetation.	-28 - -63 cal BP (AD 1978-2013)

Table 5.22. Results of DCA of SCB-1 plant macrofossil data.

	Axis 1	Axis 2	Axis 3
Eigenvalues	0.4500	0.07096	0.07701
% accounted for by axis	70.08%	11.05%	11.99%
Gradient lengths	1.8850	0.54599	0.83399

Table 5.23. Results of PCA of SCB-1 plant macrofossil data.

	Axis 1	Axis 2	Axis 3
Eigenvalues	3.392	1.351	0.955
% accounted for by axis	48.46%	19.30%	13.64%
Screeplot (Broken stick)	Significant	-	-

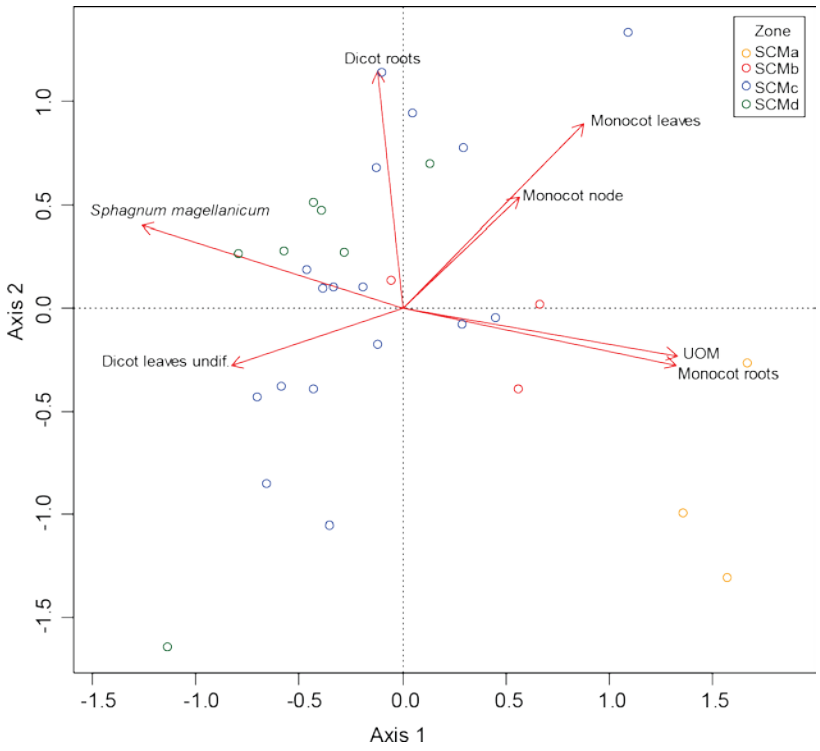

Figure 5.39. Bi-plot of PCA axis-one and -two species (Red arrows) and sample scores (points coloured according to CONISS plant macrofossil zone) of SCB-1 plant macrofossil data.

A screeplot revealed that the only significant axis resulting from the PCA of the plant macrofossil data was axis-one which accounts for 48.46% of the total variance in the data set. *S.magellanicum*, monocot roots and UOM are strongly correlated with the first principal component and dicot roots strongly correlated with axis-two. *S.magellanicum* is at the lower end of axis-one opposite to the other dominant components which are located at the higher end of the axis. Samples are coloured according to plant macrofossil zone, with samples from zones SCMa and SCMb located at the higher end of axis-one owing to higher levels of monocot roots and UOM compared with samples from zones SCMc and SCMd which are located at the lower end of the axis owing to the dominance of *S.magellanicum* in these zones. Separation of these plant components along axis-one could represent a wetness gradient The PCA axis-one scores (figure 5.40b) are compared with the Dupont Hydroclimatic Index (figure 5.40a) values of the SCB-1 plant macrofossil data. The normalised records are then compared in figure 5.40c.

DHI values are high at the base of the profile with a major shift to lower values occurring just after the zone boundary to SCMb reflecting the shift from the absence to dominance of *Sphagnum*. After the zone boundary to SCMc, values increase slightly reflecting a decrease of *Sphagnum* at this depth. Above this values decrease until ~60 cm after which values are uniform around the mean (4.27) to the surface owing to the dominance of *S.magellanicum*. The PCA axis-one scores are similar to the DHI values throughout the record (figure 5.40c) however, the presence of surface vegetation in zone SCMd which correlates with axis-two and results in lower PCA axis-one normalised values. Owing to its consideration of all species, the DHI record offers a better representation of BSW variability.

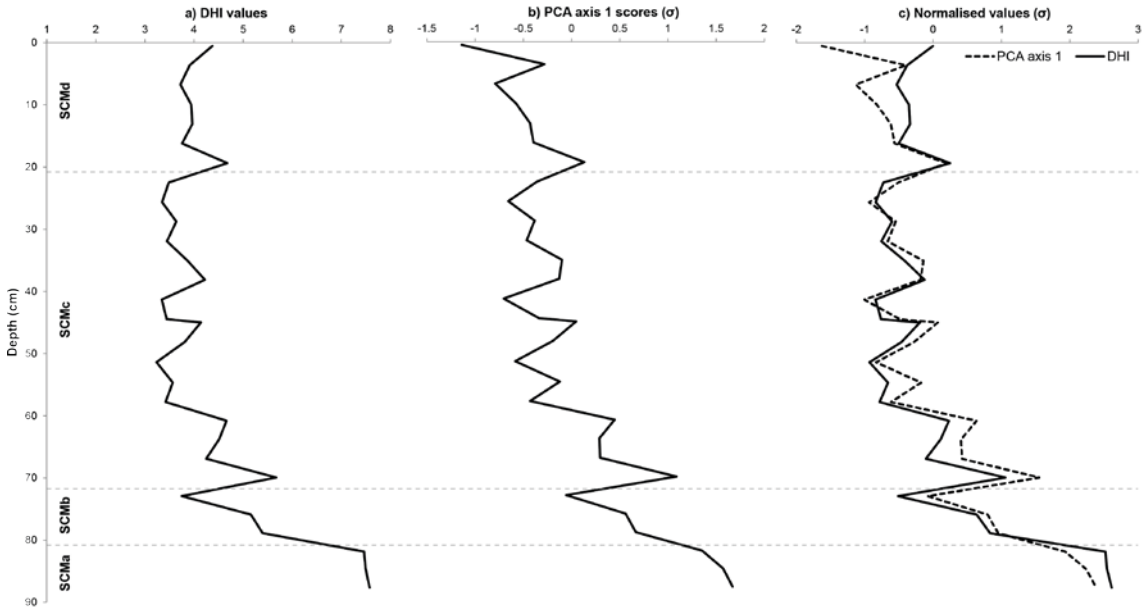

Figure 5.40. Bog surface wetness anomaly curves from the SCB-1 plant macrofossil data transformed using the Dupont Hydroclimatic Index (a) and the axis-one scores of Principal Components Analysis (b). The two records are normalised and compared (c).

5.3.1.1.2 Testate amoeba results

The SCB-1 testate amoeba results are presented in figure 5.41 with a summary description of testate amoeba zones and the depths and approximate ages of zone boundaries presented in table 5.24. From left to right on the diagram the taxa included in the transfer function and water table depth reconstruction are arranged from xerophilous to hygrophilous taxa. To the right of the diagram the test

concentration per cm^3 and taxonomic diversity are displayed. Taxonomic diversity is uniform throughout the profile. The species composition is highly variable throughout the profile.

A significant shift occurs at 70 cm when the dominance of *Centropyxis platystoma* type is replaced by the dominance of *Certesella certesi* and *Certesella martiali*. These taxa dominate until the rise of *Heleopera sylvatica* at 60 cm and subsequent shift to dominance of *D.pulex* just before the zone boundary to SCTb (AD 1884), forming the most significant shift in the profile. Test concentration is high throughout this zone and increases to >15,000 tests per cm^3 in SCTc at 38 cm, *D.pulex* dominates throughout zones SCMb and SCMc and rapidly decreases after the zone boundary to SCTd (AD 1942). *E.tuberculata* type dominates alongside *Nebela* taxa until 22 cm when *A.muscorum* and *Centropyxis cassis* type rise to dominate alongside *E.tuberculata* and *Nebela vitraea* type.

DCA was carried out on the testate amoeba data with removal from and down-weighting of rare species in the dataset to calculate the gradient length of the axes (table 5.25). In the case of an axis-one gradient length between 3 and 4σ Lepš & Šmilauer (2003) suggest that either a linear or unimodal response model can be used. For consistency with the other testate amoeba records in the investigation a linear response model was chosen for transformation of the multivariate data to a single line of BSW.

The dataset was subjected to removal of rare species and a Hellinger transformation was carried out. The results of the PCA are displayed in table 5.26 and figure 5.42, which presents a bi-plot of axis-one and -two sample and species scores.

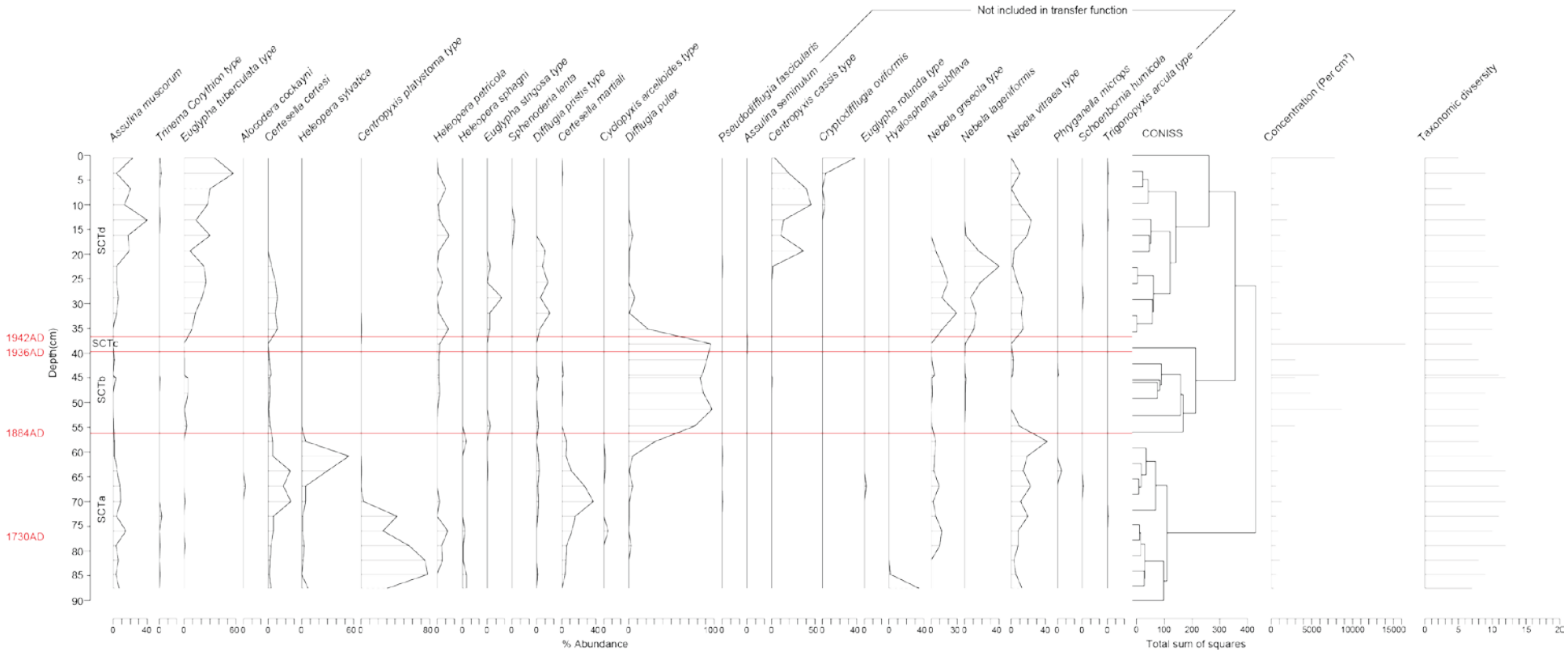

Figure 5.41. SCB-1 testate amoeba diagram plotted against depth, displaying testate amoeba zones based on CONISS with approximate ages of zone boundaries presented. Concentration and taxonomic diversity presented.

Table 5.24. Summary description of SCB-1 testate amoeba zones.

Zone	Depth (cm)	Testate amoeba zone description	Age cal BP (AD)
SCTa	88-56	There is low test concentration throughout this zone. Centropyxis platystoma type dominates until ~70 cm, after which *C.certesi* and *C.martiali* both increase then decrease ~60 cm, *H.sylvatica* dominates until just before the end of the zone where *N.vitraea* type and *D.pulex* increase.	>220 – 66 cal BP (<AD 1730 – 1884)
SCTb	56-39	Test concentration is higher in this zone throughout which *D.pulex* dominates with other taxa present only at very low abundances.	66 – 14 cal BP (AD 1884 - 1936)
SCTc	39-37	This very short zone is characterised by an increase in test concentration to >15,000 tests and the dominance of *D.pulex*.	14 – 8 cal BP (AD 1936 - 1942)
SCTd	37-0	Test concentration is low throughout the zone until the uppermost sample which has a concentration of >5000 tests. At the beginning of the zone *D.pulex* decreases rapidly after which *E.tuberculata* type increases throughout. *Nebela* taxa dominate at the beginning of the zone with N. vitraea type persisting until the surface. *C.cassis* type and *A.muscorum* increase above 22 cm and dominate alongside *E.tuberculata* and *N.vitraea* type until just below the surface when *Cryptodifflugia oviformis* increases.	8 - -63 cal BP (AD 1942 – 2013)

Table 5.25. Results of DCA of SCB-1 testate amoeba data.

	Axis 1	Axis 2	Axis 3
Eigenvalues	0.681	0.5986	0.3052
% accounted for by axis	21.22%	18.65%	9.51%
Gradient lengths	3.474	3.3135	2.12

Table 5.26. Results of PCA of SCB-1 testate amoeba data.

	Axis 1	Axis 2	Axis 3
Eigenvalues	3.982	3.333	2.364
% accounted for by axis	24.89%	20.83%	14.77%
Screeplot (Broken stick)	Significant	Significant	Significant

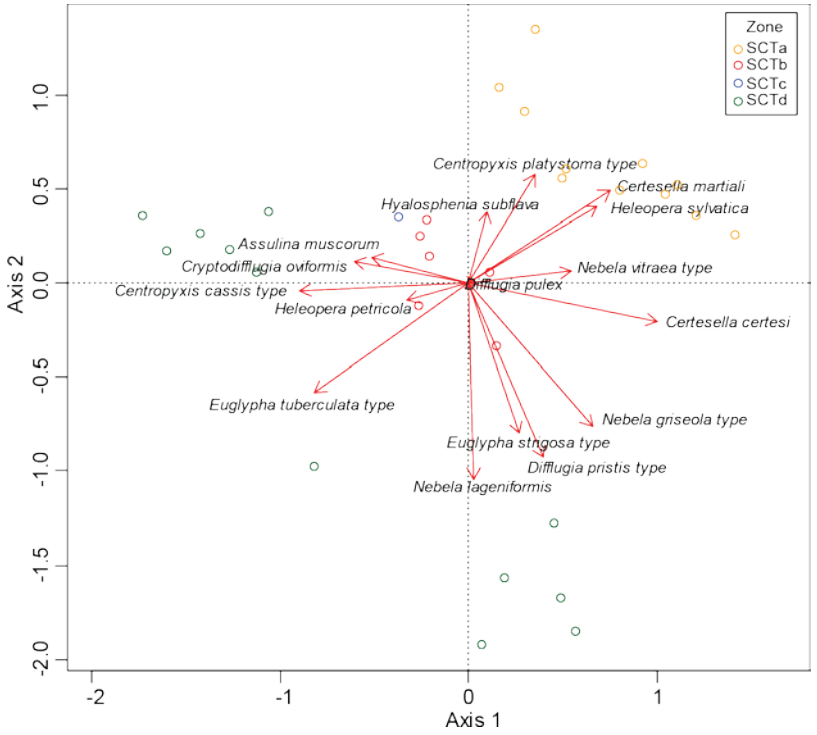

Figure 5.42. Bi-plot of PCA axis-one and -two species (Red arrows) and sample scores (points coloured according to CONISS testate amoeba zone) of SCB-1 testate amoeba data.

Three significant axes resulted from the PCA as suggested by a screeplot. The first two axes account for 45.62% of the total variance in the data. The taxa most strongly correlated with axis-one are: *C.certesi*, *C.cassis* type and *E.tuberculata* type. There is separation along this axis with *C.cassis* type and *E.tuberculata* type located at the lower end of the axis and *C.certesi* located at the higher end. Samples are coloured according to testate amoeba zone. Samples from SCTa are located at the higher ends of axis-one and -two, samples in SCTb are located close to 0 on the bi-plot

where *D.pulex* is located, whereas samples from SCTc and SCTd are spread between the lower end of axis-one and higher end of axis-two. It is clear that a well-defined wetness gradient is not represented by either of the first two axes which is also demonstrated by the Nmds (figure 5.43). Although samples are clustered based on testate amoeba zone there is high dispersal of the samples within the clusters. Samples from zones SCTd and SCTa are located at the lower end of axis-one; however, they are also dispersed along the second axis. SCTb is located at the higher end of axis-one but samples in this zone are also spread along axis-two. In this case it is difficult statistically to transform the multivariate data to a univariate line of BSW.

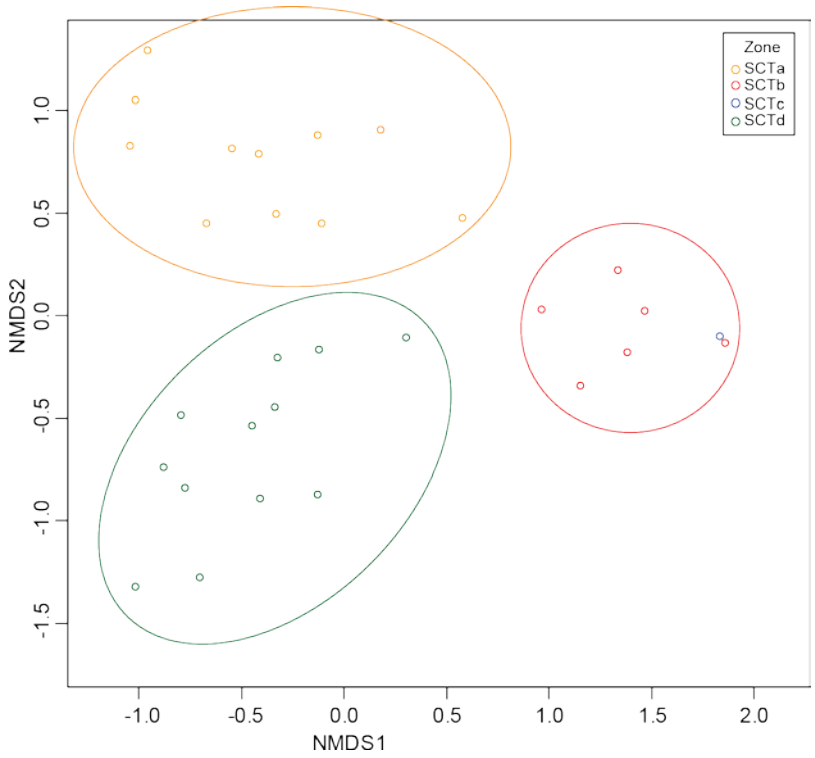

Figure 5.43. Nmds bi-plot of SCB-1 testate amoeba data (points represent sample depth and coloured according to CONISS testate amoeba zone).

Despite the absence of a wetness gradient from the PCA of the SCB-1 testate amoeba data, the PCA axis-one scores are presented in figure 5.44. The Patagonian WA-PLS transfer function was applied to this dataset and the resulting WTD reconstruction is presented in figure 5.44a. Each sample represents in cm units the

reconstructed depth to the water table from the surface. The reconstruction error (dashed lines) and testate amoeba zones are displayed on the diagram.

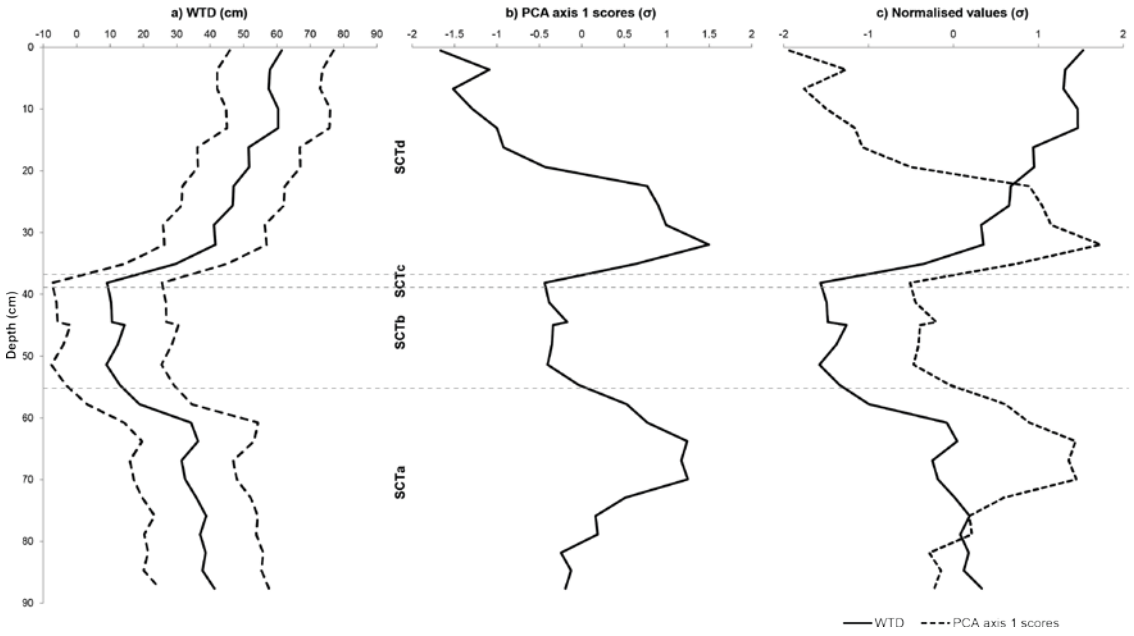

Figure 5.44. Bog surface wetness anomaly curves from the SCB-1 testate amoeba data transformed to water table depth reconstruction (a) and PCA axis-one scores (b) and the two normalised records are compared (c). Testate amoeba zones are displayed.

From the base of the profile WTD is around the mean value (35.61 cm) until ~60 cm after which WTD decreases to a level ~10 cm throughout SCTb reflecting the dominance of *D.pulex* in this zone. WTD increases in zone SCTc and values increase throughout SCTd to a value of 61.43 cm at the surface. The increase in values towards the surface reflects the increase of xerophilous taxa towards the surface.

The PCA axis-one scores (figure 5.44b) are displayed alongside the WTD reconstruction and the normalised records are compared (figure 5.44c). The absence of a wetness gradient resulting from the PCA is evident. The two records are mainly in active disagreement apart from agreement in the direction of change between 60 and 35 cm resulting from the shift to dominance of *D.pulex*. Above this,

the PCA axis-one scores move in the opposite direction to the WTD reconstruction; the lower values result from the location of the xerophilous taxa at the lower end of axis-one despite this not representing a wetness gradient. Disagreement between the records also results from the inclusion of taxa in the PCA that are excluded from the WTD reconstruction despite their importance in the species composition but lack modern hydrological preference data (e.g. *C.cassis* type and *Nebela* taxa). Despite this the WTD reconstruction is constrained by modern hydrological data and is therefore a more reliable indicator of hydrological variability. The normalised WTD record will be compared with the other proxies in this investigation.

5.3.1.2 Multi-proxy comparison of palaeoecological records

The normalised SCB-1 plant macrofossil and testate amoeba records are presented in figure 5.45. The plant macrofossil zones and stratigraphic description are displayed for reference. The records display a weak positive correlation (r_s= 0.23). From the base of the record there is a shift from high to lower DHI values from zone SCMa to SCMb reflecting the change in the stratigraphy but this is not registered in the WTD reconstruction. Above this both records move to lower values in response to a shift in the stratigraphy to less humified *Sphagnum* peat in SCMc. DHI values are uniform to the surface above 60 cm whereas the shift to lower WTD values is of a higher magnitude and persists for ~20 cm followed by an increase in values to the surface.

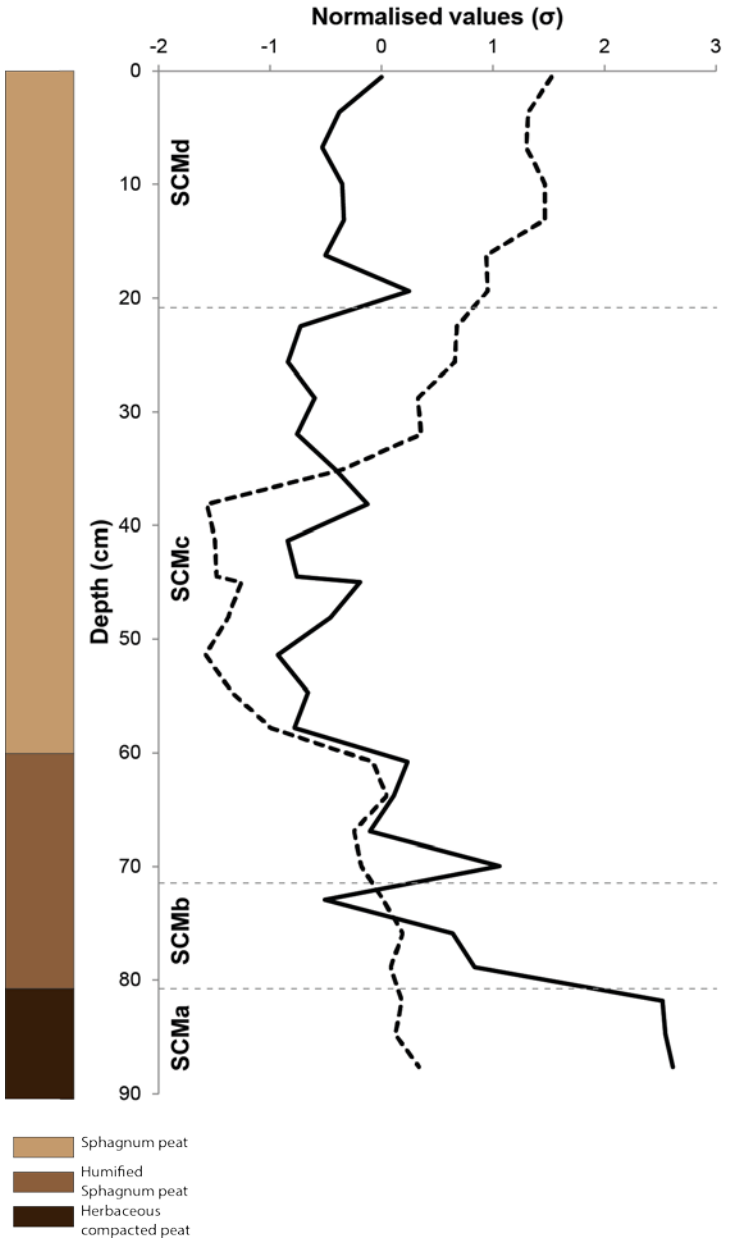

Figure 5.45. Multiproxy comparison of the SCB-1 palaeoecological records. The normalised testate amoeba and plant macrofossil records are compared.

5.3.1.3 Stable isotope results

5.3.1.3.1 Stable carbon isotope results

Figure 5.46 presents the stable carbon isotope record from SCB-1. 1σ error bars are displayed (0.19‰). The mean value of the record is -26.89‰. From the base of the record until 73 cm there is a shift to less negative values to the least negative value throughout (-24.91‰). Above this there is a shift to more negative values until 64 cm. The sampling point in closest proximity to AD 1850 was at 61 cm (AD 1855) and the record has thus been corrected above this level, removing a general trend to more negative values towards the surface. There is a slight increase in values (less negative) until 35 cm followed by a sharp shift to the most negative value at 29 cm (-28.94‰). Above this values become less negative until 13 cm, before shifting to more negative values until 4 cm before finally shifting to a less negative value of -25.43‰ at the surface.

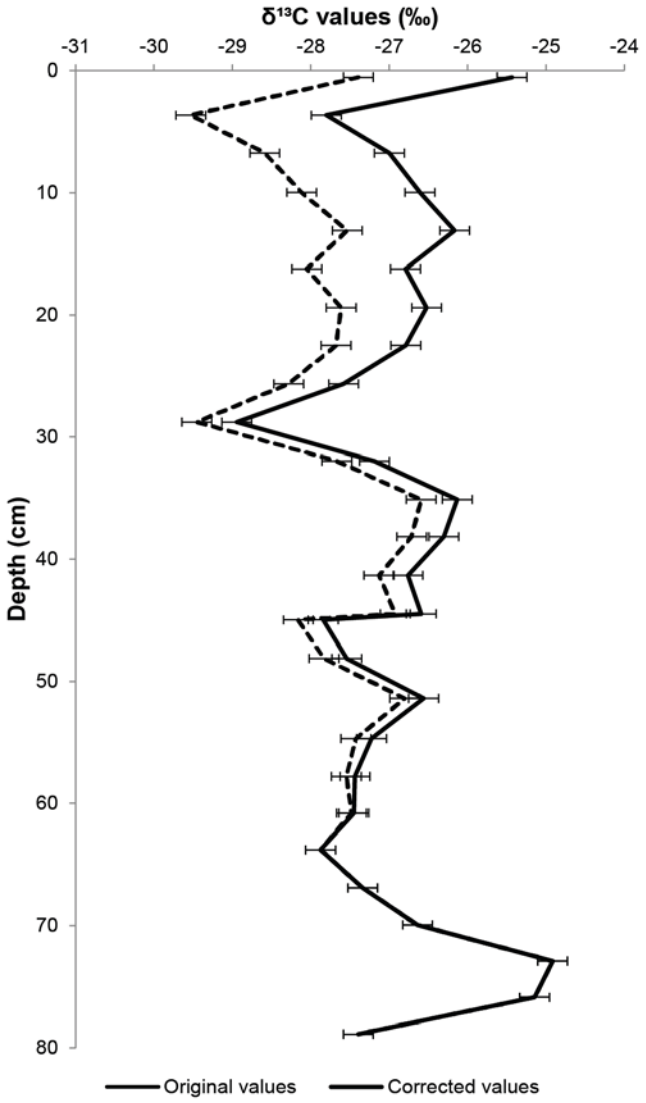

Figure 5.46. The SCB-1 corrected stable carbon isotope records. Original surface values before correction are displayed by the dashed lines.

5.3.1.3.2 Stable oxygen isotope results

Figure 5.47 presents the stable oxygen isotope record from SCB-1 with 1σ error bars displayed (0.17‰). The mean value of this record is 22.84‰. Throughout the record there is a general trend from higher to lower values. The record shifts to lower values from the base of the record until 26 cm followed by an increase in values until 19 cm to the highest value in the record (23.64‰). There is a subsequent shift to the lowest value in the record (21.50‰) at 4 cm and an increase to ~23‰ at the surface.

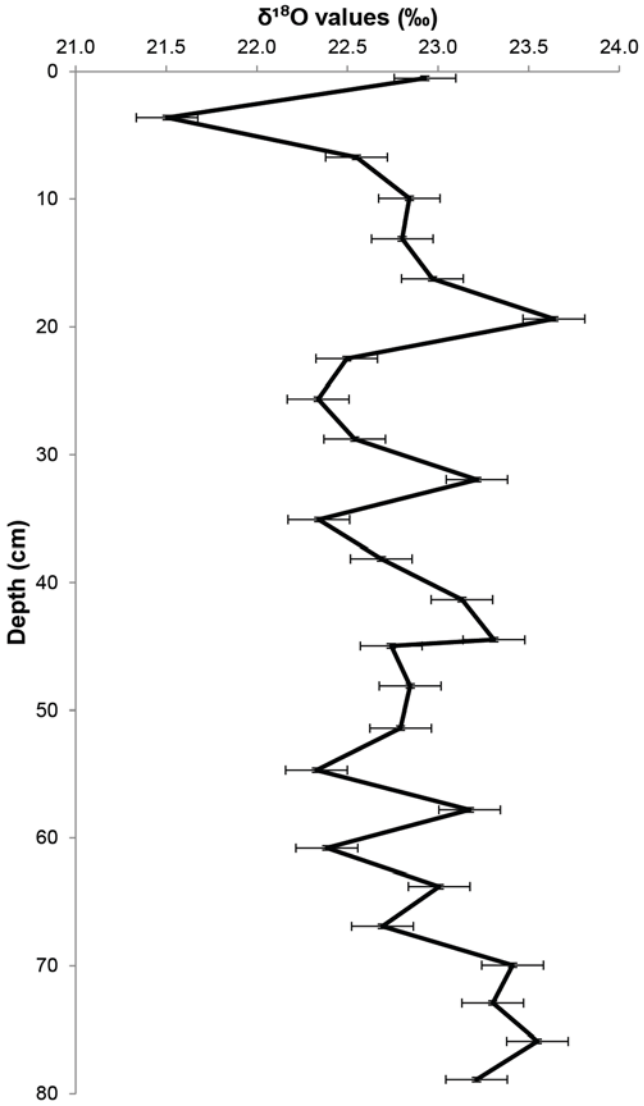

Figure 5.47. The SCB-1 stable oxygen isotope results.

5.3.1.3.3 Comparison of stable carbon and stable oxygen isotope results

The corrected stable carbon isotope record is compared with the stable oxygen isotope record in figure 5.48. A higher range of maximum variability is displayed in the stable carbon isotope record (4.03‰) compared with the stable oxygen isotope record (2.14‰). A weak positive correlation is evident (r^2=0.183) between the two records and the stable carbon isotope record is generally more variable than the stable oxygen isotope record. Excursions in the stable carbon isotope record are evident in the stable carbon isotope record at 74 cm and 30 cm which are not evident in the stable oxygen isotope record. There is agreement between the two

records in zone SCMd to the surface. Reversal of the stable carbon isotope axis results in disagreement between the two records particularly at depths where there are excursions in the stable carbon isotope record. This also results in opposite trends in the surface zone.

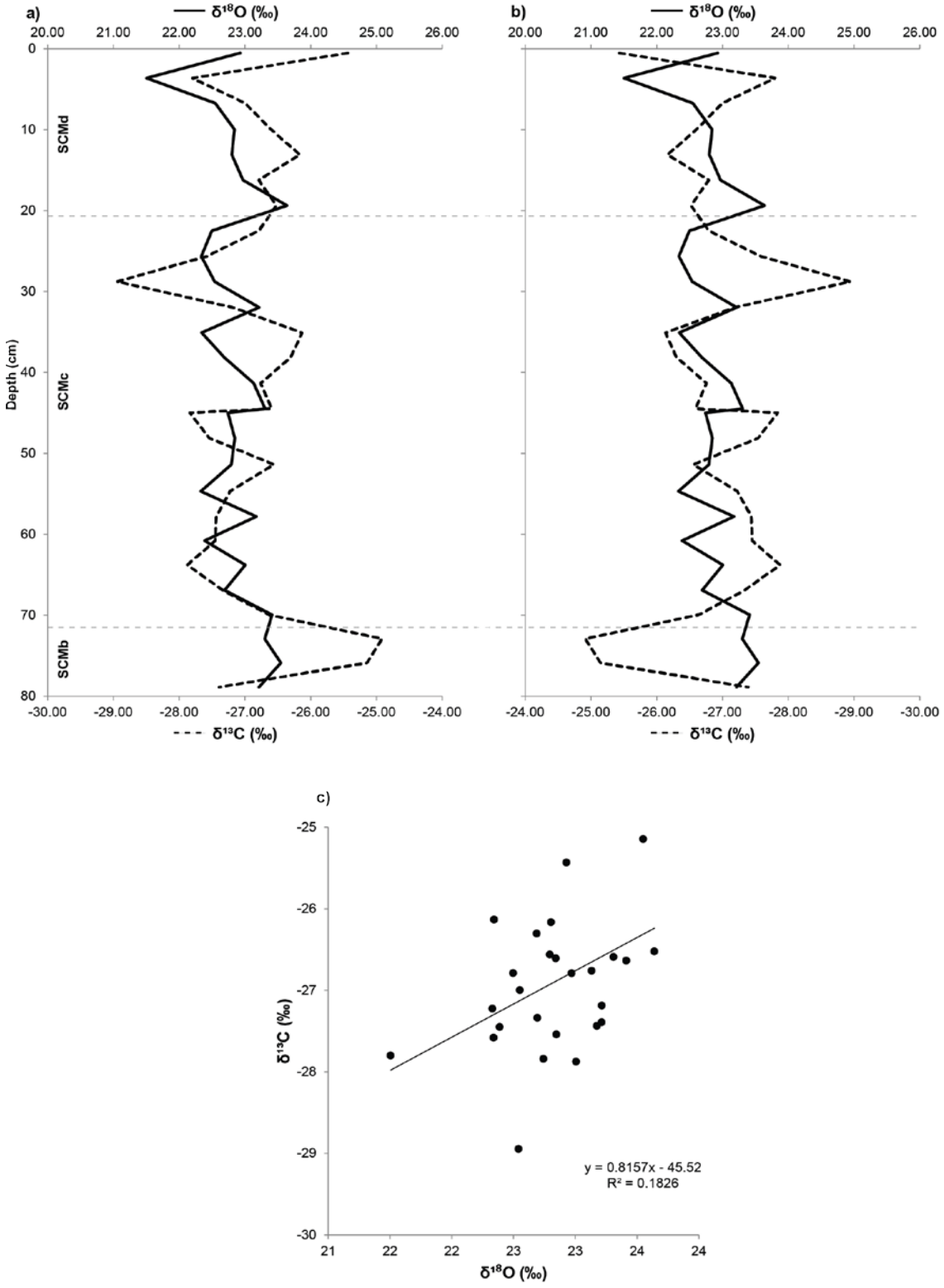

Figure 5.48. Comparison of the SCB-1 corrected stable carbon and stable oxygen isotope records (a). The stable carbon isotope axis is reversed in (b). The scatterplot compares the two records (c).

5.4 Summary of results

Figure 5.49 presents a summary of all proxy records from KAR-EM-1, KAR-EM-2 and KAR-EM-3 forming the basis of correlations between the palaeoecological and stable isotope records. Following comparison of the stable isotope records in figure 5.24 the stable carbon isotope axis has not been reversed owing to the similarity between the stable isotope records without reversal of the axis (figure 5.24, a graphs). This will allow interpretation of the stable isotope records based on the palaeoecological records from each profile rather than interpretation based on evidence from previous studies. Similarly, the stable carbon isotope axis has not been reversed in the comparison of the palaeoecological and stable isotope records from SAN-EM-2 (figure 5.50) and SCB-1 (figure 5.51).

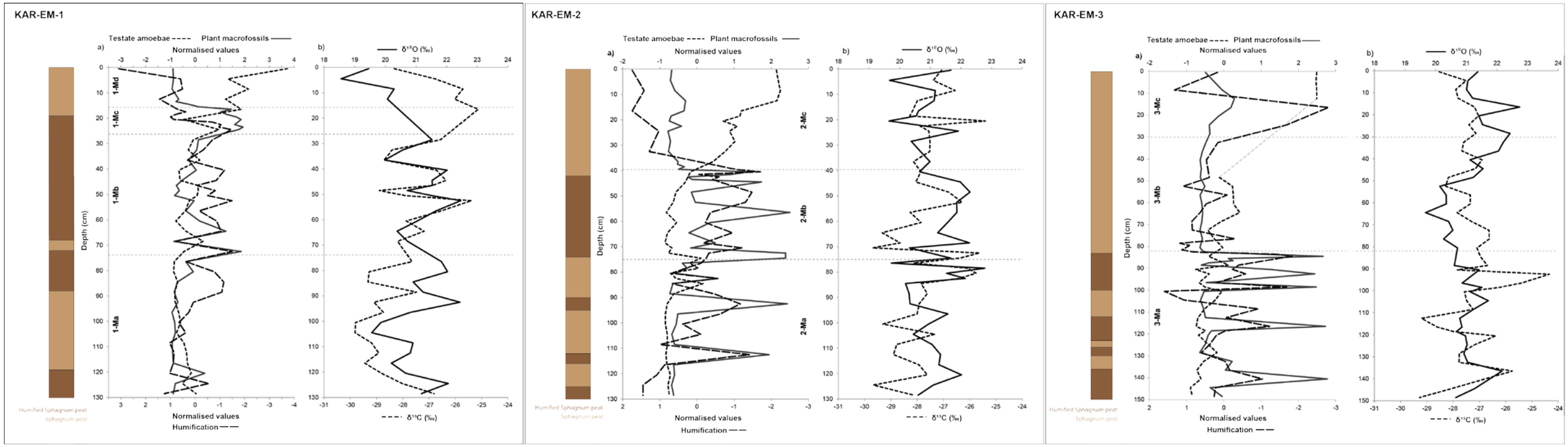

Figure 5.49. Comparison of the KAR-EM-1, KAR-EM-2 and KAR-EM-3 palaeoecological records (a graphs) and stable isotope records (b graphs).

Table 5.27. Correlation between the palaeoecological and stable isotope records from the individual KAR-EM profiles plotted against depth.

	Plant macrofossils (DHI record) vs. $\delta^{13}C$ (r_s)	Testate amoebae (WTD reconstruction) vs. $\delta^{13}C$ (r_s)	Humification values vs. $\delta^{13}C$ (r^2)	Mean correlation palaeoecological vs. $\delta^{13}C$ records	Plant macrofossils (DHI record) vs. $\delta^{18}O$ (r_s)	Testate amoebae (WTD reconstruction) vs. $\delta^{18}O$ (r_s)	Humification values vs. $\delta^{18}O$ (r^2)	Mean correlation palaeoecological vs. $\delta^{18}O$ records
KAR-EM-3	-0.056	-0.049	-0.190	-0.295	0.313	-0.253	*-0.464	-0.404
KAR-EM-2	-0.113	*0.374	0.028	0.289	*0.433	-0.233	-0.066	0.134
KAR-EM-1	0.282	*0.370	-0.147	**0.505**	0.298	*-0.495	*-0.563	**-0.760**

5.4.1 Comparison of palaeoecological and stable isotope records from KAR-EM-1, KAR-EM-2 and KAR-EM-3

The summary of records from this profile provides the basis for the following chapters and whether these records are reflective of climatic or ecohydrological variability. The stratigraphic description of each profile forms the context for the other analyses, evidencing the presence of the acrotelm-catotelm boundary and a preliminary overview of variability.

The plant macrofossil records generally reflect the stratigraphic variability with switches between low and high DHI values reflecting the presence and absence of *S.magellanicum*; whether these shifts are climatic must be assessed in subsequent chapters. The humification records also reflect the stratigraphic variability with low % transmission values in sections of humified peat and high % transmission values in sections of less humified peat. Humification values also generally reflect variability in the plant macrofossil records with higher DHI values occurring alongside lower % transmission values in sections of humified peat and lower DHI values occurring alongside higher % transmission values in sections of less humified peat.

The testate amoeba based WTD reconstructions generally reflect the shift between the dominance of *D.pulex* throughout each profile to the dominance of *A.muscorum* resulting in a WTD increase after the acrotelm-catotelm boundary in each profile. The WTD reconstructions do not generally reflect stratigraphic variability but unexpectedly positive correlations are found in each profile with humification values, with higher WTD values occurring alongside higher % transmission values in sections of less humified peat and vice versa. The relative insensitivity of the WTD reconstructions resulted in negative correlations with the plant macrofossil record in each profile with higher DHI values occurring alongside lower WTD values and vice versa and generally not reflective of variability in the plant macrofossil record.

With reference to figure 5.49 and table 5.27, in KAR-EM-3 the stable carbon isotope record does not reflect stratigraphic variability with a very weak negative correlation (r^2= -0.19) found between this and the humification record. There is no general agreement between these records with peaks to both less and more negative $\delta^{13}C$

values in sections of more humified peat (Zone 3-Ma).There is almost no correlation between the stable carbon isotope record and the plant macrofossil record (r_s = -0.06) and testate amoeba based WTD reconstruction (r_s= -0.05). In KAR-EM-2 less negative $\delta^{13}C$ values generally occur in sections of less humified peat; despite this there is no correlation between the stable carbon isotope record and humification values in this profile (r^2= 0.03). A very weak negative correlation is found between the stable carbon isotope record and plant macrofossil record in this profile (r_s= -0.11). A positive correlation is found between the stable carbon isotope record and the WTD reconstruction (r_s= *0.37) suggesting that higher WTD values occur alongside (higher) less negative $\delta^{13}C$ values. In KAR-EM-1, more negative $\delta^{13}C$ values generally occur in sections of less humified peat in this profile but there is almost no correlation between the stable carbon isotope record and humification values (r^2= -0.15). Positive correlations are however, found between this record and the plant macrofossil record (r_s= 0.28) and WTD reconstruction (r_s= *0.40).

In comparison of the stable oxygen isotope records with the palaeoecological records, in KAR-EM-3 the stable oxygen isotope record does not reflect stratigraphic variability as this record displays little variability around the mean. Despite this, a negative correlation (r^2= *-0.46) is found between these two records suggesting that higher $\delta^{18}O$ values occur alongside lower % transmission values (more humified) and vice versa. A weak positive correlation is found between the stable oxygen isotope record and plant macrofossil record (r_s= 0.31) and a weak negative correlation is found with the testate amoeba based WTD reconstruction (r_s= -0.25). In KAR-EM-2, owing to the lack of variability of the stable oxygen isotope record in this profile this record does not reflect stratigraphic variability. There is also no correlation between this record and the humification values (r^2= -0.07); however, there is a positive correlation between this record and the plant macrofossil record (r_s= *0.43) with higher $\delta^{18}O$ values generally occurring alongside higher DHI values. A weak negative correlation is found between the stable oxygen isotope record and the WTD reconstruction (r_s= -0.23) owing to the insensitivity of both records. In KAR-EM-1, lower $\delta^{18}O$ values generally occur in sections of less humified peat evidenced by the negative correlation between the stable oxygen isotope record and humification values (r^2= *-0.56). There is a positive correlation between this record and the plant

macrofossil record (r_s= 0.30) but a negative correlation is found between this record and the WTD reconstruction (r_s= *-0.49).

Three significant correlations are found in KAR-EM-1 as well as the highest positive mean correlation between the palaeoecological and $\delta^{13}C$ records and highest negative mean correlation between the palaeoecological and $\delta^{18}O$ records.

5.4.2 Comparison of palaeoecological and stable isotope records from SAN-EM-2

The stratigraphic description provided a preliminary overview of variability in this profile. The plant macrofossil record and humification values generally agree with the stratigraphic variability in this profile with higher DHI values and lower % light transmission values in more humified sections (SJMa and SJMd) and vice versa. However, lower than expected % light transmission values are found towards the end of zone SJMb suggesting a prolonged humified section (85-25 cm) which was not visibly apparent in the stratigraphy. The plant macrofossil record does not shift to higher DHI values until ~60 cm. The WTD reconstruction does not reflect stratigraphic variability in this profile and similar to the KAR-EM profiles a WTD increase results from the shift in dominance of *D.pulex* to *A.muscorum* seemingly unrelated to stratigraphic shifts. This record, therefore, is not in agreement with the plant macrofossil record or humification values.

More negative $\delta^{13}C$ values are generally found in the more humified sections (SJMa and SJMd); this is supported by the positive correlation between the stable carbon isotope record and humification values (r^2= *0.48). More negative $\delta^{13}C$ values occur alongside higher DHI values; however, there is almost no correlation between the stable carbon isotope record and the plant macrofossil record (r_s= -0.11). The positive correlation found between the stable carbon isotope record and the WTD reconstruction (r_s= *0.43) suggests that higher WTD values occur alongside (higher) less negative $\delta^{13}C$ values; despite this there is not visual similarity between these records.

The lack of a general trend in the stable oxygen isotope record makes comparison with the other records difficult. It does not reflect stratigraphic variability, there is no

correlation with the plant macrofossil record (r_s= -0.05) and weak negative correlations with the humification record (r^2= -0.30) and WTD reconstruction (r_s= -0.22).

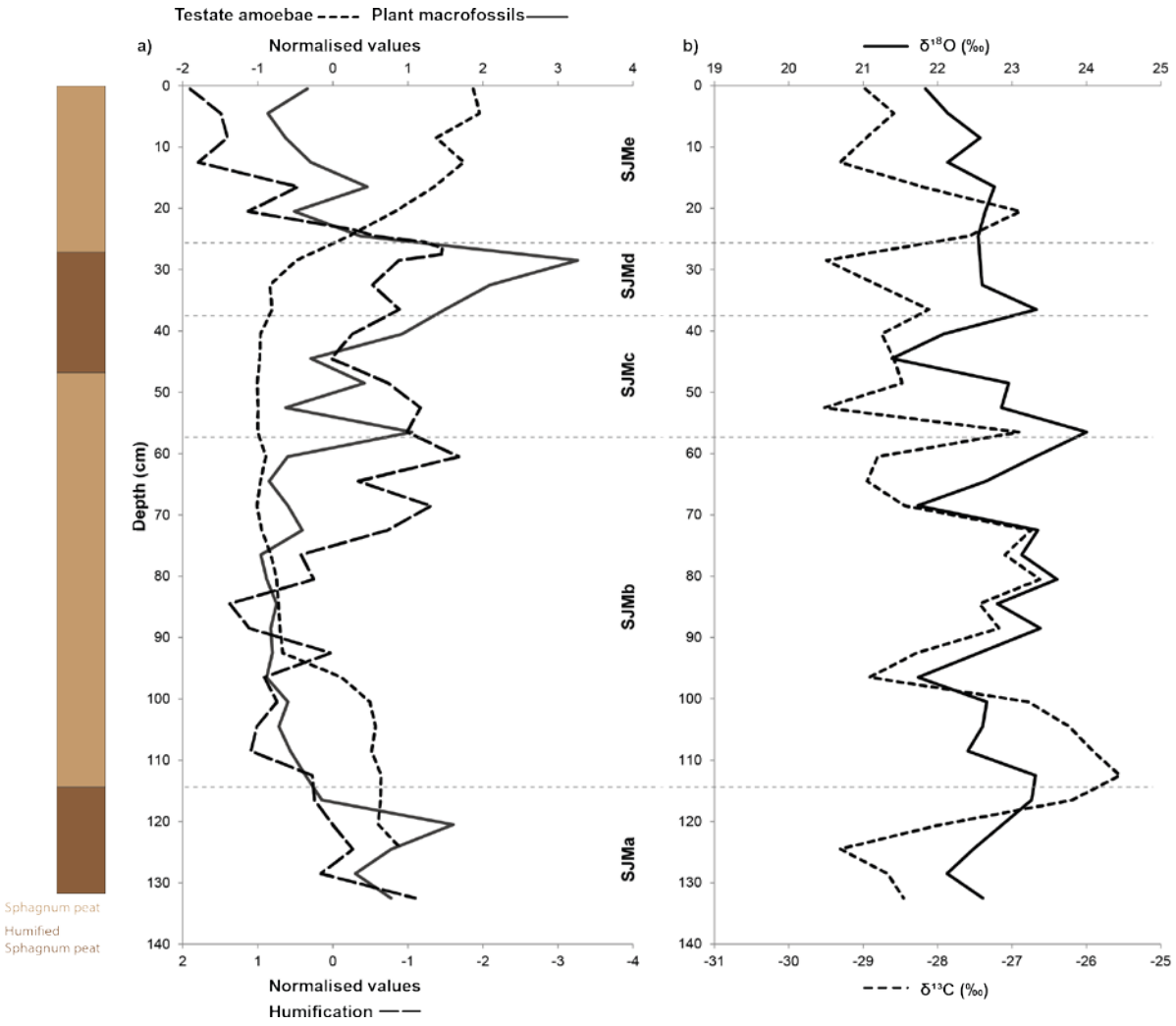

Figure 5.50. Comparison of the SAN-EM-2 palaeoecological records (a) and stable isotope records (b).

Table 5.28. Correlation between the palaeoecological and stable isotope records from SAN-EM-2 plotted against depth (α=0.05).

DHI record vs. $\delta^{13}C$ (r_s)	WTD reconstruction vs. $\delta^{13}C$ (r_s)	Humification values vs. $\delta^{13}C$ (r^2)	DHI record vs. $\delta^{18}O$ (r_s)	WTD reconstruction vs. $\delta^{18}O$ (r_s)	Humification values vs. $\delta^{18}O$ (r^2)
-0.106	*0.428	*0.484	-0.048	-0.219	-0.298

5.4.3 Comparison of palaeoecological and stable isotope records from SCB-1

In the period of interest (above 80 cm) there is a more humified section before a switch to less humified *Sphagnum* peat at 60 cm. The plant macrofossil record reflects this with higher DHI values in the more humified section and lower DHI values above this. The WTD reconstruction also reflects this shift at 60 cm. In the section of uniform stratigraphy and uniform DHI values there is a shift to higher WTD values reflecting the shift in dominance of different taxa in this record.

Less negative $\delta^{13}C$ values are found in the humified section (SCMb) and there is a shift to more negative $\delta^{13}C$ values just above 30 cm which is not found in the other proxy records. There is, therefore, almost no correlation between the stable carbon isotope record and the plant macrofossil record (r_s= 0.11) and WTD reconstruction (r^2= 0.11).

Similarly, the stable oxygen isotope record does not reflect stratigraphic variability and there is almost no correlation between this record and the plant macrofossil record (r^2= -0.14). There is however, a positive correlation between the stable oxygen isotope record and the WTD reconstruction (r^2= 0.43) which suggests that higher WTD values occur alongside higher $\delta^{18}O$ values. The stable oxygen isotope record is relatively insensitive compared with variability in the WTD reconstruction.

This chapter aimed to present the raw data from all profiles in this investigation to form the basis for subsequent chapters in which the records will be plotted against the time scales presented in chapter 4. The following chapter aims to explore further the multi-proxy and multi-profile discussion based on the intra-site comparison of the KAR-EM profiles throughout this chapter based on actual and relative depth. Chapter 7 will focus on the inter-site comparison and will consider the results from the KAR-EM profiles as well as the SAN-EM-2 and SCB-1 results (Section 5.2 and 5.3).

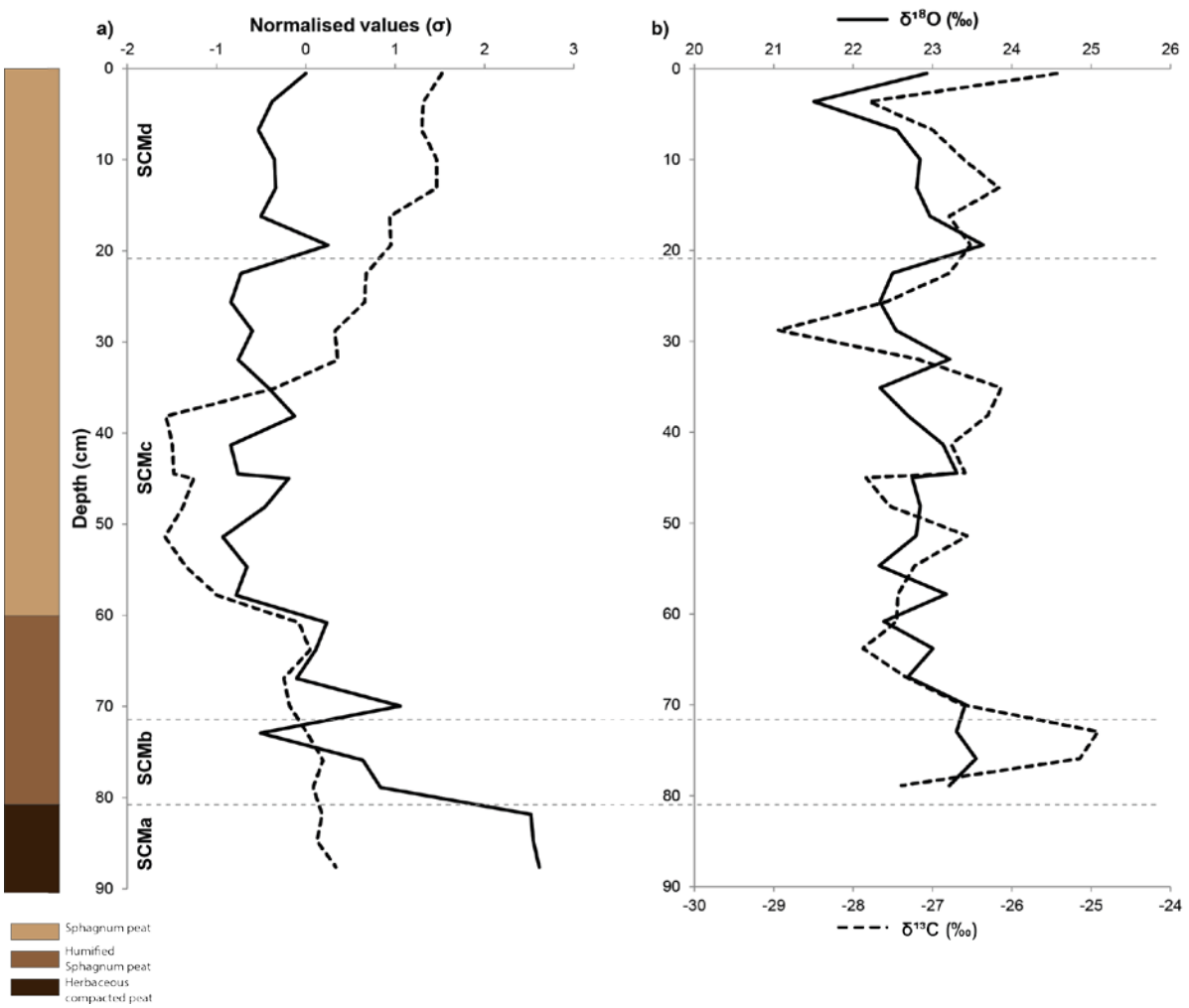

Figure 5.51. Comparison of the SCB-1 palaeoecological records (a) and stable isotope records (b).

Table 5.29. Correlation between the palaeoecological and stable isotope records from SCB-1 plotted against depth (α=0.05).

DHI record vs. $\delta^{13}C$ (r_s)	WTD reconstruction vs. $\delta^{13}C$ (r^2)	DHI record vs. $\delta^{18}O$ (r_s)	WTD reconstruction vs. $\delta^{18}O$ (r^2)
0.107	0.115	0.249	-0.137

Chapter 6: Discussion I
Intra-site comparison of multi-proxy records

This chapter focuses on answering **Research Question 1: To what extent are there correlations between multiple proxies and multiple profiles from an ombrotrophic bog, Karukinka, in southernmost Chile?** Coherence between proxies and profiles in the context of late-Holocene and recent climatic variability will be assessed. Intra-site replicability will be tested in order to assign an allogenic driver of variability and offer support for the use of SSA peatlands as reliable palaeoclimate archives. The first section focuses on the interpretation of the proxy records from Karukinka according to existing theory and presents the results plotted against age. An intra-site comparison of records is then presented in section 6.2 based on initial interpretation. An alternative approach to intra-site comparison is presented in section 6.4 owing to problems with microscale processes and chronological uncertainty. The final section (6.5) provides an overall multi-proxy intra-site comparison which forms the basis for the regional comparison in Chapter 7.

6.1 Interpretation of proxy records: Karukinka

6.1.1 Stratigraphic description and humification values

Early work (Von Post and Sernander, 1910; Osvald, 1923) proposed that switches in the peat stratigraphy were due to ontological development; however, this was falsified with such changes instead linked to climate variability (Barber, 1981). Switches between *Sphagnum* peat and humified *Sphagnum* peat were evident throughout the KAR-EM profiles with a clear acrotelm-catotelm boundary in each profile, above which undecomposed *Sphagnum* remains were visible. When plotted against age (Figure 6.1) this acrotelm zone extends from AD 1251(+144/-164years)-2013 in KAR-EM-3, AD 1929(±6years)-2013 in KAR-EM-2 and AD 1975 (±5years)-2013 in KAR-EM-1.

Section 5.1.2.2 explored options to compare the profiles based on depth. In figure 5.2b similar stratigraphic units were tied. This followed the assumption of the simultaneous deposition of distinct layers in peat profiles. The alignment of such

layers across multiple cores is common (Dachnowski, 1921; Barber *et al.*, 2000; Charman *et al.*, 2006; Blundell *et al.*, 2008; Swindles *et al.*, 2010); however, differential processes of accumulation and decomposition across the microtopography question this process of alignment (Blaauw, 2012). As an example, the Grenzhorizont, an assumed synchronous shift in peat type in European bogs, was found to be chronologically asynchronous (van den Bogaard *et al.*, 2002).

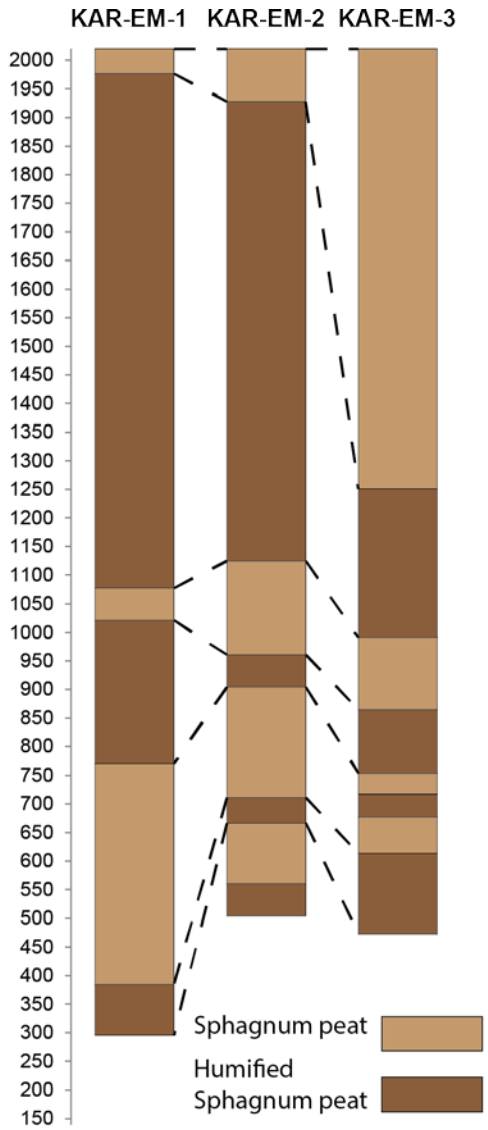

Figure 6.1. Comparison of stratigraphic changes (between Sphagnum and humified Sphagnum peat) across KAR-EM-1, KAR-EM-2 and KAR-EM-3 plotted against age.

As figure 6.1 shows, plotted against age, the stratigraphic changes are not synchronous across the profiles. The acrotelm zones are similar in KAR-EM-1 and KAR-EM-2 but this zone extends to AD 1250 in KAR-EM-3 whereas in KAR-EM-1 and KAR-EM-2 there are sections of more humified peat down to this level (~AD 1100-1950). The differences in stratigraphic variability between the profiles seem to be evidence of differential peat processes and sensitivities across the microtopography.

The degree of peat decomposition was investigated using humification analysis and the results were found to reflect the stratigraphic changes (figure 6.1). Varying peat decomposition is driven by WTD variability with the thickness of the acrotelm zone decreasing with higher water table thus exposing material in this zone to less aerobic decay before incorporation into the underlying catotelm. During periods of lowered water tables the acrotelm is exposed to more aerobic decay and material is more decomposed when incorporated into the catotelm (Borgmark and Schoning, 2006). This would suggest that the level of humification just below the acrotelm-catotelm boundary in these profiles reflects recent conditions (Blackford and Chambers, 1993; Chambers *et al.*, 2012). Decay is incomplete in the acrotelm which usually makes interpretation of proxy records from this zone difficult relative to records from the underlying catotelm which is more easily chronologically resolved (Charman *et al.*, 2015).

Based on the interpretation of humification records from the Northern Hemisphere (e.g. Charman *et al.*, 1999; Mauquoy and Barber, 1999a; Roland *et al.*, 2015) and Southern Hemisphere (e.g. Chambers *et al.*, 2014), low % light transmission values are related to more humified peat in drier periods and high % light transmission values are related to less humified peat in relatively wetter periods. Figure 6.2 shows the normalised and detrended humification values plotted against the individual age profiles; note that the axes have been reversed with this interpretation in mind. Climatic inferences are displayed and are considered further in comparison with the other proxies throughout this chapter.

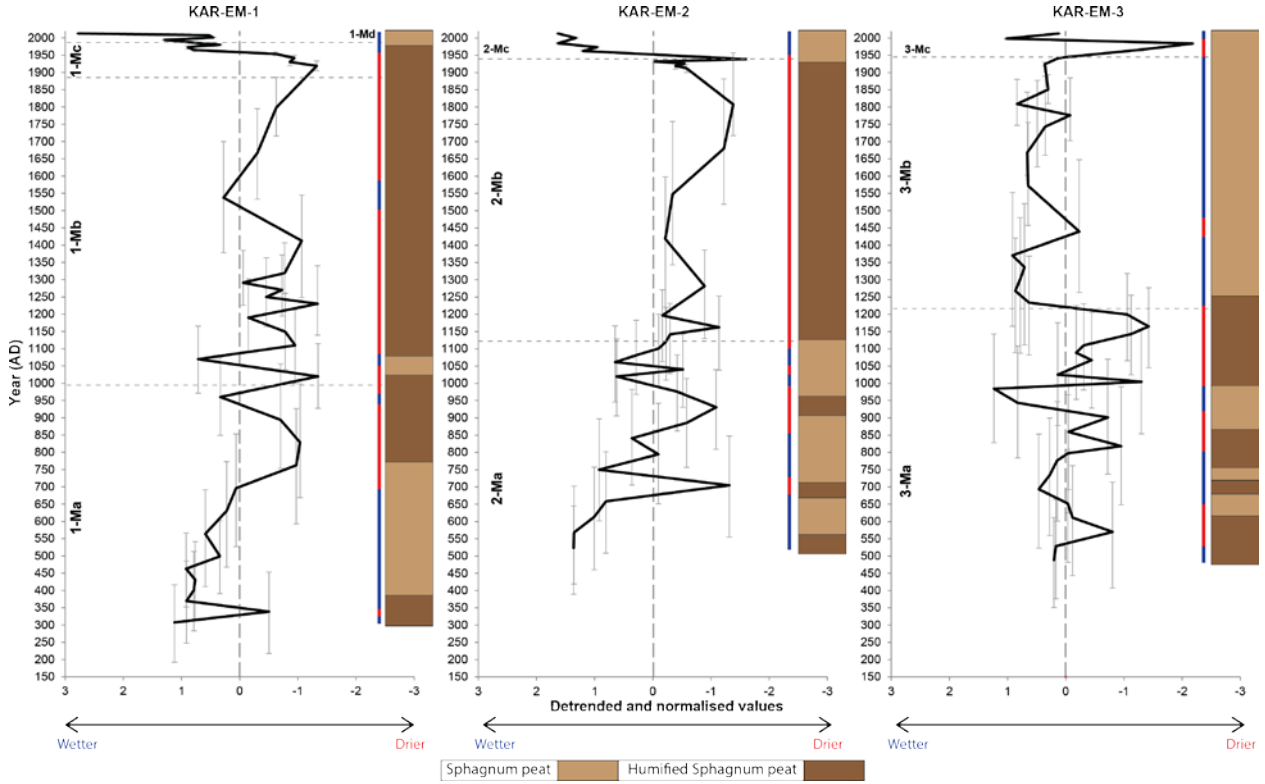

Figure 6.2. Detrended and normalised humification records from KAR-EM-1, KAR-EM-2 and KAR-EM-3 plotted against age. Stratigraphic profiles are shown alongside the graphs and the plant macrofossil zones are displayed. The chronological error is displayed by the vertical grey bars (95% confidence intervals). The horizontal axes are reversed based on the interpretation of this proxy from higher (higher % light transmission (wetter)) to lower (lower % light transmission (drier)) values. Climatic inferences based on deviation from the mean are displayed.

The humification values plotted against age do not appear to be showing consistent synchronous variability. In the acrotelm zones of KAR-EM-1 and KAR-EM-2 values are similarly high. Below this zone, low values extend to AD 1100 in both of these profiles, whereas throughout these sections in KAR-EM-3 values are high; this would indicate that conditions were drier between 1100- AD 1950 in KAR-EM-1 and KAR-EM-2 but wetter in KAR-EM-3. The shift to wetter conditions in KAR-EM-3 between AD 900-1000 may be synchronous within chronological error with a similar shift in KAR-EM-2 between AD 937-1116 and less obviously in KAR-EM-1 between AD 1000-1100.

There is generally good agreement between the humification values and the plant macrofossil records (Section 5.4.1), suggesting that the humification values may be reflecting the differential decay rates of different species (Clymo and Hayward, 1982; Rochefort *et al.*, 1990; Yeloff and Mauquoy, 2006). Hughes *et al.* (2012) recommend the use of k-values of modern plant material to correct for such species effects. Correction is not necessary here in consideration of the dominance of *S.magellanicum* in these records suggesting a uniform and species-specific decay rate (Johnson *et al.*, 1990; Johnson and Damman, 1991). The shift to lower values just below the surface in KAR-EM-3 appears to be related to the presence of roots of surface vegetation.

A species-specific record of peat humification from SSA of the last 3000 years finds evidence for a relatively dry LIA period inferred from lower % light transmission values at AD 1460 and AD 1675-1770 (Chambers *et al.*, 2014). The magnitude of variability cannot be inferred from peat humification values, owing to its semi-quantitative nature; however, Chambers *et al.* (2014) suggest that light transmission values >40% are indicative of a generally wet site and values <40% evidence dry episodes. The dry episodes of the LIA as found by Chambers *et al.* (2014) are not clearly evident in the KAR-EM humification records. This interpretation suggests that all three profile locations are wetter sites with mean values between 38 and 50% light transmission. This semi-quantitative dataset can inform on peatland functioning and forms the basis for interpretation of the other proxies.

6.1.2 Plant macrofossil records

The dominance of *S.magellanicum* in peat profiles throughout the late-Holocene is common in Patagonian peatlands (Mauquoy *et al.*, 2004; Chambers *et al.*, 2007; De Vleeschouwer *et al.*, 2014; van Bellen *et al.*, 2016) and was observed in the KAR-EM plant macrofossil records.

Such records may display climatic insensitivity in comparison with records which display high variability in *Sphagnum* species assemblage over longer time periods (Barber, 1981; Sillasoo *et al.*, 2007; Swindles *et al.*, 2007). Diverse and variable species assemblages also allow better application of statistical methods in the conversion of plant macrofossil data to a single line of BSW (Blundell and Barber, 2005; Hughes *et al.*, 2006; Daley and Barber, 2012).

The dominance of *S.magellanicum* in peat records from the region is interpreted as representing predominantly wet conditions. Periods of reduced *S.magellanicum* are interpreted as drier periods; for example, a period in which Ericaceae roots dominate is interpreted as a shift to drier climate conditions between 2820 and 2744 cal BP (Chambers *et al.*, 2007) and that between AD 1675 and 1770 (Chambers *et al.*, 2014).This species is typical of wet raised bog sites (Daniels and Eddy, 1990). Similarly, a PCA on plant macrofossil data from the same site suggests that Ericaceae roots are indicative of drier conditions and *S.magellanicum* is at the opposite end of a wetness gradient (Mauquoy *et al.*, 2004) and as such periods of low PCA axis-one scores (AD 890-950, 1030-1100 and 1830-1930) are suggested to represent wetter periods whereas higher PCA axis-one scores (AD 960-1020, 1575-1625, 1740-1830 and 1940-1950) represent dry periods. A similar gradient is evident from the axis-one scores of the PCA of the KAR-EM plant macrofossil records (figure 5.7) with low axis-one values occurring simultaneously to low DHI values and vice versa. van Bellen *et al.* (2016) from another site in the region found a similar dominance of *S.magellanicum* throughout the record apart from a period of dominance of *S.fimbriatum* between 1620 and 1370 cal BP suggesting drier conditions during this period. Loisel and Yu (2013) interpret the dominance of *S.magellanicum* to represent drier periods, whereas periods during which monocots and UOM dominate are assumed to represent wetter conditions. This interpretation

is based on the spatial separation of this vegetation across the modern microtopography and suggests that switches between the dominance and absence of *S.magellanicum* may represent shifts between drier and wetter conditions respectively.

There is no evidence for pool layers in the plant macrofossil records which would support the cyclic regeneration theory; for example, shifting to wet indicator species such as *S.falcatulum* evident in the region (Baumann, 2006). An autogenic signal may also be present in plant macrofossil records during long-term peatland development evidenced by successional vegetation (e.g. fen, raised bog vegetation) (McMullen *et al.*, 2004). The dominance of *S.magellanicum* in all profiles suggests persistence of a hummock microform and ombrotrophic conditions throughout the records.

Figure 6.3 displays the DHI values plotted against the original age profiles. In KAR-EM-3, wet conditions are inferred from the dominance of *S.magellanicum* in the periods AD 600 to 800 and AD 850 to 995. There are assumed dry shifts when the dominance of *S.magellanicum* is replaced with varying levels of Ericaceae and monocot roots and UOM, summarised into the following periods; AD 500-600, AD 800-850 and AD 995-1216. This latter period is punctuated by two short wetter periods AD 1015-1045 and AD 1090-1130. *S.magellanicum* is then dominant from AD 1216 until the surface.

In KAR-EM-2, the dominance of *S.magellanicum* similarly indicates predominantly wet conditions in this profile. These periods occur at AD 500-650, AD 750-890, AD 975-1100, AD 1160-1400 and AD 1650-1800. The wet periods are interspersed by relatively drier conditions AD 650-750 and AD 890-975 when UOM and roots replace *S.magellanicum*, AD 1100-1160 when Ericaceae roots dominate, AD 1400-1650 when monocot roots and UOM dominate and AD 1800-1942 when Ericaceae roots and UOM dominate. *S.magellanicum* dominates, after AD 1942 and after the acrotelm-catotelm boundary, until the surface. Higher apparent climatic sensitivity according to Barber's phasic theory is evident in this location.

In KAR-EM-1, wet periods dominated by *S.magellanicum* occur AD 400-850, AD 1025-1075 and AD 1150-1800. Dry periods occur AD 300-400 during which monocot roots dominate alongside *S.magellanicum*, AD 850-1025 when monocot roots and UOM dominate, AD 1075-1150 and AD 1800-1986 when monocot and Ericaceae roots and UOM dominate. *S.magellanicum* returns to dominance after AD 1986.

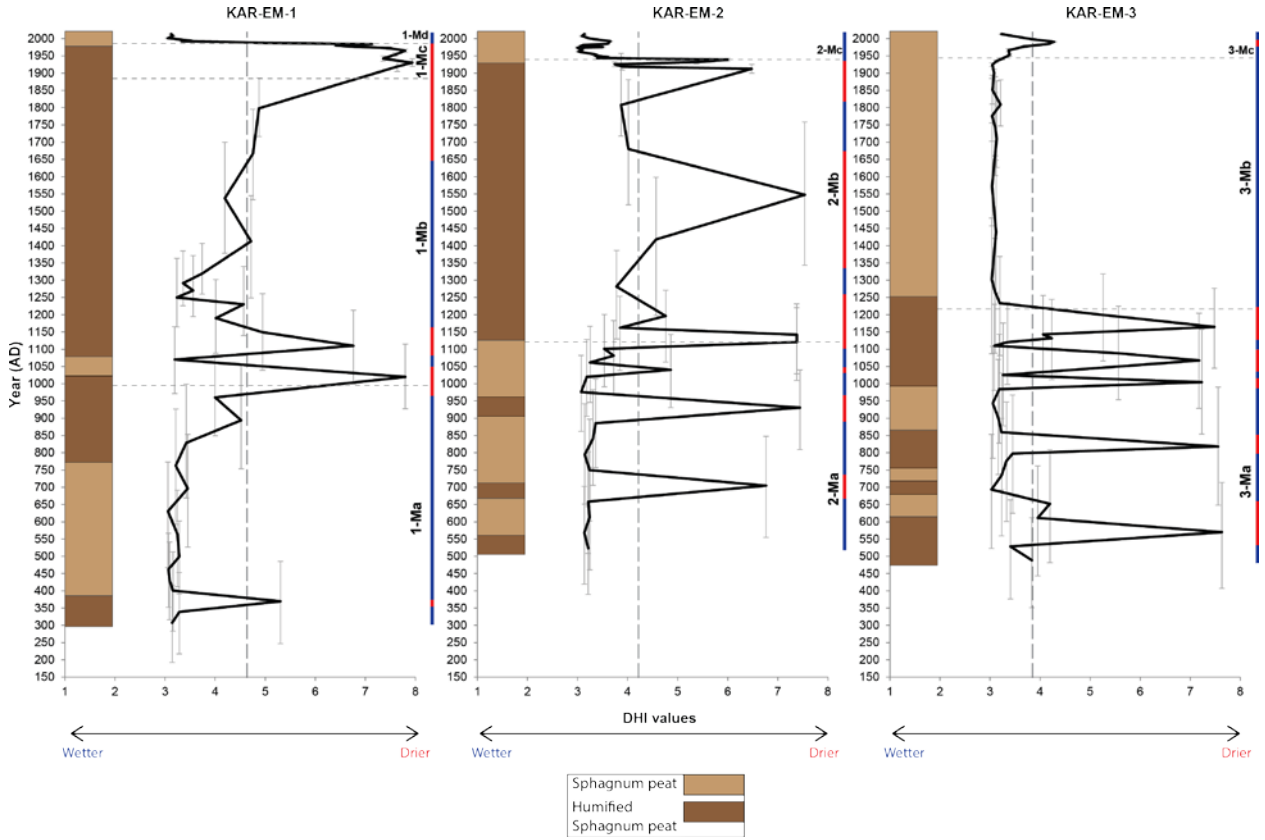

Figure 6.3. The DHI values from KAR-EM-1, KAR-EM-2 and KAR-EM-3 plotted against age. Stratigraphic profiles are shown alongside the graphs and the plant macrofossil zones are displayed. The chronological error is displayed by the vertical grey bars (95% confidence intervals). Climatic inferences based on deviation from the mean are displayed.

The switching in all profiles between the dominance of *S.magellanicum* and its disappearance or absence is to be expected if the plant macrofossil record is responding to BSW variability and this depends on the tolerance of the plant macrofossil assemblage within a certain depth to the water table (Loisel and Garneau, 2010; Morris *et al.*, 2011b). However, this proxy may display a slow or insensitive response to BSW variability, resisting external variability, owing to physiological adaptation (Daniels and Eddy, 1990). There is evidence of the resistance of *S.magellanicum* to hydrological variability through phenotype changes, regulating evapotranspiration in periods of desiccation (Li *et al.*, 1992; Joosten, 1993; Schipperges and Rydin, 1998; Köpke, 2005). This species is also able to transport water from depth, which explains its position relative to the water table and its ability to survive in drier conditions (Schipperges and Rydin, 1998; Robroek *et al.*, 2009). *S.magellanicum* forms large compact hummocks in dry conditions, which improves capillarity and prevents desiccation (Grosvenier *et al.*, 1997; Li *et al.*, 1992). Growth only occurs in the capitula of the Sphagnum where light and water availability lead to photosynthesis at the surface; therefore, capillary action does not lead to additional growth but only prevents desiccation of already formed capitula.

DHI values were found to correlate better with humification and testate amoeba records from northwestern European bogs as opposed to DCA and Nmds (Daley and Barber, 2012) and the method has been successfully used in the region. *S.magellanicum* is a wet lawn species in Northern Hemisphere bogs and is assigned a DHI value of 3 (Daley and Barber, 2012). Shifts to lower DHI values are thus assumed to represent wetter BSW conditions. However, in consideration of the dominance of this species across the microtopography (Baumann, 2006; this investigation), it displays a wide habitat tolerance via morphological differences (Daniels and Eddy, 1990; Atherton *et al.*, 2010). Therefore, this method should be applied with caution in the Southern Hemisphere. Accordingly, altering the DHI value to reflect more intermediate conditions (5) changes the apparent magnitude of variability although the non-linearity of the plant macrofossil response limits inferences on magnitudinal variability.

Switches in the plant macrofossil assemblage are inherently related to changes in the stratigraphy and thus reflect such variability. As a result, synchronous variability

in the plant macrofossil records across the profiles is not evident. Differing processes across the microtopography and lack of replicability even at the micro scale presents a problem for reconstructing climate variability (Charman *et al.*, 1999). Differences between the three profiles may be due to 'small scale patch dynamics in the bog surface vegetation' (Barber *et al.*, 1998); however, switching between the dominance and reduction of *S.magellanicum* is evident in all three profiles despite differences in the apparent timing of shifts. The mean DHI values evidence this overall difference increasing from KAR-EM-3 to KAR-EM-1 (KAR-EM-3:3.90, KAR-EM-2:4.08, KAR-EM-1:4.64) suggesting wetter to drier conditions along the microtopographic gradient. This increase reflects the higher overall abundance of *S.magellanicum* in KAR-EM-3 and as discussed above does not necessarily indicate wetter conditions.

Neither the plant macrofossil nor humification records are able to inform on the magnitude of hydroclimatic changes owing to potential insensitivity of these records, as discussed. The remaining proxies may be able to indicate magnitudinal variability but are inherently related to the plant macrofossil and humification records with regards to peat accumulation, decomposition and vegetation assemblage. The plant macrofossil and humification records provide the context for the testate amoeba and stable isotope records, which will be discussed in subsequent sections.

6.1.3 Testate amoeba records

The use of a new testate amoeba transfer function (van Bellen *et al.*, 2014) has attempted to provide a record of WTD (water table depth from the surface) variability (Figure 6.4). The summer moisture deficit (Charman, 2007; Charman *et al.*, 2009) is assumed to be the driver of hydrological variability as reconstructed by variability in testate amoeba assemblages over time. However, the relationship between climate and bog hydrology in Patagonian peatlands may differ from the Northern Hemisphere peatlands on which the summer moisture deficit theory is based (Loisel and Yu, 2013) in that precipitation may be evenly distributed throughout the year (also see section 2.3.7).

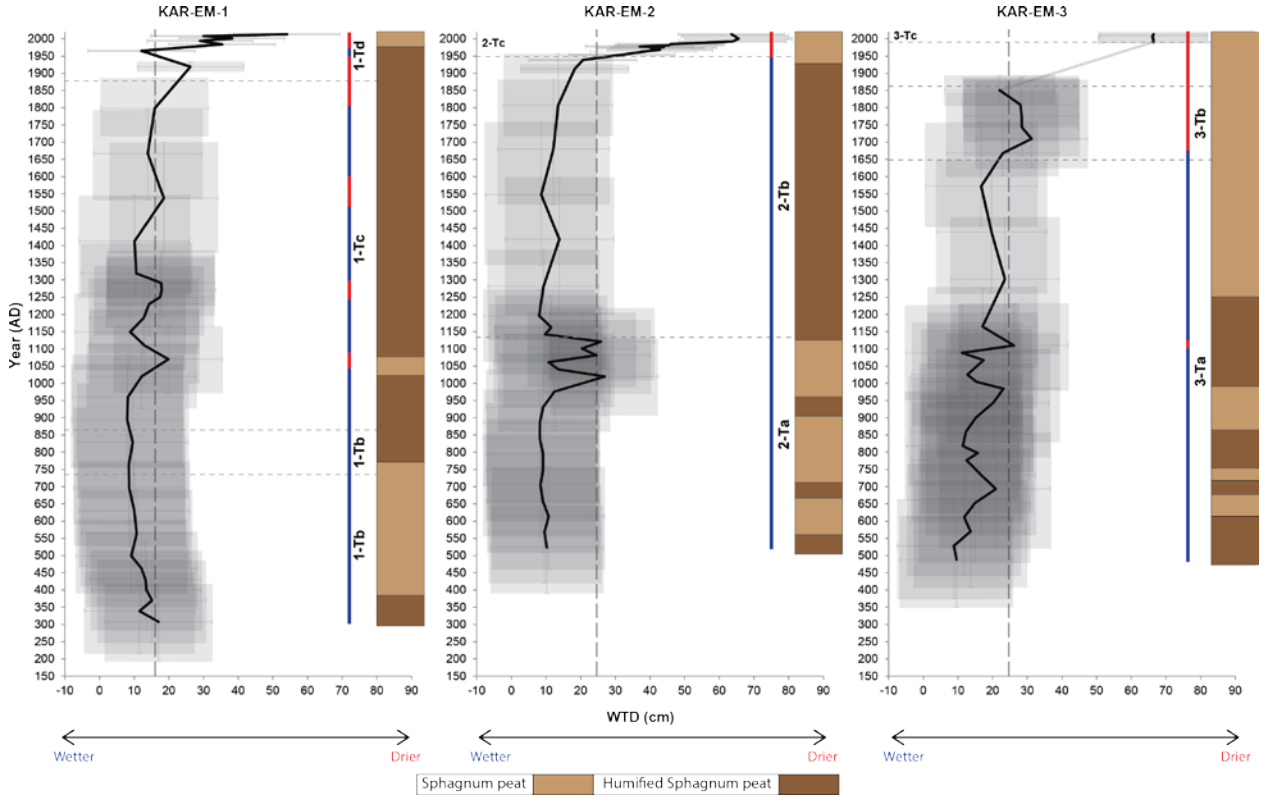

Figure 6.4. The WTD reconstructions from KAR-EM-1, KAR-EM-2 and KAR-EM-3 plotted against age. Stratigraphic profiles are shown alongside the graphs and the testate amoeba zones are displayed. The chronological error (95% confidence intervals) and reconstruction error are displayed by grey shaded areas. WTD is depth to water table with drier conditions inferred from higher WTD and wetter conditions inferred from lower WTD.

In KAR-EM-3, the WTD reconstruction is ~15 cm until AD 1093 and dominated by *D.pulex*, apart from three peaks to higher WTD at AD 694 (20 cm) and AD 984 (23 cm) where *D.pristis type* increases and AD 1109 (26 cm) where *D.pristis type* and *H.petricola* increase. The WTD is ~20 cm until AD 1652 and is higher ~30 cm until AD 1858. Above this, testate amoebae are absent until AD 1990 after which the dominance of *A.muscorum* results in WTD of 66 cm until the surface.

There is evidence of vertical zonation of testate amoebae in this profile related to different environmental factors such as light, temperature and water and oxygen availability (Booth, 2002; Mitchell and Gilbert, 2004). A lack of materials for test construction may also be a limiting factor. The absence of testate amoebae may be explained by the lack of suitable conditions in the zone between AD 1858 and 1990 (48-13 cm) in KAR-EM-3, perhaps a period of particularly dry conditions. *D.pristis type* dominates in the preceding zone suggesting higher WTD and there is a rise to dominance of *D.pulex* which appears to decrease WTD just before AD 1858. In the other profiles between AD 1850 and 1990 *D.pulex* dominates with lower WTD. *D.pulex* may too have been dominant in KAR-EM-3 during this period. Potential outgrowth of the hummock from the WTD may have led to more aerobic decay in the acrotelm zone resulting in a lack of test preservation. For example, *D.pulex* has been found to be one of the less robust tests (Swindles and Roe, 2007) potentially resulting in the absence of testate amoebae in this zone.

In KAR-EM-2, the WTD reconstruction is ~10 cm owing to dominance of *D.pulex* until AD 950 after which there are two peaks to higher WTD (~26 cm) at AD 1020 and AD 1101 where *H.petricola* increases. WTD is ~10 cm throughout zone 2-Tb increasing to ~21 cm just before the boundary to 2-Tc at AD 1949. Above this *A.muscorum* increases throughout zone 2-Tc and WTD increases to 64 cm at the surface.

In KAR-EM-1, the WTD reconstruction is ~9 cm through 1-Ta and 1-Tb until AD 950 after which at the beginning of 1-Tc there are 2 peaks to higher WTD at AD 1070 (~19 cm) where there is an increase of *H.petricola* and AD 1270 (~17 cm) where *D.pulex* decreases causing an increase in WTD. WTD remains at ~10 cm throughout 1-Tc until 1798, an increase occurs through the zone boundary to 1-Tc to ~26 cm at

AD 1919 owing to an increase of *E.tuberculata* and *H.petricola*, returning to ~10 cm at AD 1965 and increasing above this through 1-Td to ~54 cm at the surface.

The low taxonomic diversity and broad WTD tolerances of dominant taxa may have resulted in apparent climatic complacency in these records (Charman *et al.*, 2007). Indicator species may instead be used to make inferences about conditions. Some taxa are not included in the training data set despite their abundance at some levels in the records; for example, *T.arcula* and *Schwabia* sp. The presence of *T.arcula* is an indication of drier conditions (Booth, 2008); however, owing to its exclusion from the transfer function it does not affect the WTD reconstruction despite potentially lower WTD inferred from its presence at ~AD 570 in KAR-EM-3 and KAR-EM-2 and at ~AD 950 in KAR-EM-2 and KAR-EM-1. Other indicator species include *H.petricola,* which is found in hummock locations (Heal, 1962; 1964) potentially explaining the dry shifts where this taxon increases.

The dominance of *D.pulex* and *D.pristis type* is representative of stable water table levels and both dominate throughout the records in van Bellen *et al.* (2016). This dominance of *D.pulex* for long periods has been found in other studies (Hendon *et al.*, 2001; Langdon *et al.*, 2003; Blundell and Barber, 2005; Langdon and Barber, 2005; van Bellen *et al.*, 2016). Problems have arisen owing to the poor modern analogue status of this taxon (Booth, 2008; Amesbury *et al.*, 2013) assuming an intermediate-wet position on the water table depth gradient. This opposes other interpretations where it occupies an intermediate-dry position (Charman *et al.*, 2000; Booth 2008; Amesbury *et al* 2012; Lamarre *et al.*, 2013) and a very dry position (Turner *et al.*, 2013). Charman *et al.* (2007) suggest it indicates conditions with high water tables but low surface moisture. The dominance in this investigation could be due to the persistence of hummock vegetation throughout the record. Sullivan and Booth (2011) suggest that this species quickly responds to short-term fluctuations, indicating that when it is dominant highly variable environmental conditions may have occurred. Despite the lack of modern analogues in other studies this species was included in the van Bellen *et al.* (2014) training set and was found at the wet end of the gradient (21 cm) with a wide tolerance of 22 cm.

Ordinations of the training data set for the van Bellen *et al.* (2014) transfer function showed that species distribution along the principal axis was significantly related to WTD, explaining 15% of variability in the assemblage. Such percentages are usual in Northern Hemisphere transfer functions (Charman *et al.*, 2007; Amesbury *et al.*, 2013; Lamarre *et al.*, 2013). However, the transfer function has high predictive error with higher root mean square error of prediction values (14.01 cm vs 6-8 cm) than other WTD transfer functions due to the wide WTD range in the training set. Despite this, it is a regionally specific transfer function and includes rare taxa of testate amoebae that do not occur in the existing transfer functions from other regions (e.g. *Alocodera cockayni, Certesella certesi, Trigonopyxis microstoma*).

A recent assessment of how well testate amoeba transfer functions reconstruct water-table depths in peatlands was carried out on European bogs (Swindles *et al.*, 2015). Water table depths were measured over a prolonged period and compared with testate amoeba assemblages from the surface and European transfer functions were applied to these surface assemblages in order to reconstruct water table depths. From these bogs testate amoeba assemblages could not be used to reconstruct mean water tables accurately which brings into question the use of transfer functions to reconstruct the magnitude of hydrological variability over time. Given the outcomes of such studies and the wide associated errors with the WTD reconstruction in this investigation, the directional changes rather than magnitude changes may be most informative. Similarity in the direction of variability was evident in the DCA and PCA of the KAR-EM testate amoeba records (Figure 5.17) although a hydrological gradient was not clearly present in any of the ordinations. WTD is thus better represented via use of the transfer function based on the observed relationship between testate amoeba assemblages with WTD.

The PalaeoSig package in R was used to test the statistical significance of the WTD reconstructions in three testate amoeba records from peatlands in Tierra del Fuego (van Bellen *et al.*, 2016). In the only significant record (TiA12), wetter conditions are evident between AD 550 and 1050 owing to the presence of hygrophilous taxa in this period. In the testate amoeba record from Karukinka; however, significant variance in the testate assemblages could not be explained by the water depth reconstruction. Weak transfer function performance challenges the ability of the van Bellen *et al.*

(2014) transfer function to reconstruct water table depth variability reliably from this site. The lack of statistical significance and ±15 cm error in their investigation suggests that WTD variability of 5 to 10 cm may not reflect real changes but variability above 10 cm may be more reliable. This suggests that the same may be true in this investigation with ±16 cm error. The majority of variability in the records rarely exceeds 10 cm even in the zone of variability between AD 1000 and 1150.

Towards the surface the WTD increase far exceeds 10 cm suggesting recent drier conditions. Mauquoy *et al.* (2004) interpret higher levels of *A.muscorum* as an indication of low water table levels and drier conditions. Multiple studies suggest a dry optimum of this taxon (Booth, 2008; Amesbury *et al.*, 2013; Lamarre *et al.*, 2013). van Bellen *et al.* (2016) also find the recent dry shift in all three records; however, the chronological uncertainty around this period is high. In the KAR-EM WTD reconstructions there is a shift to higher percentage abundance of *A.muscorum* an assumed dry shift in all records, which is well chronologically constrained, occurring after AD 1990.

This recent drying may be related either directly or indirectly to Antarctic stratospheric ozone depletion since the 1970s/80s (See Appendix IV). Testate amoebae have been claimed to become more abundant as a result of the direct effect of UV-B and increased leaching of nutrients from leaf cells (Searles *et al.* 1999; Robson *et al.*, 2005). Numbers of *A.muscorum* were found to decrease by ~50% under reduced UV-B suggesting that the increased UV-B intensity may have increased relative numbers of this species towards the surface (Robson *et al.*, 2005). Increased test concentration is then expected in the KAR-EM records towards the surface; however, such increases are not evident (Figures 5.12-5.14) suggesting that relatively higher test concentration is not contributing to the dry shift. The increase in *A.muscorum* may be due to the ability of this taxon to withstand relatively higher UV-B. This would result in an exaggeration of the surface drying; however, van Bellen *et al.* (2016) reduced the number of *A.muscorum* in near-surface samples and applied the transfer function with the effect on the resulting WTD reconstruction still significant towards the surface. The indirect effects of stratospheric ozone depletion on the testate amoeba assemblages may be more significant than the effects of increased UV-B. The increase of *A.muscorum* may have resulted from higher WTD

due to reduced precipitation and warmer conditions at this site in recent decades. Comparison with instrumental data alongside the other proxies in this investigation will allow further assessment of the reliability of the WTD reconstructions in consideration of long-term and more recent variability.

6.1.4 Stable carbon isotope records

The stable carbon and oxygen isotope records plotted against the original age profiles are displayed in figure 6.5. The absence of *Sphagnum* at some levels, owing to potentially drier conditions, prevented stable isotopic measurements at these depths (shown by purple crosses). Despite this, measurements were available at most depths where sufficient *S.magellanicum* enabled a species-specific cellulose isotopic analysis. Although it is suggested that stable isotope records offer an independent palaeoclimate record to palaeoecological records, in this investigation they are dependent on a potentially climatically complacent plant macrofossil record through the dominance of *S.magellanicum,* which may result in higher sensitivity of the stable isotope records (Loisel *et al.*, 2009).

The Suess correction was applied to all records (See section 3.4.2.4.4) and in each case a trend to more negative $\delta^{13}C$ values (especially in KAR-EM-3 and KAR-EM-1) towards the surface, initially thought to display a shift to drier conditions in recent decades, was removed. This correction may have overwritten a potentially negative trend not an artefact of the Suess effect but may have resulted from changing climate conditions or altered plant response (physiological) both related to increased CO_2 (McCarroll and Loader, 2004).

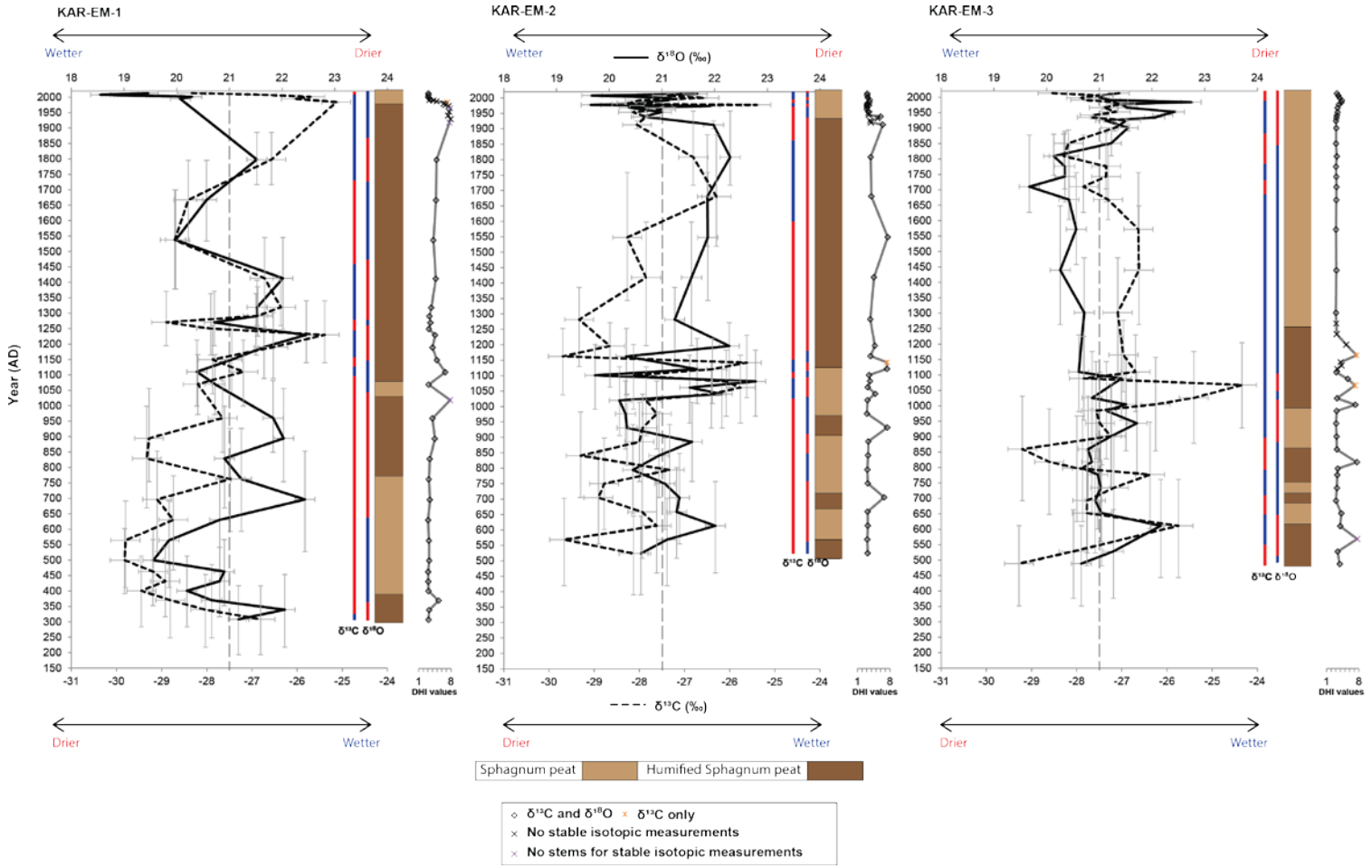

Figure 6.5. The stable carbon and oxygen isotope records from KAR-EM-1, KAR-EM-2 and KAR-EM-3 plotted against age. Stratigraphic profiles are shown alongside the graphs and the plant macrofossil zones are displayed. The chronological error (95% confidence intervals) and analytical error are displayed by the vertical grey bars. Climatic inferences based on deviation from the mean are displayed ($\delta^{13}C$ left hand bars, $\delta^{18}O$ right hand bars). The smaller graphs displayed next to the records are based on the DHI values and show where S.magellanicum was available for cellulose isotopic analysis.

The records have been interpreted based on the water film theory (Loisel *et al.*, 2009). Assuming that this is applicable at this site, less negative $\delta^{13}C$ values represent wetter periods with more negative $\delta^{13}C$ values representing drier periods. According to this interpretation the axis is usually reversed to agree with the interpretation of the direction of change of the other proxies. However, as explored in Section 5.1.4.5 reversal of this axis results in higher disagreement between the stable carbon and oxygen isotope records. Potentially wetter conditions may be evident in periods of more negative values (Nichols *et al.*, 2009; Kip *et al.*, 2012). Agreement between the stable carbon and oxygen isotope records may suggest that more negative $\delta^{13}C$ values are indicative of wetter conditions and vice versa.

Interpretation is based on the isotopic composition of differing species across the microtopography evidenced in earlier studies (e.g. Rice and Giles, 1996). The $\delta^{13}C$ values of *S.magellanicum* were found to correlate with WTD suggesting that in the absence of species differences the same relationship applied with less negative values in wetter locations and more negative values in drier locations (Loader *et al.*, 2016).

Decomposition processes may have influenced the $\delta^{13}C$ values with higher values found in the aerobic acrotelm and lower values found in the anaerobic catotelm (Lehmann *et al.*, 2002; Broder *et al.*, 2012). Such effects can be assessed based on comparison with the humification records; however, whether correlations between the two are based on climate variability or decomposition effects (higher humification, more negative $\delta^{13}C$ values and vice versa) can only be assessed by comparison with other proxies. Climatic inferences from the stable carbon isotope records are shown on figure 6.5 and are discussed further throughout the chapter.

6.1.5 Stable oxygen isotope records

As discussed in section 2.5.4.5, oxygen is incorporated into the *Sphagnum* cellulose from water on the bog surface. Variability in palaeoisotope records is assumed to follow differences in $\delta^{18}O$ values of *Sphagnum* cellulose evident across the modern microtopographic gradient in relation to the water table. Lower values (^{18}O depleted) are found in locations with low WTD and higher values (^{18}O enriched) are found in

drier microenvironments (Aravena and Warner, 1992; Tillman *et al.*, 2010) with values varying between 27±1‰ and 27±3‰ respectively (Zanazzi and Mora, 2005). These differences are based on species differences across such gradients. A similar investigation using a species-specific approach found values ranging from 19.65 to 24.90‰ across the microtopography but there was no clear relationship with WTD (Loader *et al.*, 2016). The records have been interpreted according to coherence between $\delta^{18}O$ values of precipitation (cellulose inferred) and BSW (Figure 2.23; Daley *et al.*, 2010; 2016) which also assumes that lower $\delta^{18}O$ values are indicative of negative BSW anomalies (wetter periods) and higher $\delta^{18}O$ values are indicative of positive BSW anomalies (drier periods).

This interpretation of the simple incorporation of source water into cellulose may be complicated by evidence of an evaporative signal (Price *et al.*, 2009; Royles *et al.*, 2016; Loader *et al.*, 2016). Coherence between the stable oxygen isotope records on an intra-site scale would suggest the absence of such evaporative effects. Interpretation of this proxy also requires consideration of the rainshadow effect on stable isotope records in SSA as discussed in section 2.3.7.1, which may complicate the isotope signal, potentially resulting in a different interpretation of this proxy to that in studies discussed from the Northern Hemisphere. The effect of SWW shifts on this proxy in consideration of the rainshadow effect is further discussed in section 7.3.5 (Chapter 7; Conceptual diagram Figure 7.12).

Similar to the stable carbon isotope analysis sufficient material is necessary for stable oxygen isotope analysis. With reference to figure 6.5 at some depths (purple crosses) *S.magellanicum* was not present and at others material was prioritised for stable carbon isotope analysis (orange crosses). As such, stable oxygen isotope measurements are not available at these depths. A species-specific cellulose isotopic analysis should offer a sensitive record of variability with all records displayed alongside the stable carbon isotope records in figure 6.5. Climatic inferences are displayed alongside the records for comparison with other proxies.

6.2 Intra-site proxy comparison

This section focuses on the intra-site comparison of each proxy before the final multi-proxy intra-site comparison. All records are displayed in figure 6.6 with summary

diagrams of climatic inferences presented alongside the records (discussed further in section 6.5). Tie points are displayed on the diagram and will be discussed throughout the chapter. Owing to the differences in the age of sampling points based on the individual age profiles, the proxy data have been grouped into 50- and 20-year bins to explore correlations between the profiles. These correlations are presented in table 6.1.

Table 6.1. Correlations between binned KAR-EM proxy data. Both 50- and 20-year bins are displayed. r^2 indicates where Pearson's correlation was carried out and r_s indicates where Spearman's rank was carried out. Significant correlations according to the critical values of each method are highlighted (α=0.05). The mean correlations are shown to summarise highest agreement between records.

		KAR-EM-3 vs. KAR-EM-2	**KAR-EM-3 vs. KAR-EM-1**	**KAR-EM-2 vs. KAR-EM-1**	**Mean correlation**		**KAR-EM-3 vs. KAR-EM-2**	**KAR-EM-3 vs. KAR-EM-1**	**KAR-EM-2 vs. KAR-EM-1**	**Mean correlation**
	Original chronology					**Plotted against KAR-EM-2 chronology**				
Humification	50-year bins (r^2)	-0.352	-0.174	0.236	**-0.025**	50-year bins (r^2)	0.12	*0.616	*0.607	**0.349**
	20-year bins (r^2)	-0.268	-0.223	*0.631		20-year bins (r^2)	-0.157	0.372	*0.538	
DHI values	50-year bins (r_s)	*-0.586	-0.119	0.284	**-0.116**	50-year bins (r_s)	0.478	-0.332	*0.798	**0.295**
	20-year bins (r_s)	-0.149	-0.294	0.171		20-year bins (r_s)	0.213	-0.020	*0.635	
reconstruction	50-year bins (r_s)	0.328	0.439	*0.544	**0.479**	50-year bins (r_s)	*0.543	*0.622	*0.767	**0.686**
	20-year bins (r_s)	0.385	*0.718	0.462		20-year bins (r_s)	*0.818	0.566	*0.802	
$\delta^{13}C$ values	50-year bins (r_s)	0.145	0.224	0.380	**0.202**	50-year bins (r^2)	-0.14	-0.057	0.218	**-0.019**
	20-year bins (r_s)	0.244	0.065	0.151		20-year bins (r^2)	-0.277	-0.182	0.322	
$\delta^{18}O$ values	50-year bins (r_s)	*-0.503	-0.163	0.123	**-0.070**	50-year bins (r^2)	0.394	-0.002	0.291	**0.198**
	20-year bins (r_s)	0.037	-0.160	0.247		20-year bins (r^2)	0.304	-0.141	0.344	

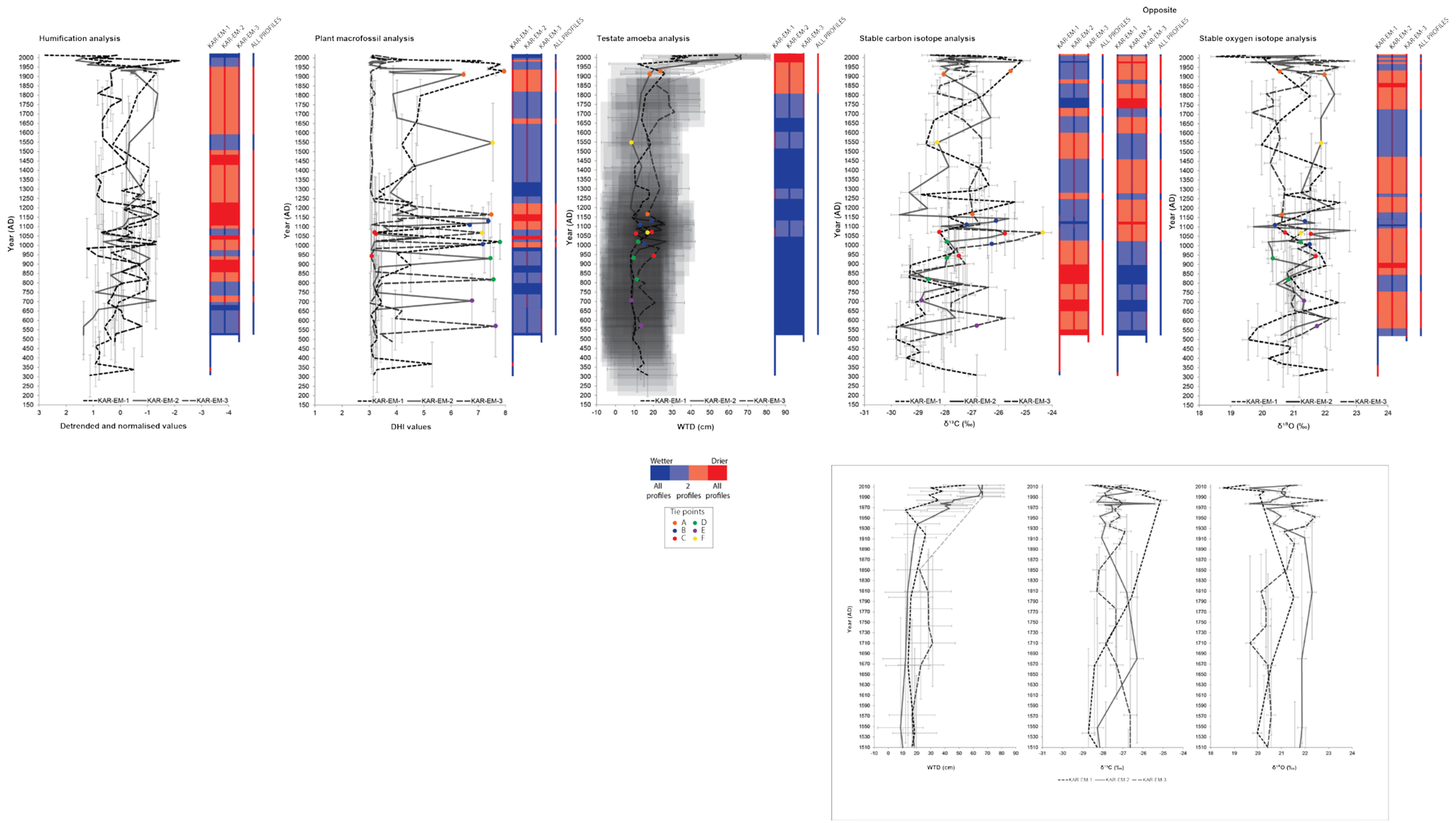

Figure 6.6. Intra-site comparison diagram displaying all records plotted against age. Climatic inferences for each record are based on deviation from the mean, the shading shows agreement of more than 2 profiles resulting in an overall climatic inference 'ALL PROFILES'. The coloured dots on the diagrams are tie points between profiles for comparison with figure 6.9. The smaller diagrams display the last 500 years of the WTD reconstructions and stable isotope records.

6.2.1 Humification records

The summarised humification analysis displays predominantly drier conditions (red shading) throughout (AD 800-1950), with KAR-EM-3 generally disagreeing with the other two profiles. Supporting this, the highest and only significant correlation is the positive correlation between KAR-EM-2 and KAR-EM-1 and this suggests that these two records are the most similar of the profiles. The humification records from these two profiles were also the most highly related in terms of depth (table 5.7).

6.2.2 Plant macrofossil records

The summarised plant macrofossil analysis shows predominantly wetter conditions (blue shading) throughout with an intervening drier period between AD 1000 and 1250. There is generally higher agreement between KAR-EM-1 and KAR-EM-2. The only significant correlation is that between KAR-EM-3 and KAR-EM-2 which shows that based on 50-year time periods there is a negative correlation between the two records;this is evidenced by the lack of correspondence between these two records. The correlation between 20-year bins includes the highest number of original observations (non-averaged see Appendix II); however, this option does not find any significant correlations between records.

6.2.3 Testate amoeba records

The WTD reconstructions from Karukinka all seem to reflect a similar dominance of *D.pulex* throughout the records and stable but low WTD with a period of WTD variability between AD 1000 and 1150 and a synchronous rise of *A.muscorum* from AD 1990 causing a rise in WTD (shown more clearly in the diagram of the last 500 years). As expected, according to a relatively wetter microhabitat, the mean WTD value of KAR-EM-1 is 16.65 cm compared with relatively drier conditions in KAR-EM-2 and KAR-EM-3. Moreover, where all profiles do not agree in the summary diagram, KAR-EM-1 disagrees with the other two profiles. The drier shifts in this record suggest the higher sensitivity of this record owing to its proximity to the water table.

At 50-year time periods there is a significant and high positive correlation between the KAR-EM-2 and KAR-EM-1 records with better correspondence between these two records in figure 6.6. At 20-year time periods a significant and high correlation is found between KAR-EM-3 and KAR-EM-1 despite the relative lack of correspondence between these two records in figure 6.6.

Intra-site replicability of testate amoeba based WTD reconstructions is found in Hendon *et al.* (2001) with synchronous variability in these records attributed to climatic variability. The records from Karukinka bog display insensitivity in comparison with the other proxies (Section 5.4.1) but all display a shift after AD 1900.

6.2.4 Stable carbon isotope records

The summarised stable carbon isotope record displays drier conditions until AD 1030 with relatively wetter conditions after this until present. The opposite interpretation of this proxy inevitably suggests the opposite direction of variability, with wetter conditions until AD 1030 and drier conditions thereafter. There is a sharp shift to more negative values in KAR-EM-2 not evident in the other two records, perhaps suggesting methanotrophic activity in this profile and wetter conditions ~AD 1150 (Nichols *et al.*, 2009; Kip *et al.*, 2012); however, this opposite interpretation is more likely in a hollow location. Despite the general agreement between the records until ~AD 1100, above this the records show no major trends towards the surface suggesting potentially climatic complacency (also shown in diagram of last 500 years). As a result, in neither the 50-year nor 20-year time periods are there significant correlations between the records. Significant correlations were also not found between the records when plotted against actual and relative depth (table 5.13).

Clear microtopographic differences are not evident between the three records. Based on the relationships evident in previous studies (Price *et al.*, 1997; Loader *et al.*, 2016) overall more negative values would be expected from KAR-EM-3 in the drier microenvironment. However, the mean values of the three records are similar (~-27‰) which may suggest that these profiles have not captured the full microtopographic gradient and may all be reflecting persistent hummock conditions.

6.2.5 Stable oxygen isotope records

The summarised stable oxygen isotope record displays drier conditions throughout with intervening wetter periods. Agreement between all three profiles is rare owing to low variability around the mean of this proxy. The direction of variability is only similar across the three records at ~AD 1100, when all records display lower values suggesting wetter conditions.

The only significant correlation between records is that between the KAR-EM-3 and KAR-EM-2 records based on 50-year time periods. A high negative correlation between the two suggests that lower $\delta^{18}O$ values in KAR-EM-3 occur alongside higher $\delta^{18}O$ values in KAR-EM-2. This may be because of the difference between these two profiles above AD 1150. A lack of significant correlations both based on 50- and 20-year time periods implies general disagreement between the records.

Similar to the mean $\delta^{13}C$ values across the profiles, the mean $\delta^{18}O$ values are similar (~21‰) suggesting potential climatic complacency. In line with assumed differences across the microtopography overall higher values with higher amplitude were expected from KAR-EM-3; however, a higher range of variability was evident in KAR-EM-1 ~4‰ (AD 1230-2008) compared with the other records (~3‰).

In consideration of more recent microtopographical differences (also with reference to the diagram showing the last 500 years) $\delta^{18}O$ values decrease in KAR-EM-1 to the surface but the lack of data points between AD 1800-1970 make it difficult to infer the beginning of this shift. Values decrease in KAR-EM-2 after AD 1900 and then fluctuate around lower values to the surface. Values in KAR-EM-3 show an earlier shift to higher values (AD 1710) until the surface.

Moreover, figure 6.7 compares the last 200 years and last 60 years of the records with GNIP precipitation $\delta^{18}O$ data. Taking the $\delta^{18}O$ values of precipitation from the Punta Arenas GNIP station (1990-2009), monthly values were averaged to estimate annual $\delta^{18}O$ values. The biochemical enrichment factor (Zanazzi and Mora, 2005) was added to these values to calculate the expected $\delta^{18}O$ values of cellulose, if this

source water has been simply incorporated into the cellulose. These values are then compared with the KAR-EM records.

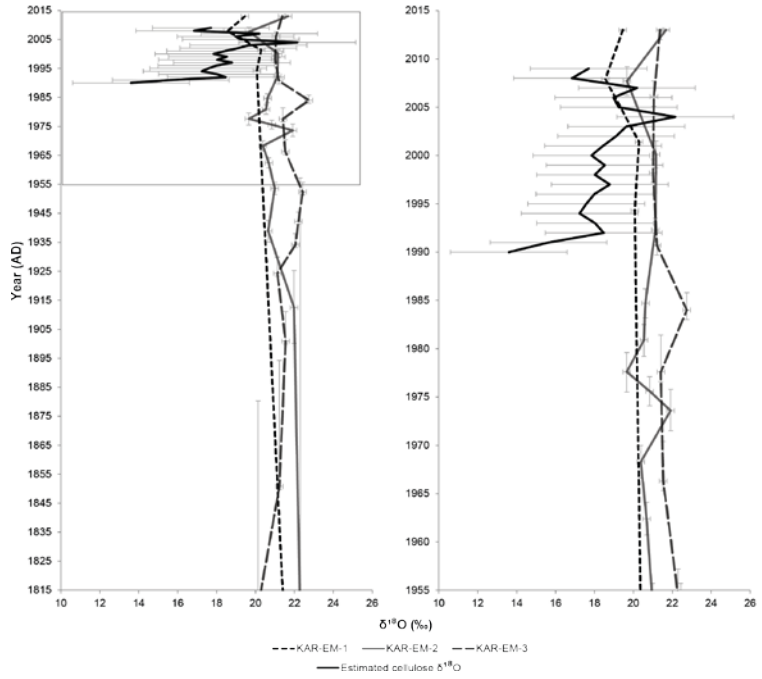

Figure 6.7. The stable oxygen isotope records plotted against age from the original chronologies. The last 200 years (left hand) and the last 60 years (right hand) are shown. The estimated cellulose $\delta^{18}O$ values (derived from GNIP precipitation $\delta^{18}O$ data from Punta Arenas 1990-2009) are displayed for comparison.

Of note are the differences between the three records in recent decades. Towards the surface, above AD 1925, KAR-EM-3 displays higher values than the other profiles, following the expected differences in $\delta^{18}O$ values according to microtopographic position.

The GNIP data show a slight shift to higher $\delta^{18}O$ values between 1990 and 2009. The KAR-EM records, not annually resolved, do not show a similar shift. Values in the records are generally higher suggesting additional enrichment perhaps as a result of the distance between the GNIP station and Karukinka bog. Inconsistencies in the GNIP data may also explain this disagreement. Daley *et al.* (2012) compared mean monthly precipitation and temperature with the $\delta^{18}O$ values of precipitation from this station and did not find any statistically significant relationships due to the paucity of data.

Variability throughout the records may reflect changes in the strength and latitude of the SWW, through changing source water and rain-out history (Cole *et al.*, 1999). This may be particularly evident in the differences between the records in recent decades. KAR-EM-1 may be reflecting large scale circulation changes as suggested by the correspondence between the $\delta^{18}O$ values in this record and the GNIP data whereas KAR-EM-3 may be responding to local processes, thus displaying higher $\delta^{18}O$ values as a result of additional evaporative enrichment. It is clear from the lack of similarity between the records that both atmospheric and local-scale factors have influenced the $\delta^{18}O$ of cellulose in these records (Loader *et al.*, 2016).

A general lack of within-site replicability based on each proxy is suggested by the absence of agreement between all profiles (summary diagrams) and by a lack of significant correlations between the profiles. Chronological uncertainty of KAR-EM-3 is evidenced by the disagreement of the records from this profile with proxy records from the other profiles. The mean of the correlations as shown in table 6.1 also highlights the overall lack of correlation with the highest correlation found between the WTD reconstructions. This results in difficulty in drawing overall climatic inferences from such records. Consideration of processes on the microscale may aid understanding of such incoherence.

6.3 Microscale processes and chronological uncertainty

As well as interpretation based on the findings of previous investigations (section 6.1), the interpretation of the proxy records relies on an understanding of how the hummock from which the profiles were taken has grown to the present day and the feedbacks influencing this growth over time. On the shorter timescale growth (NPP) is driven by water table depth (as a function of BSW) and surface temperature (van Bellen *et al.,* 2011). Feedbacks between water table depth, productivity and decay and differences in these factors across the microtopography may explain differences in the proxy records from cores taken at differing microtopographic locations (Nungesser, 2003). Related to this are also differences in chemical processes including oxygenation, redox potential, pH and nutrient availability (Weltzin *et al.*, 2001) and differences in saturated hydraulic conductivity (Branham and Strack, 2014). Horizontal temperature gradients are also evident (Kettridge and Baird, 2010)

across the microtopography which are in turn affected by BSW, water table depth and vegetation composition (Kettridge and Baird, 2008). Multiple feedbacks on the micro scale therefore complicate interpretation of proxy records from cores taken across a microtopographic gradient.

A simplistic view of the differences across the microtopography of NPP and decomposition at a single point in time assumed that there is lower NPP and higher decomposition in hollows and higher NPP and lower decomposition in hummocks (Johnson and Damman, 1991) explaining differences in the thickness of the acrotelm zones across the microtopography (Section 2.3.2). Other studies have found evidence of higher productivity of *Sphagnum* in hollows and lawns than in relatively drier hummock areas with uniformly low decomposition of *Sphagnum* across the microtopography resulting in hummock growth (Clymo and Hayward, 1982; Gunnarsson, 2005). Differences in the thickness of the acrotelm zone are explained by higher acrotelm productivity in hollow and lawn locations that does not necessarily result in higher accumulation owing to higher decomposition processes and incorporation into the catotelm (Lindsay, 2010).
As well as these differences in feedbacks across the microtopography at a single point in time, differing feedbacks act at each microtopographical location over time. Ecohydrological feedbacks have recently been investigated (Morris *et al.*, 2011b; Swindles *et al.*, 2012a) and are based on investigations from Northern Hemisphere peatlands. Such modelling studies have improved understanding of these complex adaptive systems and assist with interpretation in this investigation.

From such investigations, an example of a negative feedback is a stable water table depth over time with an NPP increase resulting in thickening of the acrotelm zone and an increase in decay; if the water table depth remains stable as the vegetation outgrows the water table the NPP decreases and the acrotelm zone thins (Weltzin *et al.*, 2001; Morris *et al.*, 2011b). This model assumes that lawn and hummock microforms have been in the same place over time with thickening and thinning of each in response to stable water table levels. Thin and thick oxic zones are under conditions of stable equilibria whereas an intermediate thickness is less stable. In this way litter addition (NPP) minus decay controls the processes in each microtopographical location (Morris *et al.*, 2011b). A positive feedback may also exist

in which stable water table levels and an increase of NPP result in acrotelm zone thickening, higher decay, peat accumulation and further thickening of the acrotelm zone. This positive feedback supports hummock growth by promoting acrotelm zone thickness suggesting that microforms have remained in the same position over time under stable water table positions. The model results of Morris *et al.* (2011b) showed that in response to net rainfall variability peatlands may be able to resist external variability owing to the aforementioned feedbacks related to acrotelm thickness. The underlying assumption of proxies of BSW/WTD is that the peatland is responding linearly to such variability (based on acrotelm thickness); however, linearity is not suggested by this model because of the possibility of both a negative and positive feedback, as discussed above (Morris *et al.*, 2011b).

Following the general assumptions proposed, two scenarios are hypothesised for hummock growth (See figure 6.8). Evidence of either a synchronous or an asynchronous acrotelm-catotelm boundary is discussed which will inevitably influence interpretation of the proxy records owing to the differences in the age of this boundary based on the two scenarios.

The first scenario assumes that the acrotelm-catotelm boundary is the same age across the microtopography. This follows the assumption that in terms of peat accumulation, just below this boundary represents recent conditions which have acted on the acrotelm zone and resulted in incorporation into the catotelm zone. According to this, the acrotelm and catotelm zones are distinct and can be treated as separate units with different peat accumulation rates. The acrotelm zone is tied across profiles assuming that when based on the KAR-EM-2 age profile, 83 cm depth in KAR-EM-3 represents ~85 years. Faster growth through the KAR-EM-3 acrotelm is suggested (~1 yr/cm) than based on the accumulation rate as calculated from the age-depth model for this profile. With reference to figure 4.5 the calculated ^{210}Pb ages suggest that the top 45 cm (AD 1900 to present) are of a similar age in KAR-EM-2 and KAR-EM-3 (~2.5 yr/cm); below this the records diverge in age. KAR-EM-3 remains relatively young until 70 cm but between 70 and 80 cm, accumulation in KAR-EM-3 is faster and below this falls into the chronological uncertainty of the KAR-EM-2 age profile, supporting the notion of a similar age of the KAR-EM-3 and KAR-EM-2 acrotelm zones.

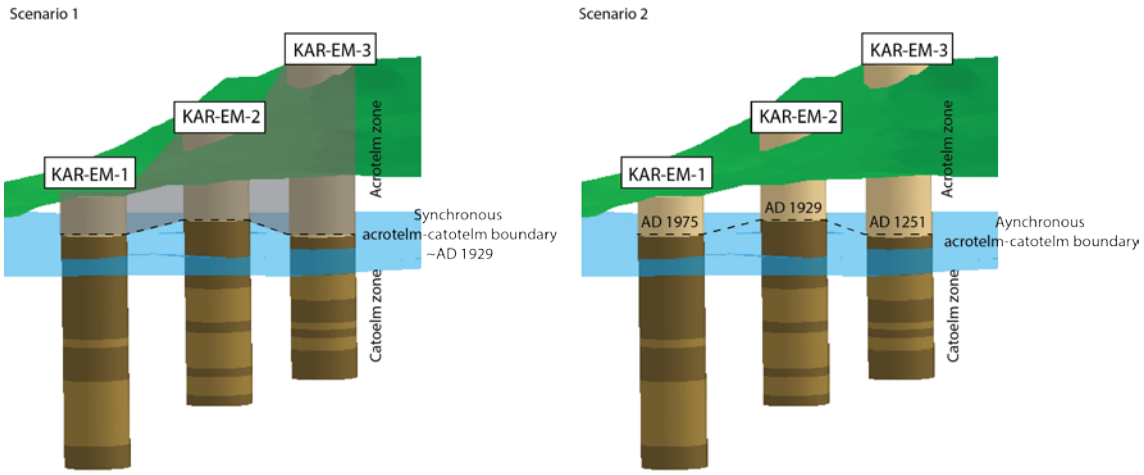

Figure 6.8. Two hypothesised scenarios for growth of the hummock from which the KAR-EM profiles were taken.

It is estimated that 50 cm of surface peat in the acrotelm zone is commonly no older than 200 years (Ohlson and Dahlberg, 1991; Ohlson and Økland, 1998) (4 yr/cm); however, dating this period presents problems. Other studies estimate that the acrotelm zone represents ~100 years of accumulation (Malmer and Wallen, 1993; Johnson and Damman, 1993; Nungesser, 2003) with an estimated rate of incorporation into the catotelm of 0.5-1mm per year (Lindsay, 2010). Ohlson and Dahlberg (1991) found generally higher annual peat increment on hummocks with an age of 50 years variably representing between 15 and 54 cm below the surface (3-1 yr/cm). However, at one site 20 years of growth on one hummock microform was found to differ between 10 and 40 cm depth (2-0.5 yr/cm) suggesting high variability even on the microscale. Gerdol (1996) found around 28-31 mm increment of *S.magellanicum* in one growing season (~3 yr/cm). Although the figures are highly variable they support the potentially fast growth of the hummock vegetation through the acrotelm zone of KAR-EM-3 (~1 yr/cm). This relatively faster growth, according to scenario one, could have been the result of a synchronous change in the water regime (either lower/higher WTD) (Malmer, 2014). In this scenario the apparent dry shift evidenced by low humification and high DHI values (dominance of UOM and root material) just below the acrotelm-catotelm boundary is assumed to have occurred simultaneously. Heijmans *et al.* (2001) suggest that at levels where vascular plants are dominant the abundance of *Sphagnum* may have been reduced owing to increased depth to water table and shading. This boundary is followed by a

period after which *S.magellanicum* was more successful than vascular plants (Grootjans *et al.*, 2010). Such dominance has been found in several cases after periods of disturbance and water table lowering (Barber *et al.*, 1998; McMullen *et al.*, 2004; Swanson, 2007). Scaffold-species such as *E.rubrum*, *N.antarctica* and *M.grandiflorum* stabilize hummocks (Baumann, 2006). This seems to be evident especially in KAR-EM-3 where there is an increase in *E.rubrum* after the acrotelm-catotelm boundary which may have supported hummock growth. Another explanation for this clear boundary may be higher nitrogen levels which resulted in more decayed plant debris (Belyea and Warner, 1996).

High productivity of *S.magellanicum* is evident on hummocks as this species is dry adapted (Wallén *et al.*, 1988) but slow to decay (Johnson *et al.*, 1990; Johnson and Damman, 1991) leading to accumulation. Baumann (2006) investigated surface patterning of nanotopes at Andorra bog (same site as Chambers *et al.*, 2014). They attribute such patterning and sustained hummocks to higher production than decomposition, a positive feedback (Morris *et al.*, 2011b). Conditions specific to Patagonian peatlands (see section 2.3.7) have resulted in higher productivity and limited decomposition in the acrotelm which has resulted in the extreme microtopographical gradients present at these sites (Loisel and Yu, 2013). Higher growth (4.42±3.28 cm and 2.31±1.85 cm) and productivity (573.10±303.33 and 342.83±217.30 $gm^{-2}year^{-1}$) of *S.magellanicum* was found in lawns than in hummocks (differentiated by a 10 cm datum height) across nine anthropogenic peatlands 'pomponales' from which the top layer of *Sphagnum* is harvested yearly for horticultural purposes (Díaz *et al.*, 2012). The growth and productivity of *S.magellanicum* was assessed across the microtopography in terms of the water table depth and a negative relationship was found between the two (as depth from the surface to the water table increases there were lower growth rates). This potentially supports slow growth of *Sphagnum* through the acrotelm zone in KAR-EM-3 with differential decay rates across the microtopography resulting in horizontal heterogeneity. The peatlands in this investigation may be affected by different processes (e.g. latitude, climate, anthropogenic influence) as those investigated by Díaz *et al.*, 2012). Also from pomponales, Tapia (2008) found variable growth of *S.magellanicum* between 1.72 and 9.53 cm in an eleven-month period, an average of 4.43 cm per year (~0.25 yr/cm). The production and decay of *Sphagnum* varies

widely amongst species and *S.magellanicum* itself has a highly variable NPP ranging from 50 to 794 g/m^2. (Nungesser, 2003). Growth rates of *S.magellanicum* have been found to be highly variable making assessment of the most likely scenario difficult, based on the rates found in other investigations.

Alternatively, a rise of the water table level may have led to the outgrowth of hummock microtopography from the water table (Swanson, 2007). *Sphagnum* productivity, and in particular of *S.magellanicum,* has been found to increase as a result of higher water tables (Li *et al.*, 1992; Bridgham *et al.*, 2008; Sulman *et al.*, 2010). Using the Morris *et al.* (2011b) model, Swindles *et al.* (2012a) found that as a result of two wet shifts as recorded in a multi-proxy record of hydrological variability there were subsequent dry shifts resulting from the faster accumulation of peat and associated feedbacks. This suggests that initial wet shifts may be climatic but subsequent dry shifts may instead be driven by resulting ecohydrological feedbacks.

Differences in CO_2 exchange across the microtopographic gradient are expressed in differences in CO_2 diffusivity. In hummock locations an increase in *Sphagnum* productivity was evident as a result of a water table rise; the same rise did not affect productivity at the lawn location and it was negative in the hollow location. It was suggested that an optimum water table position at each microform location would allow maximum productivity but above or below this, optimum productivity would be reduced (Pelletier *et al.*, 2011). This offers support for a potential water table rise which may then have resulted in the rapid formation of the hummock in this investigation. More specifically, an increase in atmospheric CO_2 was found to increase the height growth of *S.magellanicum* (Heijmans *et al.*, 2001). As the photosynthetic cells are completely enclosed by hyaline cells *S.magellanicum* has a higher diffusive resistance to CO_2 uptake so thrives under increased CO_2. The CO_2 rise since 1850 (Robertson *et al.*, 2001), and especially since 1950, may have resulted in higher growth. If this has resulted in higher growth in KAR-EM-3 it is likely that the acrotelm zone in this profile is similar in age to that in KAR-EM-2.

Effects of Antarctic stratospheric ozone depletion on climate change have particularly affected summer temperatures and precipitation and thus impact ecosystems that have summer growing seasons (Robinson and Erickson, 2015).

Natural ecosystems have been affected by the recent drying in SSA; examples include decreases in the growth rates of trees in the region and Antarctic mosses (Clarke *et al.*, 2012; Villalba *et al.*, 2012). Gehrke (1998) found UV-B radiation to reduce the growth of *Sphagnnum fuscum* as a result of the ozone hole. Conversely, increased moss growth rates have been found on the Antarctic Peninsula linked to warming (Royles *et al.*, 2012; 2013). Ozone hole related increases of UV-B radiation have had less of an effect on *S.magellanicum* than on vascular plants in an investigation on a peatland in Tierra del Fuego (Robson *et al.*, 2003). This may explain the dominance of *S.magellanicum* at the surface through this species outcompeting vascular species.

Moss increment counting has been applied to recent peats in which the well preserved stems of *Sphagnum* are analysed (Pakarinen and Tolonen, 1977). El-Daoushy *et al.* (1982) and Belyea and Warner (1994) have used this technique successfully. In KAR-EM-3 whole *Sphagnum* stems up to 15 cm in length were evident. According to the original KAR-EM-3 chronology, ~15 cm represents 27 years of growth (~2 yr/cm). If it is assumed that growth has been uniform throughout the acrotelm section of KAR-EM-3, then 83 cm represents ~760 years of growth (~9 yr/cm). This leads to the second scenario which assumes that based on the ages inferred from the original chronologies the acrotelm-catotelm boundary is asynchronous across the three profiles with a relatively older boundary in KAR-EM-3.

Scenario one suggests that the acrotelm zones of the three Karukinka profiles may be similar in age supporting plotting the KAR-EM-1 and KAR-EM-3 records against the ages inferred from the KAR-EM-2 chronology. This could result in better agreement between the records than was evident where the records are plotted against their respective age profiles according to scenario two, which will be discussed in the following section.

6.4 Intra-site proxy comparison based on Scenario one

Figure 6.9 displays all records as in figure 6.6 but instead the records are plotted against the KAR-EM-2 ages. The stratigraphic variability as displayed in figure 6.1 has formed the basis of matching between the proxy records. This is similar to the process of tuning and stacking, whereby proxy records are aligned based on

synchronous events within measurement and age error (Blaauw, 2012). Improved correlation is expected as a result of tuning but may not necessarily evidence an original relationship between records.

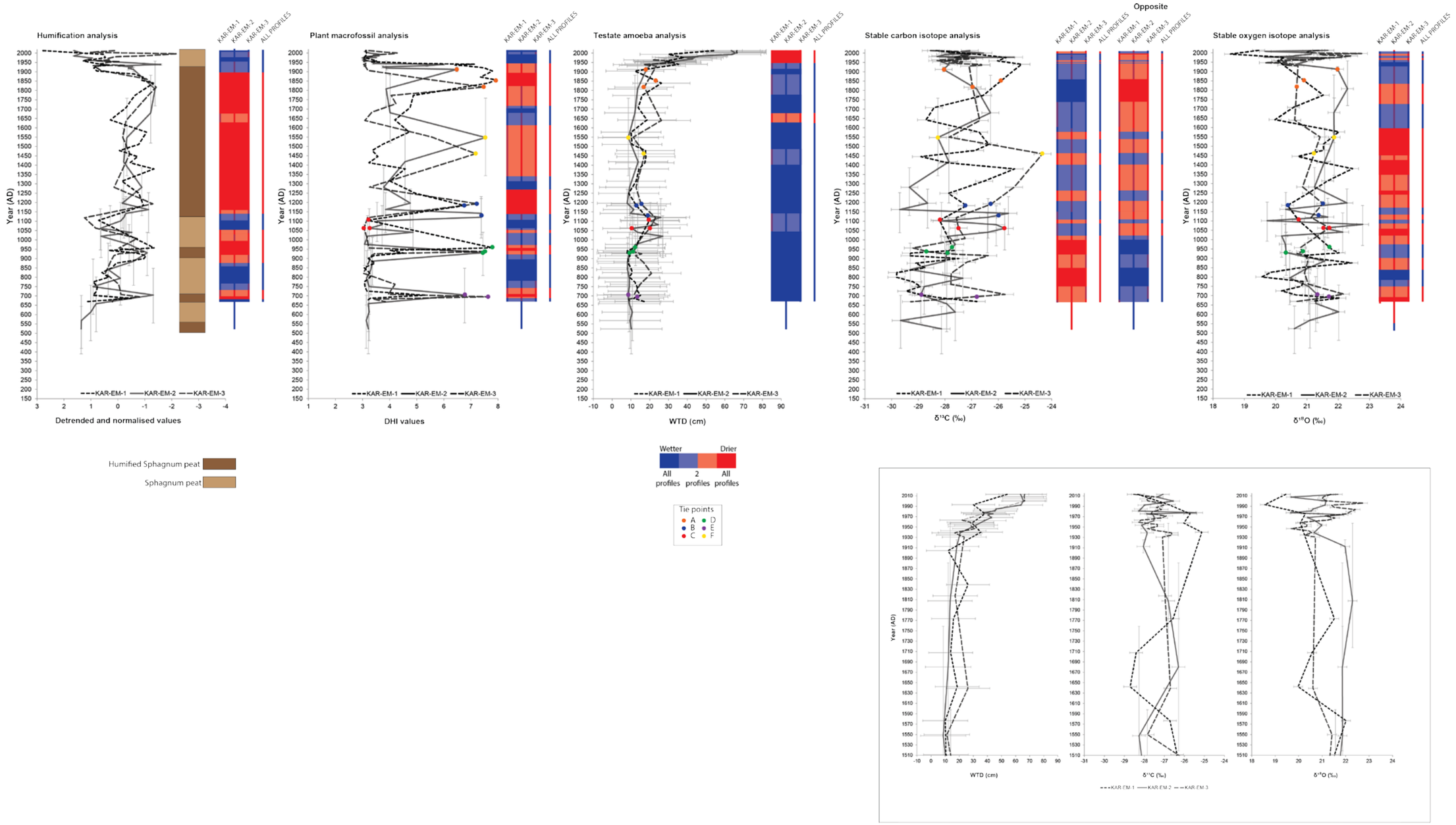

Figure 6.9. Intra-site comparison diagram displaying all records plotted against the KAR-EM-2 age profile. Climatic inferences for each record are based on deviation from the mean, the shading shows agreement of more than 2 profiles resulting in an overall climatic inference 'ALL PROFILES'. The coloured dots on the diagrams are tie points between profiles for comparison with figure 6.6. The smaller diagrams display the last 500 years of the WTD reconstructions and stable isotope records.

6.4.1 Humification records

Similarities in the pattern of shifting from inferred wetter to drier conditions preceding the acrotelm zone of each profile offers justification for aligning the acrotelm of KAR-EM-3 in timing with the acrotelm zones of KAR-EM-1 and KAR-EM-2 according to scenario one. Higher compaction is evident in hummocks (Ohlson and Dahlberg, 1991) which may explain the higher compaction of the stratigraphic unit below the acrotelm-catotelm boundary in KAR-EM-3 compared with KAR-EM-2 and KAR-EM-1 and further supports tying these units. This is a simplified interpretation of potential accumulation in this profile. If the acrotelm-catotelm boundary is assumed to be synchronous across the profiles then these distinct zones could be treated independently. This separation is necessary owing to decomposition processes still occurring in the acrotelm zone whereas material in the catotelm zone would be more representative of variability over time.

Plotted against the KAR-EM-2 age profile there is better agreement between the records evidenced by the higher number of significant correlations and darker shading on the summary diagram. However, the upper part of KAR-EM-3 and lower part of KAR-EM-1 are not within their original chronological error. This either suggests that tuning should not be carried out and that there are genuine differences between the profiles based on differing peat processes or it suggests that the original chronologies are incorrect. Higher agreement between profiles displayed in figure 6.9 would support this. This agreement will be assessed in the following sections.

6.4.2 Plant macrofossil records

Overall higher correlations were found when the DHI records were plotted against relative depth (table 5.6); this supported a synchronous acrotelm-catotelm boundary with similarity across the profiles (low values) above this. Alignment of the acrotelm zones and synchronous stratigraphic units below, following scenario one resulted in better agreement between the records. The correlations between the profiles are generally improved and there are significant and high positive correlations between KAR-EM-2 and KAR-EM-1 in both the 50- and 20-year bin options. Opposite to figure 6.6 predominantly drier conditions are evident. The tie points (B-E) are within

the KAR-EM-2 chronological error questioning the original chronologies. Despite lack of agreement of variability with previous studies (Mauquoy *et al.*, 2004; Chambers *et al.*, 2014) the shift to drier conditions between AD 1750 and 1900 in the plant macrofossil records is evident in these studies (1675-1770; 1740-1830 respectively).

6.4.3 Testate amoeba records

When plotted against relative depth significant and high positive correlations were found between all records (table 5.12) supporting tying the acrotelm zones of the three profiles because there are similarities in the direction and timing of the shift in WTD in all records above the acrotelm-catotelm boundary. Assuming scenario one (figure 6.8) there is clear agreement between the profiles and based on both 50- and 20-year time periods there are more significant and positive correlations between the records.

However, the tie points (A-F), based on similarities in the humification and plant macrofossil records, when placed on the WTD records, are at depths where similarities between the absolute WTD values are not evident (figure 6.6). For example, at tie point C a WTD value of ~20 cm in KAR-EM-1 and KAR-EM-3 is different to ~10 cm in KAR-EM-2. However, this may be reasonable owing to the large error and insignificance of variability below 10 cm. This questions the reliability of absolute values throughout the records.

After tying the records (figure 6.9) the tie points (B-E) are within the KAR-EM-2 chronological error. Tie point A in KAR-EM-3, although not within the original chronological error, is in better agreement with KAR-EM-2 and KAR-EM-1 in the tuned diagram (~20 cm) than in the original diagram (~10 cm). Based on the tuned records, between AD 1000 and 1150 there is a rise in WTD in all records suggesting relatively drier conditions in this period (although wetter conditions are still indicated by values below the mean). Below and above this period of variability, WTD is stable. The surface shift in all records occurs synchronously above AD 1900 (also see diagram showing last 500 years).

6.4.4 Stable carbon isotope records

Similarities were not evident across the records in the acrotelm zone (figure 6.6) suggesting that these records are not as well tied as the other proxies. However, for consistency the stable carbon isotope records have been plotted against the KAR-EM-2 ages. This changes the depth after which correction is necessary in KAR-EM-1 and KAR-EM-3 but results in minimal difference owing to the records fluctuating around the mean between the point of correction and the surface. Plotting against KAR-EM-2 ages does not result in improved correlations between profiles or improved agreement.

The original tuning points are placed at differing absolute values on the original records and although these fall into the chronological error of the original KAR-EM-2 chronology (B-E) after tuning there are large differences between these points. This suggests that tuning of the other records may be incorrect. Conversely, it may indicate the difficulty of this proxy in inferring BSW variability evidenced by inconsistent variability across the microtopography.

6.4.5 Stable oxygen isotope records

Plotted against relative depth (figure 5.23b), agreement above 90 cm offers support for aligning the acrotelm zones of the three profiles. There was a significant and positive correlation between KAR-EM-3 and KAR-EM-1 plotted in this way. Plotting the records against the ages inferred from the original KAR-EM-2 chronology did not however, result in any significant correlations between records. Similar to the stable carbon isotope records, the original tie points are placed on differing values and do not tie synchronous peaks. Although on the tuned records tie points B-E fall into the chronological error of KAR-EM-2 they remain on differing absolute values (figure 6.9).

The surface shift in KAR-EM-3 is sharper and larger as a result of plotting against the KAR-EM-2 age profile (see diagram of last 500 years); a later (~AD 1920) and more extreme shift to drier conditions is indicated. If tuning were correct this demonstrates how interpretation may differ based on uncertain chronologies. Tuning

also results in better correspondence between the GNIP data and the three records, particularly with KAR-EM-1 (figure 6.10).

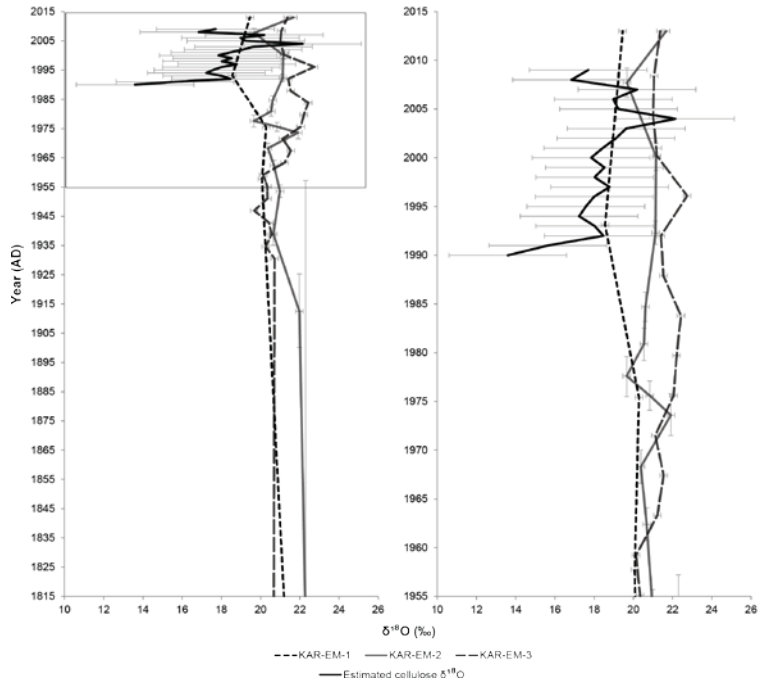

Figure 6.10. The stable oxygen isotope records plotted against the KAR-EM-2 age profile. The last 200 years (Left hand) and the last 60 years (right hand) are shown. The estimated cellulose $\delta^{18}O$ values (derived from GNIP precipitation $\delta^{18}O$ data from Punta Arenas 1990-2009) are displayed for comparison.

6.4.6 Summary diagrams

Figure 6.11 displays all of the summary diagrams from figures 6.6 and 6.9. It suggests that there is higher overall agreement when the records are plotted against the KAR-EM-2 ages as evidenced by higher periods of darker shading. These records may be able to offer more reliable climatic inferences owing to apparently higher coherence between profiles. However, plotted in this way there is improved coherence between the palaeoecological proxy records but not between the stable isotope records based on lack of improved correlations, visual agreement and in consideration of the absolute values on which the tie points were placed. Plotted in this way the proxy records also do not result in improved periods of synchronous variability.

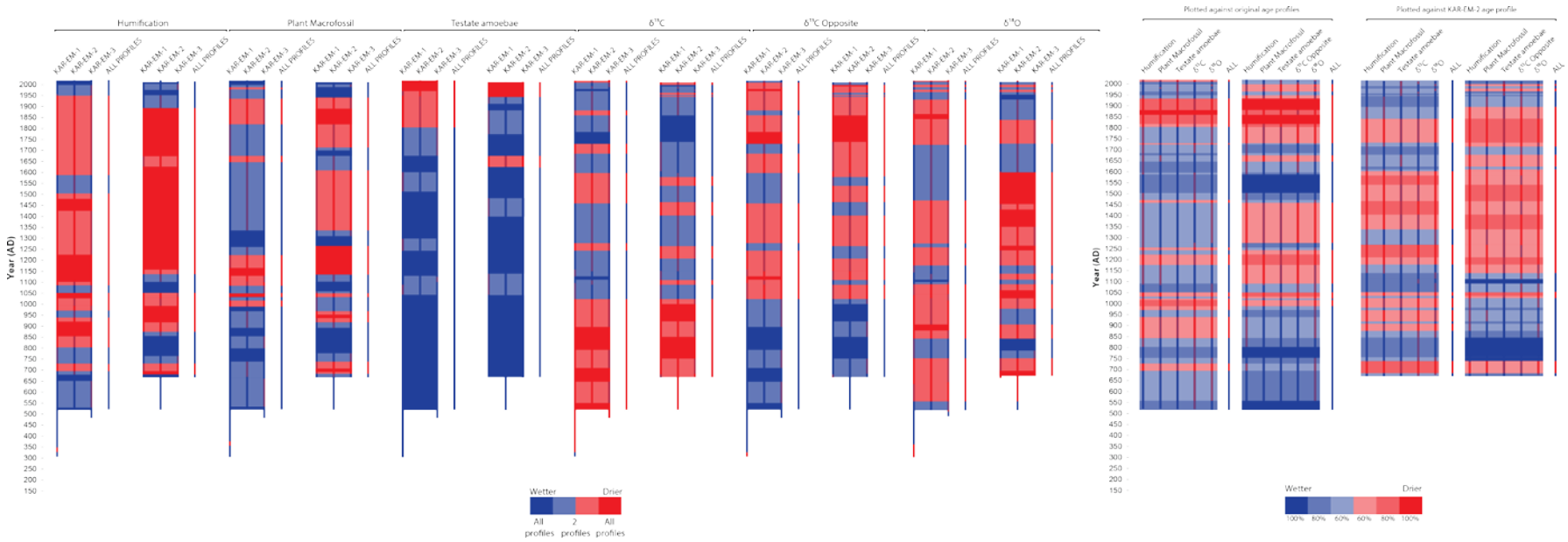

Figure 6.11. Comparison of climatic inferences from the proxy records. For each proxy the climatic inferences are shown from figure 6.6 (left of each proxy) where the records are plotted against their individual age profiles and from figure 6.9 (right of each proxy) where the records are plotted against the KAR-EM-2 age profile. Shading relates to agreement of more than 2 profiles and results in a final climatic inference 'ALL PROFILES'. The summary diagrams on the right hand side compare the climatic inferences from 'ALL PROFILES' with the shading related to the degree of overall agreement of climatic inferences from each proxy. Note that '$\delta^{13}C$ opposite' relates to the potentially opposite interpretation of this proxy (Section 6.1.4).

Figure 6.11 is an example of the potentially erroneous climatic inferences that may be made because of the lack of within-site replicability of profiles based on the individual proxies. This approach takes the majority climatic inference based on agreement of more than 2 profiles. It is clear that, based on an overall lack of agreement between the final climatic inferences, there are large intra-site differences between profiles which in turn result in differing climatic inferences being made based on plotting the records against the original and KAR-EM-2 age profiles. In summary, differing climatic inferences result from multi-profile comparisons, associated chronological uncertainty and interpretative uncertainty particularly surrounding stable carbon isotope analysis. The mean of correlations (table 6.1) suggests that the palaeoecological records are more replicable on an intra-site basis than the stable isotope records with the WTD reconstructions displaying the highest correlation and intra-site coherence. The next section further considers within-site replicability by summarising the multi-proxy records from each profile.

6.5 Multi-proxy intra-site comparison

6.5.1 Synthesis of multi-proxy records from each profile

Given that the response of peatland water tables to climate variability may not be consistent and predictable (Swindles *et al.*, 2012a) with an ultimate influence on palaeohydrological proxies, comparison and discussion on a multi-proxy and multi-profile basis is necessary in order to assess the most likely climatic inference.

This section provides a synthesis of the proxy records from each profile and summarises variability, deviation from the mean state represented by each proxy, based on age. After consideration of each proxy in the first part of this chapter, this section continues to assess **Research Question 1** relating to the use of multi-proxy and multi-profile records to explore within site replicability of peatland palaeoclimate archives.

The figures in the following sections present all proxy records from each profile plotted against age. The palaeoecological proxies are plotted as z scores for

comparison and the stable isotope records are plotted using raw values. The summary diagrams to the right of the records are based on the interpretation of each proxy as discussed earlier in the chapter. The long-term mean value of each proxy record has been used to assess deviations from this value. In the first summary diagram ('Original'), where the values of each proxy are below the mean, this is assumed to be indicative of wetter conditions and the bar is coloured blue and vice versa where the bar is coloured red. The stable carbon isotope record is the exception and where values are below the mean this is interpreted as drier conditions resulting in a red section on the bar and vice versa. This follows the interpretation of Loader *et al.* (2016). Similarities between the stable isotope records in all profiles (Section 5.1.4.5) question this interpretation and the second summary diagrams ('Opposite') compare the stable carbon isotope records interpreted to follow the direction of variability of the other proxies to assess whether there is higher agreement of all proxies as a result. Periods in which the two stable isotope records agree are presented and boxes display where the two are in agreement but are opposite in direction to the palaeoecological proxies. Correspondence between proxies and intra-site replicability may suggest that these records have responded similarly to climatic variability.

It must be noted that these diagrams do not include the chronological uncertainty and instead use the mid-point ages of each sample. Consideration of the different scenarios which includes chronological uncertainty is beyond the scope of this investigation but in some cases uncertainty can be as high as ±150 years, potentially placing a climatic period assumed to last, e.g., for 100 years in an error range of 400 years, thus making comparison with other studies difficult.

It must also be noted that the magnitude of variability is not accounted for by the summary diagrams; for example, values just above the mean appear the same as a value that is relatively higher above the mean. It is assumed that in response to allogenic variability all proxies will respond similarly. This however, does not take into consideration potentially differing response times and sensitivity of the proxies and also does not allow for non-stationarity of proxy response over time (Charman *et al.*, 1999). For example, more negative $\delta^{13}C$ values may not signify uniformly wetter or drier conditions over time; according to Nichols *et al* (2009) they may suggest

temporarily wetter conditions owing to methanotrophic activity but throughout the rest of the record may suggest drier conditions. The summary diagrams aim to provide a semi-quantitative assessment of synchronous variability, based on age, within each profile to finally assess within site replicability.

Figures 6.12-6.16 display all proxy records from each profile; the records are plotted against their original age profiles and the records from KAR-EM-3 and KAR-EM-1 are also plotted against the KAR-EM-2 age profile as was done in figure 6.9. The summary diagrams of interpretation are displayed alongside the records. Table 6.2 is an overview of these summary diagrams. There are four options from KAR-EM-3 based on the interpretation of the records plotted against the KAR-EM-3 ages (Result 1 and 2) and plotted against the KAR-EM-2 ages (Result 3 and 4) and the same for KAR-EM-1 (Result 7 and 8, 9 and 10). Two options are available for KAR-EM-2 (Result 5 and 6) since the other two profiles are plotted against this age profile. Exploring these options was necessary in choosing which option from each profile could be used in the final intra-site comparison.

Table 6.2. Overview of the summary diagrams shown alongside figures 6.12-6.16 with the corresponding results from plotting against original ages (1,2,5,6,7,8) and against KAR-EM-2 ages (3,4,5,6,9,10) and according to the differing interpretation of the stable carbon isotope records (Original and opposite).

		Result 1	**Result 2**	**Result 3**	**Result 4**
		Against KAR-EM-3 ages		Against KAR-EM-2 ages	
		Original	Opposite	Original	Opposite
KAR-EM-3		Wetter (76%)	Wetter (69%)	Wetter (58%)	Drier (63%)
	Agreement between stable isotope records	58%	51%	49%	47%
	Stable isotope records agree but disagree with palaeoecological records (Boxes)	14%	14%	30%	16%
	Stable isotope record contribution to majority indicator	$\delta^{18}O$: 27% $\delta^{13}C$: 15%	$\delta^{18}O$: 35% $\delta^{13}C$: 15%	$\delta^{18}O$: 37% $\delta^{13}C$: 14%	$\delta^{18}O$: 16% $\delta^{13}C$: 29%
	Period in which 100% of proxies agree	Wetter (33%) Drier (1%)	Wetter (11%) Drier (1%)	Wetter (8%) Drier 1%	Wetter (4%) Drier 1%
	Climatic inference	• AD 1000-1100 Drier • AD 1100-1850 Wetter • AD 1950 onwards Drier	• AD 900-1225 Drier • AD 1225-1890 Wetter • AD 2000 onwards Wetter	• AD 1150-1270 Drier • AD 1350-1590 Drier • AD 1590-1950 Wetter • AD 1950 onwards Drier	• AD 1140-1890 Drier • No clear climate periods

		Result 5	**Result 6**		
		Against KAR-EM-2 ages			
		Original	Opposite		
KAR-EM-2	Predominant conditions	Drier (62%)	Drier (55%)		
	Agreement between stable isotope records	52%	52%		
	Stable isotope records agree but disagree with palaeoecological records (Boxes)	12%	21%		
	Stable isotope record contributing most to majority indicator	$\delta^{18}O$: 29% $\delta^{13}C$: 22%	$\delta^{18}O$: 32% $\delta^{13}C$: 13%		
	Period in which	0%	Wetter (14%)		

	100% of proxies agree		Drier (0%)		
	Climatic inference	• AD 975-1100 Wetter • AD 1100-1675 Drier • AD 1940 onwards Wetter	• AD 950-1350 Fluctuation between wetter-drier • AD 1350-1940 Drier • AD 1940 onwards – wetter-drier fluctuations		

		Result 7	**Result 8**	**Result 9**	**Result 10**
		Against KAR-EM-1 ages		Against KAR-EM-2 ages	
		Original	Opposite	Original	Opposite
KAR-EM-1	Predominant conditions	Wetter (57%)	Wetter (60%)	Wetter (58%)	Drier (51%)
	Agreement between stable isotope records	39%	64%	48%	67%
	Stable isotope records agree but disagree with palaeoecological records (Boxes)	30%	22%	19%	29%
	Stable isotope record contributing most to majority indicator	$\delta^{18}O$: 38% $\delta^{13}C$: 25%	$\delta^{18}O$: 9% $\delta^{13}C$: 30%	$\delta^{18}O$: 37% $\delta^{13}C$: 27%	$\delta^{18}O$: 16% $\delta^{13}C$: 19%
	Period in which 100% of proxies agree	0%	Wetter (15%) Drier (4%)	Wetter (0%) Drier (1%)	Wetter (10%) Drier (5%)
	Climatic inference	• AD 960-1300 Variable conditions • AD 1300-1650 Wetter • AD 1950 onwards Wetter	• AD 955-1460 Drier • AD 1460-1730 Wetter • AD 1955 onwards Wetter	• AD 875-1060 Drier • AD 1060-1700 Wetter • AD 1700-1890 Wetter • AD 1890 onwards Wetter	• AD 1150-1610 Drier

6.5.2 Multi-proxy records from KAR-EM-3

In figure 6.12 of result 1 and 2, result 1 has higher overall agreement between proxies (predominantly wetter conditions) and also has the highest percentage of agreement between all proxies (33%). This high agreement occurs just above the acrotelm-catotelm boundary and, as already discussed, this zone is problematic in terms of climatic inference. Periods that are generally synchronous with the MCA and LIA occur, with drier conditions between AD 1000 and 1100 and (apparent) wetter conditions AD 1100 and 1850. Problems with the chronology of this profile are addressed by assessing agreement between the records plotted against the KAR-EM-2 age profile (figure 6.13). This did not however, result in higher agreement between the records. Of the two results, result 3 showed the highest agreement between all proxies (only 8% of the record). In this option there is high disagreement with the palaeoecological records in periods where the stable isotope records agree (30%). The stable oxygen isotope record generally agrees with the palaeoecological records where the two stable isotope records do not agree apart from result 4. This option shows predominantly drier conditions, opposite to the other options.

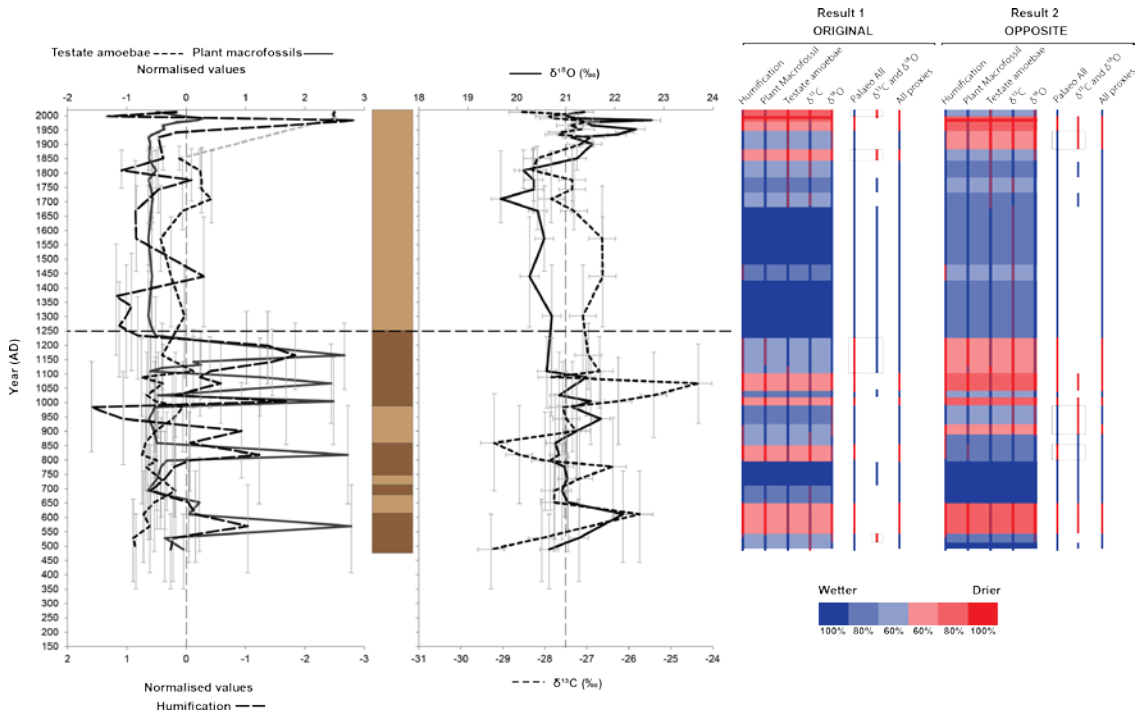

Figure 6.12. All proxy records from KAR-EM-3 plotted against age. Climatic inferences of each record are based on deviation from the mean. Result 1 and 2 relate to the differing interpretation of the stable carbon isotope record. See text for explanation. Dashed line shows the acrotelm-catotelm boundary.

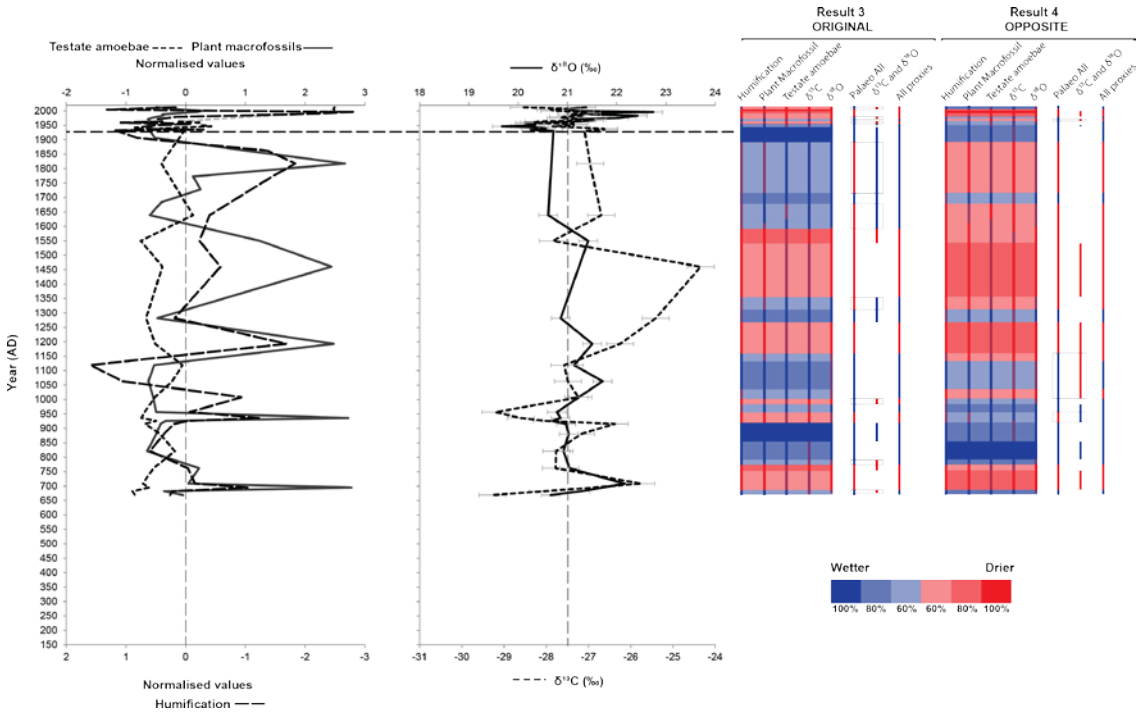

Figure 6.13. All proxy records from KAR-EM-3 plotted against the KAR-EM-2 age profile. Climatic inferences of each record are based on deviation from the mean. Result 3 and 4 relate to the differing interpretation of the stable carbon isotope record. See text for explanation. Dashed line shows the KAR-EM-2 acrotelm-catotelm boundary.

6.5.3 Multi-proxy records from KAR-EM-2

In figure 6.14, of the two options result 5 has the highest agreement between proxies (predominantly drier conditions); however, there are no periods in which 100% of proxies agree. Result 6 shows that there is proxy agreement for 14% of the record. Result 5 seems to show clearer climate periods with a wetter period AD 975-1100 and a drier period AD 1100-1675. These two options will be compared in the different final scenarios in figure 6.17.

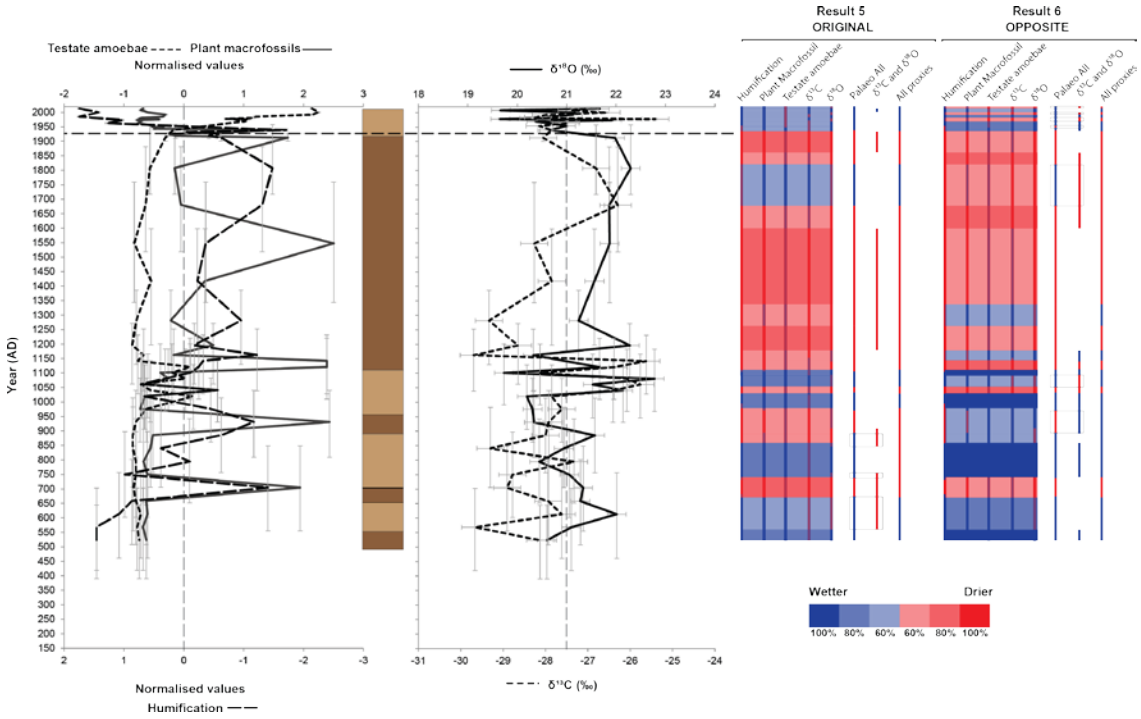

Figure 6.14. All proxy records from KAR-EM-2 plotted against age. Climatic inferences of each record are based on deviation from the mean. Result 5 and 6 relate to the differing interpretation of the stable carbon isotope record. See text for explanation. Dashed line shows the acrotelm-catotelm boundary.

6.5.4 Multi-proxy records from KAR-EM-1

In figure 6.15, result 8 has slightly higher agreement between proxies (predominantly wetter conditions) and also shows highest agreement between all proxies (15%) compared with result 7. There is also relatively higher agreement between the stable isotope records based on the opposite interpretation of the stable carbon isotope

record. The same is true for result 10, in which the KAR-EM-1 records are plotted against the KAR-EM-2 age profile. This results in predominantly drier conditions throughout and higher agreement between all proxies for 10% of the record compared with result 9. Result 8 suggests a drier period between AD 955 and 1460 followed by a wetter period until AD 1730 whereas result 10 suggests predominantly drier conditions throughout the period AD 1150 to 1610.

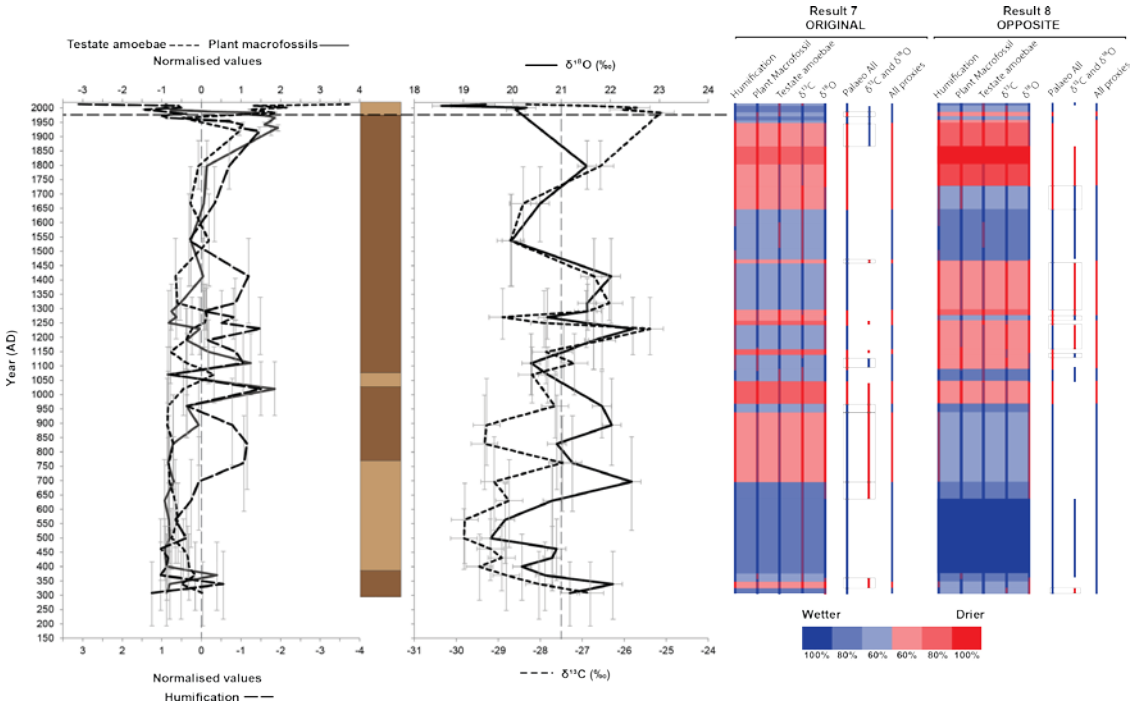

Figure 6.15. All proxy records from KAR-EM-1 plotted against age. Climatic inferences of each record are based on deviation from the mean. Result 7 and 8 relate to the differing interpretation of the stable carbon isotope record. See text for explanation. Dashed line shows the acrotelm-catotelm boundary.

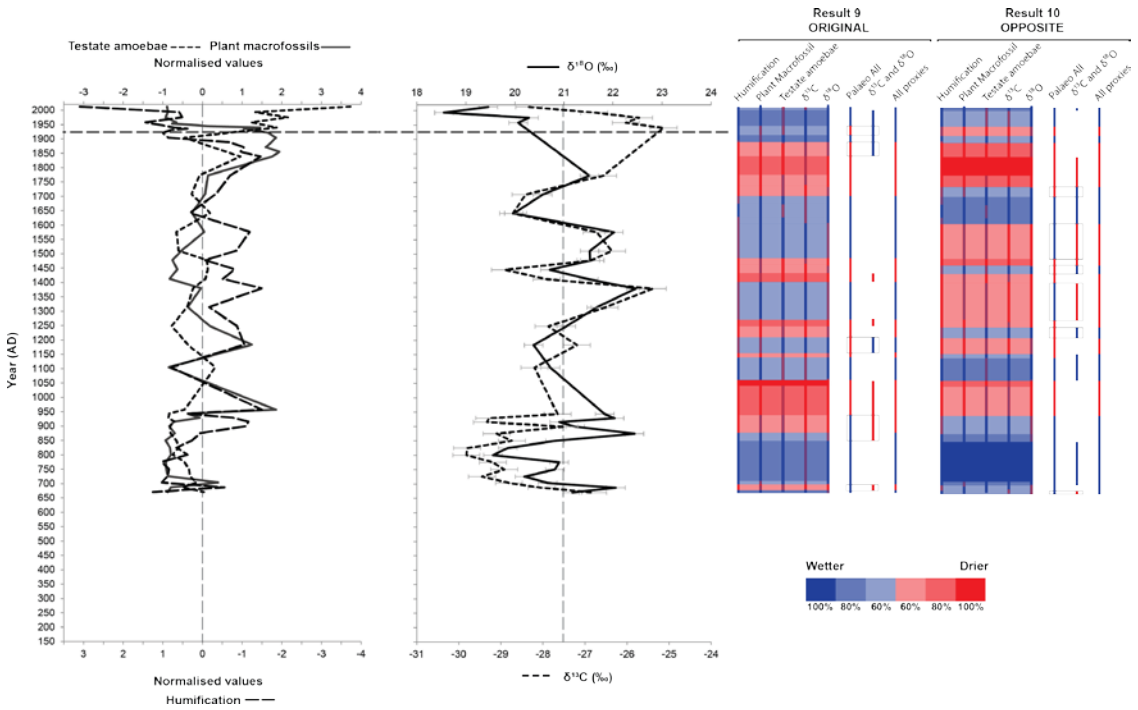

Figure 6.16. All proxy records from KAR-EM-1 plotted against the KAR-EM-2 age profile. Climatic inferences of each record are based on deviation from the mean. Result 9 and 10 relate to the differing interpretation of the stable carbon isotope record. See text for explanation. Dashed line shows the KAR-EM-2 acrotelm-catotelm boundary.

The different options based on differing interpretation in each profile reveal the difficulty of making climatic inferences from such records. Additionally, the absence of more periods in which there is 100% proxy agreement reveals that all proxies rarely reach the same conclusion.

6.5.2 Comparison of scenarios from sections 6.5.2-6.5.4

The different options from figures 6.12 – 6.16 are combined in an intra-site comparison shown in figure 6.17 which displays eight final scenarios. Scenarios 1, 2, 5 and 6 are plotted against the original age profiles and scenarios 3, 4, 7 and 8 are plotted against the KAR-EM-2 age profile to assess whether any of the scenarios resulted in higher agreement in order to make final climatic inferences. A few studies from the region have been chosen for comparison alongside the scenarios in figure 6.17. As discussed throughout chapter 2, consensus on definite climate periods in the region over the last 2000 years has yet to be reached. The timing of the LIA and MCA in the Northern Hemisphere is displayed to assess whether synchronous periods may be evident in SSA. Table 6.3 summarises figure 6.17.

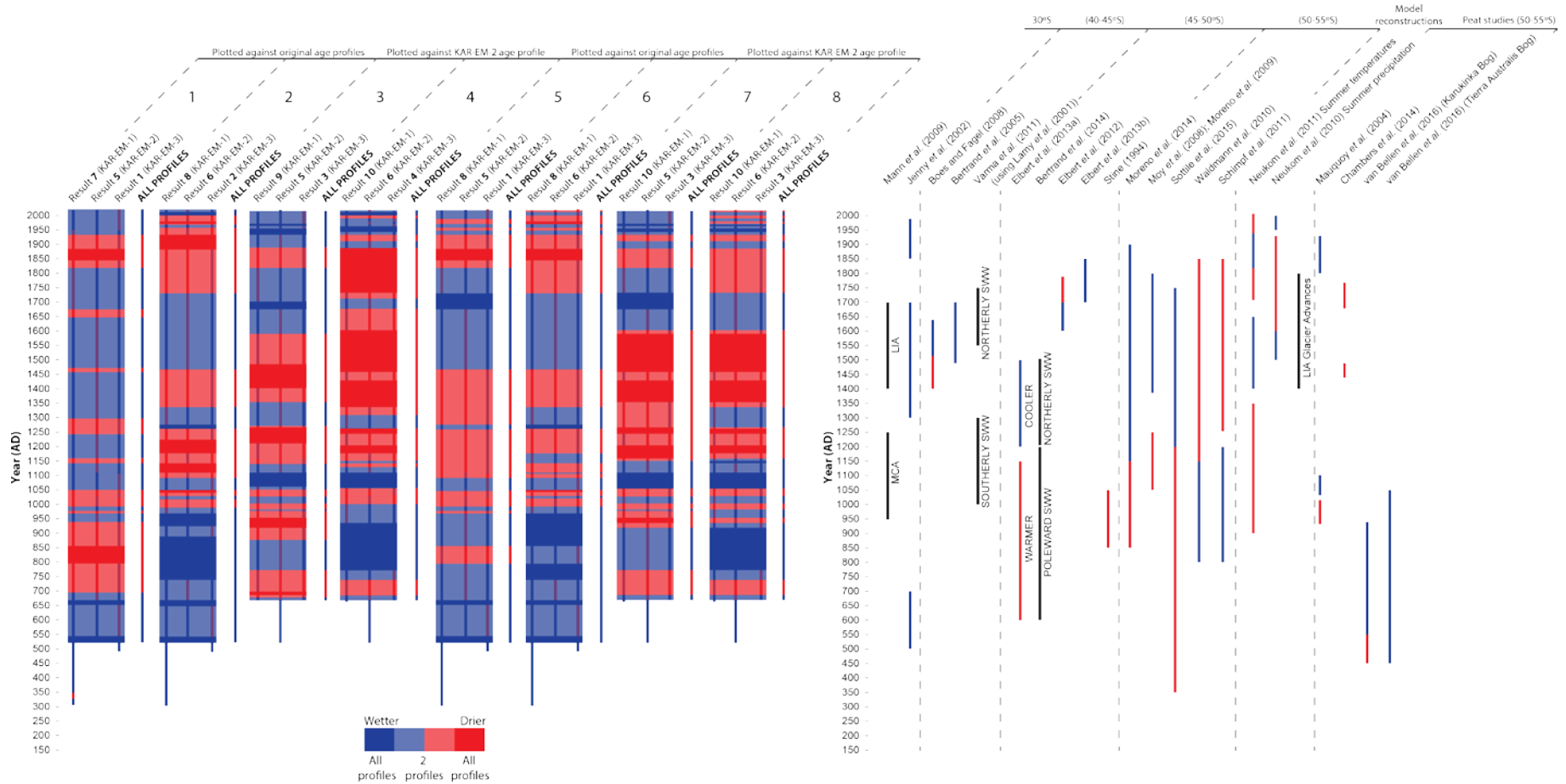

Figure 6.17. Comparison of the climatic inferences from each profile (Result 1-10 in figures 6.12-6.16) and the resulting climatic inferences from agreement between profiles. Displayed alongside the comparison of scenarios is a summary of climatic inferences from other studies in the region.

Table 6.3. A summary of the resulting eight scenarios of climatic inferences which summarises figure 6.17.

	Scenario							
	1	2	3	4	5	6	7	8
Predominant conditions	Wetter (65%)	Wetter (58%)	Wetter (51%)	Drier (60%)	Wetter (57%)	Wetter (48%)	Equal conditions	Equal conditions
Period in which all profiles agree	Wetter (3%) Drier (6%)	Wetter (17%) Drier (10%)	Wetter (8%) Drier (13%)	Wetter (19%) Drier (31%)	Wetter (7%) Drier (2%)	Wetter (15%) Drier (5%)	Wetter (10%) Drier (22%)	Wetter (17%) Drier (17%)
Climatic inference	• AD 700-1050 Drier • AD 1050-1850 Wetter	• AD 1095-1260 Drier • AD 1260-1730 Wetter	• AD 1140-(AD 1270-1350 Wetter) 1590 Drier • AD 1590-1820 Wetter	• AD 750-1130 Wetter • AD 1130-1890 Drier	• AD 960-1460 Drier • AD 1460-1820 Wetter	• AD 990-1460 predominantly dry but variable • AD 1460-1730 Wetter	• AD 1150-1600 Drier • AD 1600-1820 Wetter	• AD 1150-1600 Drier • AD 1600-1740 Wetter • AD 1740-1890 Drier

Scenario 1 has the highest overall agreement with predominantly wetter conditions (65%); however, scenario 4 (which compares Result 10, 6 and 4) has the highest percentage of agreement between all profiles (50%). This scenario assumes that the interpretation of the stable carbon isotope record is opposite to the generally accepted interpretation. Results 10 and 4 from KAR-EM-1 and KAR-EM-3 respectively, are plotted against the KAR-EM-2 age profile suggesting that this chronology may be best used for comparison with regional records. Climatic inferences associated with the MCA and LIA are opposite in direction from these two scenarios with relatively drier and wetter conditions in Scenario 1 (AD 700-1050, AD 1050-1850 respectively) and the opposite in Scenario 4 (AD 750-1130, AD 1130-1890 respectively) with implications for palaeoclimate reconstructions.

Scenario 1 would offer support for a drier MCA and wetter LIA due to a poleward and equatorward shift of the SWW respectively as evidenced in the palaeoclimate reconstructions located at the northerly extent of the modern SWW (Bertrand *et al.*, 2014; Varma *et al.*, 2011). Records from within the core of the modern SWW located to the East of the Andes also show a similar drier MCA and wetter LIA (Sottile *et al.*, 2015). A westerly response to such shifts of the SWW is thought to have resulted in a wetter MCA and drier LIA (Waldmann *et al.*, 2010; Schimpf *et al.*, 2011) which is

also generally found by the palaeoclimate reconstructions from peat studies in the same latitudinal band (Chambers *et al.*, 2014; van Bellen *et al.*, 2016) despite the location of these sites to the East of the Andes. Scenario 4 offers support for this interpretation with a wetter MCA and drier LIA suggested by the higher agreement of profiles during these periods. Within chronological and measurement error which are not accounted for by the summary diagrams differing interpretations and climatic inferences result from the proxy records from Karukinka bog in this investigation.

Owing to its general agreement with other peat studies in the region and generally higher agreement compared with the other scenarios presented, scenario 4 has been chosen for the regional comparison in Discussion II. This scenario plots all records against the KAR-EM-2 age profile and assumes the opposite interpretation of the stable carbon isotope record and is thus presented in figure 6.18 as the final intra-site comparison. Scenario 1 is also displayed and demonstrates the differing climatic inferences that result from various interpretations of the same proxy records.

Despite higher variability in Scenario 4, this overall interpretation is questioned by the validity of each proxy that was assessed in the first half of this chapter. This section has demonstrated how the use of single proxy records may be problematic for climatic interpretation and despite complexity it is more valuable to consider multiple proxies.

In previous studies testate amoeba derived WTD reconstructions have recorded higher variability than plant macrofossil records, suggesting the higher sensitivity of this proxy (McMullen *et al.*, 2004; Blundell and Barber, 2005; Loisel and Garneau, 2010). In this investigation the WTD reconstruction suggests a stable WTD or a complacent signal throughout the majority of the records. During periods where all palaeoecological proxies do not agree it is the WTD reconstruction that is usually opposite to the plant macrofossil and humification records. These two proxies are usually in agreement in this investigation and thus form the majority indicators; however, the validity of these proxies was discussed in the respective sections of this chapter and drawing climatic inferences from them may be inaccurate based on their slow response and potential resistance of *S.magellanicum* to external variability.

Despite modern correlations between the $\delta^{13}C$ values of *Sphagnum* cellulose and WTD (Loisel *et al.*, 2009; Loader *et al.*, 2016; Royles *et al.*, 2016) this proxy is problematic owing to differing interpretations and lack of coherence with other proxy records. This lack of coherence and intra-site replicability suggests that this proxy should not be taken on its own as a palaeoclimate record (Broder *et al.*, 2012) and when compared with other proxies differing interpretations result.

The stable oxygen isotope records showed generally low variation around the mean and could be considered to be relatively climatically insensitive, again suggesting that this proxy should be considered alongside other proxy records.

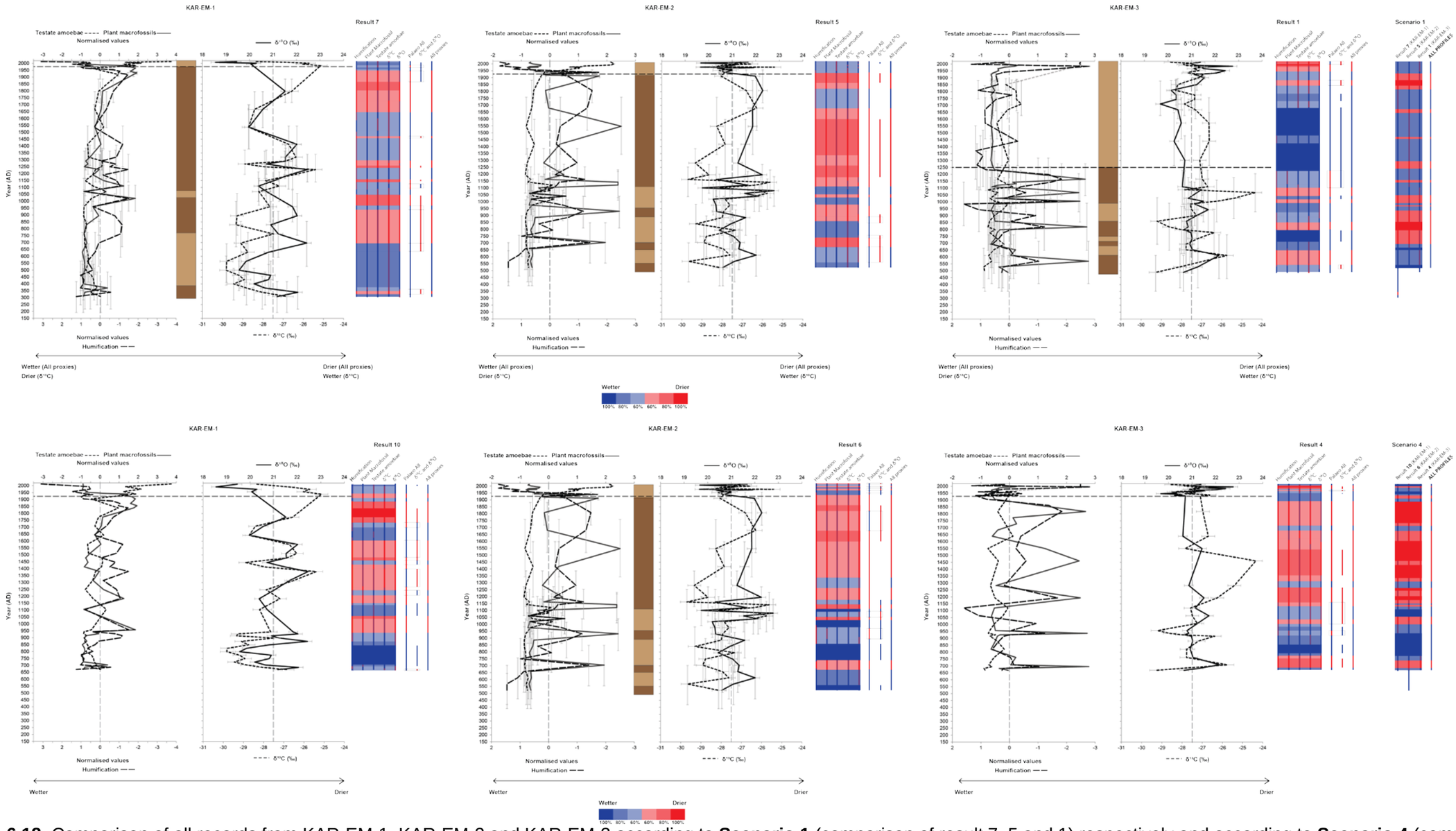

Figure 6.18. Comparison of all records from KAR-EM-1, KAR-EM-2 and KAR-EM-3 according to **Scenario 1** (comparison of result 7, 5 and 1) respectively and according to **Scenario 4** (comparison of result 10, 6 and 4) respectively.

6.6 Conclusions

When based on correlations between the different proxies table 5.27 demonstrated the varying degree of coherence between proxy records in each profile. This directly addressed **Research Question 1** and the correlation between the palaeoecological and stable isotope records. Statistically significant correlations are rarely evident between proxies suggesting that despite the objectivity of correlations a semi-quantitative method of comparison may be more useful. This has been explored throughout Chapter 6 in which deviations from the long-term mean of each proxy record have been interpreted as representing wetter or drier conditions based on the currently understood interpretation of each proxy.

It is clear that significant correlations between multi-proxy and multi-profile records are rarely present. A general lack of coherence both within individual profiles and across profiles based on multiple proxies suggested limited within site-replicability of these records. However, chronological uncertainty led to the plotting of the records against a master chronology which resulted in higher correlation (table 6.1) and increased coherence between records. It was seen that the palaeoecological records display higher agreement than the stable isotope records with the WTD reconstructions displaying higher coherence than the other proxies.

Despite clear noise in the records, general trends can be drawn offering reliable palaeoclimate records from peatlands in the region. Scenario 4 was chosen for regional comparison owing to higher agreement of climatic inferences both across records and with a selection of palaeoclimate records from the region. It has been seen that a number of scenarios of differing climatic inference are the result of differing interpretation and chronological uncertainty surrounding the peatland records from this site. These records will form part of the multi-site aspect of the investigation in the following chapter.

Chapter 7: Discussion II
Inter-site comparison of multi-proxy records

This chapter synthesises the multi-proxy records from the three sites in this investigation, San Juan bog, Karukinka bog, and San Carlos bog (Falkland Islands) (Figure 3.1) and discusses these records in the context of current understanding of regional climate variability over the last 2000 years. Sections 7.1 and 7.2 provide an interpretation of the multi-proxy records from San Juan and San Carlos which forms the basis for Section 7.3 which provides an inter-site comparison of all records. This addresses **Research Question 3: In response to recent and late-Holocene climate variability related to shifts in the SWW, to what degree are there correlations between the records from multiple sites?**

7.1 Interpretation of proxy records: San Juan Bog

Figure 7.1 displays the comparison of the proxy records from San Juan plotted against age. Similar to Karukinka, *Sphagnum magellanicum* dominates the plant macrofossil record and suggests predominantly wet conditions (Lower DHI values) throughout apart from the shift to drier conditions starting ~AD 1820 until the acrotelm-catotelm boundary ~AD 1974 which is characterised by a decrease of *S.magellanicum* and an increase of Ericaceae roots and UOM (Higher DHI values) and lower % light transmission. Drier conditions are also suggested at the beginning of the humification and plant macrofossil records until ~AD 1530. The same problems with interpretation exist surrounding the dominance of a single species in this record and potential climatic complacency. The van Bellen *et al*. (2014) transfer function was used to produce the WTD reconstruction for this site. Values are ~40 cm until AD 1640 reflecting drier conditions, followed by a shift to lower WTD (~10 cm) and wetter conditions until AD 1975, coinciding with the acrotelm-catotelm boundary. This period of lower WTD reflects the dominance of *D.pulex*. Above this, WTD values increase rapidly to 60 cm reflecting the shift to dominance of *A.muscorum* at the surface and suggesting recently drier conditions. As discussed in section 6.1.3, the dominance of this taxon at the surface may reflect increasing UV-B levels since AD 1980 (Appendix IV). Climatic insensitivity or a generally stable WTD

is suggested by this record, lacking in major WTD variability during the last ~600 years represented by the record.

The Suess correction was applied to the stable carbon isotope record above AD 1857 but generally drier conditions remain until the surface. According to the water film theory this proxy suggests predominantly drier conditions throughout (below the mean) apart from wetter periods between AD 1520 to 1625 and AD 1670 to 1765.The stable oxygen isotope record shows switching between relatively drier and wetter conditions throughout. Values are above the mean between AD 1660 and 1885 suggesting predominantly drier conditions during this time.

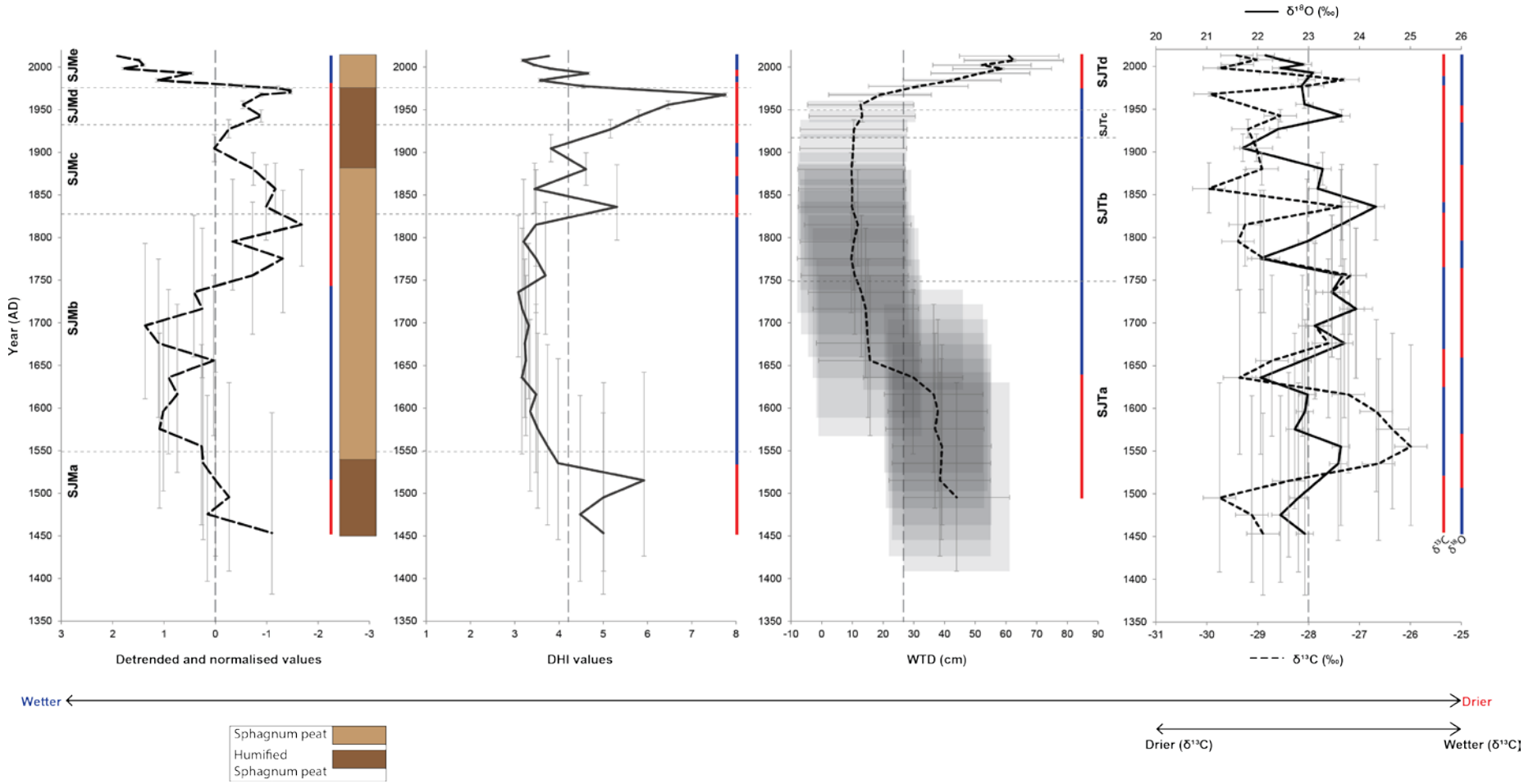

Figure 7.1. Comparison of records from SAN-EM-2 plotted against age. The plant macrofossil and testate amoeba zones are displayed. The chronological error is displayed by the grey bars (95% confidence intervals). The horizontal axis of the humification results is reversed in accordance with the other proxies. Climatic inferences based on deviation from the mean are displayed.

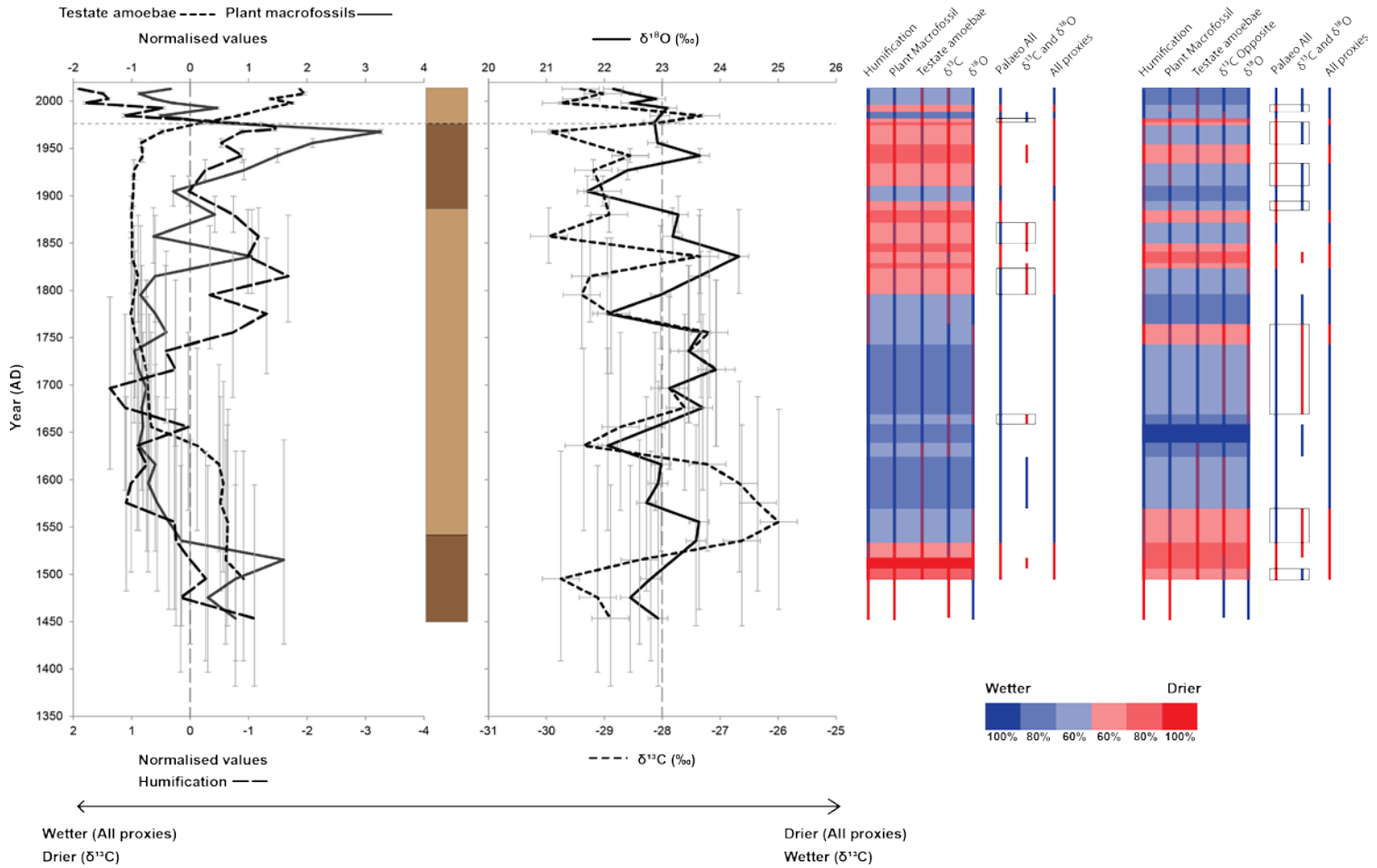

Figure 7.2. Multi-proxy comparison of records from SAN-EM-2 plotted against age. Climatic inferences are based on deviation from the mean with shading related to agreement between proxy records (see key). The boxes on the summary diagrams show periods in which there is agreement between the stable isotope records but disagreement of the two with the palaeoecological records.

Figure 7.2 compares the standardised palaeoecological records with the raw stable isotope records forming the multi-proxy comparison of records from this site. Climatic inferences are shown to the right of the diagram and follow the interpretation of the records as discussed, with the options 'Original' and 'Opposite' relating to agreement in the direction of variability of the stable carbon isotope record. Table 7.1 summarises the climatic inferences.

Table 7.1. Climatic inferences from San Juan with reference to the summary diagram in figure 7.2.

	Original	Opposite
Predominant conditions	Wetter (58%)	Wetter (69%)
Agreement between stable isotope records	33%	72%
Stable isotope records agree but disagree with palaeoecological records (Boxes)	12%	43%
Stable isotope record contribution to majority indicator	$\delta^{18}O$: 22% $\delta^{13}C$: 39%	$\delta^{18}O$: 24% $\delta^{13}C$: 6%
Period in which 100% of proxies agree	Wetter (0%) Drier (2%)	Wetter (4%) Drier (2%)
Climatic inference	• AD 1500-1530 Drier • AD 1530-1800 Wetter • AD 1800-1980 Drier • AD 1980onwards Wetter	• AD 1500-1570 Drier • AD 1570 onwards Wetter with drier intervals

The 'opposite' interpretation has higher overall agreement (69%) and the highest amount of agreement between all proxies (although this is only 4%) and also results in better agreement between the stable isotope records however, there is higher disagreement with the other proxies (shown by the boxes). These records do not extend as far back as the assumed MCA period (AD 950-1250) although both interpretations suggest an early drier period until AD 1530 and AD 1570 respectively. The 'original' interpretation suggests wetter conditions to the surface apart from a period of drier conditions AD 1800 to 1980 whereas the 'opposite' interpretation

suggests wetter conditions to the surface with intervening drier periods. The most likely interpretation in comparison with the other records will be assessed.

7.2 Interpretation of proxy records: San Carlos Bog

Figure 7.3 displays the proxy records plotted against age from San Carlos. According to the extrapolated ages the shift from the absence to presence of *Sphagnum* occurring across the zone boundary to SCMb dates to between AD 1690 (±100yrs) and AD 1710 (±100yrs), but note the large chronological uncertainty surrounding this shift. This may be associated with a fen-bog transition (Hughes *et al*., 2000; Hughes and Barber, 2004) which may have been caused by a shift from drier to wetter conditions around this time creating more favourable conditions for *Sphagnum*. The inter-site comparison will assess a climatic cause. *Sphagnum* is thought to have colonised at this time and persists during stable climatic and hydrological conditions with the establishment of ombrotrophy.

The presence of charcoal (Chapter 5, Figure 5.38) before this transition may suggest human disturbance as the cause of initiation of a *Sphagnum*-dominated peatland. The first English navigator, Captain John Strong, recorded a landing in AD 1690 and the islands were assumed to be uninhabited before this time (Falkland Islands Government, 2012). It is possible that Amerindians from Patagonia visiting the Falkland Islands before this time (Buckland and Edwards, 1998) were responsible for fire on the Islands; however, it is likely to be the result of European arrival.

This is similar in timing to the peak in charcoal flux from a peat sequence from East Falkland Island (Turney *et al*., 2016) however, these charcoal fragments are comparatively small (<106µm compared with macro-charcoal in this investigation) and are thus assumed to have been transported from Patagonia. The authors interpret the increase of micro-charcoal as a strengthening of the SWW ~AD 1500. The presence of charcoal in SCB-1 decreases to absence by ~AD 1770.

Above this boundary, *S.magellanicum* is the dominant *Sphagnum* species and is present throughout until the surface. Dominance of this species begins ~AD 1760 suggesting wetter conditions from this time. *Sphagnum* colonisation may have been allowed by introduction of spores by wind dispersal from SSA (Sundberg and Rydin,

2002; Sundberg, 2005; Whitaker and Edwards, 2010). There is knowledge of valley raised bogs where *Sphagnum* dominates (Otley, *et al*., 2008; Upson, 2012; Fenton, 2014); however, the focus of vegetation surveys has been on vascular flora (Broughton and McAdam, 2002; 2005). Despite this lack of knowledge the Falkland Islands have a peatland cover of 11,408 km^2 constituting ~94% of the land cover (Joosten, 2009). A critical knowledge gap exists surrounding the lower plant and lichen flora of the Falkland Islands (Falklands Conservation, 2012) with the biodiversity strategy aiming to address this gap between 2008 and 2018. Comparison with other sites may allow an understanding of the cause of this shift. A shift to apparently drier conditions (Higher DHI values) occurs between AD 1770 and 1860 with wetter conditions evident until the surface (Lower DHI values). The acrotelm-catotelm boundary may be present ~AD 1980 where there is a decrease of *Sphagnum* and an increase of UOM.

The same transfer function (van Bellen *et al*., 2014) was used to produce the WTD reconstruction for this site as for the other sites. Drier conditions are present at the beginning of the record with WTD ~40 cm until ~AD 1760 reflecting the dominance of *C.platystoma* and other taxa. After this, *D.pulex* rises to dominance and results in a shift of WTD to ~10 cm particularly after AD 1860. An increase of xerophilous taxa results in a rapid increase of WTD after AD 1940 reaching 61 cm at the surface.

The stable carbon isotope record suggests wetter conditions between AD 1710 and 1800 and generally drier conditions from AD 1800 and 1920. Wetter conditions persist until the surface, apart from a drier period between AD 1955 and 1975. The opposite conditions are suggested by the stable oxygen isotope record, in that drier conditions are evident until AD 1800, after which there are generally wetter conditions to the surface, apart from two short drier periods around AD 1920 and AD 1980.

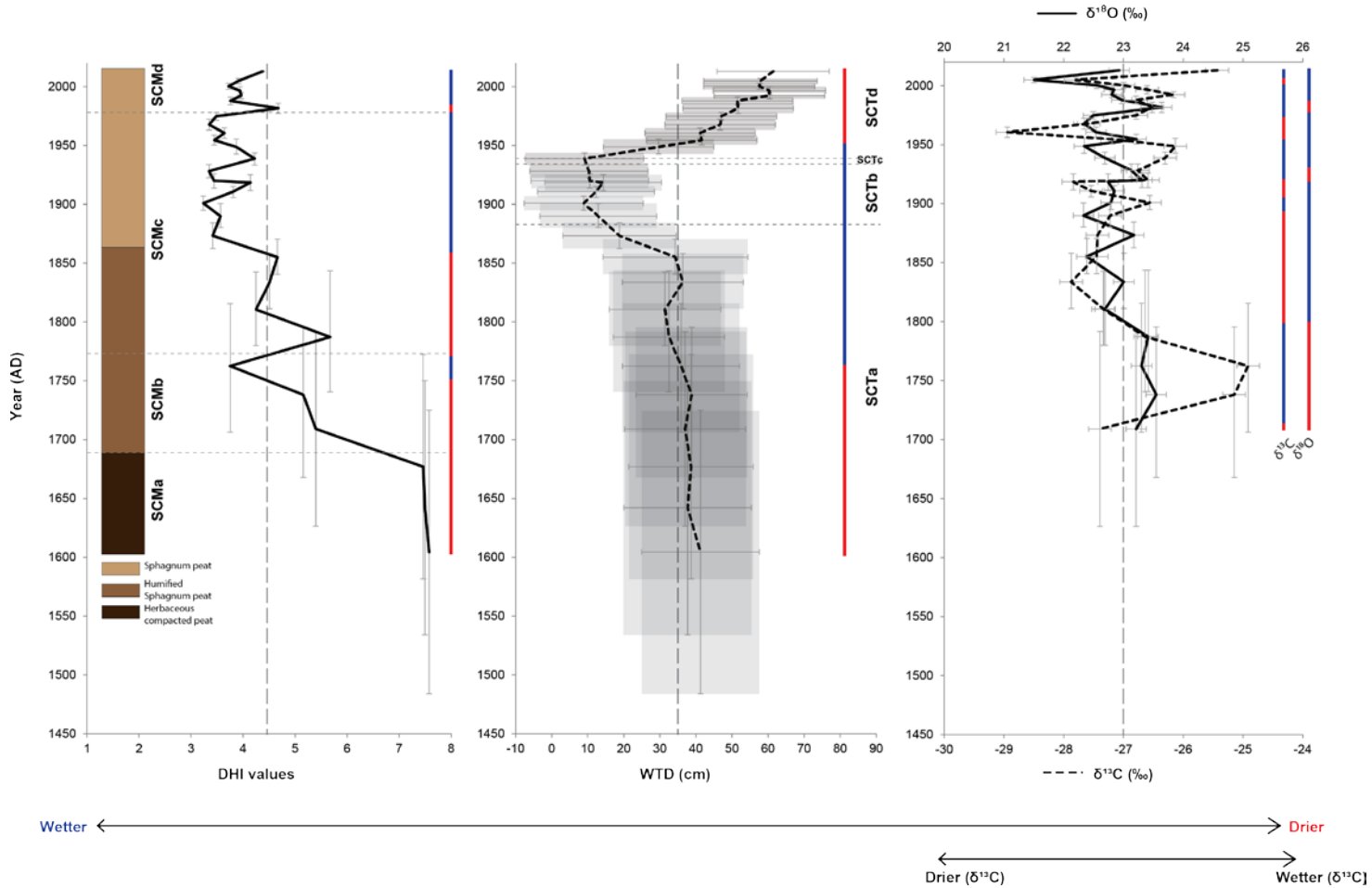

Figure 7.3. Comparison of records from SCB-1 plotted against age. The plant macrofossil and testate amoeba zones are displayed. The chronological error is displayed by the grey bars (95% confidence intervals). Climatic inferences based on deviation from the mean are displayed.

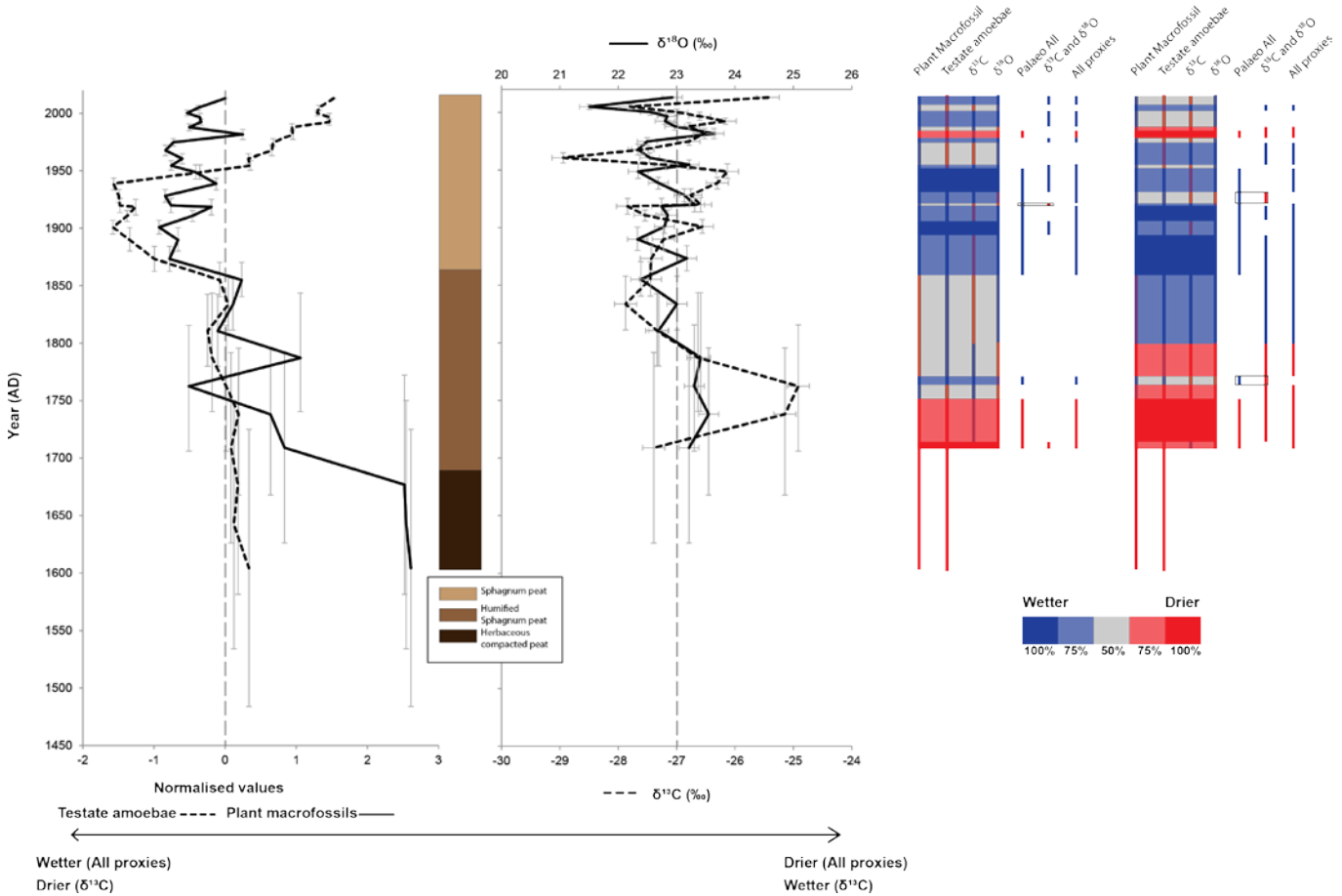

Figure 7.4. Multi-proxy comparison of records from SCB-1 plotted against age. Climatic inferences are based on deviation from the mean with shading related to agreement of more than 2 proxy records (grey shaded areas show where there is no majority agreement). The boxes on the summary diagrams show periods in which there is agreement between the stable isotope records but disagreement of the two with the palaeoecological records.

Figure 7.4 displays the multi-proxy comparison of the SCB-1 records with the climatic inferences summarised in table 7.2.

Table 7.2. Climatic inferences from San Carlos with reference to the summary diagram in figure 7.4.

	Original	Opposite
Predominant conditions	Intermediate (45%)	Wetter (54%)
Agreement between stable isotope records	19%	81%
Stable isotope records agree but disagree with palaeoecological records (Boxes)	2%	15%
Stable isotope record contribution to majority indicator	Periods of no majority indicator…	$\delta^{18}O$: 40% $\delta^{13}C$:0%
Period in which 100% of proxies agree	Wetter (10%) Drier (2%)	Wetter (16%) Drier (14%)
Climatic inference	• Until AD 1750 Drier • AD 1860-1960 Wetter	• Until AD 1800 Drier • AD 1800-1975 Wetter

Only four proxy records are available for this site as humification analysis was not carried out. As a result, there are some periods in which there is no majority inference, where two proxies suggest wetter conditions and two suggest drier conditions; these are noted as intermediate in table 7.2. These periods are marked by grey shading and result in no climatic inferences being made for these durations (see gaps in 'All proxies'). The 'opposite' interpretation has higher overall agreement (54%) with predominantly wetter conditions; the 'original' interpretation does not reach consensus on climatic inferences owing to the dominance of periods in which there is not agreement of more than two proxies. The 'opposite' interpretation also has higher periods where all proxies agree (30%) suggesting that the stable carbon isotope record is better interpreted in this way. Climatic inferences suggest drier conditions until AD 1800 and wetter conditions thereafter until the surface.

7.3 Inter-site comparison of records

This section addresses **Research Question 3** relating to the multi-site aspect of the investigation with a focus on assessing the spatial and temporal coherence between records from the three sites in terms of late-Holocene and more recent variability.

7.3.1 Multi-site comparison of raw values

The proxy records from each site plotted against age presented in figure 7.5 are compared based on the absolute values across the sites. Table 7.3 compares the mean value of each proxy record from each site.

Table 7.3. Comparison of the mean values of each proxy record from all sites. Sites are displayed from left to right, in terms of their location within the precipitation gradients, from wetter to drier location.

	SAN-EM-2	KAR-EM-1	KAR-EM-2	KAR-EM-3	SCB-1
Humification (% light transmission)	53.33%	42.38%	38.39%	49.76%	-
Plant macrofossils (DHI values)	4.14	4.64	4.08	3.90	4.27
Testate amoebae (WTD cm)	27.66 cm	16.65 cm	23.96 cm	24.02 cm	35.61 cm
$\delta^{13}C$ (‰)	-27.56‰	-27.81‰	-27.69‰	-27.36‰	-26.89‰
$\delta^{18}O$ (‰)	22.68‰	20.92‰	21.11‰	21.11‰	22.84‰

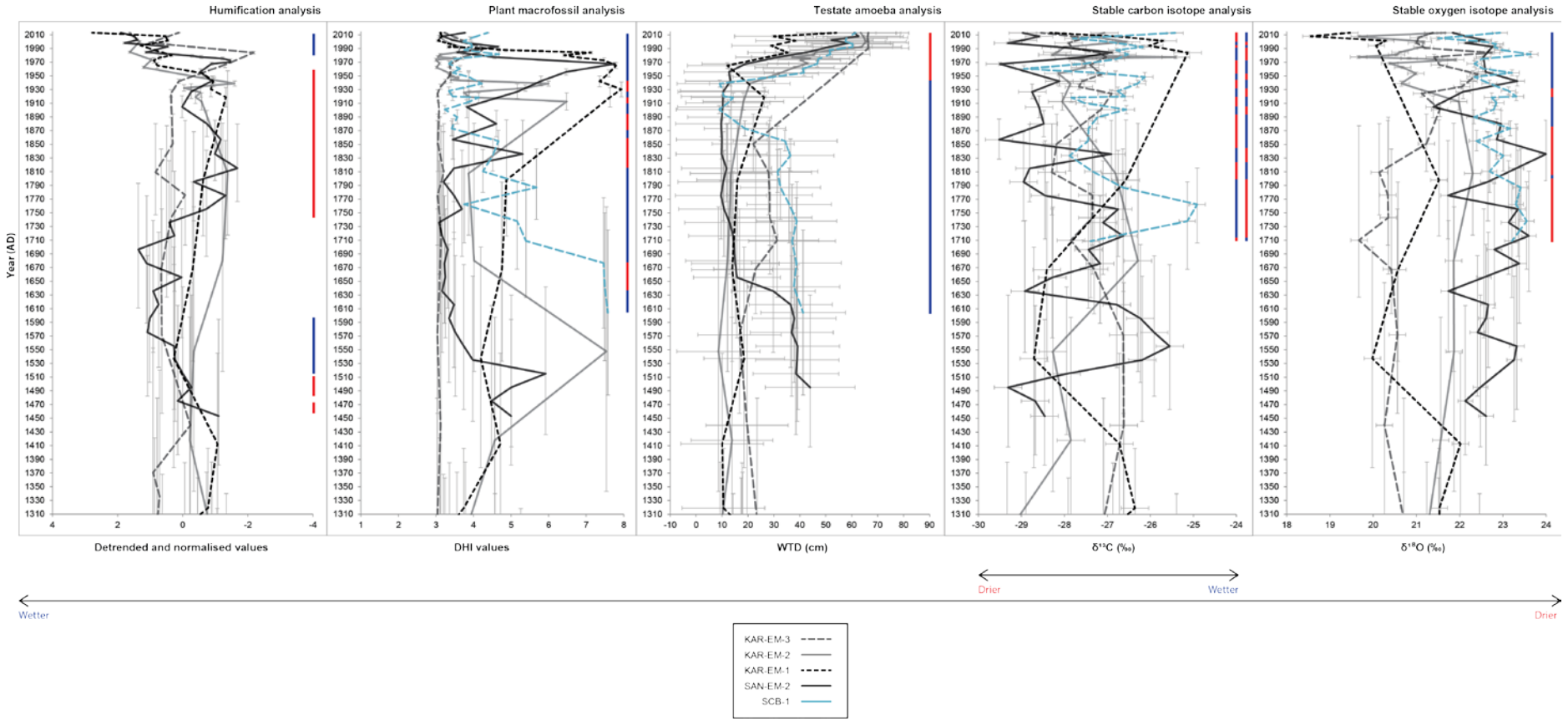

Figure 7.5. Multi-site comparison of absolute values plotted against individual age profiles.

Based on the modern correlation between wind speed and precipitation (Moy *et al*., 2009; Garreaud *et al*., 2013) and the resultant precipitation gradient (Figure 2.2) it would be expected that the records from San Juan would display overall wetter conditions in comparison with those from Karukinka, and the records from San Carlos would be expected to display overall drier conditions. When comparing the mean values of each proxy across all of the sites it can be seen that this is rarely the case.

The percentage light transmission and DHI values are similar across all sites, perhaps related to the dominance of *Sphagnum* throughout each profile. The WTD reconstructions display drier conditions at both San Juan and San Carlos compared with the reconstructions from Karukinka. This may be explained by the overall insensitivity of the Karukinka records. A period of drier conditions is evident in the San Juan record until AD 1630 which was also evident in KAR-EM-1. The mean values of the stable carbon isotope records are also similar; this may suggest that this proxy has not clearly recorded variability in terms of a wetness gradient across the region as expected, an indication of the lack of a clear relationship between $\delta^{13}C$ and WTD. The $\delta^{18}O$ records from San Juan and San Carlos show higher mean values than the records from Karukinka. According to Zanazzi and Mora (2005) and Loader *et al.* (2016) higher values are indicative of generally drier conditions on the microscale (section 6.1.5); however, according to the precipitation gradient an isotopic rainshadow is expected to result in ^{18}O-depleted samples owing to the reduction in moisture of an air mass as it moves across the Andes and across Patagonia (Stern and Blisniuk, 2002; Mayr *et al*., 2007b). Therefore, overall lower values would be expected from the San Carlos $\delta^{18}O$ record. The evidently higher values may suggest that this site is affected by air masses from the Atlantic, relatively ^{18}O enriched in comparison with lower values expected from SWW influences (Mayr *et al.*, 2007b; Agosta *et al.*, 2015). The differences between the $\delta^{18}O$ records evidence expected latitudinal effects (Royles *et al.*, 2016) with higher overall $\delta^{18}O$ values (less ^{18}O depleted samples) from San Juan and San Carlos compared with lower overall $\delta^{18}O$ values (more ^{18}O depleted samples) from Karukinka related to the location of this site at a relatively higher latitude.

General differences between the records are usually attributed to site-specific processes in response to regional climatic differences (Swindles *et al.*, 2012a; Roland *et al.*, 2015). The records also cover differing time periods with the Karukinka records representing a longer term mean than the records from the other two sites. Owing to the shorter time period covered by the records from San Juan and San Carlos, the last 400 years of the palaeoecological records and the last 300 years of the stable isotope records are considered in the climatic inferences drawn from the multi-site comparison. A general incoherence between the records plotted against their individual age profiles is suggested by the lack of significant correlations shown in table 7.4.

The intra-site comparison (Chapter 6) suggested within-site incoherence between all proxy records based on uncertain chronological control but plotting the records against a master chronology (KAR-EM-2) resulted in higher agreement (Table 6.1). Significant correlations (Table 7.4) resulted when the Karukinka records were plotted against the KAR-EM-2 age profile (Figure 7.6) between the WTD reconstructions from KAR-EM-3 and SCB-1 and between the stable oxygen isotope records from KAR-EM-1 and SCB-1. However, it must be noted that these significant correlations are based on only five observations in both cases. Significant correlations are found between the records from San Juan and San Carlos but this is related to similarities in the temporal resolution of records from these sites. Correlations were based on 20-year time periods, when based on 50-year time periods an insufficient number of original observations from San Juan and San Carlos resulted. This emphasises the importance of obtaining records of similar chronological duration in order to draw regional comparisons.

Table 7.4. Inter-site correlations between all proxy records from Karukinka, San Juan and San Carlos based on 20-year bins. r^2 indicates where Pearson's correlation was carried out and r_s indicates where Spearman's rank was carried out (α=0.05). The mean overall correlation for each proxy summarises agreement between records.

All plotted against original age profiles										
	Karukinka vs San Juan				**Karukinka vs San Carlos**				**San Juan vs San Carlos**	
	KAR-EM-3 vs. SAN-EM-2	**KAR-EM-2 vs. SAN-EM-2**	**KAR-EM-1 vs. SAN-EM-2**	**Mean correlation**	**KAR-EM-3 vs. SCB-1**	**KAR-EM-2 vs. SCB-1**	**KAR-EM-1 vs. SCB-1**	**Mean correlation**	**SAN-EM-2 vs. SCB-1**	**Mean overall correlation**
Humification (r^2)	0.322	0.159	0.628	**0.370**	-	-	-	-	-	-
Plant macrofossil (r_s)	0.126	0.033	0.714	**0.291**	-0.382	-0.048	-0.657	**-0.362**	*-0.723	**-0.036**
Testate amoebae (r_s)	0.643	0.476	0.536	**0.552**	0.821	0.679	0.600	**0.700**	*0.787	**0.626**
$\delta^{13}C$ (r^2)	0.270	-0.151	-0.375	**-0.085**	0.353	-0.110	0.578	**0.274**	*0.543	**0.094**
$\delta^{18}O$ (r^2)	0.021	-0.091	0.099	**0.010**	-0.571	0.226	1.00	**0.218**	0.040	**0.089**
Karukinka records plotted against KAR-EM-2 age profile										
	KAR-EM-3 vs. SAN-EM-2	**KAR-EM-2 vs. SAN-EM-2**	**KAR-EM-1 vs. SAN-EM-2**	**Mean correlation**	**KAR-EM-3 vs. SCB-1**	**KAR-EM-2 vs. SCB-1**	**KAR-EM-1 vs. SCB-1**	**Mean correlation**	**SAN-EM-2 vs. SCB-1**	**Mean overall correlation**
Humification (r^2)	0.269	0.159	0.260	**0.229**	-	-	-	-	-	-
Plant macrofossil (r_s)	-0.301	0.033	0.011	**-0.086**	0.285	-0.048	-0.063	**0.058**	*-0.723	**-0.014**
Testate amoebae (r_s)	0.393	0.476	0.155	**0.341**	*1.00	0.679	0.667	**0.673**	*0.787	**0.507**
$\delta^{13}C$ (r^2)	-0.172	-0.151	0.02	**-0.101**	0.310	-0.110	0.381	**0.194**	*0.543	**0.046**
$\delta^{18}O$ (r^2)	0.102	-0.091	-0.032	**-0.007**	0.387	0.226	*0.955	**0.307**	0.040	**0.113**

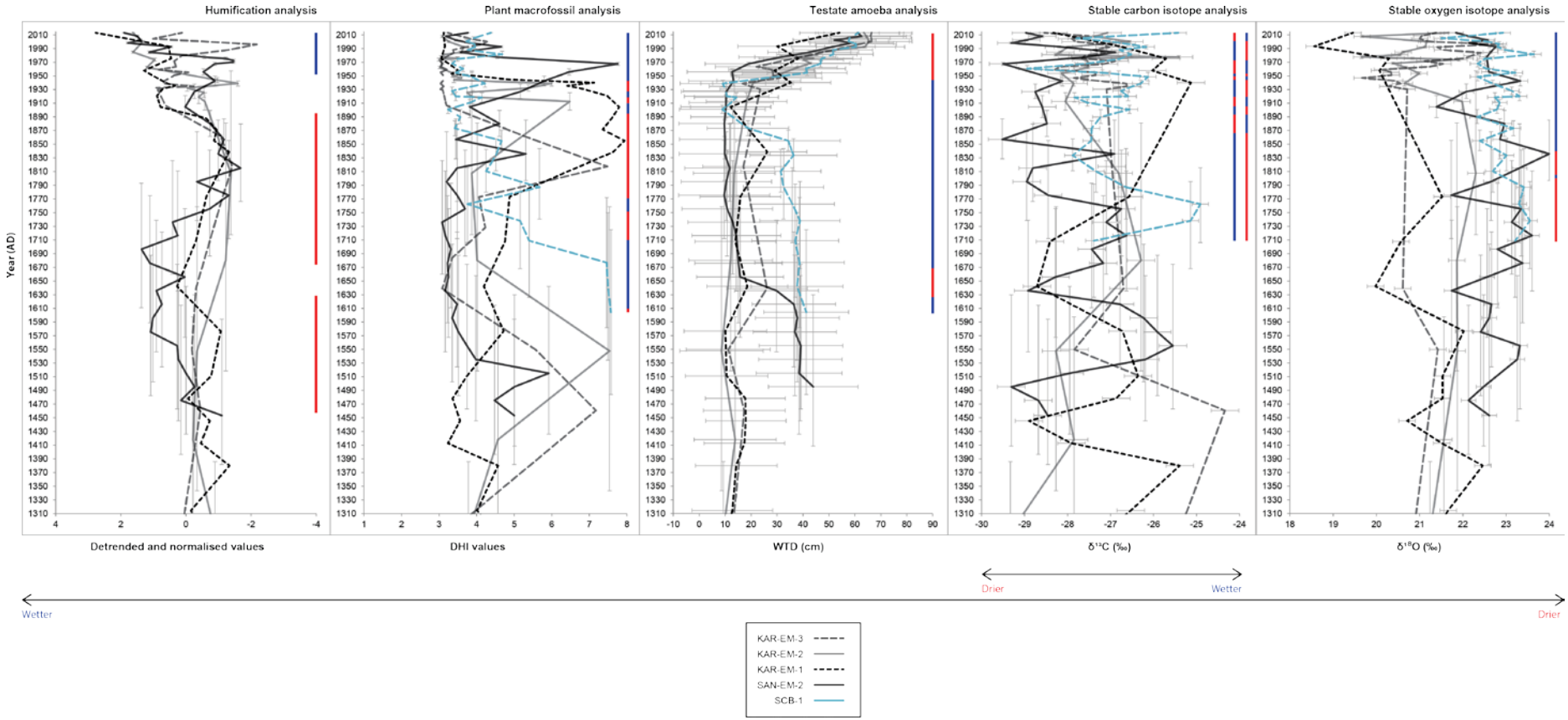

Figure 7.6. Multi-site comparison of absolute values with the Karukinka records plotted against the KAR-EM-2 age profile.

7.3.2 Incoherence between multi-site records

Before comparing the records in this investigation with others from the region it is important to consider the reasons for incoherence between the multi-site records. The difference in temporal resolution seems to be the most probable reason for the lack of correlation between the records from Karukinka with those from the other sites. As Loisel and Garneau (2010) suggest, local conditions at each site will contribute to inter-site differences; however, a regional allogenic driver would result in the similarity of records in terms of low-frequency high-magnitude variability (Daley and Barber, 2012).

The comparison of decomposition rates in peat records from three ombrotrophic bogs in Patagonia suggested that rates were strongly affected by water table level, ash deposition and sea spray input differences between sites (Broder *et al.*, 2012). Differing decomposition rates may impede the comparison of palaeoclimate records from multiple sites with San Juan potentially influenced by sea spray input (Kleinebecker *et al*., 2007; 2008); however, similarities with the Karukinka humification records especially plotted against the KAR-EM-2 age profile suggest this has not resulted in differential decomposition rates. In periods where records do not agree, authors attribute this to differential sensitivities of sites caused by oceanicity or continentality (Langdon and Barber, 2005). Precipitation with variable chloride and sodium ions affects the species composition across the sites (Moore and Bellamy, 1974) with higher concentrations in more oceanic regions. pH differences across the sites result in differences in plant macrofossil and testate amoeba species assemblages. The general dominance of *S.magellanicum* across all sites suggests this has not affected species composition at the sites in this study. This may explain minor differences in the WTD reconstructions between the sites but all records are within measurement error.

Differential productivity across sites may also present problems for multi-site proxy comparison. As well as intra-site differences in productivity and decomposition, *Sphagnum* productivity was found to decrease with latitude (Wieder and Lang, 1983) and temperature decreases (Moore, 1989). Differential productivity is important to consider with regards to the 2° latitudinal difference between Karukinka and San

Juan (~53°S) and San Carlos (51°S). Differential productivity has resulted in the differences in temporal resolution of samples. Another factor for consideration is decreasing growth rates associated with increasing altitude. This factor would suggest that San Juan and San Carlos (8 m.a.s.l) have higher growth rates than Karukinka (228 m.a.s.l.) which was evident in figure 4.20. The location of San Carlos 1200 km to the east of the other sites would suggest a spatially variable response of the records from this site. However, studies in which large spatial and altitudinal differences between sites exist have found synchronous shifts between plant macrofossil (Barber *et al*., 2000) and testate amoeba records (Booth *et al*., 2006).

The shape and size of the individual bogs may also influence the water balance and result in site-specific differences (Mauquoy and Barber, 2002). The sites in this investigation are all ombrotrophic; however, San Juan and San Carlos are relatively smaller sites perhaps explaining the discrepancies between the records from these sites and those from Karukinka. In terms of the precipitation gradient, bogs in areas of higher rainfall have been found to be more hydrologically sensitive (Mauquoy and Barber, 2002). The higher temporal resolution of the records from San Juan, the most westerly located site, suggests higher variability of the plant macrofossil and stable isotope records as compared with the other sites.

Multi-site coherence of testate amoeba inferred WTD variability (e.g. Hendon *et al*., 2001; Booth *et al*., 2006; Loisel and Garneau, 2010; Swindles *et al*., 2012a) is evidence of the sensitivity and reliability of this proxy in recording climate variability supported by the highest overall mean correlation (0.507) (table 7.4).

Differences between records can therefore be summarised as dating inconsistencies on the regional scale and ecohydrological feedbacks, ‘non-climatic’ factors, including slow peat accumulation resulting in climatic insensitivity as well as differential proxy response to regional climatic variability (Swindles *et al*., 2010; 2012a) and methodological errors (Charman *et al.*, 2006).

The low number of observations to allow correlation between records and the dissimilarity in chronological extent makes a quantitative multi-site comparison difficult. Despite this, key trends from the records can be inferred. There seems to be

general similarity between the humification records from Karukinka and San Juan, suggesting drier conditions preceding wetter conditions since ~AD 1950. The plant macrofossil records also suggest wetter conditions since this time following a period of drier conditions from ~AD 1800 in all records but that from San Carlos. There is coherence between the WTD reconstructions with all records displaying a synchronous rise in WTD from ~AD 1930. The stable carbon isotope records show a less clear trend. The stable oxygen isotope records, despite differing mean values, show a general trend to lower values to the surface, apart from in KAR-EM-3 suggesting wetter conditions to present since ~AD 1890.

It has been seen that differences in the absolute values of each proxy are expected across multiple sites (Charman *et al*., 2006). Despite this the standardised records of BSW anomaly are presented in the following section in order to compare general trends in the records to draw regional climatic inferences for comparison with other records from the region.

7.3.3 Multi-site climatic inferences

Tuning and stacking of regional peatland records is one approach to the problems presented by the incoherence of variability as discussed in section 7.3.2. Tuning is now commonly undertaken on single (Sanchez Goñi *et al*., 2002; Itambi *et al*., 2009; Swindles *et al*., 2010) and multi-proxy records (Blundell *et al*., 2008; Bokhorst and Vandenberghe, 2009). The process of tuning and stacking of regional records is fully considered in Blaauw (2012) and is carried out by aligning proxy records based on synchronous events that are matched within measurement and chronological error. Although this process is subjective and is prone to the ‘suck-in effect’ (Baillie, 1981) of potentially unrelated events, it has been successfully used. Alternatively, tuning can be avoided by inferring the timing of variability based on individual proxy records and age profiles.

Some investigations present composite BSW curves by amalgamating standardised multi-site records (Hughes *et al*., 2000; Langdon and Barber, 2005); however, this masks regional variability. This investigation has aimed to consider fully spatio-temporal variability and therefore multi-site tuning and stacking has not been carried out. Moreover, the limited extent of the San Juan and San Carlos records and

differing temporal resolution compared with Karukinka prevents the tuning of these records.

Figure 7.7 displays the proxy records from all sites, with the palaeoecological proxies standardised in order to infer BSW anomalies over time. The summary diagrams alongside the graphs show the climatic inferences, as variability above and below the mean, determined through majority agreement. The Karukinka records plotted against the KAR-EM-2 age profile are shown in figure 7.8 to assess overall agreement compared with that of the records plotted against their individual age profiles. Table 7.5 is an overview of the summary diagrams and displays the resulting climatic inferences.

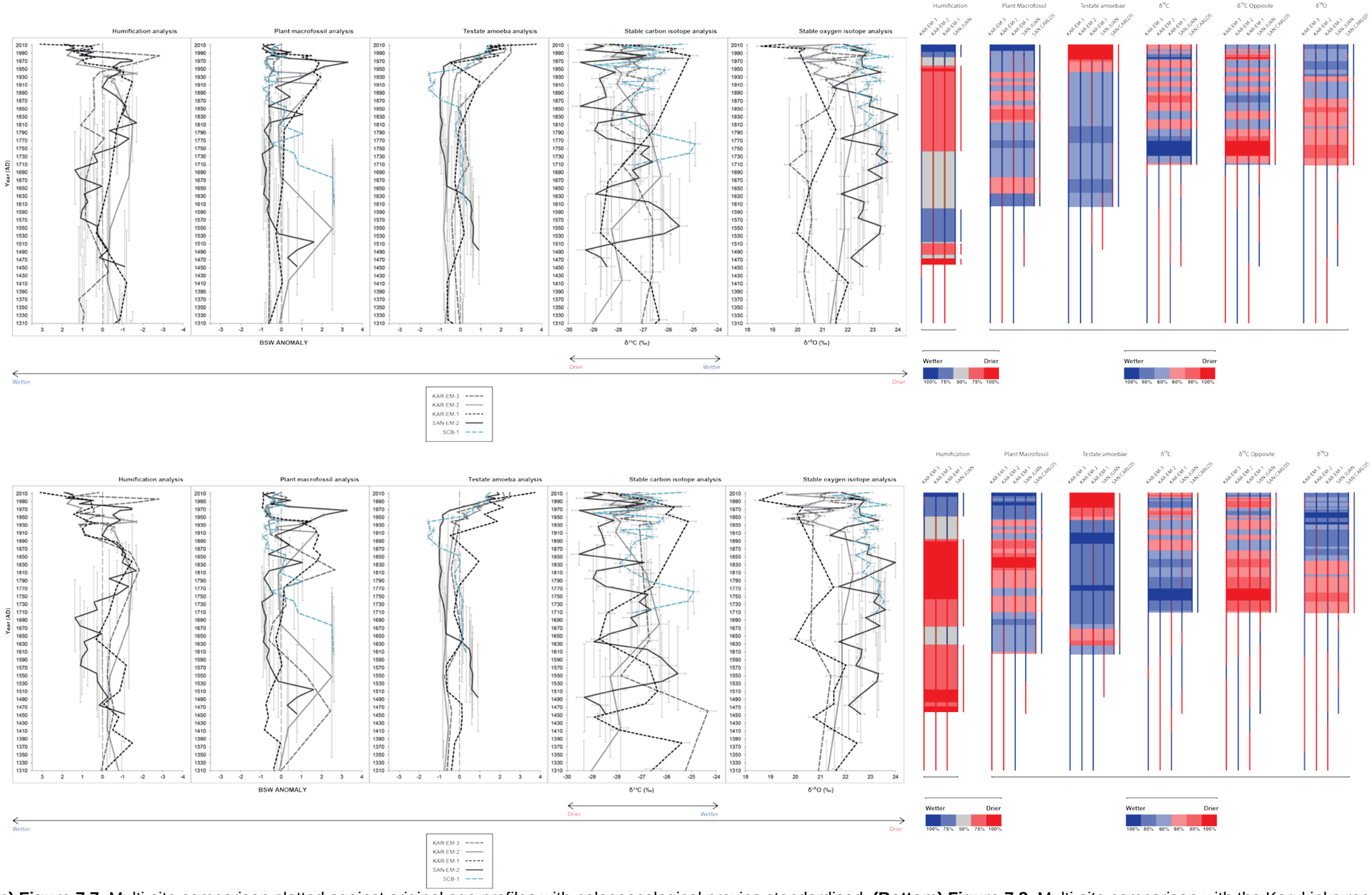

(Top) Figure 7.7. Multi-site comparison plotted against original age profiles with palaeoecological proxies standardised. **(Bottom) Figure 8.** Multi-site comparison with the Karukinka records plotted against KAR-EM-2 age profile with palaeoecological proxies standardised. Summary diagrams show climatic inferences.

Table 7.5. Overview of the summary diagrams and resulting climatic inferences with reference to figures 7.7 and 7.8.

	Plotted against original age profiles (Figure 7.7)					
	Humification	Plant macrofossil	Testate amoebae	$\delta^{13}C$	$\delta^{18}O$	$\delta^{13}C$ (Opposite)
Predominant conditions	Drier (50%)	Wetter (70%)	Wetter (83%)	Wetter (58%)	Drier (59%)	Drier (58%)
Period in which all profiles agree	Wetter (20%) Drier (30%)	Wetter (5%) Drier (0%)	Wetter (0%) Drier (9%)	Wetter (15%) Drier (0%)	Wetter (0%) Drier (0%)	Wetter (0%) Drier (15%)
Climatic inference	• AD 1745-1960 Drier • AD 1980-Present Wetter	• AD 1605-1845 Wetter • AD 1845-1945 Drier • AD 1945-Present Wetter	• AD 1605-1945 Wetter • AD 1945-Present Drier	• AD 1710-1800 Wetter • AD 1800-1975 Drier • AD 1975-1990 Wetter • AD 1990-Present Drier	• AD 1710-1875 Drier • AD 1875-Present Wetter	• AD 1710-1800 Drier • AD 1800-1975 Wetter • AD 1975-1990 Drier • AD 1990-Present Wetter
	Plotted against KAR-EM-2 age profile (Figure 7.8)					
	Humification	Plant macrofossil	Testate amoebae	$\delta^{13}C$	$\delta^{18}O$	$\delta^{13}C$ (Opposite)
Predominant conditions	Drier (71%)	Wetter (53%)	Wetter (74%)	Wetter (87%)	Wetter (58%)	Drier (87%)
Period in which all profiles agree	Wetter (2%) Drier (38%)	Wetter (4%) Drier (7%)	Wetter (12%) Drier (10%)	Wetter (13%) Drier (0%)	Wetter (5%) Drier (0%)	Wetter 0(%) Drier (13%)
Climatic inference	• AD 1675-1895 Drier • AD 1950-Present Wetter	• AD 1605-1710 Wetter • AD 1710-1945 Drier • AD 1945-Present Wetter	• AD 1625-1670 Drier • AD 1670-1945 Wetter • AD 1945-Present Drier	• AD 1710-1865 Wetter • AD 1865-1920 Drier • AD 1920-1955 Wetter • AD 1955-1970 Drier • AD 1970-2000 Wetter • AD 2000-Present Drier	• AD 1710-1840 Drier • AD 1840-Present Wetter	• AD 1710-1865 Drier • AD 1865-1920 Wetter • AD 1920-1955 Drier • AD 1955-1970 Wetter • AD 1970-2000 Drier • AD 2000-Present Wetter

Figure 7.8 has a slightly higher percentage of periods during which all profiles agree as well as generally higher agreement as suggested by the overall higher percentage of predominant conditions (where there is majority agreement). Despite this higher agreement, the overall mean correlations do not display improved multi-site correlation as a result of plotting the Karukinka records against the KAR-EM-2

age profile (table 7.4). Using the majority indicator assumes correct interpretation of variability at each site; for example, atypical records that do not agree with the majority are assumed to be incorrect and may be disregarded (Hughes *et al*., 2006; Daley, 2007); however, it may be the majority indicator that is flawed. This is demonstrated by the lack of correlation between all other proxies but the WTD reconstructions (table 7.4) and the opposite trend to the surface suggested by all other proxies forming the majority inference (wetter) to the WTD reconstruction (drier).

The majority inference is shown in figure 7.9 which compares the overall climatic inferences of each multi-site proxy comparison from the summary diagrams in figures 7.7 and 7.8. Assuming the majority indicator may be erroneous, regional variability of the multi-site records may be masked. There are four scenarios which are summarised in table 7.6.

Table 7.6. Summary of the four scenarios presented in figure 7.9 a comparison of the climatic inferences from figures 7.7 and 7.8.

	1	2	3	4
Predominant conditions	Wetter (52%)	Drier (55%)	Drier (59%)	Drier (67%)
Period in which all profiles agree	Wetter (0%) Drier (0%)	Wetter (0%) Drier (0%)	Wetter (0%) Drier (0%)	Wetter (0%) Drier (0%)
Climatic inference	• AD 1740-1805 Wetter • AD 1805-1960 Drier • AD 1980 onwards Wetter	• AD 1740-1860 Drier • AD 1860-1920 Wetter • AD 1920-1955 Drier • AD 1980 onwards Wetter	• AD 1710-1895 Drier • AD 1950 onwards Wetter	• AD 1710-1895 Drier • AD 1950 onwards Wetter

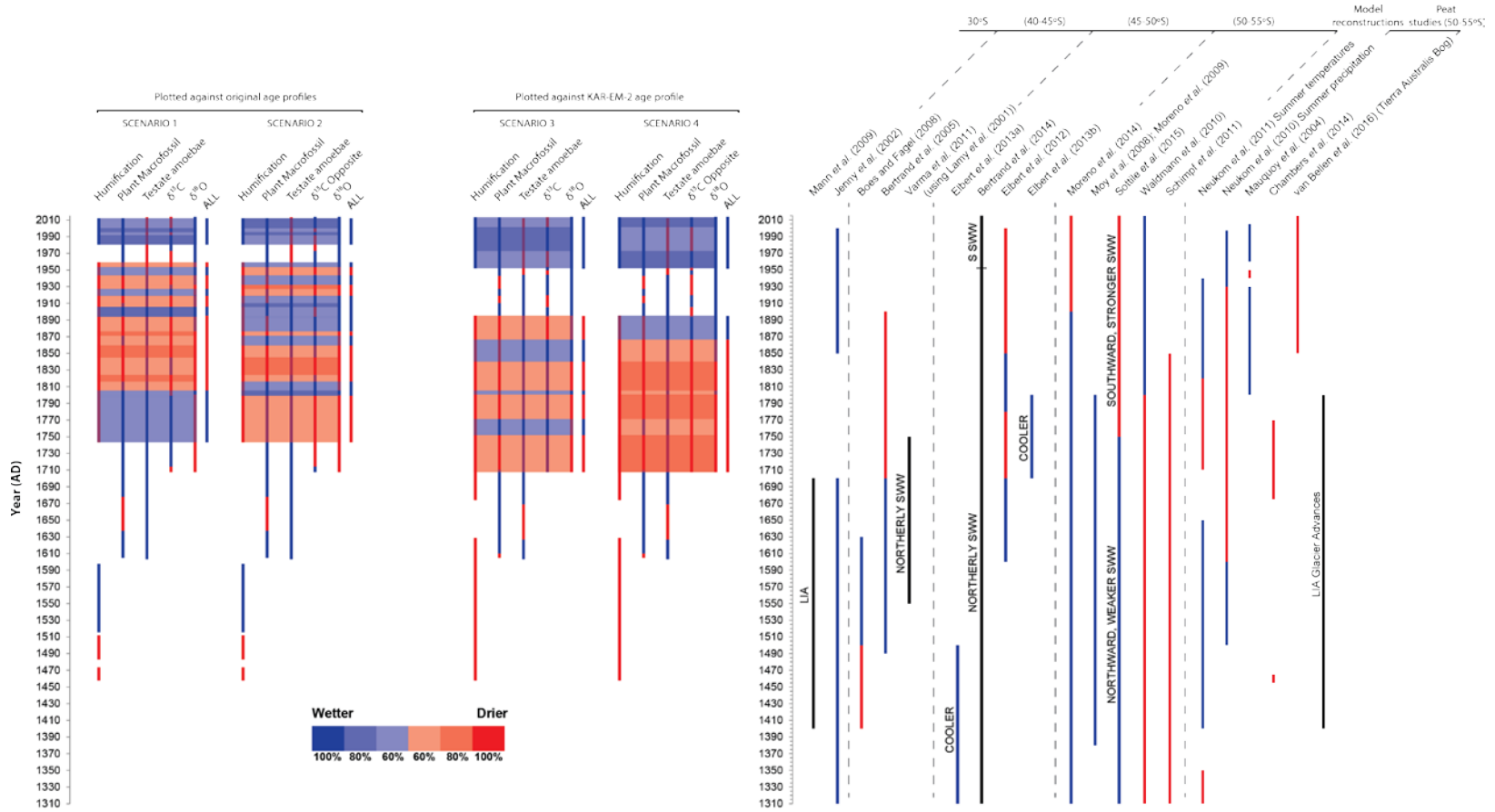

Figure 7.9. Four scenarios resulting from the comparison of the majority climatic inferences displayed in figures 7.7 (Scenario 1&2) & 7.8 (Scenario 3&4). The inferences from key palaeoclimate investigations are displayed for comparison.

Although none of the scenarios results in periods in which all inferences agree the scenario with overall highest agreement is scenario 4, which assumes the opposite interpretation of the stable carbon isotope records and plots the Karukinka profiles against the KAR-EM-2 age profile. This scenario suggests drier conditions until AD 1900 and wetter conditions from AD 1950 onwards. Despite regional variability being masked the following section compares recent trends over the last 300 years as inferred from the multi-site comparison with other records from the region.

7.3.4 Recent (from AD 1700-present)

This section compares the scenarios presented in the previous section with climate inferences from observational, reanalysis and palaeoclimate data.

An increase in the positive phase of the SAM since 1957 (Marshall, 2003; Jones *et al*., 2009; Wilmes *et al*., 2012) associated with an observed shift and intensification of the mean annual latitude of the SWW (Thompson and Solomon, 2002; Marshall, 2003; Garreaud *et al.*, 2009; Villalba *et al*., 2012) since this time has resulted in increased wind speeds between 55 and 70°S and decreased wind speeds between 35 and 55°S (Garreaud *et al.*, 2013) and resultant heterogeneity of precipitation variability (Aravena and Luckman, 2009). The latest IPCC report states that with medium confidence the positive SAM trend is anomalous within the last 400 years (Masson-Delmotte *et al*., 2013). An increase of precipitation as analysed from the Punta Arenas instrumental data (Daley *et al*., 2012) has been observed. Comparison of palaeoclimate records with instrumental data to corroborate recent trends relies on high temporal resolution of the palaeoclimate records (Charman *et al*., 2004), preferably to annual resolution. The palaeoclimate records in this investigation are at a decadal resolution preventing direct comparison with instrumental records. Moreover, the limited extent of the instrumental data to AD 1970 inhibits useful comparison of recent trends.

All scenarios presented in figure 7.9 suggest recently wetter conditions, consistent with the observed SWW shift and slight increases in precipitation at this latitude (Daley *et al*., 2012). In the model reconstruction of summer precipitation from the region (Neukom *et al.*, 2010) a slight shift to wetter conditions is evident from AD 1930; however, this ignores any spatial patterns associated with the Andes divide.

Wetter conditions to present from ~AD 1800 (Chambers *et al*., 2014) and AD 1960 (following a brief drier period) (Mauquoy *et al*., 2004) are also suggested by the dominance of *S.magellanicum* at Valle de Andorra. This would indicate a westerly response to a southerly shift of the SWW.

Despite this, the proxy with the highest correlations both based on the intra- and inter-site comparison, the testate amoeba inferred WTD reconstruction, suggests drier conditions to present, opposing expected wetter conditions from a southerly shifted SWW and a potential easterly response. Appendix V displays the interpolated temperature and precipitation records for the 0.5º grid cells in which the three sites are located (Harris *et al.*, 2014). The precipitation record suggests decreased precipitation from ~AD 1990 to present, although the paucity of data from nearby meteorological stations means such inferences are questionable.

As discussed in section 2.1.3 and 6.1.3, the recent drying trend suggested by the WTD reconstructions, also evident in the testate amoeba records from San Juan and San Carlos is thought to be linked to Antarctic stratospheric ozone depletion (van Bellen *et al.*, 2016). The increase of xerophilous species in the testate amoeba record from San Carlos, not only *A.muscorum* as with the other records, suggests that the WTD reconstructions from the three sites are recording a regional shift to drier conditions rather than a UV-B signal.

A UV-B increase would be expected to result in higher numbers of testate amoebae to the surface (Searles *et al*. 1999; Robson *et al*., 2005) however, in light of the test concentration data, an increase is not evident in any of the records (see testate amoeba diagrams). A recent dry shift in all WTD records which begins ~AD 1850 (although not well constrained) was also found in van Bellen *et al.* (2016).

In terms of agreement on the regional scale between sites, the WTD reconstructions seem to offer the most valid palaeoclimate reconstruction. Moreover, this proxy is based on actual values that are related to modern depth to water table relationships. The timing of the shift in this investigation is consistent across all sites and occurs after AD 1930. If this dating is correct, it precedes observed increases of UV-B

radiation, supporting a climatic explanation which may have been exacerbated by either direct or indirect effects of stratospheric ozone depletion.

There has been much focus on the major climate periods in terms of the MCA and LIA in existing palaeoclimate studies from SSA. As the multi-site comparison only extends 300 years, this may not encompass the whole of the assumed LIA period in the context of longer term variability.

In the absence of major climate periods in the last 300 years, apart from recent variability associated with the southerly shift of the SWW, it is difficult to compare the multi-site comparison with other records in the region. With reference to figure 7.9 which compares climate inferences with those of this investigation; of interest is the period of drier conditions in Chambers *et al*. (2014) between AD 1675 and 1770. Despite a lack of correlation between the stable carbon isotope records across the sites, there is a period of agreement centred on AD 1750 (figure 7.8) where wetter conditions are suggested by less negative $\delta^{13}C$ values across all sites. According to scenario 1 a period of wetter conditions dominates until AD 1800 whereas scenario 4 suggests drier conditions which persisted until ~AD 1860.

This drier period is also evident in the model reconstruction of summer precipitation (Neukom *et al.*, 2010) from AD 1600 until 1930 (relative to 1931-1995). The stalagmite Yttrium content record (Schimpf *et al*., 2011) demonstrates similarly drier conditions until AD 1850 as well as the iron content record from Lago Fagnano displaying drier conditions until AD 1800 (Waldmann *et al*., 2010). Drier conditions around this time are associated with a northerly SWW (Schimpf *et al*., 2011; Varma *et al*., 2011; Bertrand *et al*., 2014). Conversely, a northerly SWW is associated with wetter conditions at Lago Cipreses and Lago Guanaco (both 51ºS) around this time (Moreno *et al*., 2014; Moy *et al*., 2008; Moreno *et al*., 2009). In the synthesis of palaeoclimate records located to the east of the Andes wetter conditions are also evident until AD 1750 (Sottile *et al*., 2015).

The spatial variability evident in this period across the region suggests differing responses to the same event. Spatial variability across the sites in this investigation would therefore be expected and despite higher agreement suggested by scenario 4,

using the majority indicator from these scenarios is incorrect based on such spatial variability. However, in consideration of the last 300 years it seems that the most significant trends across the sites are those associated with a southerly shift of the SWW of which strong evidence in palaeoclimate records has been found both at the northerly limit of SWW influence (Bertrand *et al*., 2014) and in the modern core (Mauquoy *et al*., 2004). Although the humification and plant macrofossil records suggest wetter conditions to present, the WTD reconstructions suggest drier conditions from ~AD 1930. Drying preceding the acrotelm-catotelm boundary in the Karukinka and San Juan humification and plant macrofossil records may be synchronous with the WTD shift. Following this, undecomposed *Sphagnum* dominating to the surface, resulting in higher % transmission values and low DHI values in the acrotelm zone may not be indicative of wetter conditions. The stable isotope records do not confirm or refute the surface trend but it is likely that the dominant signal has been recent drying as a result of a southerly shift of the SWW. This is consistent with increased relative humidity to the west of the Andes and a decrease to the east since AD 1961 (Daley *et al*., 2012).

There is strong evidence that the southerly shift of the SWW is related to anthropogenic forcing as discussed in section 2.1.4, particularly in relation to GHG accumulation and Antarctic stratospheric ozone depletion (e.g. Marshall *et al*., 2004; Polvani *et al*., 2011). Anthropogenic forcing has exacerbated natural forcing (Moreno *et al*., 2014; Abram *et al*., 2013). This is supported by the recent model results of Berman *et al*. (2016), which suggest that insolation changes between the mid-Holocene and the pre-industrial period followed by anthropogenic forcing (GHG concentration) during the last 100 years have resulted in a decreased SLP gradient in the southeast Pacific. Polvani *et al*. (2011) found that the strongest forcing in the second half of the 20th century was due to stratospheric ozone depletion. This has also been found more recently (Swart and Fyfe, 2012; Gonzalez *et al*., 2014). This pattern of shifting to drier conditions ~AD 1930 followed by a more rapid shift to drier conditions ~AD 1960 supports the notion of anthropogenic forcing overtaking natural forcing in recent decades. The shift to a more positive SAM is present in other Southern Hemisphere locations (Nicholls, 2010; Cai *et al*., 2012; Manatsa *et al*., 2013; Purich *et al*., 2013; Cai *et al.*, 2014). Such a shift in the records is clear evidence of increasing global anthropogenic impact around this time, which is now

proposed to form a new geological epoch 'The Anthropocene' (Lewis and Maslin, 2015) starting ~AD 1950 and defined by the onset of nuclear bomb testing.

This section has addressed **Research Question 3** by synthesising the records from the multi-site comparison and assessing agreement between records based on matching periods of similar inferred variability. It has been seen that using the majority inference in this way masks spatial variability making it difficult to assess the likely final climate inferences over the last 300 years for comparison with other records from the region. Despite the potential advantage of a higher number of sites (Langdon and Barber, 2005), an additional two sites in this investigation to form a regional reconstruction has resulted in increased interpretative complexity.

It is probable that San Carlos has been influenced by air masses other than those associated with the SWW as suggested by differences between the $\delta^{18}O$ records, and its location 1200 km east of the other sites has complicated the regional signal. All records only extend to ~AD 1700 and the San Juan record only extends to AD 1450 which does not allow for consideration of long-term trends, despite this it has been possible to assess recent variability across all sites. This is confounded by consideration of proxies from the acrotelm zone, complicating climate inferences especially from humification and plant macrofossil records. As Charman *et al*. (2006) emphasised, records from closely distributed sites of similar chronological control are essential for the compilation of records. Despite the use of the same proxy records across sites, unanticipated differences in the chronological extent of the records has prevented a coherent regional picture of late-Holocene trends from the multi-site aspect of this investigation.

7.3.5 Late-Holocene SWW variability (AD 500-present)

The focus of the final section will be on the presence of the assumed MCA and LIA periods in the Karukinka records owing to the longer extent of these records. Problems associated with the acrotelm-catotelm division are avoided by considering the proxy records in the catotelm zone. As discussed in chapter 6, scenario 4 was chosen for the regional comparison owing to the highest coherence between the interpreted records. Despite higher agreement based on this interpretation in

comparison with the other proxies it is clear that there is no physical mechanism by which the stable carbon isotope records could be interpreted in the opposite manner to the commonly assumed interpretation (Loisel *et al.*, 2009). This 'opposite' interpretation was based on agreement between the stable isotope records in Section 5.1.4.5 which assumed that these proxies are controlled by the same mechanism (and were thus interpreted in agreement with the stable oxygen isotope record). However, the stable oxygen isotope records may have been incorrectly interpreted based on the interpretation of Northern Hemisphere records (See figure 7.12). As well as interpretative difficulties, the limitation of using the stable isotope records from this site is suggested by generally poor intra-site replicability and a lack of correlation between these records (table 7.4). Conversely, owing to the higher correlations between the palaeoecological records these may be used more reliably for the final regional comparison.

From the palaeoecological records, within the chronological error of the KAR-EM-2 age profile, two distinct periods can be inferred which are contemporaneous with climate periods found in other records. With reference to figure 7.10, an earlier **MCA** period seems to occur between **AD 750 and 1100** of generally wetter conditions followed by an **LIA** period of drier conditions between **AD 1100 and 1900**, as initially discussed in chapter 6. Figure 7.11 and Table 7.7 summarise these climate periods and associated shifts of the SWW. This assumes that the records from Karukinka are recording a westerly response to assumed SWW shifts. The response to the recent southerly shift of the SWW seems to be in the opposite direction with drier conditions to present which may suggest an alteration of the response to SWW shifts in recent decades.

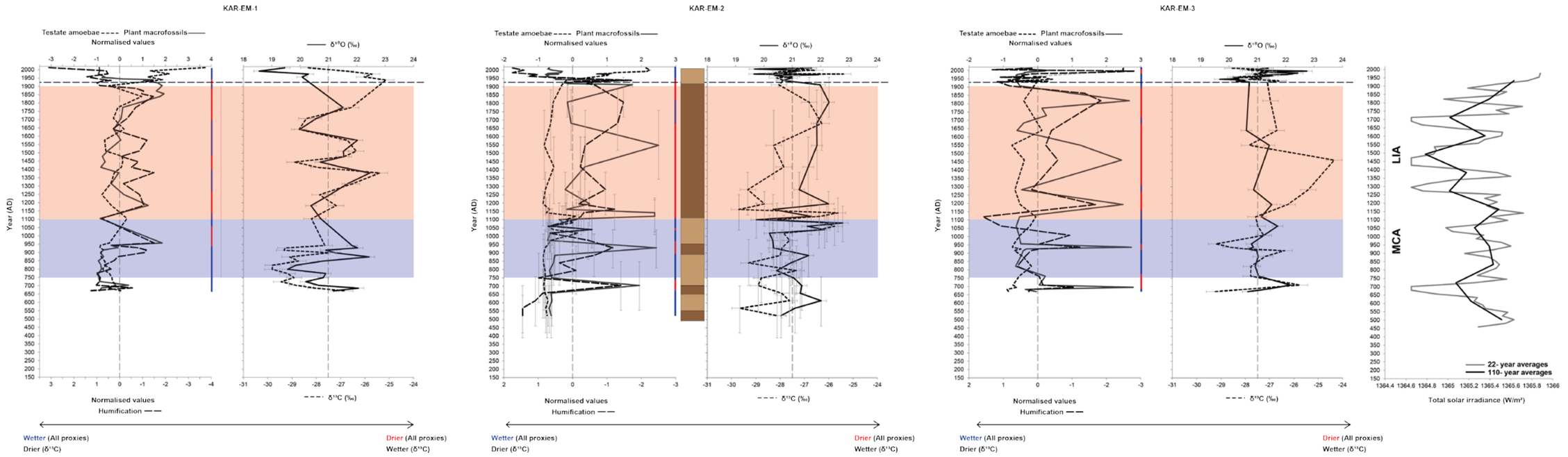

Figure 7.10. The final records from Karukinka plotted against the KAR-EM-2 age profile. Based on coherence between the palaeoecological proxies two periods were identified which broadly coincide with assumed shifts of the SWW during the MCA and LIA as inferred from other palaeoclimate records (table 7.7). The TSI data from Steinhilber et al. (2012) is displayed alongside the records to show the relatively higher (lower) solar irradiance during the MCA (LIA). Data plotted as difference from AD 1986 minimum (1365.67 w/m^2).

Figure 7.11. Graphical summary of Section 7.3.5. Displaying the records from Karukinka bog (centre) and the TSI records (**Steinhilber *et al.*, 2012**). **a)** Summer temperature reconstruction for SSA **(Neukom *et al.*, 2011)**. **b)** Fe/Al precipitation seasonality record from Quitralco Fjord (**Bertrand *et al.*, 2014**). **c)** Water balance index from Peninsula Avellaneda peatland pollen record (**Echeverria *et al.*, 2014**). **d)** Non-arboreal pollen record from Lago Cipreses (**Moreno *et al.*, 2014**). **e)** Synthesis of easterly located records (**Sottile *et al.*, 2015**). **f)** Charcoal record from Canopus Hill peatland record (**Turney *et al.*, 2016**). **g)** Yttrium content Stalagmite record from Marcelo Arevalo cave (**Schimpf *et al.*, 2011**). **h)** Testate amoeba inferred WTD record from Tierra Australis bog (**van Bellen *et al.*, 2016**). **i)** Iron content record from Lago Fagnano (**Waldmann et al., 2010**) (g,h,i graphs edited from van Bellen et al., 2016). **j)** Plant macrofossil and humification records from valle de Andorra bog (**Chambers *et al.*, 2014**). **k)** West Antarctic ice core dust flux record (**Koffman *et al.*, 2014**). Inferred SWW shifts are displayed on each graph.

Table 7.7. Summary table of assumed shifts of the SWW in the MCA and LIA. See Figure 7.11 for graphical summary.

Latitude		Figure 7.11	Timing of MCA	Direction of SWW/Inferred conditions	Timing of LIA	Direction of SWW/Inferred conditions
20-55°S	Neukom *et al*. (2011)	A		Warmer summer temperatures		Cooler summer temperatures
46°S	Bertrand *et al*. (2014)	B	< AD 1200	Strengthened (poleward)	AD 1200-1500	weakening (equatorward)
50°S	Echeverría *et al*. (2014)	C	AD 500-1500	Strengthened SWW	~AD 1400-1900	Weaker SWW
51°S	Moreno *et al*. (2014)	D	AD 900-1200	dry/warm phase positive phases of the SAM (S SWW)	AD 1200-1900	wet/cold phase negative SAM phase (N SWW)
Easterly records	Sottile *et al*. (2015)	E	AD 350-1200	S SWW	AD 1200-1750	N SWW
52°S	Turney *et al*. (2016) Falkland Islands	F	Until AD 950	Stronger SWW		
53°S	Schimpf *et al*. (2011)	G	AD 750-1250	Wetter (S SWW)	AD 1250 – 1850	relatively drier (N SWW)
Karukinka 53°S	This investigation		AD 750-1100	Wetter due to southerly SWW	AD 1100-1890	Drier due to northerly SWW
53-55°S	van Bellen *et al*. (2016)	H	AD 550-1050	Wetter		
54°S	Strother *et al*. (2015) S. Georgia	-	AD 280-1240	Warmer (weaker SWW)	AD 1240	Cooler (Associated with stronger SWW)
54°S	Waldmann *et al*. (2010)	I	AD 850-1150	Wetter S SWW	AD 1150-1850	Drier N SWW
55°S	Chambers *et al.* (2014)	J			AD 1675–1770	Drier conditions N SWW
79°S	Koffman *et al*. (2014)	K	AD 1050-1400	Southerly displaced and strengthened SWW	~AD 1430 - late 20th century	Equatorward

A period of decreased precipitation seasonality, as inferred from the Fe/Al record from Quitralco Fjord (46°S) between AD 1200 and 1500, in timing with the LIA, suggests a weakened SWW at this time (Bertrand *et al*., 2014). The mechanism for this shift from the record at 46°S is related to lower SSTs in the southeast Pacific. This is due to weakening of the Hadley cell and strengthening of the polar cell causing a northerly shift of the SWW in response to temperature gradients. This is thought to be driven by solar forcing resulting in lower Antarctic air temperatures and sea-ice expansion, as opposed to a tropical forcing mechanism (as argued by Sun *et al*., 2013). Cooler temperatures over the Antarctic Peninsula are inferred from an ice core deuterium excess record between AD 1410 and 1460 (Abram *et al*., 2013). The LIA period is also characterised by glacier advances during a period of weakened SWW between the 15th and 19th centuries (Glasser *et al.*, 2004; Masiokas *et al.*, 2009). The results from a peat record from Peninsula Avellaneda (50°S) also suggest SWW weakening associated with the LIA between AD 1400 and 1900 (Echeverría *et al*., 2014). Both studies find a preceding period representative of the MCA associated with a stronger SWW.

A record from Lago Cipreses (51°S) also supports a southerly SWW associated with a positive SAM between AD 900 and 1200 followed by a northerly SWW associated with a negative SAM until AD 1900 (Moreno *et al*., 2014). The forcing of these shifts was attributed to three potentially interlinked mechanisms; Hadley cell expansion (Previdi and Liepert, 2007), solar variability (Bond *et al*., 2001) or a SWW-SO (Southern Oscillation)-AMOC (Atlantic Meridional Overturning Circulation) link (Marini *et al*., 2011). A synthesis of records located to the east of the Andean divide also finds evidence of a southerly shifted SWW between AD 350 and 1200 and a northerly shifted SWW between AD 1200 and 1750 (Sottile *et al*., 2015) with most records displaying drier MCA and wetter LIA conditions, respectively, in contrast to westerly located records. For example, the stalagmite record from Marcelo Arevalo as investigated by Schimpf *et al*. (2011) suggested wetter conditions owing to a southerly shifted SWW between AD 750 and 1250 and drier conditions due to a northerly expansion of the SWW between AD 1250 and 1850 at this site supporting the generally assumed directional SWW shifts across the region.

A peat record from Canopus Hill, Falkland Islands finds a stronger SWW until AD 950 (Turney *et al*., 2016). During this time there is evidence of periodicity in the record (200-250 yrs) inferred from charcoal inputs which becomes less important over the last millennium, perhaps suggesting less influence of the SWW during this time at this site. Strother *et al*., (2015) in contrast to the majority of studies suggest that cooling during the LIA is associated with a stronger SWW indicated by increased long-distance transport of pollen in a record from Fan Lake, South Georgia with the authors concluding that the forcing mechanism behind this remains to be understood. The difficulty of using records from the sub-Antarctic islands to infer SWW shifts is perhaps demonstrated.

The peat records display wetter conditions between AD 550 and 1050 (Tierra Australis) (van Bellen *et al*., 2016) and drier periods at AD 1460 and AD 1675 to 1770 (Valle de Andorra) (Chambers *et al*., 2014) contemporaneous with the MCA and LIA. Consistent with the majority regional inference the iron content record from Lago Fagnano (54°S) suggests wetter MCA conditions AD 850 to 1150 and drier LIA conditions AD 1150 to 1850 a westerly response to a southerly and northerly shifted SWW respectively (Waldmann *et al*., 2010). Reconstructed temperatures from the region suggest warmer summer temperatures between AD 900 and 1350 and cooler summer temperatures between AD 1400 and 1650 (Neukom *et al*., 2011) associated with the southerly and northerly shift of the SWW. Finally, the West Antarctic ice core dust flux record (79°S) also suggests a southerly displaced and strengthened SWW in the MCA between AD 1050 and 1400 and a northerly and weakened SWW in the LIA between AD 1430 – late 20th century (Koffman *et al*., 2014).

Given the strong evidence of the direction of shifts of the SWW as discussed, with a southerly shifted SWW during the MCA and northerly shifted SWW during the LIA, it is likely that the records from Karukinka have responded to such variability. This site location was chosen because of its assumed sensitivity in terms of correlation between zonal wind speed and precipitation (Figure 2.2b), which forms the basis for palaeoclimate reconstructions aiming to infer SWW strength and location from precipitation reconstruction, despite this relationship remaining unclear based on the resolution displayed (figure 2.2b).

It was initially hypothesised based on its location on the leeward side of the Andes with relatively lower precipitation (Figure 2.2a) that southerly shifts and intensification of the SWW had resulted in lower precipitation to the East of the Andes (easterly response) due to a rainshadow effect of higher precipitation to the West of the Andes (westerly response).

Recent variability is consistent with this hypothesis in that the current conditions at the site are suggested by its location in an area of relatively lower precipitation (recent drying in response to a southerly shift of SWW). However, if this relationship had persisted over time an easterly response would be expected during the MCA (drier) and LIA (wetter). A late-Holocene westerly response was evident in the records with a wetter MCA and drier LIA and on closer inspection a positive correlation between zonal wind speed and precipitation is apparent (yellow shading) (figure 2.2b). The effects of these shifts of the SWW, as inferred from the palaeoecological records, on the stable oxygen isotope records from Karukinka, are reassessed in figure 7.12; the interpretation of this proxy assuming a rainshadow effect was not fully considered.

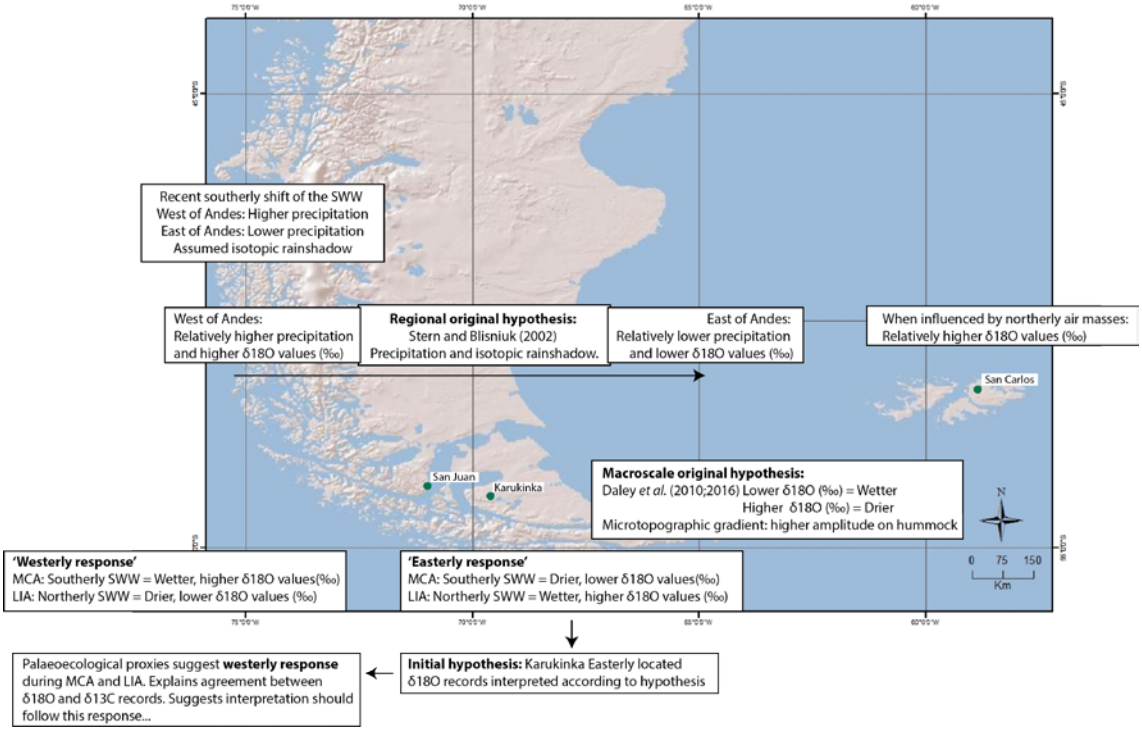

Figure 7.12. Conceptual model of the effect of shifts of the SWW on the sites in this investigation.

Anthropogenic forcing has evidently complicated the relationship between zonal wind speed and precipitation at this site. Owing to agreement with the majority of records in the direction of late-Holocene SWW shifts the forcing of such shifts is considered in the next section.

7.3.6 Late-Holocene forcing mechanisms

According to the results of this investigation, the first hypothesis proposed in section 2.2.7, that synchronous late-Holocene natural climate variability has occurred in the Northern and Southern Hemispheres as a result of solar variability, is highly likely. The timing of major climate periods is generally around AD 1000 to 1400 (MCA) and AD 1400 to 1850 (LIA) (Jansen *et al*., 2007; Mann *et al*., 2009). The mechanisms linking solar activity and volcanic forcing with late-Holocene SWW variability have recently been considered (Abram *et al*., 2014; Koffman *et al*., 2014) but remain to be understood. Many studies now incorporate palaeoclimate and reanalysis data, investigating the mechanisms via complex climate models.

The link between BSW variability and solar irradiance has been investigated from Northern Hemisphere peatland records (Mauquoy *et al*., 2004; Hughes *et al*., 2006; Swindles *et al*., 2010). Wetter conditions were evident in these records whilst lower temperatures are thought to have decreased NPP (Charman *et al*., 2013) during the LIA. The LIA was the coldest multi-centennial period in the last 2000 years and resulted from solar minima and volcanic eruptions (Gao *et al*., 2008; Wanner *et al*., 2015).

The final BSW records of this investigation are compared with TSI data (Steinhilber *et al*., 2012) in figure 7.10. These data show a period of relatively higher TSI between AD 500 and 1100 in comparison with relatively lower TSI between AD 1100 and 1800, generally coincident with the wetter and drier periods associated with the MCA and LIA in the Karukinka records. Similarly, Varma *et al*. (2010) in comparison of solar activity (100-year averaged ^{10}Be) with precipitation inferred SWW shifts (figure 2.20), relate higher solar activity with a southerly shift of the SWW AD 750 and 1250 and lower solar activity with a northerly shift of the SWW from AD 1250. Turney *et al*. (2016) linked variability in SWW strength with ^{14}C and ^{10}Be production and found evidence of a 200-250 year periodicity in their record related to the

deVries solar cycle (Leventer *et al*., 1996). Despite generally wetter conditions in the earlier part of the Karukinka records assumed to represent the MCA period there is evidence of drier peaks roughly 250 years apart which may relate to this solar cycle

Focusing on the MCA, Diaz *et al*. (2011) assess external (solar irradiance, volcanism and atmospheric turbidity) and internal variability (ocean-atmosphere interactions) as causal mechanisms of this climate period. The mean surface temperature difference between the MCA and LIA indicates a cool tropical Pacific during the MCA suggesting the dominance of La Niña-like conditions (Mann *et al*., 2009). Globally, surface warming during this period is generally found in response to increased solar irradiance; however, regional differences would have resulted from internal variability. Warmer summer temperatures are found over SSA during this period (Mann *et al*., 2009; Neukom *et al*., 2011). The 'top-down' mechanism is understood as stratospheric warming from increased solar irradiance which alters atmospheric circulation (Diaz *et al*., 2011). A 'bottom-up' mechanism is thought to act alongside this with increased solar irradiance heating the sea surface affecting ocean-atmosphere interactions (Meehl *et al*., 2009).

Chambers *et al*. (2014) attributed dry periods of the LIA to solar minima (Spörer and Maunder) which caused a reduction of Hadley cell circulation resulting in a northward expansion of the SWW. This supports the hypothesised in-phase interhemispheric coupling via atmospheric teleconnections between the Northern and Southern Hemispheres. Evidence of a globally synchronous cooling due to a solar downturn at 2800 cal BP supports the notion of in-phase interhemispheric climate variability with the forcing sustained via ocean-atmosphere feedbacks (van Geel *et al*., 2002; Renssen *et al*., 2006). The Pages 2k (2013) continental-scale temperature reconstructions; however, do not suggest globally synchronous temperature intervals during the MCA or LIA; however, it is clear that the records in that investigation are responding to solar and volcanic forcing (as summarised in figure 4 of Pages 2k, 2013) with drier conditions evident during the LIA period. Moreno *et al*. (2014), in comparison of their SAM reconstruction with Northern Hemisphere records, find common trends during the MCA and LIA between the hemispheres suggesting that it is likely, within chronological error, that these climate periods were globally synchronous.

The ITCZ is thought to have shifted southward due to cooling in the NH during the LIA (Haug *et al*., 2001); however, this would have caused a southerly shift of the SWW, opposite to the assumed northerly shift of the SWW at this time. This assumed tropical Pacific mechanism (Sun *et al*., 2013; Ding *et al*., 2014) is explained in Schneider *et al*. (2012) with the Pacific-South American Pattern (PSA) (Irving and Simmonds, 2016) the mechanism by which ENSO is propagated to the southern high latitudes. Through this mechanism, correspondence between ENSO (Yan *et al*., 2011) and SWW reconstructions in Koffman *et al*. (2014) offers strong support for a tropical Pacific forcing.

Opposing this is the forcing of the northerly shift of the SWW during the LIA through weakening of the Hadley cell and strengthening of the polar cell in response to solar forcing (Bertrand *et al*., 2014). As opposed to a tropical forcing mechanism, it is thought that lower Antarctic air temperatures and sea-ice expansion strengthened the polar cell resulting in lower SSTs in the southeast Pacific (Lamy *et al*., 2010), congruent with temperature gradients necessary for a northerly shift of the SWW.

Increasing evidence of solar forcing of climate variability offers support for globally synchronous climate periods with regards to the MCA and LIA. Although the exact mechanisms are still not fully understood a general increase in palaeoclimate data, especially from the Southern Hemisphere, for climate modelling will continue to elucidate the causes of these climate anomalies.

7.4 Conclusions

The first sections of this chapter summarised the interpretation of the San Juan and San Carlos records before comparing the records to form the multi-site aspect of the investigation. The raw values were first compared to demonstrate the regional differences in absolute values based on each proxy displaying the associated measurement errors. The WTD reconstruction suggested that conditions at San Carlos bog have been relatively drier than at the other sites, while the $\delta^{18}O$ records suggest that this site has been influenced by other air masses.

There was a lack of correlation across all sites which was not improved when the Karukinka records were plotted against the KAR-EM-2 age profile. The reasons for multi-site disagreement were explored but general trends have been inferred and the standardised records were compared with potential climatic inferences made for the last 300 years which the multi-site records encompass. The testate amoeba inferred WTD reconstructions recorded a shift to drier conditions in recent decades in response to a southerly shift of the SWW.

Regional-scale reconstructions now require a greater number of peatland sites from across the region both in terms of the precipitation gradient and latitudinal influence of the SWW. Ensuring similar chronological extent of the records is paramount for consideration of spatio-temporal variability.

Despite the interpretative difficulties of the Karukinka records, as discussed in Chapter 6, general trends over the last 1500 years were inferred from the palaeoecological proxies (humification, plant macrofossil and testate amoeba) in relation to the MCA and LIA. These periods are suggested to have occurred from AD 750 to 1100 and AD 1100 to 1890 respectively as inferred from relatively wetter and drier periods in the Karukinka records. In comparison with other records from the region there is strong evidence that these periods are broadly in keeping with a southerly and northerly shift respectively of the SWW during the MCA and LIA caused by solar variability.

Chapter 8: Conclusions

8.1 Aim and research questions

The aim of this investigation was *to* ***test the late-Holocene climate signal from ombrotrophic bogs in southernmost Chile and the Falkland Islands using a multi-proxy, multi-profile and multi-site approach.***

The following research questions were considered throughout the investigation:

1. **To what extent are there correlations between multiple proxies and multiple profiles from an ombrotrophic bog, Karukinka, in southernmost Chile?**

   Correlations were evident between the multi-proxy records within each profile from Karukinka, with the highest number of statistically significant correlations evident in the low-hummock profile, KAR-EM-1. Higher intra-site replicability of the palaeoecological records was evident after the chronological uncertainty surrounding KAR-EM-3 was addressed, a synchronous acrotelm-catotelm boundary was assumed and the records were plotted against the KAR-EM-2 ages. The highest intra-site coherence was found between the testate amoeba inferred WTD reconstructions. The stable isotope records displayed a general lack of intra-site replicability. An alternative approach to intra-site correlation was carried out based on agreement of variability above and below the mean value between the different records. This semi-quantitative approach resulted in a range of different climatic inferences based on eight scenarios. One scenario was chosen for the regional comparison addressed by Research Question 3.

2. **To what extent are there correlations between multiple proxies from San Juan bog, Chile and from San Carlos bog, Falkland Islands?**

   A lack of statistically significant correlations was evident between the multi-proxy records between San Juan and San Carlos bog. These records were

limited in duration in comparison with the records from Karukinka; however, they formed part of the inter-site comparison addressed by Research Question 3.

3. **Provided that these records have responded to recent (late 20th century) and late-Holocene (Medieval Climate Anomaly and Little Ice Age) climate variability related to shifts in the SWW, to what degree are there correlations between records from the multiple sites?**

   The comparison of records from all sites revealed a lack of significant correlations, partly owing to differences in the temporal resolution of samples. Owing to the limited duration of the San Carlos record, the last 300 years of variability were considered for inter-site comparison. The highest inter-site coherence between records was found between the testate amoeba inferred WTD reconstructions. A shift to drier conditions across all records after AD 1930 is assumed to be related to a southerly shift of the SWW, consistent with anthropogenic climate forcing. In comparison with other palaeoclimate records from the region the palaeoecological records from Karukinka were used to infer climate related variability of the SWW over the last 1500 years. Wetter conditions are suggested to have occurred during a MCA period (AD 750-1100) related to a southerly shift of the SWW, with drier conditions suggested during a LIA period (~AD 1100-1900) associated with a northerly shift of the SWW. Anthropogenic climate forcing, via stratospheric ozone depletion, seems to have altered the signal of SWW-related climate variability at this site. A continued understanding of the spatial heterogeneity of SWW influences in the region is paramount in consideration of future effects of ozone hole recovery and increasing GHG accumulation on SWW strength.

Addressing the above research questions has supported the use of ombrotrophic bogs from SSA in inferring both recent and late-Holocene climate variability related to shifts in the SWW. Despite a lack of significant correlations on the intra-site basis the semi-quantitative approach has enabled SWW related climate variability to be inferred from the palaeoecological records from Karukinka. The inter-site approach only enabled consideration of the last 300 years of climate variability, nonetheless,

the three sites recorded a surface drying trend related to a southerly shift of the SWW.

8.2 Weaknesses in the methodology

The lack of significant correlations both on an intra- and inter-site basis led to the use of a semi-quantitative approach to assess intra-site coherence. This approach did not take in to consideration chronological uncertainty or the magnitude of variability and was only based on fluctuation above or below the long-term mean. Discrete variability may have been masked in the individual profiles by taking the majority climatic indicator; however, it suggested evidence of an allogenic driver by indicating likely regional scale variability. The differences in chronological duration of the cores from the three sites prevented a more extensive assessment of regional climate on an inter-site basis, with only the last 300 years of variability considered. As a result the records from only one site, Karukinka, were used to assess longer term late-Holocene climate variability. Interpretation of the stable isotope records relied on current understanding from similar Northern Hemisphere peatland investigations although interpretation of such records in SSA is evidently complicated by the Andes climate barrier. The stable isotope records showed a general lack of coherence with the palaeoecological proxies and on an intra-site basis. A better understanding of the mechanisms influencing these proxies is required in the region.

8.3 Suggestions for future research

More high-resolution late-Holocene studies have been published since the initiation of this research which has aided comparison on the regional scale; however, there is still a lack of high-resolution climate data from across the Southern Hemisphere. Peatland palaeoclimate records in the region are far from providing quantitative inputs for palaeoclimate modelling; however, the following recommendations may further advance this area. Calibration studies from across the modern microtopographic gradient are required to understand better the relationship between the $\delta^{13}C$ and $\delta^{18}O$ composition of *Sphagnum* cellulose and WTD/BSW in the region. Further to this, studies from across the regional isotopic gradient would also lead to a better understanding of the influence of SWW shifts on the $\delta^{18}O$ composition of precipitation and *Sphagnum* cellulose. A transect of peatland study sites both across the precipitation gradient and across the meridional extent of SWW influence would

allow for improved regional comparisons. Ensuring records are of similar chronological extent and temporal resolution is paramount.

Additionally, the discovery of the *Sphagnum*-dominated San Carlos bog has opened up the opportunity to investigate the arrival of Europeans to the Falkland Islands. Despite chronological control of the surface layers of the profile from this site via ^{210}Pb dating, only one ^{14}C date was obtained on this section of the profile. Further work could be carried out to assess the timing of the beginning of the presence of charcoal in the record and the shift to *Sphagnum* dominance.

Appendix I: δ13C correction values

1850-2003 $\delta^{13}C$ (‰) values from McCarroll and Loader (2004) (Interpolated from Francey et al. (1999) 1980-1997 atmospheric $\delta^{13}C$ record from Antarctic ice cores). Values 2003-2015 interpolated from McCarroll and Loader (2004) values.

Year	Correction								
2015	2.02	**1975**	0.89	**1935**	0.39	**1895**	0.21	**1855**	0.03
2014	1.99	**1974**	0.86	**1934**	0.39	**1894**	0.21	**1854**	0.03
2013	1.96	**1973**	0.84	**1933**	0.39	**1893**	0.2	**1853**	0.03
2012	1.93	**1972**	0.81	**1932**	0.38	**1892**	0.2	**1852**	0.02
2011	1.9	**1971**	0.78	**1931**	0.38	**1891**	0.19	**1851**	0.02
2010	1.87	**1970**	0.75	**1930**	0.37	**1890**	0.19	**1850**	0.01
2009	1.85	**1969**	0.72	**1929**	0.37	**1889**	0.18		
2008	1.82	**1968**	0.7	**1928**	0.36	**1888**	0.18		
2007	1.79	**1967**	0.67	**1927**	0.36	**1887**	0.18		
2006	1.76	**1966**	0.64	**1926**	0.35	**1886**	0.17		
2005	1.73	**1965**	0.61	**1925**	0.35	**1885**	0.17		
2004	1.71	**1964**	0.58	**1924**	0.35	**1884**	0.16		
2003	1.68	**1963**	0.55	**1923**	0.34	**1883**	0.16		
2002	1.65	**1962**	0.53	**1922**	0.34	**1882**	0.15		
2001	1.62	**1961**	0.51	**1921**	0.33	**1881**	0.15		
2000	1.59	**1960**	0.51	**1920**	0.33	**1880**	0.15		
1999	1.57	**1959**	0.5	**1919**	0.32	**1879**	0.14		
1998	1.54	**1958**	0.5	**1918**	0.32	**1878**	0.14		
1997	1.51	**1957**	0.49	**1917**	0.31	**1877**	0.13		
1996	1.48	**1956**	0.49	**1916**	0.31	**1876**	0.13		
1995	1.45	**1955**	0.48	**1915**	0.31	**1875**	0.12		
1994	1.43	**1954**	0.48	**1914**	0.3	**1874**	0.12		
1993	1.4	**1953**	0.47	**1913**	0.3	**1873**	0.11		
1992	1.37	**1952**	0.47	**1912**	0.29	**1872**	0.11		
1991	1.34	**1951**	0.47	**1911**	0.29	**1871**	0.11		
1990	1.31	**1950**	0.46	**1910**	0.28	**1870**	0.1		
1989	1.29	**1949**	0.46	**1909**	0.27	**1869**	0.1		
1988	1.26	**1948**	0.45	**1908**	0.27	**1868**	0.09		
1987	1.23	**1947**	0.45	**1907**	0.26	**1867**	0.09		
1986	1.2	**1946**	0.44	**1906**	0.26	**1866**	0.08		
1985	1.17	**1945**	0.44	**1905**	0.26	**1865**	0.08		
1984	1.15	**1944**	0.43	**1904**	0.25	**1864**	0.07		
1983	1.12	**1943**	0.43	**1903**	0.25	**1863**	0.07		
1982	1.09	**1942**	0.43	**1902**	0.24	**1862**	0.07		
1981	1.06	**1941**	0.42	**1901**	0.24	**1861**	0.06		
1980	1.03	**1940**	0.42	**1900**	0.23	**1860**	0.06		
1979	1	**1939**	0.41	**1899**	0.23	**1859**	0.05		
1978	0.98	**1938**	0.41	**1898**	0.22	**1858**	0.05		
1977	0.95	**1937**	0.4	**1897**	0.22	**1857**	0.04		
1976	0.92	**1936**	0.4	**1896**	0.22	**1856**	0.04		

Appendix II: Number of pairwise observations for correlations

Intra-site correlations based on actual and relative depth (Chapter 5)

Actual depth: Synchronous observations
Relative depth: Majority of observations are interpolated two point averages

DHI values (Table 5.6)		KAR-EM-3	KAR-EM-2	KAR-EM-1
Actual depth	Observations	34	36	35
		KAR-EM-3 vs. KAR-EM-2	KAR-EM-3 vs. KAR-EM-1	KAR-EM-2 vs. KAR-EM-1
	No. of pairwise observations	34	34	35
Relative depth		KAR-EM-3	KAR-EM-2	KAR-EM-1
	Observations	37	44	35
	Original observations	10	44	14
		KAR-EM-3 vs. KAR-EM-2	KAR-EM-3 vs. KAR-EM-1	KAR-EM-2 vs. KAR-EM-1
	No. of pairwise observations	37	28	*35
Humification records (Table 5.7)		KAR-EM-3	KAR-EM-2	KAR-EM-1
Actual depth	Observations	29	30	28
		KAR-EM-3 vs. KAR-EM-2	KAR-EM-3 vs. KAR-EM-1	KAR-EM-2 vs. KAR-EM-1
	No. of pairwise observations	29	27	*28
Relative depth		KAR-EM-3	KAR-EM-2	KAR-EM-1
	Observations	26	28	30
	Original observations	10	28	10
		KAR-EM-3 vs. KAR-EM-2	KAR-EM-3 vs. KAR-EM-1	KAR-EM-2 vs. KAR-EM-1
	No. of pairwise observations	26	24	30
WTD records (Table 5.12)		KAR-EM-3	KAR-EM-2	KAR-EM-1

Actual depth	Observations	25	33	33
		KAR-EM-3 vs. KAR-EM-2	KAR-EM-3 vs. KAR-EM-1	KAR-EM-2 vs. KAR-EM-1
	No. of pairwise observations	*25	25	*33
Relative depth		KAR-EM-3	KAR-EM-2	KAR-EM-1
	Observations	31	35	30
	Original observations	9	35	6
		KAR-EM-3 vs. KAR-EM-2	KAR-EM-3 vs. KAR-EM-1	KAR-EM-2 vs. KAR-EM-1
	No. of pairwise observations	*31	*26	*30
$\delta^{13}C$ records (Table 5.13)		KAR-EM-3	KAR-EM-2	KAR-EM-1
Actual depth	Observations	33	33	30
		KAR-EM-3 vs. KAR-EM-2	KAR-EM-3 vs. KAR-EM-1	KAR-EM-2 vs. KAR-EM-1
	No. of pairwise observations	33	33	30
Relative depth		KAR-EM-3	KAR-EM-2	KAR-EM-1
	Observations	33	39	25
	Original observations	9	39	6
		KAR-EM-3 vs. KAR-EM-2	KAR-EM-3 vs. KAR-EM-1	KAR-EM-2 vs. KAR-EM-1
	No. of pairwise observations	33	19	25
$\delta^{18}O$ records (Table 5.14)		KAR-EM-3	KAR-EM-2	KAR-EM-1
Actual depth	Observations	30	32	29
		KAR-EM-3 vs. KAR-EM-2	KAR-EM-3 vs. KAR-EM-1	KAR-EM-2 vs. KAR-EM-1
	No. of pairwise observations	30	27	29
Relative depth		KAR-EM-3	KAR-EM-2	KAR-EM-1
	Observations	29	36	23
	Original observations	9	36	5
		KAR-EM-3 vs. KAR-EM-2	KAR-EM-3 vs. KAR-EM-1	KAR-EM-2 vs. KAR-EM-1
	No. of pairwise observations	29	*16	23

Intra-site correlations based on age (Chapter 6)

Observations: Data points available for correlation including averaged values where multiple data points exist in a 20-/50-year time period.
Original observations: Number of non-averaged data points used
No. of pairwise observations: Number of data points available for correlation based on 20-/50-year time period (Table 6.1).

Humification records					
			KAR-EM-3	KAR-EM-2	KAR-EM-1
Original chronology	50-year bins	Observations	27	22	25
		Original observations	16	16	18
			KAR-EM-3 vs. KAR-EM-2	KAR-EM-3 vs. KAR-EM-1	KAR-EM-2 vs. KAR-EM-1
		No. of pairwise observations	20	20	17
	20-year bins		KAR-EM-3	KAR-EM-2	KAR-EM-1
		Observations	40	31	33
		Original observations	39	27	29
			KAR-EM-3 vs. KAR-EM-2	KAR-EM-3 vs. KAR-EM-1	KAR-EM-2 vs. KAR-EM-1
		No. of pairwise observations	19	16	*15
Plotted against KAR-EM-2 chronology	50-year bins		KAR-EM-3	KAR-EM-2	KAR-EM-1
		Observations	18	22	21
		Original observations	13	16	9
			KAR-EM-3 vs. KAR-EM-2	KAR-EM-3 vs. KAR-EM-1	KAR-EM-2 vs. KAR-EM-1
		No. of pairwise observations	16	*14	*14
	20-year bins		KAR-EM-3	KAR-EM-2	KAR-EM-1
		Observations	26	31	36
		Original observations	19	27	31
			KAR-EM-3 vs. KAR-EM-2	KAR-EM-3 vs. KAR-EM-1	KAR-EM-2 vs. KAR-EM-1
		No. of pairwise observations	13	15	*14

DHI records					
	50-year bins		KAR-EM-3	KAR-EM-2	KAR-EM-1
Original chronology		Observations	27	22	25
		Original observations	16	16	18
			KAR-EM-3 vs. KAR-EM-2	KAR-EM-3 vs. KAR-EM-1	KAR-EM-2 vs. KAR-EM-1
		No. of pairwise observations	*21	19	17
	20-year bins		KAR-EM-3	KAR-EM-2	KAR-EM-1
		Observations	40	31	33
		Original observations	36	26	29
			KAR-EM-3 vs. KAR-EM-2	KAR-EM-3 vs. KAR-EM-1	KAR-EM-2 vs. KAR-EM-1
		No. of pairwise observations	21	17	15
Plotted against KAR-EM-2 chronology	50-year bins		KAR-EM-3	KAR-EM-2	KAR-EM-1
		Observations	20	22	21
		Original observations	15	16	9
			KAR-EM-3 vs. KAR-EM-2	KAR-EM-3 vs. KAR-EM-1	KAR-EM-2 vs. KAR-EM-1
		No. of pairwise observations	17	14	*14
	20-year bins		KAR-EM-3	KAR-EM-2	KAR-EM-1
		Observations	28	31	36
		Original observations	21	26	31
			KAR-EM-3 vs. KAR-EM-2	KAR-EM-3 vs. KAR-EM-1	KAR-EM-2 vs. KAR-EM-1
		No. of pairwise observations	14	15	*14

WTD reconstructions					
	50-year bins		KAR-EM-3	KAR-EM-2	KAR-EM-1
Original chronology		Observations	22	22	25
		Original observations	14	16	19
			KAR-EM-3 vs. KAR-EM-2	KAR-EM-3 vs. KAR-EM-1	KAR-EM-2 vs. KAR-EM-1
		No. of pairwise observations	17	15	*17

	20-year bins		KAR-EM-3	KAR-EM-2	KAR-EM-1
		Observations	31	30	32
		Original observations	30	27	31
			KAR-EM-3 vs. KAR-EM-2	KAR-EM-3 vs. KAR-EM-1	KAR-EM-2 vs. KAR-EM-1
		No. of pairwise observations	14	*10	13
Plotted against KAR-EM-2 chronology	50-year bins		KAR-EM-3	KAR-EM-2	KAR-EM-1
		Observations	16	22	21
		Original observations	12	16	11
			KAR-EM-3 vs. KAR-EM-2	KAR-EM-3 vs. KAR-EM-1	KAR-EM-2 vs. KAR-EM-1
		No. of pairwise observations	*14	*12	*14
	20-year bins		KAR-EM-3	KAR-EM-2	KAR-EM-1
		Observations	22	30	33
		Original observations	17	27	31
			KAR-EM-3 vs. KAR-EM-2	KAR-EM-3 vs. KAR-EM-1	KAR-EM-2 vs. KAR-EM-1
		No. of pairwise observations	*10	12	*13
δ¹³C records					
	50-year bins		KAR-EM-3	KAR-EM-2	KAR-EM-1
Original chronology		Observations	24	22	24
		Original observations	16	16	18
			KAR-EM-3 vs. KAR-EM-2	KAR-EM-3 vs. KAR-EM-1	KAR-EM-2 vs. KAR-EM-1
		No. of pairwise observations	19	13	16
	20-year bins		KAR-EM-3	KAR-EM-2	KAR-EM-1
		Observations	34	30	29
		Original observations	31	27	28
			KAR-EM-3 vs. KAR-EM-2	KAR-EM-3 vs. KAR-EM-1	KAR-EM-2 vs. KAR-EM-1
		No. of pairwise observations	17	9	11
R	50-year		KAR-EM-3	KAR-EM-2	KAR-EM-1

	bins	Observations	16	22	19
		Original observations	12	16	9
			KAR-EM-3 vs. KAR-EM-2	KAR-EM-3 vs. KAR-EM-1	KAR-EM-2 vs. KAR-EM-1
		No. of pairwise observations	14	11	12
	20-year bins		KAR-EM-3	KAR-EM-2	KAR-EM-1
		Observations	23	30	30
		Original observations	18	27	28
			KAR-EM-3 vs. KAR-EM-2	KAR-EM-3 vs. KAR-EM-1	KAR-EM-2 vs. KAR-EM-1
		No. of pairwise observations	11	12	12
$\delta^{18}O$ records					
	50-year bins		KAR-EM-3	KAR-EM-2	KAR-EM-1
Original chronology		Observations	23	22	25
		Original observations	15	16	19
			KAR-EM-3 vs. KAR-EM-2	KAR-EM-3 vs. KAR-EM-1	KAR-EM-2 vs. KAR-EM-1
		No. of pairwise observations	18	13	15
	20-year bins		KAR-EM-3	KAR-EM-2	KAR-EM-1
		Observations	32	29	28
		Original observations	29	26	27
			KAR-EM-3 vs. KAR-EM-2	KAR-EM-3 vs. KAR-EM-1	KAR-EM-2 vs. KAR-EM-1
		No. of pairwise observations	15	8	9
Plotted against KAR-EM-2 chronology	50-year bins		KAR-EM-3	KAR-EM-2	KAR-EM-1
		Observations	14	22	19
		Original observations	10	16	10
			KAR-EM-3 vs. KAR-EM-2	KAR-EM-3 vs. KAR-EM-1	KAR-EM-2 vs. KAR-EM-1
		No. of pairwise observations	*12	10	13
	20-year bins		KAR-EM-3	KAR-EM-2	KAR-EM-1
		Observations	21	29	29

		Original observations	16	26	27
			KAR-EM-3 vs. KAR-EM-2	KAR-EM-3 vs. KAR-EM-1	KAR-EM-2 vs. KAR-EM-1
		No. of pairwise observations	11	11	11

Inter-site correlations based on chronology (Chapter 7)

Observations: Data points available for correlation including averaged values where multiple data points exist in a 20-year time period.
Original observations: Number of non-averaged data points used
No. of pairwise observations: Number of data points available for correlation based on 20-year time period (Table 7.4).

All plotted against original age profiles (INTERSITECHRON20)

Humification		KAR-EM-3	KAR-EM-2	KAR-EM-1	SAN-EM-2						
	Observations	40	31	33	28						
	Original observations	39	27	29	25						
		3 v 2	3 v 1	2 v 1	3 v SEM2	2 v SEM2	1 v SEM2				
	No. of pairwise observations	19	16	15	7	9	8				
DHI		KAR-EM-3	KAR-EM-2	KAR-EM-1	SAN-EM-2			SCB-1			
	Observations	40	31	33	28			17			
	Original observations	36	26	29	25			10			
		3 v 2	3 v 1	2 v 1	3 v SEM2	2 v SEM2	1 v SEM2	3 v SCB1	2 v SCB1	1 v SCB1	SEM2 v SCB1
	No. of pairwise	19	16	15	13	9	8	11	8	6	*17

	observations										
WTD		KAR-EM-3	KAR-EM-2	KAR-EM-1	SAN-EM-2			SCB-1			
	Observations	31	30	32	25			17			
	Original observations	30	27	31	22			10			
		3 v 2	3 v 1	2 v 1	3 v SEM2	2 v SEM2	1 v SEM2	3 v SCB1	2 v SCB1	1 v SCB1	SEM2 v SCB1
	No. of pairwise observations	14	10	13	8	8	7	7	7	5	*17
$\delta^{13}C$		KAR-EM-3	KAR-EM-2	KAR-EM-1	SAN-EM-2			SCB-1			
	Observations	34	30	29	28			14			
	Original observations	31	27	28	26			7			
		3 v 2	3 v 1	2 v 1	3 v SEM2	2 v SEM2	1 v SEM2	3 v SCB1	2 v SCB1	1 v SCB1	SEM2 v SCB1
	No. of pairwise observations	17	9	11	13	8	5	11	6	3	*14
$\delta^{18}O$		KAR-EM-3	KAR-EM-2	KAR-EM-1	SAN-EM-2			SCB-1			
	Observations	32	29	28	27			14			
	Original observations	29	26	27	25			7			
		3 v 2	3 v 1	2 v 1	3 v SEM2	2 v SEM2	1 v SEM2	3 v SCB1	2 v SCB1	1 v SCB1	SEM2 v SCB1
	No. of pairwise	15	8	9	13	8	4	11	6	2	14

	observations										

Karukinka records plotted against KAR-EM-2 age profile (INTERSITECHRON20KEM2).

Humification		KAR-EM-3	KAR-EM-2	KAR-EM-1	SAN-EM-2						
	Observations	26	31	36	28						
	Original observations	19	27	31	25						
		3 v 2	3 v 1	2 v 1	3 v SEM2	2 v SEM2	1 v SEM2				
	No. of pairwise observations	13	15	14	12	9	15				
DHI		KAR-EM-3	KAR-EM-2	KAR-EM-1	SAN-EM-2			SCB-1			
	Observations	28	31	36	28			17			
	Original observations	21	26	31	25			10			
		3 v 2	3 v 1	2 v 1	3 v SEM2	2 v SEM2	1 v SEM2	3 v SCB1	2 v SCB1	1 v SCB1	SEM2 v SCB1
	No. of pairwise observations	14	15	14	14	9	15	10	8	12	*17
WTD		KAR-EM-3	KAR-EM-2	KAR-EM-1	SAN-EM-2			SCB-1			
	Observations	22	30	33	25			17			
	Original observations	17	27	31	22			10			
		3 v 2	3 v 1	2 v 1	3 v SEM2	2 v SEM2	1 v SEM2	3 v SCB1	2 v SCB1	1 v SCB1	SEM2 v SCB1

	No. of pairwise observations	10	12	13	7	8	11	*5	7	9	*17
$\delta^{13}C$		KAR-EM-3	KAR-EM-2	KAR-EM-1	SAN-EM-2			SCB-1			
	Observations	23	30	30	28			14			
	Original observations	18	27	28	26			7			
		3 v 2	3 v 1	2 v 1	3 v SEM2	2 v SEM2	1 v SEM2	3 v SCB1	2 v SCB1	1 v SCB1	SEM2 v SCB1
	No. of pairwise observations	11	12	12	9	8	10	5	6	6	*14
$\delta^{18}O$		KAR-EM-3	KAR-EM-2	KAR-EM-1	SAN-EM-2			SCB-1			
	Observations	21	29	29	27			14			
	Original observations	16	26	27	25			7			
		3 v 2	3 v 1	2 v 1	3 v SEM2	2 v SEM2	1 v SEM2	3 v SCB1	2 v SCB1	1 v SCB1	SEM2 v SCB1
	No. of pairwise observations	11	11	11	5	8	9	5	6	*5	14

Appendix III: Alternative Age-depth models

KAR-EM-3

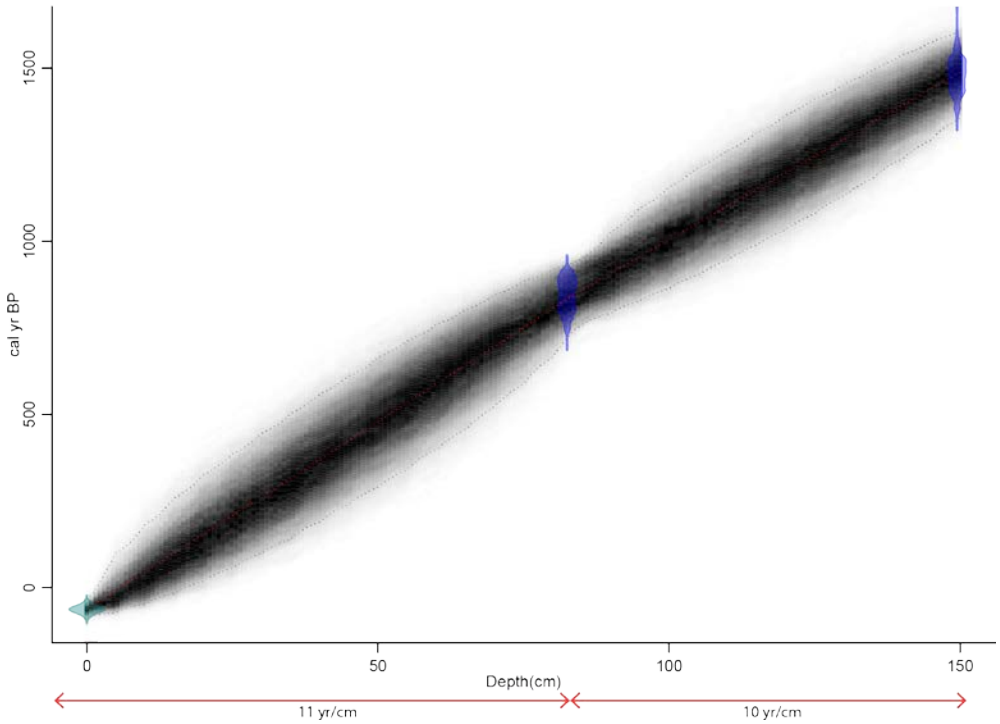

KAR-EM-2

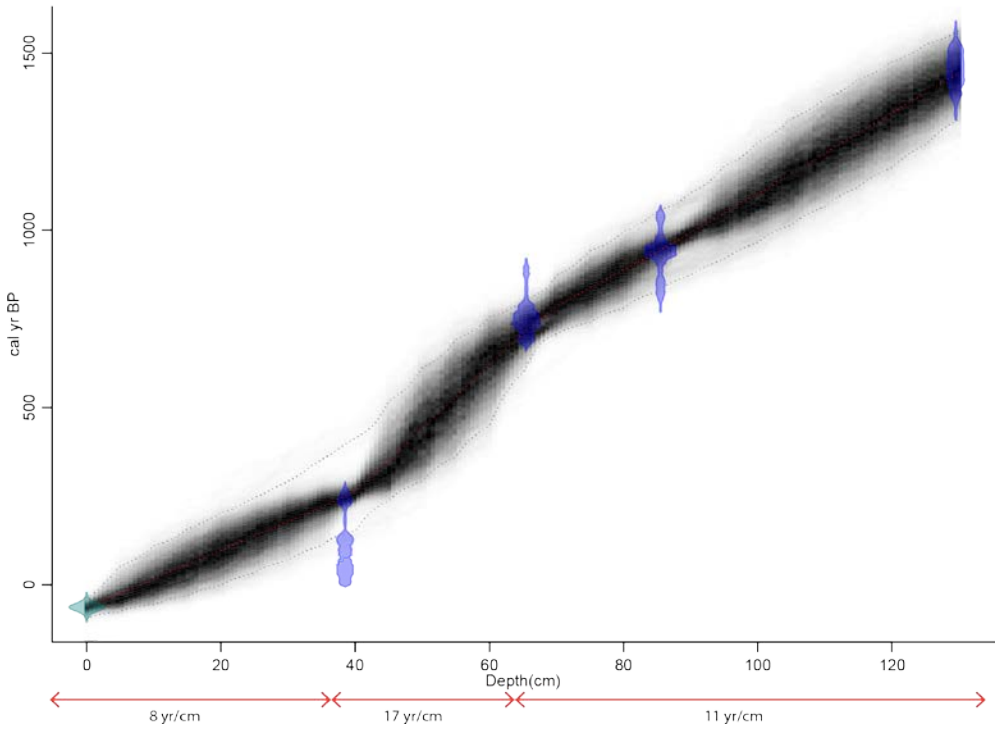

KAR-EM-1

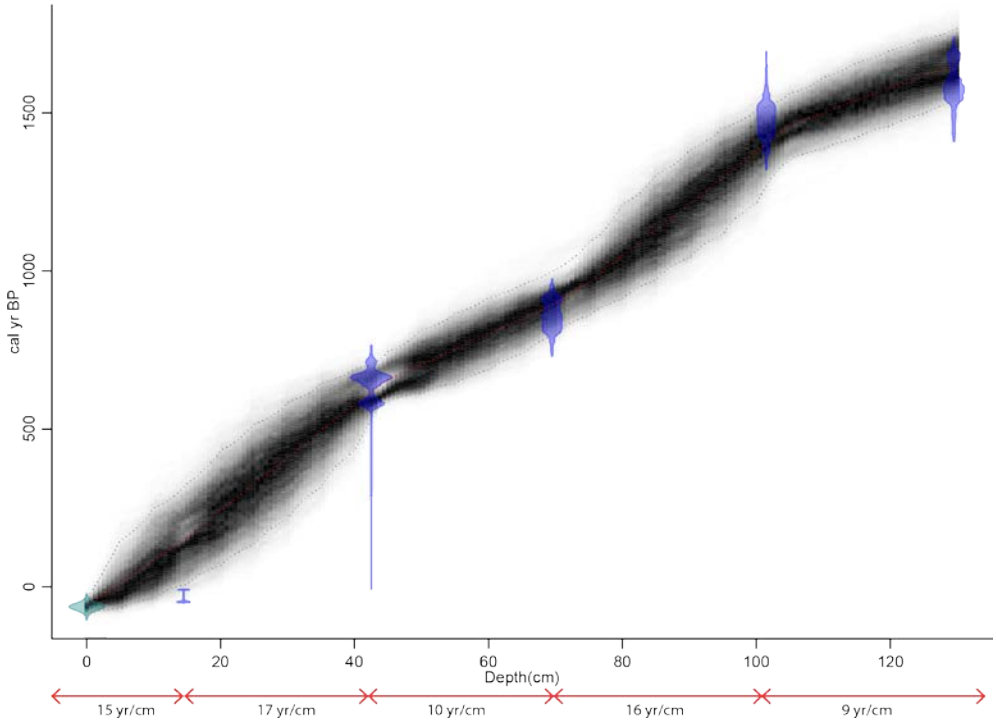

Comparison of the ages from the alternative age-depth models

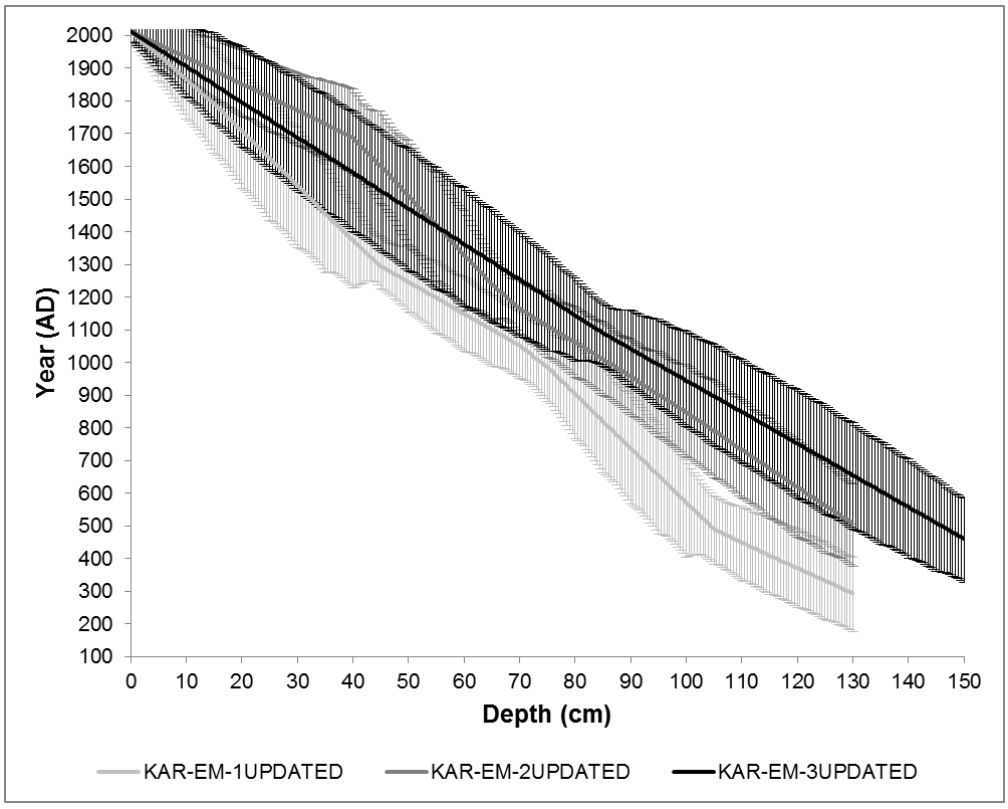

The alternative age-depth model from the KAR-EM-3 profile excludes the ^{210}PB ages and the ^{14}C date at 66.5cm (122 ± 37 ^{14}C). This displays a more uniform and continuous accumulation rate throughout the profile. Exclusion of the ^{210}Pb results in higher uncertainty around the ages towards the surface. This section was better constrained in the KAREM3FINAL model but suggested unrealistic accumulation rates (~3 yr/cm). The exclusion of the ^{14}C date at 66.5cm results in a continuous accumulation rate throughout the profile as opposed to the non-uniform accumulation rates in KAREM3FINAL. The alternative KAR-EM-2 age-depth model excludes the ^{210}PB ages and also results in more uniform and continuous accumulation than in the original age-depth model presented in Chapter 4. Removal of the ^{210}Pb from the KAR-EM-1 age-depth model also results in more continuous accumulation rates throughout the profile. The post-modern radiocarbon date at 14.5cm is outside the weighted mean age, suggesting that the accumulation rates inferred from the ^{210}Pb ages are representative of surface accumulation throughout the acrotelm zone. The comparison of the alternative age-depth models displays similarity between the profiles in accumulation rate owing to the exclusion of the ^{210}Pb ages and unrealistic accumulation rates (almost 30 yr/cm in all profiles).

Whereas Chapter 5 presents the results plotted against age, Chapters 6 and 7 are based on the ages generated from the final age-depth models presented in Chapter 4. Changes in the age-depth models inevitably alter the ages against which the proxy records are plotted and compared. The intra-site comparison of records from Karukinka would, therefore, need to be amended to match these new ages as would the inter-site comparison in Chapter 7. In particular the use of binned data based on 20 or 50 year time periods would be altered.

Alternative age-depth models have implications for the main findings of this investigation. The rise to dominance of *A.muscorum* in the Karukinka testate amoeba records occurred ~1990AD according to the final age-depth models, the alternative models suggest a very different timing in KAR-EM-3 (AD 1878 ± 120), KAR-EM-2 (AD 1913 ± 84) and KAR-EM-1 (AD 1878 ± 120) with much higher age uncertainties. Final use of the KAR-EM-2 age profile for correlation between records would suggest this shift occurred ~AD 1913 which is suggested by the inter-site comparison. The discussion around plotting against the KAR-EM-2 age profile based

on a synchronous acrotelm-catotelm boundary may also be affected by the development of alternative age-depth models. This boundary is still much older in KAR-EM-3 (82cm: AD 1122) than in the other two profiles. According to the alternative age-depth models this boundary is much older in KAR-EM-2 (AD 1652) and KAR-EM-1 (AD 1724) than was suggested by the original age-depth models (AD 1929 and 1975 respectively) which has implications for the timing of climate inferences. In particular the correction of the $\delta^{13}C$ records is affected by alternative age-depth models. The original age-depth models suggested that the records should be corrected ~AD 1850 (KAR-EM-3: 48cm, KAR-EM-2: 44cm, KAR-EM-1: 16cm) the alternative age-depth models suggest correction at AD 1850 would be at 15cm, 20cm and 11cm respectively affecting only the samples towards the surface despite there being a clear trend to negative $\delta^{13}C$ values earlier than this.

Although the alternative age-depth models offer more uniform and continuous accumulation rates the original age-depth models better explain shifts in the proxy records towards the surface evidencing the difficulties associated with dating recent material in peatland investigations.

Appendix IV: Summertime ozone and UV Index, New Zealand

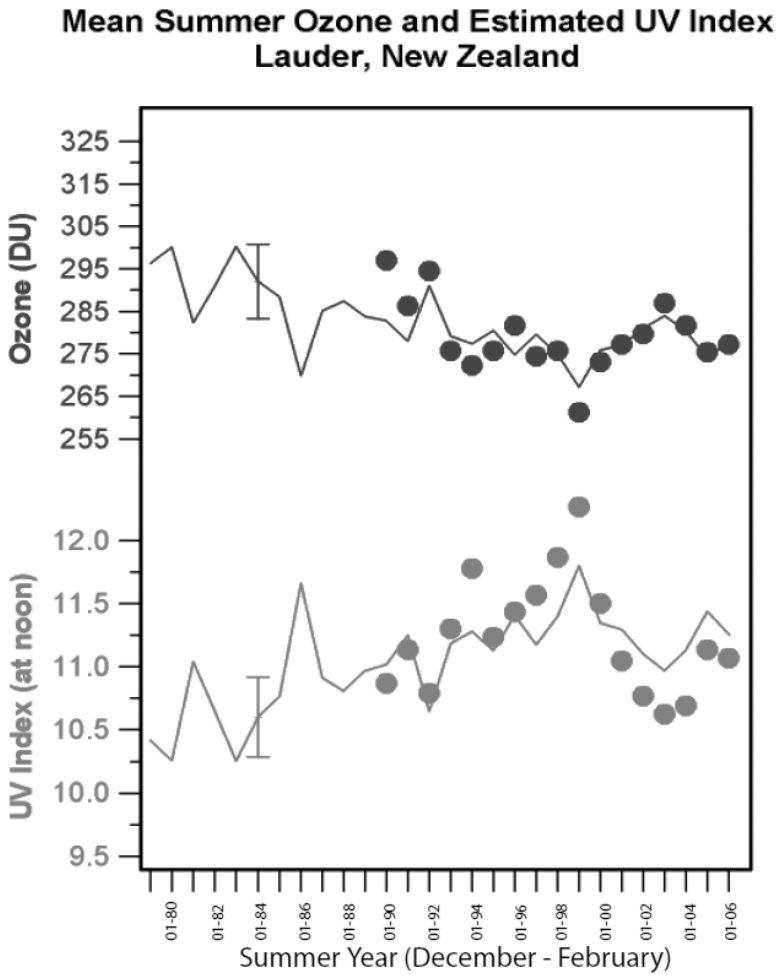

From Bais et al. (2007). Long-term changes in summertime ozone (top) and in peak UV Index (bottom) from assimilated ozone data and UV spectral measurements at Lauder, New Zealand. UV increases occur alongside Ozone depletion.

Appendix V: Interpolated temperature and precipitation records

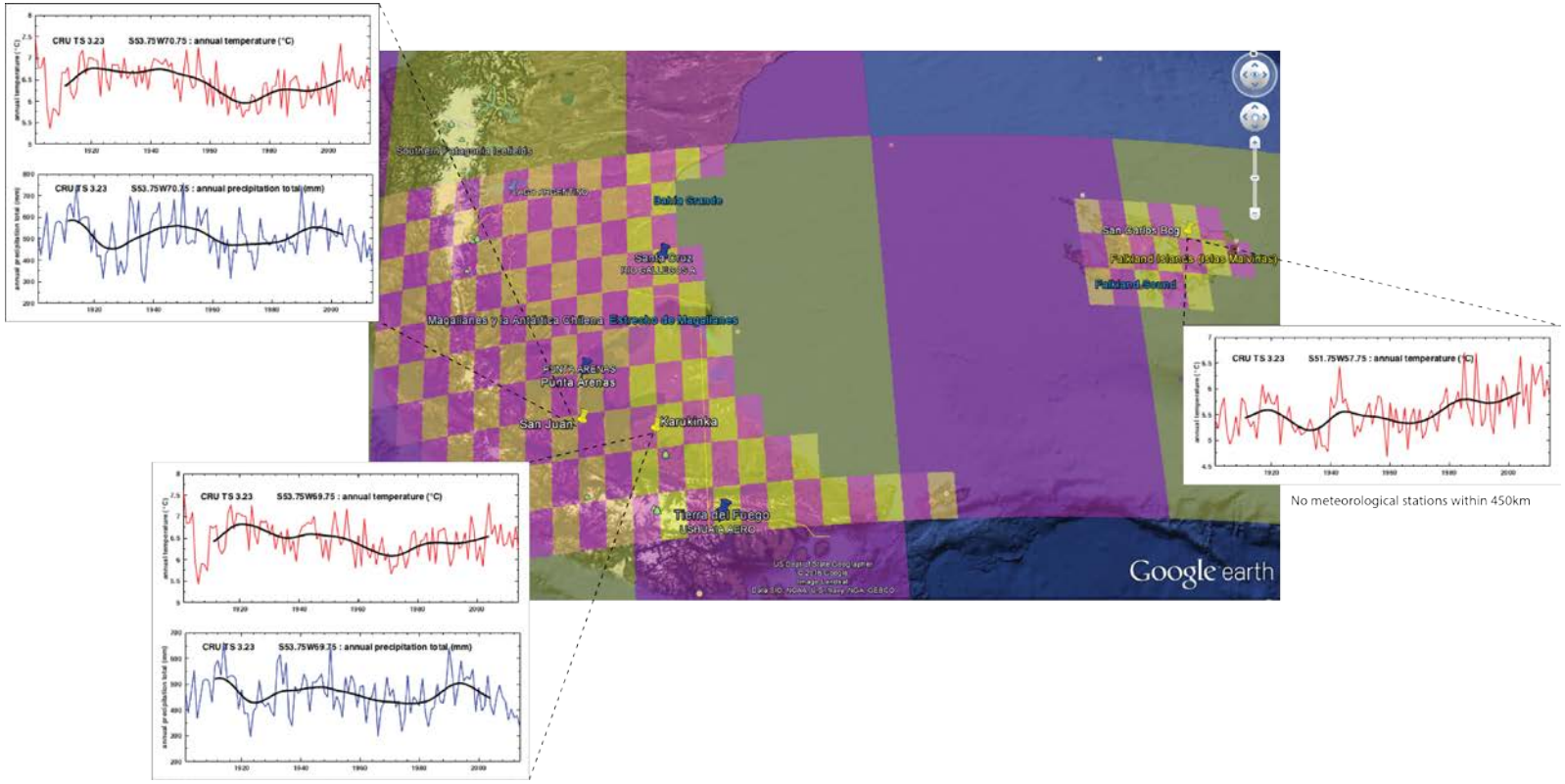

High-resolution gridded datasets (CRU TS v. 3.23) available at https://crudata.uea.ac.uk/cru/data/hrg/. Monthly observations from meteorological stations interpolated into 0.5º resolution grid cells covering the period 1901-2014 (Harris *et al.*, 2014). Interpolated annual temperature and precipitation records are the same for San Juan bog and Karukinka bog. Interpolated temperature record for San Carlos bog displayed. Precipitation record unavailable due to lack of meteorological stations within 450 km for this variable.

References

Aaby, B. (1976) 'Cyclic climatic variations in climate over the past 5,500 yr reflected in raised bogs'. *Nature*, 263, pp 281-284.

Abram, N. J., Mulvaney, R., Wolff, E. W., Triest, J., Kipfstuhl, S., Trusel, L. D., Vimeux, F., Fleet, L. & Arrowsmith, C. (2013) 'Acceleration of snow melt in an Antarctic Peninsula ice core during the twentieth century'. *Nature Geoscience*, 6 (5). pp 404-411.

Abram, N. J., Mulvaney, R., Vimeux, F., Phipps, S. J., Turner, J. & England, M. H. (2014) 'Evolution of the Southern Annular Mode during the past millennium'. *Nature Climate Change*, 4 (7). pp 564-569.

Agosta, E., Compagnucci, R. & Ariztegui, D. (2015) 'Precipitation linked to Atlantic moisture transport: clues to interpret Patagonian palaeoclimate'. *Climate Research*, 62 (3). pp 219-240.

Amesbury, M., Barber, K. & Hughes, P. (2012) 'The relationship of fine-resolution, multi-proxy palaeoclimate records to meteorological data at Fågelmossen, Värmland, Sweden and the implications for the debate on climate drivers of the peat-based record'. *Quaternary international*, 268, pp 77-86.

Amesbury, M. J., Mallon, G., Charman, D. J., Hughes, P. D., Booth, R. K., Daley, T. J. & Garneau, M. (2013) 'Statistical testing of a new testate amoeba-based transfer function for water-table depth reconstruction on ombrotrophic peatlands in north-eastern Canada and Maine, United States'. *Journal of Quaternary Science*, 28 (1). pp 27-39.

Anderson, W., Bernasconi, S., McKenzie, J., Saurer, M. & Schweingruber, F. (2002) 'Model evaluation for reconstructing the oxygen isotopic composition in precipitation from tree ring cellulose over the last century'. *Chemical geology*, 182 (2). pp 121-137.

Anderson, R., Ali, S., Bradtmiller, L., Nielsen, S., Fleisher, M., Anderson, B. & Burckle, L. (2009) 'Wind-driven upwelling in the Southern Ocean and the deglacial rise in atmospheric CO2'. *science*, 323 (5920). pp 1443-1448.

Appleby, P. (2001) *Chronostratigraphic techniques in recent sediments.* Tracking Environmental Change Using Lake Sediments. vol. 1.

Appleby, P. (2008) 'Three decades of dating recent sediments by fallout radionuclides: a review'. *The Holocene*, 18 (1). pp 83-93.

Appleby, P. & Oldfield, F. (1978) 'The calculation of 210Pb dates assuming a constant rate of supply of unsupported 210Pb to the sediments'. *Catena*, 5 pp 1-8.

Appleby, P., Jones, V. & Ellis-Evans, J. (1995) 'Radiometric dating of lake sediments from Signy Island (maritime Antarctic): evidence of recent climatic change'. *Journal of Paleolimnology*, 13 (2). pp 179-191.

Appleby, P., Oldfield, F., Thompson, R., Huttunen, P. & Tolonen, K. (1979) '210Pb dating of annually laminated lake sediments from Finland'. *Nature*, 280 pp 53-55.

Araguás-Araguás, L., Froehlich, K. & Rozanski, K. (2000) 'Deuterium and oxygen-18 isotope composition of precipitation and atmospheric moisture'. *Hydrological Processes*, 14 (8). pp 1341-1355.

Aravena, R. & Warner, B. G. (1992) 'Oxygen-18 composition of Sphagnum, and microenvironmental water relations'. *Bryologist*, pp 445-448.

Aravena, J. C. & Luckman, B. H. (2009) 'Spatio-temporal rainfall patterns in Southern South America'. *International journal of climatology*, 29 (14). pp 2106-2120.

Arblaster, J. M. & Meehl, G. A. (2006) 'Contributions of external forcings to southern annular mode trends'. *Journal of Climate*, 19 (12). pp 2896-2905.

Aristarain, A. J. & Delmas, R. J. (1993) 'Firn-core study from the southern Patagonia ice cap, South America'. *Journal of Glaciology*, 39 (132). pp 249-254.

Aristarain, A. J., Delmas, R. J. & Stievenard, M. (2004) 'Ice-core study of the link between sea-salt aerosol, sea-ice cover and climate in the Antarctic Peninsula area'. *Climatic Change*, 67 (1). pp 63-86.

Ariztegui, D., Bösch, P. & Davaud, E. (2007) 'Dominant ENSO frequencies during the Little Ice Age in northern Patagonia: the varved record of proglacial Lago Frías, Argentina'. *Quaternary international*, 161 (1). pp 46-55.

Ashworth, A. C., Markgraf, V. & Villagran, C. (1991) 'Late Quaternary climatic history of the Chilean Channels based on fossil pollen and beetle analyses, with an analysis of the modern vegetation and pollen rain'. *Journal of Quaternary Science*, 6 (4). pp 279-291.

Atherton, I., Bosanquet, S. & Lawley, M. (2010) *Mosses and liverworts of Britain and Ireland: a field guide.* British bryological society Plymouth, U. K.

Aucour, A.-M., Hillaire-Marcel, C. & Bonnefille, R. (1996) 'Oxygen isotopes in cellulose from modern and quaternary intertropical peatbogs: implications for palaeohydrology'. *Chemical geology*, 129 (3). pp 341-359.

Baertschi, P. (1976) 'Absolute18O content of standard mean ocean water'. *Earth and Planetary Science Letters*, 31 (3). pp 341-344.

Baillie, M. (1991) 'Suck-in and smear: two related chronological problems for the 90s'. *Journal of theoretical archaeology*, 2 pp 12-16.

Baird, A. J., Eades, P. A. & Surridge, B. W. (2008) 'The hydraulic structure of a raised bog and its implications for ecohydrological modelling of bog development'. *Ecohydrology*, 1 (4). pp 289-298.

Baird, A. J., Morris, P. J. & Belyea, L. R. (2012) 'The DigiBog peatland development model 1: rationale, conceptual model, and hydrological basis'. *Ecohydrology*, 5 (3). pp 242-255.

Bais, A.F., Lubin, D., Arola, A., Bernhard, G., Blumthaler, M., Chubarova, N., Erlick, C., Gies, H.P., Krotkov, N.A., Lantz, K., Mayer, B., Mckenzie, R.L., d. Piacentini, R., Seckmeyer, G., Slusser, J.R. & Zerefos, C.Z. (2007) Surface Ultraviolet Radiation: Past, Present, and Future. Scientific assessment of ozone depletion: 2006. (Organization W, Ed.) Geneva, Switzerland: World Meteorological Organization.

Bamonte, F. P. & Mancini, M. V. (2011) 'Palaeoenvironmental changes since Pleistocene–Holocene transition: Pollen analysis from a wetland in southwestern Patagonia (Argentina)'. *Review of Palaeobotany and Palynology*, 165 (1). pp 103-110.

Barber, K. E. (1981) Peat stratigraphy and climatic change: a palaeoecological test of the theory of cyclic peat bog regeneration. Balkema, Rotterdam.

Barber, D., Dyke, A., Hillaire-Marcel, C., Jennings, A., Andrews, J., Kerwin, M., Bilodeau, G., McNeely, R., Southon, J. & Morehead, M. (1999) 'Forcing of the cold event of 8,200 years ago by catastrophic drainage of Laurentide lakes'. *Nature*, 400 (6742). pp 344-348.

Barber, K. E. & Langdon, P. G. (2007) 'What drives the peat-based palaeoclimate record? A critical test using multi-proxy climate records from northern Britain'. *Quaternary Science Reviews*, 26 (25). pp 3318-3327.

Barber, K. E., Chambers, F. M. & Maddy, D. (2003) 'Holocene palaeoclimates from peat stratigraphy: macrofossil proxy climate records from three oceanic raised bogs in England and Ireland'. *Quaternary Science Reviews*, 22 (5). pp 521-539.

Barber, K. E., Chambers, F. M. & Maddy, D. (2004) 'Late Holocene climatic history of northern Germany and Denmark: peat macrofossil investigations at Dosenmoor, Schleswig-Holstein, and Svanemose, Jutland'. *Boreas*, 33 (2). pp 132-144.

Barber, K., Chambers, F., Maddy, D., Stoneman, R. & Brew, J. (1994) 'A sensitive high-resolution record of late Holocene climatic change from a raised bog in northern England'. *The Holocene*, 4 (2). pp 198-205.

Barber, K., Dumayne-Peaty, L., Hughes, P., Mauquoy, D. & Scaife, R. (1998) 'Replicability and variability of the recent macrofossil and proxy-climate record from raised bogs: field stratigraphy and macrofossil data from Bolton Fell Moss and Walton Moss, Cumbria, England'. *Journal of Quaternary Science*, 13 (6). pp 515-528.

Barber, K., Maddy, D., Rose, N., Stevenson, A., Stoneman, R. & Thompson, R. (2000) 'Replicated proxy-climate signals over the last 2000 yr from two distant UK peat bogs: new evidence for regional palaeoclimate teleconnections'. *Quaternary Science Reviews*, 19 (6). pp 481-487.

Barbour, M. M., Andrews, T. J. & Farquhar, G. D. (2001) 'Correlations between oxygen isotope ratios of wood constituents of Quercus and Pinus samples from around the world'. *Functional Plant Biology*, 28 (5). pp 335-348.

Barker, S., Diz, P., Vautravers, M. J., Pike, J., Knorr, G., Hall, I. R. & Broecker, W. S. (2009) 'Interhemispheric Atlantic seesaw response during the last deglaciation'. *Nature*, 457 (7233). pp 1097-1102.

Baumann, M. A. (2006) Water flow, spatial patterns and hydrological self-regulation of a raised bog in Tierra del Fuego (Argentina). PhD thesis. Ernst-Moritz-Arndt University Greifswald.

Belyea, L. R. (1996) 'Separating the effects of litter quality and microenvironment on decomposition rates in a patterned peatland'. *Oikos*, pp 529-539.

Belyea, L. (1999) 'A novel indicator of reducing conditions and water-table depth in mires'. *Functional Ecology*, 13 (3). pp 431-434.

Belyea, L. R. (2007) 'Revealing the Emperor's new clothes: niche-based palaeoenvironmental reconstruction in the light of recent ecological theory'. *The Holocene*, 17 (5). pp 683-688.

Belyea, L. R. (2009) 'Nonlinear dynamics of peatlands and potential feedbacks on the climate system'. *Carbon Cycling in Northern Peatlands*, pp 5-18.

Belyea, L. R. & Warner, B. G. (1994) 'Dating of the near-surface layer of a peatland in northwestern Ontario, Canada'. *Boreas*, 23 (3). pp 259-269.

Belyea, L. R. & Warner, B. G. (1996) 'Temporal scale and the accumulation of peat in a Sphagnum bog'. *Canadian Journal of Botany*, 74 (3). pp 366-377.

Belyea, L. & Clymo, R. (1999) 'Do hollows control the rate of peat bog growth'. *Patterned Mires: Origin and Development, Flora and Fauna*, pp 1-15.

Belyea, L. R. & Clymo, R. (2001) 'Feedback control of the rate of peat formation'. *Proceedings of the Royal Society of London. Series B: Biological Sciences*, 268 (1473). pp 1315-1321.

Belyea, L. R. & Malmer, N. (2004) 'Carbon sequestration in peatland: patterns and mechanisms of response to climate change'. *Global Change Biology*, 10 (7). pp 1043-1052.

Belyea, L. R. & Baird, A. J. (2006) 'Beyond "the limits to peat bog growth": cross-scale feedback in peatland development'. *Ecological Monographs*, 76 (3). pp 299-322.

Bennett, K. D. (1996) 'Determination of the number of zones in a biostratigraphical sequence'. *New phytologist*, 132 (1). pp 155-170.

Benscoter, B., Thompson, D., Waddington, J., Flannigan, M., Wotton, B., De Groot, W. & Turetsky, M. (2011) 'Interactive effects of vegetation, soil moisture and bulk density on depth of burning of thick organic soils'. *International Journal of Wildland Fire*, 20 (3). pp 418-429.

Bentley, M. J., Hodgson, D., Smith, J., Cofaigh, C. Ó., Domack, E., Larter, R., Roberts, S., Brachfeld, S., Leventer, A. & Hjort, C. (2009) 'Mechanisms of Holocene palaeoenvironmental change in the Antarctic Peninsula region'. *The Holocene*, 19 (1). pp 51-69.

Berger, A. (1988) 'Milankovitch theory and climate'. *Reviews of Geophysics*, 26 (4). pp 624-657.

Berger, A. & Loutre, M.-F. (1991) 'Insolation values for the climate of the last 10 million years'. *Quaternary Science Reviews*, 10 (4). pp 297-317.

Berman, A. L., Silvestri, G. E., Rojas, M. & Tonello, M. S. (2016) 'Accelerated greenhouse gases versus slow insolation forcing induced climate changes in southern South America since the Mid-Holocene'. *Climate dynamics*, pp 1-18.

Bertrand, S., Boës, X., Castiaux, J., Charlet, F., Urrutia, R., Espinoza, C., Lepoint, G., Charlier, B. & Fagel, N. (2005) 'Temporal evolution of sediment supply in Lago Puyehue (Southern Chile) during the last 600 yr and its climatic significance'. *Quaternary Research*, 64 (2). pp 163-175.

Bertrand, S., Hughen, K., Sepúlveda, J. & Pantoja, S. (2014) 'Late Holocene covariability of the southern westerlies and sea surface temperature in northern Chilean Patagonia'. *Quaternary Science Reviews*, 105. pp 195-208.

Biester, H., Hemmerich, S. & Petri, M. (2006) 'Halogens in pore water of peat bogs? the role of peat decomposition and dissolved organic matter'. *Biogeosciences*, 3 (1). pp 53-64.

Biester, H., Kilian, R., Franzen, C., Woda, C., Mangini, A. & Schöler, H. (2002) 'Elevated mercury accumulation in a peat bog of the Magellanic Moorlands, Chile (53 S)–an anthropogenic signal from the Southern Hemisphere'. *Earth and Planetary Science Letters*, 201 (3). pp 609-620.

Biester, H., Martinez-Cortizas, A., Birkenstock, S. & Kilian, R. (2003) 'Effect of peat decomposition and mass loss on historic mercury records in peat bogs from Patagonia'. *Environmental science & technology*, 37 (1). pp 32-39.

Birks, H. J. B. & Birks, H. H. (1980) 'Principles and methods of pollen analysis'. *Birks, HJA, Birks, HH Quaternary palaeoecology. London, Edward Arnold*, pp 156-176.

Birks, H. B., Heiri, O., Seppä, H. & Bjune, A. E. (2010) 'Strengths and weaknesses of quantitative climate reconstructions based on late-Quaternary biological proxies'. *Open Ecology Journal*, 3 pp 68-110.

Björck, S., Rundgren, M., Ljung, K., Unkel, I. & Wallin, Å. (2012) 'Multi-proxy analyses of a peat bog on Isla de los Estados, easternmost Tierra del Fuego: a unique record of the variable Southern Hemisphere Westerlies since the last deglaciation'. *Quaternary Science Reviews*, 42 pp 1-14.

Björck, S., Olsson, S., Ellis-Evans, C., Håkansson, H., Humlum, O. & de Lirio, J. M. (1996) 'Late Holocene palaeoclimatic records from lake sediments on James Ross Island, Antarctica'. *Palaeogeography, Palaeoclimatology, Palaeoecology*, 121 (3). pp 195-220.

Blaauw, M. (2010) 'Methods and code for 'classical'age-modelling of radiocarbon sequences'. *Quaternary Geochronology*, 5 (5). pp 512-518.

Blaauw, M. (2012) 'Out of tune: the dangers of aligning proxy archives'. *Quaternary Science Reviews*, 36 pp 38-49.

Blaauw, M. & Christen, J. A. (2005) 'Radiocarbon peat chronologies and environmental change'. *Journal of the Royal Statistical Society: Series C (Applied Statistics)*, 54 (4). pp 805-816.

Blaauw, M. & Christen, J. A. (2011) 'Flexible paleoclimate age-depth models using an autoregressive gamma process'. *Bayesian Analysis*, 6 (3). pp 457-474.

Blaauw, M. & Mauquoy, D. (2012) 'Signal and variability within a Holocene peat bog—chronological uncertainties of pollen, macrofossil and fungal proxies'. *Review of Palaeobotany and Palynology*, 186 pp 5-15.

Blaauw, M., Heuvelink, G., Mauquoy, D., van der Plicht, J. & van Geel, B. (2003) 'A numerical approach to ^{14}C wiggle-match dating of organic deposits: best fits and confidence intervals'. *Quaternary Science Reviews*, 22 (14). pp 1485-1500.

Blackford, J. & Chambers, F. (1993) 'Determining the degree of peat decomposition for peat-based palaeoclimatic studies'. *International peat journal*, 5 (7.24).

Blackwell, P. & Buck, C. (2008) 'Estimating radiocarbon calibration curves'. *Bayesian Analysis*, 3 (2). pp 225-248.

Blundell, A. & Barber, K. (2005) 'A 2800-year palaeoclimatic record from Tore Hill Moss, Strathspey, Scotland: the need for a multi-proxy approach to peat-based climate reconstructions'. *Quaternary Science Reviews*, 24 (10). pp 1261-1277.

Blundell, A., Charman, D. J. & Barber, K. (2008) 'Multiproxy late Holocene peat records from Ireland: towards a regional palaeoclimate curve'. *Journal of Quaternary Science*, 23 (1). pp 59-71.

Bobrov, A. A., Charman, D. J. & Warner, B. G. (1999) 'Ecology of testate amoebae (Protozoa: Rhizopoda) on peatlands in western Russia with special attention to niche separation in closely related taxa'. *Protist*, 150 (2). pp 125-136.

Boës, X. & Fagel, N. (2008) 'Relationships between southern Chilean varved lake sediments, precipitation and ENSO for the last 600 years'. *Journal of Paleolimnology*, 39 (2). pp 237-252.

Bokhorst, M. P. & Vandenberghe, J. (2009) 'Validation of wiggle matching using a multi-proxy approach and its palaeoclimatic significance'. *Journal of Quaternary Science*, 24 (8). pp 937-947.

Bond, G., Kromer, B., Beer, J., Muscheler, R., Evans, M. N., Showers, W., Hoffmann, S., Lotti-Bond, R., Hajdas, I. & Bonani, G. (2001) 'Persistent solar influence on North Atlantic climate during the Holocene'. *science*, 294 (5549). pp 2130-2136.

Boninsegna, J., Argollo, J., Aravena, J., Barichivich, J., Christie, D., Ferrero, M., Lara, A., Le Quesne, C., Luckman, B. & Masiokas, M. (2009) 'Dendroclimatological reconstructions in South America: A review'. *Palaeogeography, Palaeoclimatology, Palaeoecology*, 281 (3). pp 210-228.

Booth, R. K. (2002) 'Testate amoebae as paleoindicators of surface-moisture changes on Michigan peatlands: modern ecology and hydrological calibration'. *Journal of Paleolimnology*, 28 (3). pp 329-348.

Booth, R. K. (2008) 'Testate amoebae as proxies for mean annual water-table depth in Sphagnum-dominated peatlands of North America'. *Journal of Quaternary Science*, 23 (1). pp 43-57.

Booth, R. K. (2010) 'Testing the climate sensitivity of peat-based paleoclimate reconstructions in mid-continental North America'. *Quaternary Science Reviews*, 29 (5). pp 720-731.

Booth, R. K., Jackson, S. T. & Notaro, M. (2010) 'Using peatland archives to test paleoclimate hypotheses'. *science*, 22 pp 209-221.

Booth, R. K., Notaro, M., Jackson, S. T. & Kutzbach, J. E. (2006) 'Widespread drought episodes in the western Great Lakes region during the past 2000 years: geographic extent and potential mechanisms'. *Earth and Planetary Science Letters*, 242 (3). pp 415-427.

Borgmark, A. & Schoning, K. (2006) 'A comparative study of peat proxies from two eastern central Swedish bogs and their relation to meteorological data'. *Journal of Quaternary Science*, 21 (2). pp 109-114.

Borgmark, A. & Wastegård, S. (2008) 'Regional and local patterns of peat humification in three raised peat bogs in Värmland, south-central Sweden'. *Gff*, 130 (3). pp 161-176.

Borromei, A. M., Coronato, A., Franzén, L. G., Ponce, J. F., Sáez, J. A. L., Maidana, N., Rabassa, J. & Candel, M. S. (2010) 'Multiproxy record of Holocene paleoenvironmental change, Tierra del Fuego, Argentina'. *Palaeogeography, Palaeoclimatology, Palaeoecology*, 286 (1). pp 1-16.

Branham, J. E. & Strack, M. (2014) 'Saturated hydraulic conductivity in Sphagnum-dominated peatlands: do microforms matter?'. *Hydrological Processes*, 28 (14). pp 4352-4362.

Brenninkmeijer, C., Van Geel, B. & Mook, W. (1982) 'Variations in the D/H and$^{18}O/^{16}$ O ratios in cellulose extracted from a peat bog core'. *Earth and Planetary Science Letters*, 61 (2). pp 283-290.

Bridgham, S. D., Pastor, J., Dewey, B., Weltzin, J. F. & Updegraff, K. (2008) 'Rapid carbon response of peatlands to climate change'. *Ecology*, 89 (11). pp 3041-3048.

Broder, T., Blodau, C., Biester, H. & Knorr, K. (2012) 'Peat decomposition records in three pristine ombrotrophic bogs in southern Patagonia'. *Biogeosciences*, 9 (4). pp 1479-1491.

Bronk Ramsey, C. (1995) 'Radiocarbon calibration and analysis of stratigraphy; the OxCal program'. *Radiocarbon*, 37 (2). pp 425-430.

Bronk Ramsey, C. (2008) 'Deposition models for chronological records'. *Quaternary Science Reviews*, 27 (1). pp 42-60.

Bronk Ramsey, C. (2013) 'OxCal v4.2.4' Available online: https://c14.arch.ox.ac.uk/oxcal.html

Broughton, D. & McAdam, J. (2002) 'A red data list for the Falkland Islands vascular flora'. *Oryx*, 36 (03). pp 279-287.

Broughton, D. A. & McAdam, J. H. (2005) 'A checklist of the native vascular flora of the Falkland Islands (Islas Malvinas): New information on the species present, their ecology, status and distribution 1'. *The Journal of the Torrey Botanical Society*, 132 (1). pp 115-148.

Buckland, P. C. & Edwards, K. J. (1998) 'Palaeoecological evidence for possible pre-European settlement in the Falkland Islands'. *Journal of archaeological science*, 25 (6). pp 599-602.

Cai, W., Cowan, T. & Thatcher, M. (2012) 'Rainfall reductions over Southern Hemisphere semi-arid regions: the role of subtropical dry zone expansion'. *Scientific reports*, 2 pp 702.

Cai, W., Purich, A., Cowan, T., van Rensch, P. & Weller, E. (2014) 'Did climate change–induced rainfall trends contribute to the Australian Millennium Drought?'. *Journal of Climate*, 27 (9). pp 3145-3168.

Cambray, R. S., Fisher, E., Playford, K., Eakins, J. & Peirson, D. (1980) *Radioactive fallout in air and rain: results to end of 1979.* UKAEA Atomic Energy Research Establishment.

Caniupán, M., Lamy, F., Lange, C. B., Kaiser, J., Kilian, R., Arz, H. W., León, T., Mollenhauer, G., Sandoval, S. & De Pol-Holz, R. (2014) 'Holocene sea-surface temperature variability in the Chilean fjord region'. *Quaternary Research*, 82 (2). pp 342-353.

Caseldine, C., Baker, A, Charman, D. J and Hendon, D (2000) 'A comparative study of optical properties of NaOH peat extracts: implications for humification studies.'. *The Holocene*, 10 (5). pp 649-658.

Cavalieri, D. & Parkinson, C. (2012) 'Arctic sea ice variability and trends, 1979-2010'. *The Cryosphere, Volume 6, Issue 4, 2012, pp. 881-889*, 6 pp 881-889.

Chambers, F., Barber, K., Maddy, D. & Brew, J. (1997) 'A 5500-year proxy-climate and vegetation record from blanket mire at Talla Moss, Borders, Scotland'. *The Holocene*, 7 (4). pp 391-399.

Chambers, F. M., Mauquoy, D., Brain, S. A., Blaauw, M. & Daniell, J. R. G. (2007) 'Globally synchronous climate change 2800 years ago: proxy data from peat in South America'. *Earth and Planetary Science Letters*, 253 (3). pp 439-444.

Chambers, F., Beilman, D. & Yu, Z. (2011) 'Methods for determining peat humification and for quantifying peat bulk density, organic matter and carbon content for palaeostudies of climate and peatland carbon dynamics'. *Mires and Peat*, 7 (10).

Chambers, F. M., Booth, R. K., De Vleeschouwer, F., Lamentowicz, M., Le Roux, G., Mauquoy, D., Nichols, J. E. & van Geel, B. (2012) 'Development and refinement of proxy-climate indicators from peats'. *Quaternary international*, 268 pp 21-33.

Chambers, F. M., Brain, S. A., Mauquoy, D., McCarroll, J. & Daley, T. (2014) 'The 'Little Ice Age'in the Southern Hemisphere in the context of the last 3000 years: Peat-based proxy-climate data from Tierra del Fuego'. *The Holocene*, pp 1-8.

Charman, D. J. (1997) 'Modelling hydrological relationships of testate amoebae (Protozoa: Rhizopoda) on New Zealand peatlands'. *Journal of the Royal Society of New Zealand*, 27 (4). pp 465-483.

Charman, D. J. (1999) 'Testate amoebae and the fossil record: issues in biodiversity'. *Journal of Biogeography*, 26 (1). pp 89-96.

Charman, D. J. (2001) 'Biostratigraphic and palaeoenvironmental applications of testate amoebae'. *Quaternary Science Reviews*, 20 (16). pp 1753-1764.

Charman, D. (2002) *Peatlands and environmental change.* John Wiley & Sons Ltd.

Charman, D. J. (2007) 'Summer water deficit variability controls on peatland water-table changes: implications for Holocene palaeoclimate reconstructions'. *The Holocene*, 17 (2). pp 217-227.

Charman, D. & Warner, B. (1997) 'The ecology of testate amoebae(Protozoa: Rhizopoda) in oceanic peatlands in Newfoundland, Canada: Modelling hydrological relationships for palaeoenvironmental reconstruction'. *Ecoscience*, 4 (4). pp 555-562.

Charman, D. J., Hendon, D. & Packman, S. (1999) 'Multiproxy surface wetness records from replicate cores on an ombrotrophic mire: implications for Holocene palaeoclimate records'. *Journal of Quaternary Science*, 14 (5). pp 451-463.

Charman, D. J., Hendon, D. & Woodland, W. A. (2000) *The identification of testate amoebae (Protozoa: Rhizopoda) in peats.* Quaternary Research Association.

Charman, D. J., Brown, A. D., Hendon, D. & Karofeld, E. (2004) 'Testing the relationship between Holocene peatland palaeoclimate reconstructions and instrumental data at two European sites'. *Quaternary Science Reviews*, 23 (1). pp 137-143.

Charman, D. J., Blundell, A., Chiverrell, R. C., Hendon, D. & Langdon, P. G. (2006) 'Compilation of non-annually resolved Holocene proxy climate records: stacked Holocene peatland palaeo-water table reconstructions from northern Britain'. *Quaternary Science Reviews*, 25 (3). pp 336-350.

Charman, D. J. ,Blundell, A. & ACCROTELM members (2007) 'A new European testate amoebae transfer function for palaeohydrological reconstruction on ombrotrophic peatlands'. *Journal of Quaternary Science*, 22 (3). pp 209-221.

Charman, D. J., Barber, K. E., Blaauw, M., Langdon, P. G., Mauquoy, D., Daley, T. J., Hughes, P. D. & Karofeld, E. (2009) 'Climate drivers for peatland palaeoclimate records'. *Quaternary Science Reviews*, 28 (19). pp 1811-1819.

Charman, D. J., Hohl, V., Blundell, A., Mitchell, F., Newberry, J. & Oksanen, P. (2012) 'A 1000-year reconstruction of summer precipitation from Ireland: Calibration of a peat-based palaeoclimate record'. *Quaternary international*, 268 pp 87-97.

Charman, D. J., Beilman, D. W., Jackson, S., Korhola, A., Mauquoy, D., Mitchell, F., Prentice, I., van der Linden, M., De Vleeschouwer, F. & Yu, Z. (2013) 'Climate-related changes in peatland carbon accumulation during the last millennium'. *Biogeosciences*, 10 pp 929-944.

Charman, D. J., Amesbury, M. J., Hinchliffe, W., Hughes, P. D., Mallon, G., Blake, W. H., Daley, T. J., Gallego-Sala, A. V. & Mauquoy, D. (2015) 'Drivers of Holocene peatland carbon accumulation across a climate gradient in northeastern North America'. *Quaternary Science Reviews*, 121 pp 110-119.

Chavaillaz, Y., Codron, F. & Kageyama, M. (2013) 'Southern westerlies in LGM and future (RCP4. 5) climates'. *Climate of the Past*, 9 (2). pp 517-524.

Chiang, J. C. & Bitz, C. M. (2005) 'Influence of high latitude ice cover on the marine Intertropical Convergence Zone'. *Climate dynamics*, 25 (5). pp 477-496.

Chiverrell, R. (2001) 'A proxy record of late Holocene climate change from May Moss, northeast England'. *Journal of Quaternary Science*, 16 (1). pp 9-29.

Christen, J. A. & Fox, C. (2012) 'Markov chain Monte Carlo using an approximation'. *Journal of computational and graphical statistics*, 14 (4). pp 795-810.

Chylek, P., Folland, C. K., Lesins, G. & Dubey, M. K. (2010) 'Twentieth century bipolar seesaw of the Arctic and Antarctic surface air temperatures'. *Geophysical research letters*, 37 (8).

Clapperton, C. M. & Sugden, D. E. (1988) 'Holocene glacier fluctuations in South America and Antarctica'. *Quaternary Science Reviews*, 7 (2). pp 185-198.

Clark, I. & Fritz, P. (1997) *Environmental isotopes in hydrology.* Lewis Publishers, Boca Raton, Florida.

Clarke, L. J., Robinson, S. A., Hua, Q., Ayre, D. J. & Fink, D. (2012) 'Radiocarbon bomb spike reveals biological effects of Antarctic climate change'. *Global Change Biology*, 18 (1). pp 301-310.

Climate Prediction Center (2005) http://www.cpc.ncep.noaa.gov/products/analysis_monitoring/ensocycle/soi.shtml

Clymo, R. S. (1965) 'Experiments on breakdown of Sphagnum in two bogs'. *The Journal of Ecology*, pp 747-758.

Clymo, R. S. (1984) 'The limits to peat bog growth'. *Philosophical Transactions of the Royal Society of London B*, 303. pp 605–654.

Clymo, R. & Hayward, P. (1982) 'The ecology of Sphagnum'. *Bryophyte ecology.* Springer, pp 229-289.

Clymo, R. & Bryant, C. (2008) 'Diffusion and mass flow of dissolved carbon dioxide, methane, and dissolved organic carbon in a 7-m deep raised peat bog'. *Geochimica et Cosmochimica Acta*, 72 (8). pp 2048-2066.

Clymo, R., Oldfield, F., Appleby, P., Pearson, G., Ratnesar, P. & Richardson, N. (1990) 'The record of atmospheric deposition on a rainwater-dependent peatland'. *Philosophical Transactions of the Royal Society of London. B, Biological Sciences*, 327 (1240). pp 331-338.

Cobb, K. M., Charles, C. D., Cheng, H. & Edwards, R. L. (2003) 'El Niño/Southern Oscillation and tropical Pacific climate during the last millennium'. *Nature*, 424 (6946). pp 271-276.

Cole, J. E., Rind, D., Webb, R. S., Jouzel, J. & Healy, R. (1999) 'Climatic controls on interannual variability of precipitation δ18O: Simulated influence of temperature, precipitation amount, and vapor source region'. *Journal of Geophysical Research*, 104 (D12). pp 14223-14235.

Comas, X. & Slater, L. D. (2009) 'Noninvasive field-scale characterization of gaseous-phase methane dynamics in peatlands using the ground-penetrating radar method'. *Geophysical Monograph Series*, 184 pp 159-171.

Coplen, T. B. (1995) 'Discontinuance of SMOW and PDB'. *Nature*, 375 pp 285

Coplen, T. B., Böhlke, J. K., De Bievre, P., Ding, T., Holden, N., Hopple, J., Krouse, H., Lamberty, A., Peiser, H. & Revesz, K. (2002) 'Isotope-abundance variations of selected elements (IUPAC Technical Report)'. *Pure and Applied Chemistry*, 74 (10). pp 1987-2017.

Coronato, A., Roig, C., Collado, L. & Roig, F. (2006) 'Geomorphologic emplacement and vegetation characteristics of Fuegian peatlands, southernmost Argentina, South America'. *Developments in Earth Surface Processes*, 9 pp 111-128.

Couwenberg, J. & Joosten, H. (2005) 'Self-organization in raised bog patterning: The origin of microtope zonation and mesotope diversity'. *Journal of Ecology*, 93 (6). pp 1238-1248.

Craig, H. (1961a) 'Standard for reporting concentrations of deuterium and oxygen-18 in natural waters'. *Science (New York, NY)*, 133 (3467). pp 1833.

Craig, H. (1961b) 'Isotopic variations in meteoric waters'. *Science (New York, NY)*, 133 (3465). pp 1702.

Crann, C. A., Patterson, R. T., Macumber, A. L., Galloway, J. M., Roe, H. M., Blaauw, M., Swindles, G. T. & Falck, H. (2015) 'Sediment accumulation rates in subarctic lakes: Insights into age-depth modeling from 22 dated lake records from the Northwest Territories, Canada'. *quaternary geochronology*, 27 pp 131-144.

Criss, R. (1999) *Principles of stable isotope distribution.* vol. 254. Oxford University Press New York.

Dachnowski, A. P. (1921) 'Peat deposits and their evidence of climatic changes'. *Botanical Gazette*, pp 57-89.

Daley, T. (2007) Tracking Holocene climate change using peat bog stable isotopes. PhD thesis, University of Southampton.

Daley, T. & Barber, K. (2012) 'Multi-proxy Holocene palaeoclimate records from Walton Moss, northern England and Dosenmoor, northern Germany, assessed using three statistical approaches'. *Quaternary international*, 268 pp 111-127.

Daley, T. J., Street-Perrott, F. A., Loader, N. J., Barber, K. E., Hughes, P. D., Fisher, E. H. & Marshall, J. D. (2009) 'Terrestrial climate signal of the “8200 yr BP cold event” in the Labrador Sea region'. *Geology*, 37 (9). pp 831-834.

Daley, T., Barber, K., Street-Perrott, F., Loader, N., Marshall, J., Crowley, S. & Fisher, E. (2010) 'Holocene climate variability revealed by oxygen isotope analysis of *Sphagnum* cellulose from Walton Moss, northern England'. *Quaternary Science Reviews*, 29 (13). pp 1590-1601.

Daley, T. J., Thomas, E. R., Holmes, J. A., Street-Perrott, F. A., Chapman, M. R., Tindall, J. C., Valdes, P. J., Loader, N. J., Marshall, J. D. & Wolff, E. W. (2011) 'The 8200yr BP cold event in stable isotope records from the North Atlantic region'. *Global and Planetary Change*, 79 (3). pp 288-302.

Daley, T., Mauquoy, D., Chambers, F., Street-Perrott, F., Hughes, P., Loader, N., Roland, T., van Bellen, S., Garcia-Meneses, P. & Lewin, S. (2012) 'Investigating late Holocene variations in hydroclimate and the stable isotope composition of precipitation using southern South American peatlands: a hypothesis'. *Climate of the Past Discussions*, 8 pp 595-620.

Daley, T., Barber, K., Hughes, P., Loader, N., Leuenberger, M. & Street-Perrott, F. (2016) 'The 8.2-ka BP event in north-eastern North America: first combined oxygen and hydrogen isotopic data from peat in Newfoundland'. *Journal of Quaternary Science*, 31 (4). pp 416-425.

Daniels, R. E. & Eddy, A. (1990) *Handbook of European sphagna.* HMSO.

Dansgaard, W. (1964) 'Stable isotopes in precipitation'. *Tellus*, 16 (4). pp 436-468.

Darling, W. & Talbot, J. (2003) 'The O and H stable isotope composition of freshwaters in the British Isles. 1. Rainfall'. *Hydrology and Earth System Sciences Discussions*, 7 (2). pp 163-181.

Deflandre G. 1936. 'Etude monographique sur le genre Nebela Leidy'. *Annales de Protistologie,* 5, pp201–286.

DeNiro, M. J. & Epstein, S. (1979) 'Relationship between the oxygen isotope ratios of terrestrial plant cellulose, carbon dioxide, and water'. *science*, 204 (4388). pp 51-53.

DeNiro, M. J. & Epstein, S. (1981) 'Isotopic composition of cellulose from aquatic organisms'. *Geochimica et Cosmochimica Acta*, 45 (10). pp 1885-1894.

Deser, C. & Phillips, A. S. (2009) 'Atmospheric circulation trends, 1950-2000: The relative roles of sea surface temperature forcing and direct atmospheric radiative forcing'. *Journal of Climate*, 22 (2). pp 396-413.

de Vernal, A., Gersonde, R., Goosse, H., Seidenkrantz, M.-S. & Wolff, E. W. (2013) 'Sea ice in the paleoclimate system: the challenge of reconstructing sea ice from proxies–an introduction'. *Quaternary Science Reviews*, 79 pp 1-8.

De Vleeschouwer, F., Chambers, F. & Swindles, G. (2010a) 'Coring and sub-sampling of peatlands for palaeoenvironmental research'. *Mires and Peat*, 7 (01). pp 1-10.

De Vleeschouwer, F., Pazdur, A., Luthers, C., Streel, M., Mauquoy, D., Wastiaux, C., Le Roux, G., Moschen, R., Blaauw, M. & Pawlyta, J. (2012) 'A millennial record of environmental change in peat deposits from the Misten bog (East Belgium)'. *Quaternary international*, 268 pp 44-57.

De Vleeschouwer, F., Vanneste, H., Mauquoy, D., Piotrowska, N., Torrejón, F., Roland, T., Stein, A. & Le Roux, G. (2014) 'Emissions from Pre-Hispanic Metallurgy in the South American Atmosphere'. *PloS one*, 9 (10). pp e111315.

De Witt, J., Straaten, C. & Mook, W. (1980) 'Determination of the Absolute Hydrogen Isotopic Ratio of V-SMOW and SLAP'. *Geostandards Newsletter*, 4 (1). pp 33-36.

Diaz, H. F., Trigo, R., Hughes, M. K., Mann, M. E., Xoplaki, E. & Barriopedro, D. (2011) 'Spatial and temporal characteristics of climate in medieval times revisited'. *Bulletin of the American Meteorological Society*, 92 (11). pp 1487.

Diaz, M. F., Tapia, C., Jiménez, P. & Bacigalupe, L. (2012) 'Sphagnum magellanicum growth and productivity in Chilean anthropogenic peatlands'. *Revista chilena de historia natural*, 85 (4). pp 513-518.

Ding, Q. & Steig, E. J. (2013) 'Temperature change on the Antarctic Peninsula linked to the tropical Pacific'. *Journal of Climate*, (26). pp 7570-7585.

Ding, Q., Steig, E. J., Battisti, D. S. & Wallace, J. M. (2012) 'Influence of the tropics on the Southern Annular Mode'. *Journal of Climate*, 25 (18). pp 6330-6348.

Ding, H., Greatbatch, R. J. & Gollan, G. (2014) 'Tropical influence independent of ENSO on the austral summer Southern Annular Mode'. *Geophysical research letters*, 41 (10). pp 3643-3648.

Dise, N. B. (2009) 'Peatland response to global change'. *science*, 326 (5954). pp 810.

Dragović, S., Nedić, O., Stanković, S. & Bačić, G. (2004) 'Radiocesium accumulation in mosses from highlands of Serbia and Montenegro: chemical and physiological aspects'. *Journal of environmental radioactivity*, 77 (3). pp 381-388.

Dupont, L. M. (1986) 'Temperature and rainfall variation in the Holocene based on comparative palaeoecology and isotope geology of a hummock and a hollow (Bourtangerveen, The Netherlands)'. *Review of Palaeobotany and Palynology*, 48 (1). pp 71-159.

Dupont, L. M. & Brenninkmeijer, C. (1984) 'Palaeobotanic and isotopic analysis of late Subboreal and early Subatlantic peat from Engbertsdijksveen VII, The Netherlands'. *Review of Palaeobotany and Palynology*, 41 (3). pp 241-271.

Dupont, L. M. & Mook, W. G. (1987) 'Palaeoclimate analysis of 2H1H ratios in peat sequences with variable plant composition'. *Chemical Geology: Isotope Geoscience section*, 66 (3). pp 323-333.

Ebaid, Y. & Khater, A. (2006) 'Determination of 210Pb in environmental samples'. *Journal of radioanalytical and nuclear chemistry*, 270 (3). pp 609-619.

Echeverria, M. E., Sottile, G. D., Mancini, M. V. & Fontana, S. L. (2014) 'Nothofagus forest dynamics and palaeoenvironmental variations during the mid and late Holocene, in southwest Patagonia'. *The Holocene*, 24 (8). pp 957-969.

Eggelsman, R., Heathwaite, A. L., Grosse-Brauckmann, G., Kuster, E., Naucke, W., Schuch, M. & Shweickle, V. (1993) Physical processes and properties of mires. In: Mires: Process, Exploitation and Conservation (eds. Heathwaite, A. L. & Gottlich, K.). pp 171-262. Wiley,Chichester.

Elbert, J., Grosjean, M., von Gunten, L., Urrutia, R., Fischer, D., Wartenburger, R., Ariztegui, D., Fujak, M. & Hamann, Y. (2012) 'Quantitative high-resolution winter (JJA) precipitation reconstruction from varved sediments of Lago Plomo 47 S, Patagonian Andes, AD 1530–2002'. *The Holocene*, 22 (4). pp 465-474.

Elbert, J., Wartenburger, R., von Gunten, L., Urrutia, R., Fischer, D., Fujak, M., Hamann, Y., Greber, N. D. & Grosjean, M. (2013a) 'Late Holocene air temperature variability reconstructed from the sediments of Laguna Escondida, Patagonia, Chile (45° 30'S)'. *Palaeogeography, Palaeoclimatology, Palaeoecology*,

Elbert, J., Jacques-Coper, M., Van Daele, M., Urrutia, R. & Grosjean, M. (2013b) 'A 1500 yr warm-season temperature record from varved Lago Plomo, Northern Patagonia (47◦ S) and implications for the Pacific Decadal Oscillation (PDO)'. *Past Discuss*, 9 pp 1771-1801.

Ellis, C. J. & Tallis, J. H. (2000) 'Climatic control of blanket mire development at Kentra Moss, north-west Scotland'. *Journal of Ecology*, 88 (5). pp 869-889.

El Bilali, H. & Patterson, R. T. (2012) 'Influence of cellulose oxygen isotope variability in sub-fossil *Sphagnum* and plant macrofossil components on the reliability of paleoclimate records at the Mer Bleue Bog, Ottawa, Ontario, Canada'. *Organic geochemistry*, 43 pp 39-49.

El-Daoushy, F., Tolonen, K. & Rosenberg, R. (1982) 'Lead 210 and moss-increment dating of two Finnish Sphagnum hummocks'. *Nature*, 296 (5856). pp 429-431.

Emile-Geay, J., Cobb, K. M., Mann, M. E. & Wittenberg, A. T. (2013) 'Estimating central equatorial Pacific SST variability over the past millennium. Part II: Reconstructions and implications'. *Journal of Climate*, 26 (7). pp 2329-2352.

Eppinga, M. B., De Ruiter, P. C., Wassen, M. J. & Rietkerk, M. (2009a) 'Nutrients and hydrology indicate the driving mechanisms of peatland surface patterning'. *The American Naturalist*, 173 (6). pp 803-818.

Eppinga, M. B., Rietkerk, M., Wassen, M. J. & De Ruiter, P. C. (2009b) 'Linking habitat modification to catastrophic shifts and vegetation patterns in bogs'. *Plant Ecology*, 200 (1). pp 53-68.

Epstein, S. & Mayeda, T. (1953) 'Variation of O content of waters from natural sources'. *Geochimica et Cosmochimica Acta*, 4 (5). pp 213-224.

Falklands Conservation (2012) Available online: http://www.falklandsconservation.com/projects/lower-plants

Falkland Islands Government (2012) Available online: http://www.falklands.gov.fk/

Faure, G. and Mensing, T. M. (2005) *Isotopes Principles and Applications*.Third edition.John Wiley & Sons, Inc. Hoboken, New Jersey.

Farquhar, G. D. & Sharkey, T. D. (1982) 'Stomatal conductance and photosynthesis'. *Annual review of plant physiology*, 33 (1). pp 317-345.

Feng, X., Krishnamurthy, R. & Epstein, S. (1993) 'Determination of DH ratios of nonexchangeable hydrogen in cellulose: A method based on the cellulose-water exchange reaction'. *Geochimica et Cosmochimica Acta*, 57 (17). pp 4249-4256.

Fenton, J. (2014) Observations on Falkland Islands peat including long-term dynamics.

Fey, M., Korr, C., Maidana, N. I., Carrevedo, M. L., Corbella, H., Dietrich, S., Haberzettl, T., Kuhn, G., Lücke, A. & Mayr, C. (2009) 'Palaeoenvironmental changes during the last 1600 years inferred from the sediment record of a cirque lake in southern Patagonia (Laguna Las Vizcachas, Argentina)'. *Palaeogeography, Palaeoclimatology, Palaeoecology*, 281 (3). pp 363-375.

Fiałkiewicz-Kozieł, B., Kołaczek, P., Piotrowska, N., Michczyński, A., Łokas, E., Wachniew, P., Woszczyk, M. & Sensuła, B. (2014) 'A high resolution age-depth model of a peat bog in Poland as an important basis for palaeoenvironmental studies'. *Radiocarbon*, 56 (1). pp 109-125.

Filot, M. S., Leuenberger, M., Pazdur, A. & Boettger, T. (2006) 'Rapid online equilibration method to determine the D/H ratios of non-exchangeable hydrogen in cellulose'. *Rapid Communications in Mass Spectrometry*, 20 (22). pp 3337-3344.

Fogt, R. L., Perlwitz, J., Monaghan, A. J., Bromwich, D. H., Jones, J. M. & Marshall, G. J. (2009) 'Historical SAM Variability. Part II: Twentieth-Century Variability and Trends from Reconstructions, Observations, and the IPCC AR4 Models*'. *Journal of Climate*, 22 (20). pp 5346-5365.

Fogt, R. L., Bromwich, D. H. & Hines, K. M. (2011) 'Understanding the SAM influence on the South Pacific ENSO teleconnection'. *Climate dynamics*, 36 (7-8). pp 1555-1576.

Forster, P. M. d. F. & Shine, K. P. (1999) 'Stratospheric water vapour changes as a possible contributor to observed stratospheric cooling'. *Geophysical research letters*, 26 (21). pp 3309-3312.

Flantua, S. G., Hooghiemstra, H., Vuillle, M., Behling, H., Carson, J., Gosling, W., Hoyos, I., Ledru, M.-P., Montoya, E. & Mayle, F. (2015) 'Climate variability and human impact on the environment in South America during the last 2000 years: synthesis and perspectives'. *Climate of the Past Discussions*, 11 (4). pp 3475-3565.

Fletcher, M. S. & Moreno, P. I. (2012) 'Have the Southern Westerlies changed in a zonally symmetric manner over the last 14,000 years? A hemisphere-wide take on a controversial problem'. *Quaternary international*, 253 pp 32-46.

Francey, R., Allison, C., Etheridge, D., Trudinger, C., Enting, I., Leuenberger, M., Langenfelds, R., Michel, E. & Steele, L. (1999) 'A 1000-year high precision record of δ13C in atmospheric CO2'. *Tellus B*, 51 (2). pp 170-193.

Gao, C., Robock, A. & Ammann, C. (2008) 'Volcanic forcing of climate over the past 1500 years: An improved ice core-based index for climate models'. *Journal of Geophysical Research: Atmospheres*, 113 (D23).

Garreaud, R. D. (2007) 'Precipitation and circulation covariability in the extratropics'. *Journal of Climate*, 20 (18). pp 4789-4797.

Garreaud, R. (2009) 'The Andes climate and weather'. *Advances in Geosciences*, 22 pp 3-11.

Garreaud, R. D. & Aceituno, P. (2007) 'Atmospheric circulation over South America: mean features and variability'. *The physical geography of South America. Oxford University Press, Oxford, England*

Garreaud, R. D., Vuille, M., Compagnucci, R. & Marengo, J. (2009) 'Present-day South American climate'. *Palaeogeography, Palaeoclimatology, Palaeoecology*, 281 (3). pp 180-195.

Garreaud, R., Lopez, P., Minvielle, M. & Rojas, M. (2013) 'Large-Scale Control on the Patagonian Climate'. *Journal of Climate*, 26 pp 215-230.

Gat, J. R. (1996) 'Oxygen and hydrogen isotopes in the hydrologic cycle'. *Annual Review of Earth and Planetary Sciences*, 24 (1). pp 225-262.

Gehrke, C. (1998) 'Effects of enhanced UV-B radiation on production-related properties of a Sphagnum fuscum dominated subarctic bog'. *Functional Ecology*, 12 (6). pp 940-947.

Gerdol, R. (1996) 'The seasonal growth pattern of Sphagnum magellanicum Brid. in different microhabitats on a mire in the southern Alps (Italy)'. *Oecologia Montana*, 5 (1). pp 13-20.

Gille, S. T. (2014) 'Meridional displacement of the Antarctic Circumpolar Current'. *Philosophical Transactions of the Royal Society A: Mathematical, Physical and Engineering Sciences*, 372 (2019). pp 20130273.

Gillett, N. P. & Thompson, D. W. J. (2003) 'Simulation of recent Southern Hemisphere climate change'. *science*, 302 (5643). pp 273-275.

Gilli, A. P. (2003) *Tracking late Quaternary environmental change in southernmost South America using lake sediments of Lago Cardiel (49 S), Patagonia, Argentina*. Diss., Eidgenössische Technische Hochschule ETH Zürich.

Gilli, A., Ariztegui, D., Anselmetti, F. S., McKenzie, J. A., Markgraf, V., Hajdas, I. & McCulloch, R. D. (2005) 'Mid-Holocene strengthening of the southern westerlies in South America—sedimentological evidences from Lago Cardiel, Argentina (49 S)'. *Global and Planetary Change*, 49 (1). pp 75-93.

Givelet, N., Le Roux, G., Cheburkin, A., Chen, B., Frank, J., Goodsite, M. E., Kempter, H., Krachler, M., Noernberg, T. & Rausch, N. (2004) 'Suggested protocol for collecting, handling and preparing peat cores and peat samples for physical, chemical, mineralogical and isotopic analyses'. *Journal of Environmental Monitoring*, 6 (5). pp 481-492.

Glasser, N. F., Harrison, S., Winchester, V. & Aniya, M. (2004) 'Late Pleistocene and Holocene palaeoclimate and glacier fluctuations in Patagonia'. *Global and Planetary Change*, 43 (1). pp 79-101.

Glasser, N., Harrison, S., Jansson, K. N., Anderson, K. & Cowley, A. (2011) 'Global sea-level contribution from the Patagonian Icefields since the Little Ice Age maximum'. *Nature Geoscience*, 4 (5). pp 303-307.

Godwin, H. (1962) 'Half-life of radiocarbon'. *Nature*, 195

Gong, D. & Wang, S. (1999) 'Definition of Antarctic oscillation index'. *Geophysical research letters*, 26 (4). pp 459-462.

Gonzalez, P. L., Polvani, L. M., Seager, R. & Correa, G. J. (2014) 'Stratospheric ozone depletion: a key driver of recent precipitation trends in South Eastern South America'. *Climate dynamics*, 42 (7-8). pp 1775-1792.

Green, D. G. & Dolman, G. S. (1988) 'Fine resolution pollen analysis'. *Journal of Biogeography*, pp 685-701.

Green, D., Singh, G., Polach, H., Moss, D., Banks, J. & Geissler, E. A. (1988) 'A fine-resolution palaeoecology and palaeoclimatology from south-eastern Australia'. *The Journal of Ecology*, pp 790-806.

Grimm, E. C. (1987) 'CONISS: a FORTRAN 77 program for stratigraphically constrained cluster analysis by the method of incremental sum of squares'. *Computers & Geosciences*, 13 (1). pp 13-35.

Grimm, E. (1991) *Tilia and Tiliagraph*. Illinois State Museum, Springfield.

Grootjans, A., Iturraspe, R., Lanting, A., Fritz, C. & Joosten, H. (2010) 'Ecohydrological features of some contrasting mires in Tierra del Fuego, Argentina'. *Mires and Peat*, 6 (01). pp 1-15.

Grosvernier, P., Matthey, Y. & Buttler, A. (1997) 'Growth potential of three Sphagnum species in relation to water table level and peat properties with implications for their restoration in cut-over bogs'. *Journal of applied ecology*, pp 471-483.

Gunnarsson, U. (2013) 'Global patterns of Sphagnum productivity'. *Journal of Bryology*, 27 pp 269-279.

Haberzettl, T., Fey, M., Lücke, A., Maidana, N., Mayr, C., Ohlendorf, C., Schäbitz, F., Schleser, G. H., Wille, M. & Zolitschka, B. (2005) 'Climatically induced lake level changes during the last two millennia as reflected in sediments of Laguna Potrok Aike, southern Patagonia (Santa Cruz, Argentina)'. *Journal of Paleolimnology*, 33 (3). pp 283-302.

Haberzettl, T., Wille, M., Fey, M., Janssen, S., Lücke, A., Mayr, C., Ohlendorf, C., Schäbitz, F., Schleser, G. H. & Zolitschka, B. (2006) 'Environmental change and fire history of southern Patagonia (Argentina) during the last five centuries'. *Quaternary international*, 158 (1). pp 72-82.

Haberzettl, T., Corbella, H., Fey, M., Janssen, S., Lücke, A., Mayr, C., Ohlendorf, C., Schäbitz, F., Schleser, G. H. & Wille, M. (2007) 'Lateglacial and Holocene wet—dry cycles in southern Patagonia: chronology, sedimentology and geochemistry of a lacustrine record from Laguna Potrok Aike, Argentina'. *The Holocene*, 17 (3). pp 297-310.

Haberzettl, T., Kück, B., Wulf, S., Anselmetti, F., Ariztegui, D., Corbella, H., Fey, M., Janssen, S., Lücke, A. & Mayr, C. (2008) 'Hydrological variability in southeastern Patagonia and explosive volcanic activity in the southern Andean Cordillera during Oxygen Isotope Stage 3 and the Holocene inferred

from lake sediments of Laguna Potrok Aike, Argentina'. *Palaeogeography, Palaeoclimatology, Palaeoecology*, 259 (2). pp 213-229.

Hancock, G., Leslie, C., Everett, S., Tims, S., Brunskill, G. & Haese, R. (2011) 'Plutonium as a chronomarker in Australian and New Zealand sediments: a comparison with 137 Cs'. *Journal of environmental radioactivity*, 102 (10). pp 919-929.

Hansson, S. V., Rydberg, J., Kylander, M., Gallagher, K. & Bindler, R. (2013) 'Evaluating paleoproxies for peat decomposition and their relationship to peat geochemistry'. *The Holocene*, 0 (0). pp 1-6.

Harris, I., Jones, P., Osborn, T. & Lister, D. (2014) 'Updated high-resolution grids of monthly climatic observations–the CRU TS3. 10 Dataset'. *International journal of climatology*, 34 (3). pp 623-642.

Hartmann, D. L., Wallace, J. M., Limpasuvan, V., Thompson, D. W. & Holton, J. R. (2000) 'Can ozone depletion and global warming interact to produce rapid climate change?'. *Proceedings of the National Academy of Sciences*, 97 (4). pp 1412-1417.

Haug, G. H., Hughen, K. A., Sigman, D. M., Peterson, L. C. & Röhl, U. (2001) 'Southward migration of the Intertropical Convergence Zone through the Holocene'. *science*, 293 (5533). pp 1304-1308.

Heal, O. (1962) 'The abundance and micro-distribution of testate amoebae (Rhizopoda: Testacea) in Sphagnum'. *Oikos*, pp 35-47.

Heal, O. (1964) 'Observations on the seasonal and spatial distribution of testacea (Protozoa: Rhizopoda) in Sphagnum'. *The Journal of Animal Ecology*, pp 395-412.

Heijmans, M. M., Berendse, F., Arp, W. J., Masselink, A. K., Klees, H., De Visser, W. & Van Breemen, N. (2001) 'Effects of elevated carbon dioxide and increased nitrogen deposition on bog vegetation in the Netherlands'. *Journal of Ecology*, 89 (2). pp 268-279.

Hendon, D. & Charman, D. J. (2004) 'High-resolution peatland water-table changes for the past 200 years: the influence of climate and implications for management'. *The Holocene*, 14 (1). pp 125-134.

Hendon, D., Charman, D. & Kent, M. (2001) 'Palaeohydrological records derived from testate amoebae analysis from peatlands in northern England: within-site variability, between-site comparability and palaeoclimatic implications'. *The Holocene*, 11 (2). pp 127-148.

Hermanns, Y. & Biester, H. (2011) 'A Holocene record of mercury accumulation in a pristine lake in Southernmost South America (53 S)–climatic and environmental drivers'. *Biogeosciences Discussions*, 8 (4). pp 6555-6588.

Heusser, C. J. (1989) 'Late Quaternary vegetation and climate of southern Tierra del Fuego'. *Quaternary Research*, 31 (3). pp 396-406.

Heusser, C. (1995) 'Three late Quaternary pollen diagrams from southern Patagonia and their palaeoecological implications'. *Palaeogeography, Palaeoclimatology, Palaeoecology*, 118 (1). pp 1-24.

Heusser, C. (1998) 'Deglacial paleoclimate of the American sector of the Southern Ocean: Late Glacial–Holocene records from the latitude of Canal Beagle (55 S), Argentine Tierra del Fuego'. *Palaeogeography, Palaeoclimatology, Palaeoecology*, 141 (3). pp 277-301.

Heusser, C. J., Heusser, L. E. & Lowell, T. V. (2000) 'Deglacial palaeoclimate at Puerto del Hambre, subantarctic Patagonia, Chile'. *Journal of Quaternary Science*, 15 (2). pp 101-114.

Hill, M. O. & Gauch Jr, H. (1980) 'Detrended correspondence analysis: an improved ordination technique'. *Vegetation*, 42 (1-3). pp 47-58.

Holynska, B., Ostachowicz, B., Ostachowicz, J., Samek, L., Wachniew, P., Obidowicz, A., Wobrauschek, P., Streli, C. & Halmetschlager, G. (1998) 'Characterisation of 210 Pb dated peat core by various X-ray fluorescence techniques'. *Science of the Total Environment*, 218 (2). pp 239-248.

Huber, U. M. & Markgraf, V. (2003) 'European impact on fire regimes and vegetation dynamics at the steppe-forest ecotone of southern Patagonia'. *The Holocene*, 13 (4). pp 567-579.

Huber, U. M., Markgraf, V. & Schäbitz, F. (2004) 'Geographical and temporal trends in Late Quaternary fire histories of Fuego-Patagonia, South America'. *Quaternary Science Reviews*, 23 (9). pp 1079-1097.

Hogg, A. G., Hua, Q., Blackwell, P. G., Niu, M., Buck, C. E., Guilderson, T. P., Heaton, T. J., Palmer, J. G., Reimer, P. J. & Reimer, R. W. (2013) 'SHCal13 Southern Hemisphere calibration, 0–50,000 years cal BP'. *Radiocarbon*, 55 (2). pp 1-15.

Holdsworth, G., Fogarasi, S. & Krouse, H. (1991) 'Variation of the stable isotopes of water with altitude in the Saint Elias Mountains of Canada'. *Journal of Geophysical Research*, 96 (D4). pp 7483-7494.

Hong, Y., Jiang, H., Liu, T., Zhou, L., Beer, J., Li, H., Leng, X., Hong, B. & Qin, X. (2000) 'Response of climate to solar forcing recorded in a 6000-yearδ18O time-series of Chinese peat cellulose'. *The Holocene*, 10 (1). pp 1-7.

Hong, Y., Wang, Z., Jiang, H., Lin, Q., Hong, B., Zhu, Y., Wang, Y., Xu, L., Leng, X. & Li, H. (2001) 'A 6000-year record of changes in drought and precipitation in northeastern China based on a $\delta^{13}C$ time series from peat cellulose'. *Earth and Planetary Science Letters*, 185 (1). pp 111-119.

Horita, J. & Wesolowski, D. J. (1994) 'Liquid-vapor fractionation of oxygen and hydrogen isotopes of water from the freezing to the critical temperature'. *Geochimica et Cosmochimica Acta*, 58 (16). pp 3425-3437.

Hughes, P. & Barber, K. (2004) 'Contrasting pathways to ombrotrophy in three raised bogs from Ireland and Cumbria, England'. *The Holocene*, 14 (1). pp 65-77.

Hughes, P., Mauquoy, D., Barber, K. & Langdon, P. (2000) 'Mire-development pathways and palaeoclimatic records from a full Holocene peat archive at Walton Moss, Cumbria, England'. *The Holocene*, 10 (4). pp 465-479.

Hughes, P., Blundell, A., Charman, D., Bartlett, S., Daniell, J., Wojatschke, A. & Chambers, F. (2006) 'An 8500cal. year multi-proxy climate record from a bog in eastern Newfoundland: contributions of meltwater discharge and solar forcing'. *Quaternary Science Reviews*, 25 (11). pp 1208-1227.

Hughes, P., Mallon, G., Essex, H., Amesbury, M., Charman, D., Blundell, A., Chambers, F., Daley, T. & Mauquoy, D. (2012) 'The use of *k*-values to examine plant 'species signals' in a peat humification record from Newfoundland'. *Quaternary international*, 268 pp 156-165.

Hua, Q. & Barbetti, M. (2004) 'Review of tropospheric bomb ^{14}C data for carbon cycle modeling and age calibration purposes'. *Radiocarbon*, 46 (3). pp 1273-1298.

Hua, Q., Barbetti, M. & Rakowski, A. Z. (2013) 'Atmospheric radiocarbon for the period 1950–2010'. *Radiocarbon*, 55 (4). pp 2059-2072.

Ingraham, N. L. & Taylor, B. E. (1986) 'Hydrogen isotope study of large-scale meteoric water transport in northern California and Nevada'. *Journal of Hydrology*, 85 (1). pp 183-197.

Ingraham, N. L. & Taylor, B. E. (1991) 'Light stable isotope systematics of large-scale hydrologic regimes in California and Nevada'. *Water Resources Research*, 27 (1). pp 77-90.

Ingram, H.A.P. (1978) 'Soil layers in mires: function and terminology'. *Journal of Soil Science,* 29. pp 224–227.

Ingram, H.A.P. (1982) 'Size and shape in raised mire ecosystems: a geophysical model.' *Nature*, 297. pp 300–303.

Irving, D. & Simmonds, I. (2016) 'A new method for identifying the Pacific-South American pattern and its influence on regional climate variability'. *Journal of Climate*,

Ise, T., Dunn, A. L., Wofsy, S. C. & Moorcroft, P. R. (2008) 'High sensitivity of peat decomposition to climate change through water-table feedback'. *Nature Geoscience*, 1 (11). pp 763-766.

Itambi, A., Von Dobeneck, T., Mulitza, S., Bickert, T. & Heslop, D. (2009) 'Millennial-scale northwest African droughts related to Heinrich events and Dansgaard-Oeschger cycles: Evidence in marine sediments from offshore Senegal'. *Paleoceanography*, 24 (1).

Ivanov, K. E. (1953) Gidrologiya Bolot (The Hydrology of Mires). Gidrometeoizdat: Leningrad.

Jansen, E., Overpeck, J., Briffa, K. R., Duplessy, J.-C., Joos, F., Masson-Delmotte, V., Olago, D., Otto-Bliesner, B., Peltier, W. & Rahmstorf, S. (2007) 'Palaeoclimate'. *Climate change*, pp 433-497.

Janssens, J. A. (1983) 'A quantitative method for stratigraphic analysis of bryophytes in Holocene peat'. *The Journal of Ecology*, pp 189-196.

Jardine, T. D. & Cunjak, R. A. (2005) 'Analytical error in stable isotope ecology'. *Oecologia*, 144 (4). pp 528-533.

Jędrysek, M.-O. & Skrzypek, G. (2005) 'Hydrogen, carbon and sulphur isotope ratios in peat: the role of diagenessis and water regimes in reconstruction of past climates'. *Environmental Chemistry Letters*, 2 (4). pp 179-183.

Johnson, L. C. & Damman, A. W. (1991) 'Species-controlled Sphagnum decay on a south Swedish raised bog'. *Oikos*, pp 234-242.

Johnson, L. & Damman, A. (1993) 'Decay and its regulation in Sphagnum peatlands'. *Advances in bryology*, 5 pp 249-296.

Johnson, L. C., Damman, A. W. & Malmer, N. (1990) 'Sphagnum macrostructure as an indicator of decay and compaction in peat cores from an ombrotrophic south Swedish peat-bog'. *The Journal of Ecology*, pp 633-647.

Jones, A. & Shanklin, J. (1995) 'Continued decline of total ozone over Halley, Antarctica, since 1985'. *Nature*, 376 pp 409 - 411.

Jones, P. & Mann, M. (2004) 'Climate over past millennia'. *Reviews of Geophysics*, 42 (2). pp RG2002.

Jones, J. M. & Widmann, M. (2004) 'Atmospheric science: Early peak in Antarctic oscillation index'. *Nature*, 432 (7015). pp 290-291.

Jones, J. M., Fogt, R. L., Widmann, M., Marshall, G. J., Jones, P. D. & Visbeck, M. (2009) 'Historical SAM Variability. Part I: Century-Length Seasonal Reconstructions*'. *Journal of Climate*, 22 (20). pp 5319-5345.

Joosten, H. (1993) 'Denken wie ein hochmoor: hydrologische Selbstregulation von hochmooren und deren Bedeutung für Wiedervernässung und Restauration'. *Telma*, 23 pp 95-115.

Joosten, H. (2009) 'The Global Peatland CO2 Picture: peatland status and drainage related emissions in all countries of the world'. Wetlands International; UNFCC Barcelona.

Juggins, S. (2015) Package 'rioja'. Available online: ftp://156.56.247.196/pub/CRAN/web/packages/rioja/rioja.pdf

Kang, S., Polvani, L., Fyfe, J. & Sigmond, M. (2011) 'Impact of polar ozone depletion on subtropical precipitation'. *Science*, 332 (6032). pp 951-954.

Ke, L., Lin, Z and Guoxing, Z (2014) 'Study of normalization method of isotopic compositions to isotope reference scales'. *Journal of Chemical and Pharmaceutical Research*, 6 (4). pp 1-5.

Keeling, C. D. (1979) 'The Suess effect: 13 carbon-14 carbon interrelations'. *Environment International*, 2 (4-6). pp 229-300.

Kenny, R., Markgraf, V. & White, J. (1999) 'Palaeotemperature estimates for the last 14,000 (radiocarbon) years BP from D/H isotopes in peat in southern South America'. *Modern Geology*, 21 (4). pp 365-378.

Kettridge, N. & Baird, A. (2008) 'Modelling soil temperatures in northern peatlands'. *European journal of soil science*, 59 (2). pp 327-338.

Kettridge, N. & Baird, A. J. (2010) 'Simulating the thermal behavior of northern peatlands with a 3-D microtopography'. *Journal of Geophysical Research: Biogeosciences (2005–2012)*, 115 (G3).

Kettridge, N., Binley, A., Comas, X., Cassidy, N. J., Baird, A. J., Harris, A., van der Kruk, J., Strack, M., Milner, A. M. & Waddington, J. M. (2012) 'Do peatland microforms move through time? Examining the developmental history of a patterned peatland using ground-penetrating radar'. *Journal of Geophysical Research*, 117 (G3). pp G03030.

Kidson, J. W. (1999) 'Principal modes of Southern Hemisphere low-frequency variability obtained from NCEP-NCAR reanalyses'. *Journal of Climate*, 12 (9). pp 2808-2830.

Kilian, R. & Lamy, F. (2012) 'A review of Glacial and Holocene paleoclimate records from southernmost Patagonia (49–55° S)'. *Quaternary Science Reviews*, 53 pp 1-23.

Kilian, M., Van der Plicht, J. & Van Geel, B. (1995) 'Dating raised bogs: New aspects of AMS ^{14}C wiggle matching, a reservoir effect and climatic change'. *Quaternary Science Reviews*, 14 (10). pp 959-966.

Kilian, M., Van Geel, B. & Van der Plicht, J. (2000) '14C AMS wiggle matching of raised bog deposits and models of peat accumulation'. *Quaternary Science Reviews*, 19 (10). pp 1011-1033.

Kilian, R., Hohner, M., Biester, H., Wallrabe-Adams, H. J. & Stern, C. R. (2003) 'Holocene peat and lake sediment tephra record from the southernmost Chilean Andes (53-55 S)'. *Revista geológica de Chile*, 30 (1). pp 23-37.

Kindt, R. & Coe, R. (2005) 'Analysis of ecological distance by ordination'. *Tree diversity analysis: a manual and software for common statistical methods for ecological and biodiversity studies.* World Agroforestry Centre.

Kip, N., Fritz, C., Langelaan, E., Pan, Y., Bodrossy, L., Pancotto, V., Jetten, M., Smolders, A. & Camp, H. (2012) 'Methanotrophic activity and diversity in different Sphagnum magellanicum dominated habitats in the southernmost peat bogs of Patagonia'. *Biogeosciences*, 9 (1). pp 47-55.

Kleinebecker, T., Hölzel, N. & Vogel, A. (2007) 'Gradients of continentality and moisture in South Patagonian ombrotrophic peatland vegetation'. *Folia Geobotanica*, 42 (4). pp 363-382.

Kleinebecker, T., Hölzel, N. & Vogel, A. (2008) 'South Patagonian ombrotrophic bog vegetation reflects biogeochemical gradients at the landscape level'. *Journal of Vegetation Science*, 19 (2). pp 151-160.

Koch, J. & Kilian, R. (2005) ''Little Ice Age'glacier fluctuations, Gran Campo Nevado, southernmost Chile'. *The Holocene*, 15 (1). pp 20-28.

Koffman, B., Kreutz, K., Breton, D., Kane, E., Winski, D., Birkel, S., Kurbatov, A. & Handley, M. (2014) 'Centennial-scale variability of the Southern Hemisphere westerly wind belt in the eastern Pacific over the past two millennia'. *Climate of the Past*, 10 (3). pp 1125-1144.

Kohfeld, K., Graham, R., de Boer, A., Sime, L., Wolff, E., Le Quéré, C. & Bopp, L. (2013) 'Southern Hemisphere westerly wind changes during the Last Glacial Maximum: paleo-data synthesis'. *Quaternary Science Reviews*, 68 pp 76-95.

Köpke, K. (2005) *Musterbildung in einem feuerländischen Regenmoor*. MSc thesis, Greifswald.

Kreutz, K., Mayewski, P., Meeker, L., Twickler, M., Whitlow, S. & Pittalwala, I. (1997) 'Bipolar changes in atmospheric circulation during the Little Ice Age'. *science*, 277 (5330). pp 1294-1296.

Kuylenstierna, J., Rosqvist, G. & Holmlund, P. (1996) 'Late-Holocene glacier variations in the Cordillera Darwin, Tierra del Fuego, Chile'. *The Holocene*, 6 (3). pp 353-358.

Kwok, R. & Comiso, J. C. (2002) 'Spatial patterns of variability in Antarctic surface temperature: Connections to the Southern Hemisphere Annular Mode and the Southern Oscillation'. *Geophysical research letters*, 29 (14). pp 51-54

Langdon, P., Barber, K. & Lomas-Clarke, S. (2004) 'Reconstructing climate and environmental change in northern England through chironomid and pollen analyses: evidence from Talkin Tarn, Cumbria'. *Journal of Paleolimnology*, 32 (2). pp 197-213.

Langdon, P. G. & Barber, K. E. (2005) 'The climate of Scotland over the last 5000 years inferred from multiproxy peatland records: inter-site correlations and regional variability'. *Journal of Quaternary Science*, 20 (6). pp 549-566.

Langdon, P., Barber, K. & Hughes, P. (2003) 'A 7500-year peat-based palaeoclimatic reconstruction and evidence for an 1100-year cyclicity in bog surface wetness from Temple Hill Moss, Pentland Hills, southeast Scotland'. *Quaternary Science Reviews*, 22 (2). pp 259-274.

Lamarre, A., Magnan, G., Garneau, M. & Boucher, É. (2013) 'A testate amoeba-based transfer function for paleohydrological reconstruction from boreal and subarctic peatlands in northeastern Canada'. *Quaternary international*, 306, pp88-96.

Lamb, H. H. (1977) Climate: Past, Present and Future. Volume 2. Methuen, London.

Lamentowicz, M., Cedro, A., Gałka, M., Goslar, T., Miotk-Szpiganowicz, G., Mitchell, E. & Pawlyta, J. (2008) 'Last millennium palaeoenvironmental changes from a Baltic bog (Poland) inferred from stable isotopes, pollen, plant macrofossils and testate amoebae'. *Palaeogeography, Palaeoclimatology, Palaeoecology*, 265 (1). pp 93-106.

Lamentowicz, M., Van Der Knaap, W., Lamentowicz, Ł., Van Leeuwen, J. F., Mitchell, E. A., Goslar, T. & Kamenik, C. (2010) 'A near-annual palaeohydrological study based on testate amoebae from a sub-alpine mire: surface wetness and the role of climate during the instrumental period'. *Journal of Quaternary Science*, 25 (2). pp 190-202.

Lamy, F., Hebbeln, D., Röhl, U. & Wefer, G. (2001) 'Holocene rainfall variability in southern Chile: a marine record of latitudinal shifts of the Southern Westerlies'. *Earth and Planetary Science Letters*, 185 (3). pp 369-382.

Lamy, F., Rühlemann, C., Hebbeln, D. & Wefer, G. (2002) 'High-and low-latitude climate control on the position of the southern Peru-Chile Current during the Holocene'. *Paleoceanography*, 17 (2). pp 1028.

Lamy, F., Kaiser, J., Arz, H. W., Hebbeln, D., Ninnemann, U., Timm, O., Timmermann, A. & Toggweiler, J. (2007) 'Modulation of the bipolar seesaw in the Southeast Pacific during Termination 1'. *Earth and Planetary Science Letters*, 259 (3). pp 400-413.

Lamy, F., Kilian, R., Arz, H. W., Francois, J. P., Kaiser, J., Prange, M. & Steinke, T. (2010) 'Holocene changes in the position and intensity of the southern westerly wind belt'. *Nature Geoscience*, 3 (10). pp 695-699.

Law, R. M., Matear, R. J. & Francey, R. J. (2008) 'Comment on" Saturation of the Southern Ocean CO2 Sink Due to Recent Climate Change"'. *science*, 319 (5863). pp 570.

Legendre, P. & Gallagher, E. D. (2001) 'Ecologically meaningful transformations for ordination of species data'. *Oecologia*, 129 (2). pp 271-280.

Legendre, P. & Legendre, L. F. (2012) *Numerical ecology.* vol. 24. Elsevier.

Lehmann, M. F., Reichert, P., Bernasconi, S. M., Barbieri, A. & McKenzie, J. A. (2003) 'Modelling nitrogen and oxygen isotope fractionation during denitrification in a lacustrine redox-transition zone'. *Geochimica et Cosmochimica Acta*, 67 (14). pp 2529-2542.

Lepš, J. & Šmilauer, P. (2003) *Multivariate analysis of ecological data using CANOCO.* Cambridge university press.

Le Quéré, C., Rödenbeck, C., Buitenhuis, E. T., Conway, T. J., Langenfelds, R., Gomez, A., Labuschagne, C., Ramonet, M., Nakazawa, T. & Metzl, N. (2007) 'Saturation of the Southern Ocean CO2 sink due to recent climate change'. *science*, 316 (5832). pp 1735-1738.

Le Roux, G. & Marshall, W. (2011) 'Constructing recent peat accumulation chronologies using atmospheric fall-out radionuclides'. *Mires and Peat*, 7 (08). pp 1-14.

Leventer, A., Domack, E. W., Ishman, S. E., Brachfeld, S., McClennen, C. E. & Manley, P. (1996) 'Productivity cycles of 200–300 years in the Antarctic Peninsula region: understanding linkages among the sun, atmosphere, oceans, sea ice, and biota'. *Geological Society of America Bulletin*, 108 (12). pp 1626-1644.

Lewis, S. L. & Maslin, M. A. (2015) 'Defining the anthropocene'. *Nature*, 519 (7542). pp 171-180.

L'Heureux, M. L. & Thompson, D. W. (2006) 'Observed relationships between the El Nino-Southern Oscillation and the extratropical zonal-mean circulation'. *Journal of Climate*, 19 (2). pp 276-287.

Li, Y., Glime, J. & Liao, C. (1992) 'Responses of two interacting Sphagnum species to water level'. *Journal of Bryology*, 17 (1). pp 59-70.

Limpasuvan, V. & Hartmann, D. L. (1999) 'Eddies and the annular modes of climate variability'. *Geophysical research letters*, 26 (20). pp 3133-3136.

Lindsay, R. (2010) 'Peatbogs and carbon: A Critical synthesis'. *Unpublished report to RSPB Scotland*.

Lindsay, R. A., Charman, D. J., Everingham, F., O'Reilly, R. M., Palmer, M. A., Rowell, T. A. & Stroud, D. A. (1988) The Flow Country: the Peatlands of Caithness and Sutherland. NCC, Peterborough.

Ljung, K., Björck, S., Renssen, H. & Hammarlund, D. (2008) 'South Atlantic island record reveals a South Atlantic response to the 8.2 kyr event'. *Climate of the Past*, 4 (1). pp 35-45.

Loader, N., McCarroll, D., Van der Knaap, W., Robertson, I. & Gagen, M. (2007) 'Characterizing carbon isotopic variability in Sphagnum'. *The Holocene*, 17 (3). pp 403-410.

Loader, N., Young, G. H., McCarroll, D. & Wilson, R. J. (2013) 'Quantifying uncertainty in isotope dendroclimatology'. *The Holocene*, 0 (0). pp 1-6.

Loader, N., Street-Perrott, F., Daley, T., Hughes, P., Kimak, A., Levanič, T., Mallon, G., Mauquoy, D., Robertson, I. & Roland, T. (2014) 'Simultaneous determination of stable carbon, oxygen, and hydrogen isotopes in cellulose'. *Analytical chemistry*, 87 (1). pp 376-380.

Loader, N., Street-Perrott, F., Mauquoy, D., Roland, T., van Bellen, S., Daley, T., Davies, D., Hughes, P., Pancotto, V. & Young, G. (2016) 'Measurements of hydrogen, oxygen and carbon isotope variability in Sphagnum moss along a micro-topographical gradient in a southern Patagonian peatland'. *Journal of Quaternary Science*, 31 (4). pp 426-435.

Loisel, J. (2012) Autogenic and allogenic controls on carbon dynamics in peatlands from Alaska and Patagonia. PhD Thesis paper. Paper 1124, Lehigh University

Loisel, J. & Garneau, M. (2010) 'Late Holocene paleoecohydrology and carbon accumulation estimates from two boreal peat bogs in eastern Canada: Potential and limits of multi-proxy archives'. *Palaeogeography, Palaeoclimatology, Palaeoecology*, 291 (3). pp 493-533.

Loisel, J. & Yu, Z. (2013) 'Surface vegetation patterning controls carbon accumulation in peatlands'. *Geophysical research letters*, 40 (20). pp 5508-5513.

Loisel, J., Garneau, M. & Hélie, J. F. (2009) 'Modern Sphagnum δ13C signatures follow a surface moisture gradient in two boreal peat bogs, James Bay lowlands, Québec'. *Journal of Quaternary Science*, 24 (3). pp 209-214.

Luckman, B. & Villalba, R. (2001) 'Assessing the synchroneity of glacier fluctuations in the western cordillera of the Americas during the last millennium'. *Interhemispheric Climate Linkages. Academic Press, San Diego, CA*, pp 119-140.

Luterbacher, J. R. G., Neukom, R., Gonzalez-Rouco, F., Fernandez-Donado, L., Raible, C. & Zorita, E. (2011) 'Reconstructed and simulated Medieval Climate Anomaly in southern South America'. *Pages Newsletter*, 19 pp 20-21.

MacKenzie, A., Logan, E., Cook, G. & Pulford, I. (1998) 'Distributions, inventories and isotopic composition of lead in 210 Pb-dated peat cores from contrasting biogeochemical environments: implications for lead mobility'. *Science of the Total Environment*, 223 (1). pp 25-35.

Majoube, M. (1971a) Fractionation in O18 Between ice and water vapor. *Journal de Chimie Physique et de Physico-Chimie Biologique*, 68(4). pp 625.

Majoube, M. (1971b) Oxygen18 and Deuterium fractionation between water and steam. *Journal de Chimie Physique et de Physico-Chimie Biologique*, 68(10). pp 1423

Malmer, N. (2014) 'On the relations between water regime, mass accretion and formation of ombrotrophic conditions in Sphagnum mires'. *Mires and Peat*, 14 (7). pp 1-23.

Malmer, N. & Wallén, B. (1993) 'Accumulation and release of organic matter in ombrotrophic bog hummocks-processes and regional variation'. *Ecography*, 16 (3). pp 193-211.

Malmer, N. & Wallén, B. (1999) 'The dynamics of peat accumulation on bogs: mass balance of hummocks and hollows and its variation throughout a millennium'. *Ecography*, 22 (6). pp 736-750.

Manatsa, D., Morioka, Y., Behera, S. K., Yamagata, T. & Matarira, C. H. (2013) 'Link between Antarctic ozone depletion and summer warming over southern Africa'. *Nature Geoscience*, 6 (11). pp 934-939.

Mancini, M. V. (2009) 'Holocene vegetation and climate changes from a peat pollen record of the forest–steppe ecotone, Southwest of Patagonia (Argentina)'. *Quaternary Science Reviews*, 28 (15). pp 1490-1497.

Mancini, M. V., Páez, M. & Prieto, A. R. (2002) 'Cambios paleoambientales durante los últimos 7000 14 C años en el ecotono bosque-estepa, 47-48 S, Santa Cruz, Argentina'. *Ameghiniana*, 39 (2). pp 151-162.

Mann, M. E. & Jones, P. D. (2003) 'Global surface temperatures over the past two millennia'. *Geophysical research letters*, 30 (15). pp 1820.

Mann, M. E., Zhang, Z., Hughes, M. K., Bradley, R. S., Miller, S. K., Rutherford, S. & Ni, F. (2008) 'Proxy-based reconstructions of hemispheric and global surface temperature variations over the past two millennia'. *Proceedings of the National Academy of Sciences*, 105 (36). pp 13252-13257.

Mann, M. E., Zhang, Z., Rutherford, S., Bradley, R. S., Hughes, M. K., Shindell, D., Ammann, C., Faluvegi, G. & Ni, F. (2009) 'Global signatures and dynamical origins of the Little Ice Age and Medieval Climate Anomaly'. *science*, 326 (5957). pp 1256-1260.

Marden, C. J. & Clapperton, C. M. (1995) 'Fluctuations of the South Patagonian Ice-field during the last glaciation and the Holocene'. *Journal of Quaternary Science*, 10 (3). pp 197-209.

Marini, C., Frankignoul, C. & Mignot, J. (2011) 'Links between the southern annular mode and the Atlantic meridional overturning circulation in a climate model'. *Journal of Climate*, 24 (3). pp 624-640.

Markgraf, V. (1993) 'Paleoenvironments and paleoclimates in Tierra del Fuego and southernmost Patagonia, South America'. *Palaeogeography, Palaeoclimatology, Palaeoecology*, 102 (1). pp 53-68.

Markgraf, V. & Huber, U. M. (2010) 'Late and postglacial vegetation and fire history in Southern Patagonia and Tierra del Fuego'. *Palaeogeography, Palaeoclimatology, Palaeoecology*, 297 (2). pp 351-366.

Markgraf, V., White, J., Figge, R. & Kenny, R. (1995) 'Multivariate climate reconstruction for the last 14,000 years in southernmost South America', *Proceedings of the 11th Annual Pacific Climate, Workshop, Interagency Ecological Program, California Water Resources. Technical Report*. pp. 21-28.

Markgraf, V., Bradbury, J. P., Schwalb, A., Burns, S. J., Stern, C., Ariztegui, D., Gilli, A., Anselmetti, F. S., Stine, S. & Maidana, N. (2003) 'Holocene palaeoclimates of southern Patagonia: limnological and environmental history of Lago Cardiel, Argentina'. *The Holocene*, 13 (4). pp 581-591.

Marshall, G. J. (2003) 'Trends in the Southern Annular Mode from observations and reanalyses'. *Journal of Climate*, 16 (24). pp 4134-4143.

Marshall, J. & Speer, K. (2012) 'Closure of the meridional overturning circulation through Southern Ocean upwelling'. *Nature Geoscience*, 5. pp 171-180.

Marshall, G. J., Stott, P. A., Turner, J., Connolley, W. M., King, J. C. & Lachlan-Cope, T. A. (2004) 'Causes of exceptional atmospheric circulation changes in the Southern Hemisphere'. *Geophysical research letters*, 31 (14).

Marshall, J. D., Lang, B., Crowley, S. F., Weedon, G. P., van Calsteren, P., Fisher, E. H., Holme, R., Holmes, J. A., Jones, R. T. & Bedford, A. (2007) 'Terrestrial impact of abrupt changes in the North Atlantic thermohaline circulation: Early Holocene, UK'. *Geology*, 35 (7). pp 639-642.

Markel, E. R., Booth, R. K. & Qin, Y. (2010) 'Testate amoebae and δ13C of Sphagnum as surface-moisture proxies in Alaskan peatlands'. *The Holocene*, 20 (3). pp 463-475.

Masiokas, M. H., Rivera, A., Espizua, L. E., Villalba, R., Delgado, S. & Aravena, J. C. (2009) 'Glacier fluctuations in extratropical South America during the past 1000years'. *Palaeogeography, Palaeoclimatology, Palaeoecology*, 281 (3). pp 242-268.

Massaferro, J. & Brooks, S. J. (2002) 'Response of chironomids to Late Quaternary environmental change in the Taitao Peninsula, southern Chile'. *Journal of Quaternary Science*, 17 (2). pp 101-111.

Masson-Delmotte, V., Schulz, M., Abe-Ouchi, A., Beer, J., Ganopolski, A., González Rouco, J.F., Jansen, E., Lambeck, K., Luterbacher, J., Naish, T., Osborn, T., Otto-Bliesner, B., Quinn, T., Ramesh, R., Rojas, M., Shao X. and Timmermann A. (2013) 'Information from Paleoclimate Archives'. in Stocker, T.F., Qin, D., Plattner, G.-K., Tignor, M., Allen, S.K., Boschung, J., Nauels, A., Xia, Y., Bex, V. and Midgley, P.M. (ed.) *Climate Change 2013: The Physical Science Basis. Contribution of Working Group I to the Fifth Assessment Report of the Intergovernmental Panel on Climate Change.* Cambridge, United Kingdom and New York, NY, USA: Cambridge University Press.

Matsuoka, K. & Naruse, R. (1999) 'Mass balance features derived from a firn core at Hielo Patagonico Norte, South America'. *Arctic, Antarctic, and Alpine Research*, pp 333-340.

Mauquoy, D. & Barber, K. (1999a) 'A replicated 3000 yr proxy-climate record from Coom Rigg Moss and Felecia Moss, the Border Mires, northern England'. *Journal of Quaternary Science*, 14 (3). pp 263-275.

Mauquoy, D. & Barber, K. (1999b) 'Evidence for climatic deteriorations associated with the decline of Sphagnum imbricatum Hornsch. ex Russ. in six ombrotrophic mires from northern England and the Scottish Borders'. *The Holocene*, 9 (4). pp 423-437.

Mauquoy, D. & Barber, K. (2002) 'Testing the sensitivity of the palaeoclimatic signal from ombrotrophic peat bogs in northern England and the Scottish Borders'. *Review of Palaeobotany and Palynology*, 119 (3). pp 219-240.

Mauquoy, D. & Bennett, K. (2006) Chapter 11: Peatlands in Tierra del Fuego. In: The biology of peatlands. (eds Rydin, H. & Jeglum, J.) Oxford University Press.

Mauquoy, D. & Van Geel, B. (2007) 'Mire and peat macros'. *Encyclopedia of quaternary science*, 3 pp 2315-2336.

Mauquoy, D. & Yeloff, D. (2008) 'Raised peat bog development and possible responses to environmental changes during the mid-to late-Holocene. Can the palaeoecological record be used to predict the nature and response of raised peat bogs to future climate change?'. *Biodiversity and conservation*, 17 (9). pp 2139-2151.

Mauquoy, D., Hughes, P. & van Geel, B. (2010) 'A protocol for plant macrofossil analysis of peat deposits'. *Mires and Peat*, 7 (06). pp 1-5.

Mauquoy, D., Engelkes, T., Groot, M., Markesteijn, F., Oudejans, M., Van Der Plicht, J. & Van Geel, B. (2002) 'High-resolution records of late-Holocene climate change and carbon accumulation in two north-west European ombrotrophic peat bogs'. *Palaeogeography, Palaeoclimatology, Palaeoecology*, 186 (3). pp 275-310.

Mauquoy, D., Blaauw, M., van Geel, B., Borromei, A., Quattrocchio, M., Chambers, F. M. & Possnert, G. (2004) 'Late Holocene climatic changes in Tierra del Fuego based on multiproxy analyses of peat deposits'. *Quaternary Research*, 61 (2). pp 148-158.

Mauquoy, D., Yeloff, D., Van Geel, B., Charman, D. J. & Blundell, A. (2008) 'Two decadally resolved records from north-west European peat bogs show rapid climate changes associated with solar variability during the mid–late Holocene'. *Journal of Quaternary Science*, 23 (8). pp 745-763.

Mayewski, P. A., Meredith, M., Summerhayes, C., Turner, J., Worby, A., Barrett, P., Casassa, G., Bertler, N. A., Bracegirdle, T. & Naveira Garabato, A. (2009) 'State of the Antarctic and Southern Ocean climate system'. *Reviews of Geophysics*, 47 (1).

Mayr, C., Fey, M., Haberzettl, T., Janssen, S., Lücke, A., Maidana, N. I., Ohlendorf, C., Schäbitz, F., Schleser, G. H. & Struck, U. (2005) 'Palaeoenvironmental changes in southern Patagonia during the last millennium recorded in lake sediments from Laguna Azul (Argentina)'. *Palaeogeography, Palaeoclimatology, Palaeoecology*, 228 (3). pp 203-227.

Mayr, C., Wille, M., Haberzettl, T., Fey, M., Janssen, S., Lücke, A., Ohlendorf, C., Oliva, G., Schäbitz, F. & Schleser, G. H. (2007a) 'Holocene variability of the Southern Hemisphere westerlies in Argentinean Patagonia (52 S)'. *Quaternary Science Reviews*, 26 (5). pp 579-584.

Mayr, C., Lücke, A., Stichler, W., Trimborn, P., Ercolano, B., Oliva, G., Ohlendorf, C., Soto, J., Fey, M. & Haberzettl, T. (2007b) 'Precipitation origin and evaporation of lakes in semi-arid Patagonia (Argentina) inferred from stable isotopes ($\delta^{18}O$,$\delta^{2}H$)'. *Journal of Hydrology*, 334 (1). pp 53-63.

Mayr, C., Lücke, A., Maidana, N. I., Wille, M., Haberzettl, T., Corbella, H., Ohlendorf, C., Schäbitz, F., Fey, M. & Janssen, S. (2009) 'Isotopic fingerprints on lacustrine organic matter from Laguna Potrok Aike (southern Patagonia, Argentina) reflect environmental changes during the last 16,000 years'. *Journal of Paleolimnology*, 42 (1). pp 81-102.

Mayr, C., Lücke, A., Wagner, S., Wissel, H., Ohlendorf, C., Haberzettl, T., Oehlerich, M., Schäbitz, F., Wille, M. & Zhu, J. (2013) 'Intensified Southern Hemisphere Westerlies regulated atmospheric CO2 during the last deglaciation'. *Geology*, 41 (8). pp 831-834.

McCarroll, D. (2010) 'Future climate change and the British Quaternary research community'. *Quaternary Science Reviews*, 29 (13). pp 1661-1672.

McCarroll, D. & Loader, N. J. (2004) 'Stable isotopes in tree rings'. *Quaternary Science Reviews*, 23 (7). pp 771-801.

McClymont, E., Pendall, E. & Nichols, J. (2010) 'Stable isotopes and organic geochemistry in peat: tools to investigate past hydrology, temperature and biogeochemistry'. *PAGES news.*, 18 (1). pp 15-18.

McCormac, F. G., Hogg, A. G., Blackwell, P. G., Buck, C. E., Higham, T. F. & Reimer, P. J. (2004) 'SHCal04 Southern Hemisphere calibration, 0–11.0 cal kyr BP'.

McCulloch, R. D. & Davies, S. J. (2001) 'Late-glacial and Holocene palaeoenvironmental change in the central Strait of Magellan, southern Patagonia'. *Palaeogeography, Palaeoclimatology, Palaeoecology*, 173 (3). pp 143-173.

McMullen, J. A., Barber, K. E. & Johnson, B. (2004) 'A paleoecological perspective of vegetation succession on raised bog microforms'. *Ecological Monographs*, 74 (1). pp 45-77.

Meehl, G. A., Covey, C., Taylor, K. E., Delworth, T., Stouffer, R. J., Latif, M., McAvaney, B. & Mitchell, J. F. (2007) 'The WCRP CMIP3 multimodel dataset: A new era in climate change research'. *Bulletin of the American Meteorological Society*, 88 (9). pp 1383-1394.

Meehl, G. A., Arblaster, J. M., Matthes, K., Sassi, F. & van Loon, H. (2009) 'Amplifying the Pacific climate system response to a small 11-year solar cycle forcing'. *science*, 325 (5944). pp 1114-1118.

Mendes, M. C. D., Trigo, R. M., Cavalcanti, I. F. & DaCamara, C. C. (2008) 'Blocking episodes in the Southern Hemisphere: Impact on the climate of adjacent continental areas'. *Pure and Applied Geophysics*, 165 (9-10). pp 1941-1962.

Ménot, G. & Burns, S. J. (2001) 'Carbon isotopes in ombrogenic peat bog plants as climatic indicators: calibration from an altitudinal transect in Switzerland'. *Organic geochemistry*, 32 (2). pp 233-245.

Ménot-Combes, G., Burns, S. J. & Leuenberger, M. (2002) 'Variations of $^{18}O/^{16}O$ in plants from temperate peat bogs (Switzerland): implications for paleoclimatic studies'. *Earth and Planetary Science Letters*, 202 (2). pp 419-434.

Menounos, B., Clague, J. J., Osborn, G., Davis, P. T., Ponce, F., Goehring, B., Maurer, M., Rabassa, J., Coronato, A. & Marr, R. (2013) 'Latest Pleistocene and Holocene glacier fluctuations in southernmost Tierra del Fuego, Argentina'. *Quaternary Science Reviews*, 77 pp 70-79.

Merlivat, L. & Jouzel, J. (1979) 'Global climatic interpretation of the deuterium-oxygen 18 relationship for precipitation'. *Journal of Geophysical Research: Oceans (1978–2012)*, 84 (C8). pp 5029-5033.

Mertens, K. N., Verhoeven, K., Verleye, T., Louwye, S., Amorim, A., Ribeiro, S., Deaf, A. S., Harding, I. C., De Schepper, S. & González, C. (2009) 'Determining the absolute abundance of dinoflagellate cysts in recent marine sediments: the Lycopodium marker-grain method put to the test'. *Review of Palaeobotany and Palynology*, 157 (3). pp 238-252.

Meyer, I. & Wagner, S. (2008) 'The Little Ice Age in southern Patagonia: Comparison between paleoecological reconstructions and downscaled model output of a GCM simulation'. *PAGES news*, 16 (2). pp 12-13.

Min, S.-K., Zhang, X., Zwiers, F. W. & Hegerl, G. C. (2011) 'Human contribution to more-intense precipitation extremes'. *Nature*, 470 (7334). pp 378-381.

Minchin, P. R. (1987) 'An evaluation of the relative robustness of techniques for ecological ordination'. *Theory and models in vegetation science.* Springer, pp 89-107.

Mitchell, E. A. (2003) 'The identification of Nebela and similar species with indications on their ecology and distribution'. *University of Anchorage, Alaska*

Mitchell, E. A. D. & Gilbert, D. (2004) 'Vertical Micro-Distribution and Response to Nitrogen Deposition of Testate Amoebae in Sphagnum'. *Journal of Eukaryotic Microbiology*, 51 (4). pp 480-490.

Mitchell, E. A., Payne, R. J. & Lamentowicz, M. (2008) 'Potential implications of differential preservation of testate amoeba shells for paleoenvironmental reconstruction in peatlands'. *Journal of Paleolimnology*, 40 (2). pp 603-618.

Mitchell, E. A., Payne, R. J., van der Knaap, W. O., Lamentowicz, Ł., Gąbka, M. & Lamentowicz, M. (2013) 'The performance of single-and multi-proxy transfer functions (testate amoebae, bryophytes, vascular plants) for reconstructing mire surface wetness and pH'. *Quaternary Research*, 79 (1). pp 6-13.

Mohtadi, M., Romero, O. E., Kaiser, J. & Hebbeln, D. (2007) 'Cooling of the southern high latitudes during the Medieval Period and its effect on ENSO'. *Quaternary Science Reviews*, 26 (7). pp 1055-1066.

Montecinos, A. & Aceituno, P. (2003) 'Seasonality of the ENSO-related rainfall variability in central Chile and associated circulation anomalies'. *Journal of Climate*, 16 (2). pp 281-296.

Moore, P. (1977) 'Stratigraphy and pollen analysis of Claish Moss, north-west Scotland: significance for the origin of surface-pools and forest history'. *The Journal of Ecology*, pp 375-397.

Moore, T. (1989) 'Growth and net production of Sphagnum at five fen sites, subarctic eastern Canada'. *Canadian Journal of Botany*, 67 (4). pp 1203-1207.

Moore, P. D. & Bellamy, D. J. (1974) *Peatlands.* London, England:

Moreno, P. I. (2004) 'Millennial-scale climate variability in northwest Patagonia over the last 15 000 yr'. *Journal of Quaternary Science*, 19 (1). pp 35-47.

Moreno, P., Francois, J., Moy, C. & Villa-Martínez, R. (2010) 'Covariability of the Southern Westerlies and atmospheric CO2 during the Holocene'. *Geology*, 38 (8). pp 727-730.

Moreno, P., François, J., Villa-Martínez, R. & Moy, C. (2009) 'Millennial-scale variability in Southern Hemisphere westerly wind activity over the last 5000 years in SW Patagonia'. *Quaternary Science Reviews*, 28 (1). pp 25-38.

Moreno, P. I., Vilanova, I., Villa-Martínez, R., Garreaud, R., Rojas, M. & De Pol-Holz, R. (2014) 'Southern Annular Mode-like changes in southwestern Patagonia at centennial timescales over the last three millennia'. *Nature communications*, 5 pp 1-7.

Morris, P. J., Waddington, J. M., Benscoter, B. W. & Turetsky, M. R. (2011a) 'Conceptual frameworks in peatland ecohydrology: looking beyond the two-layered (acrotelm–catotelm) model'. *Ecohydrology*, 4 (1). pp 1-11.

Morris, P. J., Belyea, L. R. & Baird, A. J. (2011b) 'Ecohydrological feedbacks in peatland development: a theoretical modelling study'. *Journal of Ecology*, 99 (5). pp 1190-1201.

Morris, P., Baird, A. & Belyea, L. (2013) 'The role of hydrological transience in peatland pattern formation'. *Earth Surface Dynaics Discussions*, 1 pp 31-66.

Moschen, R., Kühl, N., Rehberger, I. & Lücke, A. (2009) 'Stable carbon and oxygen isotopes in sub-fossil *Sphagnum*: Assessment of their applicability for palaeoclimatology'. *Chemical geology*, 259 (3). pp 262-272.

Moy, C. M., Seltzer, G. O., Rodbell, D. T. & Anderson, D. M. (2002) 'Variability of El Niño/Southern Oscillation activity at millennial timescales during the Holocene epoch'. *Nature*, 420 (6912). pp 162-165.

Moy, C. M., Dunbar, R. B., Moreno, P. I., Francois, J. P., Villa-Martínez, R., Mucciarone, D. M., Guilderson, T. P. & Garreaud, R. D. (2008) 'Isotopic evidence for hydrologic change related to the westerlies in SW Patagonia, Chile, during the last millennium'. *Quaternary Science Reviews*, 27 (13). pp 1335-1349.

Moy, C. M., Moreno, P. I., Dunbar, R. B., Kaplan, M. R., Francois, J.-P., Villalba, R. & Haberzettl, T. (2009) 'Climate change in southern South America during the last two millennia'. *Past Climate Variability in South America and Surrounding Regions.* Springer, pp 353-393.

Moy, C. M., Dunbar, R. B., Guilderson, T. P., Waldmann, N., Mucciarone, D. A., Recasens, C., Ariztegui, D., Austin, J. A. & Anselmetti, F. S. (2011) 'A geochemical and sedimentary record of high southern latitude Holocene climate evolution from Lago Fagnano, Tierra del Fuego'. *Earth and Planetary Science Letters*, 302 (1). pp 1-13.

Mühlinghaus, C., Scholz, D. & Mangini, A. (2008) 'Temperature and precipitation records from stalagmites grown under disequilibrium conditions: a first approach'. *Earth and Planetary Science Letters*, 233 pp 17-32.

Mundo, I. A., Junent, F. A. R., Villalba, R., Kitzberger, T. & Barrera, M. D. (2012) 'Araucaria araucana tree-ring chronologies in Argentina: spatial growth variations and climate influences'. *Trees*, 26 (2). pp 443-458.

Musotto, L. L., Borromei, A. M., Coronato, A., Menounos, B., Osborn, G. & Marr, R. (2016) 'Late Pleistocene and Holocene palaeoenvironmental changes in central Tierra del Fuego (~ 54° S) inferred from pollen analysis'. *Vegetation history and archaeobotany*, 25 (2). pp 117-130.

Myrhe, G., Shindell, D., Bréon, F-M., Collins, W., Fuglestvedt, J., Huang, J., Koch, D., Lamarque, J-F., Lee, G., Mendoza, B., Nakajima, T., Robock, Stephens, G., Takemura, T. and Zhang, H. (2013) 'Anthropogenic and Natural Radiative Forcing' in Stocker, T.F., Qin, D., Plattner, G.-K., Tignor, M., Allen, S.K., Boschung, J., Nauels, A., Xia, Y., Bex, V. and Midgley, P.M. (ed.) *Climate Change 2013: The Physical Science Basis. Contribution of Working Group I to the Fifth Assessment Report of the Intergovernmental Panel on Climate Change.* Cambridge, United Kingdom and New York, NY, USA: Cambridge University Press.

Neukom, R., Luterbacher, J., Villalba, R., Küttel, M., Frank, D., Jones, P., Grosjean, M., Esper, J., Lopez, L. & Wanner, H. (2010) 'Multi-centennial summer and winter precipitation variability in southern South America'. *Geophysical research letters*, 37 (14). pp L14708.

Neukom, R., Luterbacher, J., Villalba, R., Küttel, M., Frank, D., Jones, P., Grosjean, M., Wanner, H., Aravena, J. C. & Black, D. (2011) 'Multiproxy summer and winter surface air temperature field reconstructions for southern South America covering the past centuries'. *Climate dynamics*, 37 (1). pp 35-51.

Neukom, R. & Gergis, J. (2012) 'Southern Hemisphere high-resolution palaeoclimate records of the last 2000 years'. *The Holocene*, 22 (5). pp 501-524.

Nichols, J. E., Walcott, M., Bradley, R., Pilcher, J. & Huang, Y. (2009) 'Quantitative assessment of precipitation seasonality and summer surface wetness using ombrotrophic sediments from an Arctic Norwegian peatland'. *Quaternary Research*, 72 (3). pp 443-451.

Nicholls, N. (2010) 'Local and remote causes of the southern Australian autumn-winter rainfall decline, 1958–2007'. *Climate dynamics*, 34 (6). pp 835-845.

Nilsson, M., Klarqvist, M., Bohlin, E. & Possnert, G. (2001) 'Variation in 14C age of macrofossils and different fractions of minute peat samples dated by AMS'. *The Holocene*, 11 (5). pp 579-586.

Noller, J. (2000) 'Lead-210 Geochronology, chapter Noller, JS, and Sowers, JM, and Lettis, WR'. *AGU Reference Shelf.* pp 115-120.

Nungesser, M. K. (2003) 'Modelling microtopography in boreal peatlands: hummocks and hollows'. *Ecological Modelling*, 165 (2). pp 175-207.

Ohlson, M. & Dahlberg, B. (1991) 'Rate of peat increment in hummock and lawn communities on Swedish mires during the last 150 years'. *Oikos*, pp 369-378.

Ohlson, M. & Halvorsen Økland, R. (1998) 'Spatial variation in rates of carbon and nitrogen accumulation in a boreal bog'. *Ecology*, 79 (8). pp 2745-2758.

Oldfield, F., Richardson, N. & Appleby, P. (1995) 'Radiometric dating (210Pb, 137Cs, 241Am) of recent ombrotrophic peat accumulation and evidence for changes in mass balance'. *The Holocene*, 5 (2). pp 141-148.

Olsson, I. U. (1986) 'A study of errors in 14 C dates of peat and sediment'. *Radiocarbon*, 28 (2A). pp 429-435.

Osvald, H. (1923) *Die Vegetation des Hochmoores Komosse*. Uppsala University.

Otley, H., Munro, G., Clausen, A. & Ingham, B. (2008) 'Falkland Islands state of the environment report 2008'. *Falkland Islands Government and Falklands Conservation, Stanley*.

Pages 2k (2013) 'Continental-scale temperature variability during the past two millennia'. *Nature Geoscience*, 6. 339-346.

Pakarinen, P. & Tolonen, K. (1977) 'On the growth-rate and dating of surface peat'. *Suo*, 28 pp 19-24.

Pancost, R. D., van Geel, B., Baas, M. & Damsté, J. S. S. (2000) 'δ13C values and radiocarbon dates of microbial biomarkers as tracers for carbon recycling in peat deposits'. *Geology*, 28 (7). pp 663-666.

Parker, D. (1983) 'Documentation of a Southern Oscillation index'. *Meteorol. Mag*, 112 pp 184-188.

Parkinson, C. & Cavalieri, D. (2012) 'Antarctic sea ice variability and trends, 1979–2010'. *The Cryosphere Discussions*, 6 (2). pp 931-956.

Parry, L. E., Charman, D. J. & Blake, W. H. (2013) 'Comparative dating of recent peat deposits using natural and anthropogenic fallout radionuclides and Spheroidal Carbonaceous Particles (SCPs) at a local and landscape scale'. *quaternary geochronology*, 15 pp 11-19.

Paruelo, J. M., Beltran, A., Jobbagy, E., Sala, O. E. & Golluscio, R. A. (1998) 'The climate of Patagonia: general patterns and controls on biotic'. *Ecol Austral*, 8 pp 85-101.

Payne, R. J. & Mitchell, E. A. (2007) 'Ecology of testate amoebae from mires in the Central Rhodope Mountains, Greece and development of a transfer function for palaeohydrological reconstruction'. *Protist*, 158 (2). pp 159-171.

Payne, R. J. & Mitchell, E. A. (2009) 'How many is enough? Determining optimal count totals for ecological and palaeoecological studies of testate amoebae'. *Journal of Paleolimnology*, 42 (4). pp 483-495.

Pelletier, L., Garneau, M. & Moore, T. (2011) 'Variation in CO2 exchange over three summers at microform scale in a boreal bog, Eastmain region, Québec, Canada'. *Journal of Geophysical Research: Biogeosciences*, 116 (G3).

Pendall, E., Markgraf, V., White, J. W. C., Dreier, M. & Kenny, R. (2001) 'Multiproxy record of late Pleistocene–Holocene climate and vegetation changes from a peat bog in Patagonia'. *Quaternary Research*, 55 (2). pp 168-178.

Pennington, W. (1974) The History of British Vegetation. The English Universities Press Ltd., London.

Philander, S. G. (1990) *El Niño, La Niña, and the southern oscillation.* vol. 46. Academic press San Diego.

Pike, J., Swann, G. E., Leng, M. J. & Snelling, A. M. (2013) 'Glacial discharge along the west Antarctic Peninsula during the Holocene'. *Nature Geoscience*, 6 (3). pp 199-202.

Piotrowska, N., Blaauw, M., Mauquoy, D. & Chambers, F. (2011) 'Constructing deposition chronologies for peat deposits using radiocarbon dating'. *Mires and Peat*, 7 pp 1-14.

Planas, X., Ponsa, À., Coronato, A. & Rabassa, J. (2002) 'Geomorphological evidence of different glacial stages in the Martial cirque, Fuegian Andes, southernmost South America'. *Quaternary international*, 87 (1). pp 19-27.

Polvani, L. M. & Kushner, P. J. (2002) 'Tropospheric response to stratospheric perturbations in a relatively simple general circulation model'. *Geophysical research letters*, 29 (7). pp 1114.

Polvani, L. M., Waugh, D. W., Correa, G. J. & Son, S.-W. (2011) 'Stratospheric ozone depletion: The main driver of twentieth-century atmospheric circulation changes in the Southern Hemisphere'. *Journal of Climate*, 24 (3). pp 795-812.

Ponce, J. F., Borromei, A., Rabassa, J. & Martinez, O. (2011) 'Late Quaternary palaeoenvironmental change in western Staaten Island (54.5 S, 64 W), Fuegian Archipelago'. *Quaternary international*, 233 (2). pp 89-100.

Preiss, N., Mélières, M.-A. & Pourchet, M. (1996) 'A compilation of data on lead 210 concentration in surface air and fluxes at the air-surface and water-sediment interfaces'. *Journal of Geophysical Research*, 101 (D22). pp 28847-28862.

Previdi, M. & Liepert, B. G. (2007) 'Annular modes and Hadley cell expansion under global warming'. *Geophysical research letters*, 34 (22). pp L22701.

Price, G. D., McKenzie, J. E., Pilcher, J. R. & Hoper, S. T. (1997) 'Carbon-isotope variation in Sphagnum from hummock-hollow complexes: implications for Holocene climate reconstruction'. *The Holocene*, 7 (2). pp 229-233.

Purich, A., Cowan, T., Min, S.-K. & Cai, W. (2013) 'Autumn precipitation trends over Southern Hemisphere midlatitudes as simulated by CMIP5 models'. *Journal of Climate*, 26 (21). pp 8341-8356.

Ramette, A. (2007) 'Multivariate analyses in microbial ecology'. *FEMS Microbiology Ecology*, 62 (2). pp 142-160.

Reimer, P. J., Brown, T. A. & Reimer, R. W. (2004) 'Discussion: reporting and calibration of post-bomb 14C data'. *Radiocarbon*, 46 (3). pp 1299-1304.

Reimer, P. J., Bard, E., Bayliss, A., Beck, J. W., Blackwell, P. G., Bronk Ramsey, C., Buck, C. E., Cheng, H., Edwards, R. L. & Friedrich, M. (2013) 'IntCal13 and Marine13 radiocarbon age calibration curves 0-50,000 years cal BP'. *Radiocarbon*, 55 (4). pp 1869-1887.

Rein, B., Lückge, A. & Sirocko, F. (2004) 'A major Holocene ENSO anomaly during the Medieval period'. *Geophysical research letters*, 31 (17).

Renssen, H., Goosse, H. & Muscheler, R. (2006) 'Coupled climate model simulation of Holocene cooling events: oceanic feedback amplifies solar forcing'. *Climate of the Past*, 2 (2). pp 79-90.

Rice, S. K. (2000) 'Variation in carbon isotope discrimination within and among Sphagnum species in a temperate wetland'. *Oecologia*, 123 (1). pp 1-8.

Rice, S. & Giles, L. (1996) 'The influence of water content and leaf anatomy on carbon isotope discrimination and photosynthesis in Sphagnum'. *Plant, Cell & Environment*, 19 (1). pp 118-124.

Rignot, E., Rivera, A. & Casassa, G. (2003) 'Contribution of the Patagonia Icefields of South America to sea level rise'. *science*, 302 (5644). pp 434-437.

Rind, D., Chandler, M., Lerner, J., Martinson, D. & Yuan, X. (2001) 'Climate response to basin-specific changes in latitudinal temperature gradients and implications for sea ice variability'. *Journal of Geophysical Research: Atmospheres (1984–2012)*, 106 (D17). pp 20161-20173.

Rinne, K., Boettger, T., Loader, N., Robertson, I., Switsur, V. & Waterhouse, J. S. (2005) 'On the purification of α-cellulose from resinous wood for stable isotope (H, C and O) analysis'. *Chemical geology*, 222 (1). pp 75-82.

Robertson, A., Overpeck, J., Rind, D., Mosley-Thompson, E., Zielinski, G., Lean, J., Koch, D., Penner, J., Tegen, I. & Healy, R. (2001) 'Hypothesized climate forcing time series for the last 500 years'. *Journal of Geophysical Research: Atmospheres*, 106 (D14). pp 14783-14803.

Robson, T. M., Pancotto, V. A., Flint, S. D., Ballaré, C. L., Sala, O. E., Scopel, A. L. & Caldwell, M. M. (2003) 'Six years of solar UV-B manipulations affect growth of Sphagnum and vascular plants in a Tierra del Fuego peatland'. *New phytologist*, 160 (2). pp 379-389.

Robson, T. M., Pancotto, V. A., Scopel, A. L., Flint, S. D. & Caldwell, M. M. (2005) 'Solar UV-B influences microfaunal community composition in a Tierra del Fuego peatland'. *Soil Biology and Biochemistry*, 37 (12). pp 2205-2215.

Robinson, S. A. & Erickson, D. J. (2015) 'Not just about sunburn–the ozone hole's profound effect on climate has significant implications for Southern Hemisphere ecosystems'. *Global Change Biology*, 21 (2). pp 515-527.

Robroek, B. J., Schouten, M. G., Limpens, J., Berendse, F. & Poorter, H. (2009) 'Interactive effects of water table and precipitation on net CO2 assimilation of three co-occurring sphagnum mosses differing in distribution above the water table'. *Global Change Biology*, 15 (3). pp 680-691.

Rochefort, L., Vitt, D. H. & Bayley, S. E. (1990) 'Growth, production, and decomposition dynamics of Sphagnum under natural and experimentally acidified conditions'. *Ecology*, 71 (5). pp 1986-2000.

Roden, J. S., Lin, G. & Ehleringer, J. R. (2000) 'A mechanistic model for interpretation of hydrogen and oxygen isotope ratios in tree-ring cellulose'. *Geochimica et Cosmochimica Acta*, 64 (1). pp 21-35.

Roig, C. (2004). Antecedentes sobre turberas en Tierra del Fuego. In D. E. Blanco, & V. M. de la Balze (Eds.), *Los Turbales de la Patagonia: Bases para su inventario y la conservación de su biodiversidad* (pp. 33–43). Buenos Aires, Argentina: Wetlands International.

Roland, T., Caseldine, C., Charman, D., Turney, C. & Amesbury, M. (2014) 'Was there a '4.2 ka event'in Great Britain and Ireland? Evidence from the peatland record'. *Quaternary Science Reviews*, 83 pp 11-27.

Roland, T., Daley, T., Caseldine, C., Charman, D., Turney, C., Amesbury, M., Thompson, G. & Woodley, E. (2015) 'The 5.2 ka climate event: Evidence from stable isotope and multi-proxy palaeoecological peatland records in Ireland'. *Quaternary Science Reviews*, 124 pp 209-223.

Rose, N., Harlock, S., Appleby, P. & Battarbee, R. (1995) 'Dating of recent lake sediments in the United Kingdom and Ireland using spheroidal carbonaceous particle (SCP) concentration profiles'. *The Holocene*, 5 (3). pp 328-335.

Rosén, K., Vinichuk, M. & Johanson, K. (2009) '137 Cs in a raised bog in central Sweden'. *Journal of environmental radioactivity*, 100 (7). pp 534-539.

Royles, J., Ogée, J., Wingate, L., Hodgson, D. A., Convey, P. & Griffiths, H. (2012) 'Carbon isotope evidence for recent climate-related enhancement of CO 2 assimilation and peat accumulation rates in Antarctica'. *Global Change Biology*, 18 (10). pp 3112-3124.

Royles, J., Amesbury, M. J., Convey, P., Griffiths, H., Hodgson, D. A., Leng, M. J. & Charman, D. J. (2013a) 'Plants and soil microbes respond to recent warming on the Antarctic Peninsula'. *Current Biology*, 23 (17). pp 1702-1706.

Royles, J., Sime, L. C., Hodgson, D. A., Convey, P. & Griffiths, H. (2013b) 'Differing source water inputs, moderated by evaporative enrichment, determine the contrasting d18O CELLULOSE signals in maritime Antarctic moss peat banks.'. *Journal of Geophysical Research*, 118 pp 1-11.

Royles, J., Amesbury, M. J., Roland, T. P., Jones, G. D., Convey, P., Griffiths, H., Hodgson, D. A. & Charman, D. J. (2016) 'Moss stable isotopes (carbon-13, oxygen-18) and testate amoebae reflect environmental inputs and microclimate along a latitudinal gradient on the Antarctic Peninsula'. *Oecologia*, pp 1-15.

Rozanski, K. (1985) 'Deuterium and O-18 in European Groundwaters - Links to Atmospheric Circulation in the Past'. *Chemical geology*, 52 pp 349-363.

Rozanski, K., Araguás-Araguás, L. & Gonfiantini, R. (1992) 'Relation between long-term trends of oxygen-18 isotope composition of precipitation and climate'. *science*, 258 (5084). pp 981-985.

Rozanski, K., Araguás-Araguás, L. & Gonfiantini, R. (1993) 'Isotopic patterns in modern global precipitation'. *Geophysical Monograph Series*, 78 pp 1-36.

Rozanski, K. & Araguás-Araguás, L. (1995) 'Spatial and temporal variability of stable isotope composition of precipitation over the South American continent'. *Bull. Inst. fr. études andines*, 24 (3). pp 379-390.

Rozanski, K., Johnsen, S. J., Schotterer, U. & Thompson, L. (1997) 'Reconstruction of past climates from stable isotope records of palaeo-precipitation preserved in continental archives'. *Hydrological sciences journal*, 42 (5). pp 725-745.

Rull, V. (2010) 'Ecology and palaeoecology: two approaches, one objective'. *Open Ecology Journal*, 3 pp 1-5.

Russell, A. & McGregor, G. R. (2010) 'Southern hemisphere atmospheric circulation: impacts on Antarctic climate and reconstructions from Antarctic ice core data'. *Climatic Change*, 99 (1-2). pp 155-192.

Rydin, H. & Jeglum, J. (2006) *The biology of peatlands.* Oxford University Press.

Salati, E., Dall'Olio, A., Matsui, E. & Gat, J. R. (1979) 'Recycling of water in the Amazon basin: an isotopic study'. *Water Resources Research*, 15 (5). pp 1250-1258.

Sallée, J., Speer, K. & Rintoul, S. (2010) 'Zonally asymmetric response of the Southern Ocean mixed-layer depth to the Southern Annular Mode'. *Nature Geoscience*, 3 (4). pp 273-279.

Sanchez-Goñi, M., Cacho, I., Turon, J.-L., Guiot, J., Sierro, F., Peypouquet, J., Grimalt, J. & Shackleton, N. (2002) 'Synchroneity between marine and terrestrial responses to millennial scale climatic variability during the last glacial period in the Mediterranean region'. *Climate dynamics*, 19 (1). pp 95-105.

Sapkota, A., Cheburkin, A. K., Bonani, G. & Shotyk, W. (2007) 'Six millennia of atmospheric dust deposition in southern South America (Isla Navarino, Chile)'. *The Holocene*, 17 (5). pp 561-572.

Saurer, M., Siegwolf, R. T. & Schweingruber, F. H. (2004) 'Carbon isotope discrimination indicates improving water-use efficiency of trees in northern Eurasia over the last 100 years'. *Global Change Biology*, 10 (12). pp 2109-2120.

Schäbitz, F., Wille, M., Francois, J.-P., Haberzettl, T., Quintana, F., Mayr, C., Lücke, A., Ohlendorf, C., Mancini, V. & Paez, M. M. (2013) 'Reconstruction of palaeoprecipitation based on pollen transfer functions–the record of the last 16 ka from Laguna Potrok Aike, southern Patagonia'. *Quaternary Science Reviews*, 71 pp 175-190.

Schimpf, D., Kilian, R., Kronz, A., Simon, K., Spötl, C., Wörner, G., Deininger, M. & Mangini, A. (2011) 'The significance of chemical, isotopic, and detrital components in three coeval stalagmites from the superhumid southernmost Andes (53° S) as high-resolution palaeo-climate proxies'. *Quaternary Science Reviews*, 30 (3). pp 443-459.

Schipperges, B. & Rydin, H. (1998) 'Response of photosynthesis of Sphagnum species from contrasting microhabitats to tissue water content and repeated desiccation'. *New phytologist*, 140 (4). pp 677-684.

Schneider, C. & Gies, D. (2004) 'Effects of El Niño–Southern Oscillation on southernmost South America precipitation at 53° S revealed from NCEP–NCAR reanalyses and weather station data'. *International journal of climatology*, 24 (9). pp 1057-1076.

Schneider, D. P., Okumura, Y. & Deser, C. (2012) 'Observed Antarctic interannual climate variability and tropical linkages'. *Journal of Climate*, 25 (12). pp 4048-4066.

Schnitzer, M. (1982) Organic matter characterization. In: Page A.L. (Ed) Methods of Soil Analysis, Part 2. Chemical and Microbiological Properties – Agronomy Monograph 9 (pp 581–593). American Society of Agronomy, Inc. and Soil Science of Society of America, Inc., Madison.

Schoning, K., Charman, D. J. & Wastegoard, S. (2005) 'Reconstructed water tables from two ombrotrophic mires in eastern central Sweden compared with instrumental meteorological data'. *The Holocene*, 15 (1). pp 111-118.
Searles, P. S., Flint, S. D., Díaz, S. B., Rousseaux, M. C., Ballaré, C. L. & Caldwell, M. M. (1999) 'Solar ultraviolet-B radiation influence on Sphagnum bog and Carex fen ecosystems: first field season findings in Tierra del Fuego, Argentina'. *Global Change Biology*, 5 (2). pp 225-234.

Searles, P. S., Kropp, B. R., Flint, S. D. & Caldwell, M. M. (2001) 'Influence of solar UV-B radiation on peatland microbial communities of southern Argentinia'. *New phytologist*, 152 (2). pp 213-221.

Sexton, D. (2001) 'The effect of stratospheric ozone depletion on the phase of the Antarctic Oscillation'. *Geophysical research letters*, 28 (19). pp 3697-3700.

Sime, L. C., Kohfeld, K. E., Le Quéré, C., Wolff, E. W., de Boer, A. M., Graham, R. M. & Bopp, L. (2013) 'Southern Hemisphere westerly wind changes during the Last Glacial Maximum: model-data comparison'. *Quaternary Science Reviews*, 64 pp 104-120.

Sharp, Z. (2007) *Principles of stable isotope geochemistry.* Pearson Education Upper Saddle River, NJ, USA.

Shindell, D. T. & Schmidt, G. A. (2004) 'Southern Hemisphere climate response to ozone changes and greenhouse gas increases'. *Geophysical research letters*, 31 (18). pp L18209.

Shiraiwa, T., Kohshima, S., Uemura, R., Yoshida, N., Matoba, S., Uetake, J. & Godoi, M. A. (2002) 'High net accumulation rates at Campo de Hielo Patagonico Sur, South America, revealed by analysis of a 45.97 m long ice core'. *Annals of Glaciology*, 35 (1). pp 84-90.

Shotyk, W., Weiss, D., Appleby, P., Cheburkin, A., Frei, R., Gloor, M., Kramers, J., Reese, S. & Van Der Knaap, W. (1998) 'History of atmospheric lead deposition since 12,370 14C yr BP from a peat bog, Jura Mountains, Switzerland'. *science*, 281 (5383). pp 1635-1640.

Shulmeister, J., Goodwin, I., Renwick, J., Harle, K., Armand, L., McGlone, M., Cook, E., Dodson, J., Hesse, P. & Mayewski, P. (2004) 'The Southern Hemisphere westerlies in the Australasian sector over the last glacial cycle: a synthesis'. *Quaternary international*, 118 pp 23-53.

Siegenthaler, U. & Oeschger, H. (1980) 'Correlation of 18O in precipitation with temperature and altitude'. *Nature*, 285 pp 314 – 317

Sigmond, M., Fyfe, J. & Scinocca, J. (2010) 'Does the ocean impact the atmospheric response to stratospheric ozone depletion?'. *Geophysical research letters*, 37 (12). pp L12706.

Sillasoo, U., Mauquoy, D., Blundell, A., Charman, D., Blaauw, M., Daniell, J. R., Toms, P., Newberry, J., Chambers, F. M. & Karofeld, E. (2007) 'Peat multi-proxy data from Männikjärve bog as indicators of late Holocene climate changes in Estonia'. *Boreas*, 36 (1). pp 20-37.

Silvestri, G. E. & Vera, C. S. (2003) 'Antarctic Oscillation signal on precipitation anomalies over southeastern South America'. *Geophys. Res. Lett*, 30 (21). pp 2115.

Sime, L. C., Kohfeld, K. E., Le Quéré, C., Wolff, E. W., de Boer, A. M., Graham, R. M. & Bopp, L. (2013) 'Southern Hemisphere westerly wind changes during the Last Glacial Maximum: model-data comparison'. *Quaternary Science Reviews*, 64 pp 104-120.

Skrzypek, G., Kałużny, A. & Jędrysek, M. O. (2007a) 'Carbon stable isotope analyses of mosses—comparisons of bulk organic matter and extracted nitrocellulose'. *Journal of the American Society for Mass Spectrometry*, 18 (8). pp 1453-1458.

Skrzypek, G., Kałużny, A., Wojtuń, B. & Jędrysek, M.-O. (2007b) 'The carbon stable isotopic composition of mosses: a record of temperature variation'. *Organic geochemistry*, 38 (10). pp 1770-1781.

Skrzypek, G. & Sadler, R. (2011) 'A strategy for selection of reference materials in stable oxygen isotope analyses of solid materials'. *Rapid Communications in Mass Spectrometry*, 25 (11). pp 1625.

Smart, P. (1982) 'Stratigraphy of a site in the Munsary Dubh Lochs, Caithness, northern Scotland: development of the present pattern'. *The Journal of Ecology*, pp 549-558.

Smart,P.L. & Frances, P.D. (Eds.) (1991) *Quaternary dating methods a user's guide, QRA Technical Guide 4*. Quaternary Research Association, London.

Solanki, S. K., Usoskin, I. G., Kromer, B., Schüssler, M. & Beer, J. (2004) 'Unusual activity of the Sun during recent decades compared to the previous 11,000 years'. *Nature*, 431 (7012). pp 1084-1087.

Son, S.-W., Polvani, L., Waugh, D., Akiyoshi, H., Garcia, R., Kinnison, D., Pawson, S., Rozanov, E., Shepherd, T. & Shibata, K. (2008) 'The impact of stratospheric ozone recovery on the Southern Hemisphere westerly jet'. *science*, 320 (5882). pp 1486-1489.

Son, S. W., Gerber, E., Perlwitz, J., Polvani, L., Gillett, N., Seo, K. H., Eyring, V., Shepherd, T., Waugh, D. & Akiyoshi, H. (2010) 'Impact of stratospheric ozone on Southern Hemisphere circulation change: A multimodel assessment'. *Journal of Geophysical Research: Atmospheres (1984–2012)*, 115 (D3).

Sonntag, C., Münnich, K., Jacob, H. & Rozanski, K. (1983) 'Variations of deuterium and oxygen-18 in continental precipitation and groundwater, and their causes'. *Variations in the global water budget.* Springer, pp 107-124.

Sottile, G., Echeverria, M., Mancini, M., Bianchi, M., Marcos, M. & Bamonte, F. (2015) 'Eastern Andean environmental and climate synthesis for the last 2000 years BP from terrestrial pollen and charcoal records of Patagonia'. *Climate of the Past Discussions*, 11 pp 2121-2157.

Spence, P., Griffies, S. M., England, M. H., Hogg, A. M., Saenko, O. A. & Jourdain, N. C. (2014) 'Rapid subsurface warming and circulation changes of Antarctic coastal waters by poleward shifting winds'. *Geophysical research letters*, 41 (13). pp 4601-4610.

Stammerjohn, S., Martinson, D., Smith, R., Yuan, X. & Rind, D. (2008) 'Trends in Antarctic annual sea ice retreat and advance and their relation to El Niño–Southern Oscillation and Southern Annular Mode variability'. *Journal of Geophysical Research: Oceans (1978–2012)*, 113 (C3).

Steig, E. J., Mayewski, P. A., Dixon, D. A., Kaspari, S. D., Frey, M. M., Schneider, D. P., Arcone, S. A., Hamilton, G. S., Spikes, V. & Albert, M. (2005) 'High-resolution ice cores from US ITASE (West Antarctica): Development and validation of chronologies and determination of precision and accuracy'. *Annals of Glaciology*, 41 (1). pp 77-84.

Steinhilber, F., Beer, J. & Fröhlich, C. (2009) 'Total solar irradiance during the Holocene'. *Geophysical research letters*, 36 (19). pp L19704.

Steinhilber, F., Abreu, J. A., Beer, J., Brunner, I., Christl, M., Fischer, H., Heikkilä, U., Kubik, P. W., Mann, M. & McCracken, K. G. (2012) '9,400 years of cosmic radiation and solar activity from ice cores and tree rings'. *Proceedings of the National Academy of Sciences*, 109 (16). pp 5967-5971.

Sternberg, L. D. S., Deniro, M. J. & Savidge, R. A. (1986) 'Oxygen isotope exchange between metabolites and water during biochemical reactions leading to cellulose synthesis'. *Plant Physiology*, 82 (2). pp 423-427.

Stern, C. (1990) 'Tephrochronology of southernmost Patagonia'. *National Geographic Research*, 6 (1). pp 110-126.

Stern, C. R. (2008) 'Holocene tephrochronology record of large explosive eruptions in the southernmost Patagonian Andes'. *Bulletin of Volcanology*, 70 (4). pp 435-454.

Stern, L. A. & Blisniuk, P. M. (2002) 'Stable isotope composition of precipitation across the southern Patagonian Andes'. *Journal of Geophysical Research*, 107 (D23). pp 4667.

Stine, S. (1994) 'Extreme and persistent drought in California and Patagonia during mediaeval time'. *Nature*, 369 (6481). pp 546-549.

Stocker, T.F., Qin, D., Plattner, G.-K., Tignor, M., Allen, S.K., Boschung, J., Nauels, A., Xia, Y., Bex, V. and Midgley, P.M. (ed.) *Climate Change 2013: The Physical Science Basis. Contribution of Working Group I to the Fifth Assessment Report of the Intergovernmental Panel on Climate Change.* Cambridge, United Kingdom and New York, NY, USA: Cambridge University Press.

Stockmarr, J. (1971) 'Tablets with spores used in absolute pollen analysis'. *Pollen et spores*, 13 pp 615-621.

Strelin, J. & Iturraspe, R. (2007) 'Recent evolution and mass balance of Cordón Martial glaciers, Cordillera Fueguina Oriental'. *Global and Planetary Change*, 59 (1). pp 17-26.

Strelin, J., Denton, G., Vandergoes, M., Ninnemann, U. & Putnam, A. (2011) 'Radiocarbon chronology of the late-glacial Puerto Bandera moraines, southern Patagonian Icefield, Argentina'. *Quaternary Science Reviews*, 30 (19). pp 2551-2569.

Strother, S. L., Salzmann, U., Roberts, S. J., Hodgson, D. A., Woodward, J., Van Nieuwenhuyze, W., Verleyen, E., Vyverman, W. & Moreton, S. G. (2015) 'Changes in Holocene climate and the intensity of Southern Hemisphere Westerly Winds based on a high-resolution palynological record from sub-Antarctic South Georgia'. *The Holocene*, 25 (2). pp 263-279.

Stuiver, M. & Reimer, P. J. (2006) 'Extended (super 14) C data base and revised CALIB 3.0 (super 14) C age calibration program'. *Radiocarbon*, 35 (1). pp 215-230.

Stuiver, M., Reimer, P. J., Bard, E., Beck, J. W., Burr, G. S., Hughen, K. A., Kromer, B., McCormac, G., Van Der Plicht, J. & Spurk, M. (1998) 'INTCAL98 radiocarbon age calibration, 24,000-0 cal BP'. *Radiocarbon*, 40 (3). pp 1041-1083.

Sturm, C., Zhang, Q. & Noone, D. (2010) 'An introduction to stable water isotopes in climate models: benefits of forward proxy modelling for paleoclimatology'. *Clim. Past*, 6 pp 115-129.

Sullivan, M. E. & Booth, R. K. (2011) 'The potential influence of short-term environmental variability on the composition of testate amoeba communities in Sphagnum peatlands'. *Microbial ecology*, 62 (1). pp 80-93.

Sulman, B. N., Desai, A. R., Saliendra, N. Z., Lafleur, P. M., Flanagan, L. B., Sonnentag, O., Mackay, D. S., Barr, A. G. & van der Kamp, G. (2010) 'CO2 fluxes at northern fens and bogs have opposite responses to inter-annual fluctuations in water table'. *Geophysical research letters*, 37 (19).

Sun, L., Chen, G. & Lu, J. (2013) 'Sensitivities and mechanisms of the zonal mean atmospheric circulation response to tropical warming'. *Journal of the Atmospheric Sciences*, 70 (8). pp 2487-2504.

Sundberg, S. (2005) 'Larger capsules enhance short-range spore dispersal in Sphagnum, but what happens further away?'. *Oikos*, 108 (1). pp 115-124.

Sundberg, S. & Rydin, H. (2002) 'Habitat requirements for establishment of Sphagnum from spores'. *Journal of Ecology*, 90 (2). pp 268-278.

Svensson, G. (1988a) 'Bog development and environmental conditions as shown by the stratigraphy of Store Mosse mire in southern Sweden'. *Boreas*, 17 (1). pp 89-111.

Svensson, G. (1988b) 'Fossil plant communities and regeneration patterns on a raised bog in South Sweden'. *The Journal of Ecology*, pp 41-59.

Swanson, D. K. (2007) 'Interaction of mire microtopography, water supply, and peat accumulation in boreal mires'. *Suo*, 58 (2). pp 37-47.

Swart, N. & Fyfe, J. (2012) 'Observed and simulated changes in the Southern Hemisphere surface westerly wind-stress'. *Geophysical research letters*, 39 (16).

Swindles, G. T. & Roe, H. M. (2007) 'Examining the dissolution characteristics of testate amoebae (Protozoa: Rhizopoda) in low pH conditions: implications for peatland palaeoclimate studies'. *Palaeogeography, Palaeoclimatology, Palaeoecology*, 252 (3). pp 486-496.

Swindles, G. T., Plunkett, G. & Roe, H. M. (2007) 'A delayed climatic response to solar forcing at 2800 cal. BP: multiproxy evidence from three Irish peatlands'. *The Holocene*, 17 (2). pp 177-182.

Swindles, G., De Vleeschouwer, F. & Plunkett, G. (2010) 'Dating peat profiles using tephra: stratigraphy, geochemistry and chronology'. *Mires and Peat*, 7 (05). pp 1-9.

Swindles, G., Charman, D., Roe, H. & Sansum, P. (2009) 'Environmental controls on peatland testate amoebae (Protozoa: Rhizopoda) in the North of Ireland: implications for Holocene palaeoclimate studies'. *Journal of Paleolimnology*, 42 (1). pp 123-140.

Swindles, G. T., Morris, P. J., Baird, A. J., Blaauw, M. & Plunkett, G. (2012a) 'Ecohydrological feedbacks confound peat-based climate reconstructions'. *Geophysical research letters*, 39 (11). pp L11401.

Swindles, G. T., Patterson, R. T., Roe, H. M. & Galloway, J. M. (2012b) 'Evaluating periodicities in peat-based climate proxy records'. *Quaternary Science Reviews*, 41 pp 94-103.

Swindles, G. T., Holden, J., Raby, C. L., Turner, T. E., Blundell, A., Charman, D. J., Menberu, M. W. & Kløve, B. (2015) 'Testing peatland water-table depth transfer functions using high-resolution hydrological monitoring data'. *Quaternary Science Reviews*, 120 pp 107-117.

Tans, P., De Jong, A. & Mook, W. (1979) 'Natural atmospheric 14C variation and the Suess effect'. *Nature*, 280 pp 826-828.

Tapia, C (2008) Crecimiento y productividad del musgo Sphagnum magellanicum Brid. En turberas secundarias de la provincia de Llanquihue, Chile. PhD thesis. Universidad Austral de Chile.

Telford, R. J., Heegaard, E. & Birks, H. J. B. (2004a) 'All age–depth models are wrong: but how badly?'. *Quaternary Science Reviews*, 23 (1). pp 1-5.

Telford, R. J., Heegaard, E. & Birks, H. J. B. (2004b) 'The intercept is a poor estimate of a calibrated radiocarbon age'. *The Holocene*, 14 (2). pp 296-298.

ter Braak, C. J. & Prentice, I. C. (1988) 'A theory of gradient analysis'. *Advances in Ecological Research*, 18 pp 271-317.

Thomas, E. R., Marshall, G. J. & McConnell, J. R. (2008) 'A doubling in snow accumulation in the western Antarctic Peninsula since 1850'. *Geophysical research letters*, 35 (1).

Thompson, D. W. J. & Solomon, S. (2002) 'Interpretation of recent Southern Hemisphere climate change'. *science*, 296 (5569). pp 895-899.

Thompson, D. W., Wallace, J. M. & Hegerl, G. C. (2000) 'Annular modes in the extratropical circulation. Part II: Trends'. *Journal of Climate*, 13 (5). pp 1018-1036.

Tillman, P. K., Holzkämper, S., Kuhry, P., Sannel, A. B. K., Loader, N. J. & Robertson, I. (2010) 'Stable carbon and oxygen isotopes in *Sphagnum fuscum* peat from subarctic Canada: Implications for palaeoclimate studies'. *Chemical geology*, 270 (1). pp 216-226.

Toggweiler, J. (2009) 'Shifting westerlies'. *science*, 323 (5920). pp 1434-1435.

Toggweiler, J. & Russell, J. (2008) 'Ocean circulation in a warming climate'. *Nature*, 451 (7176). pp 286-288.

Toggweiler, J., Russell, J. L. & Carson, S. (2006) 'Midlatitude westerlies, atmospheric CO2, and climate change during the ice ages'. *Paleoceanography*, 21 (2). pp PA2005.

Tolonen, K., Warner, B. G. & Vasander, H. (1992) 'Ecology of testaceans (Protozoa: Rhizopoda) in mires in southern Finland: I. Autecology'. *Archiv für Protistenkunde*, 142 (3). pp 119-138.

Tolonen, K., Warner, B. G. & Vasander, H. (1994) 'Ecology of testaceans (Protozoa: Rhizopoda) in mires in southern Finland: II. Multivariate analysis'. *Archiv für Protistenkunde*, 144 (1). pp 97-112.

Tonello, M. S., Mancini, M. V. & Seppä, H. (2009) 'Quantitative reconstruction of Holocene precipitation changes in southern Patagonia'. *Quaternary Research*, 72 (3). pp 410-420.

Trenberth, K. E. (1997) 'The definition of el nino'. *Bulletin of the American Meteorological Society*, 78 (12). pp 2771-2777.

Trenberth, K. E., Olson, J. G. & Large, W. G. (1989) *A global ocean wind stress climatology based on ECMWF analyses.* Climate and Global Dynamics Division, National Center for Atmospheric Research.

Turetsky, M. R., Manning, S. W. & Wieder, R. K. (2004) 'Dating recent peat deposits'. *Wetlands*, 24 (2). pp 324-356.

Turner, J. (2004) 'The El Niño–Southern Oscillation and Antarctica'. *International journal of climatology*, 24 (1). pp 1-31.

Turner, J., Comiso, J. C., Marshall, G. J., Lachlan-Cope, T. A., Bracegirdle, T., Maksym, T., Meredith, M. P., Wang, Z. & Orr, A. (2009) 'Non-annular atmospheric circulation change induced by stratospheric ozone depletion and its role in the recent increase of Antarctic sea ice extent'. *Geophysical research letters*, 36 (8).

Turner, T. E., Swindles, G. T., Charman, D. J. & Blundell, A. (2013) 'Comparing regional and supra-regional transfer functions for palaeohydrological reconstruction from Holocene peatlands'. *Palaeogeography, Palaeoclimatology, Palaeoecology*, 369, 395-408.

Turney, C., Jones, R., Fogwill, C., Hatton, J., Williams, A., Hogg, A., Thomas, Z., Palmer, J. & Mooney, S. (2015) 'A 250-year periodicity in Southern Hemisphere westerly winds over the last 2600 year'. *Climates of the Past Discussions*, 11 pp 2159-2180.

Upson, R.(2012) 'Important Plant Areas of the Falkland Islands'. Report, Falklands Conservation.

van Bellen, S., Garneau, M. & Booth, R. K. (2011) 'Holocene carbon accumulation rates from three ombrotrophic peatlands in boreal Quebec, Canada: impact of climate-driven ecohydrological change'. *The Holocene*, 21 (8). pp 1217-1231.

van Bellen, S., Mauquoy, D., Payne, R. J., Roland, T. P., Daley, T. J., Hughes, P. D., Loader, N. J., Street-Perrott, F. A., Rice, E. M. & Pancotto, V. A. (2014) 'Testate amoebae as a proxy for reconstructing Holocene water table dynamics in southern Patagonian peat bogs'. *Journal of Quaternary Science*, 29 (5). pp 463-474.

van Bellen, S., Mauquoy, D., Hughes, P. D., Roland, T. P., Daley, T. J., Loader, N. J., Street-Perrott, F. A., Rice, E. M., Pancotto, V. A. & Payne, R. J. (2016) 'Late-Holocene climate dynamics recorded in the peat bogs of Tierra del Fuego, South America'. *The Holocene*, pp 1-13.

van den Bogaard, C., Dörfler, W., Glos, R., Nadeau, M.-J., Grootes, P. M. & Erlenkeuser, H. (2002) 'Two tephra layers bracketing late Holocene paleoecological changes in northern Germany'. *Quaternary Research*, 57 (3). pp 314-324.

Van der Molen, P. & Hoekstra, S. (1988) 'A palaeoecological study of a hummock-hollow complex from Engbertsdijksveen, in the Netherlands'. *Review of Palaeobotany and Palynology*, 56 (3). pp 213-274.

van der Plicht, J., Yeloff, D., Linden, M. v. d., Geel, B. v., Brain, S., Chambers, F. M., Webb, J. & Toms, P. (2013) 'Dating recent peat accumulation in European ombrotrophic bogs'. *Radiocarbon*, 55 (2-3). pp 1763-1778.

Van der Putten, N., Verbruggen, C., Ochyra, R., Spassov, S., de Beaulieu, J. L., De Dapper, M., Hus, J. & Thouveny, N. (2009) 'Peat bank growth, Holocene palaeoecology and climate history of South Georgia (sub-Antarctica), based on a botanical macrofossil record'. *Quaternary Science Reviews*, 28 (1). pp 65-79

Van der Putten, N., Mauquoy, D., Verbruggen, C. & Björck, S. (2012) 'Subantarctic peatlands and their potential as palaeoenvironmental and palaeoclimatic archives'. *Quaternary international*, 268 pp 65-76.

van Geel, B. & Middeldorp, A. (1988) 'Vegetational history of Carbury Bog (Co. Kildare, Ireland) during the last 850 years and a test of the temperature indicator value of 2H/1H measurements of peat samples in relation to historical sources and meteorological data'. *New phytologist*, 109 (3). pp 377-392.

van Geel, B. & Mook, W. (1989) 'High-resolution C-14 dating of organic deposits using natural atmospheric C-14 variations'. *Radiocarbon*, 31 (2). pp 151-155.

van Geel, B. & Renssen, H. (1998) 'Abrupt climate change around 2,650 BP in North-West Europe: evidence for climatic teleconnections and a tentative explanation'. *Water, environment and society in times of climatic change.* Springer, pp 21-41.

van Geel, B., Buurman, J. & Waterbolk, H. T. (1996) 'Archaeological and palaeoecological indications of an abrupt climate change in The Netherlands, and evidence for climatological teleconnections around 2650 BP'. *Journal of Quaternary Science*, 11 (6). pp 451-460.

van Geel, B., Heusser, C. J., Renssen, H. & Schuurmans, C. J. (2000) 'Climatic change in Chile at around 2700 BP and global evidence for solar forcing: a hypothesis'. *The Holocene*, 10 (5). pp 659-664.

Väliranta, M., Korhola, A., Seppä, H., Tuittila, E.-S., Sarmaja-Korjonen, K., Laine, J. & Alm, J. (2007) 'High-resolution reconstruction of wetness dynamics in a southern boreal raised bog, Finland, during the late Holocene: a quantitative approach'. *The Holocene*, 17 (8). pp 1093-1107.

Väliranta, M., Blundell, A., Charman, D., Karofeld, E., Korhola, A., Sillasoo, Ü. & Tuittila, E.-S. (2012) 'Reconstructing peatland water tables using transfer functions for plant macrofossils and testate amoebae: a methodological comparison'. *Quaternary international*, 268 pp 34-43.

Varma, V., Prange, M., Lamy, F., Merkel, U. & Schulz, M. (2010) 'Solar-forced shifts of the Southern Hemisphere Westerlies during the late Holocene'. *Climate of the Past Discussions*, 6 pp 369-384.

Vieira, L. E. A., Solanki, S. K., Krivova, N. A. & Usoskin, I. (2011) 'Evolution of the solar irradiance during the Holocene'. *Astronomy & Astrophysics*, 531

Vile, M. A., Wieder, R. K. & Novák, M. (1999) 'Mobility of Pb inSphagnum-derived peat'. *Biogeochemistry*, 45 (1). pp 35-52.

Villagrán, C. & Barrera, E. (2002) 'Musgos del archipiélago de Chiloé, Chile'. *Corporación Nacional Forestal CONAF.(Chile)*

Villalba, R. (1994) 'Tree-ring and glacial evidence for the Medieval Warm Epoch and the Little Ice Age in southern South America'. *Climatic Change*, 26 (2). pp 183-197.

Villalba, R., Grosjean, M. & Kiefer, T. (2009) 'Long-term multi-proxy climate reconstructions and dynamics in South America (LOTRED-SA): State of the art and perspectives'. *Palaeogeography, Palaeoclimatology, Palaeoecology*, 281 (3). pp 175-179.

Villalba, R., Lara, A., Boninsegna, J. A., Masiokas, M., Delgado, S., Aravena, J. C., Roig, F. A., Schmelter, A., Wolodarsky, A. & Ripalta, A. (2003) 'Large-scale temperature changes across the southern Andes: 20th-century variations in the context of the past 400 years'. *Climatic Change*, 59 (1). pp 177-232.

Villa-Martínez, R. & Moreno, P. I. (2007) 'Pollen evidence for variations in the southern margin of the westerly winds in SW Patagonia over the last 12,600 years'. *Quaternary Research*, 68 (3). pp 400-409.

Vimeux, F., De Angelis, M., Ginot, P., Magand, O., Casassa, G., Pouyaud, B., Falourd, S. & Johnsen, S. (2008) 'A promising location in Patagonia for paleoclimate and paleoenvironmental reconstructions revealed by a shallow firn core from Monte San Valentín (Northern Patagonia Icefield, Chile)'. *Journal of Geophysical Research: Atmospheres (1984–2012)*, 113 (D16).

Vimeux, F., Ginot, P., Schwikowski, M., Vuille, M., Hoffmann, G., Thompson, L. G. & Schotterer, U. (2009) 'Climate variability during the last 1000 years inferred from Andean ice cores: A review of methodology and recent results'. *Palaeogeography, Palaeoclimatology, Palaeoecology*, 281 (3). pp 229-241.

Vinichuk, M., Dahlberg, A. & Rosén, K. (2011) 'Cesium (137Cs and 133Cs), potassium and rubidium in macromycete fungi and sphagnum plants'. INTECH. [Online]. Available at:

http://www.intechopen.com/books/radioisotopes-applications-in-physical-sciences/cesium-137cs-and-133cspotassium-and-rubidium-in-macromycete-fungi-and-sphagnum-plants.

Vonmoos, M., Beer, J. & Muscheler, R. (2006) 'Large variations in Holocene solar activity: Constraints from 10Be in the Greenland Ice Core Project ice core'. *Journal of Geophysical Research: Space Physics (1978–2012)*, 111 (A10).

von Post, L. & Sernander, R. (1910) *Guides des excursions en Suède: Pflanzen-Physiognomische Studien auf Torfmooren in Närke. Excursion A7.* Norstedt.

Waldmann, N., Ariztegui, D., Anselmetti, F. S., Austin Jr, J. A., Moy, C. M., Stern, C., Recasens, C. & Dunbar, R. B. (2010) 'Holocene climatic fluctuations and positioning of the Southern Hemisphere Westerlies in Tierra del Fuego (54 S), Patagonia'. *Journal of Quaternary Science*, 25 (7). pp 1063-1075.

Wallén, B., Falkengren-Grerup, U. t. & Malmer, N. (1988) 'Biomass, productivity and relative rate of photosynthesis of Sphagnum at different water levels on a South Swedish peat bog'. *Ecography*, 11 (1). pp 70-76.

Walling, D. E., Quine, T. A. (1992) 'The use of caesium-137 measurements in soil erosion surveys'. *Erosion and sediment transport monitoring programmes in river basins*, 210 pp 143-152.

Walling, D. E., Quine, T.A. (1995) 'Use of fallout radionuclide measurements in soil erosion investigations'. [Online]. Available at: http://www.fao.org/docrep/x5313e/x5313e00.htm.

Wang, G. & Cai, W. (2013) 'Climate-change impact on the 20th-century relationship between the Southern Annular Mode and global mean temperature'. *Scientific reports*, 3

Wang, Y.-M., Lean, J. & Sheeley Jr, N. (2005) 'Modeling the Sun's magnetic field and irradiance since 1713'. *The Astrophysical Journal*, 625 (1). pp 522.

Wanner, H., Mercolli, L., Grosjean, M. & Ritz, S. (2015) 'Holocene climate variability and change; a data-based review'. *Journal of the Geological Society*, 172 (2). pp 254-263.

Warner, B. (1990) 'Testate amoebae (protozoa)'. *Geoscience Canada Reprint Series*, 5 pp 65-74.

Warner, B. G. & Charman, D. J. (1994) 'Holocene changes on a peatland in northwestern Ontario interpreted from testate amoebae (Protozoa) analysis'. *Boreas*, 23 (3). pp 270-279.

Warner, B. G., Nobes, D. C. & Theimer, B. D. (1990) 'An application of ground penetrating radar to peat stratigraphy of Ellice Swamp, southwestern Ontario'. *Canadian Journal of Earth Sciences*, 27 (7). pp 932-938.

Waterhouse, J. S., Switsur, V., Barker, A., Carter, A. & Robertson, I. (2002) 'Oxygen and hydrogen isotope ratios in tree rings: how well do models predict observed values?'. *Earth and Planetary Science Letters*, 201 (2). pp 421-430.

Weltzin, J. F., Harth, C., Bridgham, S. D., Pastor, J. & Vonderharr, M. (2001) 'Production and microtopography of bog bryophytes: response to warming and water-table manipulations'. *Oecologia*, 128 (4). pp 557-565.

Whitaker, D. L. & Edwards, J. (2010) 'Sphagnum moss disperses spores with vortex rings'. *science*, 329 (5990). pp 406-406.

White, J., Ciais, P., Figge, R., Kenny, R. & Markgraf, V. (1994) 'A high-resolution record of atmospheric CO2 content from carbon isotopes in peat'. *Nature*, 367 pp 153-156.

Wieder, R. K. & Lang, G. E. (1983) 'Net primary production of the dominant bryophytes in a Sphagnum-dominated wetland in West Virginia'. *Bryologist*, pp 280-286.

Wilmes, S., Raible, C. & Stocker, T. (2012) 'Climate variability of the mid-and high-latitudes of the Southern Hemisphere in ensemble simulations from 1500 to 2000 AD'. *Climate of the Past*, 8 pp 373-390.

Woodland, W. A. (1996) 'Holocene palaeohydrology from testate amoebae analysis: developing a model for British peatlands'.

Woodland, W. A., Charman, D. J. & Sims, P. C. (1998) 'Quantitative estimates of water tables and soil moisture in Holocene peatlands from testate amoebae'. *The Holocene*, 8 (3). pp 261-273.

Woodley, E. J., Loader, N. J., McCarroll, D., Young, G. H., Robertson, I., Heaton, T. H., Gagen, M. H. & Warham, J. O. (2012) 'High-temperature pyrolysis/gas chromatography/isotope ratio mass spectrometry: simultaneous measurement of the stable isotopes of oxygen and carbon in cellulose'. *Rapid Communications in Mass Spectrometry*, 26 (2). pp 109-114.

Worsfold, R. D., Parashar, S. K. & Perrott, T. (1986) 'Depth profiling of peat deposits with impulse radar'. *Canadian Geotechnical Journal*, 23 (2). pp 142-154.

Yan, H., Sun, L., Wang, Y., Huang, W., Qiu, S. & Yang, C. (2011) 'A record of the Southern Oscillation Index for the past 2,000 years from precipitation proxies'. *Nature Geoscience*, 4 (9). pp 611-614.

Yeloff, D. & Mauquoy, D. (2006) 'The influence of vegetation composition on peat humification: implications for palaeoclimatic studies'. *Boreas*, 35 (4). pp 662-673.

Young, G. H., Loader, N. J. & McCarroll, D. (2011) 'A large scale comparative study of stable carbon isotope ratios determined using on-line combustion and low-temperature pyrolysis techniques'. *Palaeogeography, Palaeoclimatology, Palaeoecology*, 300 (1). pp 23-28.

Yu, Z., Loisel, J., Brosseau, D. P., Beilman, D. W. & Hunt, S. J. (2010) 'Global peatland dynamics since the Last Glacial Maximum'. *Geophysical research letters*, 37 (13). pp L13402.

Yuan, X. (2004) 'ENSO-related impacts on Antarctic sea ice: a synthesis of phenomenon and mechanisms'. *Antarctic Science*, 16 (4). pp 415-425.

Yurtsever, Y. & Gat, J. R. (1981) 'Atmospheric waters'. *Stable isotope hydrology: deuterium and oxygen-18 in the water cycle*, 210 pp 103-142.

Zanazzi, A. & Mora, G. (2005) 'Paleoclimatic implications of the relationship between oxygen isotope ratios of moss cellulose and source water in wetlands of Lake Superior'. *Chemical geology*, 222 (3). pp 281-291.

Zhang, R. & Delworth, T. L. (2005) 'Simulated tropical response to a substantial weakening of the Atlantic thermohaline circulation'. *Journal of Climate*, 18 (12). pp 1853-1860.

Zhang, X., Zwiers, F. W., Hegerl, G. C., Lambert, F. H., Gillett, N. P., Solomon, S., Stott, P. A. & Nozawa, T. (2007) 'Detection of human influence on twentieth-century precipitation trends'. *Nature*, 448 (7152). pp 461-465.

Zhou, S., Gelman, M. E., Miller, A. J. & McCormack, J. P. (2000) 'An inter-hemisphere comparison of the persistent stratospheric polar vortex'. *Geophysical research letters*, 27 (8). pp 1123-1126.

Zolitschka, B., Schäbitz, F., Lücke, A., Corbella, H., Ercolano, B., Fey, M., Haberzettl, T., Janssen, S., Maidana, N. & Mayr, C. (2006) 'Crater lakes of the Pali Aike Volcanic Field as key sites for paleoclimatic and paleoecological reconstructions in southern Patagonia, Argentina'. *Journal of South American Earth Sciences*, 21 (3). pp 294-309.